Half-Round Bearing Stiffeners for Skewed Steel I-Girders

Project No. BED65-DOT-RFP-22-9068-SD

Final Report
December 2024

Principal Investigator: Armin Mehrabi
Co-PI: Todd Helwig
Co-PI: Kingsley Lau
Co-PI: Atorod Azizinamini

Graduate Assistants: Dariya Tabiatnejad
Seyed Saman Khedmatgozar Dolati

Department of Civil and Environmental Engineering
Florida International University
Miami, FL

Authors
Dariya Tabiatnejad
Armin Mehrabi
Todd Hewig
Kingsley Lau
Seyed Saman Khedmatgozar Dolati

Sponsored by

FDOT
Florida Department of Transportation

A report from

FIU | FLORIDA INTERNATIONAL UNIVERSITY

DISCLAIMER

This research is funded by the Florida Department of Transportation. The opinions, findings, and conclusions expressed in this publication are those of the authors and not necessarily those of the Florida Department of Transportation.

Technical Report Documentation Page

1. Report No. : FIU-BED65-06	2. Government Accession No.	3. Recipient's Catalog No.	
4. Title and Subtitle **Half-Round Bearing Stiffeners for Skewed Steel I-Girders**		5. Report Date December 2024	
		6. Performing Organization Code	
7. Author(s) Armin Mehrabi https://orcid.org/0000-0003-4736-850X Dariya Tabiatnejad https://orcid.org/0000-0002-1643-2743 Seyed Saman Khedmatgozar Dolati https://orcid.org/0000-0002-6016-9030 Atorod Azizinamini Todd Helwig Kingsley Lau		8. Performing Organization Report No.	
9. Performing Organization Name and Address Department of Civil and Environmental Engineering Florida International University 10555 West Flagler Street, EC 3680 Miami, FL 33174		10. Work Unit No. (TRAIS)	
		11. Contract or Grant No. BED65-DOT-RFP-22-9068-SD	
12. Sponsoring Organization Name and Address FDOT Research Center Phone: (850) 414-5260 605 Suwannee Street Tallahassee, Florida 32399-0450 Email: research.center@dot.state.fl.us		13. Type of Report and Period Covered Final Report	
		14. Sponsoring Agency Code	
15. Supplementary Notes			
16. Abstract A new connection type, Half-Round Bearing Stiffener (HRBS) connection, has been developed and investigated by others as an alternative to bent plate connection for joining end cross-frames to steel girders in skewed bridges. The configuration of this connection assures the connection stiffener plate is perpendicular to the HRBS regardless of the skew angle and avoids the use of bent connection plates. Higher stiffness of girders against lateral deflection provided by HRBS has been also recognized as positive for construction phase fit-up activities. The buckling strength of girders has been found to improve because of the restraint against warping provided by the HRBS, and less twist and less cross-frame force will be the consequence. Over the intermediate support and negative moment region in continuous bridges, the upper flanges of the girders experience tensile stress variations from the live load, and therefore, create susceptibility to fatigue at the connection of the HRBS to the tension flange at that location. This also generates potential stress risers and concentration adding to the overall concerns about the fatigue behavior of this connection detail. A more in-depth investigation of the fatigue behavior of the HRBS connection and its variations is therefore desirable. The objective of this research project is to develop a testing program for determining the fatigue sensitivity of the HRBS connection over the intermediate support in continuous skewed steel girder bridges and to categorize the detail in accordance with the AASHTO LRFD existing fatigue categories. The project also evaluated the effect of welding the stiffener (connection) plate to the flange. This will be accomplished through a review of the literature on the skew bridge and cross-frame connections, selection of candidate bridges in Florida for parametric studies, identifying the factors affecting the fatigue behavior of this connection detail, and establishing a test matrix, plan, and setup for laboratory fatigue testing that accounts for these parameters. A corrosion study plan will also be developed to review the effects of material type and sizes, application of coatings, use of fillers, and venting by analysis or testing for this configuration.			
17. Key Words Skewed Bridges, Half-Round Bearing Connection, Steel Girders, Cross Frames, Connections, Fatigue, Corrosion, Test Plan		18. Distribution Statement	
19. Security Classification	20. Security Classification (of this page)	21. No. of Pages 378	22. Price

ACKNOWLEDGMENTS

The authors would like to acknowledge the support provided by the Florida Department of Transportation Research Center.

The author would like to extend special appreciation to Ms. Vickie Young, the Project Manager, and the FDOT Research Technical Committee members, Ms. Christina Freeman, Mr. Timothy McCullough, and Mr. Dennis Golabek, for their guidance throughout the project.

The author would like to acknowledge Midasoft company for generously providing their software, which significantly contributed to the success of this research.

Executive Summary

The 10th Edition of the AASHTO Bridge Design Specifications (2024) include Half-Round Bearing Stiffeners (HRBS) that can provide improvements in connections between cross-frame or diaphragms in steel bridge systems. The improvements are particularly present in bridges with skewed supports since they provide an alternative to bent plate connections for joining end cross-frames to the steel girders. Although bent plates provide a simple means of accommodating the skew angle during fabrication, the plates result in eccentricities in the connection that reduce the effectiveness of the cross-frames due to flexibility in the plate. The HRBS detail assures the connection stiffener plate is perpendicular to the rounded plate regardless of the skew angle and avoids the need for flexible bent connection plates. Higher stiffness against lateral deflection and buckling strength of girders has been found to improve because of the restraint against rotation and warping provided by the HRBS. However, before the HRBS is widely utilized in practice, a closer evaluation of the behavior under in-service conditions of the detail is warranted to ensure potential maintenance issues do not arise. One area of the bridge deserving closer study is at interior supports of continuous bridges where the upper girder flanges experience tensile stress variations from the live load, and therefore, create potential susceptibility to fatigue at the connection of the rounded plate to the tension flange at that location. This also generates potential stress concentration adding to the overall concerns about the fatigue behavior of this connection detail. A more in-depth investigation of the fatigue behavior of the half-round bearing stiffener connection and its variations is therefore desirable.

The objective of this research project is to develop a testing program for determining the fatigue sensitivity of the half-round bearing stiffener connection over the intermediate support in continuous skewed steel girder bridges, to evaluate the effect of welding the stiffener (connection) plate to the flange, and to categorize the detail through testing in accordance with the AASHTO LRFD existing fatigue categories. The goals of the study were accomplished through i) a review of the literature on the skew bridge and cross-frame connections, ii) evaluation of plans of existing bridges in Florida for detailed parametric studies, iii) identifying the factors affecting the fatigue behavior of the connection detail, and iv) establishing a test matrix, plan,

and setup for laboratory fatigue testing of the HRBS detail. A corrosion study plan will also be developed to review the effects of material type and sizes, application of coatings, use of fillers, and venting by analysis or testing for this configuration.

Background

Figure E-1 depicts a bridge with skewed supports and includes an isometric and plan view of the bridge system. The skewed geometry results in a condition in which the longitudinal axis of the girder that is not perpendicular to abutments or pier supports. The resulting geometry presents unique structural challenges. The skew angle, defined as the angle between the end support centerline and a line perpendicular to the longitudinal axis of the bridge, significantly influences the resulting structural behavior. Skewed bridges require specialized design considerations due to the complexity of the load paths. This complexity leads to uneven force distribution across the structure, increasing the potential for over-stress and fatigue. Therefore, it is crucial to design these bridges with an understanding of their unique demands to ensure structural integrity and longevity.

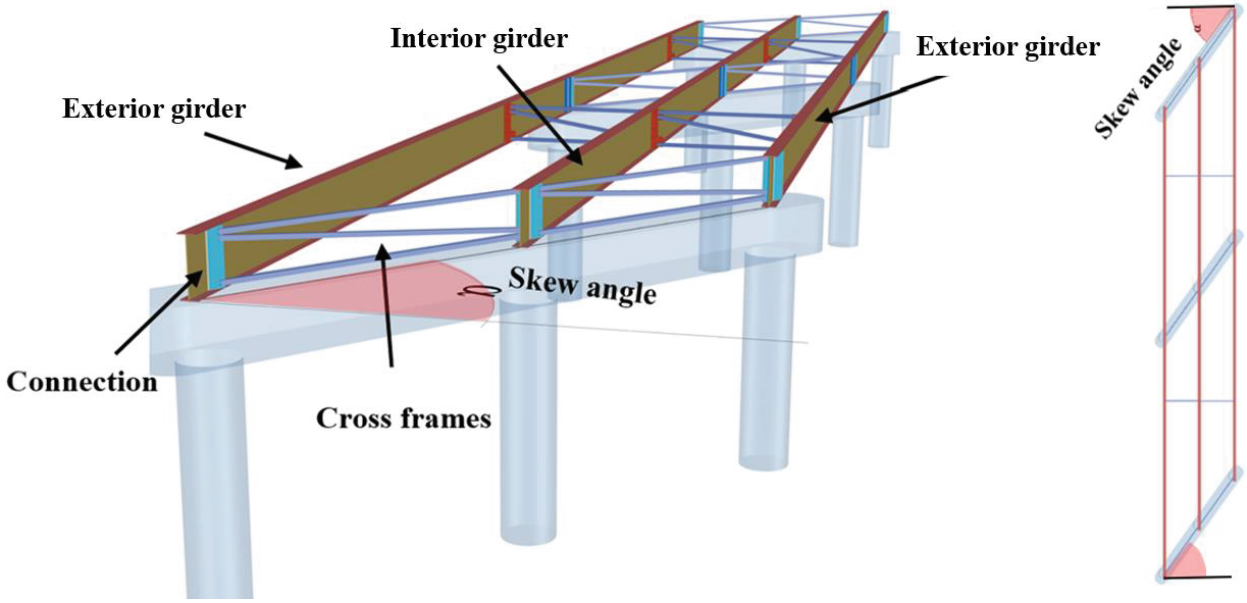

Figure E-1 Overall view of a skewed bridge

Steel girders are often used in the construction of skewed bridges with I-shaped girder configurations. These girders are connected by cross-frames or diaphragms, which are essential

for stability during construction. The interaction between girders and cross-frames becomes more complex, with larger skew angles resulting in higher live load-induced stresses. This increased stress can increase the fatigue demands in both the braces and the girders.

A significant concern in skewed steel girder bridges is the behavior during the construction phase. During this time, girders are subject to substantial loads, including the weight of the concrete deck and construction equipment. Cross-frames, which act as torsional braces, play a vital role in preventing the girders from twisting and primary source of girder stability. Various cross-frame configurations, such as X-type, K-type, and plate diaphragms, are designed to enhance stability and reduce torsional deformations.

End cross-frames, located at the bridge's supports, are critical in controlling girder twist and transferring lateral loads from sources such as seismic or wind events. Design and construction of end cross-frames in skewed bridges is challenging due to the complex interaction between adjacent girders. During construction, the complex skewed geometry results in the girders rotating with the application of the applied load and the fit-up condition for the cross-frames is a major consideration during fabrication and erection. Two primary sources of twist in skewed bridge girders include the rotation of cross-frames at the bearing line and differential deflection of girders in between the supports. Addressing these issues requires precise detailing and fit-up strategies during construction to ensure that girders are plumb at the desired load level and that additional stresses caused by support skew are effectively managed.

Skewed connections, which join structural elements at angles other than 90 degrees, require unique design considerations to ensure both safety and structural integrity. In skewed bridges, the connections between end cross-frames and girders are of special interest. Two connection types in these scenarios are the commonly used bent plate and newly introduced Half-Round Bearing Stiffener (HRBS) details. Bent plates, while flexible and easier to construct, can reduce the stiffness of cross-frames and therefore impact girder stability. HBRS, on the other hand, provide higher stiffness and improved the girder warping restraint, thereby resulting in benefits for systems with highly skewed applications.

Various analytical methods have been used to analyze the complex behavior of skewed bridges, ranging from simple line-girder analyses to more sophisticated 3D Finite Element Analysis (FEA). The choice of method depends on the complexity of the bridge design and the required level of accuracy. While line-girder analysis might suffice for simple bridges, more intricate designs, particularly those with significant skew angles, often require the detailed insights provided by advanced computational models. Selecting the appropriate analysis method is crucial for accurately predicting the bridge's behavior under various loads and conditions.

Fatigue considerations are another critical aspect of designing skewed bridges. Understanding the fatigue behavior of these structures, particularly at the connections of HRBS to tension flanges, is essential. Continuous girders at interior supports often experience significant moments, making fatigue performance a concern.

The unique geometry and exposure conditions for some HRBS applications may also require tailored corrosion protection strategies. Selecting steel with improved corrosion resistance combined with appropriate coatings and sealants can effectively improve the corrosion performance of the connections. Proper detailing, such as venting and drainage, is also crucial in preventing moisture and corrosive agents from accumulating within the connections, which can lead to accelerated corrosion.

Analytical Study

The design and analysis of skewed bridges require specialized techniques to account for the effects of support skew, which can significantly influence the performance of critical structural elements. This study focuses on the design and evaluation of Half-Round Bearing Stiffener (HRBS) connections in skewed bridges.

The primary objective of the analytical study in this project was to develop a comprehensive understanding of the behavior of HRBS connections under various loading conditions and to provide representative detailing and sizing for bridges with the range of parameters considered in the study and for use in future fatigue testing. This objective was achieved through a rigorous

analytical approach combining global and local analyses utilizing advanced finite element modeling techniques to simulate the structural behavior of representative skewed bridges.

A key aspect of the study was the selection of a population of 26 skewed bridges by the FDOT Project Technical Committee, identified as being representative of the practical range of parameters observed in continuous skewed steel girder bridges and for which HRBS connections could offer an alternative. The parameters considered include the skew angle, span length, bridge width, number of steel girders, cross-frame configuration, and girder spacing. The selected bridges encompass a variety of geometrical configurations and structural characteristics, ensuring that the analysis covers a broad spectrum of real-world scenarios.

The analysis was divided into two levels. The Level I analyses focused on modeling the entire bridge systems to assess stress variations in girder flanges and forces in the end cross-frame members. This analysis utilized Midas Civil software for 3D FEM analyses and provided data on the envelope of forces that are crucial for the subsequent, more detailed analysis. The Level II analyses consisted of a refined analysis of the HRBS connections using Midas FEA NX software, emphasizing local stress distributions and the sizing of HRBS connections for various detailing options.

Level I Analyses

The Level I analyses involved developing models of the entire bridge systems, with the primary focus on assessing stress variations in the girder tension flanges and forces in the end cross-frame members. This analysis was essential for understanding the overall behavior of the bridge under various load conditions and for identifying the critical forces that must be considered in the subsequent, more detailed analyses.

A preliminary literature review pointed to modeling methods, including 2D or 3D grids for bridge modeling on a global scale. Despite these recommendations, the research group decided that the Level I analyses could be more effectively performed using improved 3D FEM analysis models. These models provide a more accurate representation of the structural behavior when compared to grid models, allowing for better and more refined evaluation of the forces and stresses that

develop in the critical components. Among several FE programs, the study identified Midas Civil, a sophisticated finite element analysis (FEA) program, as the most suitable tool for conducting these analyses due to the advanced modeling capabilities and ease of use. Figure E-2 shows a sample Level I model of one of the bridges analyzed in the study. All elements of the girders were modeled using plate elements, and the cross-frame members were modeled using beam elements.

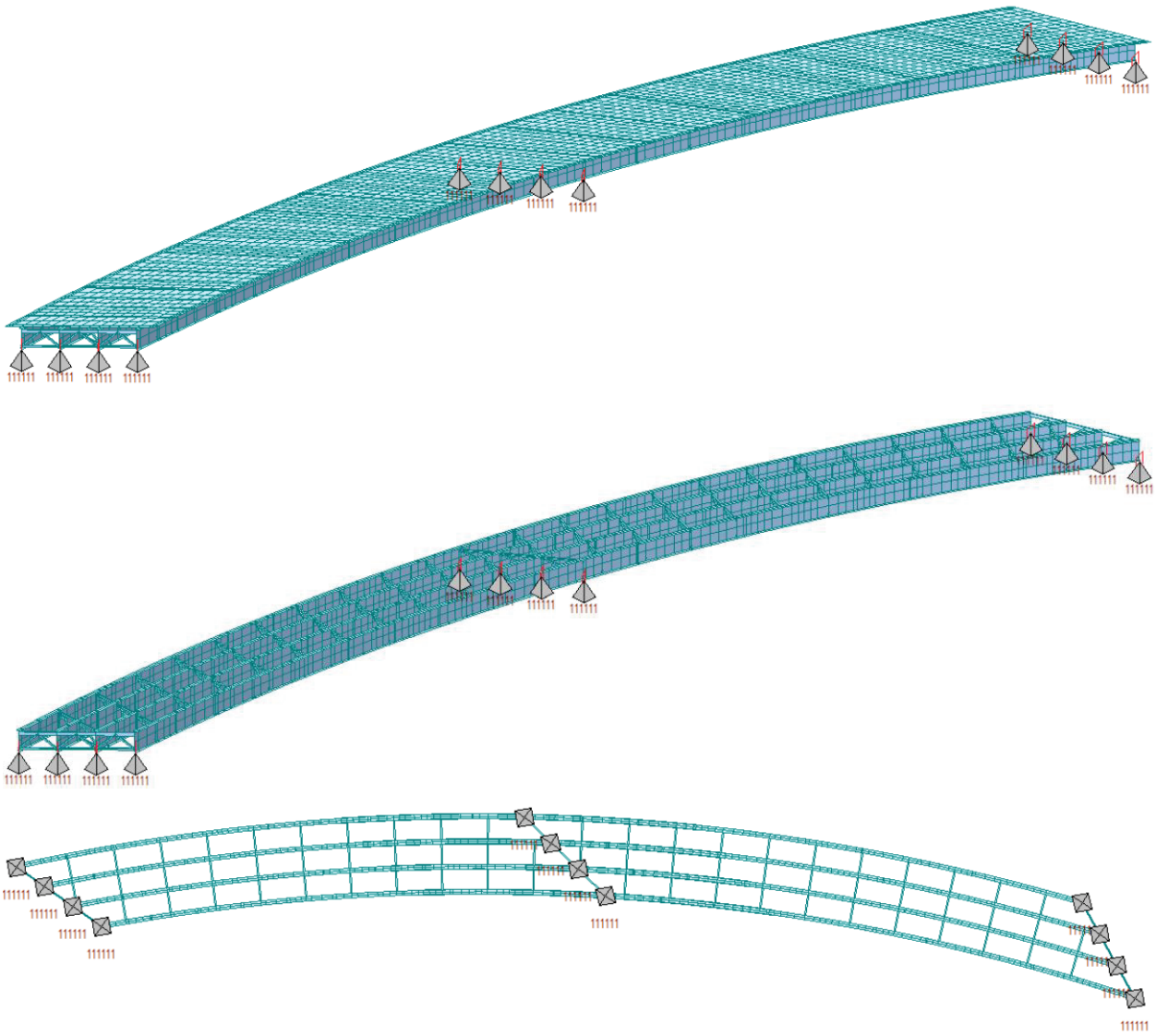

Figure E-2- Bridge 70 FEM Model at Level I

The Level I analyses produced two sets of critical information: the tensile stress variation in the girder top flange over the intermediate pier, which is crucial for planning fatigue tests, and the

forces in the end cross-frame members, which are necessary for sizing and detailing the HRBS connections. These outputs provide the foundation for the Level II analyses focused on the local connection behavior and were, therefore, more refined than the Level I analyses. Figure E-3 shows a histogram of factored tensile stresses in the top flange over the intermediate piers for the population of bridges analyzed in the study.

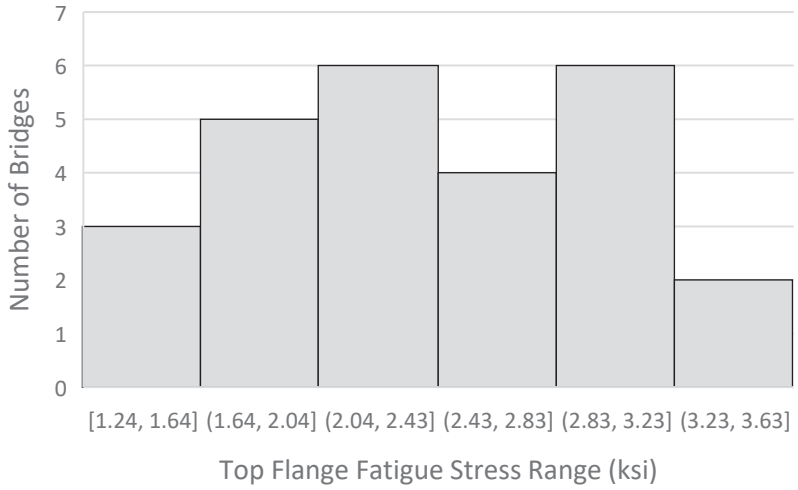

Figure E-3- Histogram for top flange fatigue stress range (ksi)

Selection of Representative Bridges

The main goal of the analyses was to select representative bridges that reflect the characteristics of all 26 bridges, focusing on their geometric configurations. Critical parameters for selecting these representative bridges include the Skew Index, cross-frame member forces, the moment of inertia of steel I-girders, and bridge curvature. These parameters capture essential aspects of the bridge performance and properties. The selection process involved sorting the bridges based on each parameter in ascending order and dividing them into groups: Group 1 with lower parameter values, Group 2 with intermediate values, and Group 3 with higher values. After grouping the bridges based on the skew index, cross-frame member forces, and girder moment of inertia, Venn diagrams were used to identify bridges common to each group for all three parameters. From there, Bridge 65 was selected as the representative for bridges with lower parameter values, Bridge 25 for those with intermediate values, and Bridge 72 for higher parameter values. These bridges also vary in terms of curvature. To ensure the representative

bridge adequately covers all bridges in its group, force envelopes were developed within a given grouping of the bridges, and the connections were designed to handle the highest forces in the group. Table E-1 shows the envelope of design and Fatigue-I forces for the three representative bridges used in the Level II analyses.

Table E-1-Cross-frame internal forces used for analysis Level II

		Cross-frame Member Forces								
		Design Envelope (Kips)						Fatigue I Force Range (Kips)		
	Alternative	TOP CHORD		DIAGONAL		BOT CHORD		TOP CHORD	DIAGONAL	BOT CHORD
#	Bridge #	min	max	min	max	min	max			
24	**65**	-12.6	27.8	-47.7	41.3	-43.4	34.9	22.1	27.7	18.3
23	**25**	-21.4	27.7	-73.2	65.9	-16.1	50.5	13.3	16.1	34.8
9	**72**	-64.2	68.4	-110.0	102.0	-155.6	145.9	17.3	13.3	53.0

Level II Analyses

The Level II analyses build on the results of the Level I analyses by focusing on refined models of the girder and HRBS details. The primary objective of this analysis is to obtain detailed stress distributions within the HRBS connection details for proper sizing and design of the components. The Level II analyses employed Midas FEA NX, a more advanced FEA program that creates highly detailed models capable of capturing local stress concentrations and other critical phenomena. Figure E-4 shows a sample Level II model of the focus region. The level of detail in this model is obviously much more significant than in the Level 1 analyses due to the interest in localized stress concentrations. Such a level of detail in the Level 1 analyses is not generally feasible due to the size of such a model – nor warranted. Because the force ranges used in the Level II analyses were based upon the findings in the Level I analyses – the results obtained from the Level II analyses are representative and encompass the behavior of all 26 bridges considered in the study.

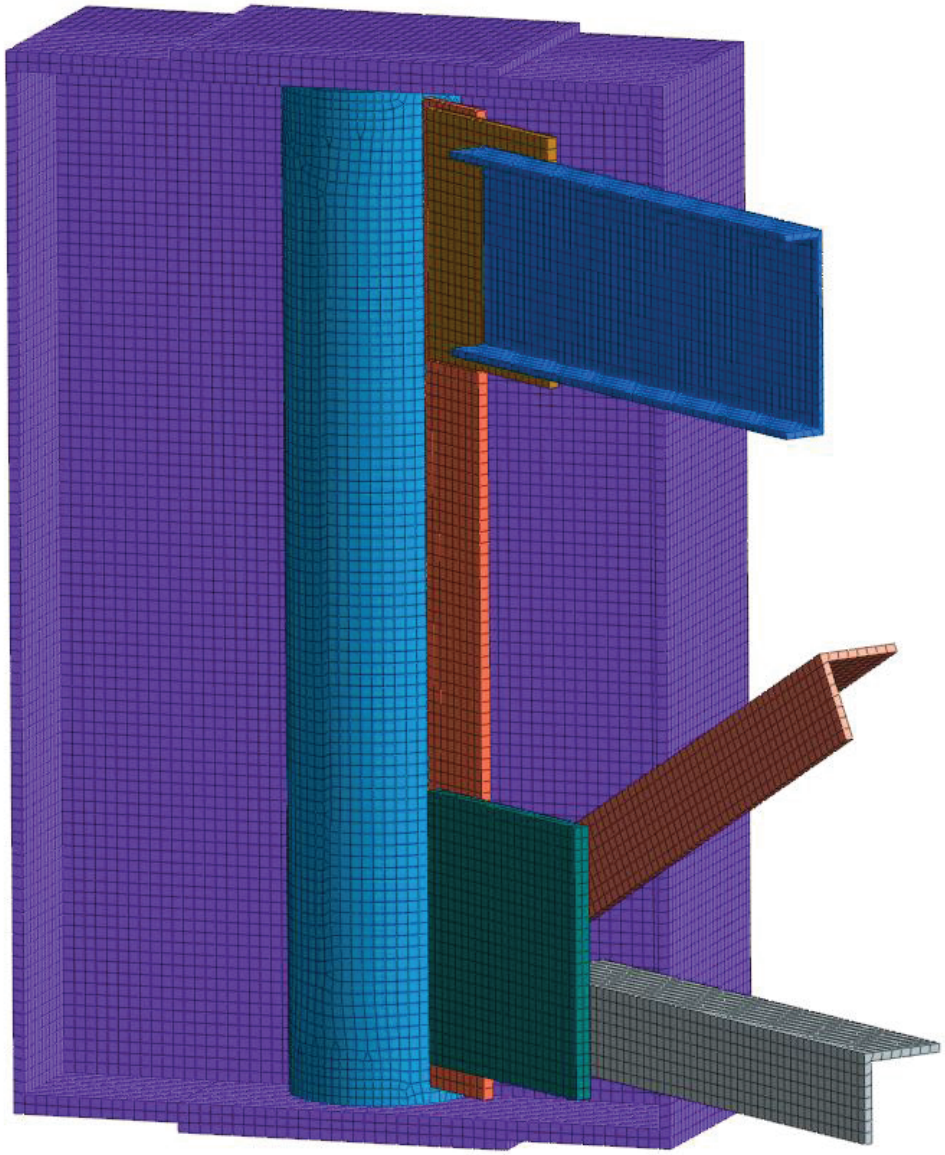

Figure E-4-A Sample FEM HRBS Connection Detail Model at Level II

In the Level II analysis, the study investigates the effects of various design parameters on the performance of HRBS connections, including the influence of connection stiffness, the presence of HRBS corner clipping, and the attachment of stiffener plates to the flanges. The analysis also considers the effects of different loading conditions, including static loads (e.g., self-weight, dead load, barrier load, and wind load) and moving loads (e.g., live loads and fatigue loads).

Results and Design Recommendations

The results of the Level I and Level II analyses provide a wealth of information on the behavior of HRBS connections under various load conditions. The study identified the maximum forces and stress ranges that these connections are likely to experience and used this information to develop detailed design recommendations. Table E-2 shows a summary of sizing for the representative bridges.

Table E-2- Summary of HRBS sizing suggested for representatives of three bridge groups

Bridge #	**Stiffener Welded to Flanges**	**Clipping Type**	**HRBS Plate Dimensions** (in.)	
			D	**t**
Bridge 72	Unwelded	Non-Clipped	16	3/4
		Clipped		3/4
	Welded	Non-Clipped	16	1/2
		Clipped		1/2
Bridge 25	Unwelded	Clipped	16	5/8
	Welded	Clipped		3/8
Bridge 65	Unwelded	Clipped	11	5/8

Comparison of Welded and Unwelded Stiffener Conditions:

A significant part of the study compares the performance of welded and unwelded stiffener conditions. The analysis shows that welding the stiffener plate to the flanges significantly reduces the stress, strain, and displacement in the HRBS connections compared to unwelded conditions. This finding highlights the importance of proper connection detailing in ensuring the long-term performance and durability of the HRBS connections. Figure E-5 provides sample FE results showing the deformed shape of the HRBS connection in Bridge 72 for the clipped and unwelded stiffener plate condition. Table E-3 compares the stresses and displacements for welded and unwelded stiffener plate conditions for Bridge 72.

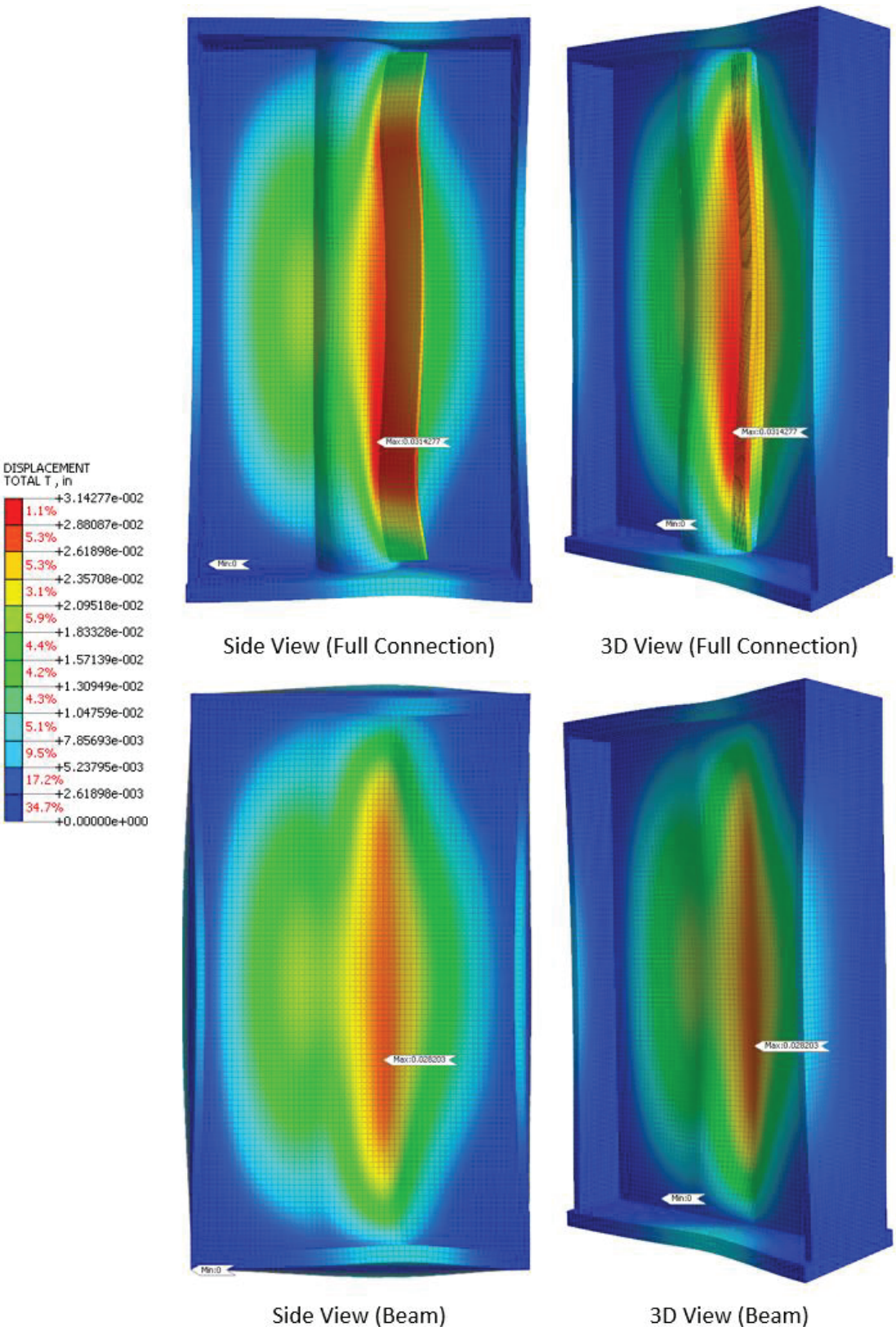

Figure E-5- Deformed shape with displacement contours in HRBS connection for clipped and unwelded condition in Bridge 72 under critical design envelope Load

Table E-3- FEA results in HRBS connection components due to Design Envelope forces, Bridge 72

HRBS Dimensions (in.)		Condition	Variables	Stiffener Plate	Half-Round Plate	Girder Web
D	t					
16	3/4	Unwelded & Clipped	Von-Mises Stress (ksi)	46.36	50.62	7.52
			Von-Mises Strain	0.001385	0.00151	0.000225
			Displacement (in.)	0.03085	0.03142	0.0282
	1/2	Welded & Clipped	Von-Mises Stress (ksi)	34.34	37.50	5.95
			Von-Mises Strain	0.001026	0.00112	0.000178
			Displacement (in.)	0.0383	0.0394	0.0319

For instance, in Bridge 72, the study showed that the von Mises stress in the HRBS plates under the unwelded condition is significantly higher than under the welded condition. This difference in stress levels suggests that the welded condition is more effective in distributing the forces and reducing the likelihood of failure in the HRBS connections. However, in some cases, the unwelded condition may be necessary due to geometric constraints or other design considerations and the results provide an indication of the likely change in behavior.

Fatigue Considerations

The half-round bearing stiffener connection models were also analyzed using the refined Finite Element Method (FEM) of the connection details under various Fatigue I load ranges. The applied forces represent the full range from compression to tension calculated by adding the absolute values of the minimum (compression) and maximum (tension) envelope forces. While there is debate over which stress type is more critical for fatigue, most support the principal stress as key. To provide a complete picture, Table E-4 presents the absolute values of both the highest Von Mises and principal stress concentration ranges observed in the connections of the three bridge models. Table E-5 shows the maximum fatigue principal stress concentration ranges and their locations for the connections corresponding to all three bridges.

Table E-4- FEA maximum von Mises and principal fatigue I stress concentration ranges for bridge models

Bridge No.	**Weld Condition**	**Clipping Condition**	**HRBS thickness** (in.)	**Max Fatigue I Stress Range in I-girder (ksi)**		**Max Fatigue I Stress Concentration Range in Stiffener** (ksi)		**Max Fatigue I Stress Concentration Range in Half Round** (ksi)	
				$\sigma_{von\ Misses}$	$\sigma_{Principal}$	$\sigma_{von\ Misses}$	$\sigma_{Principal}$	$\sigma_{von\ Misses}$	$\sigma_{Principal}$
72	Unwelded	NC	3/4	2.14	2.47	13.71	16.58	11.27	11.48
		C		2.34	2.62	13.46	16.42	15.12	14.71
	Welded	NC	1/2	3.38	4.60	11.87	14.54	7.56	8.83
		C		3.22	4.33	11.21	13.71	7.49	8.00
25	Unwelded	C	5/8	3.36	3.52	19.66	24.45	21.09	18.1
	Welded		3/8	3.86	3.55	9.64	9.93	13.59	8.25
65	Unwelded	C	5/8	3.50	3.22	18.93	25.47	27.95	26.86

Table E-5- SCR and positions in HRBS, Stiffener Plate, and Girder from Fatigue I for representative bridges

Bridge #	Stiffener Welded to Flanges	Clipping Type	HRBS Plate Dimensions (inch)		Maximum Principal Stress Concentration Range and Position in I-girder	Maximum Principal Stress Concentration Range and Position in Stiffener Plate	Maximum Principal Stress Concentration Range and Position in HRBS
			D	t			
Bridge 72	Unwelded	Non-Clipped	16	3/4	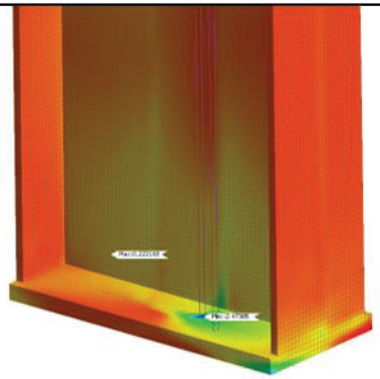 Max SCR = 2.47 (ksi)	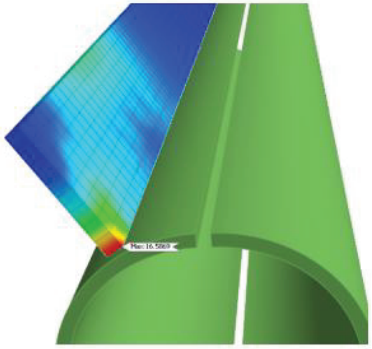 Max SCR = 16.58 (ksi)	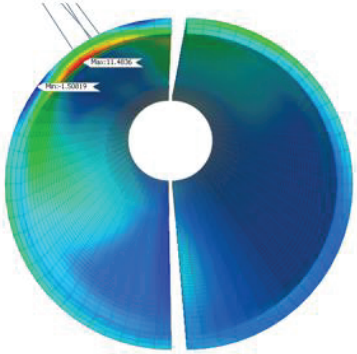 Max SCR = 11.48 (ksi)
		Clipped		3/4	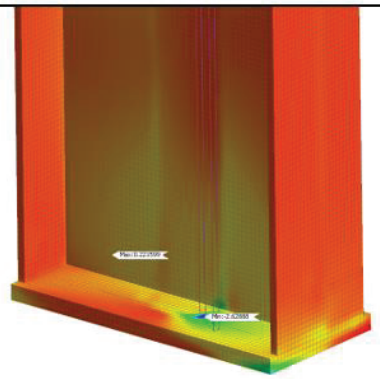 Max SCR = 2.62 (ksi)	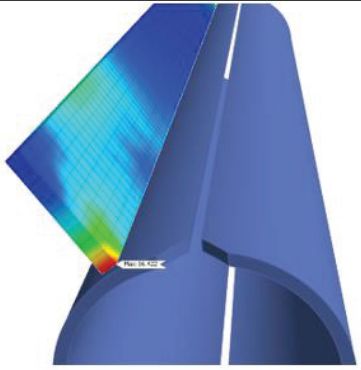 Max SCR = 16.42 (ksi)	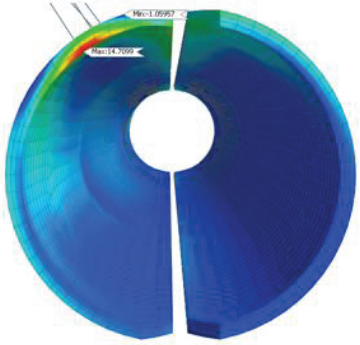 Max SCR = 14.71 (ksi)

Bridge #	Stiffener Welded to Flanges	Clipping Type	HRBS Plate Dimensions (inch)		Maximum Principal Stress Concentration Range and Position in I-girder	Maximum Principal Stress Concentration Range and Position in Stiffener Plate	Maximum Principal Stress Concentration Range and Position in HRBS
			D	t			
	Welded	Non-Clipped	16	1/2	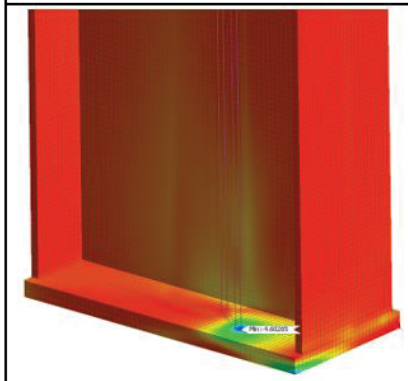 Max SCR = 4.60 (ksi)	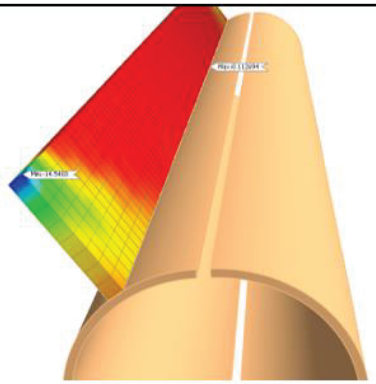 Max SCR = 14.54 (ksi)	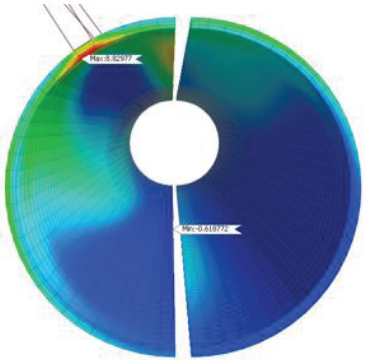 Max SCR = 8.83 (ksi)
		Clipped		1/2	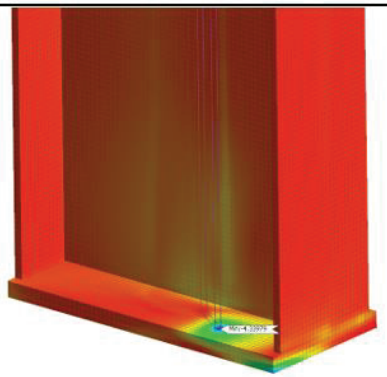 Max SCR = 4.34 (ksi)	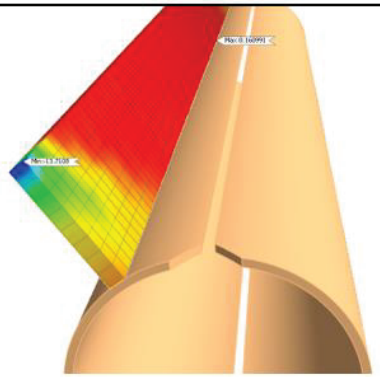 Max SCR = 13.71 (ksi)	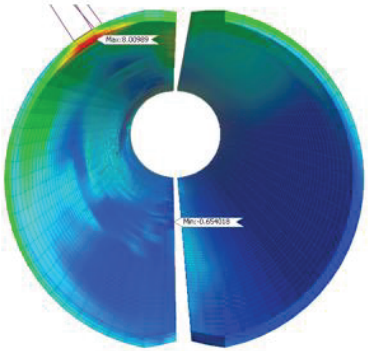 Max SCR = 8.00 (ksi)

Bridge #	Stiffener Welded to Flanges	Clipping Type	HRBS Plate Dimensions (inch)		Maximum Principal Stress Concentration Range and Position in I-girder	Maximum Principal Stress Concentration Range and Position in Stiffener Plate	Maximum Principal Stress Concentration Range and Position in HRBS
			D	t			
Bridge 25	Unwelded	Clipped	16	5/8	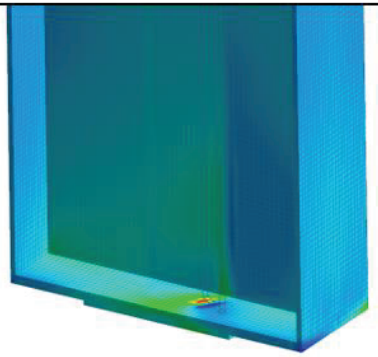 Max SCR = 3.52 (ksi)	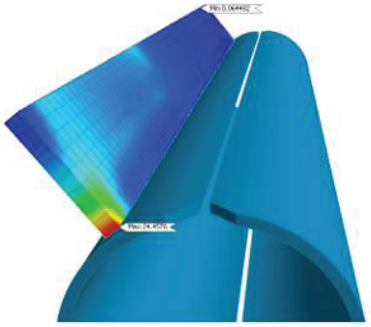 Max SCR = 24.45 (ksi)	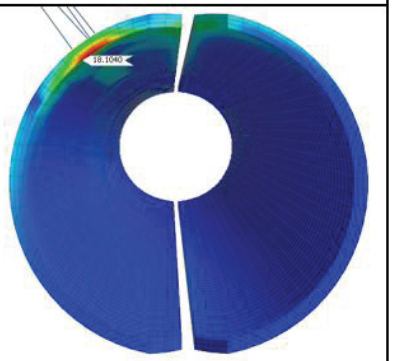 Max SCR = 18.10 (ksi)
	Welded	Clipped		3/8	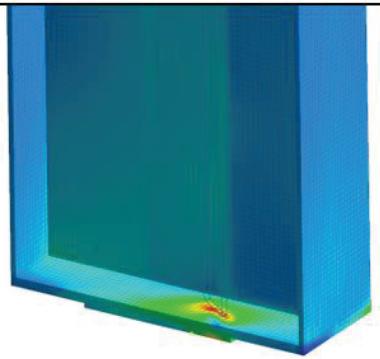 Max SCR = 3.55 (ksi)	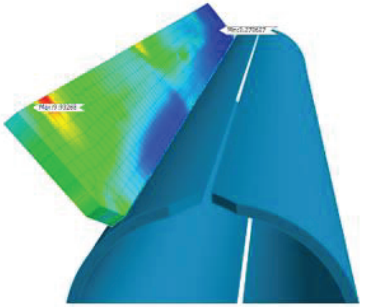 Max SCR = 9.93 (ksi)	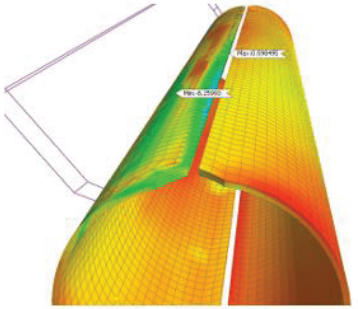 Max SCR = 8.25 (ksi)

Bridge #	Stiffener Welded to Flanges	Clipping Type	HRBS Plate Dimensions (inch)		Maximum Principal Stress Concentration Range and Position in I-girder	Maximum Principal Stress Concentration Range and Position in Stiffener Plate	Maximum Principal Stress Concentration Range and Position in HRBS
			D	t			
Bridge 65	Unwelded	Clipped	11	5/8	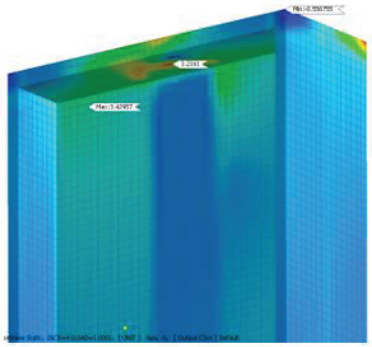 Max SCR = 3.22 (ksi)	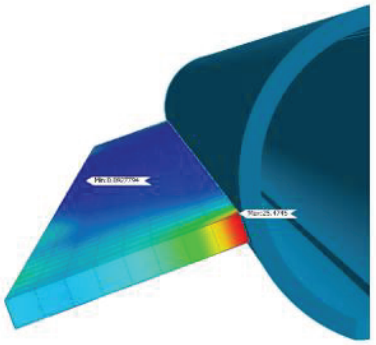 Max SCR = 25.47 (ksi)	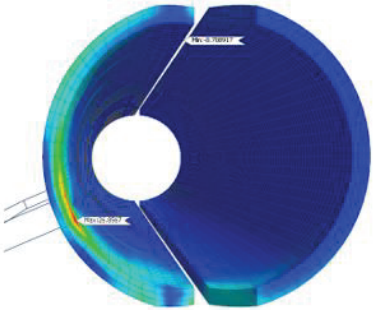 Max SCR = 26.86 (ksi)

To study the distortional effects, the stress and strain concentration ranges for the condition of unwelded stiffener plates were calculated and compared to corresponding values in the welded condition to provide a measure of the effects of distortion for Bridge 72 with the highest level of cross-frame member forces. The results, including the maximum principal stress and principal strain are summarized in Table E-6. The results show that welding the stiffener plate to the flanges considerably reduces the stress and strain when compared to the unwelded condition. Another observation is that the stress and strain ranges in the web of the girder in both conditions are relatively low. Based on the results of Level II analyses, it is the recommendation of this study to use welded stiffener plates wherever possible. This is because the fatigue stress ranges in the top flange estimated in this study are relatively low, minimizing the effects of inclined weld on the flange, and the welded stiffeners will perform better in regards with distortion fatigue in the connection itself. In addition, welding the stiffener plates is consistent with past details that have been used on cross-frame connection plates to avoid distortional-induced fatigue.

Table E-6- FEA results in HRBS connection components due to Fatigue-I force range for Bridge 72

HRBS Dimensions (in.)		**Condition**	**Variables with max. Absolute value**	**Stiffener Plate**	**Half-Round Plate**	**Girder Web**
D	**t**					
16	**3/4**	**Unwelded & Clipped**	Principal Stress Concentration Range (ksi)	16.42	14.7	1.3372
			Principal Strain Concentration Range	0.0005042	0.0005062	0.0000600
	1/2	**Welded & Clipped**	Principal Stress Concentration Range (ksi)	-13.71	8.01	-1.049
			Principal Strain Concentration Range	0.000421	0.000265	0.00004565

Corrosion Study

A comprehensive corrosion testing plan was developed for the steel half-round bearing stiffeners that are likely to be used in bridge construction, emphasizing the evaluation of methods for assessing and improving corrosion performance. The plan focuses on key aspects such as

environmental exposure, material corrosion performance, stiffener connection details, and preventative measures.

The test plan includes a rigorous testing regime to assess the effectiveness of the identified methods for improving the corrosion performance. Specific tests include assessments of seal venting and drainage efficacy, corrosion development on internal and external surfaces, and the impact of different welding techniques on corrosion resistance. The materials selected for testing were also identified including various grades of carbon steel and weathering steel plates and pipes, and the rationale behind these choices.

Test Plan

A detailed experimental testing plan aimed at determining the most appropriate fatigue category for the Half-Round Bearing Stiffener (HRBS) connection detail in steel girder designs was developed in the study. The test matrix was outlined in accordance with the variables involved, the prototypes used, and the scaling options. The targeted goal was developed to follow a statistically valid approach that minimizes the number of experiments while ensuring that the results are reliable and applicable.

The study first identified the test variables, focusing particularly on the geometry and configurations of the HRBS and girder cross-sections. The test prototypes were chosen based on a representative sample of bridges. Development of the representative test specimens was organized to cover all significant variables, such as sizes and configurations. This structured approach is essential to the effectiveness of the test plan.

Scaling is an essential aspect of the testing program due to limitations in the experimental facilities, specifically regarding space and loading capacities. Two scaling options are considered: Option 1 involves a girder depth of 34 inches, while Option 2 proposes a depth of 50 inches. Figure E-6 shows the schematic configuration of the HRBS detail for both test plan options. Detailed dimensions are shown in Table E-7 and E-8 for Options 1 and 2, respectively. The choice between these options is based on the need to balance practical dimension-scaling and weld-size

considerations, ensuring the test specimens are as representative as possible of real-world conditions while fitting to the limitations of the testing facility.

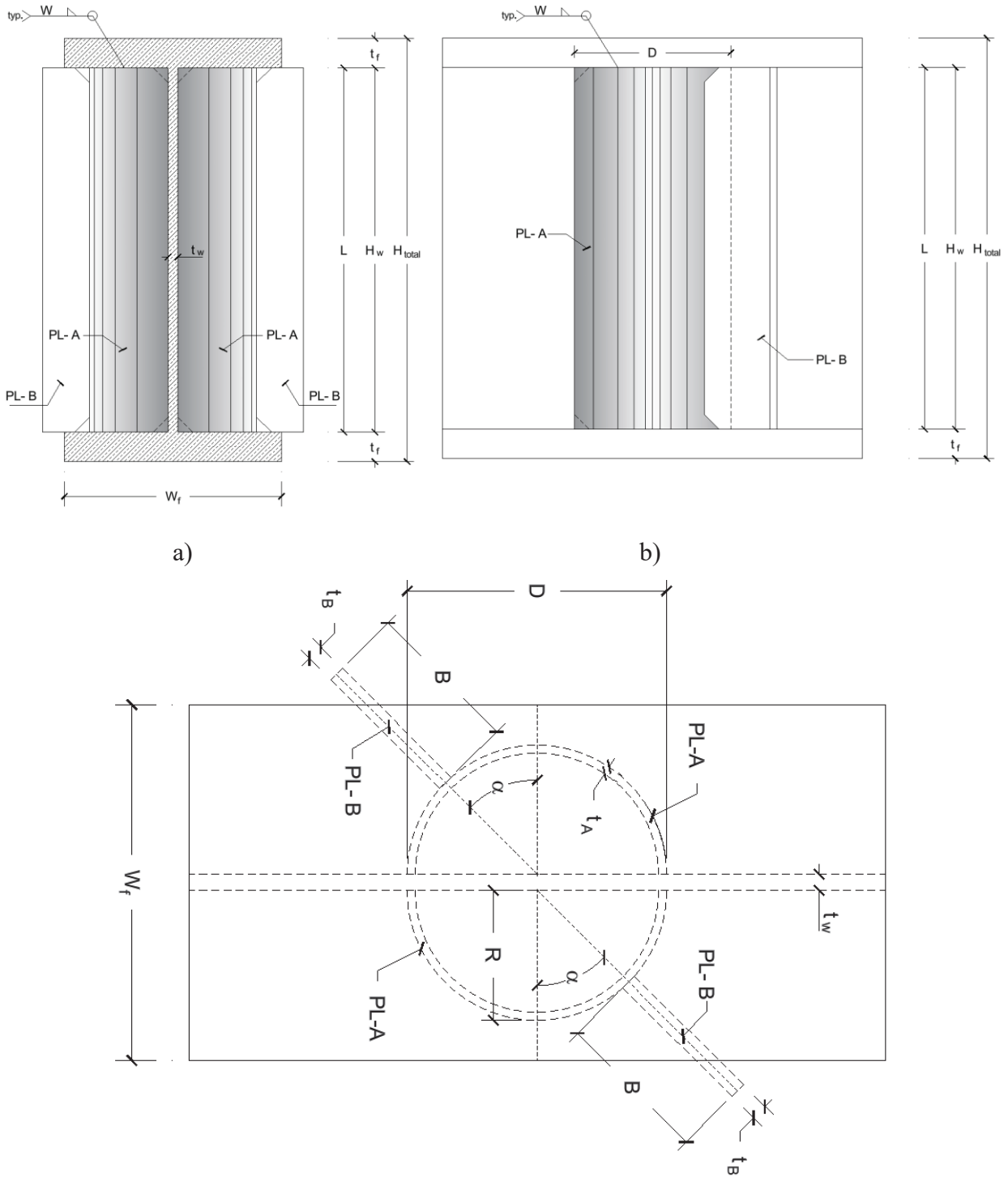

Figure E-6- HRBS skewed connection parametric details a) Front view, b) Top view, and c) Side view

Table E-7- Test specimen sizing details for the total height of 34 inches (Option 1)

Detail #	Case	Steel I-girder in.				Weld Size (Typ.) in.	Stiffener Welded to Flanges	Clipping Type	PL-A (HRBS) in.			PL-B (Stiffener) in.			
		W_f	t_f	H_w	t_w	w			D	R	t_A	L	B	t_B	α
1	1	8	1	32	1/4	1/8	Unwelded	Non-Clipped	5.5	2.75	1/4	30	3	0.4	30°
	2							Clipped	5.5	2.75	1/4	30	3	0.4	30°
2	1						Welded	Non-Clipped	5.5	2.75	3/16	32	3	0.35	60°
	2							Clipped	5.5	2.75	3/16	32	3	0.35	60°
3	1							Non-Clipped	5.5	2.75	3/16	32	3	0.35	30°
	2							Clipped	5.5	2.75	3/16	32	3	0.35	30°

Table E-8- Test specimen sizing details for the total height of 50 inches (Option 2)

Detail #	Case	Steel I-girder in.				Weld Size (Typ.) in.	Stiffener Welded to Flanges	Clipping Type	PL-A (HRBS) in.			PL-B (Stiffener) in.			
		W_f	t_f	H_w	t_w	w			D	R	t_A	L	B	t_B	α
1	1	12	1.5	47	3/8	5/16	Unwelded	Non-Clipped	8	4	3/8	45	4	0.5	30°
	2							Clipped	8	4	3/8	45	4	0.5	30°
2	1						Welded	Non-Clipped	8	4	1/4	47	4	0.5	60°
	2							Clipped	8	4	1/4	47	4	0.5	60°
3	1							Non-Clipped	8	4	1/4	47	4	0.5	30°
	2							Clipped	8	4	1/4	47	4	0.5	30°

The proposed test setup, shown in Figure E-7, is described in detail in the report, with specific attention given to the space and load level limitations inherent to the FDOT structures laboratory. The setup includes the arrangement of the girder specimens and the positioning of the HRBS details. The application of cyclic loading is described to simulate stress ranges intended for the fatigue categorization process. An elaborate instrumentation plan was also developed for the

fatigue testing. In addition to monitoring stresses and displacement, the plan calls for automated crack detection monitoring methods and appropriate pauses in test cycles to apply NDT crack detection techniques.

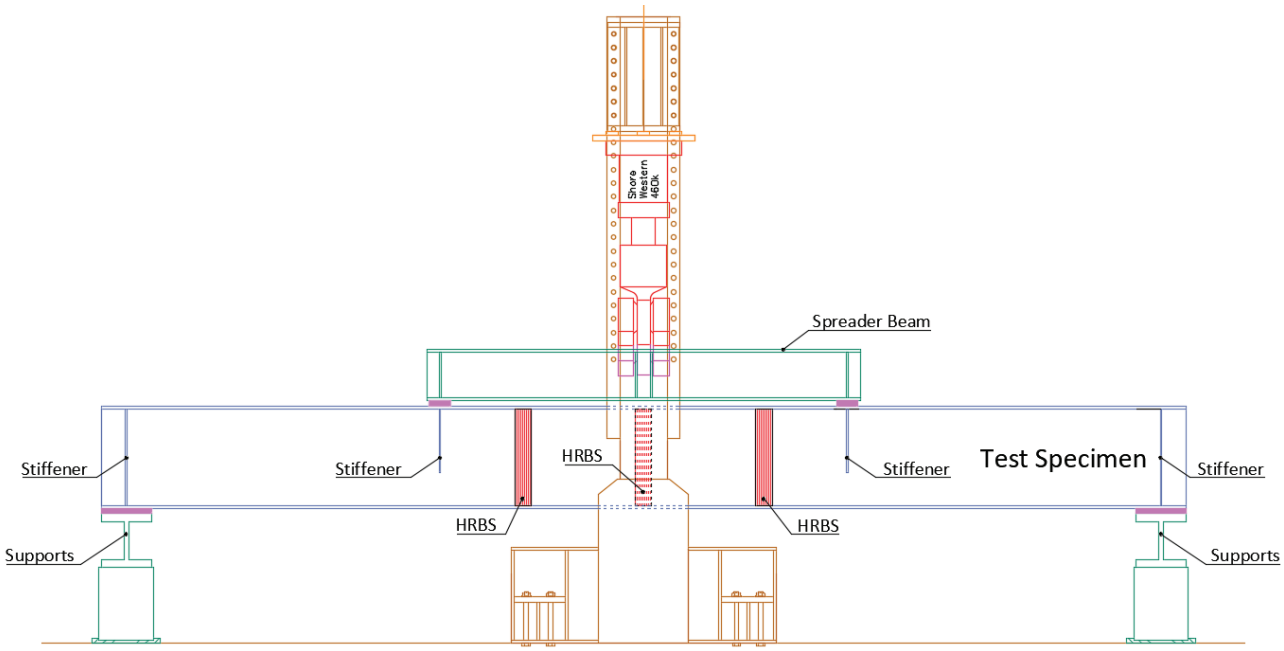

Figure E-7- Test setup

Regardless of which option is selected between Options 1 and 2, it is recommended to start with the cases that are presumed to be the most critical with respect to performance. The case of unwelded connection stiffener plate (PL-B) with non-clipped HRBS (PL-A) that is Detail 1 - Case 1 in Table E-7 and Table E-8, and the case of welded stiffener plate with non-clipped half-round stiffener and skew angle of 60 degrees that is Detail 2 - Case 1 in Table E-7 and Table E-8, are expected to generate more critical details for fatigue testing among 6 cases.

As stated earlier, the objective of the test plan is to assess the appropriate AASHTO fatigue category for the HRBS detail. An essential part of the experimental design is the stochastic approach to fatigue testing. A “design allowable test plan” was recommended in this study, which is deemed appropriate for the objectives. This plan involves selecting two stress range levels, as defined in Table E-9, for the linear descending region of the S-N bilinear curves, with a specified number of replications to ensure statistically significant results. The testing strategy also includes

provisions for reducing the total test duration by adjusting the number of tests at each stress level, demonstrating a practical approach to balancing thoroughness with efficiency.

Table E-9- Test matrix for each detail configuration (multiply this table by the number of details selected for testing)

Item	Purpose	Stress levels	Cycles	Min. Number of tests	
				Option A	Option B
1	Inclined Line portion	S1	Determined by test	6	3
2		S2	Determined by test	6	9

While this study notes that determining the descending line is sufficient for the project purpose, it provides a detailed description of the process for those cases where a more precise threshold determination might be necessary.

Safety is a paramount concern throughout the testing process, as outlined in a dedicated section on safety protocols. This section covers pre-test preparations, personal protective equipment (PPE), test setup, monitoring during the test, and post-test procedures.

The importance of data collection, management, and quality control is also emphasized through a comprehensive data management plan. The study provides a detailed and methodologically rigorous experimental testing plan designed to determine the appropriate fatigue category for HRBS connection details in steel girders among those established by AASHTO LRFD.

Table of Contents

List of Figures

List of Tables

Chapter 1- Background and Literature Review

1.1 Skewed Bridges

1.1.1 Introduction

According to the FHWA 2022, the US has approximately 619,622 bridges in service, and referencing the FDOT Bridge Inventory annual report 2021, the state of Florida has 12595 bridges, many of which can be categorized as skewed bridges. Skewed bridges, as shown in Figure 1.1, are bridges whose longitudinal axis (parallel to traffic direction) is not perpendicular to the abutment or pier support necessitated by geometrical constraints, intersecting roads, and local terrain. The skew angle is defined as the angle between the end support centerline (bridge abutment or piers center line) of the bridge and a line that is perpendicular to the bridge's longitudinal axis [1].

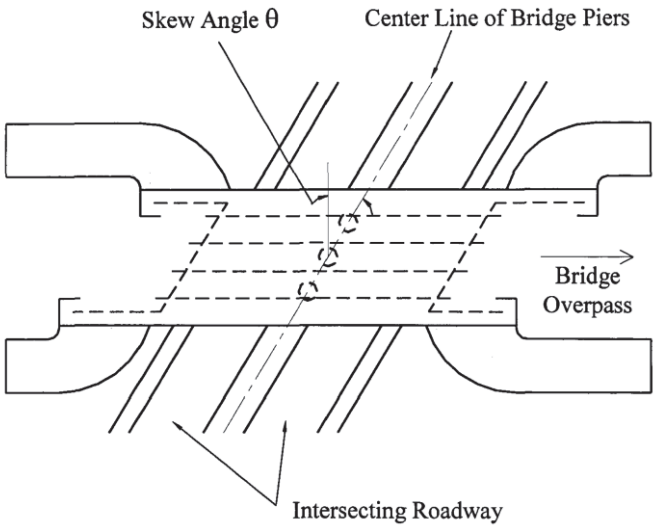

Figure 1.1 Plan View of Skewed Bridge[2]

Skewed bridge design requires extra care because the structural behavior of skewed bridges can differ significantly from non-skewed bridges [3, 4]. Unlike non-skewed bridges, the deck slab of a skewed bridge is not perpendicular to the abutment, and therefore, the load paths can be more complicated [5]. Skew effects depend on many factors, including the skew angle, span length, and spaces between girders [6]. As shown in Figure 1.2, in skewed bridge decks, the forces flow from the unsupported sides parts C and D) toward the center of the deck (part E) and then travel

from the center to the supported edges within the shortest path (parts A and B). As a result, the maximum support reaction generally happens at skewed corners [7].

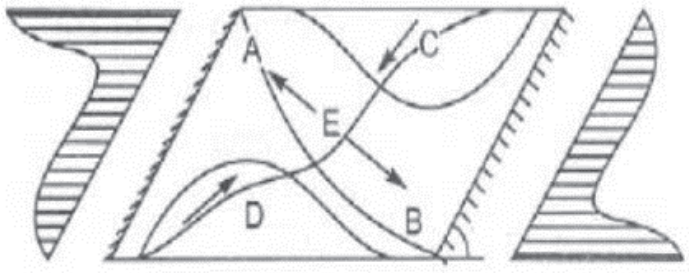

Figure 1.2 Force Flow Skewed Bridges Deck[7]

1.1.2 Skewed Steel Girder Bridges

Steel girders are often selected for the superstructure system. The steel girders can consist of either I-shaped sections or box beams that act compositely with the concrete bridge deck. Cross-frames or diaphragms generally frame between adjacent girders and serve as essential structural elements for the overall stability of the bridges, especially during construction [8]. In Figure 1.3, a skewed steel girder bridge is shown with its structural elements, such as girders, cross-frames, and piers. Larger skew angles generally increase the interaction between cross-frames and the girders, leading to more complicated structural behavior that tends to increase the live load-induced stresses in the cross-frames and their connections. Larger live-load stresses increase the potential for fatigue in the braces or the girders [2]. Several previous investigations have been conducted in relation to skewed bridges [9-16], and NCHRP Report 725 provides guidelines for analysis and construction methods for curved and skewed steel girder bridges [11]. However, among those, a recent analytical investigation performed by FDOT and the members of the research team provides a good summary of prior studies and also discusses the potentially complex behavior, and offers a simple analysis method [17, 18].

Figure 1.3 A skew bridge under construction (Roads & Bridges, November 2015)

1.1.3 Cross-frames in Steel Girder Bridges

1.1.3.1 Structural Functions of Cross-frames

One of the main controlling parameters in designing steel girder bridges is Lateral Torsional Buckling (LTB), especially during the construction phase when the steel girders support the entire construction load, including the weight of the concrete deck and forming system, the steel girder self-weight, and the weight of construction equipment and personnel. As depicted in Figure 1.4, Lateral Torsional Buckling is an instability mode involving a lateral translation and twist of the cross-section. In most situations involving gravity loading, the compression flange experiences the largest lateral deformation (Δ) while the tension flange usually experiences a smaller deformation, leading to twisting of the girder cross-section (θ) [19].

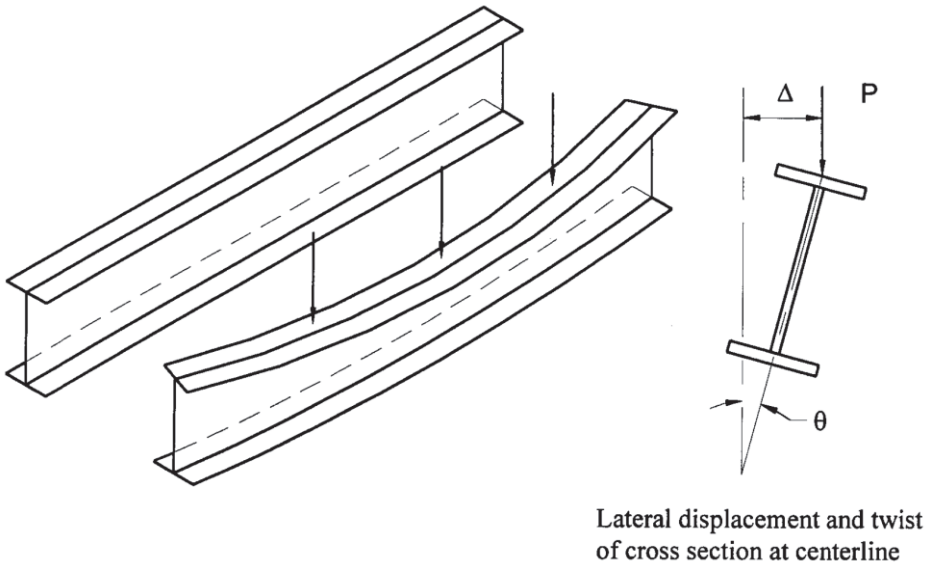

Figure 1.4 Lateral Torsional Buckling in a Steel Girder [19]

The LTB capacity of a steel girder can be increased by providing an intermediate bracing system along the length of the steel girders [19]. Effective bracing can be achieved by either stopping the lateral movement of the compression flange (lateral bracing) or by preventing the twist of the section (torsional bracing). In straight girder bridges, these bracing systems are often considered secondary members. The classification as "secondary" does not imply the braces are not important; however, in contrast to primary structural members, stringent material tests such as Charpy V-Notch (CVN) specimens are not generally required for secondary structural members. The primary bracing system utilized in steel bridges consists of cross frames or diaphragms categorized as torsional bracing systems since these members primarily provide bracing by restricting the twist of the adjacent girders that the braces frame between. Although torsional bracing systems can be categorized as either continuous or discrete bracing systems, cross-frames are categorized as discrete systems since the braces are spaced intermittently along the girder length [20]. Cross-frames generally consist of diagonal and horizontal steel truss members in the X or K shape (Figure 1.4). The truss members can typically be a channel, angle, double angle, W-shapes, or WT-Shapes [21]. Some bridge owners include details without a top strut such as those shown in Figures 5a and 5b. However, as shown in subsequent sections, many bridge owners include a top strut. For K-frame systems, the presence of the top strut can be very important since the strut ensures a deformational mode with the top flanges moving in the same direction. Without a top strut for a K-frame, a mode in which the top flanges move in opposite directions is possible, which results in a reduction in the effectiveness of the brace.

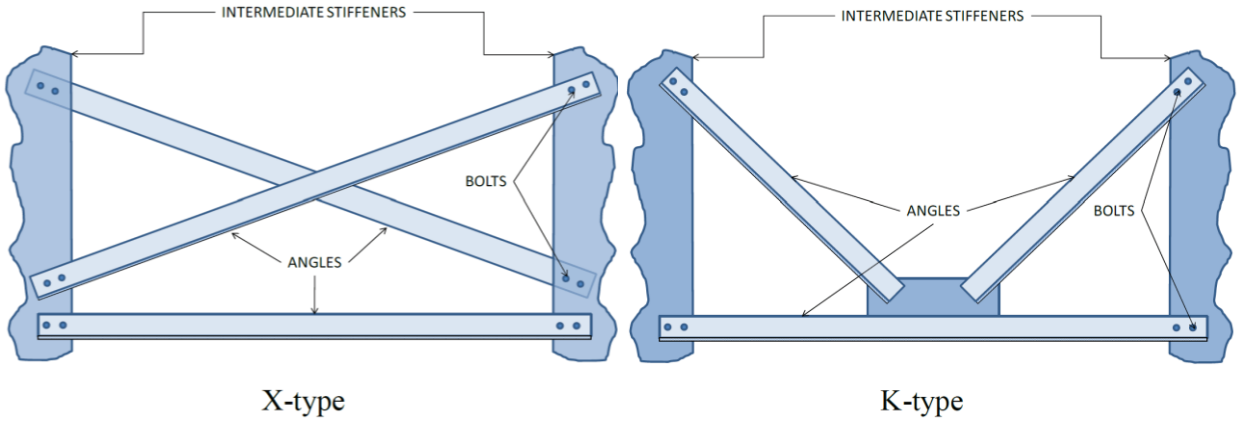

Figure 1.5 Cross-frame configuration [22]

1.1.3.2 X-type Cross-frames

As noted in the last subsection, many common cross-frame details include a top strut, as depicted in Figure 1.6 and Figure 1.7, which show X-type truss-type layouts with a top chord, a bottom chord, and two diagonals. Including both top and bottom struts makes the cross frames easier to handle during shipping and erection. The diagonal members are generally the most important members concerning the stiffness of the cross-frames. From a stability bracing perspective, the distribution of forces/stresses in the cross frames will result in compression in one diagonal and tension in the other. Some design philosophies idealize the cross frame as a "tension-only" diagonal system and conservatively neglect the compression diagonal, thereby sizing the diagonal members to fully stabilize the girders based on the tension diagonal and the top and bottom compression struts. Alternatively, both diagonals can be relied upon; however, the compression diagonal must be properly sized with adequate buckling strength for the compression force. With regards to an unbraced length, provided the two diagonals are connected at the middle, the tension diagonal braces the compression diagonal. Channels, angles (single or double), W-shapes, or WT-shapes are the most common types of sections used as members for cross frames.

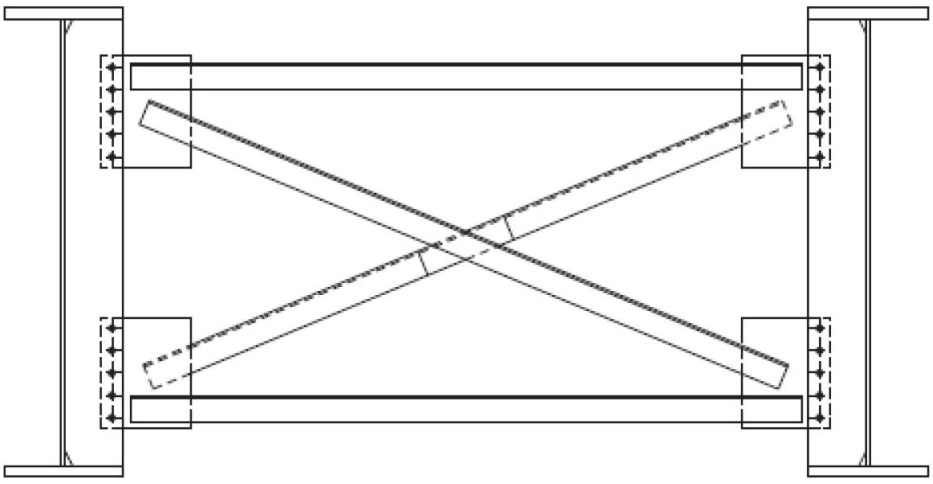

Figure 1.6 X-Type Crossframe Configuration[21]

Figure 1.7 X- shape Cross-frame in Steel Girder Bridges[23]

1.1.3.3 K-type Cross-frames

Both regular and inverted K-type truss-type are often utilized. A top chord, a bottom chord, and two diagonals that converge in the middle of one of the chords are the usual components of these chords. The intersection of the two diagonals occurs in the middle of the bottom chord in a typical arrangement. The two diagonals meet at the upper chord's center in an inverted configuration. These are shown in Figure 1.8 and Figure 1.9. In the inverted arrangement, diagonals connect the two bottom corners to the cross-frame, increasing girder stability in the completed bridge superstructure. This is because the deck offers a rigid connecting component at the top of the girders. Channels, (single and double) angles, W-shapes, or WT-shapes are the most common types of members.

1.1.3.4 Diaphragms

While cross-frames are widely used in steel bridge systems, diaphragms are also commonly used. Whereas cross-frames are “trusses”, diaphragms provide their stiffness through either flexural stiffness for shallow systems – or shear stiffness for deeper braces. The diaphragms can consist of either channel sections, wide flanges or built-up I-sections (often requiring a flange to be coped at the connection), or bent plates. Diaphragms are usually used as a bracing system in steel

girders with lower depth (i.e., less than 4 feet). Figure 1.10 and Figure 1.11 show some diaphragm applications.

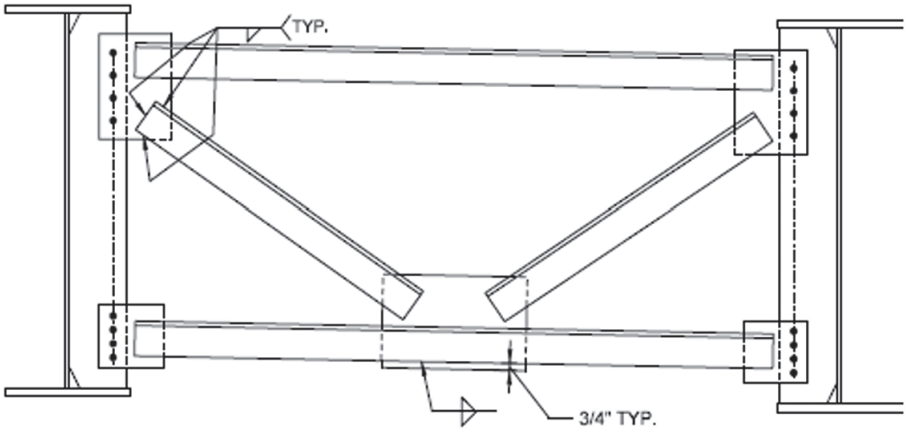

Figure 1.8 K-type Cross-frame Configuration [21, 24]

Figure 1.9 K-type Cross-frame in Steel Girder Bridge

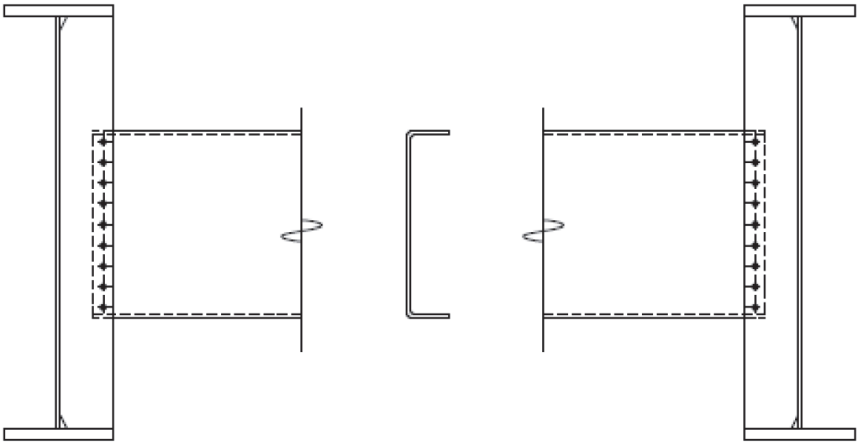

Figure 1.10 Diaphragm Members Detailing [21]

Figure 1.11 Diaphragm in Steel Girder Bridges

1.1.4 Cross-Frame in Skewed Bridges

1.1.4.1 Cross-Frame Layouts

The layout of cross frames is generally a function of the magnitude of the skew angle. The American Association of State Highway and Transportation Officials (AASHTO) only permits intermediate cross-frames to be oriented parallel to the abutment and piers centerline when the skew angle is less than 20 degrees. In this case (Figure 1.12), steel girders are connected at a relative distance to the end of the steel girder, which reduces the possible differential deflection under live loads.

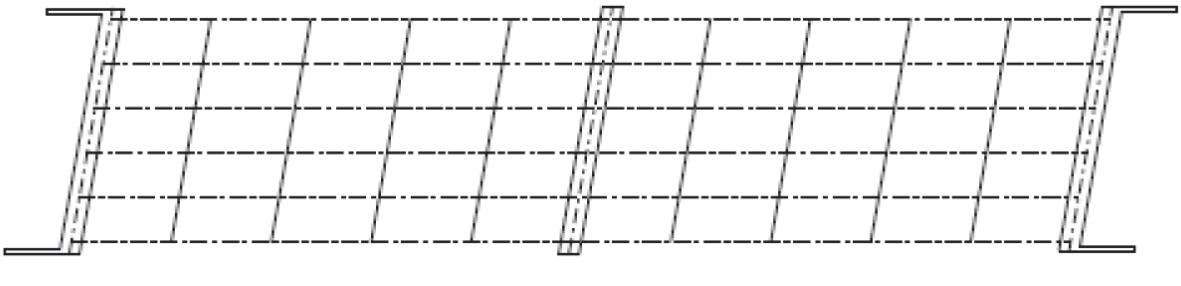

Figure 1.12 Slightly Skewed Bridge with Skewed Crossframes (Skew angle <20 degrees)[21]

By increasing the skew angle, the length of the skewed cross-frames will be increased, and as a result, the cross-frame stiffness will decrease. For skew angles greater than 20 degrees, cross-frames must be aligned normal to the girder axis in accordance with the AASHTO specifications. Three major framing plan options for the cross-frames can be observed: contiguous, staggered, and lean-on frames. Figure 1.13 depicts contiguous perpendicular cross-frames throughout the

bridge width. Each bracing line in Figure 1.13 represents a line of full cross frames. In skewed bridges, the bracing line provides a direct load path to the supports. With significant support skew, a bracing line may frame into support at one end of the bridge and a point well into the span at the opposing end, leading to large differential deflections at the two ends of the bracing line. In these situations, relatively large live-load-induced stresses can result in the braces.

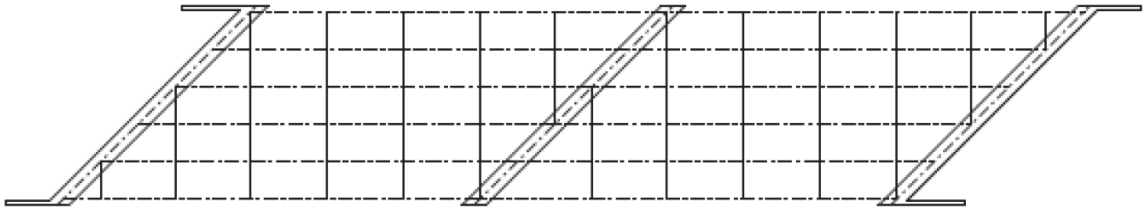

Figure 1.13 Highly Skewed Bridge with Non-skewed, Contiguous Crossframes(Skew >20 degrees) [21]

Figure 1.14 depicts an alternative framing plan design with perpendicular cross frames. While staying perpendicular to the girders, these cross frames are spaced apart and staggered along the skew angle. Although differential deflections occur at the two ends of a single cross frame, the staggered layout results in a "softening" of the bracing system that reduces live load-induced stresses. The staggered layout tends to mimic the parallel layout of the cross frames, which can be envisioned by considering the midpoint of each cross-frame relative to the bracing line at the piers or abutments. One drawback to the staggered layout is that connection plates (web stiffeners that connect the cross-frame to the girders) are offset on either side of the girder web. For these cases, the fabricator has to layout more stations along the bridge length for the cross-frame connection plates.

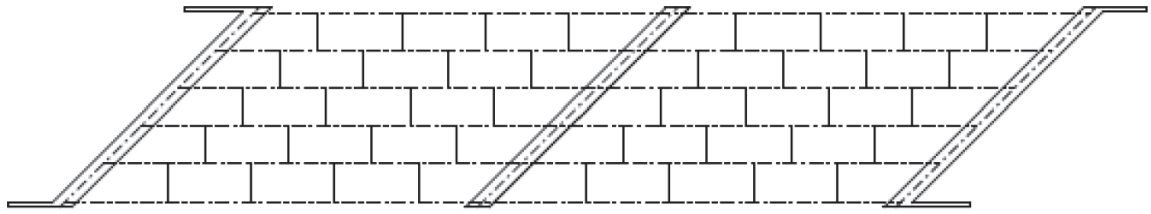

Figure 1.14 Highly Skewed Bridge with Non-skewed, Staggered Crossframes(Skew angle >20 degrees) [21]

Figure 1.15 illustrates a lean-on bracing system, which is a relatively new framing plan design for severely skewed steel girder bridges. Although lean-on bracing systems have been used in bridges with normal supports, the layout has significant advantages in bridges with skewed supports. Considering the continuous line of braces from Figure 1.15, cross-frame lines that

frame directly into support regions are particularly susceptible to large live-load-induced forces since one end of the cross-frame essentially experiences no deformation. As shown in Figure 15, lean-on bracing systems make use of full cross frames in combination with some bays that only include top and bottom struts. In a given line, the cross frame is typically positioned so that it is the furthest away from the support leading to smaller live-load induced forces. Near mid-span, it is often advisable to provide nearly a full line of cross frames to fully engage the girders to act as a system.

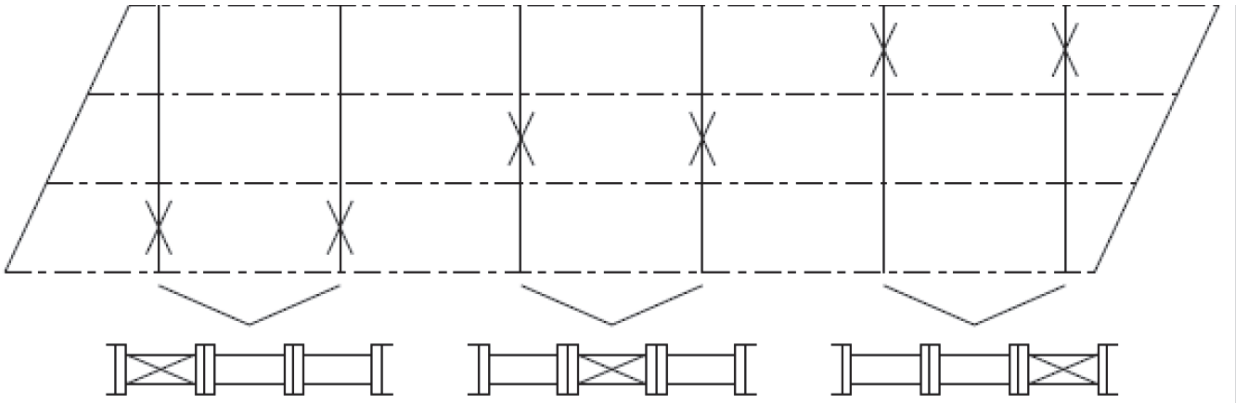

Figure 1.15 Highly Skewed Bridge with Nonskewed, Contiguous, Lean-On Bracing System (Adapted from Herman, 2007) (Skew angle >20 degrees)[25]

While the details discussed thus far have focused on straight bridge systems, cross frames also play a critical role in horizontally curved applications. In these cases, the cross-frames are primary structural members. The radially oriented cross-frames are the most typical framing plan design for curved steel girder bridges. Because the torsional forces on the girder apply radially along the curve on which the girder geometry is constructed, as seen in Figure 1.16, the cross-frames aligned in this direction will produce the most efficient arrangement.

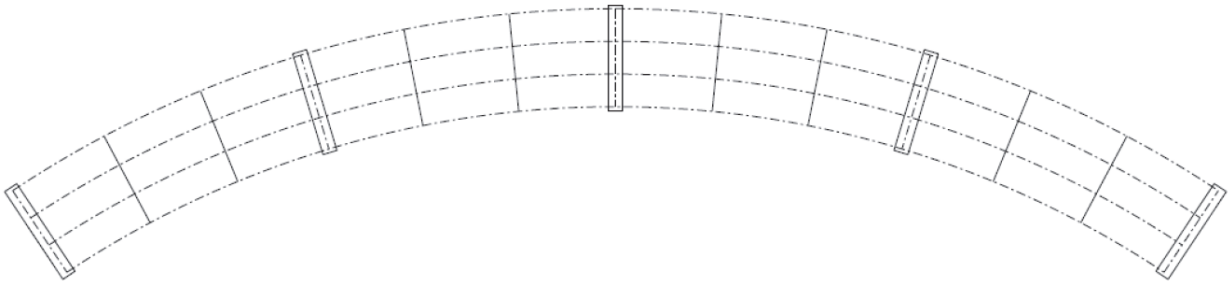

Figure 1.16 Curved Bridge with Radially Contiguous Crossframes[21]

Steel girder bridges that are both skewed and curved must utilize a combination of the above-mentioned frame plan configurations, which may necessitate a more thorough study.

1.1.4.2 Forces and Stress Concentration

Cross-frames for steel girder bridges serve several purposes during construction. While the primary purpose is to stabilize the girders during erection and construction, the braces also assist in distributing the forces from the slab and finishing machine that is often transmitted through the overhang brackets. The braces also help transmit lateral loads from the wind on the bridge. The critical stage for the cross frames generally occurs during construction before the concrete in the deck is hardened. They experience a variety of forces and effects primarily because of lack-of-fit and fit-up forces. On the other hand, usually, the cross-frames are there to stay during the service life of the bridge and, therefore, attract live load forces. In the case of bridges with their axis perpendicular to the abutment line (non-skew bridges), these forces are developed because of the contribution of cross-frames to lateral load distribution. Stress variation in the cross-frame members has the potential for fatigue in the cross-frame connections and the connection zone in the girders and necessitates periodic inspection for fatigue.

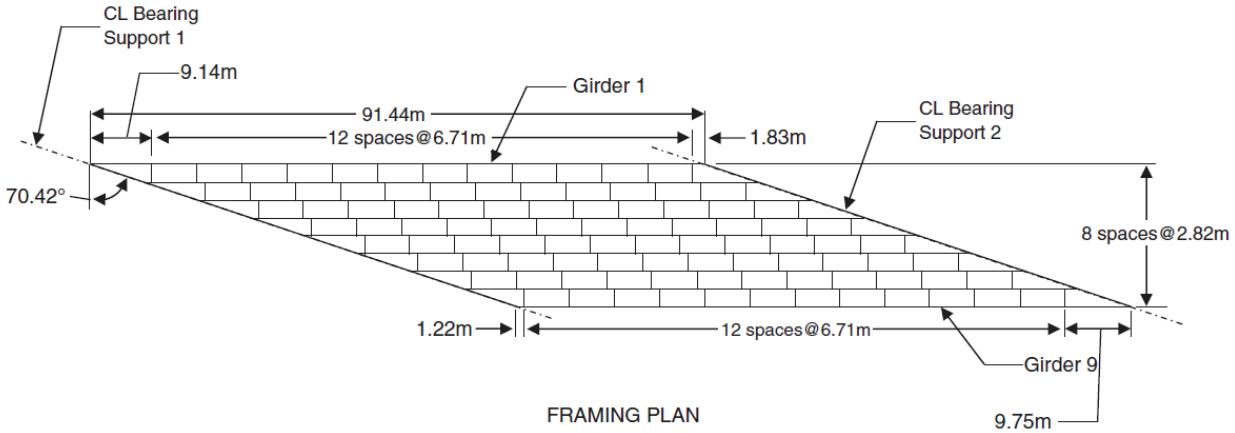

Figure 1.17 Plan of a skewed straight bridge, Up [18], and an example of connections at abutment [13]

For the case of skewed bridges, the live load effects and fatigue issues are exacerbated because the skewness of the supports creates a much different structural response, adding to the effect of live load. Figure 1.17 shows a plan view of a skewed straight bridge and some details of the girder-cross-frame-diaphragm connection.

As it was discussed earlier, by increasing the bridge skew angle, the interaction between adjacent girders is more significant since the cross frames connect to adjacent girders at different longitudinal locations. As a result, the cross-frames experience differential vertical displacements at the two ends from truck traffic on the bridge. This behavior leads to more complicated structural behavior and an increase in stresses in cross-frame members and their connections. These concentrated stresses can play an important role in the design procedure and may exacerbate potential in-service fatigue issues [2]. Therefore, it is vital to study the structural behavior of cross-frames in skewed bridges during construction and service and to investigate the fatigue consequences. Some studies have been conducted focusing on stress concentration in cross-frame members, steel girders, and their connection in skewed bridges. Bishara et al. [26] and McConnel et al. [27] studied the relationship between the skew angle and the internal forces within cross-frame members and found that as the skew angle increases, the internal forces in cross-frame members increase. For very large skew angles, the internal force demand in cross-frame members can become more critical than the demand on steel girders. The fatigue concerns for cross-frames have intensified in recent years with the designation of Category E' for single-angle members (Battistini et al. 2016) [27].

It has also been reported that when comparing the cross-frame stresses in its members, the diagonal members of K-types are exposed to noticeably lower stresses than the diagonal members of X-type frames [28]. Ozgur [10] demonstrated that the lateral load transmission increases with the bridge skew angle, affecting bottom flange lateral bending stresses. When Krupicka and Poellot [29] investigated the effects of cross-frames on steel girder stresses, they found that the placement and stiffness of cross-frames usually affect the stiffness in girders, especially near the skewed supports of the bridge. The bottom flange of the girder may experience stresses that are not normally taken into account if cross-frames are designed with

stiffness that is similar to or greater than those of the girders. This is known as nuisance stiffness. McConnell et al. [30] demonstrated how bridge skew angle and cross-frame location affect noticeably the bottom flange lateral bending stress. They also demonstrated that using staggered cross-frame configurations is one way to lessen the bridge transverse stiffness. Cross-frame forces are decreased by adopting this form of cross-frame location, but bottom flange lateral bending stresses are increased as a result.

1.1.4.3 End Cross-frames

End Cross-frames are typically defined as truss members located at the end of each bridge span. In a multi-span bridge, end cross-frames would be located at the end supports (abutments) and intermediate supports (piers). On the other hand, other cross-frames located in between the bridge supports along the bridge spans are defined as intermediate cross-frames. If the bridge skew angle is more than 20°, intermediate cross-frames must be placed perpendicular to the steel girders (AASHTO 6.7.4.2), while end cross-frames should be in line with the support centerline (Figure 1.18).

Figure 1.18 60° Skewed Steel Bridge in Lubbock. TX with End Cross-frames[31]

Major roles of end cross-frames include controlling the twist of the girders, supporting the deck and expansion joint, and transferring lateral loads such as seismic and wind loads from the bridge deck to the bearings. Astaneh-Asl [32], Bruneau [33], and Shinozuka [34] have shown seismic load transferring and the importance of the end cross-frame design [35], by reporting damages within end cross-frames during severe earthquakes. In terms of design, there are essentially two options. The first approach introduced by Itani [36] is designing the end cross-frames in the elastic region protected by substructure capacity design. The second approach is considering ductility for the end cross-frames to protect the superstructure and substructure by dissipating energy during severe earthquakes. Carden [36] and Zahrai [37, 38] have studied the possibility of using cross frames as ductile parts by using different systems such as special cross braces, shear panel systems (SPS), eccentric braced frames (EBF), and triangular plate with added damping and stiffness (TADAS) device. They showed that if the substructure is not overly flexible, using the ductile end cross-frames is feasible.

1.1.4.4 Design and Construction Challenges

Skewed supports in steel girder bridges introduce issues and complications during design and more importantly the construction phase stemming from the torsional deformation of girders because of interaction between cross-frames and adjacent steel girders. For the stability of steel girders, especially during construction and before the deck concrete is hardened, the cross-frames and diaphragms play an important role. Large twists of girders, support uplift, flange lateral bending stresses, and fitting difficulties have been mentioned as skewness-related construction issues by the references.

One of the factors contributing to excessive girder twists in systems with skewed supports is the relatively low torsional stiffness of the steel I-shape section during construction. There are two main sources of girder twist in straight skewed I-girder bridges: 1) twist induced by the skewed cross-frame line at the supports, and 2) twist induced by the differential girder deflection that occurs at the two ends of cross-frames located at intermediate locations along the bridge length. Figure 1.19(a) depicts a cross-frame located at the exterior support of a skewed girder system. Major axis bending of the girders from gravity loads results in girder rotations at the supports.

Because the skewed cross-frames attached to these ends have components in the longitudinal and transverse direction, the in-plane girder rotation results in a force in the cross-frame. The induced cross-frame forces essentially lead to a twist of the girder. Figure 1.19(b) shows an intermediate cross-frame that connects to two adjacent skewed girders at different locations along the length of the individual girders. As the girder deflects from the applied dead load, the two ends of the cross-frame experience a differential vertical displacement that leads to torsional deformations in the girders. Previous studies have produced analytical expressions for both the twist caused by rotation of the cross-frame at the bearing line and the twist caused by a differential deflection by assuming the cross-frame to be rigid[18].

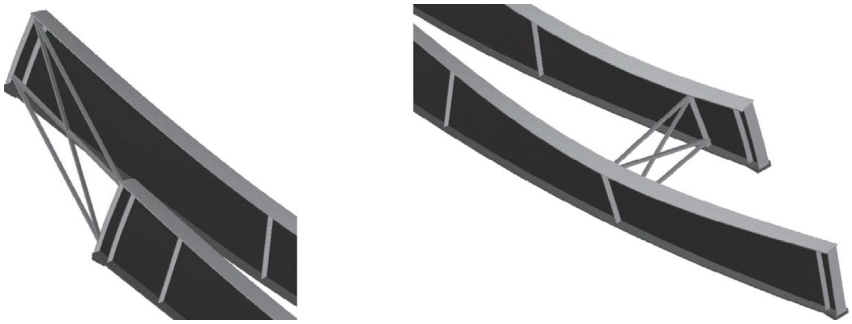

a) b)

Figure 1.19 Main sources of twist in straight skew bridges; a) Rotation of end cross-frames at bearing line, b) Differential deflection of girders[18]

The estimate of skewed steel girder deformations during erection and construction can be challenging in terms of when the girder webs should be plumb and the potential for lack-of-fit of the cross-frame connections. The cross-frames are generally installed when the loads on girders consist only of the girder self-weight. However, the cross frames must be detailed for a specific fit condition that might be 1) no-load fit, 2) steel dead-load fit, or 3) total load fit. This poses a serious issue to the construction process for plumbing the girder webs (lack-of-fit) let alone the additional stresses to the girder, cross-frames, and of course their connections. Girder web can only be plumbed either at the stage that steel dead load is applied or when concrete is placed and hardened. FDOT Standard Design Guidelines (SDG) include guidance for addressing fit-up for bridges with a steel superstructure. According to SDG, the design, and detail of the cross-frames

are to be performed for Steel Dead Load Fit (SDLF). No Load Fit (NLF) and Erected Fit (EF) may be used where appropriate. The SDG does not permit Total Dead Load Fit (TDLF) unless approved by the Structures Design Office (SDO). For phase or widening construction in which the cross-frames are located in the closure pour bay, detailing must be performed for TDLF [39].

As noted above, there are 3 distinct stages of construction for steel girder composite bridges where the girder webs can be plumbed. These are no-load, steel dead load, and total dead load, referring to when the girders are totally or partially supported along their length, when the girders are erected and carry their weight, and when the concrete deck is cast on top with girders carrying the entire dead load, respectively. Detailing of cross-frame depends on the stage that it is desired to have the girder web plumbed. The accuracy of this process depends on the correct method of analysis to predict girder displacement and forces in the cross frames. To be consistent with industry, these three stages are truncated to two including erected fit and final fit, with detailing of cross frames to fit between girders at erection (steel self-weight) and for when the fresh concrete is placed on the girder (total dead load), respectively. Figure 1.20 shows these two detailing methods.

Regardless of which stage the detailing is implemented for, additional forces are applied to the girder due to fit-up of the cross-frames (fit-up force) if the detailing for the girder plumb is done for a later stage and/or additional forces from the additional dead load when detailing is done for plumb in an earlier stage. In general, additional structural effects/responses should be expected in the skew bridges stemming from the lack-of-fit of cross frames in between girders. These can include layovers (see Figure 1.20), deflections, reactions, girder flanges lateral bending, and force in cross-frames and their connections. It should also be pointed out that for example in the case of erected fit, the detailing for fit can be applied in two ways, change in length of cross-frames or shifting the connection points such as bolt holes (see Figure 1.21).

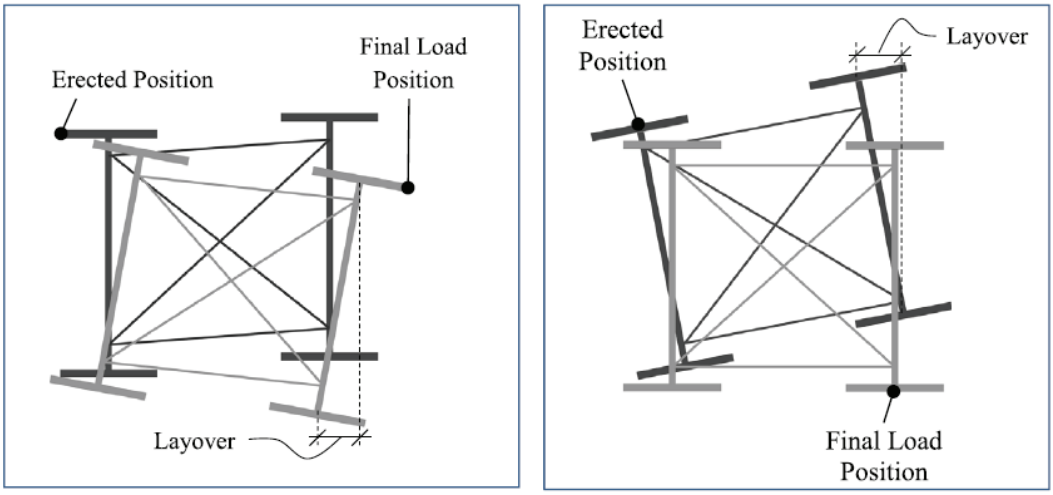

(a) Erected fit detailing method (b) Final fit detailing method

Figure 1.20 Two common and distinct detailing methods[18]

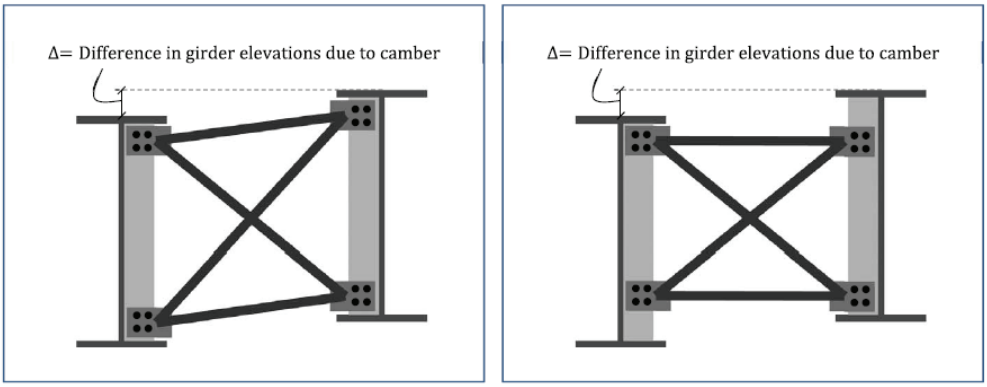

(a) Change lengths of cross-frame members (b) Change location of connection of points

Figure 1.21 Ways detailing can be applied for erected fit case[18]

1.1.5 Skewed Connections

In a standard steel connection such as cross-beam to girder, beam to girder, or beam to column, the structural elements are generally connected at an angle of 90 degrees. However, some structures and bridges in certain circumstances have elements that do not have a perpendicular connection to other elements. A connection that links two elements at an angle other than a right angle is called a skewed connection. To ensure safety and economical construction, the application of skew connections needs unique design considerations [40].

1.1.5.1 Skewed Connections in Buildings

Sometimes, architectural demands necessitate skew connections in buildings. Some building shear connections for beams and columns are discussed here. For beam-to-girder connection, single plates (Figure 1.22) and end plates (Figure 1.23) are the ideal skewed connections for both being economical and safe. At high skew angles, single bent plates and eccentric end plates also perform well. Single plates (Figure 1.22) have an eccentricity equal to “a”, the distance between bolts and the weld, and can be used for skew angles between 0 to 60 degrees. Whereas end plates (Figure 1.23) that do not have eccentricity can provide higher capacities compared to shear tabs (single plates). It is possible to impose an eccentricity (e) to this type of connection as required geometrically as shown in Figure 1.24 [40].

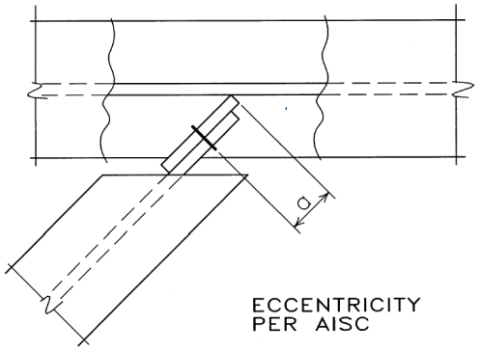

Figure 1.22 Shear Tab (Single Plate) [40]

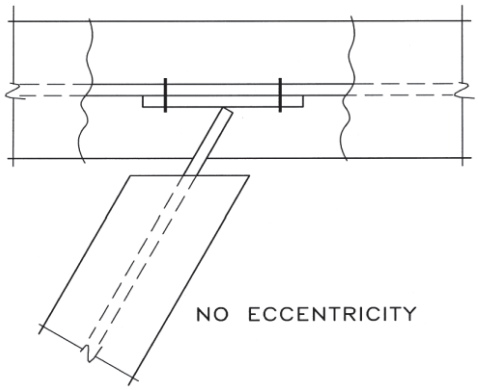

Figure 1.23 Shear End Plate [40]

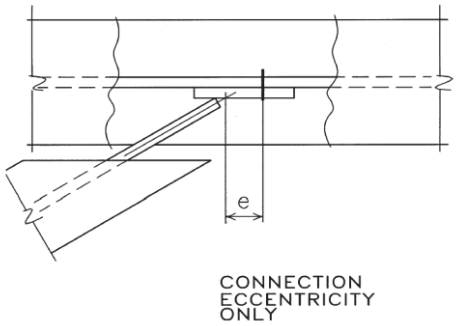

Figure 1.24 Eccentric End Plate [40]

Single bent plates, as shown in Figure 1.25, is another type of beam-to-beam skewed connection designed for shear with two eccentricities, e1 and e2 measured from the bend line. The eccentricity should be measured from the bending line because the out-of-plane bending strength is assumed negligible. It is possible to use an angle section instead of the bent plate in this type of connection as well (Figure 1.26). Connections with eccentricity should be designed by considering additional load effects due to these eccentricities [40].

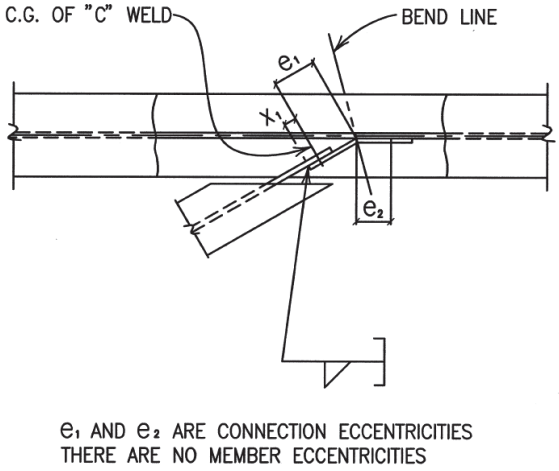

Figure 1.25 Bent Plate [40]

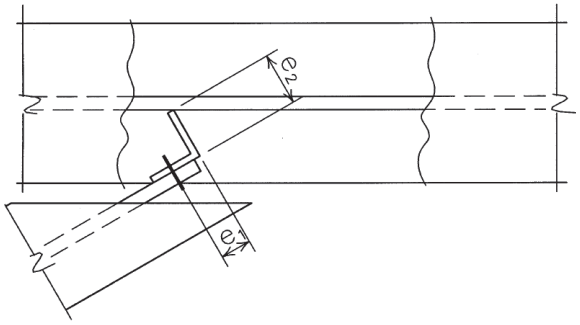

Figure 1.26 Single Bent Plate with Angle Section

Another basic connection in buildings is the connection between the beam and the column. In some cases, it is inevitable for this connection to have a skew angle. The use of skewed connections in a wide flange column introduces some challenges. In this type of connection, access to the connection details for erection and welding is limited. Except for columns with section depth over flange width ratio of more than one or for skew angle less than 30 degrees, it is better for accessibility and simpler details to connect the beam to the column flange instead of the column web. When it is possible to connect the beam to the column web, a standard end plate (Figure 1.27) and an eccentric end plate (Figure 1.28) can be used. The use of a single plate for the shear connection is another type of skewed connection (Figure 1.29). In this connection type, bolts should be placed outside of the column flanges for accessibility, which can increase connection eccentricity. As a result, there may be a need to add two plates to the top and bottom of the connection. This eccentricity (e in Figure 1.29) can also change the column design and increase the overall cost of the connection [40].

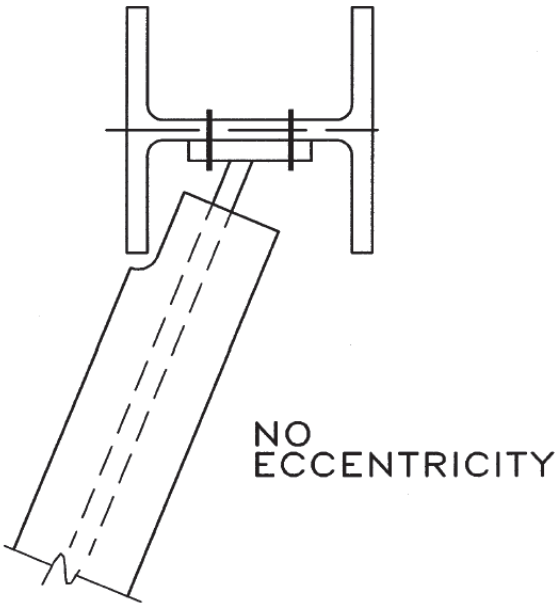

Figure 1.27 Standard End Plate [40]

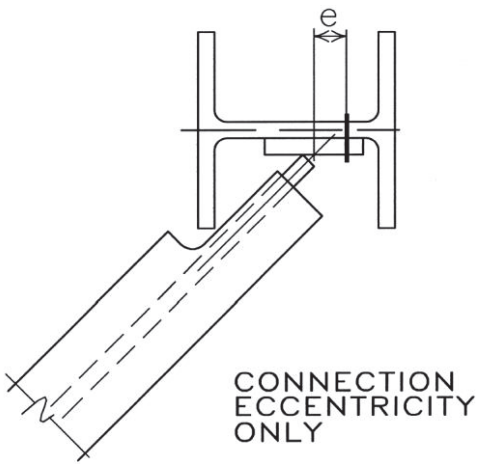

Figure 1.28 Eccentric End Plate [40]

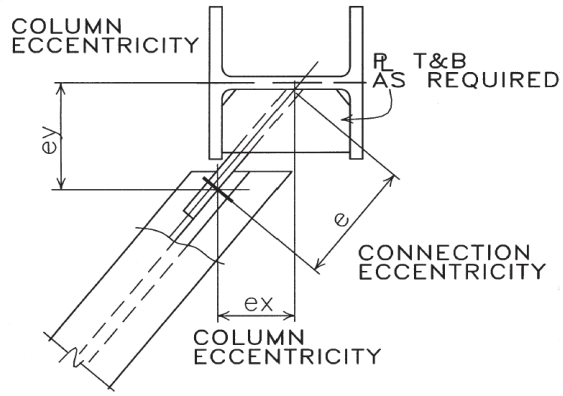

Figure 1.29 Single Plate with Extended Shear Tab [40]

In a skewed connection, the beams can also be connected to the column flange. In these connections, the alignment of the beam plays an important role in the eccentricity of the connection. For example, when the beam centerline alignment passes through the centroid of the column section (Figure 1.30), the skewed connection creates a column eccentricity (e_y) that can affect the column design, and if it passes the flange center point, the column eccentricity would be negligible (Figure 1.31) [40].

If the beam centerline passes through the column section centroid, it is possible to use single plates (Figure 1.30), eccentric end plates (Figure 1.32 and Figure 1.33), or single bent plates (Figure 1.34) for skewed beam-to-column shear connections [40].

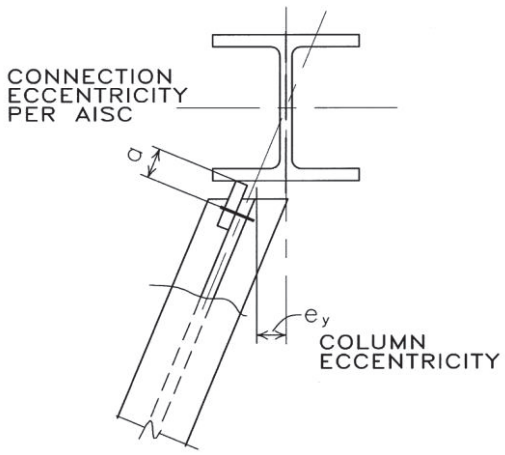

Figure 1.30 Beam-to-Column Skewed Connection with a Single Plate [40]

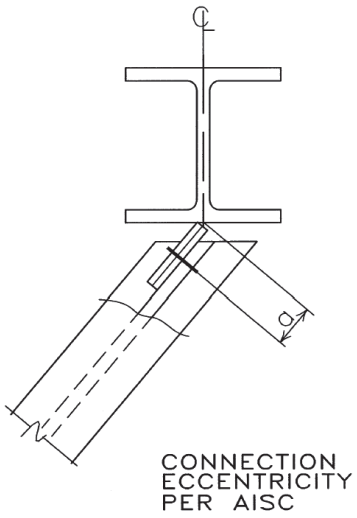

Figure 1.31 Beam-to-Column Flange Skewed Connection with Single Plate [40]

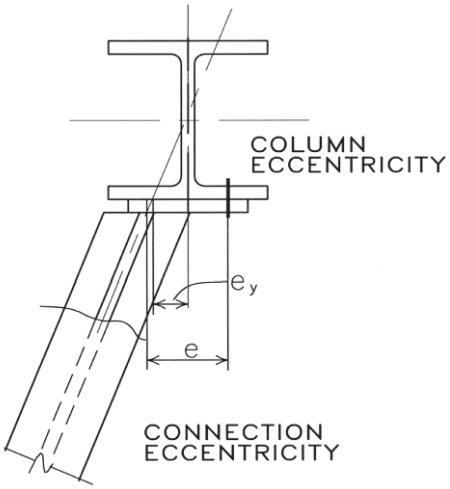

Figure 1.32 Eccentric End Plate for Beam to Column Shear Skewed Connection [40]

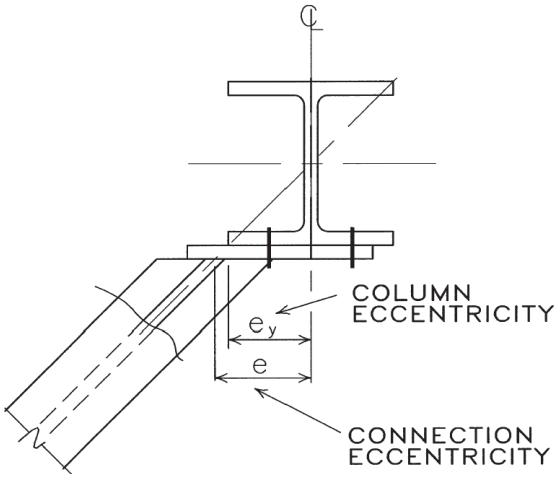

Figure 1.33 Eccentric End Plate for Beam to Column Shear High Skewed Connection [40]

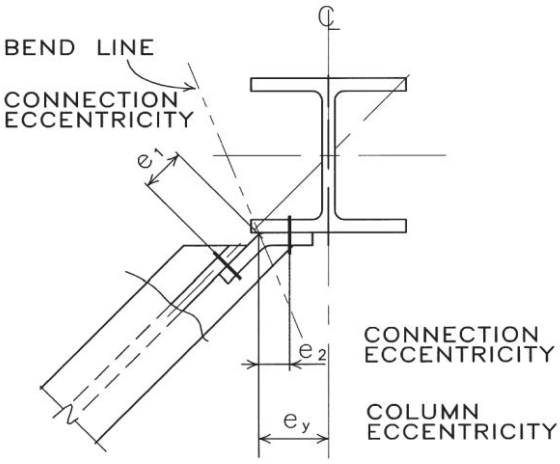

Figure 1.34 Single Bent Plate in Beam to Column Skewed Shear Connection [40]

1.1.5.2 Skewed Connections in Bridges

In skewed bridges, where the bridge longitudinal axis (traffic direction) is not perpendicular to abutment or piers, skewed connections between end cross-frames and girders become necessary. As noted earlier, when the skew angle is larger than 20 degrees, intermediate cross-frames are normally kept perpendicular to the girder, either contiguous or staggered, but the end cross-frame or diaphragm must be connected to the girder at an angle equal to the skew angle. The following sub-sections describe skewed connections for steel girder bridges.

1.1.5.2.1 Bent Plate Connection

As noted above, for skew angles larger than 20 degrees, AASHTO [41] requires intermediate cross-frames to be aligned perpendicular to the girders. End cross-frames, regardless of skew angle, must be parallel to the skew and hence in line with the supports or abutment center line [42]. This implies that the end cross-frames will connect the girder at a non-perpendicular angle, potentially causing welding and fit-up complications. Bent plates (as shown in Figure 1.35 and Figure 1.36) between the cross-frame braces and stiffeners are commonly used to solve the connection issue [43]. Although bent plates make construction easier, they can reduce cross-frame effectiveness due to their flexibility.

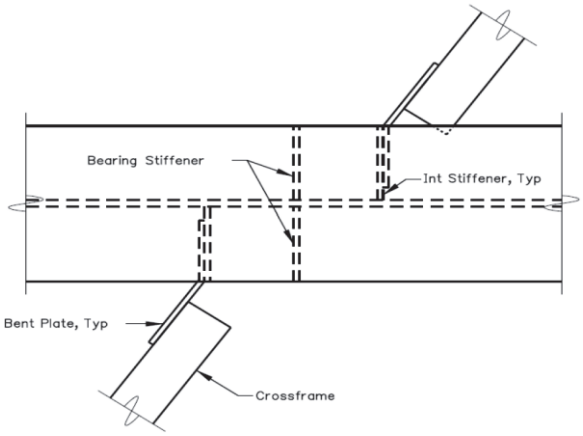

Figure 1.35 Skewed End Crossframe Bent Plate Connection[44]

Figure 1.36 Bent plate end cross-frame connection[45]

Sufficient strength and stiffness are required for effective bracing for stability [46]. Yura (2001)[47] showed that the conventional series springs formulas can be used for the relationship between the overall system stiffness to individual stiffness components. There are several stiffness components in the torsional bracing system that can be included in the stiffness for bridges as represented in the following expression:

$$\frac{1}{\beta_{system}} = \frac{1}{\beta_{web}} + \frac{1}{\beta_{brace}} + \frac{1}{\beta_{girder}} + \frac{1}{\beta_{connection}} \quad (1.1)$$

The mathematical nature of this expression necessitates that the overall system stiffness is always less than the smallest stiffness component. For instance, the bent plate connection introduces significant flexibility and will most often have the least stiffness in the cross-frame system and will often be the limiting element in the overall bracing system stiffness. Furthermore, since end cross-frames in skewed steel bridges do not connect to the girders perpendicularly, they have a lower effective stiffness, and it is necessary to multiply the end cross-frame stiffness by the square of the cosine of the skew angle [48]. Although a bent plate will often suffice for small skew angles, significant issues can arise for highly skewed bridges [44]. Experimental studies and Finite Element Modeling (FEM) results have shown that the main cause for the out-of-plane bending and deformation of the elements is the eccentricity of the bent plate connection [49]. Eccentric connections cause member bending, which has a negative impact on stiffness, fatigue, and strength.

1.1.5.2.2 Half-Round Bearing Stiffness Connections

In an extensive research study, Quadrato et al. (2010) [44, 50] investigated the existing connection details for end-cross frames to steel girders in heavily skewed systems and considered new details. The study focused on bent plate connections and proposed a new Half-Round Bearing stiffener detail to facilitate connection fabrication in skewed girder applications. The configuration of this connection assures the connection stiffener plate is perpendicular to the half-round bearing stiffener regardless of the skew angle and avoids using a bent connection plate. Their investigation first reviewed current AASHTO and TxDOT code provisions and

construction practices [42, 51, 52]. They tested a series of small- and large-scale skew connections using a bent plate and half-round bearing stiffener details of carrying angles, as shown in Figure 1.37, the tests showed that the half-round bearing stiffener detail is significantly stiffer than bent plate details, and no rotation of connection was registered for half-round bearing stiffener detail.

Figure 1.37 Small-scale connection test specimens by Quadrato et al.[44]

The investigation also tested large-scale specimens that included single, double, and three-girder systems. The testing targeted both the behavior of the girders (mostly buckling) with a variety of connections and measured brace forces and girder end twist. The tests were performed with bent plate and half-round bearing stiffener connections. One main reason for large-scale tests was for validation of the finite element methods to be used for parametric study. Figure 1.38 shows one of the large-scale test specimens with the half-round bearing stiffener connection for the end cross-frames. Also, in this figure, a half-round bearing stiffener detail is prepared for welding. The skew angle used for the three-girder test specimens was 53 degrees. In addition to improved constructability, there are also structural advantages to utilizing half-round bearing stiffeners. The large-scale test demonstrated the effect of half-round bearing stiffener in increasing the warping restraint for the girder, therefore, increasing buckling capacity. half-round bearing stiffener also showed that lower end twist for the girder in comparison with the bent

plate. Also, staggering the intermediate cross-frames showed to have reduced the intermediate cross-frame forces but did not significantly impact the girder end twist.

Figure 1.38 Large-scale test specimen with half-round bearing stiffener (left) and a single stiffener prepared for welding (right) Quadrato et al.[44]

Quadrato et al. also utilized finite element (FE) models of the connections and combination of cross-frames and girders similar to the test specimens to validate the models using experimental results. An example of FE models is shown in Figure 1.39. Three types of analysis were conducted: 1st order elastic, elastic-critical load (eigenvalue buckling), and geometric non-linear analyses (large-displacement. The models were validated against the tests and shown to be in good agreement.

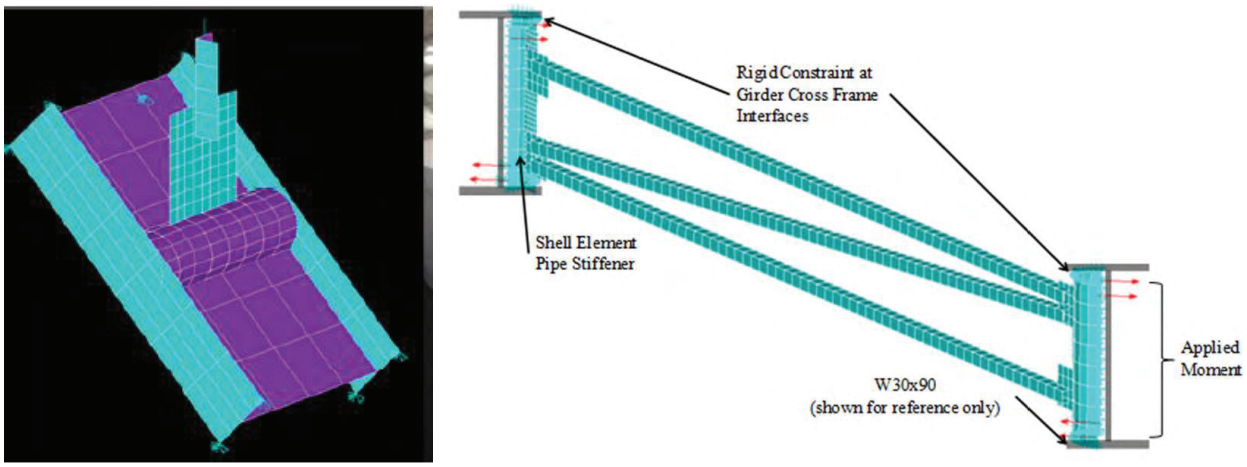

Figure 1.39 Finite element models of half-round bearing stiffener connection (left) and an end cross-frame to girders (right) Quadrato et al.[44]

The models were used to perform a series of parametric studies to develop guidelines for the design of end cross-frame connections. Reviewing the TxDOT plans for skewed bridges and previous work performed on the topic, the research study evaluated five girder cross-sections in the study. The parametric study began by varying the skew angle for the bent plate connection and determining at what angle (critical angle) the bent plate will influence the stiffness of the cross frame. Simulations to demonstrate the positive effects of half-round bearing stiffener compared to bent plate connections. Equations were developed, and refined by the FE modeling, to predict the effects of the bent plate on the stiffness of cross-frames. Plate thickness, bend radius, and skew angle were found to be the main factors impacting the stiffness effects. Similar analyses were performed for half-round bearing stiffener details. The effect of pipe diameters was examined on the resulting warping stiffness. Recommendations for the reduction of cross-frame stiffness from the half-round bearing stiffener connection were also developed. Overall, the half-round bearing stiffener connection offered significantly higher connection stiffness than the bent plate. The tests and computational studies demonstrated that improved warping stiffness of the girders provided by half-round bearing stiffener were recognized as positive for construction phase fit-up activities. The effects of the reduction in girder end twist provided by the half-round bearing stiffener on girder buckling strength were investigated in the parametric studies, which demonstrated improvements in the buckling strength of girders due to the higher warping restraint provided by the half-round bearing stiffener. The improved warping stiffness resulted in less girder twist and smaller cross-frame forces. In addition to the improved constructability, increases in warping restraint for girder ends were emphasized as an added advantage of using half-round bearing stiffener detail, providing higher buckling capacity for the girder and allowing the first line of intermediate cross-frames to move farther from the end.

Quadrato et al. also considered the fatigue performance of half-round bearing stiffener connections. Although there are no significant fatigue concerns in the girders at exterior supports due to the lack of girder moments, at interior supports the girders often experience the largest moments. Therefore, the fatigue performance of the girders at interior supports was a major consideration. The study focused on the stress concentrations in the half-round bearing stiffener detail compared to both normal and inclined plate stiffeners. With bent plates, the web

stiffeners are generally normal to the webs, while for smaller skew angles, the web stiffener might be inclined. The study focused on identifying the proper fatigue category for the half-round bearing stiffener detail that is in accordance with the AASHTO categories. Previous investigations have considered the half-round bearing stiffener connection for applications in buildings where fatigue is not a serious issue [53]. Earlier work [54] identified a Fatigue Category C for stiffener plates. In addition, other studies identified the susceptibility of cross-frame connections to fatigue damage and considered retrofitting methods for fatigue damage [55, 56]. Limited laboratory tests were performed that included half-round bearing stiffener and plate stiffeners installed along the length of girders subjected to moment variations developing a predefined stress variation in the girder. The FE modeling plan was designed to demonstrate that the half-round bearing stiffener does not create a fatigue condition worse than the bent plate. Accordingly, and conservatively, the recommended fatigue designation for the half-round bearing stiffener detail was identified as Category C.

1.1.5.2.3 Implementation of Half-Round Bearing Stiffeners

TxDOT has allowed the use of half-pipe stiffeners and included the detail in Standard Miscellaneous Details [52]. Although the recommended TxDOT detail has recommended half pipe and connection plates are both welded to the top and bottom flanges as shown in Figure 1.40, the original researchers do not recommend welding connection plates to the flanges. His research demonstrated the worst performance in fatigue was inclined plates welded to the flanges and therefore, the original researchers do not recommend any connection between the inclined stiffeners and the flanges. The recommended detail from the researchers consists of the half-round bearing stiffener welded to the flanges and the connection plates only welded to the half-round bearing stiffener. The half-round bearing stiffener is completely sealed against the web and flanges creating a closed space.

Recently, for a design-build project for FDOT, the designer proposed the half-round bearing stiffener detail with some variation from that of the TxDOT detail. For this case, the connection plate at the continuous bearing (over piers) is not welded to the top flange (tension flange) and is only connected with bolted tabs, due to fatigue concerns at that location. Also, for corrosion

consideration, weathering steel for the connecting parts and clipped pipe corners as a vent for the closed space were used. AASHTO Bridges and Structures Committee has addressed the incorporation of this detail but with connection plates not attached to the flanges, based upon recommendations from the researchers. Based upon the recommended TxDOT standards and the recommendations in the AASHTO Bridges and Structures Committee, there seems to be discord on at least some of the details considered by different sources.

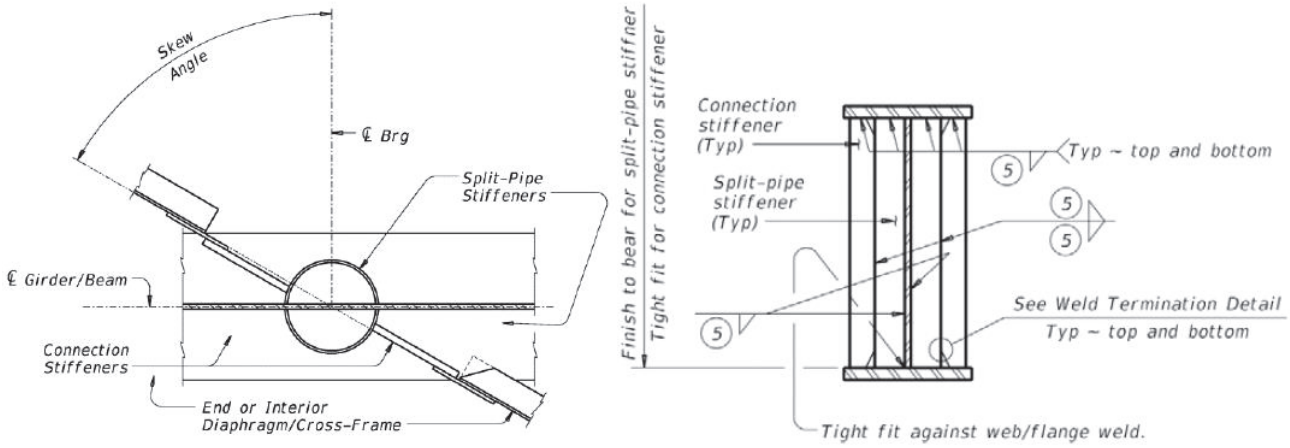

Figure 1.40 TxDOT half pipe detail [52]

1.1.6 Analysis methods

White et al [11] studied various analysis methods for steel girder bridges and especially for cross-frames and diaphragms. Some of the common methods consist of the following:

1- Calculation of Flange Lateral Bending Stresses, f_ℓ
2- Line girder analysis (1D) methods
3- Traditional 2D-grid or grillage methods
4- Traditional 2D-frame methods
5- Improved 2D-grid method
6- Plate and eccentric beam models
7- Traditional 3D-frame methods
8- Thin-walled open-section (TWOS) 3D-frame methods

9- 3D Finite Element Analysis (FEA) methods

In the following subsections, a summary of simplifications and approximations for each of the methods based on White et al [11] research is provided. It is important to consider that cross-frames and diaphragms play a key role in the structural system, especially in load transferring to the supports. As a result, in many instances, analyzing the cross-frames and diaphragms is equivalent to analyzing the bridge superstructure.

1.1.6.1 Calculation of Flange Lateral Bending Stresses

Warping torsion leads to lateral bending stresses in the flanges of I-girders. Torsional stresses in the girders are the result of multiple sources, including the following:

- Eccentric overhang bracket loads
- Horizontal curvature effects
- Support skew effects

The lateral bending stresses resulting from these sources must be taken into account in the construction evaluations, according to the AASHTO Specifications [42]. In the following subsections, a brief description of procedures for estimating the flange lateral bending stresses is provided. The stresses estimated using the outlined procedures do not include the second-order effects between cross-frames and the girder. NCHRP [11] suggests multiplying the estimated stresses by the amplification factor referenced in AASHTO Article 6.10.1.6.

Loading from eccentric overhang brackets is a major source that can cause lateral bending stresses in steel girders. Care should be taken to ensure that the bottom reaction point of the bracket (Figure 1.41) is located on the web near the bottom flange to minimize web deformation [57]. According to FDOT standard specification Section 400-4.4, the bracket should be placed within approximately 6 inches of the bottom flange [58]. Otherwise, it may be necessary to ensure that the load from the bracket will not cause the web to deform or that additional bracing support may be needed, based on recommendations from Roddis et al. (2002) [57] and NCHRP Report 725 [11].

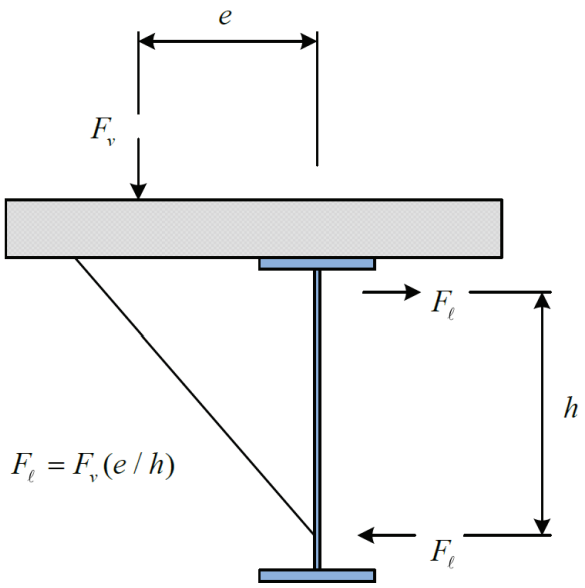

Figure 1.41 A schematic of overhang bracket [59]

Another potential source for lateral bending stresses occurs in girders with horizontally curved geometries. The lateral bending moments of girder flanges caused by the effects of horizontal curvature should be considered. The V-load approach described in later sections provides a relatively simple method for estimating the effects of horizontal curvature. Calculating the forces applied to the cross-frame and diaphragm from the girders can be complex, as described in the following sections where the V-Load method is explained as part of Line-Girder (1D) analytical techniques.

Another source leading to lateral bending in the flanges of steel I-girders is the effects of support skew. For the case of evaluating I-girder bridges using a line-girder or classic 2D-grid analysis, there is limited guidance on calculating lateral bending moments of the girder flanges from skew effects. Although the AASHTO LRFD Article C6.10.1 does not provide methods for the exact girder stresses, the provisions provide upper-bound values of the girder flange lateral bending stresses caused by skew effects. These estimates are based on a small set of analytical results for skew angles of 60 degrees and an average girder depth/flange width ratio of roughly 4.0. One

interesting point from the results is that increasing the girder flange widths does not always result in reductions in the lateral bending stress on flanges.

Furthermore, in order to calculate the minimum cross-frame or diaphragm forces for the bridges with skew indices larger than 0.30, NCHRP 725 [11] suggests using improved 2D-grid analyses. The bridge skew index can be defined as $I_s = w_g \tan\theta \,/\, L_s$, where w_g is the framing width between the fascia girders, θ is the bridge skew angle, and L_s is the bridge span length. Following estimates of the cross-frame or diaphragm forces based on the analysis, NCHRP 725 suggests a process for approximating the girder flange lateral bending moments based on statics for the analysis methods rather than determining the flange lateral bending stresses in a direct manner. A more recent study (NCHRP report 962) suggests that even after these improvements some errors may persist.

1.1.6.2 Line-Girder (1D) Analysis

The simplest method for structural analysis of steel girder bridges is a line-girder (1D) analysis. According to this approach, each bridge girder is analyzed separately, and the interaction of the girders with the secondary elements (cross-frames or diaphragms) is either disregarded or only loosely considered. Considering the recommended procedures for a line-girder analysis, loadings for each steel girder should be calculated and applied separately. Some loads, such as erection loads, are applied directly on each steel girder, while other loads, such as the deck dead load, are recommended to be distributed in a realistic manner. According to U.S. National Highway Institute (NHI) [60], the dead load of the wet concrete deck may be transferred equally to each of the steel girders if the width of the deck is constant, the girders are parallel, and if the number of girders is not fewer than four. In addition, AASHTO (Article 4.6.2.2.4) [42] suggests that distributed and surface loads transfer to each steel girder in curved steel bridges. On the other hand, NHI [61] advises that heavy line loads, such as parapets, barriers, walkways, or sound walls, shouldn't be distributed uniformly to all the girders. A common method of treating the overhang loads is the use of the lever rule[42] to distribute heavy concrete barrier loads and the overhangs to the girders. The lever rule increases the fraction of the dead load given to the fascia girders while decreasing the loads on the interior girders. Meanwhile, some state DOTs suggest that

designers apply 60% and 40% of the barrier dead load to the exterior and interior girders, respectively[60]. Furthermore, NHI [60] reveals that for skews greater than 10 degrees, the equal distribution of loads might be unrealistic. It is important to note that each of these assumptions results in different analyzed dead load forces in the cross-frame members. To account for the significant impact that may not be automatically taken into account in the 1D idealization, many extra computations are typically applied to basic line-girder estimations. In the following sections, different common methods in 1-D Line-girder analysis are briefly explained.

1.1.6.2.1 V-Load Method

The V-load method enhances the capabilities of 1D line-girder analysis by addressing the impacts of horizontal curvature in steel girder bridges [62]. For over 40 years, the preliminary and final designs of curved I-girder bridges have utilized the V-load method. In this method, the effect of the horizontal curvature in the bridge can be seen as vertical shear forces in the position of the cross-frame to the steel girder connection called V-Load (Figure 1.42). After considering these approximations, the line-girder analysis method can be used to analyze the curved girders separately. In this method, the curved girders are considered equivalent to straight girders with both the gravity and V-loads applied to them.

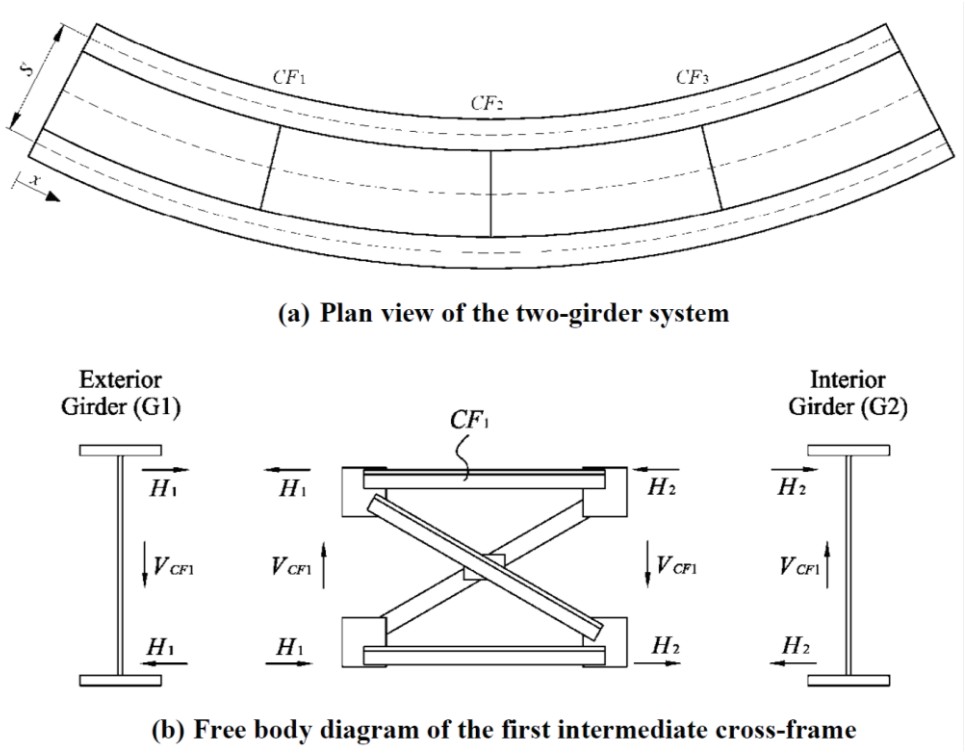

Figure 1.42 Interaction of Forces in V-Load Method in a Curved Girder System [11]

The basic assumptions in this method are:

1- All the steel girders have almost identical vertical stiffness.
2- Vertical displacement along the bridge length varies linearly due to overall torsion.

For the cases where these assumptions are satisfied, the V-load method provides reasonably accurate results. Therefore, for skewed bridges with staggered cross-frame layouts, the V-load method is not a proper analysis method. Instead, the 3D Finite Element Method (3D FEM) or Improved 2D-grid model considering the interaction between structural elements can bring improved accuracy [11]. NCHRP Report 725 [11] states the Strengths and limitations of the V-load method as below[11]:

Strength:

- Simplicity
- Widely used
- The approach is most effective for the initial design.

Limitations:

- Does not explicitly account for sources of torsion other than curvature. The horizontal shear stiffness of the concrete deck is considered by the approach.
- Not applicable for extraordinary loadings.
- The technique assumes a linear distribution of shear in the girders over the bridge section; and, as a result, the vertical stiffness of the girders at a given cross-section should be nearly the same.
- Not directly applicable to bridges with reverse curvature or a closed-framed system with horizontal lateral bracing close to, or in the plane of one or both flanges.
- The lateral deflections, which become significant on bridges with long spans and/or high skews and vertical deflections, may be significantly underestimated since the approach does not explicitly account for girder twists.
- Might not always be able to identify uplift at the end bearings.

1.1.6.2.2 M/R-Load Method

The M/R load method offers a way to account for the effects of curvature in curved box girder bridges. However, both the V-load and M/R-load approaches may significantly underestimate the vertical responses at the interior supports on the concave side of continuous-span bridges. Despite this possibility, there are no clear guidelines or restrictions on the use of any of these approximations, and it is at the discretion of the engineer to decide which approximation is acceptable [63].

1.1.6.3 2D-Grid Methods

Another commonly used method to analyze steel girder bridges with an acceptable approximation is the 2D Grid method. In this method, steel girders and cross-frames are represented with two nodes and a line element. As can be seen in Figure 1.43 each node has three degrees of freedom, DOFs (one transitional and two rotational). The translational DOF correlate to the vertical displacements, whereas the rotational DOFs record the girder major axis

bending and torsional reaction. Figure 1.44 is an example of utilizing the 2D-grid method for modeling a curved and skewed steel bridge [11].

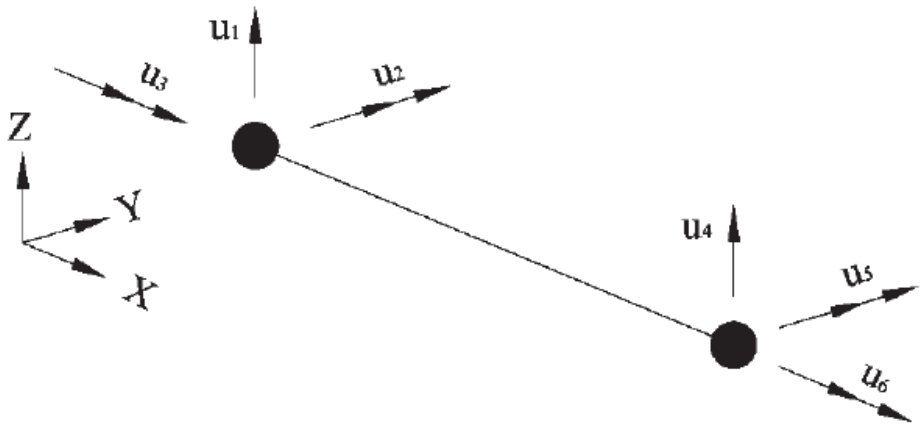

Figure 1.43 Two Node Element Degrees of Freedom (DOF) used in 2D Grid Analysis [11]

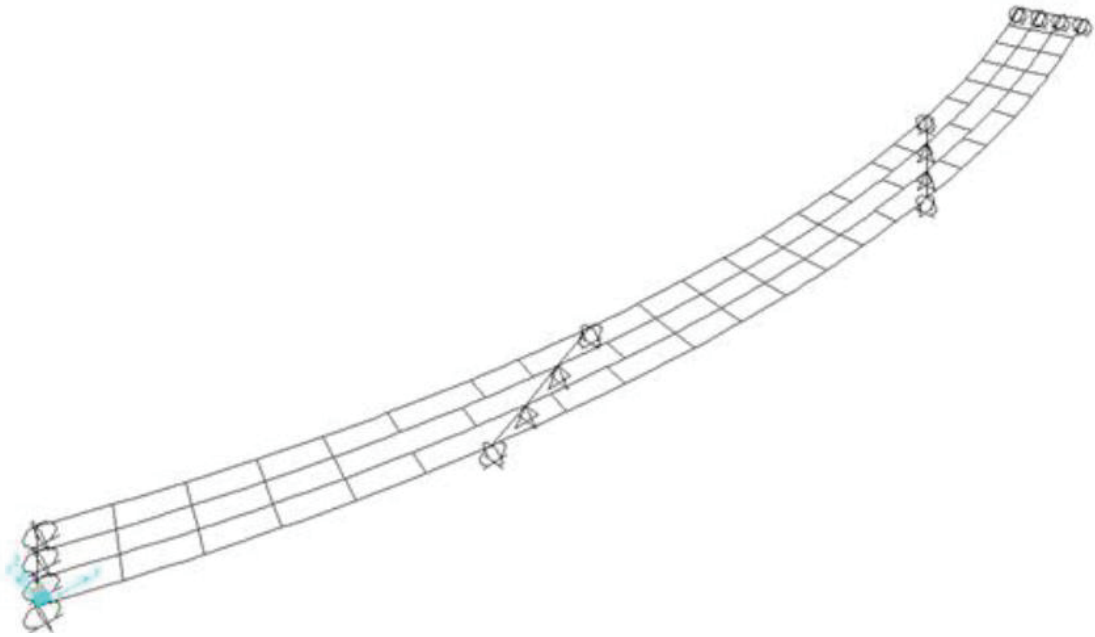

Figure 1.44 An Example of 2D-Grid Model of a Steel Bridge[11]

In 2D-grid models, the vertical depth of the superstructure is ignored. The girders are theoretically joined to their cross-frames or diaphragms at a single common height, which is implicitly assumed the girders' centroidal axis. In other words, even if the centroids of various girders, cross-frames, and diaphragms are at different depths, it is expected that all of the girders bend without any longitudinal or lateral displacement at the connections with the diaphragms or

cross-frames. Theoretically, in the model, all the girders, diaphragms, cross-frames, loads, and bearings are placed at this same height. This method simply evaluates the nodal vertical displacements and in-plane rotations. The 2D-Grid method is used in some commercial programs such as DESCUS (developed at the University of Maryland) and MDX software. NCHRP 725[11] utilized this method with the help of MDX and LARSA 4D software in their report. Some of the advantages and disadvantages of the 2D-Grid method are mentioned below [11]:

Strength:

- Simplicity in modeling compared to 3D methods
- Utilizing readily accessible, straightforward commercial software allows for speedy modeling and analysis.
- The results of a 2D analysis can be comparable to those of a 3D study if the stiffness matrix is constructed to include the warping stiffness of the cross-frame.

Limitations:

- It may become exceedingly difficult to reflect the geometry of the members that are in the third dimension, such as cross-frames.
- For skewed bridges, in particular, the mechanism of Load transmission between girders may be oversimplified.
- For complex structures, the results may not have acceptable accuracy.

1.1.6.4 2D-Frame Methods

The 2D-Frame Method is the same as the 2D-Grid method but with a greater number of DOFs for its elements. Structural elements in 2D-Frame methods, are frames or beam elements with 6 DOF (3 translational and 3 rotational) for each node (Figure 1.45).

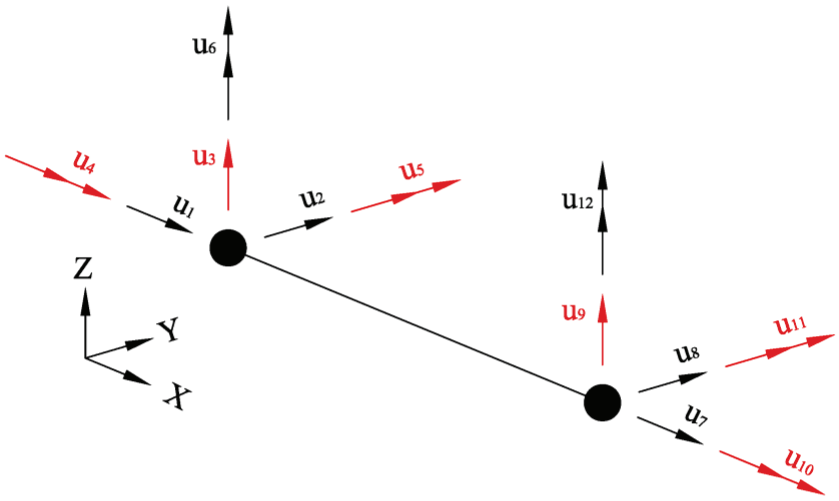

Figure 1.45 Degrees of Freedom (DOF) for a Two-Node Element used in 2D Frame Analysis [11]

The 2D-frame models do not provide any further information beyond the 2D-grid analysis. if the structural model is built entirely in one plane and if the element formulations do not include any interaction between the 2D-grid DOFs and the additional DOFs [11].

1.1.6.5 Improved 2D-Grid Method

To optimize the accuracy of the standard 2D-grid analysis methods, NCHRP 725[11] highlighted some particular flaws that needed to be addressed. They offered enhancements in each of these areas that are rather easy to put into practice and offer significant advantages with little need for additional computation.

The first problem in the 2D-Grid method was determined as underestimating the torsional stiffness of the steel girders because of the flange lateral bending effect or warping of the flanges on the girder torsional stiffness. White et al. [11] observed that the result accuracy in the 2D-Grid method can significantly improve by utilizing an equivalent torsion constant, J_{eq}, determined by equating the stiffness GJ_{eq}/L_b (G is the shear modulus of the material and L_b is the distance between cross-frames) with the analytical torsional stiffness associated with assuming warping fixity at the intermediate cross-frame locations and warping free conditions at the simply-supported ends of a bridge girder. This observation was partially based on earlier research advancements made by Ahmed and Weisgerber [64].

Another issue that affects negatively the results is the misrepresentation of the cross-frames by an equivalent beam element. The equivalent beam element that represents the cross-frames in the 2D-Grid models is calculated by using the flexural stiffness and shear stiffness methods defined by AASHTO/NSBA. White et al. [11] demonstrated that the true cross-frame flexural stiffness can be significantly greater than that obtained using either the conventional flexural or shear stiffness approaches. For the modeling of cross-frames and diaphragms, they suggested the simplified use of a Timoshenko beam element. Except for K-type cross-frames without top chords, the Timoshenko beam element offers high accuracy for almost all cross-frame types.

The third limitation that the conventional 2D-Grid method faces is that it is unable to calculate flange lateral bending stresses directly. According to NCHRP 725 study [11], grid analysis models can predict the results with close approximation compared to more complex 3D FEA solutions for the entire bridge reactions, including the diaphragm and cross-frame forces. Relying on these statically equivalent cross-frame or diaphragm forces and it is possible to calculate equivalent flange lateral loads [11]. NCHRP report 962 [65], provided a summary of the improvement techniques for 2D grid analysis methods and the related effect on bridge elements as shown in Figure 1.46.

Element	2D Analysis Improvement Techniques		
	Improve Equivalent Cross-Frame Beams[a]	**Equivalent Torsional Constant for Girders[a]**	**Equivalent Cross-Frame Beams[b]**
Concrete deck	--[c]	--[c]	Consider with equivalent cross-frame beam
Girders	--[c]	Assign J_{eq} to girder properties	--[c]
Cross-frames	Use Timoshenko beam approach	--[c]	Adjust equivalent section properties to include deck

Notes:
[a]Applies to both grillage and PEB models.
[b]Applies to grillage models only.
[c]Blank cells indicate that the improvement technique does not directly apply to that structural element.

Figure 1.46 Summary of improved 2D analysis methods

1.1.6.6 Plate and Eccentric Beam (PEB) Models

A Plate and Eccentric Beam (PEB) model is implemented by the MDX Software for the analysis of composite bridges with steel girders in their final construction stage. In this method, plate and frame elements are used for modeling the composite bridge deck and the steel girders, respectively. Frame elements as we have discussed before, have 6 DOF per node (Figure 1.45) and are modeled with a relative offset to the plate (deck) elements. As can be seen in Figure 1.47, the deck elements are connected to the frame elements with rigid links.

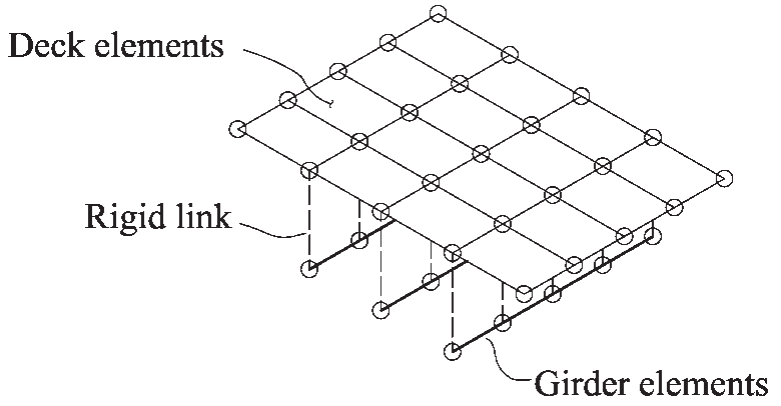

Figure 1.47 Schematic Illustration of Plate and Eccentric Beam Elements [11]

It should be highlighted that the PEB technique frequently fails to take into consideration the composite I-girders' tendency to distort into an S shape when subjected to torsional stresses. This can occasionally result in a considerable overestimation of the torsional stiffness [66]. PEB method was used in White et al. [11] and Chang et al. [66] research to study and design steel girder bridges in their final construction stage. They showed that some simplified approximations and adjustments can improve the modeling of the torsional stiffness in steel girders[66].

1.1.6.7 Traditional 3D-Frame Methods

Another method in modeling the steel girder bridges is a traditional 3D-Frame method. According to the NCHRP 725 [11], an analysis model might be referred to as a "Traditional 3D-Frame" if the following conditions are met:

- Frame elements modeled at their real spatial locations of the centroid and shear center of the girders.
- The precise placement of the cross-frames or diaphragms throughout the depth is modeled (Each complete cross-frame or diaphragm is normally represented by a single frame element)
- Rigid offsets are used to describe changes in the girder, cross-frame, and bridge's bearing depths.

Employing accurate cross-frame stiffness and girder torsional stiffness is very important in the 3D-Frame method. Otherwise, this method cannot add any further accuracy to the results. In reality, the torsional stiffness in steel girders is dominated by the non-uniform torsion linked to cross-frames warping related to Lateral Bending of the Flanges (LBF). The torsional stiffness in the frame elements defined just by Saint-Venant torsional stiffness cannot completely represent the torsional stiffness in the steel girders and in most cases that stiffness is too small compared to the actual torsional stiffness of the girder [11].

1.1.6.8 Thin-Walled Open-Section (TWOS) 3D-Frame Methods

The Thin-Walled Open-Section (TWOS) 3D-frame model is identified as the most accurate frame element model for steel girder bridges [11]. In this bridge modeling, the frame elements are constructed with two nodes. As we can see in Figure 1.48, each node in the TWOS frame element has three translations (u_1, u_2, and u_3 or u_8, u_9 and u_{10}), three rotations (u_4, u_5 , and u_6, or u_{11}, u_{12} and u_{13}) and one warping degree of freedom (u_7 or u_{14}). In this 3D method, frame elements are modeled in their accurate spatial positions. Chang et al. [67] used GT-Sabre software to study different steel bridges with this method. They modeled cross-frames completely by modeling all the components like diagonal elements and horizontal chords individually with frame elements.

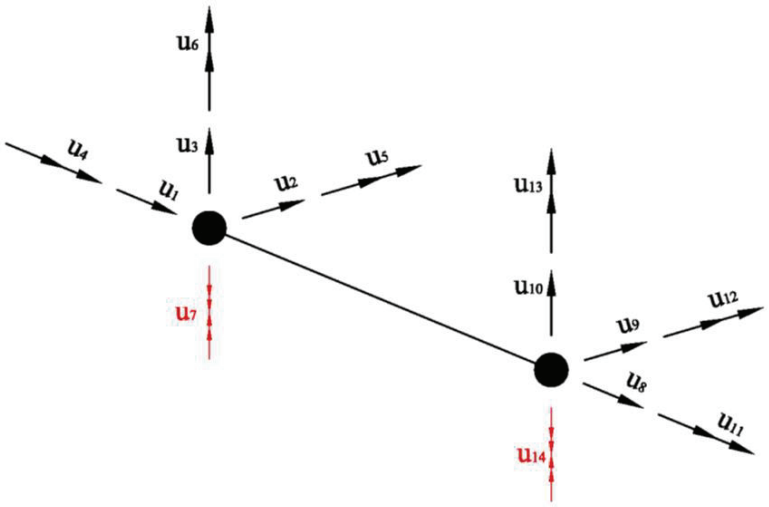

Figure 1.48 Schematic Illustration of DOF in TWOS Frame Elements [11]

Studies show that the results in TWOS 3D-Frame models have a good agreement with 3D Finite Element Method (3D FEM) models. However, this method cannot capture the effects of web distortion in steel girders. Considering that web distortion plays an important role in the results, this may be an impediment. In other words, if a TWOS frame element is connected to the concrete deck by rigid elements like in the PEB method, the lateral bending of the bottom flange would be constrained wrongly by the concrete deck. Chang [67] suggested some modeling techniques in his research to solve the issue. According to his research, there are other difficulties in using the 3D TWOS method such as continuity conditions at locations of the changing cross-sections such as changes in the width or the thickness of the web of the steel girders, and the continuity conditions for multi-branched elements (several girder elements connecting into a same node). Furthermore, Chang [67] asserts that the analysis program that can accurately represent the intricate three-dimensional deformed geometry from a TWOS 3D-frame analysis is GT-Sabre. ABAQUS as an advanced simulation software can display the 3D elements' geometry, however, it does not graphically show the exact warping deformations of 3D TWOS frame components in the deformed structure. NCHRP report 725 [11] suggests that thanks to high-speed computers, utilizing 3D Finite Element Analysis (3D FEA) with larger DOFs are superior to the TWOS 3D-frame analysis for the design of steel girder bridges when the 1D-Girder or 2D-Grid methods cannot bring satisfactory results.

1.1.6.9 Advanced 3D Finite Element Analysis (FEA) Methods

The term “3D Finite Element Analysis (3D FEA)” can be used to refer to any matrix analysis method, which has a three-dimensional modeling capability. However, AASHTO/NSBA G13.1 [68] narrowed the definition of the 3D Finite Element Analysis conditions as below:

- Having a three-dimensional model for the superstructure
- Beam, shell or solid-type elements should be used for modeling the girder flanges
- Shell or solid-type elements should be used for girder webs
- Truss, beam, shell, or solid-type elements should be used for the cross-frames or diaphragms
- Shell or solid-type elements should be used for the concrete deck modeling when the response of the composite system is needed

Compared to other analysis methods for the bridges, the finite element method utilizes a great number of relatively small elements interacting with each other for modeling a subject. Various parameters can affect the analysis results such as modeling techniques and elements size. Therefore, each finite element model may have its unique solution and results that could vary from the others at various levels. In this method, the user has a major role in choosing a theoretical representation for each component of the structure (such as 3D solid, shell, Timoshenko beam, and Euler-Bernoulli beam while creating a 3D FEA model), selecting the order of the interpolation for the elements shape function, mesh sizes and density for analysis convergence, a calling for a numerical integration scheme for evaluation of the element nodal forces and stiffnesses (e.g., standard Gauss quadrature, Gauss-Lobatto integration, etc.), and finally, employing procedures for calculating, extrapolating, and smoothening or averaging of element internal stresses and strains. To reach a proper model in the 3D FEA method, one should be aware of the assumptions, the limitations, and their effects on the results. Furthermore, the final model should be validated with experimental results [11].

The main goal of 3D FEA models is the computation of all the bridge responses with good precision that can be used in conjunction with the AASHTO LRFD Specifications for the overall

design. Even for the same structure, various analytical objectives often need different finite element models. For instance, 3D FEA may be particularly beneficial for studying detailed local stress analysis of sophisticated structural elements. This is not the usual goal of a 3D Finite Element (3D FE) design analysis. According to NCHRP Report 725 [11] a 3D FE design analysis often seeks to calculate:

- Elastic vertical and lateral deflections and rotations in the girders
- Flange lateral bending, elastic major axis bending, and web shear stresses
- Web shear forces
- Cross-frame axial elastic forces
- Elastic concrete deck normal and shear stresses and strains while considering the steel girder and the concrete deck as a composite system

Several 3D FEA modeling techniques can achieve these goals. Figure 1.49 depicts a portion of a 3D finite element model of a steel girder bridge with three steel I girders. The nominal dimensions are used to simulate all the bridge components at their physical geometric positions [11].

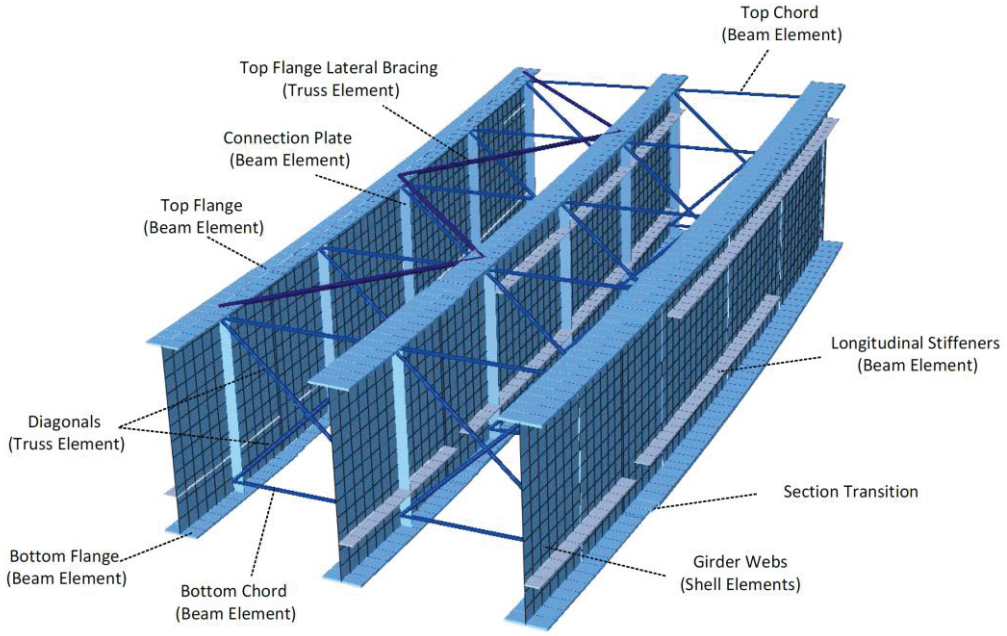

Figure 1.49 A Portion of a 3D Finite Element Model for a Steel Girder Bridge [11]

NCHRP project 12-113 [65] investigated the possibility of a simpler 3D Finite Element modeling to propose modifications to AASHTO cross-frame analysis and design. To avoid limitations to computational cost and time in the case of the extensive parametric study, they suggest the use of truss elements for modeling cross-frame members. However, they pointed out that using truss elements for the cross-frames has three major shortcomings in representing the in-plane flexural, out-of-plane flexural, and axial rigidity of cross-frame systems caused by the connection rigidity, the eccentric end connections, and the cross-frame member axial rigidity.

To overcome these limitations, they proposed two different modeling methods consisting of the Stiffness Modification Approach (R-factor) and the Eccentric-Beam Approach (Figure 1.50). The Stiffness Modification Approach corrects the effect of these limitations by approximately modifying the axial rigidity of the truss elements to accurately represent the actual stiffness of the cross-frames [49, 69]. They also proposed the eccentric-beam modeling approach that addresses the limitations by modeling the cross-frame systems (cross-frame members along with their connections and gusset plates) using beam elements with an eccentricity which can be defined in three ways with different levels of details (Figure 1.51).

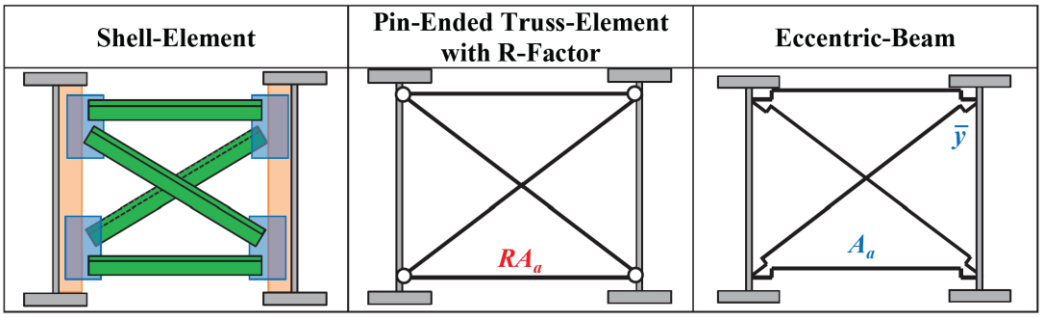

Figure 1.50 Cross-frame modeling in skewed bridges proposed by NCHRP report 962 [65]

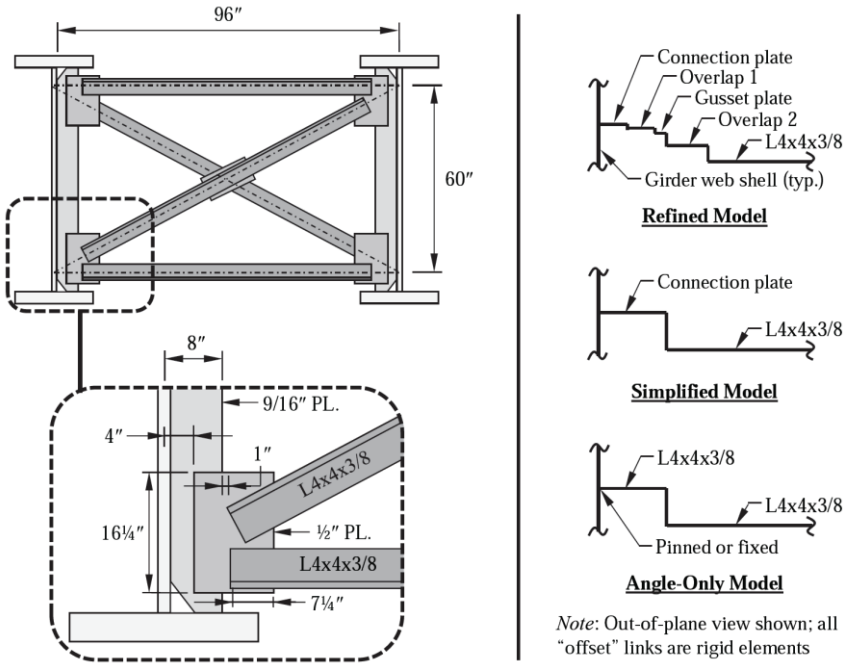

Figure 1.51 Eccentric-Beam Approach and the corresponding eccentricity definition ways for a sample cross-frame panel [65]

Various considerations must be made in addition to direct modeling of the components that are typically necessary for steel girder bridge design. These include [11]:

- Considering the sources of flexibility in the model (i.e., connection flexibility and additional flexibility of cross-frame elements because of bending under eccentric axial loads)
- modeling of the effects of bearing limitations, including guided and fixed bearings, on the 3D response under vertical load, especially for curved steel girder systems
- modeling of particular sources of added stiffness, such as restraint of anticipated movements at bearings
- Modeling of substructure deformations and their influence on the superstructure
- Potential bearings uplift
- Geometric nonlinear effects (Important for overall stability)

Suggestions for managing these and other structural features are given in the AASHTO/NSBA G13.1 [68]. Here, some of the advantages and disadvantages of 3D FEM analysis are shown below [11].

Strength:

- In contrast to 2D analysis, frame components in 3D may be represented with better geometrical placements and properties.
- It is beneficial for bridges with intricate superstructures.

Limitations:

- 3D analysis requires more effort and expertise than 2D analysis.
- Using this method can increase the project cost

1.2 Fatigue

1.2.1 Introduction

Fatigue is considered a failure mechanism developed by the initiation and propagation of cracks as a result of repetitive stresses, especially in tensile elements [41]. The fatigue issue in steel structures and welded joints has been recognized as a major problem right after World War II. It can be caused in tension elements by any repetitive loadings with different magnitudes called fatigue loadings such as varying live loads in bridges, environmental phenomena like winds or waves, vibrating equipment, and fluctuating pressure or temperature [70]. It is critical to recognize the possible fatigue loading in the design phase and to design the structure with fatigue consideration. More importantly, the designers should give careful consideration to the design of connections in accordance with codes and specifications for fatigue [70]. According to the NCHRP Report 102 [71], fatigue strength at connections mostly relies on joint geometry configuration and stress range. Experiments have shown that other variables such as the strength of the parent material, minimum stress, and size variation have a minor effect on fatigue strength in welded joints and that they can be ignored [70, 72]. Unlike column buckling strength, fatigue strength for a specific welded joint cannot be calculated solely based on geometry and basic material properties. In other words, the only reliable means to determine the fatigue strength of a joint is the experimental fatigue test. Fatigue standards based on experimental results provide helpful information for designing various types of joint details with different geometry, especially for high-stress ranges [70].

1.2.2 Methods for Developing S-N Curves and AASHTO Fatigue Categorization

Most of the fatigue specifications use S-N curves in their fatigue design process which have been constructed based on statistical analysis conducted on experimental fatigue test results under constant amplitude fatigue loading, The S-N curves are normally represented in equally spaced curves on a logarithmic scale plot in which Y-axis is $\log_{10}$ stress range (S) and X-axis is $\log_{10}$ endurance (N). Each group of S-N curves can be used for defining fatigue strength for materials or configuration/connections, and usually are made with two straight lines. The first line has a negative slope until reaching a threshold. The curve slope becomes zero after reaching the

threshold. Basically, a certain configuration can experience infinite cycles of stress ranges that are below the threshold stress range identified for that configuration. The governing equation would be similar to Eq. 1.2 with a constant slope of the curve (m) and C for each connection type (configuration) and the endurance range cycles (N).

$$\log N = \log C - m \log S \quad (1.2)$$

In fatigue analysis, there are two ways to define the slope of m (negative slope of the inclined line) for Eq. 1.2. One way is to calculate the slope of a statistically best-fit line to the available test results. Alternatively, a pre-defined slope can be adopted consistent with the slope of the line in comparable configurations or applications. The position of the line can then be adjusted in the best fit to the test results. For steel structures, it is recommended to use a pre-defined m=3.0, while for higher-strength connections and some types of continuous longitudinal welds, it is realistic to use higher values for the line slope such as 3.5 or 4 [70]. With an increasing slope of the inclined line (m), the fatigue strength would decrease, and the connection would fail in lower cycles compared to those of smaller slopes. In another word, a higher m would result in steeper slopes in S-N curves and less fatigue strength in the connection in each stress range. Fisher et al. in their study reported in NCHRP Report 147 [72], found that the slope of the mean regression curves varies slightly from -2.82 to -3.25 for steel plate attachments to the flange with different lengths, and is equal to -3.5 for stiffener welded to both flanges and web of the beam. The latter seems to be the most consistent configuration for the half-round stiffener connections.

The AASHTO LRFD Specification [73] provides ratings/categories for structural steel details ranging from A to E'. The S-N curves corresponding to these categories are shown in Figure 1.52. As it was stated earlier, prior investigations [54] have suggested a Category C (C' according to 9th edition AASHTO) for the case of stiffener plates welded perpendicularly to the flange, represented in Section 4.1 of AASHTO [73] fatigue details (Table 6.6.1.2.3-1) for welded joints transverse to the direction of stress.

Based on work conducted at Purdue University (Connor and Korkmaz, 2020), a new provision is proposed outlining the behavior of obliquely oriented welded attachments such as web stiffeners

with orientations ranging from 0 degrees (perpendicular orientation) to 90 degrees (longitudinal orientation) [74]. The provisions will apply to obliquely oriented stiffeners with a plate length (stiffener length), L<4.0 inches, and a thickness t < 1.0 inches. Stiffener orientations from 0-20 deg. are Category C' matching results from Case 4.1 for stiffeners with a perpendicular orientation and transition to Category E for stiffeners with a 90-degree orientation (matching Case 4.4 - 9th edition Case 4.3) for longitudinal stiffeners. For small angles (up to 20 degrees), the effect of the orientation is minimal. Figure 1.53 describes transition between categories for orientations between 20 and 90 degrees.

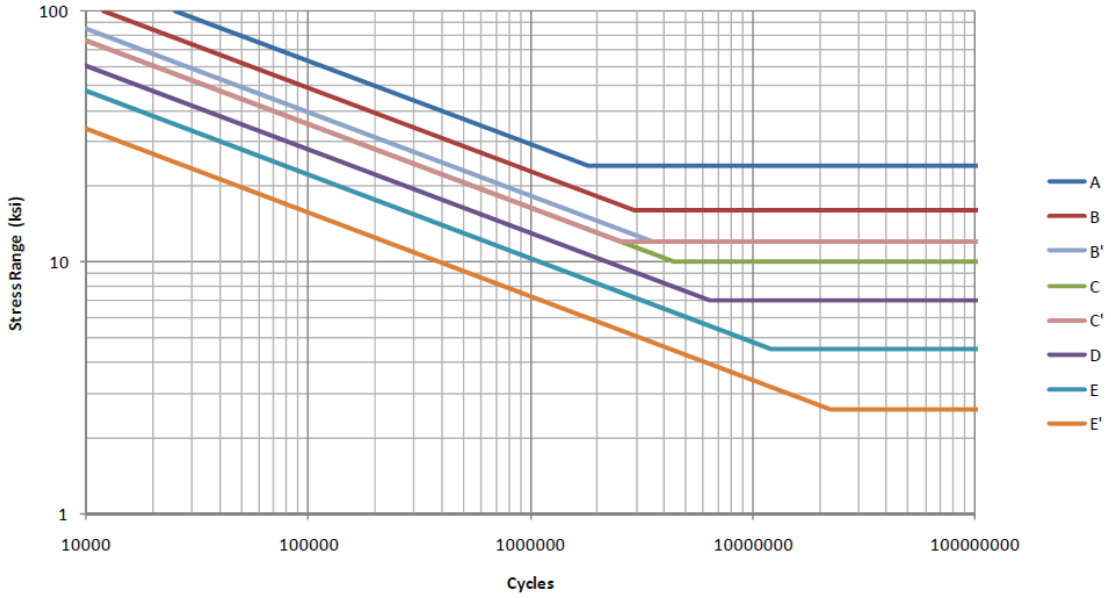

Figure 1.52 S-N curves corresponding to AASHTO fatigue categories [44]

Description	Category	Constant A (ksi^3)	Threshold $(\Delta F)_{TH}$ (ksi)	Potential Crack Initiation Point	Illustrative Examples
Base metal in a longitudinally loaded component at an obliquely oriented detail with an effective length $L > 4$ in. and a thickness t less than 1 in. attached by groove or fillet welds.					
$90° > \theta \geq 70°$	C′	44×10^8	12	In the primary member at the weld toe	
$70° > \theta \geq 60°$	C	44×10^8	10		
$60° > \theta \geq 45°$	D	22×10^8	7		
$0° < \theta < 45°$	E	11×10^8	4.5		

Figure 1.53 Recommended AASHTO provisions for skewed plates based on the angle [74]

1.2.3 Statistical Planning Guidelines for Fatigue Experiments

Planning a fatigue test requires an understanding of the two main parameters, the test program objectives and the effect of test program constraints. The fundamental concepts stipulated in the ASTM Report STP588-EB/Nov. 1975 [75], hereafter called STP588, though in general terms, can be adapted with adjustments to satisfy the two main objectives of each specific project.

1.2.3.1 Fundamental Concepts in the Statistical Planning of Fatigue Experiments

Any successful experimental planning shall have the following elements,

Organizational Structure- A descriptive combination of charts, figures, and tables showing the interrelation of all variables in a test program, the order of testing, and the type of statistical analysis required for deductions.

Experimental Units- Generally the individual specimens are to be tested. These may be grouped in a certain manner according to the variables important to the objective of the program.

Blocks- A group of test specimens that are more uniform within the block than those in the other blocks. Grouping in this manner is with the objective of masking the effect of nuisance/distracting variables so that the effect of the variable of interest can be pronounced.

Treatment - Major variables whose effects are of interest to the program. Assigning treatments to test specimens may follow certain procedures including *Mechanical Randomization* which is choosing randomly which specimen would be subject to a certain stress range. The variables of interest may need to be considered only with a certain range of interest under certain amounts or *Treatment Levels* (e.g., certain stress range in fatigue test). Treatments can also be combined within the same specimen, *Treatment Combination*, as per the organizational structure.

Nuisance Variables- Variables that may affect the fatigue response but are the focus of the testing program.

Replication- Replicate is the collection of observations including one observation on each treatment (e.g., results for specimens tested under the same stress range). *Replication* is the number of replicates in the program.

Depending on the objectives, a variety of test programs can be adopted. These include Paired Comparison Test Program (when the effect of two treatments is of concern and all other variables are kept constant), Elementary Uniformity Trial Test Program (when studying the influence of nuisance parameters are the target), Completely Randomized Design (CRD) Test Program and Randomized Complete Block (RCB) Test Program (where the specimens are randomly grouped for each level of a treatment), and Elementary Split Test Program (where CRD and RCB organizational structure is modified to overcome statistical difficulties).

Normally, organizational structures that could be represented in simple diagrams and address the objectives are indications of well-planned test programs. The plan shall be compatible with test objectives, the number and nature of blocking variables, logic in processing and preparation of specimens, and as importantly, economical and practical constraints. The plan should also consider the statistical analysis to be used for the test results and attempt to accommodate a straightforward statistical analysis method. Such analysis will involve analysis of variance or covariance.

1.2.3.2 Planning S-N Tests

The first step in designing a fatigue test and creating the related S-N curve is defining the objective of the tests and selecting the type of test that best addresses the objectives. There are four types of fatigue tests, namely, preliminary and exploratory, research and development testing of components and specimens, design allowable data, and reliability data. These four test types are different in the number of test specimens, replication percent, test costs, and reliability level of the results. STP588 [75] has elaborated on the preliminary and exploratory test types and consequently issued guidelines and recommendations for other test types as well.

The objective for the preliminary and exploratory tests is normally to learn as much as possible about the fatigue behavior of a material or component with respect to large fatigue effects in the

shortest time and with fewer specimens. It is usually adopted when there are strict limitations on the number of specimens and cost.

When the overall shape of the S-N curve is not known as per the previously available results, the number of stress range levels should be high enough., six or eight different levels, to be able to trace the shape of the curve (Figure 1.54a). When the overall shape of the S-N curve is already known, there is no need to trace every point along the S-N curve, and normally two stress ranges would be sufficient, and it is not necessary to have more ranges (Figure 1.54c). Therefore, the remaining tests can be used as a replication for those stress ranges. In general, since the data variability for specimens with longer fatigue life located on the right side of the S-N curve is more than shorter fatigue life located on the left side of the curve, it is better to allocate more replication for longer fatigue life parts. However, when the number of specimens is twice the number of stress range levels, uniform replication by having two specimens for each stress range level would generate satisfactory results. After the preliminary and exploratory tests have identified the main fatigue effects and the overall S-N curve shape with approximate values, the replication becomes the main issue. Figure 1.55 shows an acceptable compromise between the number of stress range levels and the replication at each of those stress range levels for a fatigue test program considering two treatments with fretting and without fretting effects. For the S-N curve with a straight-line shape, the middle stress range level tests can be eliminated without a negative effect on the curve fitting.

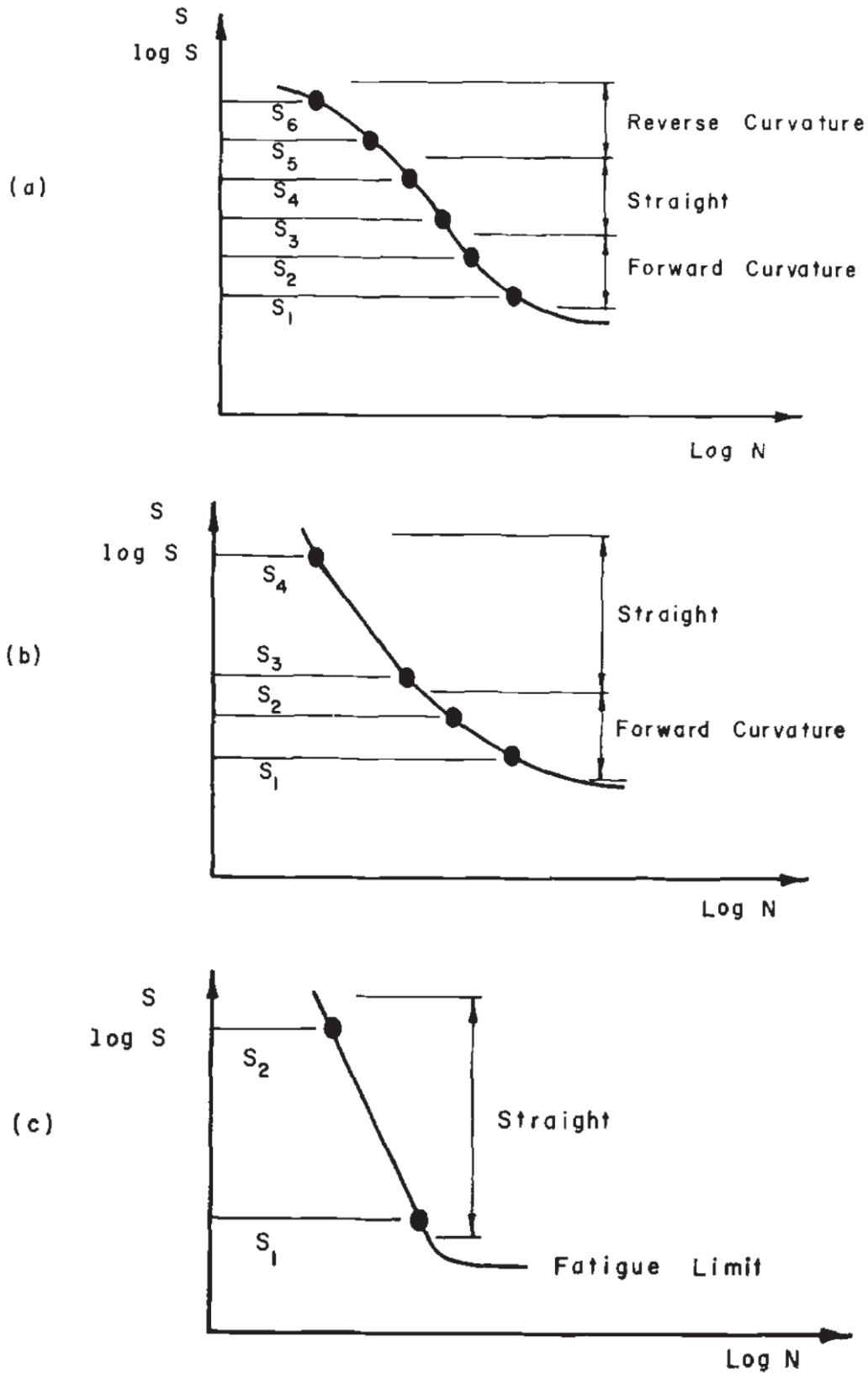

Figure 1.54 Elementary types of S-N curves with straight and curved shapes [75]

1.2.3.2.1 Recommendation for the Number of Stress Levels and Replication

Regardless of what type of test is used (Preliminary, R&D, Design Allowables, and Reliability), STP588 [75] links the number of stress range levels to the shape of the S-N curve in the desired region and introduces four different scenarios. When the difference between the desired stress range levels is sufficiently small, it can be concluded that the S-N curve in that part would be a straight line, and as a result, only two stress range levels should be used. Three stress range levels with equally divided intervals are recommended when the experimental results have shown that the S-N curve in the desired region is smooth with a gradual forward curvature. It is also beneficial to use three stress range levels when the linearity of the S-N curve in the region of concern needs to be checked for increased accuracy [76-78]. It is worthwhile to mention that, in 50 percent of the repeated tests, when the true model of the S-N curve is linear, the results would show a slight forward or reverse in the S-N curve. Finally, when the fatigue life (Log N) of the region of concern has a wide range that is required to use a second-order expression to model the S-N curve, it is recommended to use at least four stress range levels.

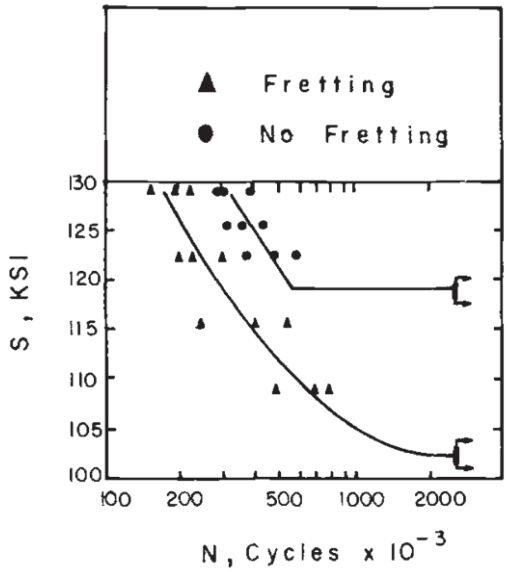

Figure 1.55 Acceptable compromise between the number of stress levels and replication at each level [75]

STP588 [75] proposes a guideline for the recommended minimum replication percentage and the minimum number of total specimens based on test types (Figure 1.56 and Figure 1.57, respectively). The percent replication is defined as,

$$\%\ Replication = 100\left[1 - \frac{\begin{array}{c}Total\ number\ of\\ different\ stress\ levels\\ used\ in\ testing\end{array}}{\begin{array}{c}Total\ number\ of\\ specimens\ tested\end{array}}\right] \quad (1.3)$$

Generally, when the shape of the S-N curve based on previous tests is known, minimum 50% of replication is recommended by the guideline, and when the shape of the S-N curve is unknown, the percent replication should be increased significantly. For example, the minimum percent replication should be 75%, when six to eight stress range levels are used.

Type of Test	Percent Replication[A]
Preliminary and exploratory (research and development tests)	17 to 33 min
Research and development testing of components and specimens	33 to 50 min
Design allowables data	50 to 75 min
Reliability data	75 to 88 min

[A] Note that percent replication indicates the portion of the total number of specimens tested that may be used for obtaining an estimate of the variability of replicate tests.

Figure 1.56 Replication Percentage Based on the Test Types [75]

Type of Test	Minimum Number of Specimens[A]
Preliminary and exploratory (exploratory research and development tests)	6 to 12
Research and development testing of components and specimens	6 to 12
Design allowables data	12 to 24
Reliability data	12 to 24

[A] If the variability is large, a wide confidence band will be obtained unless a large number of specimens are tested

Figure 1.57 Minimum Number of Specimens Based on the Test Types [75]

Strzelecki and Sempruch (2016) reviewed available requirements for the number of fatigue test specimens required for S-N curve estimation. Polish Committee for Standardization suggested at least 15 specimens at 5 stress levels [79]. ISO-12107 recommends a minimum of 28 specimens for determining the S-N curve, specifying 7 for the preliminary test but gives no number of load levels [80]. Meanwhile, the ASTM E-739 standard introduces Eq. 1.4 for finding the total number of specimens (n_a) based on the replication percentage (PR) and the number of stress levels (Sl) [81]. This equation is practically the same as Eq. 1.3.

$$PR = 100\left[1 - \left(\frac{Sl}{n_a}\right)\right] \ [\%] \tag{1.4}$$

The ASTM E-739 standard then recommends replication percentages for the type of tests being conducted referencing the STP588 [75]. Strzelecki and Sempruch (2016) also reviewed the available analytical methods for determining the S-N curve and considered a combination of experimental and analytical methods for reducing the number of tests without much sacrifice in the level of error/confidence.

1.2.3.2.2 Fatigue Strength and Fatigue Limit Tests

STP588 [75] introduces three different methods for fatigue strength and fatigue limit tests: the Probit Method, the Up-and-Down Method, and the Two-Point Method. In a historical review of fatigue testing methods, Kuroda et al., 2021, has pointed out the use of two methods, the Probit and Staircase Methods [82]. The staircase method basically refers to both up-and-down and two-point methods. In the Probit method, fatigue tests are planned for a group of specimens for each of uniformly spaced stress range levels. The results are then used to calculate the mean and standard deviation for each stress level. Kuroda et al., 2021, provided a descriptive example shown in Figure 1.58. Assuming that the run-out number (limit on the life cycles, N_f) to be 10^7 (as it normally is set), the probability of fracture at each stress level can be estimated by dividing the number of fractured specimens by the total number of specimens. Figure 1.59 shows the plot of fracture probability versus the stress level for three closely spaced 25, 26, and 27 ksi at $N_f = 10^7$. The regression line in this plot confirms the normal distribution of the fatigue fracture probability,

according to which, the stress level corresponding to F = 50% which is 25.9 ksi, represents the mean value for fatigue strength at $N_f = 10^7$.

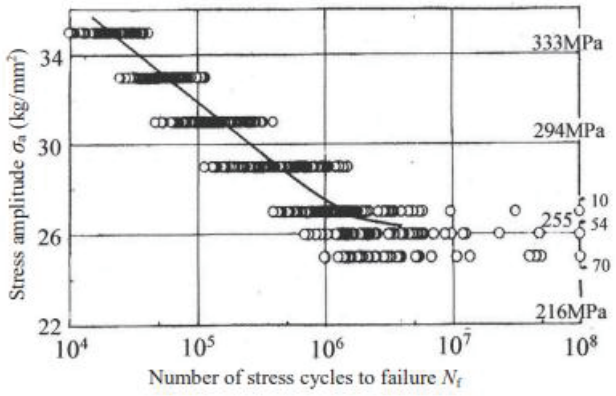

Figure 1.58 A sample fatigue testing results for the Probit method [82]

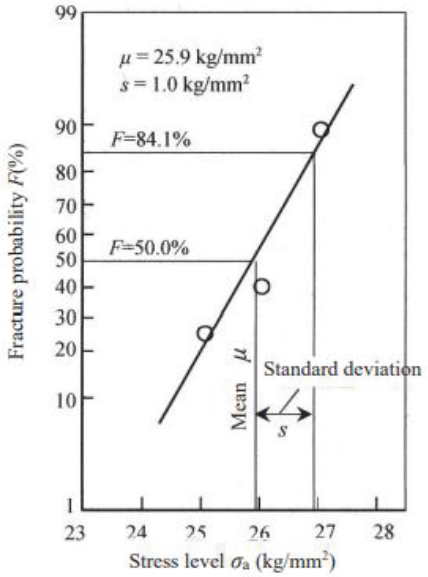

Figure 1.59 Determination of fatigue limit distribution and parameter determination [82]

According to STP588 [75], the Probit method is not statistically efficient and it is not recommended especially when the number of specimens is limited. Another method for finding fatigue limit is an up-and-down method in which specimens are tested in sequence. Figure 1.60 shows an illustration of the up-and-down method. The first specimen is tested at a stress level that is approximately equivalent to the median fatigue limit estimated by previous tests' data or the S-N curve produced by the preliminary test type. If this specimen survives during the fatigue

test for a specified number of cycles (N*), the stress range level would be increased, otherwise it would be decreased. For example, in Figure 1.60, the first specimen survived after a specific number of cycles (N*) in a fatigue test for a stress range level of 62.5 ksi. Therefore, the stress range level for the second specimen was increased to 65 ksi. Since the second specimen did not fail at 65 ksi again, the stress range level was increased another time for the following specimens until a failure occurred for the fifth specimen. As a result, with this method, a number of fatigue tests are performed hovering around the fatigue median limit and based on the collected data, the fatigue limit is defined statistically with a prescribed procedure. The up-and-down method can estimate the fatigue limit faster than the Probit method. However, this method loses its benefit and may even turn out to be quite ineffective once the approximate median fatigue limit has been determined through up-and-down testing.

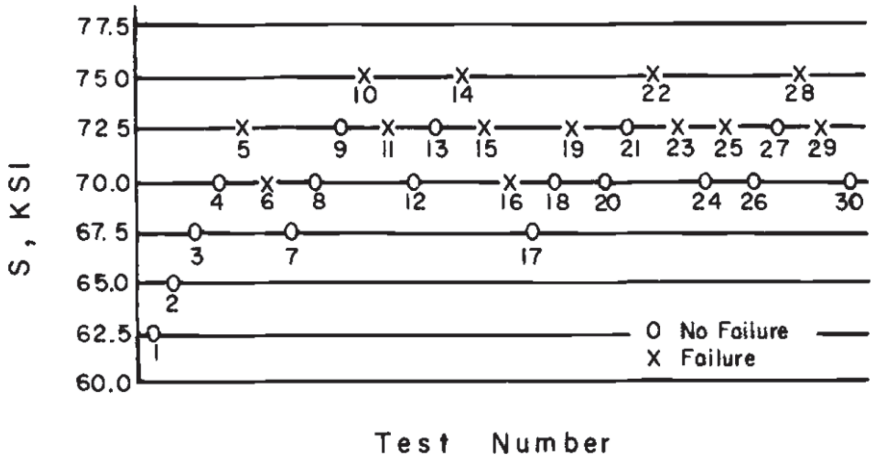

Figure 1.60 Elementary Illustration of Up-and-Down Fatigue Strength Limit Test Method [75]

Another method for estimating the fatigue limit is a two-point method [75, 76]. This method is the same as the up-and-down method until the first test result shows two nonzero and non-unity proportions failed, following which specimens are examined exclusively at the two corresponding stress levels. For instance, in Figure 1.60 the second nonzero, non-unity proportion fails at the ninth specimen. Therefore, all tests should be performed at either S_1 (70.0 ksi) or S_2 (72.5 ksi). The median fatigue can be estimated statistically between these two stress range level points (S_1 and S_2). By doing this, the inefficient specimens such as Specimens 10, 14, 22, 28, and 17 would eliminate from the test program. Accordingly, the two-point method is identified to be more

efficient. It is recommended that when the number of specimens is limited, the two-point method should be used. Generally, eight to ten specimens are needed to find the two nonzero, non-unity points. In the case that the number of specimens is very limited or the spacing of the conducted tests is so wide, it is not straightforward to find two nonzero, non-unity points. In this case, the median fatigue limit can be estimated only if the standard deviation is known from previous experiments.

Strzelecki and Sempruch (2016) have provided a very helpful summary of the methods for determining the S-N curves for metals in general [83]. The $\log_{10}$ linear equation between the stress amplitude (S) and endurance range cycles (N) is normally used for both limited and unlimited fatigue life regimes. They noted that the classic procedure for plotting the S-N curve, depicted in Figure 1.61, utilizes the linear regression for limited fatigue life and the staircase method for unlimited fatigue life portion. This is consistent with the procedure described above. The linear regression with the least square method is the most common method for stress ranges larger than the threshold stress (Z_G). From a large number of available data (91 material data sets for steel), they also discussed the number of tests required for obtaining a certain confidence level for the derivation of the S-N curve parameters.

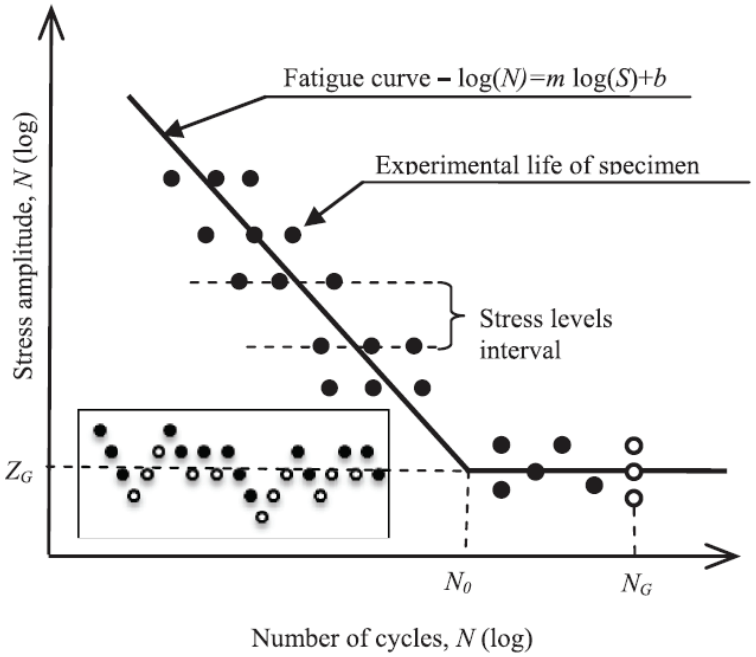

Figure 1.61 Scheme of estimated fatigue curve in high cycle range and fatigue limit [83]

1.2.3.3 Summary of Statistical Planning

Development of the S-N curve can be costly, as many parameters affect the cyclic life of the test specimens. Among these are surface condition, temperature, size, type of steel used, etc. As a result, a statistical approach needs to be used in the development of the S-N curve. For a given stress range, cyclic life can vary significantly, especially in the high fatigue cycle regime, where life is many millions. It is established that for fatigue design in accordance with AASHTO, it is necessary to subject a large-scale version of the desired detail to cyclic loading. This is reflected in AASHTO LRFD Bridge Design Specification in the form of several tables identifying the fatigue categories (Table 6.6.1.2.3-1). Therefore, a major decision to make when estimating the S-N curve or verifying the applicability of one to the case in hand is how many specimens should be tested, for how many stress ranges, and the upper and lower boundary for stresses. The latter can be determined during the analytical studies for this project.

In general, an effective test plan requires an organizational structure described by charts, figures, and tables showing in a simple manner the specimens, treatments (major variables), blocks (groups), stress levels, and replications (number of specimens at each block for each stress level). It should also suggest the statistical analysis method that would use the test data to develop the required results. There are several types of test plans that address different objectives. Preliminary, exploratory, and research test plan is used for determining the overall behavior and trends with respect to major effects. Design allowables test plan has the objective of developing results to be used in the design of structures or components. A reliability data test plan is used to determine the probability of failure normally in mass production and similar operations. Since the objective of the current project is to determine the fatigue category of half-round stiffener connection for design purposes, the design allowables test plan seems to be the proper type to choose.

The number of test specimens depends on the number of required stress levels and replications. The number of stress range levels can be reduced if the shape of the S-N curve is known. As few as two stress levels can be used for a linear behavior which is the common trend for fatigue categorization. The replication percentage and number of replications for the design allowables

test plan has been recommended by the guidelines in STP588 to be 50 to 75% and 12 to 24 specimens, respectively. Accordingly, if the S-N curve can be assumed linear, then two stress levels and 6 replications can be used to match this recommendation.

For determining the fatigue strength of a material or component, STP588 [75] and Kuroda et al., 2021 [84], described Probit and Staircase (including Two-Point Method) methods, recommending the Two-point method as a more efficient way to determine the mean fatigue strength for the specified life cycle. Considering the objective of the current project which is determining which fatigue category applies to the half-round stiffener connection, a test plan using a two-level stress range with a sufficient number of replications for each distinct configuration seems reasonable. The number of replications needs to be estimated carefully to balance the desire for a high confidence level and the economical constraint on the number of specimens. The STP588 [75] guidelines and Strzelecki et al. [83] recommendations will be used to find the proper number of replications.

1.2.4 Fatigue Mechanisms and Sources for Half-Round Bearing Stiffener Connection

It is understood that fatigue becomes a concern for an element under tension that experiences stress variation. For a half-round bearing stiffener connecting a skewed end cross-frame to the girder (Figure 1.62), one major fatigue concern at this connection is the distortional fatigue in the pipe and the stiffener plate (and perhaps the girder flanges) from the thrust of the cross-frame aiming to distort the connection tied to the girder web and flanges. In this case, stress concentration occurs at the welded joint of the flange to pipe, flange to stiffener plate, stiffener plate to the half pipe, and cross frame elements to stiffener plate. This increases the joint sensitivity to the fatigue from distortional effect. A finite element display (Figure 1.63) from work by Quadrato et al. [44] shows the stress concentration because of the application of force and distortions. Distortional effects can occur at the skewed end cross-frame connection regardless of whether the span is continuous or not. On the other hand, in the case of half-round stiffeners at the skewed continuous span bearing, in addition to distortional fatigue, there is another mechanism perhaps more important than the distortional effect. The girder flange at the pipe-to-flange weld (as well as stiffener plate-to-flange weld if welded to the flange) experiences stress

variation from live loading and therefore prone to fatigue. This is exacerbated by the fact that the tension flange is constrained against bending at a finite length by the pipe stiffener; hence, stress concentration occurs at the welded joint of the flange to pipe, (and flange to stiffener plate, if welded). This also increases the joint sensitivity to the fatigue. Another FE display from Quadrato et al.'s work shows this effect in Figure 1.64. Quadrato et al. identified hot spots in the line of contact at about 45 degrees. This is quite similar to a previous work by Anami and Sauseb, 2005 [85, 86] that pointed to stress risers at the connection of corrugated girder webs to the flange.

The degree of complexity of any fatigue testing will depend heavily on which mechanism should be considered in testing. Quadrato et al. [44], in their laboratory testing, considered only the tension flange bending mechanism. They conducted FE analysis separately for distortion fatigue. In the current study, to propose a reliable design for the laboratory specimens and a realistic setup for fatigue testing, the analysis will be performed to determine which mechanism would be the most representative of the half-round stiffener skewed connection over continuous bearing. The ideal would be to include a combination of all applicable mechanisms in the laboratory testing. This may prove to be complex and costly. The next best option would be to conduct the tests only for the most dominant mechanism or test under separate mechanisms and combine the results. In this, the FE analysis will be a key element first for determining the effect from each mechanism, and then for developing means to combine the effects if tested separately.

The following describes some studies related to testing and fatigue categorization of steel girder stiffeners with a scope similar to that being considered for this study. A review of these and other relevant prior work will help in devising a more pointed analysis and testing plan for fatigue investigation and AASHTO categorization of the half-round bearing stiffeners, including a better understanding of fatigue categories, S-N curves estimation methods, and the type and number of tests and stress ranges required for the categorization.

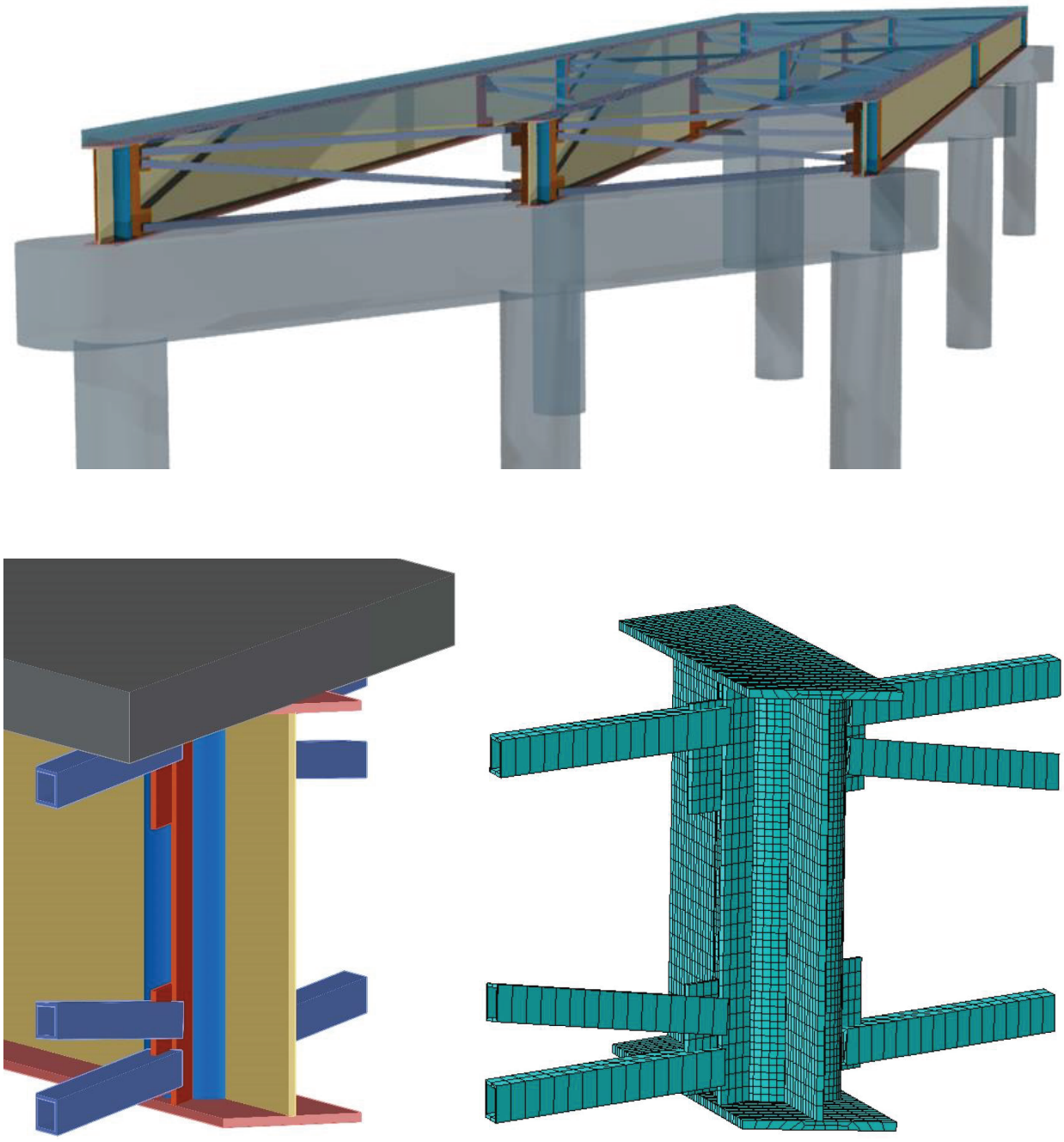

Figure 1.62 CAD models for multi-girder, continuous span structure & connection detail

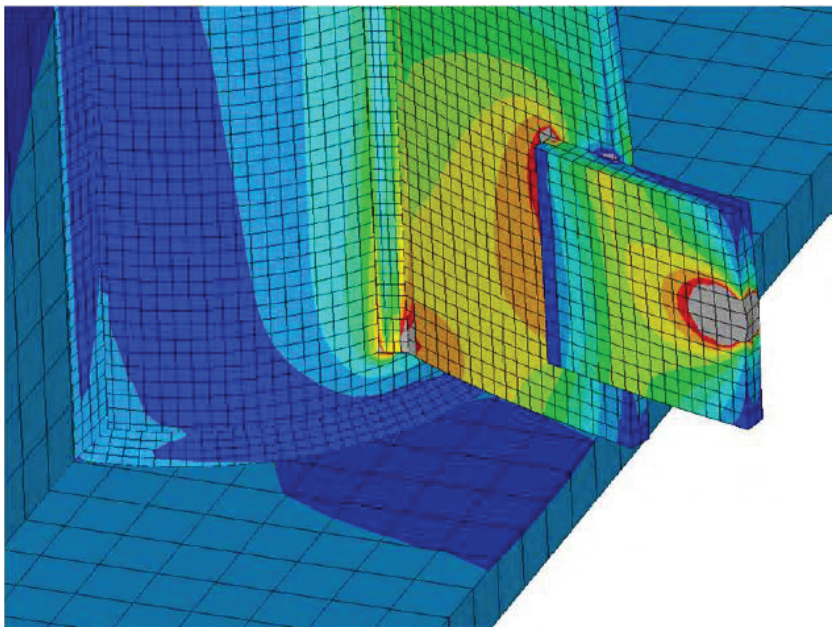

Figure 1.63 Stress concentration causing distortional fatigue within the connection [44]

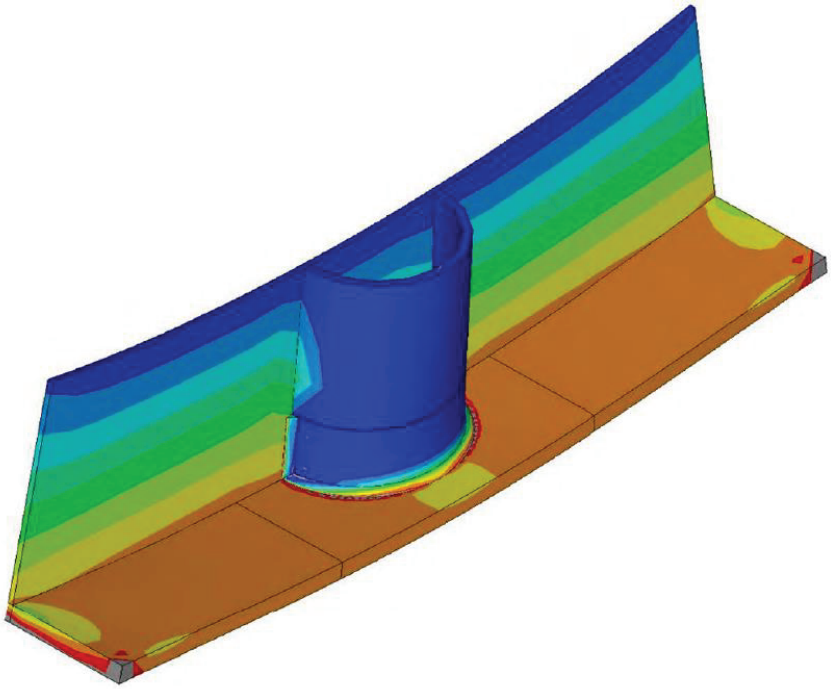

Figure 1.64 Girder flange fatigue from pipe constraint (bending constraints) [44]

1.2.5 Prior Similar Work on Fatigue Categorization for Stiffeners

Numerous experimental researches has been conducted to classify different types of steel connections based on AASHTO fatigue categories.

Fisher et al. (1974) conducted comprehensive research on the fatigue strength of steel beams with welded transverse stiffeners and attachments [72]. For this project, they tested 157 beams equipped with stiffeners or attachments. For the stiffener tests, as can be seen in Figure 1.65 and Figure 1.66, they tested three types of one-sided stiffeners on a beam. These included full-depth stiffeners welded to the web only in moment gradient and constant moment regions (Types 1 and 2), and full-depth stiffeners welded to the web and the flanges in moment gradient region (Type 3). When stiffeners are welded to the web and the flanges, the out-of-plane stiffness of the web would increase. A514 plain rolled beams with sections of W14X30 and W10X25 were used for 10 ft and 7½ ft spans, respectively. For the W10X25 beams, diagonal bracing was used as shown in Figure 1.66. The test procedure was such that the out-of-plane displacement caused by the diagonal braces was proportionate to the girder's vertical displacement.

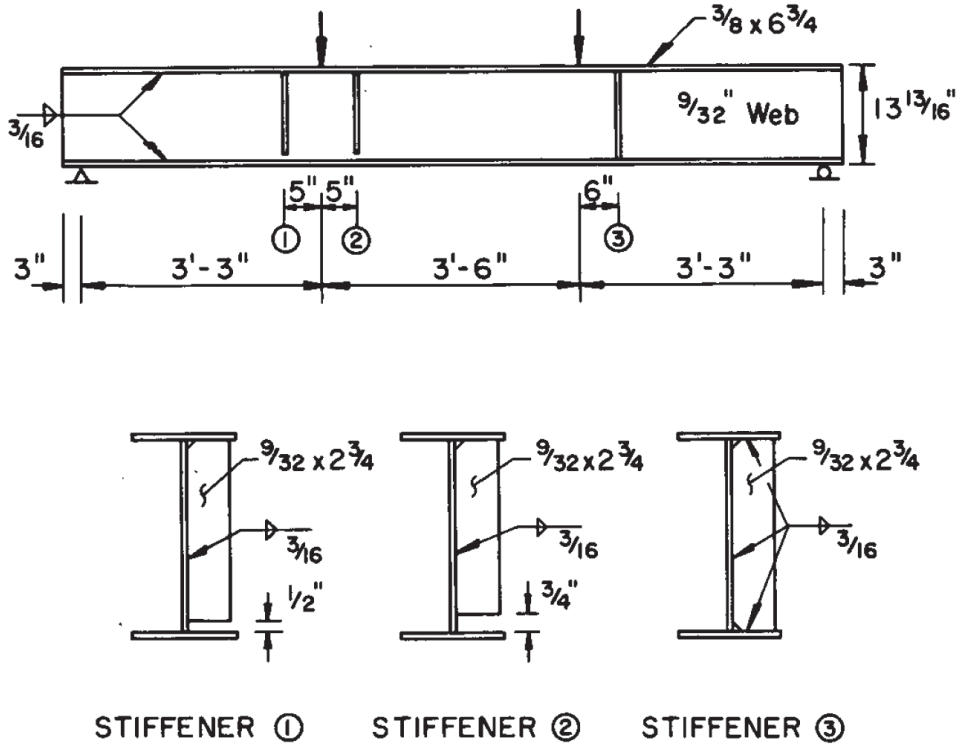

Figure 1.65 Fatigue Test Specimens for W14X30 Beams with Stiffeners [72]

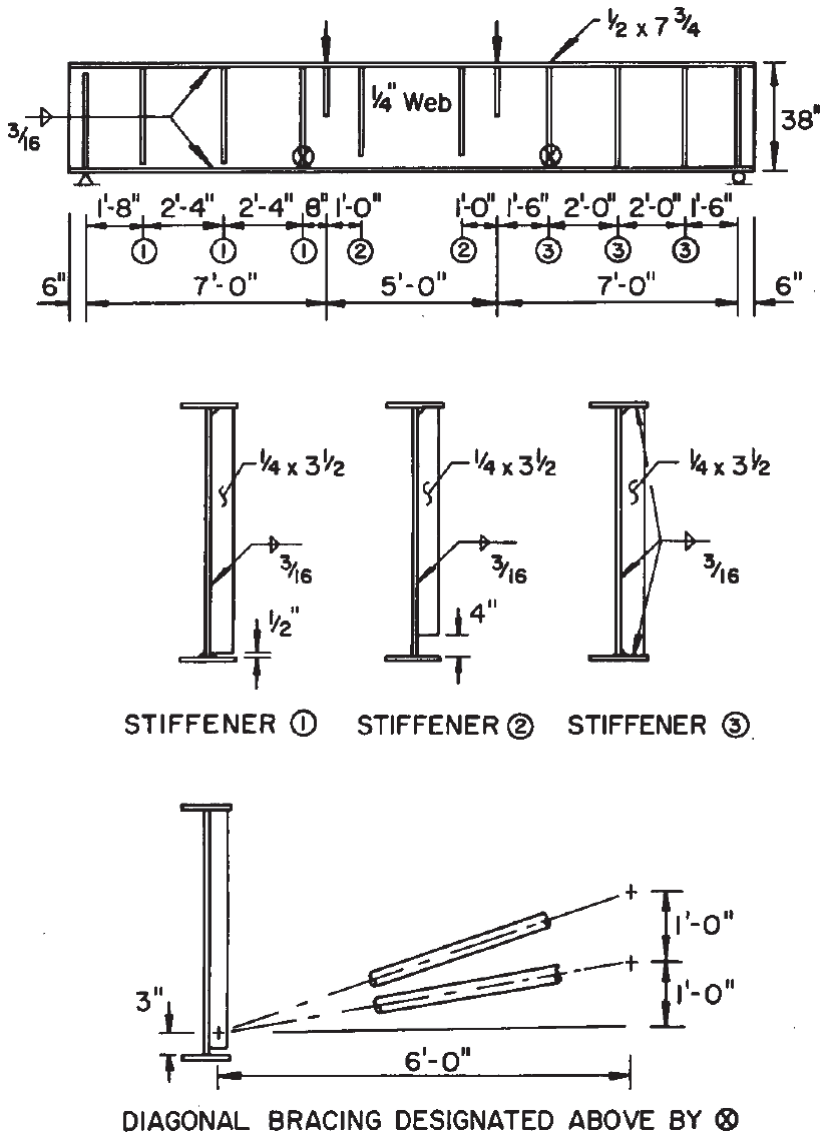

Figure 1.66 Fatigue Test Specimens for W10X25 Beams with Stiffeners [72]

Fisher et al. (1974) used the stress range and the minimum stress values as their test control variables. The formation and extension of cracks to different lengths (i.e., 2 or 4 in.) were defined as failure points in their report. They found that for the types of stiffeners, they included in the study, the stress range is the only important variable in fatigue and the grade of the base steel material, presence or absence of out-of-plane lateral forces from the braces, the bracing angle and specimen size had no significant effect on the final fatigue strength. They also asserted that the flexural stress range at the toe of the flange to the web weld in Type 3 and at the toe of the web weld termination in Types 1 and 2 was the dominant parameter in fatigue. The tests' cycles

were between 10^5 to 10^7 and the stress range varied between 13.7 to 28.7 ksi. In stiffeners Types 1 and 2, the cracks initiated at the terminating toe of the weld connecting the web and the stiffeners, while in stiffeners Type 3, the crack started at the toe of the weld between the stiffeners and the flange. The test results and deducted S-N curves for stiffeners Types 1, 2, and 3 are shown in Figure 1.67, Figure 1.68, and Figure 1.69, respectively. The data points, mean regression line, and confidence limits at two standard deviations from the mean are displayed in each S-N curve [72]. In Figure 1.70, Figure 1.71, and Figure 1.72, the statistical analysis of this study are summarized.

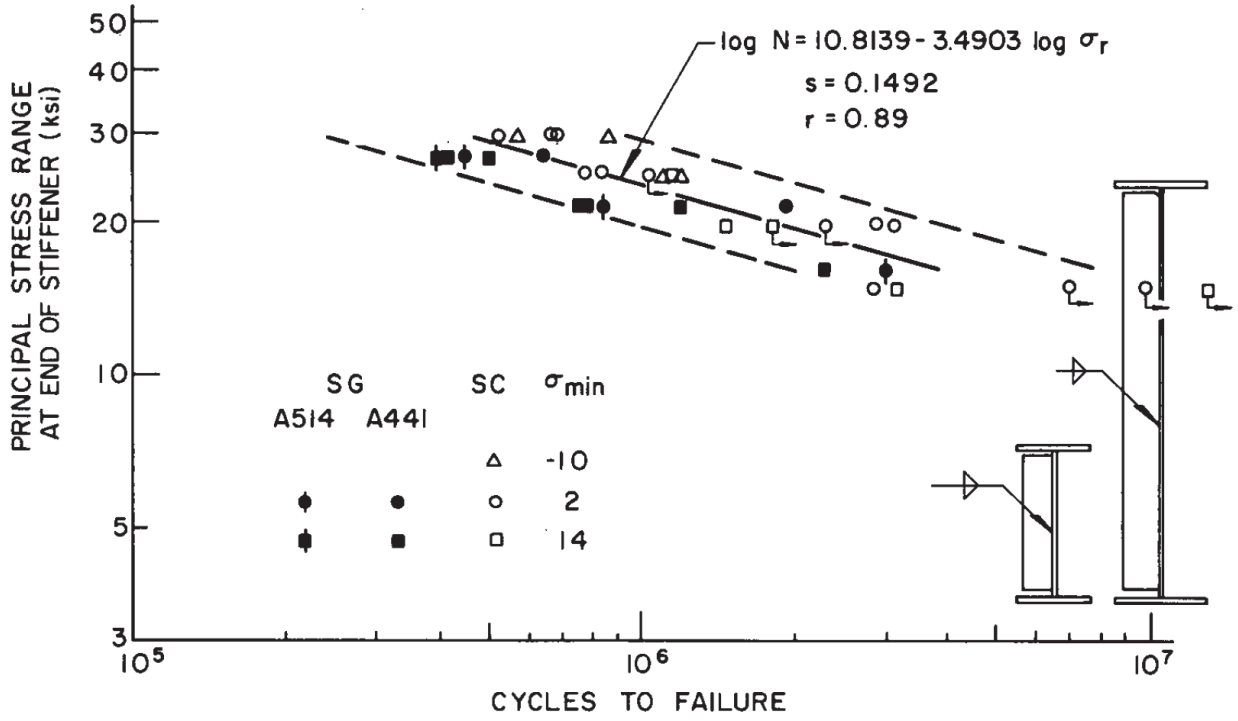

Figure 1.67 S-N Curve for Stiffeners Type 1 [72]

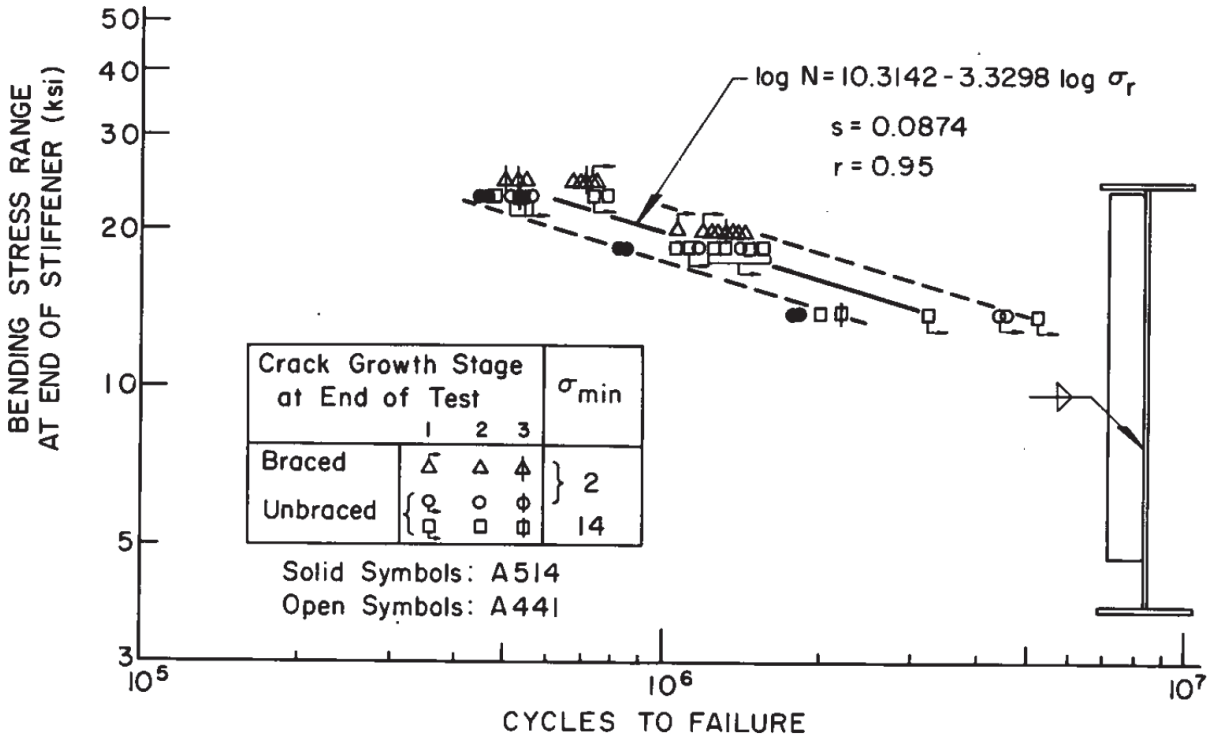

Figure 1.68 S-N Curve for Stiffeners Type 2 [72]

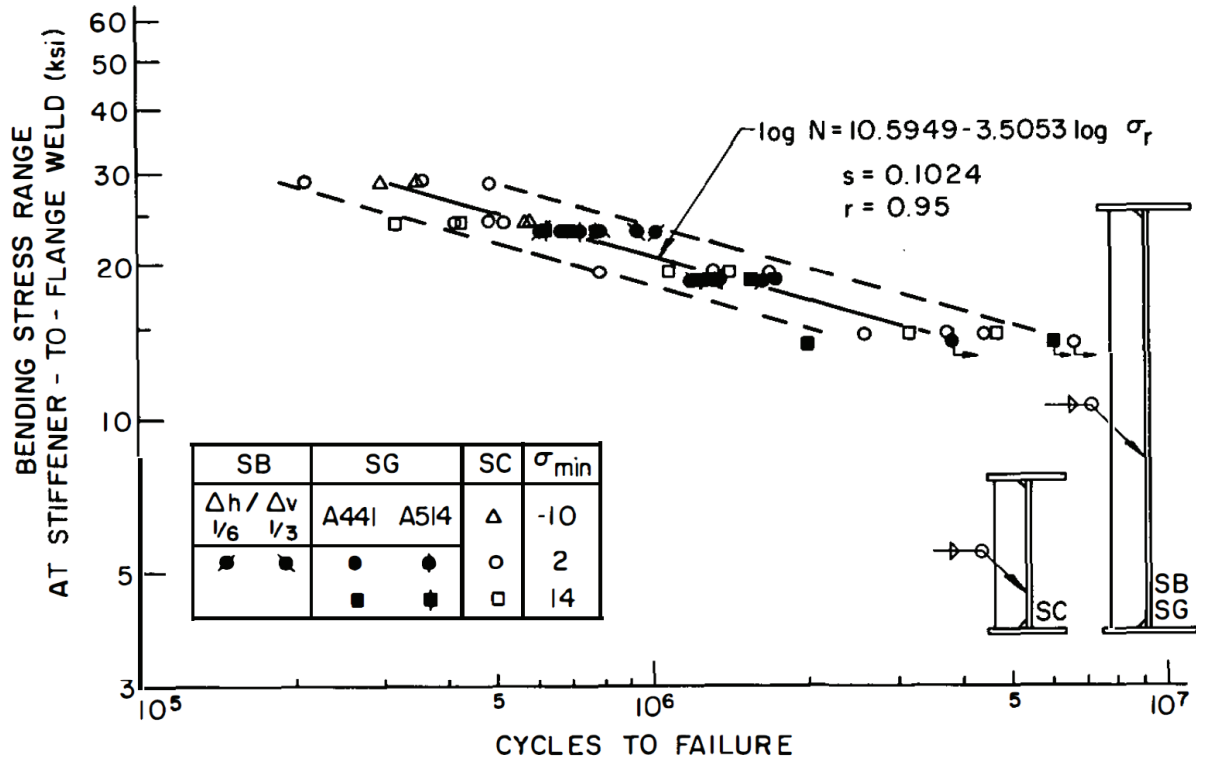

Figure 1.69 S-N Curve for Stiffeners Type 3 [72]

SERIES	SPECIMENS INCL.	SPECIMENS EXCL.	SOURCE OF VARIATION	CALC. F-RATIO	F-RATIO AT $\alpha=0.05$	VAR. SIGN.
SC	17	5 spec. at $\sigma_r=18$ ksi	Stress range	101.4	4.5	Yes
			Min. stress	6.7	4.5	Yes
			Interaction	1.1	3.8	No
SA	8	None	Stress range	96.2	7.7	Yes
			Min. stress	0.0	7.7	No
SG	6	8 spec. at $\sigma_{min}=14$ ksi	Stress range	49.7	19.0	Yes
			A441 vs A514	11.2	18.5	No
	14	None	Stress range	50.2	4.5	Yes
			Min. stress	1.9	5.3	No
			Interaction	0.1	4.5	No
SB	8	None	Stress range	21.9	7.7	Yes
			Bracing angle	0.7	7.7	No
			Interaction	1.2	7.7	No
SG, SB	22	None	Stress range	112.2	3.6	Yes
			SG vs SB	7.7	4.5	Yes
			Interaction	0.0	3.6	No
SG, SB	18	4-A514	Stress range	72.6	3.9	Yes
			SG vs SB	3.2	4.7	No
			Interaction	0.0	3.9	No

Figure 1.70 Summary of Tests Statistical Analysis of Stiffener Type 1 [72]

SERIES	SPECIMENS INCL.[a]	SPECIMENS EXCL.	SOURCE OF VARIATION	CALC. F-RATIO	F-RATIO AT $\alpha=0.05$	VAR. SIGN.
SG	6	8 spec. at $\sigma_{min}=14$ ksi	Stress range	19.7	19.0	Yes
			A441 vs A514	4.0	18.5	No
	14	None	Stress range	95.1	3.4	Yes
			Min. stress	2.5	4.3	No
			Interaction	0.2	3.4	No
SB	8	None	Stress range	123.2	4.8	Yes
			Bracing angle	2.1	4.8	No
			Interaction	0.8	4.8	No
SG, SB	22	None	Stress range	216.9	3.3	Yes
			SG vs SB	2.8	4.1	No
			Interaction	0.1	3.3	No

[a] One data point per specimen in test for effect of steel quality; two data points per specimen in all other tests.

Figure 1.71 Summary of Tests Statistical Analysis of Stiffener Type 2 [72]

SERIES	SPECIMENS INCL.	SPECIMENS EXCL.	SOURCE OF VARIATION	CALC. F-RATIO	F-RATIO AT $\alpha=0.05$	VAR. SIGN.
SC	22	None	Stress range	108.4	3.7	Yes
			Min. stress	1.2	4.1	No
			Interaction	0.2	3.2	No
SG	6	8 spec. at $\sigma_{min}=14$ ksi	Stress range	39.9	19.0	Yes
			A441 vs A514	1.7	18.5	No
	10	4 spec. at $\sigma_r=18$ ksi	Stress range	108.8	6.0	Yes
			Min. stress	0.8	6.0	No
			Interaction	0.4	6.0	No
SB	8	None	Stress range	9.9	7.7	Yes
			Bracing angle	0.0	7.7	No
			Interaction	0.5	7.7	No
SG, SB	18	4 spec. at $\sigma_r=18$ ksi	Stress range	82.6	4.6	Yes
			SG vs SB	0.7	4.6	No
			Interaction	2.5	4.6	No

Figure 1.72 Summary of Tests Statistical Analysis of Stiffener Type 3 [72]

In 1977, Robert et al. [87] studied fatigue in full-size welded cover plated beams and used 24 beam specimens. Fisher et al. (1979) [88], conducted experimental research on 60 small cover plated beams to define the AASHTO category for this type of connection. They used a specified stress range and minimum stress level for controlling stress variables. Roy et al. [54] in 2003, studied stiffener plate (and cover plate) fatigue resistance and defined the AASHTO fatigue category when using Ultrasonic Impact Treatment (UIT) for the welds. Aside from showing the benefits of UIT, their investigation provides valuable insight into fatigue testing of transverse stiffeners. It is notable that they collected test results from other sources and compared them to their results. They tested 18 full-scale girder specimens for fatigue tests with various stress range levels at two minimum stress levels and compared their findings with previous studies mostly to show the improvement resulting from UIT. Each girder combined various end plate configurations and had stiffeners in the constant moment zone as shown in Figure 1.73. Previous research [71, 72] had determined that the fatigue performance was not affected noticeably by the type of steel but by the type of details and stress range. It was also concluded that the post-weld treated details for fatigue improvement show sensitivity to minimum stress, hence, Roy et al. tested for two different minimum stresses [54]. No more than 4 specimens (stiffener or end plate) of similar configuration and stress range/Minimum stress were included. This study was not to obtain fatigue category or S-N curve but to show improvement with respect to earlier

tests. Only one stiffener detail showed a crack, but even this case exceeded Category B (originally rated in Category C by AASHTO and another test). Figure 1.74 includes the results for stiffener details considered in their study and their comparison with the previous results all on AASHTO category scales. The “run-out” in this figure indicates substantial improvement in the fatigue resistance of the treated details.

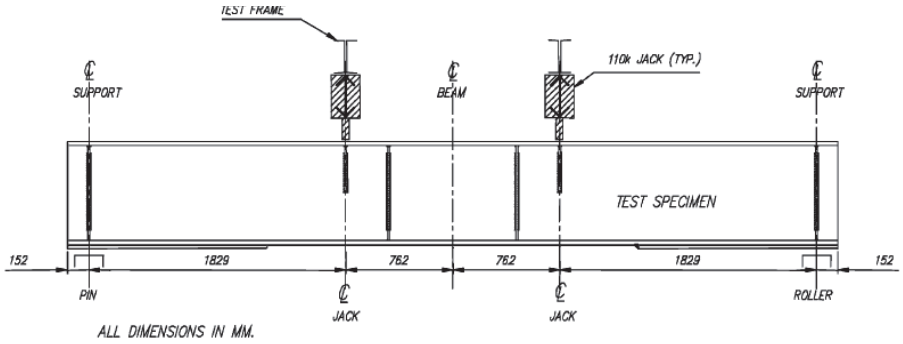

Figure 1.73 Schematic of the fatigue test for transverse stiffeners [54]

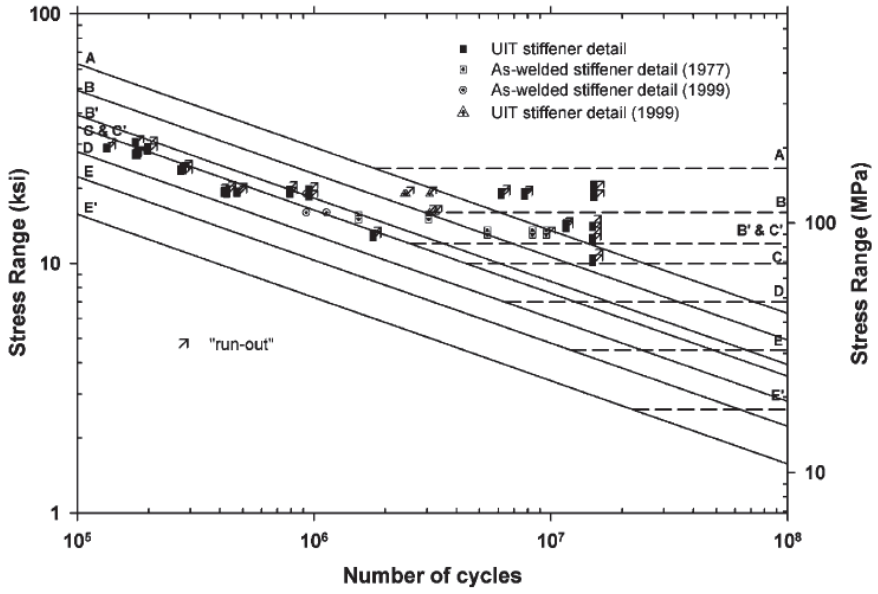

Figure 1.74 S-N curve - stiffener details [54] (filled squares [54], squares [87], circles and triangles [89])

1.2.6 Summary of Fatigue Considerations

The test matrix and the test plan to be developed in this study can be developed and adjusted considering the information provided in this literature review with the objective of determining the category of the half-round bearing stiffener consistent with the AASHTO fatigue categories.

It is understood that the verification of a specific S-N curve for the case of half-round bearing stiffeners should be achieved against two standard deviations below the mean for the collected test data, which is consistent with the development of the LRFD fatigue life curves. This means the level of conservatism will depend on the spread of standard deviation that would in turn be dependent on the number of tests at each stress range.

The earlier work has shown that for the types of stiffeners considered in those studies, the stress range is the main variable in fatigue, and that the minimum stress level, the grade of the base steel material, presence or absence of out-of-plane lateral forces from the braces, the bracing angle and specimen size did not have a significant effect on the final fatigue strength. In addition, it can be inferred that for having effective and efficient planning for the fatigue tests for connections, it is important to determine the region of concern on the S-N curve framework. This can be achieved through analysis for the truck traffic load anticipated for the bridge. The upper bound of the stress ranges obtained from this analysis will help construct the boundaries of the region of interest. One major determining factor for the scope of the testing program will be whether defining the threshold stress range (lower bound) would be necessary or not. Verification or estimation of the fatigue category for a certain connection could limit itself to the low-cycle region and avoid otherwise considerable efforts to estimate a threshold line (for the high-cycle region). On the other hand, it could include both low- and high-cycle regions to also verify compliance with the threshold values. The main objective of this study is to verify that the half-round bearing stiffener connection for skewed girders would comply with an existing AASHTO fatigue category and not necessarily the development of a new category.

After determining the region of interest, the number of stress ranges within that region under which the specimens should be tested as well as the number of tests at each stress range needs to be determined. This can be approached in two ways. One is a smaller number of stress ranges but a larger number of tests at each stress range, and the other is a smaller number of tests at a larger number of stress ranges. Regardless of which option is selected, consistent with the AASHTO approach in developing S-N curves, it is also important to find the number of tests/samples that would result in a statistically reliable linear regression corresponding to the

95% confidence level. A general approach, therefore, is that by obtaining the band at the desired confidence level from the test results, one can define the applicable category by choosing the closest AASHTO category S-N curve line that is located below the band of that confidence level.

1.2.7 Fatigue Loading Study

The goal of the Fatigue Loading Study is to investigate and answer two major questions: (i) what is the relationship between bridge geometry and fatigue force effects on end cross-frames and girder top flange at the intermediate supports for a continuous skewed bridge? (ii) What should be the design truck load properties and its position to maximize the fatigue stress range?

To address these questions as it concerns the cross-frames in general, NCHRP report 962 [65] reviewed the current fatigue load model in terms of truck position, cross-frame details, and bridge geometry for fatigue consideration. The effect of the design truck load position and the bridge geometry such as girder spacing, deck thickness, skewed angle, horizontal curvature, and cross-frame details (i.e., cross-frame type, layout, stiffness, and spacing) on the internal forces induced in cross-frame members were investigated by generating an influence-surface analysis. In this way, to find the most critical positions of the truck load for the cross-frame elements, a series of separate analyses were performed on the bridge structure under a point unit load with varying locations within a grid mesh extended over the bridge deck surface. By doing this, they could evaluate the effect of truck load in all possible positions on cross-frame forces [65].

In their research, they used a comprehensive measured Weigh-in-Motion (WIM) dataset collected throughout the US to gain a good vision of the real traffic load and conditions (Figure 1.76). This dataset provided a chance to assess the necessity of considering the Multiple Presence Factor for the fatigue effects on cross-frames, and the appropriateness of the AASHTO LRFD Fatigue I and II load factors for the design of the cross-frames. The Weigh-in-Motion (WIM) study confirmed that the presence of the dual truck at the same time on the bridge is unlikely. They concluded that using the AASHTO 9th edition [73] fatigue criteria which allows considering a single design truck positioned in all longitudinal and transverse locations (truck confined to one critical transverse position per each longitudinal position) is more appropriate. In general, they showed

that the transverse position of the design truck would affect the cross-frame response and that the influence of the longitudinal position of the design truck depends significantly on the skew angle and the horizontal curvature of the bridge. Also, they showed that the most significant force effects in cross-frame members (especially in bottom struts near skewed supports) would be in bridges with high skew angles or curvature, especially in those with contiguous lines of braces [65]. Furthermore, the WIM study indicated that the Fatigue I and II Load Factors presented in AASHTO LRFD are conservative for the fatigue limit state by at least 35% and it is possible to apply adjustment factors of 0.65 and 0.8 to Fatigue I and II load factors respectively.

State	Initial Number of Records (Before Filtering)	Records Including Light Vehicles		Records After Removing Light Vehicles	
		Total Number of Records	Lane ADT	Total Number of Truck Records	Lane ADTT
AR	3,529,952	3,414,934	9,356	1,704,481	4,670
AZ	2,711,532	2,626,954	7,704	1,227,567	3,600
CA	4,873,640	4,779,602	13,167	1,380,075	3,802
CO	1,675,744	1,645,722	4,509	352,198	965
IL	2,807,183	2,707,469	7,584	798,935	2,238
IN (Lane 1)	1,886,428	1,865,543	5,111	370,241	1,014
IN (Lane 2)	500,621	471,291	1,302	21,340	59
IN (Lane 3)	1,843,395	1,802,053	4,937	360,458	988
IN (Lane 4)	548,382	524,003	1,460	20,158	56
KS	2,312,975	2,262,526	6,199	436,913	1,197
LA	1,734,519	1,722,311	4,719	76,547	210
MD	3,040,831	3,005,933	8,564	108,881	310
MN	864,803	857,522	2,349	52,757	145
NM1	1,018,250	1,005,887	2,786	147,077	407
NM2	1,675,090	1,609,947	4,485	892,295	2,486
PA	2,292,235	2,251,316	8,187	873,903	3,178
TN (Lane 1)	2,792,715	2,120,750	7,913	550,858	2,055
TN (Lane 2)	1,945,926	1,842,295	6,874	118,000	440
TN (Lane 3)	2,042,591	1,942,114	7,247	191,330	714
TN (Lane 4)	2,757,569	2,690,197	10,038	1,182,136	4,411
VA (Lane 1)	1,462,016	1,445,614	3,961	224,928	616
VA (Lane 2)	438,126	430,438	1,179	19,300	53
WI	1,468,798	1,358,660	5,435	120,079	480
Total	**46,223,321**	**44,383,081**		**11,230,457**	

Figure 1.75 SPS sites from which WIM data was obtained by FHWA [65]

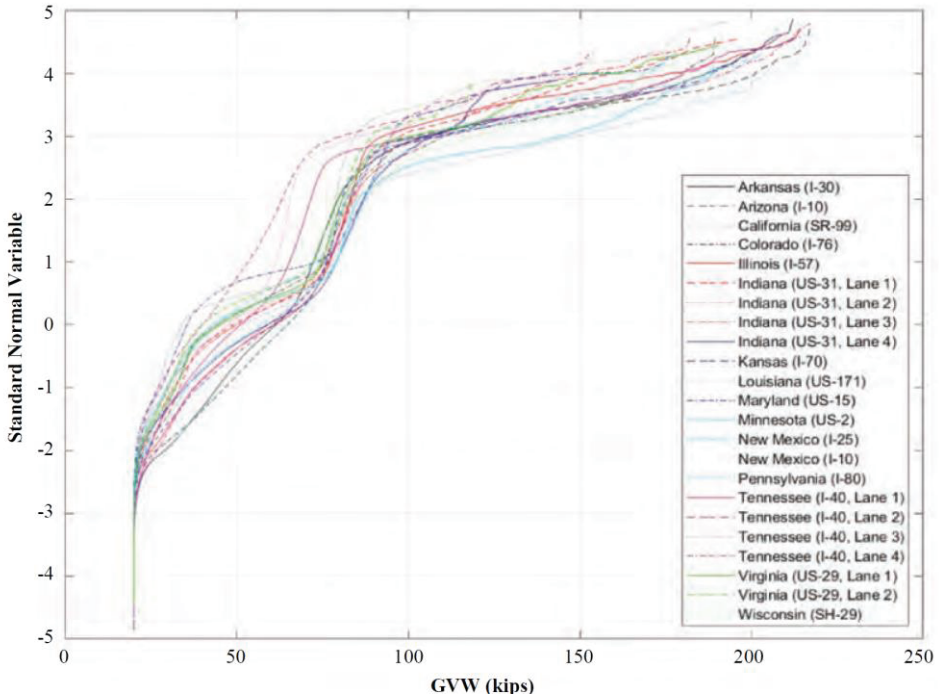

Figure 1.76 CDF of GVWs from FHWA 2014 data (Excluding light vehicles) [65]

Since the focus of this study is on bridges in the state of Florida, a reliable data-driven loading model is necessary for an accurate analysis and force demand for the connections. For an FDOT-sponsored project performed by the authors, the Weight-in-Motion (WIM) data containing data from the years 2013 – 2016 was obtained from FHWA, with 32 stations located in Florida shown in Figure 1.77. The truck weight data format was used as it contains information such as, but not limited to, the number of axles, the spacing between axles, axle weights and gross vehicle weight (GVW), and the exact time of measurement for each recorded vehicle at each location [90].

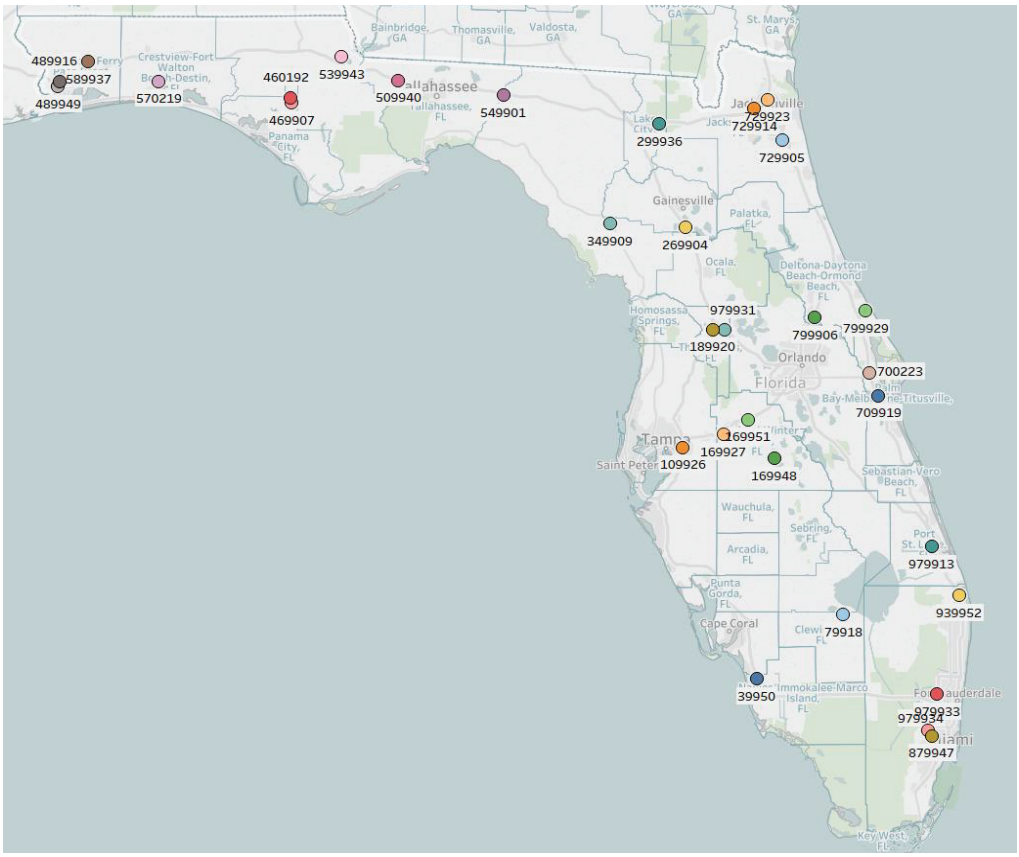

Figure 1.77 WIM stations studied in the State of Florida [90]

The data left after filtering out vehicles less than 20-kip GVW are used for further analysis. The Cumulative Distribution Function (CDF) of GVWs is plotted on probability paper. An example is shown in Figure 1.78 for the data from the year 2014. Each curve on the plot is data from each WIM station in Florida. Using a simple analytical model, these curves can be translated to show the probability distribution with respect to a specified structural response parameter such as moment and shear. For example, as shown in Figure 1.79, the above study calculated the CDF plot similar to that shown in Figure 1.78 for the moment ratio of all WIM stations for the year 2014 translated into the equivalent multiple of HS-20 truck for a 120-ft span bridge.

To obtain the loading configuration resulting in the most relevant responses, truck type, number, and position on the bridge will be determined using the information provided by the relevant literature.

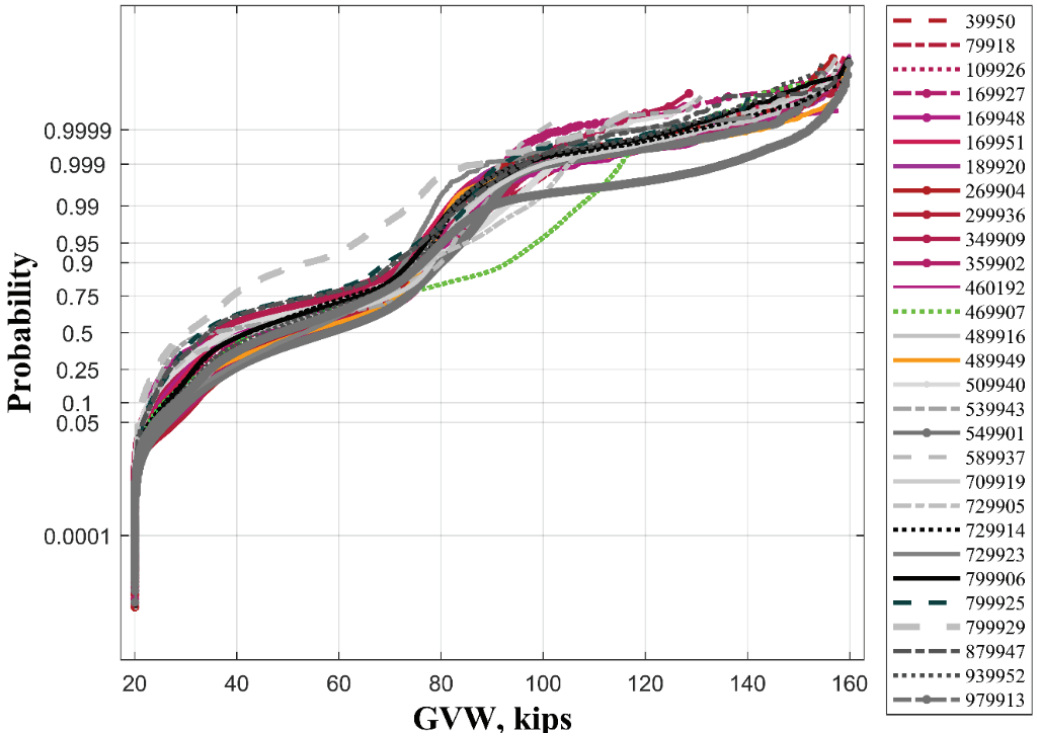

Figure 1.78 CDF plot of GVW of all WIM stations in Florida for the year 2014. [90]

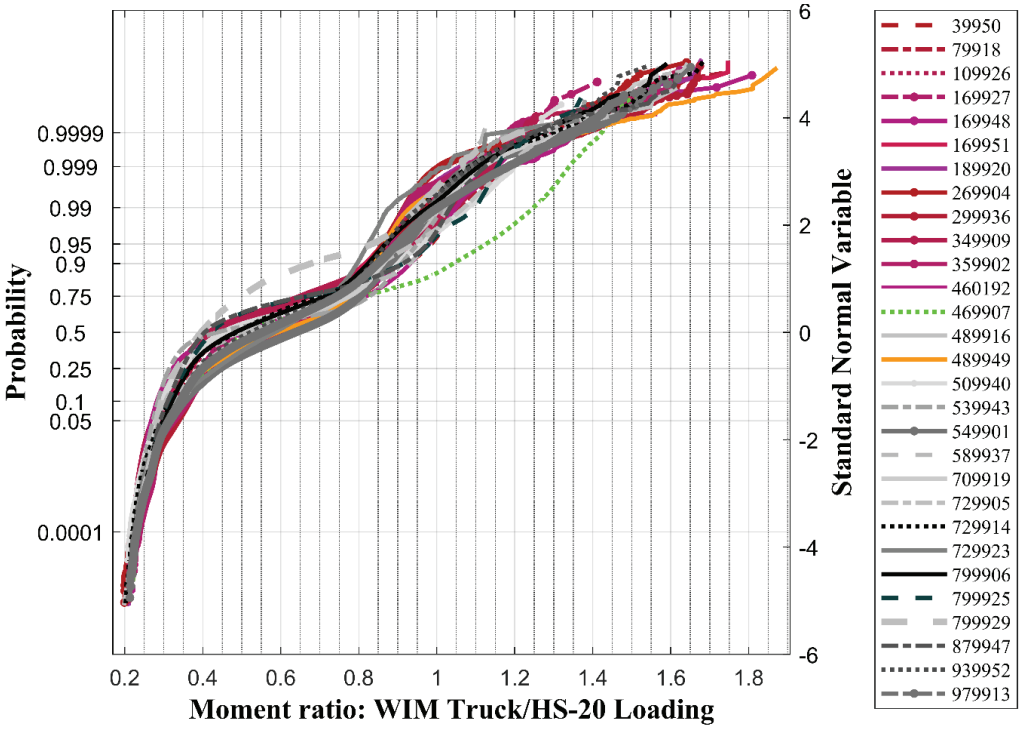

Figure 1.79 CDF plot of the moment ratio of all WIM stations in Florida for the Year 2014.

1.3 Review of Automatic/Real-time Detection Strategies for Crack Initiation and Progress Employing Instrumentation

Various means and techniques have been implemented for the detection of crack initiation and monitoring its development. These methods can be categorized into real-time monitoring and at-interval (non-real-time) monitoring techniques. Real-time methods continuously monitor the status and can be programmed to automatically signal the initiation and/or progression of the cracks, whereas the at-interval methods require stoppage of the test to allow the inspection of the location of interest for enabling detection of the crack and its growth. Therefore, in the latter, there is a chance that the exact time of the crack initiation is missed. Visual examination, dye penetrant, magnetic particle and electromagnetic, Eddy current, infrared imaging, radiography, and ultrasonic testing are among the at-interval monitoring techniques [91, 92], while acoustic emission, laser vibrometer, and strain gage or piezoelectric tapes/coating are techniques with the potential ability to detect in real-time the crack initiation and crack activity [93-95]. As it is the focus of this project, the detection of fatigue cracks during test procedure (under cyclic loadings), the methods with potential capability for real-time monitoring are described in more detail in the following. The work by Khedmatgozar Dolati et al. (2021, 2022) can be referenced to obtain more detailed information about all available methods for damage detection in steel bridges with applicability to crack detection [91, 92].

1.3.1 Acoustic Emission (AE)

AE is a non-destructive testing technique that has been significantly used for the detection of cracks in steel elements. The methodology of this technique works according to acoustic emissions generated as elastic waves by the onset or progression of cracks and other discontinuities in steel elements (Figure 1.80). These waves are radiated outward from the vicinity of crack tips in a circular pattern and are sensed by the sensors (transducers) attached to the surface of the test piece and relayed to the AE monitor. For the application of this method, the coating at the attachment locations should be removed prior to installing the transducers. In some circumstances, magnetic hold-downs need to be used to connect the transducers to a test component. The AE method typically uses multiple transducers to locate and monitor bridge

components at different locations. The transducers should be positioned on a test piece in geometric arrays to locate cracks and remove interference signals from noise sources [91, 96].

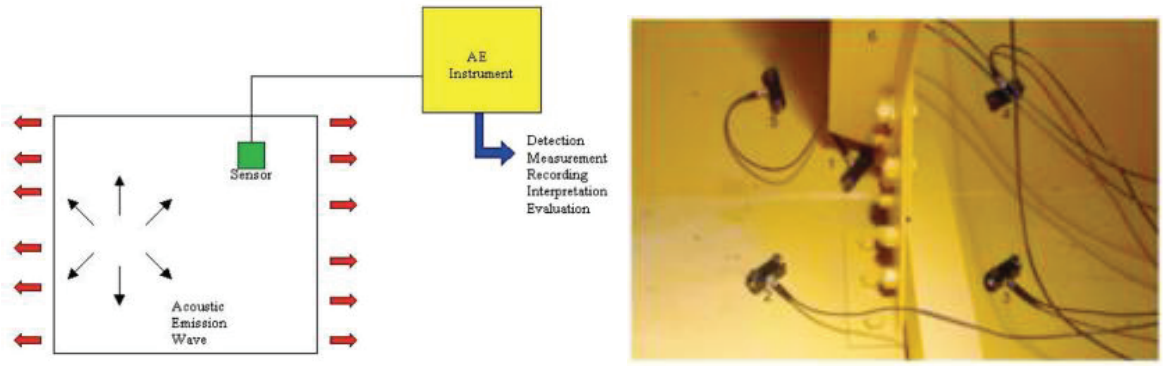

Figure 1.80 Acoustic emission testing [91]

This method can detect the initiation of a defect or the progression of existing anomalies; however, it cannot be utilized to detect existing defects without significant activity. The AE method has been used successfully for detecting fatigue cracking in orthotropic bridge decks [97]. It should be noted that this technique requires special training and equipment for the inspectors.

1.3.2 Laser Vibrometer

The application of noncontact laser-based vibration technology for bridge damage detection has increased over the years [98, 99]. This technique was initially developed for cable-stayed bridges; however, soon after, it was adapted for other types of bridges. Several bridges in the US and abroad have employed this technology for the inspection of their elements. Although the laser vibrometer technique has been used for detecting damages in engines and other mechanical systems, this method was first introduced by Mehrabi and Tabatabai in 1998 [100] for structural damage detection, and its main initial usage was for assessing tension elements and cables in bridges. In this technique, by targeting the element with the laser beam, the elements vibration from ambient (or other) sources can be recorded from a distance. The element vibration characteristics, such as the frequencies, velocities, and damping ratio, are then compared to the previously measured or expected vibration characteristics to establish a pattern of changes

indicating the intensity, location, and initiation of damage to the elements. Accordingly, this method, let it be with some modifications, has the potential to detect fatigue cracks during cyclic loading simply by targeting the desired part, and by recording and comparing the frequency (or velocities) patterns. Initiation of a crack on the element would cause a sudden change in the recorded frequencies (or velocities) and hence would be detectable.

In 2006, Staszewski et al. investigated the application of ultrasonic guided wave lamb and multi-position scanning laser vibrometer for the detection of fatigue cracks in metallic elements. In their work, a tri-axis, multi-position scanning laser vibrometer was utilized to sense the lamb waves produced by a low-profile, surface-bonded piezoceramic transducer (Figure 1.81). They indicated the effectiveness of this method by detecting fatigue cracks on their test specimens made of aluminum plates. They concluded that this method is a rapid, simple, and accurate technique for real-time fatigue crack detection[94].

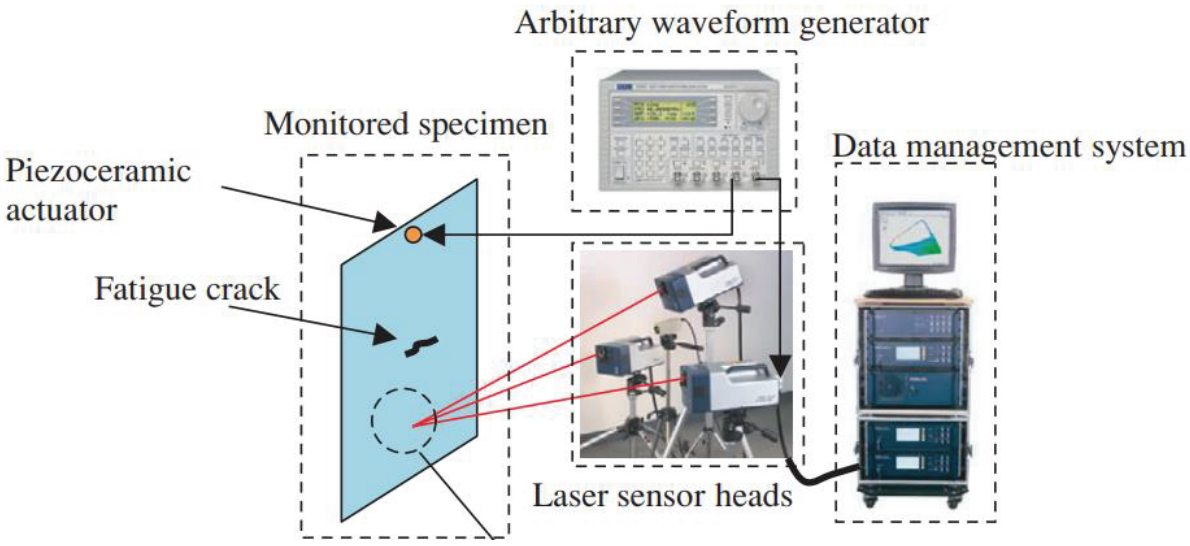

Figure 1.81 Damage detection using 3D laser vibrometer [94]

1.3.3 Vision-Based Inspection Methods

The application of vision-based methods for damage detection in structures goes back decades. Early applications of this approach have included static and dynamic monitoring of bridges [101]. Numerous vision-based monitoring techniques have been developed and employed to measure

structural displacement, monitor vibration response, measure stress/strain, and detect cracks and other anomalies [102]. Xu et al., in 2018, conducted a thorough review of vision-based structural health monitoring systems [103]. Their review has indicated the growing use of vision-based methods for damage detection and structural health monitoring for bridges and buildings. They also proposed a simple vision-based method based on two major abilities: non-contacting and multipoint simultaneous sensing. A vision-based measurement system normally includes an image acquisition device (digital camera, lens, and image grabber), software for image processing, and a computer. This technology relies heavily on image processing software, which is combined with a specific computational algorithm to acquire the mechanical parameters in structural monitoring. Figure 1.82 shows the methodology of this method, in which the images consist of some predefined targets captured by the digital camera. By implementing a pattern-matching algorithm and digital image processing, the targets are tracked, and therefore the displacement at the target positions on the structure is determined. As such, this technique can be used to detect cracks and tiny flaws in structural elements [104]. In 2022, Zhuang et al., in a comprehensive literature review, investigated computer vision-based inspection techniques for measuring structural deformation and indicated its effectiveness for real-time monitoring and damage detection. This method has great potential for detecting crack initiation and activity in real-time [102]. For the potential application of vision-based methods for detecting crack initiation and progression at the steel connections, it may be helpful to cover the target region with a coating to enhance the visibility and surface changes.

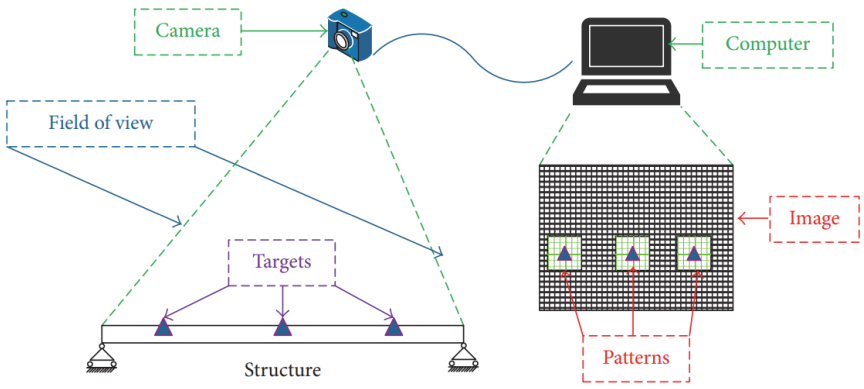

Figure 1.82 Methodology for vision-based displacement measurement technique [105]

1.3.4 Piezoelectric Sensor and Strain Gauge

Piezoelectric materials can be categorized into three main classifications: piezoelectric polymers, piezoelectric composites, and ferroelectric ceramics. Piezoelectric materials are able to sense changes in their environment due to their electromechanical coupling properties. They have been utilized for measuring the strain or physical movement in host structures by bonding them on their surfaces. The methodology for this method is that voltage signals are produced when mechanical strain is applied to the film plane of the piezoelectric sensor. Piezoelectric ceramics can be considered the most prevalent piezoelectric materials for sensing applications. Several researchers implemented sensors made of piezoelectric ceramic patches for the detection of cracks on structural members [106-108]. Zhang et al., in 2006, investigated the applicability of piezoelectric paint sensors (coating) for real-time detection of fatigue cracks. In their work, several piezoelectric paint coatings were placed on the surface of the steel beam to detect the initiation of fatigue cracks. They concluded that this method is very practical for real-time monitoring of surface cracks caused by fatigue. An example of a piezoelectric paint sensor is shown in Figure 1.83. The drawback of this method is that the cracks may not be detected if they do not cross the sensor electrodes [95].

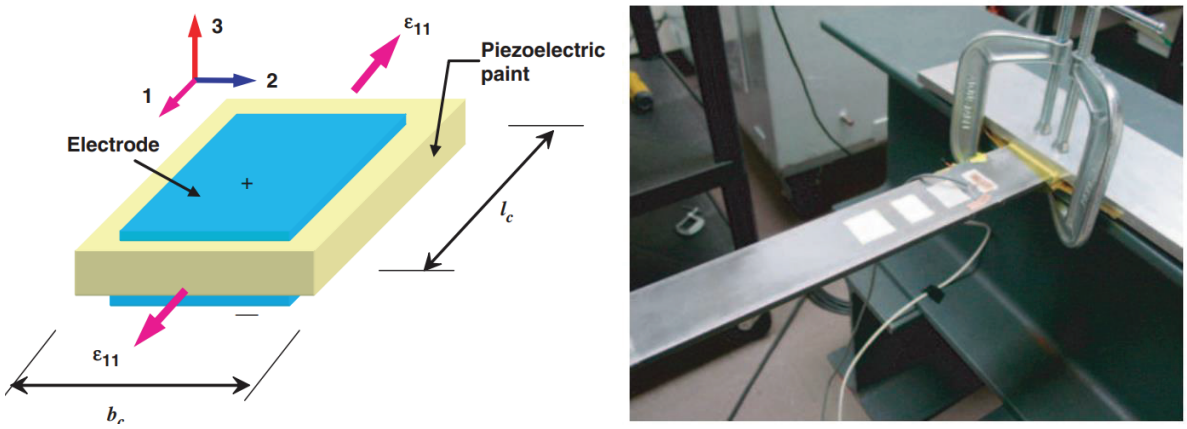

Figure 1.83 piezoelectric paint sensor [95]

Strain gauges have also been implemented for continuous online crack monitoring in structural elements [109, 110]. In 2021, Al-Karawi et al. investigated the effectiveness of strain gauges for detecting fatigue cracks in transversal non-load-carrying welded attachments. They concluded that strain gauges could be used to detect the initiation of fatigue cracks. Also, they indicated that the size and depth of the crack and its progression would be determined if this method be combined with Finite Element (FE) analysis [110].

1.3.5 Summary

The literature review has indicated that there are methods available with great potential for real-time detection of the onset and propagation of fatigue cracks. The more promising methods, especially those with a better availability to testing researchers, could be used for one or more of the tests at the beginning of the experimental program in conjunction with hands-on inspection methods at intervals to validate the application and accuracy of such methods.

1.4 Review of Corrosion Protection Measures for Half-Round Bearing Stiffeners or Similar Details

1.4.1 Introduction

Corrosion of structural steel elements is a major concern in Florida bridges. In the state, there are approximately 1,200 steel bridges over aggressive coastal water environments. Corrosion mitigation of these structural steel components has been made by application of protective coatings, but repair of these systems accounts for the largest number of repair actions (see Figure 1.84) with annual costs exceeding $25 million. The durability of half-round steel pipe stiffeners used for lateral steel cross-frame connections can be impaired by corrosion of the outer surface area of the element as well as corrosion of the interior surface area within the confined space of the element. The corrosion of the steel pipe stiffener can vary by mechanism and rate of degradation depending on its exposure condition (including moisture availability, contaminants, and pollutants) and its materials (including alloy type, fabrication, and connections). The following is a review of concepts that can be involved in the corrosion and the mitigation of corrosion of the element.

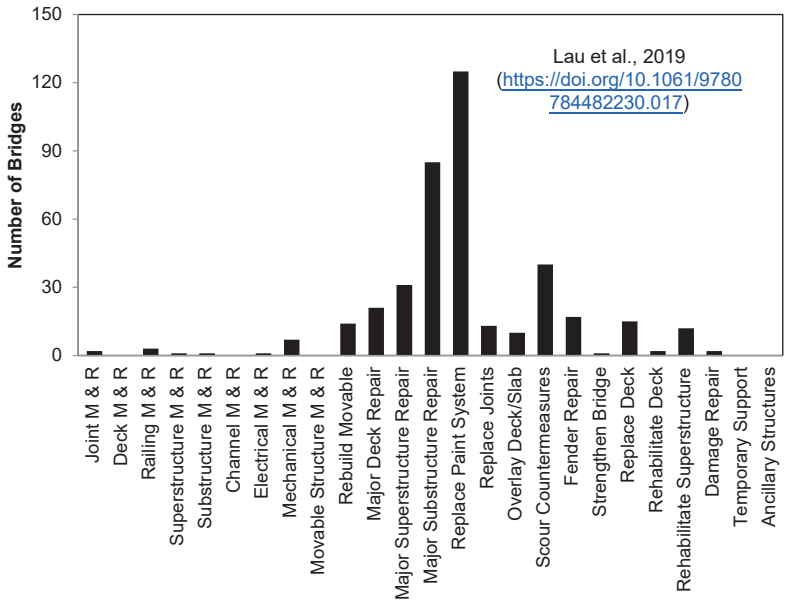

Figure 1.84 Example of FDOT Bridge Work Plan

1.4.2 Atmospheric Corrosion and Moisture

The outer surface of the stiffener can be generally considered to be subject to atmospheric corrosion. Corrosion in the atmospheric condition is largely related to the available moisture from wetting from rain, runoff, and condensation. High humidity also presents conditions to provide moisture on the steel surface. The time of wetness has often been used as a metric for corrosive environments. Critical relative humidity conditions above 60%RH have often been cited. However, due to the intermittent availability of moisture, corrosion is typically slow and uniform. The corrosion loss of steel in atmospheric exposure has often been expressed in terms of a power law function with time. However, it has been reported that steel exhibits two stages with a time of exposure where the corrosion rate initially increases but later subsequently decreases [111]. Others have challenged the conventional characterization of atmospheric corrosion behavior. Melchers (2007) [112] suggested the importance of anaerobic corrosion processes in long-term corrosion behavior as the corrosion product can form a layer on the steel surface. The corrosion behavior largely depends on the composition and stability of the corrosion product and its layered characteristics on the surface of the metal. Steel in marine atmospheric environments would develop goethite, akaganeite, lepidocrocite, magnetite, and amorphous phases. The reduction of ferrous ions may be significant in conjunction with oxygen and hydrogen reduction reactions.

1.4.3 Air Contaminants and Pollutants

The presence of contaminants such as certain corrosion products and salts and pollutants such as sulfur dioxide can greatly increase the severity of atmospheric corrosion. Hygroscopic SO_2 and salts allow condensation on steel surface at lower RH and provide moisture for corrosion to develop by increasing its time of wetness. For example, the presence of 0.01% SO_2 causes elevated corrosion rates of steel above 60% whereas corrosion in humidity in absence of pollutants remains low even up to 100%RH. Other pollutants that can elevate corrosion rates include particulate matter (from windblown soil, industrial processes, and vehicular traffic) and

nitric acid [113]. Schindenholz et al., 2014 [114] addressed the hygroscopic effect of salt contamination and the relative humidity to the level of corrosion. Deliquescence of deposited salts on the metal surface allows water to be absorbed to form an electrolyte at a specific relative humidity. However, corrosion can occur as relative humidity levels are below the deliquescence relative humidity. Corrosion of steel contaminated with NaCl was reported to corrode at relative humidity levels below its deliquescence humidity of 76%, as low as 27%RH. It was thought the corrosion at these low relative humidity levels resulted from moisture trapped between the salt and steel surface as well as the deliquescence of iron chloride salts that form after the initial steel corrosion. In $MgCl_2$ salt contamination, corrosion was sustained at relative humidity levels as low as 11% and whether ambient conditions with salt contamination can ever be considered dry is a matter of debate [115]. Deposition of airborne marine salts is most concentrated adjacent to water bodies and large particles greater than 10um may not widely deposit further inland, although some levels of smaller salt particles can be found significant distances from the coast [116]. As shown in Figure 1.85, Alcantara et al., 2015 described a decreasing exponential function of salinity (and corresponding corrosion rates) with distance from the coast [117].

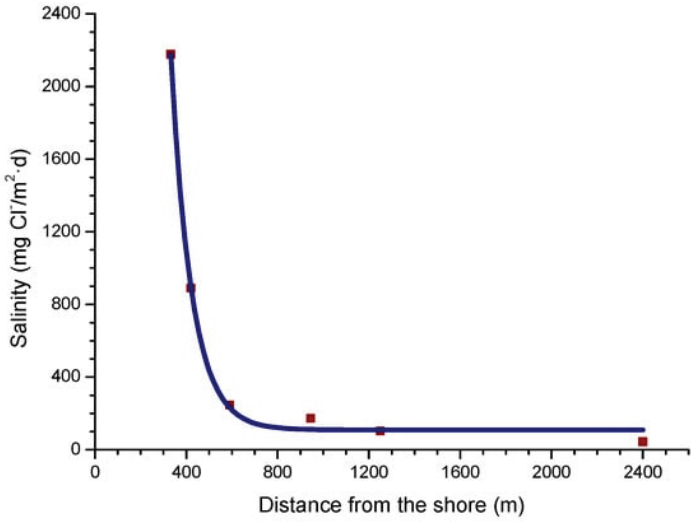

Figure 1.85 Atmospheric salinity with distance from shore [118]

1.4.4 Material Detailing, Drainage, and Moisture Retention

Repeated wetting and drying cycles can allow aggravated corrosion [118]. Corrosion is also exacerbated in conditions where moisture is retained. In conditions where water may be collected, adequate drainage should be made so that the time of wetness is minimized. Moisture should not be retained within the enclosed space of the half-round stiffener as elevated corrosion rates of the element cannot be easily detected or mitigated. Drains should be located at the lowest point of the confined space where water can be retained and large flat surfaces that are difficult to drain should be avoided [119]. Therefore, the detailing of the connection should be mindful for adequate drainage at the bottom flange (including surface inclination) as well as consideration of debris accumulation at the stiffener and the effect of inadequate drying due to sheltering. Crevices due to incomplete weld penetration such as the circumference of the pipe to the steel web and flanges should be avoided. Wallinder and Legraf, 2017 describe the role of the corrosion product patina of galvanized steel on the dissolution of the metal in a runoff with its exposure to water (rain characteristics and flow rate) in marine environments [113].

1.4.5 Corrosion of Welds

Welds to adjoin steel components can be made by an electric arc or combustible gas methods. The application of the weld causes changes in the metallurgy of the base steel as well as the weld material itself during the heating and cooling cycle. Heterogeneities in the microstructure develop in the transition zone between the steel substrate and weld that can be susceptible to preferential corrosion attack (see Figure 1.86). Distinct regions including the fusion zone, unmixed region, partially melted zone, heat-affected zone, and base metal are often observed [120]. Differential metals in the weld consumable and steel substrate can develop galvanic corrosion. Residual stresses that develop during the welding due to thermal expansion and cooling may allow for the development of stress corrosion cracking and hydrogen-induced cracking in certain aggressive corrosion conditions and subsequent localized failures. Several welding practices can be made to minimize corrosion including appropriate selection of welding consumables to minimize adverse galvanic coupling, surface preparation and cleaning to remove

contaminants, welding design to minimize crevices, post-weld inspection, and cleaning, application of protective coatings, post-weld heat treatment to reduce residual stress gradients, among others [120].

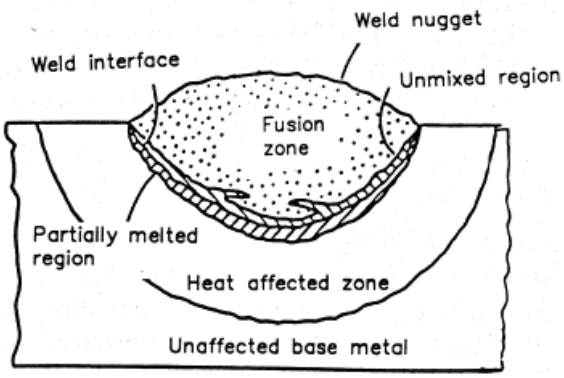

Figure 1.86 Schematic of heterogeneous structure of weldment [120]

Jiang et al, 2022 [121] described fatigue assessment of steel bridge crossbeams with corrosion of its welds. After 16 years, significant corrosion of the fillet welds of the steel crossbeams in a bridge in China was observed. The corrosion of the material in conjunction with the high-stress concentrations and residual stresses in the weld could allow crack propagation in the heat-affected zone and reduce its fatigue performance. Uniform corrosion can reduce the cross-sectional area of the steel elements and localized corrosion can increase localized stresses. The bridge tower crossbeams contained vents and drains for venting and minimizing water accumulation; however, corrosion of the welds of the vertical stiffeners and the beam occurred. Fatigue cracking could develop at the weld toe into the beam steel substrate. Their finite element fatigue analysis considered the competitive processes of pitting corrosion growth and corrosion fatigue crack growth. Results of their analysis indicated that if pitting corrosion was the dominant process, the fatigue life decreased with greater corrosion depth such that structural deficiencies would develop. If corrosion-assisted crack growth was the dominant process in severe conditions,

the fatigue life could be severely impacted with fatigue service life reduced to up to 25% of its non-corroded fatigue life.

1.4.6 Pipe Material Considerations (Fabricated plate and extruded pipe)

The use of steel pipes and fabricated steel plate may have different corrosion performances due to the differences in their microstructure and defects introduced in the fabrication process. For example, pipes with longitudinal welds or spiral welds can have varying levels of susceptibility at the welds as described earlier. For fabricated plates, physical damage to the mill scale on steel plates in the fabrication process may provide adverse galvanic coupling of the exposed steel substrate to the surface of the mil scale.

Nyrkova, 2020 [122] assessed stress-corrosion cracking of X70 steel rolled pipe. Test parameters included cyclic stresses, periodic wetting, and the application of protective coatings. Testing results indicated that the stress concentrators and periodic wetting had an effect on the sensitivity to stress corrosion cracking, but the load cycling and application of protective coatings did not have a significant effect. Gkatzogiannis, 2019 [123] attempted to correlate the corrosion of steel to fatigue behavior. Testing of steel specimens including those with butt-welds was tested in salt-fog, artificial sea water, and an accelerated electrochemical polarization method was employed. Fatigue testing was conducted until failure at the weld toe or in the substrate. Results indicated that the increase in surface roughness due to corrosion caused a reduction in the SN curve by facilitating crack initiation.

1.4.7 Corrosion mitigation and vapor-phase inhibitor

Protective coatings have been often employed to mitigate atmospheric corrosion. The 3-coat system comprised of a zinc-rich primer, epoxy midcoat, and polyurethane topcoat has been widely used after the discontinuation of older chromate paints and coatings due to environmental concerns [124]. The zinc-rich primer is placed in an inorganic silicate binder or an

organic epoxy binder. The midcoat provides an additional barrier layer and the topcoat provides UV protection. The coating system provides barrier protection and beneficial coupling of the zinc pigments to the steel substrate when subjected to chloride environments at coating defect sites. The dispersed zinc pigments require good electrical coupling to themselves as well as to the steel substrate.

Metallic coatings include hot-dipped galvanizing (HDG) and arc-sprayed zinc metallizing. HDG is made by placing the steel structural element in molten zinc so that the zinc can diffuse in the steel matrix and develop zinc and iron alloy layers. These galvanizing layers of decreasing zinc concentration by depth provide barrier protection and beneficial galvanic coupling when subjected to coating damage and moisture. In chloride environments, the outer zinc-rich layers may be subject to fast early corrosion but barrier protection can remain intact by the deposition of non-reactive zinc corrosion products [125].

Vapor phase inhibitors can mitigate the corrosion of steel in enclosed environments by the volatilization of the inhibitor and condensation of a protective film on the exposed steel surface. The vapor phase inhibitor should allow adequate coverage yet maintain adequate service life. Volatile corrosion inhibitors are organic chemicals with appreciable saturated vapor pressure to allow vapor transport of the inhibitor and the subsequent formation of a barrier film on the metal surface [126]. The inhibitor either can dissociate and saturates the air space prior to contact with the metal or dissociates on contact with the metal.

1.4.8 Summary

In summary and according to previous experiences, determination of the corrosion durability of the half-round bearing stiffener should include consideration of the selected material, connection detail, drainage detail, exposure environment, and the use of corrosion mitigation technologies as described earlier in the technical approach. A summary framework for corrosion study based on these considerations is outlined in Figure 1.87.

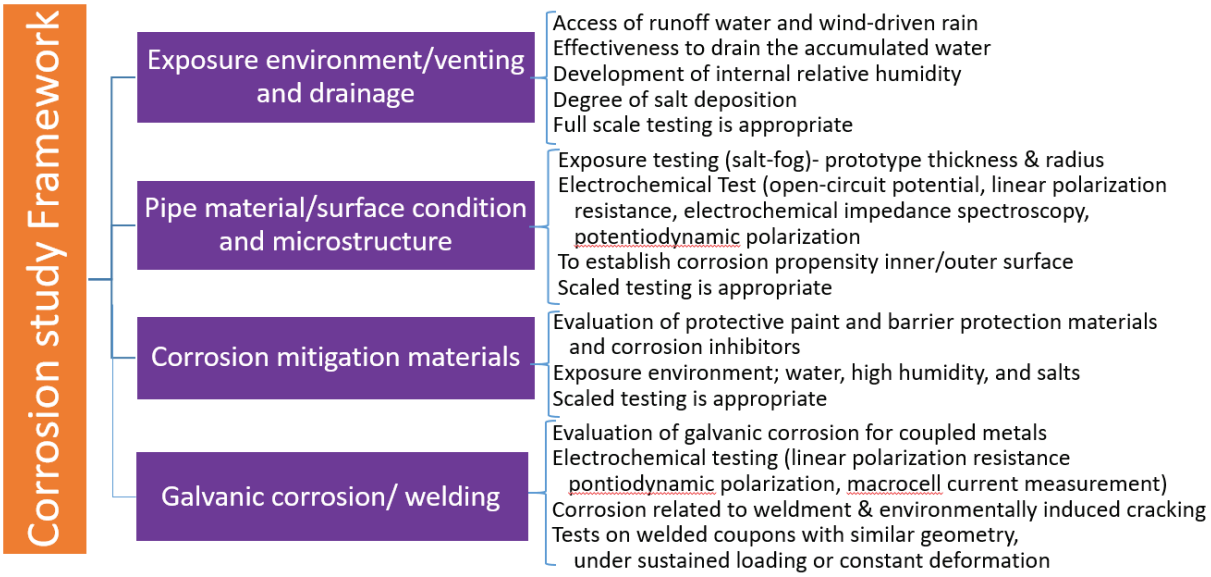

Figure 1.87 Summary framework for corrosion study

1.5 The Plan for Analytical Investigation

The main objectives of the analytical investigation planned in this study for continuous skew steel girder bridges are:

a) Tensile stress ranges from live load effects expected for the top flange of continuous steel girders over intermediate supports,
b) Force ranges from live load effects expected in the end cross-frame members over intermediate support in continuous span,
c) Forces in the end cross-frame members from construction (fit-up), dead load, and live load effects,
d) Design and detailing of half-round stiffeners for the end cross-frame connection to girders,
e) Investigating the effect of stress variations caused by the cross-frame member forces on the stress variation of the top girder flange; welded, bolted, or detached stiffener plates.

To achieve these objectives, a two-level analytical approach will be adopted; Level I analysis for obtaining the stress variations in the girder tension flange (Item a) and forces and force variations in the end cross-frame members (Items b and c), and Level II analysis for designing and detailing of the half-round stiffener connections (Item d) and investigating the effect of stress variations in the top flange caused by the cross-frame member's force variations (Item e).

1.5.1 Selection of the Representative Bridges or the Practical Range of Major Parameters

Before the analytical investigation can begin, the representative bridges to be analyzed that cover the practical range of the major parameters of continuous skewed steel girder bridges need to be identified. These parameters may include skew angle, type of continuous spans (one-sided or two-sided continuity), span length, bridge width or the number of steel girders, cross-frame configuration and spacing. The FDOT Project Technical Committee has identified 26 bridges to be investigated as representative bridges. The list of bridges adopted for this study with the alternative numbering to be referred by hereafter is shown in the table below.

Table 1.1 List of representative bridges

Bridge Item	Alternate Bridge Number
1	44
2	15
3	43
4	41
5	60
6	45
7	42
8	8
9	46
10	61
11	24
12	25
13	62
14	63
15	12
16	64
17	9
18	65
19	66
20	67
21	13
22	68
23	69
24	70
25	71
26	72

1.5.2 Loading Model

Another major step required before the analysis can commence is determining the loading model. This includes loading effects from construction (fit-up), dead load, and live loads. The application of the construction and dead load effects relies on the construction sequence as discussed above. The live load, mainly truck loading, however, has the determining effect on fatigue considerations. Therefore, the truck loading that each of the representative bridges may experience needs to be determined. Since the focus of this study is on bridges in the state of Florida, a reliable data-driven loading model is necessary for an accurate analysis and force demand for the connections. For an FDOT-sponsored project performed by the authors, the WIM data containing data from the years 2013 – 2016 was obtained from FHWA, with 32 stations located in Florida. The truck weight data format was used as it contains information such as, but not limited to, the number of axles, the spacing between axles, axle weights and gross vehicle weight (GVW), and the exact time of measurement for each recorded vehicle at each location [127]. The data left after filtering out vehicles less than 20-kip GVW are used for further analysis. The Cumulative Distribution Function (CDF) of GVWs was obtained based on the gross vehicle weight (GVW) and was translated based on multiple of design HS20 truck load for moment and shear effects for a certain span. These results can be used as much as possible for determining the truck loading effects in the analysis.

1.5.3 Analysis for Stress Variations in Girder Tension Flange and Forces in End Cross-frame Members– Level I Analysis

With the representative bridges identified and the loading model determined, analysis can be performed to calculate the stresses in the tension flange at the continuous end location. Under the same analyses, the forces in the end cross-frame members that is the loading demand on the connection to the girder can be determined. Before the analysis however the analytical software to be used will be determined. The literature search described above has determined that for the purpose of the Level I analysis, the Improved Grid Model will provide the desired results with acceptable accuracy. It is envisioned that the improved grid models will be implemented in MBrace3D finite element programs. Regardless of which software to be used, the analytical

model can be validated if experimental results are available at the level of multi-girder structure as well as at the connection detail level. A sensitivity analysis will be also performed to measure the effect of including half-round connections within the bridge model. It is understood that half-round bearing stiffeners increase the torsional stiffness of the steel girder ends, therefore, may alter the force distribution to the cross-frame members. If this effect is globally significant, means for accounting for this effect in the analysis will be studied and preferably, a simple method will be implemented to avoid further complexity of the models. This can be achieved by conducting a limited number of Level I analyses, using detailed FE analysis if needed, with and without a detailed half-round bearing stiffener connection model to investigate the effects and then devise a method to include the effect without the need for a refined connection modeling.

1.5.4 Analysis for Stress Distribution- Level II Analysis

After determining the cross-frame forces with respect to varying parameters, e.g., skew angle, Level II refined analysis using the refined finite element model of the half-round stiffener connection can be performed to obtain the stress distribution in the connection detail. This level of analysis can be used to first design the connection and provide details for the half-round pipe, the stiffener plate, and the welds joining these parts together and to the steel girder. The connection designs implemented or developed by TxDOT and FDOT will be used as a baseline for preliminary detailing. After designing and detailing the connection, Level II analysis with forces obtained from Level I analysis can also identify stress concentration points and the corresponding stress variation due to variation of live load. The latter information will be needed to provide stress range boundaries and increments for tests in determining the fatigue category for the half-round bearing stiffener within the existing S-N curves presented for AASHTO categories. Furthermore, this type of analysis will also be used to determine whether combining the steel girder tension flange bending and cross-frame member forces applied to the connection would in any way increase the susceptibility of the connection detail to fatigue. This is very important since it has a direct effect on the scheme to be considered for laboratory fatigue testing.

It is envisioned that Level II analysis will be performed using detailed finite element modeling using the ANSYS FE Program which is capable of refined modeling of steel connections.

1.6 Summary of the Literature Review and Inferences

The observations from the literature review can be summarized in the following.

Skew Bridges- In general, additional structural effects/responses should be expected in the skew bridges stemming from the lack-of-fit of cross frames in between girders. Consistent with the industry practice, there are two stages of construction for steel girder composite bridges where the girder webs are plumbed. These are erected fit and final fit, with detailing of cross frames to fit between girders at erection (steel self-weight) and when the fresh concrete is placed on the girder (total dead load), respectively. The fit-up forces need to be accounted for the design and detailing of the cross-frame connections. The live load effects and fatigue issues for cross frames are also exacerbated because of the skewness of the supports and differential deflection of the girders. The skewness creates a different structural response than that of the straight bridges. It is also understood that some of these effects dissipate for the end cross-frame over the intermediate supports of a continuous bridge where there would be no differential deflection.

The overall behavior of the skewed steel girder bridges under the fit-up, dead-load, and live-load effects can be captured with a good approximation using improved 2D grid analysis where the member properties are modified to address the shortcomings of the traditional 2D grid analysis. For the detailed design of cross-frame connections and their effects on the girder stresses, however, requires more sophisticated analytical modeling such as the 3D Finite Element method.

Half-round Stiffener Connection- To address some of the shortcomings of the existing bent-plate connections for skewed end cross-frame connections, including the detrimental flexibility of the connection, the half-round stiffener connection has been proposed. This connection configuration allows establishing a stiffener plate perpendicular to the pipe element at any skew angle. It has also been shown to improve also the warping restrain of the girder and therefore increase the girder buckling capacity.

Fatigue- The fatigue behavior of the end cross-frame skewed connections can be influenced by the stress concentration from two mechanisms, the distortional effects and the effect of the half-round pipe constraining the tension flange. Prior fatigue investigations on similar connections

have shown that for the types of stiffeners considered in those studies, the stress range is the main variable in fatigue, and that the minimum stress level, the grade of the base steel material, presence or absence of out of plane lateral forces from the braces, the bracing angle and specimen size did not significantly affect the final fatigue strength. A limited fatigue study on half-round stiffener connections has proposed an AASHTO Fatigue Category C for this connection configuration.

Fatigue categorization approach and Test Plan- In general, an effective test plan requires an organizational structure described by charts, figures, and tables showing in a simple manner the specimens, treatments (major variables), blocks (groups), stress levels, and replications (number of specimens at each block for each stress level). It should also suggest the statistical analysis method that would use the test data to develop the required results. There are several types of test plans that address different objectives including Preliminary-exploratory, Research, Design Allowables, and Reliability Data test plans. Since the objective of the current project is to determine the fatigue category of half-round stiffener connection for design purposes, the design allowables test plan seems to be the proper type to choose.

Accordingly, the number of the stress ranges and the number of specimens to be tested at each stress range need to be defined. The number of test specimens depends on the number of required stress levels and replications. The number of stress range levels can be reduced if the shape of the S-N curve is known. As few as two stress levels can be used for a linear behavior which is the common trend for fatigue categorization. The replication percentage and number of replications for the design allowables test plan has been recommended by the guidelines in STP588 to be 50 to 75% and 12 to 24 specimens, respectively. Accordingly, if the S-N curve can be assumed linear, then two stress levels and 6 replications can be used to match this recommendation.

Automated Monitoring of Cracks- The literature review has indicated that there are methods available with great potential for real-time detection of the onset and propagation of the fatigue cracks. These include the acoustic emission method, the use of laser vibrometer, vision-based methods, and piezoelectric sensors and strain gages. The more promising methods, especially

those with a better availability to testing researchers, could be used for one or more of the tests at the beginning of the experimental program in conjunction with hands-on inspection methods at intervals to validate the application and accuracy of such methods.

Corrosion Consideration- According to previous experiences, determination of the corrosion durability of the half-round bearing stiffener should include consideration of the selected material, connection detail, drainage detail, exposure environment, and the use of corrosion mitigation technologies as described earlier in the technical approach. A series of small- and large-scale testing schemes can be devised to study these effects.

1.7 Inferences and Suggestions

The results of investigations and observations from a variety of sources point to the following inferences. These are described here as hypotheses that may require verification through analytical and experimental investigations.

- The distortional effect on the fatigue behavior of the end-cross frames would not be significant and could be ignored. In another word, the effect of cross-frame forces on the stress variation in the tension flange of the girder could be negligible. Accordingly, fatigue testing may include only the girder bending effect. This will be verified through analysis in the next task.
- The fatigue performance of the half-round stiffener connections for skewed end cross-frames as it concerns the girder tension flange could be equal or better than the traditional stiffener connection perpendicular to the girder web. Analysis and fatigue testing can verify this.
- Tensile stress variation in the girder top flange above the intermediate support of the continuous spans would be small and there could be no fatigue issues for the half-round stiffener connection for the end cross-frames. The steel girders in the continuous moment region work compositely with the reinforced concrete deck, completely or partially, therefore reducing the tension stresses in the girder top flange. This can be verified using detailed finite element analysis with a model “calibrated” for the level of composite

action between the bridge deck and girder. The calibration can be accomplished with a supplementary field-testing for the instrumentation of a skewed bridge in the negative moment region over the intermediate support.

Chapter 2- Analytical Study

2.1 Bridge Matrix

2.1.1 Selection of the Representative Bridges for Analytical Study

Before the analytical investigation can begin, the representative bridges to be analyzed that cover the practical range of the major parameters of continuous skewed steel girder bridges need to be identified. These parameters include skew angle, type of continuous spans (one-sided or two-sided continuity), span length, bridge width, number of steel girders, cross-frame configuration and girder spacing. The FDOT Project Technical Committee has identified 26 bridges to be investigated as representative bridges. The list of bridges adopted for this study with the alternative numbering to be referred by hereafter is shown in Table 2.1 below. These bridges are those for which a half-round stiffener connection has been recognized as an appropriate detail for end cross-frames.

Design drawings for the representative bridges were provided to the research team. According to the information in the design drawings, specific information about the selected bridges is summarized in Table 2.1. The information includes number of spans, span lengths, skew angle and index at piers and abutments, curvature (angle, radius, and span/radius ratio), total width, framing width, number of girders, and number of lanes. Some of the longer bridges were specified for the analysis to be performed for certain unit containing limited number of spans. These are identified in the table with the unit number. The table also identifies bridges included in earlier investigations by Georgia Tech and one bridge that has been designed with half-round stiffener connection. It also notes whether a skewed cross-frame/diaphragm has been used over the intermediate supports. The type of fit, the fit condition for detailing of cross-frames, was also included in the table if prescribed specifically by the drawings.

2.1.2 Histograms of Bridges Main Variables

Using the data provided in Table 2.1, histograms were produced for main variables of the bridge including:

1- Span lengths for all spans, interior and exterior- Figure 2.1
2- Interior span lengths – Figure 2.2- Interior spans are continuous at both ends and supported by intermediate pier at both ends.
3- Exterior span lengths- Figure 2.3- Exterior spans are continuous only on one end and are supported by an intermediate pier at one end and an abutment at the other.
4- Bridge width- Figure 2.4
5- Number of girders- Figure 2.5
6- Number of lanes- Figure 2.6
7- Skew angle at all supports- Figure 2.7
8- Skew angle at intermediate pier supports- Figure 2.8
9- Skew index for all spans - Figure 2.9

   The Skew index (Is) can be defined based on the formula $\mathrm{Is} = w_g \tan(\theta) / Ls$, where w_g is the framing width between the fascia girders, θ is the skew angle, and Ls is the span length under consideration.
10- bridge skew index - Figure 2.10
11- Bridge Curvature- Figure 2.11
12- Span Length over Curvature Radius (L/R)- Figure 2.12

Note: In figures 2.1 through 2.12, the unit for the horizontal is in the form of range, for example, (150, 180] is equivalent to $150 < \mathrm{Range} \leq 180$.

Table 2.1 Bridge Matrix and Information to be used for Analytical Study

FDOT Bridge #	Alternative Bridge #	Unit	Span Length (ft)													Skewed Cross-frame over intermediate pier	Fit-up type	Existing Plans Cross-Frame Configuration
			1	2	3	4	5	6	7	8	9	10	11	12	SUM			
871018	64	-	190.0	140.0	-	-	-	-	-	-	-	-	-	-	330.0	No	SDLF	4
871020[1]	9	-	204.0	160.0	-	-	-	-	-	-	-	-	-	-	364.0	No	SDLF	4
871033	65	-	123.1	137.1	-	-	-	-	-	-	-	-	-	-	260.2	No	N/A	4
920192	66	-	216.5	233.5	-	-	-	-	-	-	-	-	-	-	450.0	Yes	SDLF	5
920193	67	-	210.4	234.4	-	-	-	-	-	-	-	-	-	-	444.8	Yes	SDLF	6
100676-1	68	1	186.3	166.7	155.8	167.3	208.3	169.0	170.6	170.6	170.6	-	-	-	1634.2	No	N/A	5
100833	69	-	218.3	250.0	-	-	-	-	-	-	-	-	-	-	468.3	Yes	N/A	5
750604-3	71	3	165.7	180.0	156.5	156.5	180.0	151.8	187.1	154.4	149.0	145.9	167.0	116.0	1910.0	Yes	N/A	5
770132[3]	72	-	158.9	239.1	234.6	176.0	-	-	-	-	-	-	-	-	808.6	Yes	NLF	5
871044	70	-	197.6	213.3			-	-	-	-	-	-	-	-	410.9	Yes	SDLF	5
924179[1]	13	-	171.6	253.0	253.0	202.4	-	-	-	-	-	-	-	-	880.0	Yes	N/A	5
100691[1]	15	-	189.3	156.7	158.8	227.7	-	-	-	-	-	-	-	-	732.4	Yes	TDLF	5
140086[2]	44	-	156.1	145.0	-	-	-	-	-	-	-	-	-	-	301.1	Yes	SDLF	5
140088[2]	43	-	171.6	171.6	-	-	-	-	-	-	-	-	-	-	343.3	Yes	SDLF	5
150281[2]	41	-	262.2	255.0	-	-	-	-	-	-	-	-	-	-	517.2	No	SDLF	5 (SC)
160323	60	-	177.5	177.5	-	-	-	-	-	-	-	-	-	-	355.0	Yes (Diaphragm)	N/A	6
160325[2]	45	-	252.5	252.5	-	-	-	-	-	-	-	-	-	-	505.0	No	N/A	4
160327[2]	42	-	251.5	251.5	-	-	-	-	-	-	-	-	-	-	503.0	No	TDLF	4
160330[1][2]	8	-	149.1	173.8	-	-	-	-	-	-	-	-	-	-	322.9	Yes	TDLF	7
750594[2]	46	-	230.0	209.8	-	-	-	-	-	-	-	-	-	-	439.8	No	NLF-SDLF	4
750739	61	-	207.9	208.5	-	-	-	-	-	-	-	-	-	-	416.4	Yes	TDLF	5
754147[1]	24	-	169.8	169.8	-	-	-	-	-	-	-	-	-	-	339.6	Yes	N/A	5
790212[1]	25	-	199.0	199.0	-	-	-	-	-	-	-	-	-	-	398.0	No	NLF	4
860656[4]	62[4]	-	181.0	174.0	-	-	-	-	-	-	-	-	-	-	355.0	N/A	N/A	6 (SC)
870988-2	63	2	100.1	167.3	185.4	-	-	-	-	-	-	-	-	-	452.8	Yes	N/A	5
871016[1]	12	-	204.4	196.0	184.9	-	-	-	-	-	-	-	-	-	585.3	No	SDLF	4

Notes: **(1) Part of BE535 Study (GeorgiaTech) (2) Part of BEB13 Study (GeorgiaTech) (3) Bridge designed with half-pipe stiffener (4) Intermediate pier for this bridge is not skewed**

Cross-Frame Configuration (Framing System Type):

1- Skew is less than 20 deg, cross-frames parallel to skew
2- Skew is less than 20 deg, cross-frames perpendicular to girder with non-continues frame line near supports
3- Skew is greater than 20 deg, cross-frames perpendicular to girder tied into bearings with pier cross-frame
4- Skew is greater than 20 deg, cross-frames perpendicular to girder tied into bearings without pier cross-frame
5- Skew is greater than 20 deg, cross-frames perpendicular to girder with non-continuous frame line near support (with pier cross-frame)
6- Skew is greater than 20 deg, cross-frames perpendicular to girder away from bearings (with pier cross-frame)
7- Skew is greater than 20 deg, cross-frames staggered

Table 2.1 (Continued) Bridge Matrix and Information to be used for Analytical Study

FDOT Bridge #	Alternative Bridge #	Unit	Skew Angle at Pier													Curvature			Case[5] Number
			Pier 1	Pier 2	Pier 3	Pier 4	Pier 5	Pier 6	Pier 7	Pier 8	Pier 9	Pier 10	Pier 11	Pier 12	Pier 13	θ	R (ft)	L/R	
871018	64	-	52° 48' 30"	56° 7' 33"	57° 14' 16"	-	-	-	-	-	-	-	-	-	-	1° 44' 46"	3281.4	0.058	4
871020[1]	9	-	56° 11' 41"	56° 11' 41"	56° 11' 41"	-	-	-	-	-	-	-	-	-	-	-	-	0.000	4
871033	65	-	23°	23°	23°	-	-	-	-	-	-	-	-	-	-	-	-	0.000	3
920192	66	-	39° 45' 14"	39° 45' 14"	39° 45' 14"	-	-	-	-	-	-	-	-	-	-	-	-	0.000	2
920193	67	-	36° 3' 12"	39° 12' 31"	42° 43' 29"	-	-	-	-	-	-	-	-	-	-	1° 30' 0"	3819.7	0.061	N/A
100676-1	68	1	40° 46' 32	27°	0	0	0	0	0	0	0	-	-	-	-	4° 45' 0"	738.2	0.282	N/A
100833	69	-	40° 38' 7"	45°	45°	-	-	-	-	-	-	-	-	-	-	1° 59'59"	2865.0	0.087	N/A
750604-3	71	3	15° 12' 11"	0	0	0	0	0	41° 3' 26"	50° 54' 36"	34° 42' 0"	0	25° 57' 36"	0	0	5°	1145.9	0.163	N/A
770132[3]	72	-	0	57°	50° 31' 41"	39° 44' 40"	0	-	-	-	-	-	-	-	-	8° 14' 38"	695.0	0.344	N/A
871044	70	-	44° 5' 22"	48° 40' 43"	46° 45' 41"	-	-	-	-	-	-	-	-	-	-	7° 04' 25"	810.0	0.263	N/A
924179[1]	13	-	0	50° 5' 38"	50° 5' 38"	50° 5' 38"	0	-	-	-	-	-	-	-	-	-	-	0.000	4
100691[1]	15	-	53°	36°	8°	45°	45°	-	-	-	-	-	-	-	-	15° 34' 32"	5725.1	0.040	4
140086[2]	44	-	40° 28' 39"	40° 28' 39"	40° 28' 39"	-	-	-	-	-	-	-	-	-	-	-	-	0.000	2
140088[2]	43	-	55° 1' 43"	55° 1' 43"	55° 1' 43"	-	-	-	-	-	-	-	-	-	-	-	-	0.000	4
150281[2]	41	-	52° 9' 41"	53° 18' 35"	54° 40' 54"	-	-	-	-	-	-	-	-	-	-	0° 29' 14"	11758.0	0.022	4
160323	60	-	25° 38' 1"	25° 38' 1"	25° 38' 1"	-	-	-	-	-	-	-	-	-	-	-	-	0.000	2
160325[2]	45	-	50° 22' 8"	50° 22' 8"	50° 22' 8"	-	-	-	-	-	-	-	-	-	-	-	-	0.000	4
160327[2]	42	-	50° 11' 3"	50° 11' 3"	50° 11' 3"	-	-	-	-	-	-	-	-	-	-	-	-	0.000	4
160330[1][2]	8	-	23° 25' 29"	23° 25' 29"	23° 25' 29"	-	-	-	-	-	-	-	-	-	-	-	-	0.000	3
750594[2]	46	-	43° 49' 50"	43° 49' 50"	43° 49' 50"	-	-	-	-	-	-	-	-	-	-	-	-	0.000	3
750739	61	-	36° 40' 17"	35° 58' 14"	35° 16' 4"	-	-	-	-	-	-	-	-	-	-	-	-	0.000	2
754147[1]	24	-	52° 39' 37"	52° 39' 37"	52° 39' 37"	-	-	-	-	-	-	-	-	-	-	-	-	0.000	4
790212[1]	25	-	54° 27' 11"	54° 27' 11"	54° 27' 11"	-	-	-	-	-	-	-	-	-	-	-	-	0.000	4
860656[4]	62[4]	-	25°	0	25°	-	-	-	-	-	-	-	-	-	-	1° 48'	3183.1	0.057	3
870988-2	63	2	35° 30' 0"	35° 30' 0"	35° 30' 0"	35° 35' 24"	-	-	-	-	-	-	-	-	-	-	-	0.000	2
871016[1]	12	-	44° 14' 24"	44° 39' 44"	58° 43' 49"	58° 43' 49"	-	-	-	-	-	-	-	-	-	-	-	0.000	4

Notes: **(1) Part of BE535 Study (GeorgiaTech) (2) Part of BEB13 Study (GeorgiaTech) (3) Bridge designed with half-pipe stiffener (4) Intermediate pier for this bridge is not skewed**
(5) Bridges that fall under 'N/A' have 0.06 ≤ L/R and must use SDG Section 5.1.B: Horizontally Curves Steel I-Girder Bridges.

Table 2.1 (Continued) Bridge Matrix and Information to be used for Analytical Study

FDOT Bridge #	Alternative Bridge #	Unit	No. of Lanes	No. of Girders	Deck Width (ft)	w_g (ft)	Skew Index (Is) $Is = w_g \cdot \tan\theta / Ls$									Max Skew Index (Is)
							Span 1	Span 2	Span 3	Span 4	Span 5	Span 6	Span 7	Span 8	Span 9	
871018	64	-	3	6	58.21	51.25	0.40	0.57								0.57
871020[1]	9	-	3	6	54.27	47.50	0.35	0.44								0.44
871033	65	-	2	4	37.08	30.00	0.10	0.09								0.10
920192	66	-	3	5	56.08	48.00	0.18	0.17								0.18
920193	67	-	4	6	67.08	60.00	0.23	0.24								0.24
100676-1	68	1	2	4	48.39	37.40	0.17	0.11								0.17
100833	69	-	1	3	30.08	22.00	0.10	0.09								0.10
750604-3	71	3	2	5	43.08	37.00							0.24	0.29	0.17	0.29
770132[3]	72	-	1	4	44.00	36.00	0.35	0.23	0.19	0.17						0.35
871044	70	-	1	4	37.29	29.00	0.17	0.15								0.17
924179[1]	13	-	2	4	43.08	36.00	0.25	0.17	0.17	0.21						0.25
100691[1]	15	-	3	5	60.20	49.21	0.35	0.23	0.31	0.22						0.35
140086[2]	44	-	2	5	47.08	39.00	0.21	0.23								0.23
140088[2]	43	-	2	4	47.08	37.50	0.31	0.31								0.31
150281[2]	41	-	2	4	43.08	36.00	0.18	0.20								0.20
160323	60	-	2	4	50.17	40.25	0.11	0.11								0.11
160325[2]	45	-	2	6	65.00	58.33	0.28	0.28								0.28
160327[2]	42	-	2	5	59.00	51.00	0.24	0.24								0.24
160330[1][2]	8	-	4	8	101.08	93.31	0.27	0.23								0.27
750594[2]	46	-	4	7	71.08	63.38	0.26	0.29								0.29
750739	61	-	3	6	59.08	52.92	0.19	0.18								0.19
754147[1]	24	-	2	7	55.25	48.25	0.37	0.37								0.37
790212[1]	25	-	2	4	43.08	35.25	0.25	0.25								0.25
860656[4]	62[4]	-	1	4	30.08	24.00	0.06	0.06								0.06
870988-2	63	2	3	6	54.37	45.11		0.19	0.17							0.19
871016[1]	12	-	2	5	42.46	35.00	0.17	0.29	0.31							0.31

Notes: **(1) Part of BE535 Study (GeorgiaTech) (2) Part of BEB13 Study (GeorgiaTech) (3) Bridge designed with half-pipe stiffener**
(4) Intermediate pier for this bridge is not skewed

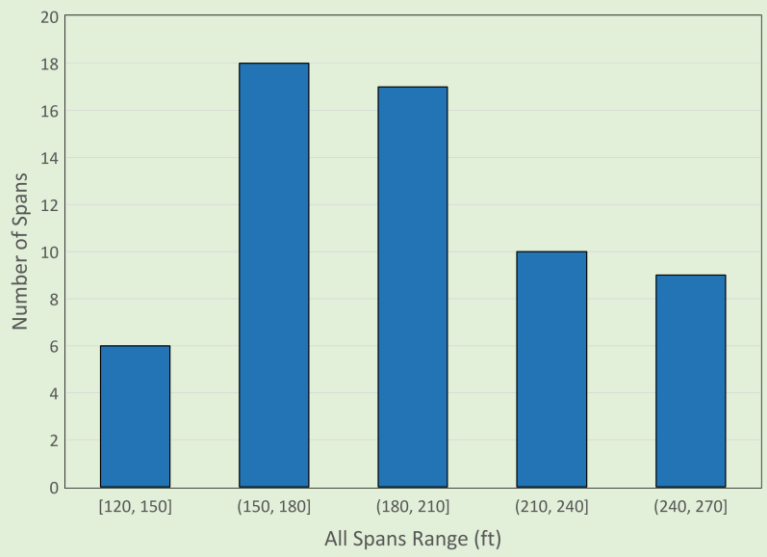

Figure 2.1 Histogram for span lengths for all spans

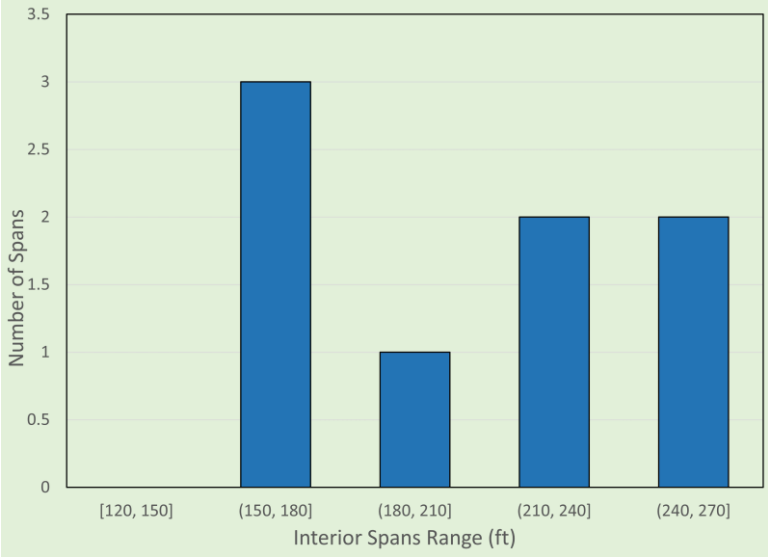

Figure 2.2 Histogram for interior span lengths

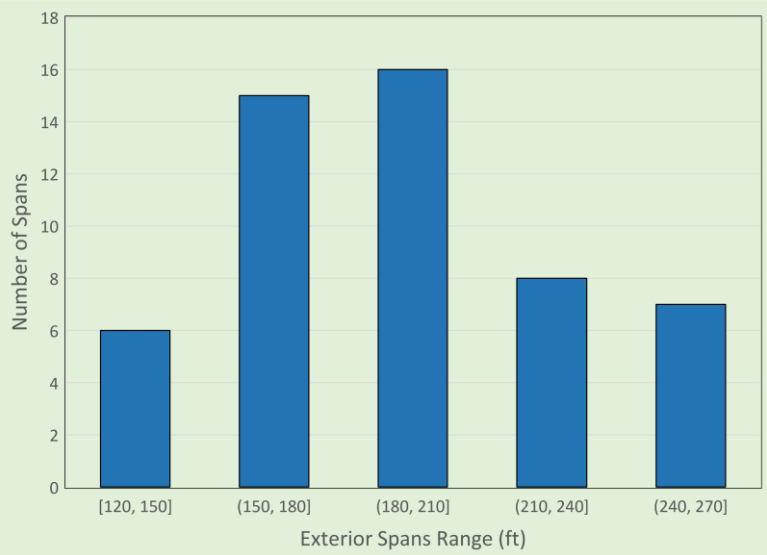

Figure 2.3 Histogram for exterior span lengths

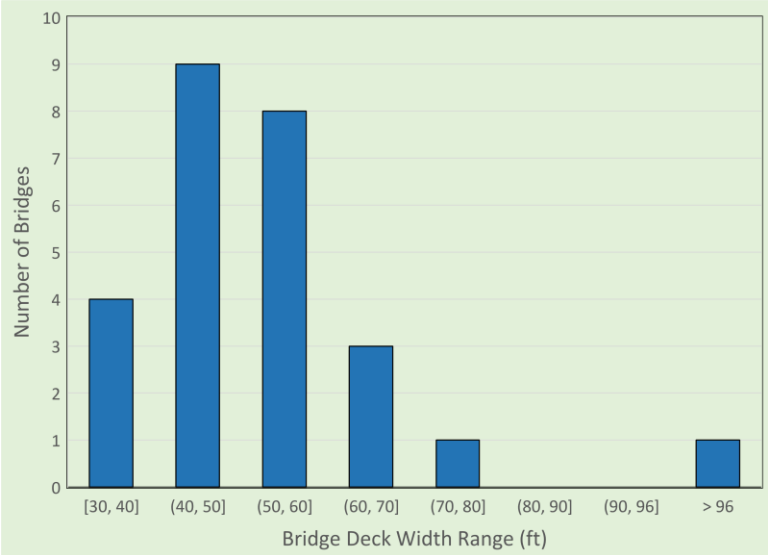

Figure 2.4 Histogram for bridge deck width

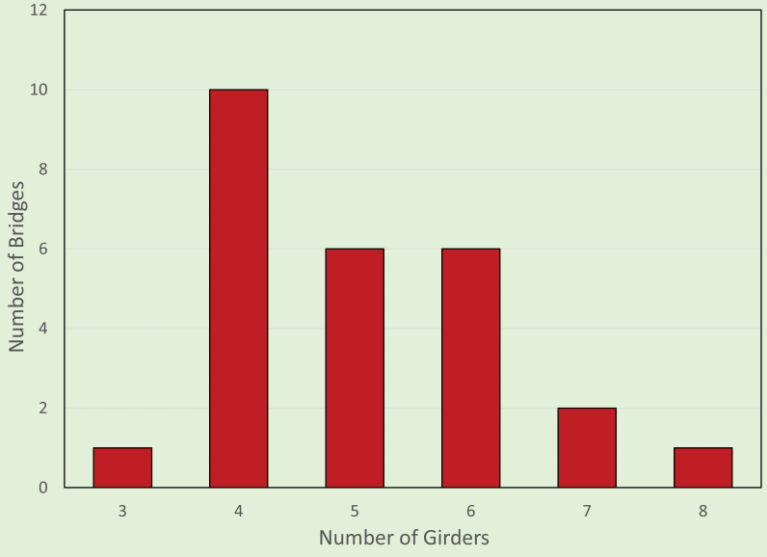

Figure 2.5 Histogram for number of girders

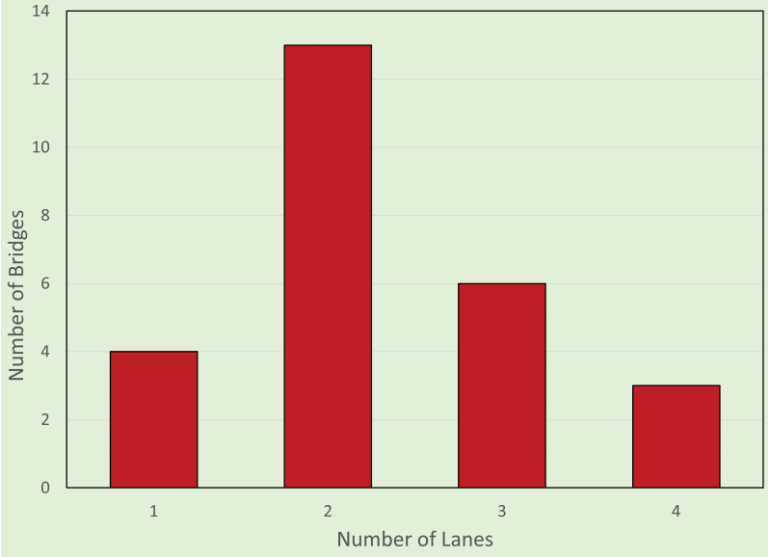

Figure 2.6 Histogram for number of lanes

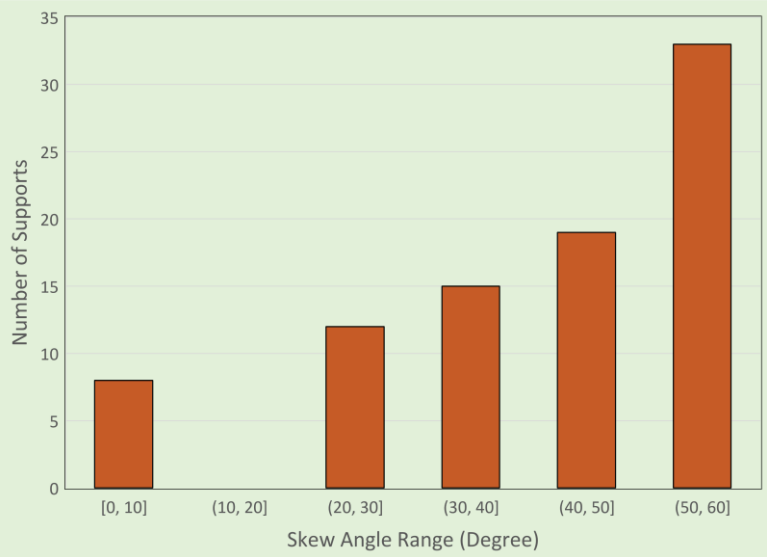

Figure 2.7 Histogram for skew angle at all supports

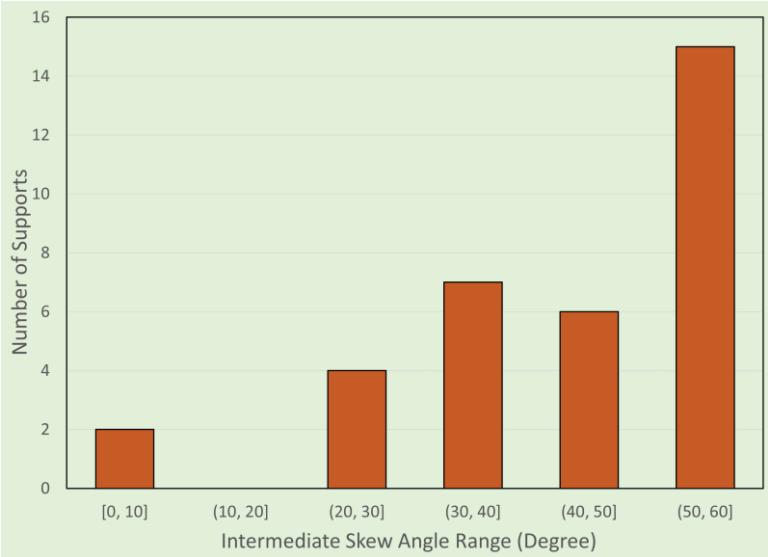

Figure 2.8 Histogram for skew angle at intermediate pier supports

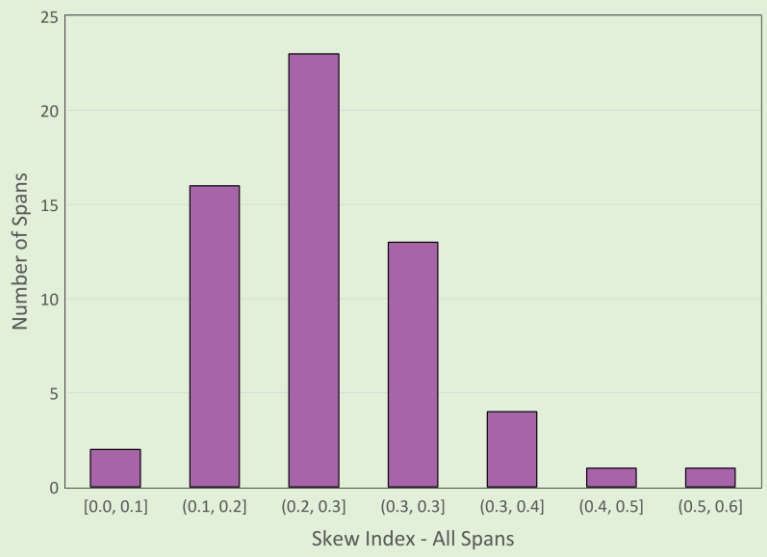

Figure 2.9 Histogram for skew index for all spans

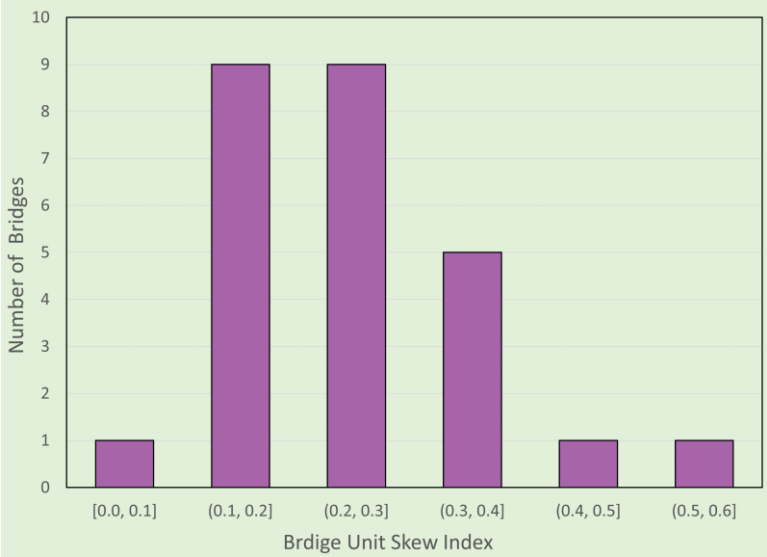

Figure 2.10 Histogram for bridge unit skew index

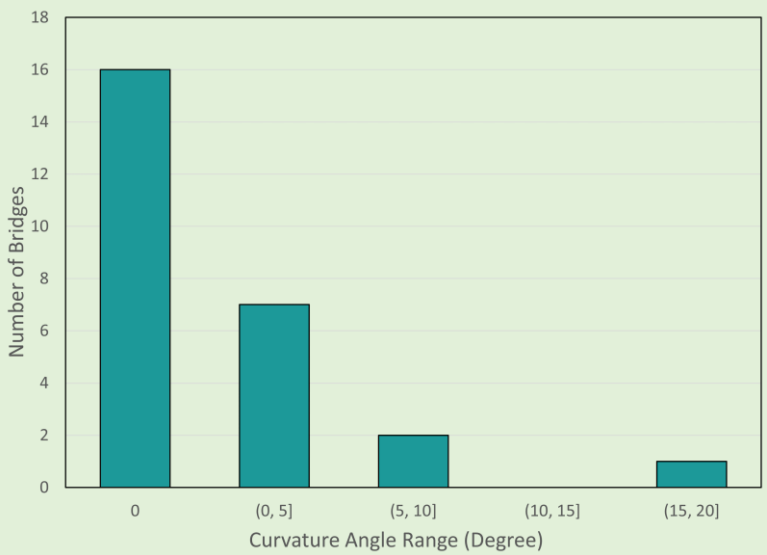

Figure 2.11 Histogram for bridge curvature

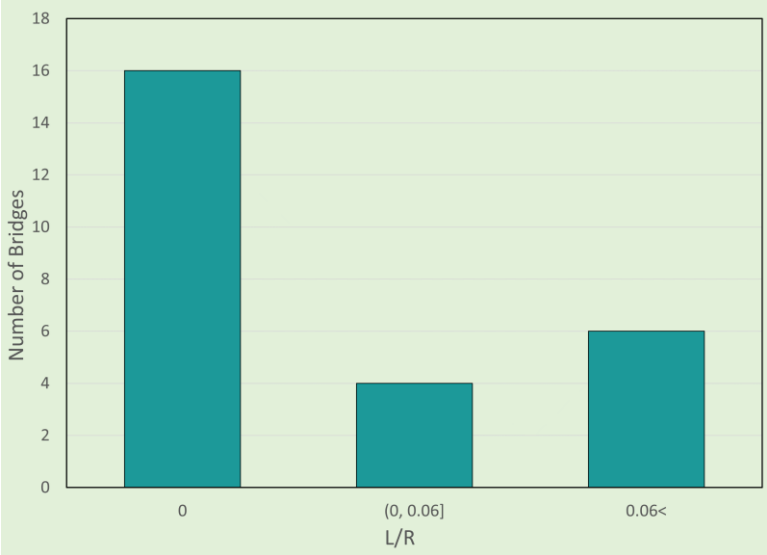

Figure 2.12 Histogram for Span Length over Curvature Radius

2.2 Analytical Study

As per the literature review performed in Task 1, it was determined that two analysis levels are required in this study, which are referred to as Level I and Level II analyses. Level I analyses consist of models of the entire bridge systems and focus on stress variations in the girder tension flanges and forces in the end cross-frame members, while the Level II analyses consist of refined models of the girder and Half-Round Bearing Stiffener (HRBS) details to focus on local stress distributions.

2.2.1 Analytical Study – Level I

Preliminary analyses demonstrated that the Level I analyses can be performed using improved 2D grid analysis models and that the Level II analyses required a more sophisticated finite element program. A review of commercially available software for these analyses, allowed the research team to identify a suitably sophisticated analytical program developed specifically for bridges that can be used for both levels of analyses with a reasonable effort. Therefore, a single FEA platform, Midas, was used for modeling and simulations. Midas Civil [128] and Midas FEA NX [129] programs were used to create the Level I and Level II finite element (FE) models, respectively. The following sub-section provides an overview of the review of a few viable software programs that were considered.

There are two sets of information expected from the analytical studies:

- Tensile stress variation in the girder top flange over the intermediate pier for the purpose of fatigue test planning, and
- End cross-frame member forces for the purpose of:
    - Sizing and detailing of the HRBS connection
    - Stress concentration considerations for the connection

2.2.1.1 Preliminary Review of Viable Analysis Programs

The research team gained access to a few viable finite element analysis programs for consideration of use in the Level I and II analyses. Two of the programs that were considered consist of mBrace3D [130] and MIDAS Civil [128]. Bridge No. 25 was selected as a benchmarking case to evaluate the programs. The bridge is a two-span bridge with a total length of 398 feet

and equal spans measuring 199 feet. The bridge has a width of 43 feet with two striped lanes of traffic. The straight bridge has abutments and intermediate piers skewed at an angle of 54.45 degree. Figure 2.13 and Figure 2.14 show a view of the bridge model using Midas and mBrace3D programs, respectively.

Preliminary analyses were performed to compare the modeling process and results from these programs. The results from the two programs agreed well. For the purpose of this study, because of the easier input along with better modeling options, the MIDAS program was selected for the Level I and Level II analysis in this project.

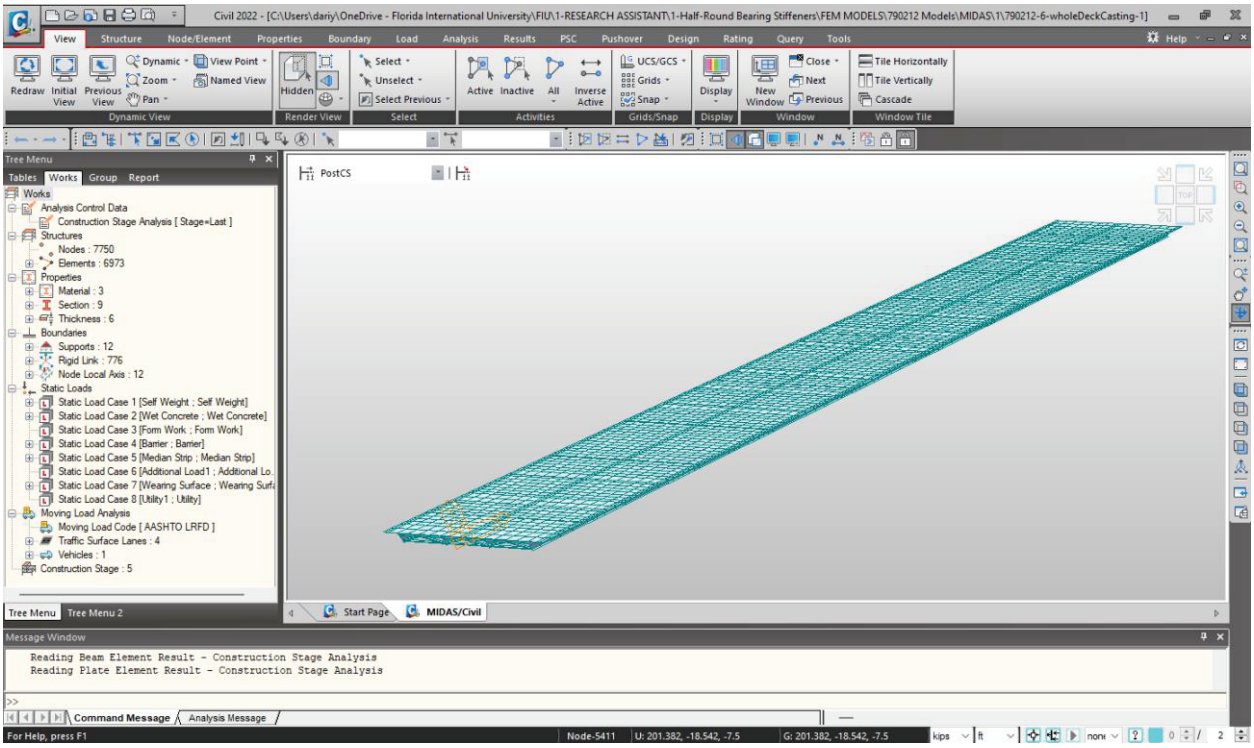

Figure 2.13- Bridge 25 FEM model in MIDAS Civil software

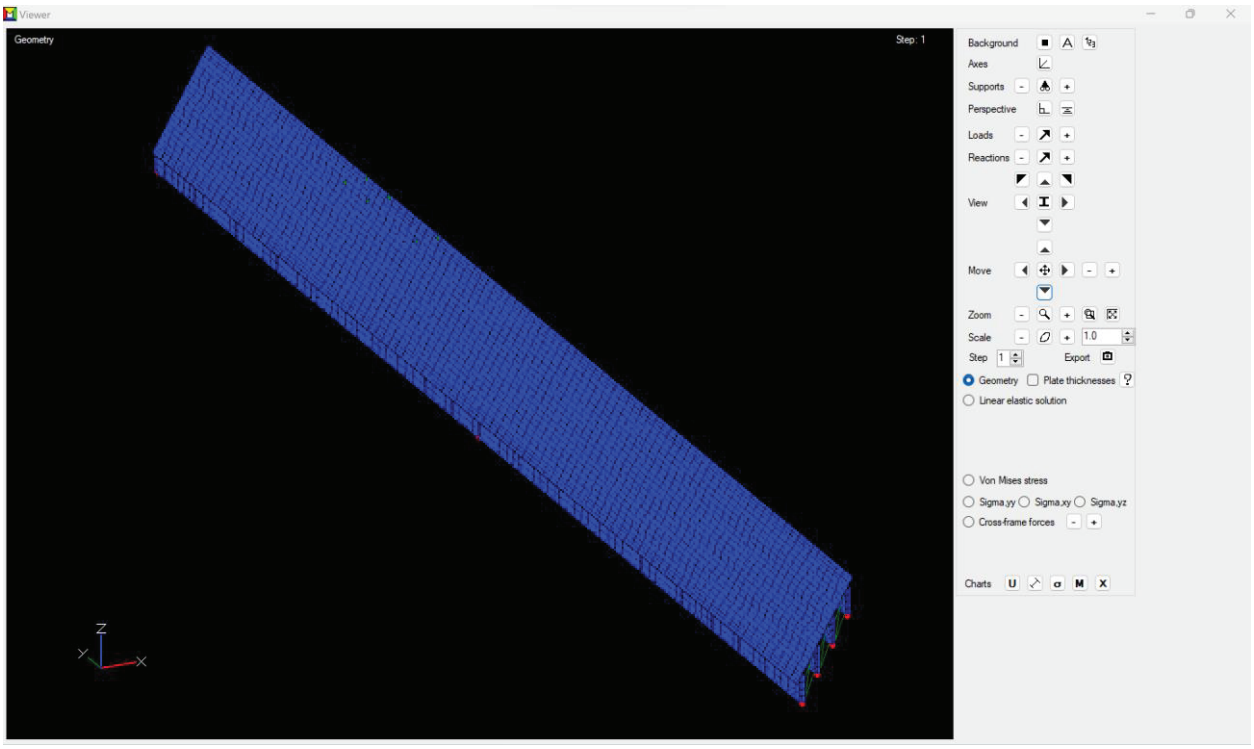

Figure 2.14- Bridge 25 FEM model in MBrace3d software

2.2.1.2 End Cross-Frame Forces Required for Design of HRBS Connections in Skewed Bridges

The primary bracing system that is utilized in steel bridges consists of cross frames or diaphragms that are categorized as torsional bracing systems since these members primarily provide bracing by restricting the twist of the adjacent girders. Steel I-girder bridges feature three distinct types of cross-frames: intermediate, abutment end, and pier end cross-frames serving to connect the steel I-girders at different location along the bridge span. Intermediate cross-frames are located within the span of the bridge and are normally perpendicular to the girders. Abutments end cross-frames (a.k.a. diaphragms) are used at the abutments where the girders are discontinued. Lastly, pier end cross-frames (a.k.a. diaphragms) are employed at the support over the intermediate piers where the bridge deck and girders are continuous. End cross-frames are aligned with the skewed direction of the supports. Cross-frames for steel girder bridges serve several purposes during construction and in service. While the primary purpose of the braces is to stabilize the girders during erection and construction, the cross-frames also assist in distributing the construction stage forces and deck finishing machine that are often transmitted through the overhang brackets. The cross-frames also distribute lateral loads from sources such

as the wind on the bridge and live load effects among steel girders. The critical stage for most cross frames generally occurs during construction before the concrete deck is hardened. In addition to the forces induced during deck placement, the cross-frames also develop forces associated with lack-of-fit and fit-up. The cross-frames generally remain throughout the service life of the bridge and therefore attract live load and wind load forces. Accordingly, the forces cross-frame members experience in skewed bridges include those listed below:

- Fit-up and lack-of fit forces.
- Dead load forces from weight of steel and miscellaneous dead load such as barriers and wearing surface,
- Live load forces from design loading,
- Forces from lateral loading such as wind, and
- Forces from fatigue truck loading.

A primary goal of the Level I analyses was to determine the maximum range of forces that develop in the pier end cross-frame components and girders that can be used in the refined models that are used in the Level II analyses to obtain an indication of the maximum stresses in the HRBS and associated connections. Results from these analyses provide important input towards the design of the connections between the pier end cross-frames, HRBS, and the girders.

2.2.1.2.1 Lack-of-Fit Forces

Normally, detailing for cross-frames is performed for erected-fit or final-fit conditions (see report for Task 1 for detailed explanation). Accordingly, cross-frame member forces at the stage of construction for which they are detailed is generally minimal but will be more significant in other construction stages. Table 2.2 adopted from [131] gives a qualitative assessment of the cross-frame member forces for various construction stages.

As a general rule in the case of erected-fit detailing [18], the lack-of-fit forces are minimal under girder dead load since the cross-frames have been detailed to fit at the stage they are installed; however the braces will generally develop larger forces as the girders deform during the placement of the additional dead load. On the contrary, when final-fit detailing is utilized, the forces are generally minimal under final dead load conditions; however significant lack-of-fit

forces may develop during installation/erection specially for intermediate cross-frames since the girders must be pulled into a suitable position. However, for end cross-frames these forces would be smaller because there is no differential vertical displacement among girders. Figure 2.15 and Figure 2.16 shows an example for better explaining the condition at different construction stages for an end cross-frame. Figure 2.15 relates to erected-fit condition. In this figure, the left figure shows the position of girders at erection stage under girder dead load before connecting the cross-frames. Because of differential cambers in adjacent girders, the girders stand plumb at different levels. The middle figure shows these two girders after connecting the cross-frames. Because the cross-frames are detailed for erected-fit, there should be no or little force in the cross-frame members and no fit-up forces are required.

Table 2.2-Structural problems related with assembly fit and final fit detailing approach

	Erected fit	**Final fit**	**Comments**
Cross-frame forces	• Small at erection • Can be significant when wet concrete is placed over girders	• Can be significant at the erection due to lack of fit of cross-frames between the girders • Small after completing casting the deck	No field problems reported for the cross-frames during construction of skew bridges

According to the schemes discussed above, the cross-frame member forces can be obtained simply by applying concrete dead-load weight to the bridge model that contains fully assembled girders and cross-frames. Table 2.3 summarizes the methods for estimation of lack-of-fit forces for various fit conditions.

Coletti et al. (2018) [131] investigated the lack-of-fit and fit-up forces with a more detailed approach that included construction-stage considerations and provided an estimation of lack of forces as a conservative approach as shown in Table 2.4 to be followed in this study.

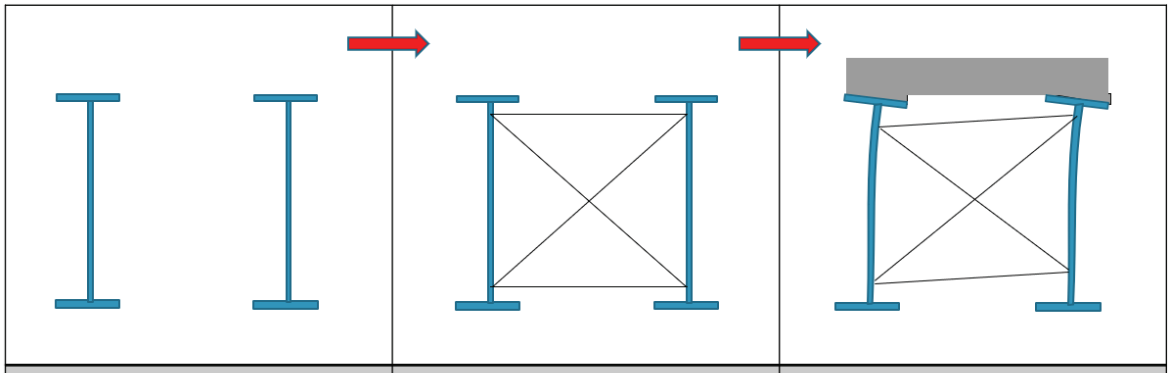

Placement of Girders on support	Attaching cross frames-Erected Position	Final load position- after Placement of Concrete Deck
	Cross Frame Forces: Minor/zero	Cross Frame Forces : Can be Significant

Figure 2.15- Erected fit detailing method for end cross-frames

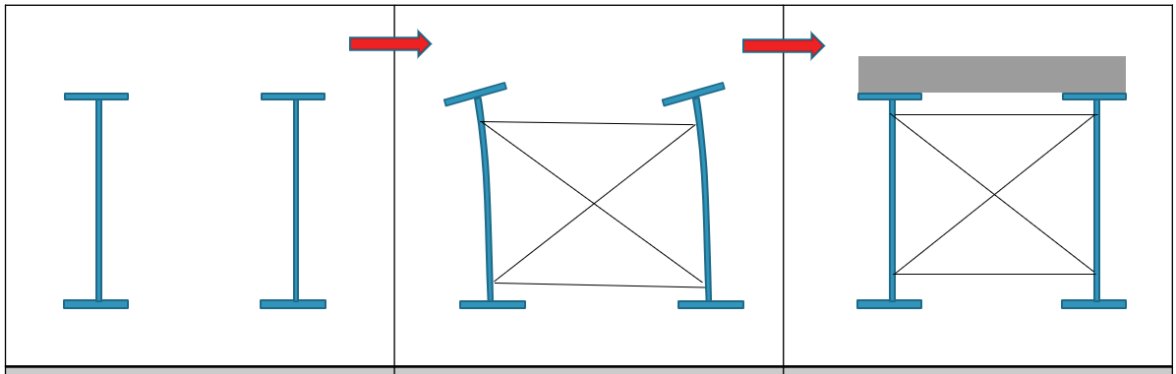

Placement of Girders on support	Fitting cross frames-Erected Position	Final load position- after Placement of Concrete Deck
	Cross Frame/fit up Forces: Can be significant	Cross Frame Forces: Minor/Zero

Figure 2.16- Final fit detailing method for end cross-frames

Table 2.3- Methods for calculating cross-frame forces based on fit condition using 3D FE

Fit Condition/Assumption	Construction Stage Cross-Frame Forces	Cross-Frame Forces when deck is cast	Method for Calculating Cross-Frame Forces for Connection Design using 3D FE Model	Notes
NLF – No-Load Fit	SDL at erection TDL at Completion	**TDL**	Build the girder and cross-frame model, then apply steel weight to obtain SDL forces and then apply wet concrete weights additionally to obtain TDL	NLF is not common, however, the forces calculated can be used conservatively for all other cases
SDLF – Erected Fit	Zero or minimal at erection (TDL – SDL) at completion	**(TDL – SDL)**	Build the girder and cross-frame model, then apply wet concrete weights to obtain (TDL-SDL) forces	Most common
TDLF – Final Fit	(SDL-TDL) at erection Zero or minimal at completion	**Zero or minimal**	(SDL-TDL) forces are equal and in the opposite direction with the forces calculated in above row	Accidental forces can be generated during construction and some locked in, making this an non-conservative option
Full member capacity			Connections are designed for the full capacity of the cross-frame members	Regardless of how members are designed, connections should not fail before the members

Table 2.4- Estimation of lack-of-fit forces for curved and/or skewed bridges [131]

Responses	(1) Curved Radially-Supported	(2) Straight Skewed	(3) Curved and Skewed
Cross-frame forces	γ_p (2.0 SDL + ADL) for SDLF [a], except γ_p (SDL + ADL) for chords of X-Type cross-frames	γ_p TDL for SDLF, (γ_p – 0.4) TDL for TDLF	Same as (1)

Definitions and Acronyms:

- SDL = Steel Dead Load, SDLF = Steel Dead Load Fit
- TDL = Total Dead Load, TDLF = Total Dead Load Fit
- ADL = Additional Dead Load = TDL – SDL
- LGA = Line Girder Analysis
- γ_p = Permanent Dead Load Factor

Their findings and conclusions are summarized below:

- Refined analysis methods allow for direct consideration of cross-frame forces and girder lateral bending.
- In straight skewed bridges with SDLF or TDLF detailing, dead load relieves the stress in cross-frame members.
- In curved radially supported bridges, the fit-up forces pulling and twisting the girders against their natural rolling therefore adding to the other dead load forces.
- In straight skewed bridges, it is conservative to neglect both SDLF and TDLF relieving effects (Equivalent to NLF) when using 3D FEA model. (i.e., Start the 3D model at NLF without locked-in forces)
- NCHRP Project 20-07 allows reduction factors for highly conservative cases.
- NCHRP Project 20-07 provides detailed procedures and benchmark calculations for straight and curved bridges and explains how results can be included in design load combinations to satisfy AASHTO LRFD requirements.
- NCHRP Project 20-07 recommends an estimate of locked-in effects associated with SDLF and TDLF detailing.
- In lieu of including lack-of-fit effects in the analysis, Coletti et al. recommend load factors for a conservative estimate of cross-frame forces (see Table 2.4)

Accordingly, Coletti et al. (2018) [131] provided an estimation of lack-of-fit forces as a conservative approach that is followed in the present study (Table 2.4).

2.2.1.2.2 Forces from Miscellaneous Dead Loads

After the concrete deck has cured, additional dead load from sources such as barriers and a wearing surface will generate additional forces in the cross-frame members. A first-order analysis

of the finished bridge system can predict the forces induced in the cross-frames from these additional loads.

2.2.1.2.3 Live Load Forces from HL-93 Loading

Design live load will generally induce additional forces in the cross-frames. The magnitudes of these live-load induced forces are generally larger in bridges with skewed supports, especially for the intermediate cross-frames that contribute to load distribution. End cross-frames do not generally experience forces from differential vertical displacements since the girders are supported vertically by the bearings and further restrained laterally by the concrete deck. However, the end cross-frames can potentially develop large forces from other sources since these braces generally account for unbalanced forces from adjacent girders and further distribute forces from the deck/girder down to the bearings, which is discussed in subsequent sections of this chapter.

2.2.1.2.4 Forces from Lateral Loading Such as Wind

Cross-frames provide important load path for the distribution of large lateral forces from sources such as wind. The magnitudes of forces in the braces from lateral loads can be significant. The primary lateral loads (in the transverse direction of the bridge, perpendicular to the girders)in Florida is generally wind loads, which is, therefore, the primary focus of the present study.

2.2.1.2.5 Forces from Fatigue Truck Loading

The fatigue evaluation of the connections to the HRBS necessitate determining the forces from the passage of the fatigue truck on the bridge. The 3D Finite Element (FE) analytical models were used for this process. In this process, the fatigue truck is moved along various lanes, and maximum and minimum forces developed in the cross-frame members during the truck passage are obtained.

2.2.1.2.6 Load Factors and Load Combinations

AASHTO LRFD load combinations as shown in Table 2.5 were used to verify the design of cross-frame members. This table includes SDL (Steel Dead Load) and CDL (Concrete Dead Load) required for calculation of lack-of-fit forces under heading of "non-Composite" referring to the fact that these loads are applied when the concrete deck is absent or in wet condition.

Table 2.5- Load combinations according to AASHTO LRFD

Load Combination Limited State		Non-Composite		Composite					
		SDL	CDL	SDL + CDL (Composite)	DLBarrier	DW	LL	IM	Wind on Structure
Strength I	max	1.25	1.25	1.25	1.25	1.5	1.75	1.75	----
	min	0.9	0.9	0.9	0.9	0.65			
Strength I I	max	1.25	1.25	1.25	1.25	1.5	1.35	1.35	----
	min	0.9	0.9	0.9	0.9	0.65			
Strength I I I	max	1.25	1.25	1.25	1.25	1.5	----	----	1 (V=180 mph)
	min	0.9	0.9	0.9	0.9	0.65			
Strength I V	max	1.5	1.5	1.5	1.5	1.5	----	----	----
	min	0.9	0.9	0.9	0.9	0.65			
Strength V	max	1.25	1.25	1.25	1.25	1.5	1.35	1.35	1 (V=80 mph)
	min	0.9	0.9	0.9	0.9	0.65			
Extreme I						----	γ_{EQ}	γ_{EQ}	----
Extreme I I						----	0.5	0.5	----
Service I						1	1	1	1
Service I I						1	1.3	1.3	----
Service I I I						1	0.8	0.8	----
Service I V						1	----	----	----
Fatigue I (LL,IM & CE only)						----	1.75	1.75	----
Fatigue I I (LL,IM & CE only)						----	0.8	0.8	----

2.2.1.3 FE Modeling Information

As it was described earlier, because of modeling advantages, the MIDAS programs including Midas Civil and Midas FEA NX were selected for the Level I and Level II analyses respectively in the study. The FDOT project technical committee identified 26 bridges to be investigated for the

Level I analyses as the representative bridges. Therefore, 3D FEM models were developed and analyzed to determine the appropriate cross-frame internal forces based on AASHTO LRFD for designing the HRBS connections. In this section, Bridge 25 was selected to demonstrate the general modeling assumptions and to provide a representative model that was developed in the Midas Civil software. The structural configuration of the bridges are comprised of continuous composite steel I-girders interconnected by intermediate cross-frames and end cross-frames. The geometry of the different bridges varies including the number of spans, span length, number of girders, girder spacing, cross sections, skew angle, curvature and bearing details.

2.2.1.3.1 General Assumptions

2.2.1.3.1.1 Materials

Representative properties of the primary structural materials, steel and concrete, were used to model these bridges. Both materials were assumed to be linear elastic, which was deemed consistent with the observation that force distributions would not be significantly impacted by inelasticity with in-service conditions and therefore, the analysis is representative of the expected behavior. Based on the general information in the plans provided by the FDOT project technical committee, material properties consistent with ASTM A 709 GRADE 50 structural steel was used for the I-girders and cross-frame elements. Similarly, properties consistent with ASTM Grade C4500 concrete with minimum 28 days compressive strength $f_c' = 4500$ psi were utilized for concrete decks. The properties of these materials are shown in Table 2.6.

Table 2.6- Material properties

Material	**Standard**	**Strength** (ksi)	**Modulus of Elasticity** (kips/in^2)	**Poisson's Ratio**	**Weight Density** (kips/in^3)	**Damping Ratio**
Steel	ASTM A709-50	F_y=50	2.90 e+4	0.3	2.84 e-4	0.02
Concrete	ASTM Grade C4500	f'_c=4.5	3.86 e+3	0.2	8.68 e-5	0.05

2.2.1.3.1.2 Structural Elements

In this study, the modeling of all 26 bridges was conducted using Advanced 3D Finite Element Analysis (FEA) methods in Midas Civil Software, which were recommended based on the

literature review. The element library provided by Midas Civil encompasses a diverse range of element types, including truss elements, tension-only elements (Hook), cable elements, beam elements, plane stress elements, plate elements, two-dimensional plan strain elements, two-dimensional axisymmetric elements, and solid elements. In this study, as illustrated in Figure 2.17, all bridges were modeled using plate elements to accurately represent the concrete decks, top and bottom flanges, and the web of the steel I-girder. Additionally, beam elements were employed for the cross-frame members, encompassing the top and bottom chords along with diagonal members. The study also incorporated the specific cross-frame configurations as depicted in the Plans, which included various types of braces such as X-braces, V-braces, or inverted V-braces. To assess the structural response and stability of these bridges, a thorough linear static analysis was methodically carried out.

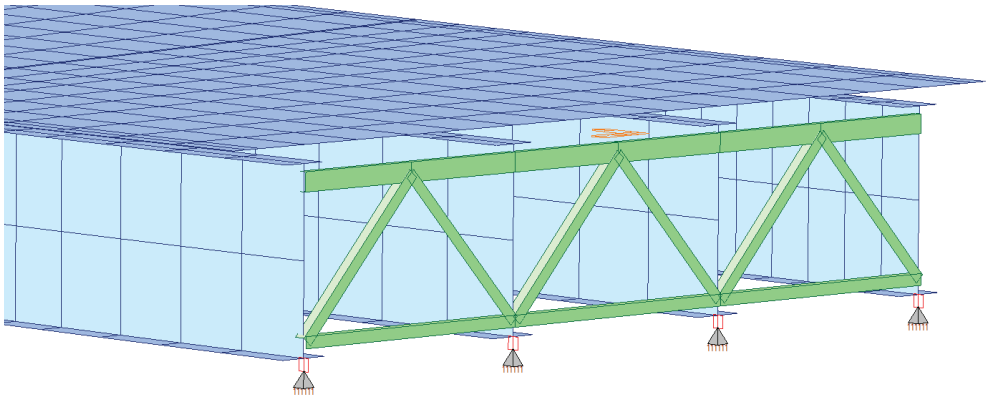

Figure 2.17- 3D FEM steel I-girder bridge model using plate and beam elements

In the development of the 3D models, careful consideration was given to the eccentricity effects on axial rigidity, as illuminated by the works of Wang et al. (2012) and the National Cooperative Highway Research Program Report No. 962 (NCHRP, 2021)[132]. This included cross-frames comprised of single angles, WT sections, or other sections causing eccentric loading at connections. These studies underscored the impact of end connection eccentricities on the axial rigidity of single-angle and flange-connected tee-section cross-frame members, leading to a reevaluation of stiffness parameters in bridge analysis. Consequently, modifications to the axial rigidity were incorporated into the models, adhering closely to the guidelines set forth in AASHTO LRFD [73] Article 4.6.3.3.4c and its associated commentary. In this context, the focus was primarily on the composite condition of the structures in service. An axial stiffness modification

factor of 0.75, as recommended for composite conditions, was uniformly applied to all relevant cross-frame members. This approach was selected based on the reasonable level of accuracy obtained from the previous studies the recommended modification factor for composite conditions, aligning with the specific requirements and characteristics of the bridges under consideration.

2.2.1.3.1.3 Dimensions and Quantities

For all bridges, the dimensions for span length, support skew angle, radius for curved bridges, deck width, girder spacing, deck thickness and haunch heights were taken into account in accordance with the plans as much as possible. The top 0.5 inch of the bridge deck slab thickness was considered sacrificial and included in the dead load of the deck slab but was not considered in the computation of the section properties of the slab or the composite section properties of the beams.

Additionally, the number of girders matched the number specified in the plans. These girders were assumed to be the same in terms of their cross-sections and lengths within each span. Detailed information on superstructure geometry, girder and support properties for each bridge used in the FE modeling are tabulated in Appendix A.

All these bridges were modeled with intermediate cross-frames and end cross-frames over piers and abutments. It is important to note that in some of the selected bridges, design drawings did not indicate any skewed cross-frames over the piers. Consequently, skewed cross-frame members were added, containing the exact same members as those in the cross-frames over the abutments in the specific bridges. For all cross-frames, the gaps between the top chord and top girder flange and between the bottom chord and bottom girder flange were considered based on the drawings. Furthermore, the number of intermediate cross-frames was the same as the number of cross-frame drawings outlined in the plans. However, in the Plans, the spacing between these intermediate cross-frames was often not uniform. This study operated under the assumption of equal spacing between these perpendicular intermediate cross-frames. This allowed the effective use of the software in accelerating the modeling. The small discrepancies

between the actual and simulated spacings will not significantly affect the internal forces of end cross-frames that is the focus of this study.

2.2.1.4 Loading

2.2.1.4.1 Static Loads

In this study, loads were applied to the bridge both during its construction phase and long-term. Accordingly, the AASHTO LRFD specification was utilized for the loading. The loadings can be categorized into two main groups: static loadings and moving loadings. Static loadings encompass the Steel Self weight Load, wet concrete load (during Construction), stay-in-place form load, Hardened Concrete Self Weight Load (long-term), traffic barrier loading, and wearing surface loading. For wind loading an equivalent static loading was used.

a) Steel Self Weight Load

In the Midas Civil program, Steel Self weight Load is computed by multiplying the volume of the steel element by its density, and it is then assigned to its actual location within the model.

b) Hardened Concrete Self Weight Load

In the Midas Civil program, Hardened Concrete Self Weight Load is computed by multiplying the volume of the hardened concrete element by its density, and it is then assigned to its actual location within the model, without the consideration of a 0.5-inch sacrifice surface.

c) Wet Concrete Load

In the Midas Civil program, this type of pressure load is determined by calculating the product of the wet concrete element's volume and its density, after which it is allocated to the top flange of the closest girder, taking into account the tributary area, with full thickness of the deck. Figure 2.18 through Figure 2.20, illustrates the loading method for the wet concrete load in Midas Civil program from different views.

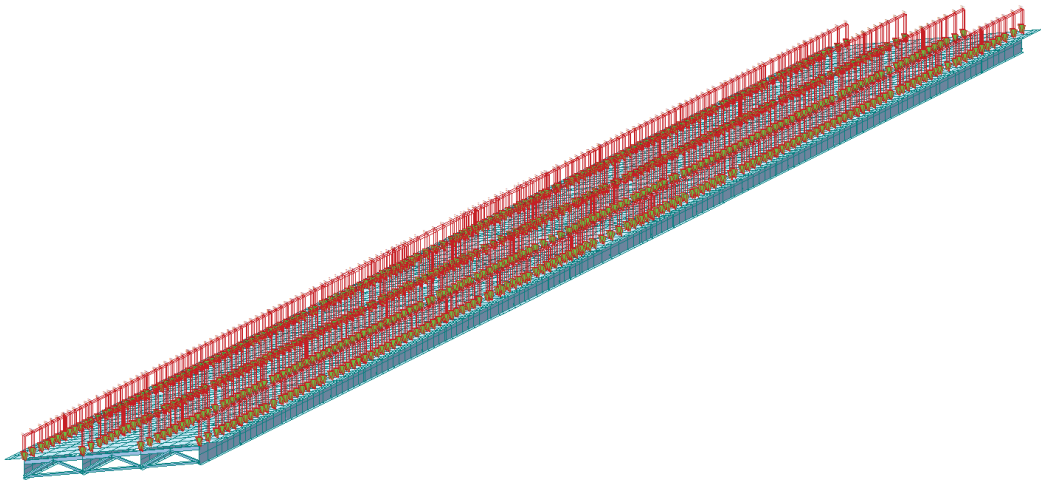

Figure 2.18- Wet concrete loading 3D view

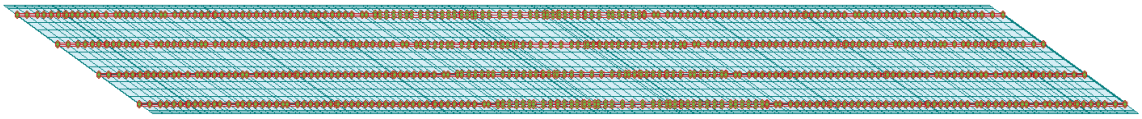

Figure 2.19- Wet concrete loading top view

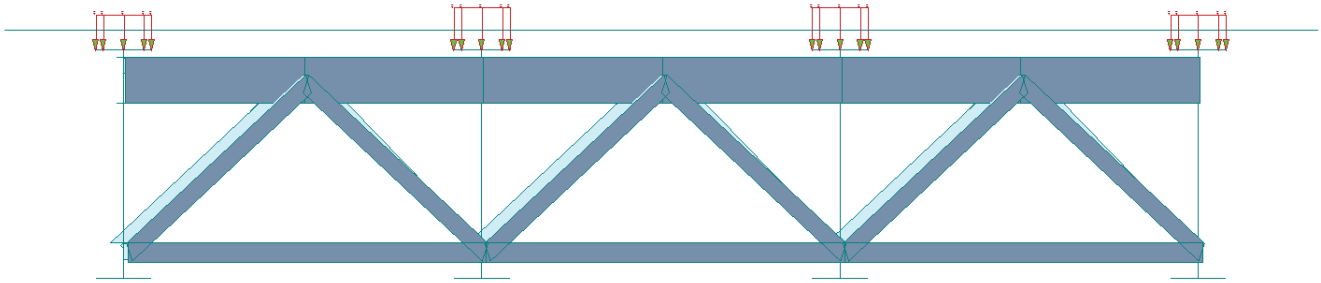

Figure 2.20- Wet concrete loading front view

d) Stay-in-Place Form Load

In the Midas Civil program, this type of load is considered as pressure load and is determined by calculating the product of 20 (psf) and the deck area (ft^2), after which it is allocated to the top

flange of the closest girder, taking into account the tributary area. The loading method for the Stay-in-Place Form load in the Midas Civil program is illustrated in Figure 2.21 through Figure 2.23.

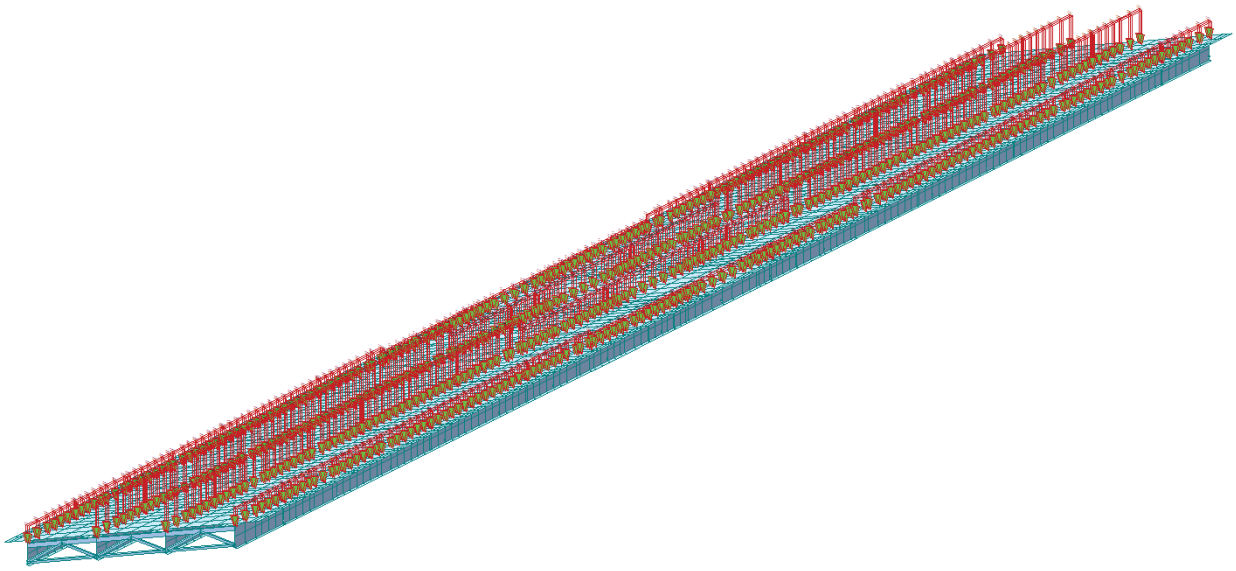

Figure 2.21- Stay-in-place form loading 3D view

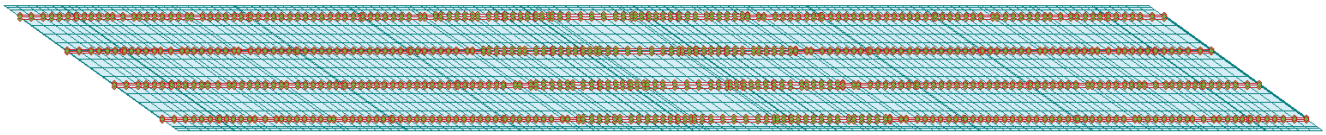

Figure 2.22- Stay-in-place form loading top view

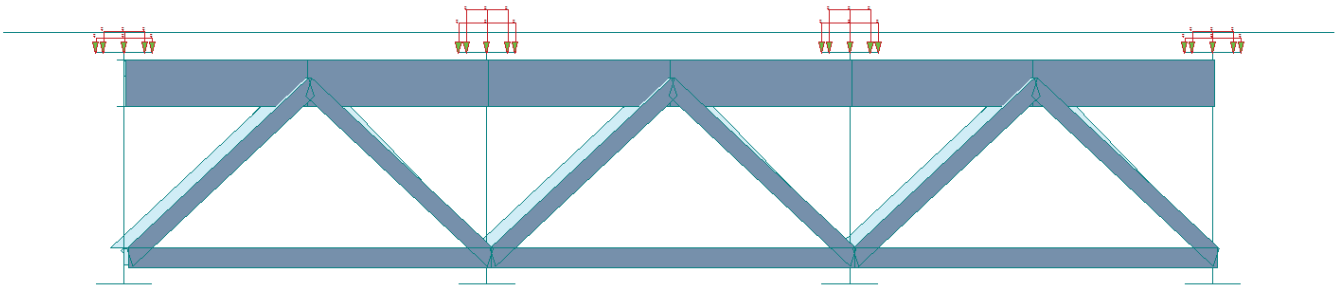

Figure 2.23- Stay-in-place form loading front view

e) Barrier Load

It was assumed that a 32" F-shaped barrier (Figure 2.24) was installed on both sides of the bridge. The determination of the Barrier Load was achieved by calculating the product of the volume of the 1-foot-long 32" F-shaped barrier and the concrete density, which was equal to 420 (plf). Subsequently, this load was allocated as a pressure load to two narrow bands on each side of the deck. Figure 2.25 through Figure 2.27, shows the loading method for the Barrier load in Midas Civil program from different views.

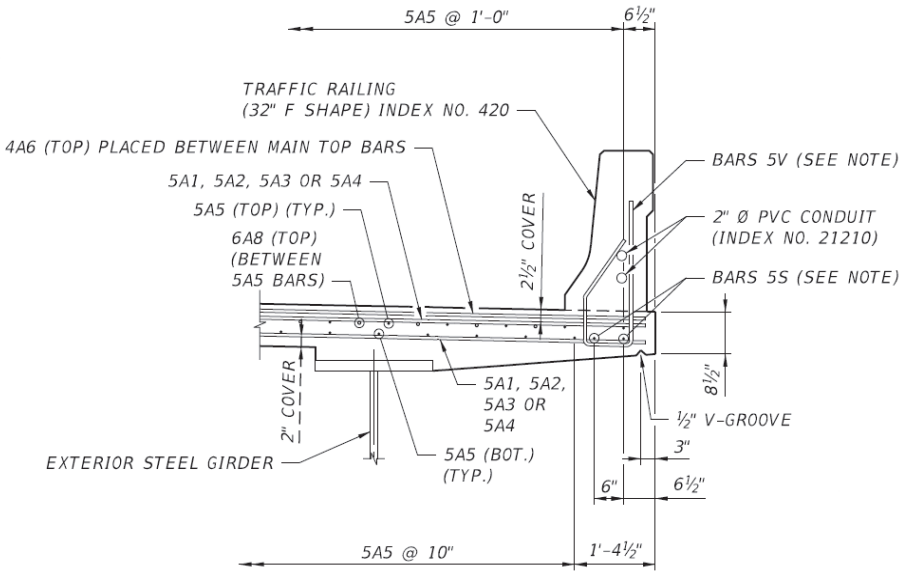

Figure 2.24- 32 inches F shape barrier

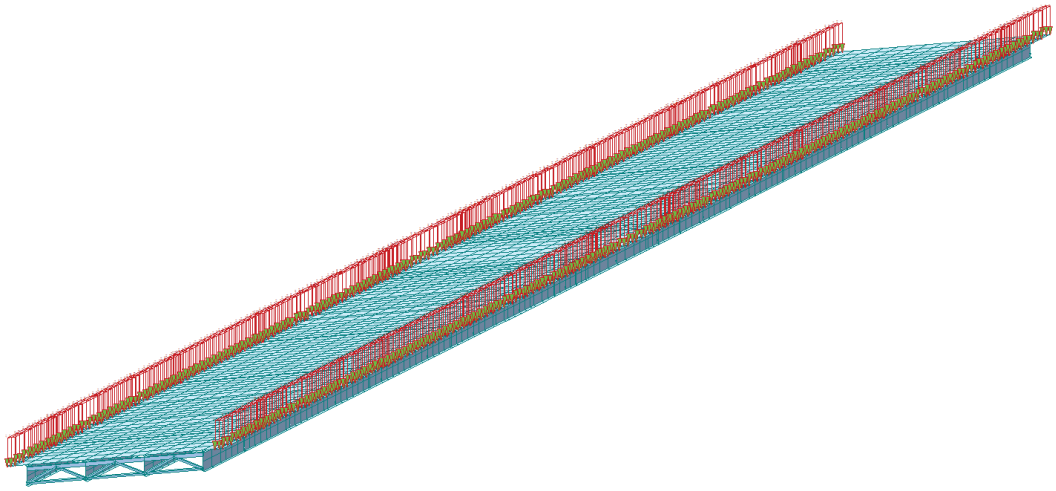

Figure 2.25- Barrier loading 3D view

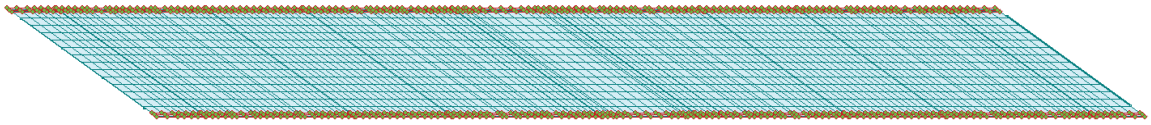

Figure 2.26- Barrier loading top view

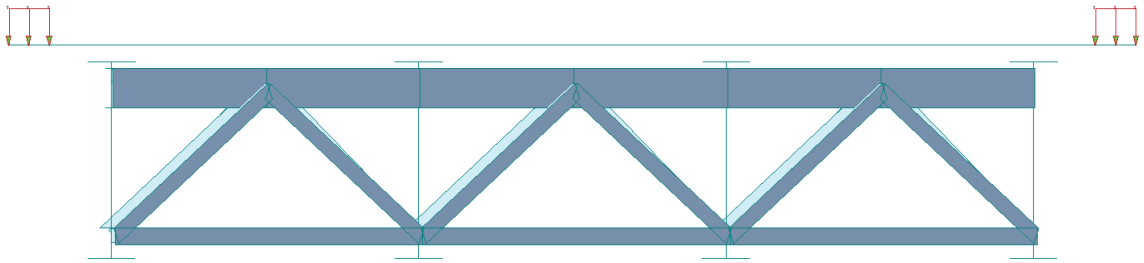

Figure 2.27- Barrier loading front view

f) Wind Load

The structural wind load is determined using the highest wind speed recorded in a 3-second gust. Per the Structures Design Guideline (SDG)[133], this peak 3-second gust speed in South Florida reaches 170 mph. In accordance with the Structures Design Guideline (SDG) [133], AASHTO LRFD's Category C, has been specifically adopted for the calculation of wind pressure. Therefore, the 3-sec gust wind speed for Strength III is considered 170 mph and for Strength V, 80 mph resulting in 82 psf and 21.3 psf static pressure, respectively, calculated using the AASHTO LRFD 3.8.1.2.1 equation to be applied to the side profile of the bridge, including the exterior girder, deck, and barrier. This loading is applied as an equivalent static pressure load to the web plate of the exterior girder from one side of the bridge. In this study, for calculation of the loading, the height of the side barrier was added to the exterior girder.

2.2.1.4.2 Moving Loads

One of the primary types of loads that a bridge experiences throughout its operational lifespan is live loads or moving loads. The loadings specified in the AASHTO LRFD guidelines including HL-93 loading and HS-20 Fatigue loading have been utilized.

2.2.1.4.2.1 HL-93 Loading

HL-93 loading represents the live load as outlined in AASHTO LRFD §3.6.1.2. This load comprises of a design truck or design tandem in addition to a design lane load of 0.64 k/ft. The specifications for the design truck and design tandem are detailed as follows.

Table 2.7- Design wind speed, V [133]

County (Dist)	Design Wind Speed (mph)	County (Dist)	Design Wind Speed (mph)	County (Dist)	Design Wind Speed (mph)
Alachua (2)	130	Hardee (1)	150	Okaloosa (3)	150
Baker (2)	130	Hendry (1)	150	Okeechobee (1)	150
Bay (3)	150	Hernando (7)	150	Orange (5)	150
Bradford (2)	130	Highlands (1)	150	Osceola (5)	150
Brevard (5)	170	Hillsborough (7)	150	Palm Beach (4)	170
Broward (4)	170	Holmes (3)	150	Pasco (7)	150
Calhoun (3)	130	Indian River (4)	170	Pinellas (7)	150
Charlotte (1)	170	Jackson (3)	130	Polk (1)	150
Citrus (7)	150	Jefferson (3)	130	Putnam (2)	130
Clay (2)	130	Lafayette (2)	130	St. Johns (2)	150
Collier (1)	170	Lake (5)	150	St. Lucie (4)	170
Columbia (2)	130	Lee (1)	170	Santa Rosa (3)	150
DeSoto (1)	150	Leon (3)	130	Sarasota (1)	170
Dixie (2)	130	Levy (2)	150	Seminole (5)	150
Duval (2)	130	Liberty (3)	130	Sumter (5)	150
Escambia (3)	170	Madison (2)	130	Suwannee (2)	130
Flagler (5)	150	Manatee (1)	150	Taylor (2)	130
Franklin (3)	150	Marion (5)	150	Union (2)	130
Gadsden (3)	130	Martin (4)	170	Volusia (5)	150
Gilchrist (2)	130	Miami-Dade (6)	170	Wakulla (3)	130
Glades (1)	150	Monroe (6)	170	Walton (3)	150
Gulf (3)	150	Monroe Islands (6)[1]	180	Washington (3)	150
Hamilton (2)	130	Nassau (2)	130		

1 For non-bridge structures use 170 mph or as modified by Vol. 3

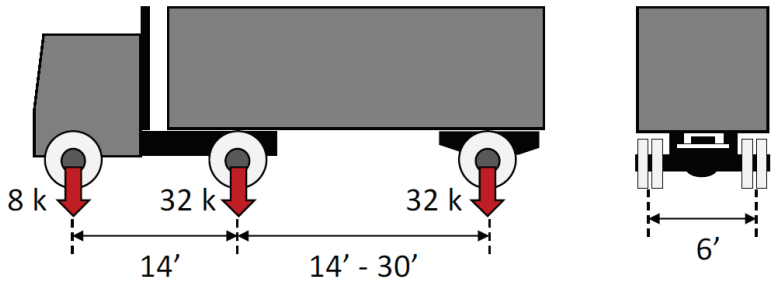

Figure 2.28- HS-20 desgin truck load

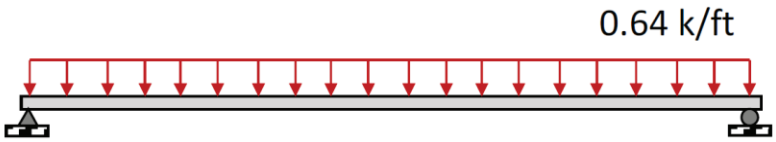

Figure 2.29- Design lane load

There are three primary methods by which the combination of the design truck, tandem, and lane load can be performed. In the first case, the effect of the design tandem and lane load together has been considered (Figure 2.30). In the second case, the effect of one design truck with the variable axle spacing, as specified in Article 3.6.1.2.2 (ranging from 14 to 30 ft), has been combined with the effect of the design lane load (Figure 2.31). In the final case, for negative moment between points of contraflexure under a uniform load on all spans, and reaction at interior piers only, 90 percentage of the effect of two design trucks spaced a minimum of 50 ft between the lead axle of one truck and the rear axle of the other truck, combined with 90 percentage of the effect of the design lane load. The 32-kip axles of each truck shall be placed in adjacent spans so that to produce maximum force effects (Figure 2.32).

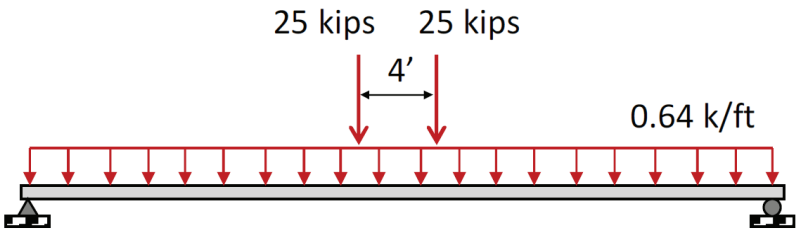

Figure 2.30- Design tandem and lane load (Case 1)

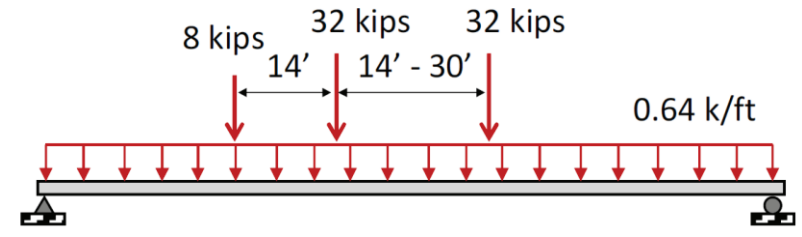

Figure 2.31- Design truck and lane load (Case 2)

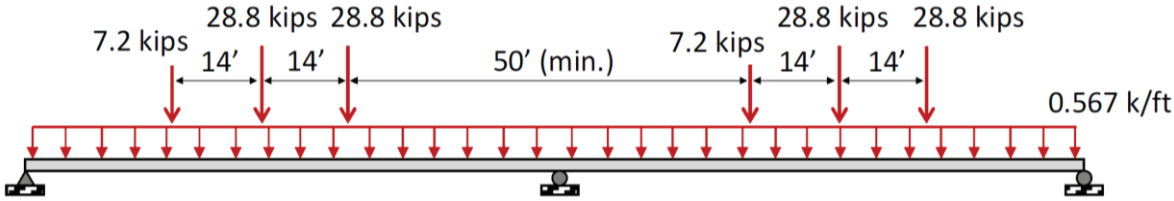

Figure 2.32- 90 percent of two design trucks and lane load (Case 3)

To account for the vertical accelerations made by unsmooth road surfaces, a dynamic load allowance factor of 33 percent has been considered for all these cases based on AASHTO LRFD 3.6.2.1.

The analysis also considered the possible combinations of the number of lanes loaded. To account for the probability of the multiple presence of heavy trucks simultaneously on the bridge and in adjacent lanes, the Multiple Presence Factor based on AASHTO LRFD article 3.6.1.1.2 was used (Table 2.8).

Table 2.8- Multiple presence factors table (AASHTO LRFD 3.6.1.1.2)

# of Loaded Lanes	Multiple Presence Factors, *m*
1	1.20
2	1.00
3	0.85
> 3	0.65

2.2.1.4.2.2 Fatigue Load

Variation of tensile stress under live loading is the main precursor for the fatigue concern for the top flange of a girder at the negative moment region over an intermediate pier as well as design of cross-frame connections at this location. While for Strength 1 design as per the AASHTO LRFD [73], loading consisting of multiple trucks on either side of the negative moment region and in multiple lanes is required. However, fatigue design focuses on the repetitive cycles of stress that occur throughout the service life of the bridge. For the purposes of evaluating the design stress range of specific components of the bridge, AASHTO LRFD considers the corresponding stress change from the passage of a single design fatigue truck. The AASHTO identifies the fatigue truck as an HS20 truck with a total weight of 72 kips distributed over three axles (Figure 2.28). The first axle carries 8 kips and the other two carry 32 kips each. The spacing between the first and second axles is 14 ft and the spacing between the second and third axles is 30 ft. The truck is positioned to cause the worst stress range in the girder from the passage over the bridge in a fixed transverse position. This position is not based upon striped lanes but the position that creates the most critical results. Normally, for the girder stress, the worst case would be for the truck centered over the girder line since that girder would see the largest portion of the truck load.

According to Section 3.4.1 of the AASHTO LRFD Bridge Design Specifications, it is required that the stresses obtained from fatigue truck loading be multiplied by a factor of 1.75 for Fatigue I, which pertains to the combination of fatigue and fracture loads related to infinite load-induced fatigue life, and a factor of 0.8 for Fatigue II, which relates to the combination of fatigue and fracture loads related to finite load-induced fatigue life. Furthermore, to design for fatigue stress range, it is necessary to take into account the Dynamic Load Allowance (IM) multiplier, which is equal to 1.15.

2.2.1.5 Level I Analysis Results for Bridge 25

For the first attempt, Bridge 25 was modeled and analyzed with the details described above and for the various load combinations. The results were analyzed and communicated with research

team (FDOT and FIU) to establish all modelling parameters and assumptions before undertaking the analysis of all bridges in the bridge matrix.

The results are included in Table 2.9 through Table 2.11. As noted in these tables, the abutment and pier end cross-frame member forces calculated for lack-of-fit case are negligible when compared to other load combinations. The cross-frame member forces from fatigue loading are also considerably lower than forces from other load combinations. For reference, positive force values indicate tension while negative values denote compression.

Table 2.9- Axial forces for abutment and pier end cross-frame members for Bridge 25 and unfactored loadings

		LOAD	SDL	(CDL + SDL) Non-Composite Stage	(CDL + SDL) Composite Stage	Barrier	Live Load (TRK & TDM)	Wind (V=170mph) (STR III)	Wind (V=80mph) (STR V)
Element			(kips)	(kips)	(kips)	(kips)	(kips)	(kips)	(kips)
Pier End Cross-frame	Top Chord	max	0.19	-0.94	0.23	2.36	18.88	55.00	10.86
		min	-0.61	-3.22	-2.30	-0.08	-5.43	-53.73	-10.61
	Diagonal	max	-1.09	-3.01	-2.48	0.70	8.96	59.77	11.80
		min	-2.08	-5.06	-5.40	-0.37	-10.78	-62.08	-12.26
	Bot Chord	max	1.44	4.85	5.47	-0.21	17.26	15.22	3.01
		min	0.78	3.29	3.71	-0.75	-5.01	-28.65	-5.66
Abutment End Cross-frame	Top Chord	max	0.70	1.86	2.95	0.15	12.71	31.46	6.21
		min	0.00	0.00	-2.07	-5.96	-8.45	-25.06	-4.95
	Diagonal	max	-0.69	-1.01	-2.36	2.33	8.05	69.39	13.70
		min	-1.71	-3.22	-5.50	-0.54	-18.10	-64.86	-12.81
	Bot Chord	max	1.11	2.50	3.46	-1.59	18.80	19.17	3.79
		min	0.49	1.03	1.98	-2.06	-3.56	-19.99	-3.95

Table 2.10- Axial forces for abutment and pier end cross-frame members for Bridge 25 and factored loadings

Element		FACTORED LOAD	1.25 X SDL	1.25 X (CDL + SDL) Non-Composite Stage	1.25 X (CDL + SDL) Composite Stage	1.25 X Barrier	1.75 X Live Load (TRK & TDM)	Wind (V=170mph) (STR III)	Wind (V=80mph) (STR V)
			(kips)	(kips)	(kips)	(kips)	(kips)	(kips)	(kips)
Pier End Cross-frame	Top Chord	max	0.2	-1.2	0.3	3.0	33.0	55.0	10.86
		min	-0.8	-4.0	-2.9	-0.1	-9.5	-53.7	-10.61
	Diagonal	max	-1.4	-3.8	-3.1	0.9	15.7	59.8	11.80
		min	-2.6	-6.3	-6.8	-0.5	-18.9	-62.1	-12.26
	Bot Chord	max	1.8	6.1	6.8	-0.3	30.2	15.2	3.01
		min	1.0	4.1	4.6	-0.9	-8.8	-28.7	-5.66
Abutment End Cross-frame	Top Chord	max	0.9	2.3	3.7	0.2	22.2	31.5	6.21
		min	0.0	0.0	-2.6	-7.5	-14.8	-25.1	-4.95
	Diagonal	max	-0.9	-1.3	-2.9	2.9	14.1	69.4	13.70
		min	-2.1	-4.0	-6.9	-0.7	-31.7	-64.9	-12.81
	Bot Chord	max	1.4	3.1	4.3	-2.0	32.9	19.2	3.79
		min	0.6	1.3	2.5	-2.6	-6.2	-20.0	-3.95

Table 2.11- Axial forces for abutment and pier end cross-frame members for Bridge 25 and factored load combinations and stability

Element		FACTORED LOAD COMBOS	1.25 X (CDL + SDL) Non-Composite Stage	Strength I	Strength II	Strength III	Strength IV	Strength V	Stability	Envelope
			(kips)	(kips)	(kips)	(kips)	(kips)	(kips)	(kips)	(kips)
Pier End Cross-frame	Top Chord	max	-1.2	31.4	23.9	34.6	3.1	33.3	6.6	34.6
		min	-4.0	-9.6	-7.5	-37.2	-1.8	-18.0	-6.6	-37.2
	Diagonal	max	-3.8	10.0	6.4	33.7	-4.0	16.6	---	33.7
		min	-6.3	-21.3	-17.0	-43.4	-4.5	-32.0	---	-43.4
	Bot Chord	max	6.1	34.5	27.6	16.3	7.4	26.9	6.6	34.5
		min	4.1	-5.3	-3.5	-14.6	2.8	-9.4	-6.6	-14.6
Abutment End Cross-frame	Top Chord	max	2.3	26.1	21.0	23.3	4.6	26.1	6.6	26.1
		min	0.0	-13.8	-10.6	-16.7	-7.2	-16.6	-6.6	-16.7
	Diagonal	max	-1.3	6.7	4.5	38.4	-1.1	15.4	---	38.4
		min	-4.0	-35.0	-27.9	-43.5	-5.4	-44.1	---	-44.1
	Bot Chord	max	3.1	32.8	25.3	14.6	2.2	26.0	6.6	32.8
		min	1.3	-6.3	-4.9	-12.7	-0.10	-9.1	-6.6	-12.7

As per AASHTO LRFD Article 6.13 on connection design, when cross-frames are part of the structural model for straight or horizontally curved bridges, end connections for these bracing members shall be designed for the calculated factored member force effects.

2.2.1.6 Level I Results for All Bridges

Table 2.12 and Table 2.13 provide the results for axial forces for skewed cross-frame members under two distinct loadings: the Design Envelope and the Fatigue I Envelope forces. Table 2.13 also shows the top flange stress range over the intermediate supports for the Fatigue I Envelope. Envelope forces in bridge engineering encompass the comprehensive range of forces and moments that a bridge structure is anticipated to endure throughout its operational life. These forces cover the envelope of forces from different Strength Limit States calculated for each bridge. Designing for the envelopes ensures that the bridge can withstand its intended loads. The histogram for "Top Flange Fatigue Stress Range" (Figure 2.33) shows that its range is between 1.24 to 3.57 ksi, while the average is 2.34 ksi. Figure 2.34 through Figure 2.36 show the histograms for cross-frame member forces for top chords, diagonal members, and bottom chords of the end cross-frames, respectively.

Table 2.12- Axial forces in end cross-frame members for design envelope effect

#	Alternative Bridge #	DESIGN Envelope ---- Axial FORCE (kips)					
		TOP CHORD		DIAGONAL		BOT CHORD	
		min	max	min	max	min	max
1	**64**	-21.7	40.5	-31.6	22.3	-8.3	41.9
2	**9**	-30.8	44.2	-43.7	29.2	-18.0	62.8
3	**65**	-9.9	29.9	-23.5	13.0	-17.2	26.2
4	**66**	-12.6	22.3	-24.3	25.0	-32.5	36.6
5	**67**	-15.9	24.1	-25.6	29.6	-32.3	54.3
6	**68**	-25.7	30.0	-52.3	60.7	-32.9	70.4
7	**69**	-34.0	25.2	-95.7	103.4	-91.6	84.6
8	**71**	-16.5	31.1	-30.9	38.1	-20.1	50.8
9	**72**	-64.2	68.4	-110.0	102.0	-155.6	145.9
10	**70**	-21.4	27.7	-73.2	65.9	-16.1	50.5
11	**13**	-35.9	30.7	-57.2	60.5	-69.9	117.9
12	**15**	-80.7	36.0	-46.8	40.9	-26.9	64.4
13	**44**	-12.1	25.7	-24.6	16.6	-25.1	36.3
14	**43**	-43.4	34.9	-47.7	41.3	-12.6	27.8
15	**41**	-46.0	37.1	-66.8	66.1	-27.5	74.9
16	**60**	-29.9	28.2	-39.9	21.5	-7.1	32.9
17	**45**	-49.8	39.5	-35.3	32.7	-13.9	50.1
18	**42**	-30.8	40.4	-37.6	35.3	-12.8	50.0
19	**8**	-17.5	32.3	-38.8	8.9	-9.8	25.3
20	**46**	-17.6	28.8	-30.4	18.1	-5.5	15.1
21	**61**	-20.3	27.9	-30.7	13.7	-18.0	41.1
22	**24**	-14.1	34.0	-24.4	13.7	-9.8	24.3
23	**25**	-37.2	34.6	-44.7	40.6	-14.6	34.5
24	**62**	-27.8	11.7	-32.9	16.6	-6.4	26.0
25	**63**	-26.1	30.1	-24.2	14.6	-16.4	25.3
26	**12**	-36.3	30.3	-33.1	27.2	-13.6	38.1

Table 2.13- Axial forces in end cross-frame members and maximum top flange stress range for Fatigue I effect

#	Alternative Bridge #	FATIGUE I Envelope--- Axial Force (kips)						Maximum Top Flange FATIGUE Stress Range (ksi)
		TOP CHORD		DIAGONAL		BOT CHORD		
		min	max	min	max	min	max	
1	**64**	-7.6	14.0	-15.8	4.7	-8.8	10.5	2.24
2	**9**	-8.9	10.3	-19.5	8.3	-11.5	18.0	1.24
3	**65**	-4.5	16.2	-8.0	4.9	-4.4	26.2	1.53
4	**66**	-6.8	15.9	-6.0	5.6	-17.4	14.5	1.67
5	**67**	-9.5	19.6	-5.7	5.7	-10.7	12.4	1.94
6	**68**	-8.5	16.2	-6.0	6.1	-17.4	25.6	2.92
7	**69**	-18.6	12.7	-12.5	9.1	-32.1	36.5	3.57
8	**71**	-4.8	17.1	-3.8	3.8	-11.4	13.9	3.17
9	**72**	-6.6	12.6	-20.3	6.3	-25.1	36.1	2.85
10	**70**	-6.5	7.7	-10.3	9.8	-13.7	21.1	3.17
11	**13**	-11.7	20.8	-12.8	12.2	-22.3	27.5	1.86
12	**15**	-7.1	16.1	-20.2	4.9	-9.2	16.1	2.27
13	**44**	-6.2	18.8	-9.0	6.6	-8.9	13.2	2.27
14	**43**	-7.6	14.2	-26.1	7.8	-9.4	20.9	2.43
15	**41**	-4.6	8.5	-24.5	7.4	-18.1	23.4	2.34
16	**60**	-6.3	17.0	-15.3	2.9	-5.2	12.4	1.76
17	**45**	-5.2	9.2	-14.7	5.1	-7.1	8.8	1.91
18	**42**	-6.0	11.5	-12.6	4.0	-8.8	9.9	1.42
19	**8**	-8.3	13.4	-13.8	5.5	-2.9	10.9	2.03
20	**46**	-5.8	11.9	-11.7	3.0	-2.1	7.2	2.47
21	**61**	-7.0	11.0	-14.2	5.2	-11.2	12.0	2.38
22	**24**	-5.1	8.9	-15.5	4.1	-4.3	8.8	1.52
23	**25**	-9.4	11.0	-16.9	7.1	-8.8	13.8	3.07
24	**62**	-13.0	10.0	-11.0	3.6	-8.9	12.5	3.44
25	**63**	-9.7	10.4	-11.3	4.6	-8.2	9.0	2.68
26	**12**	-7.7	9.7	-12.4	10.3	-13.2	16.9	2.78

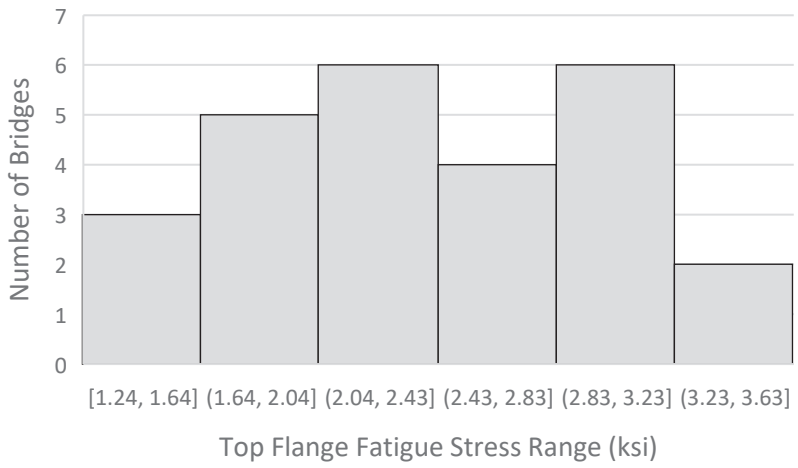

Figure 2.33- Histogram for top flange fatigue stress range (ksi)

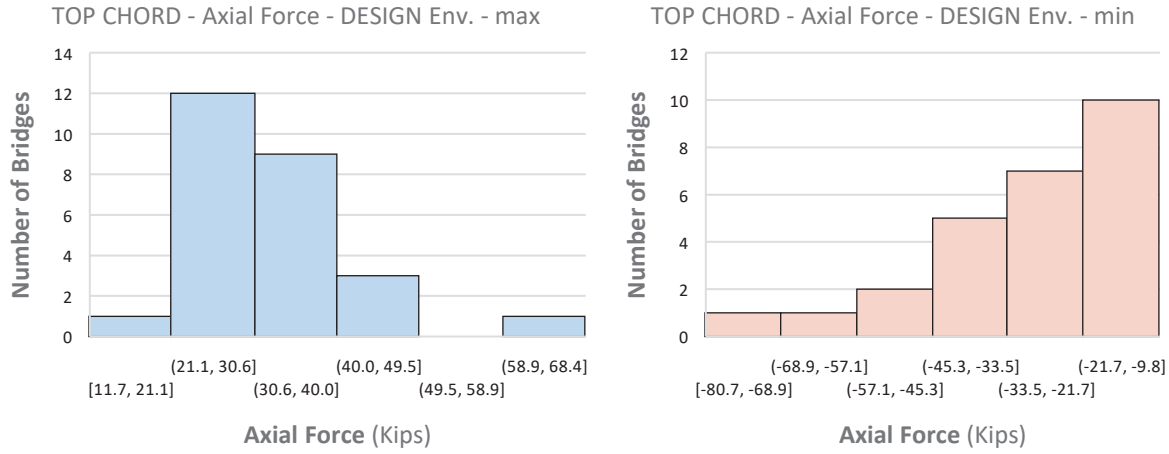

Figure 2.34- Histogram for maximum tensile and compressive axial force distribution in top chord elements for design envelope

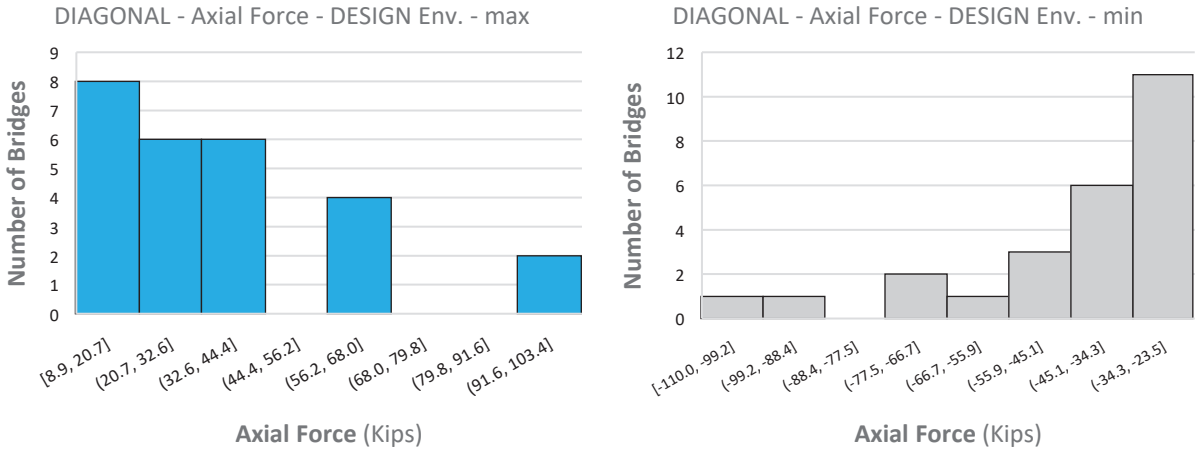

Figure 2.35- Histogram for maximum tensile and compressive axial force distribution in diagonal elements for design envelope

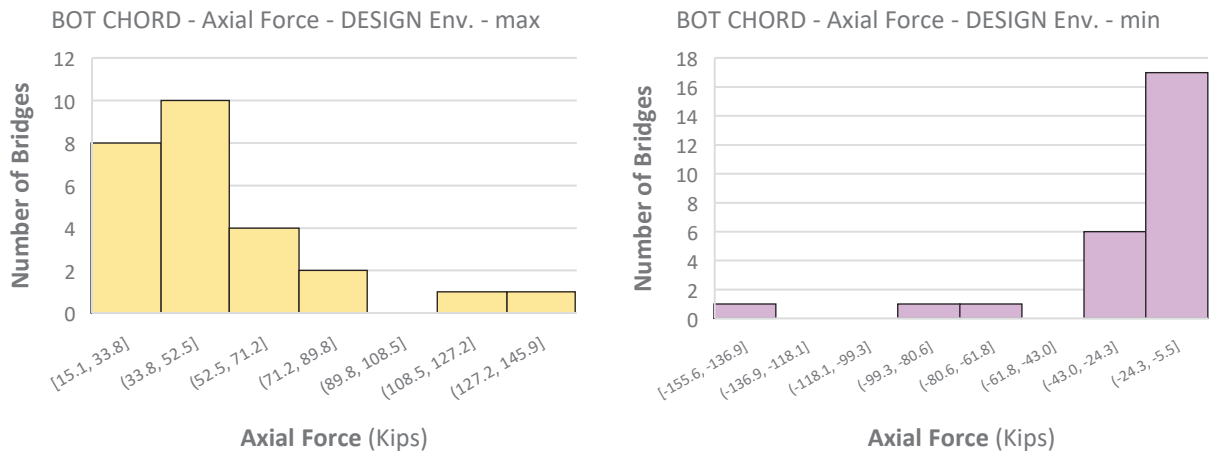

Figure 2.36- Histogram for maximum tensile and compressive axial force distribution in bottom chord elements for design envelope

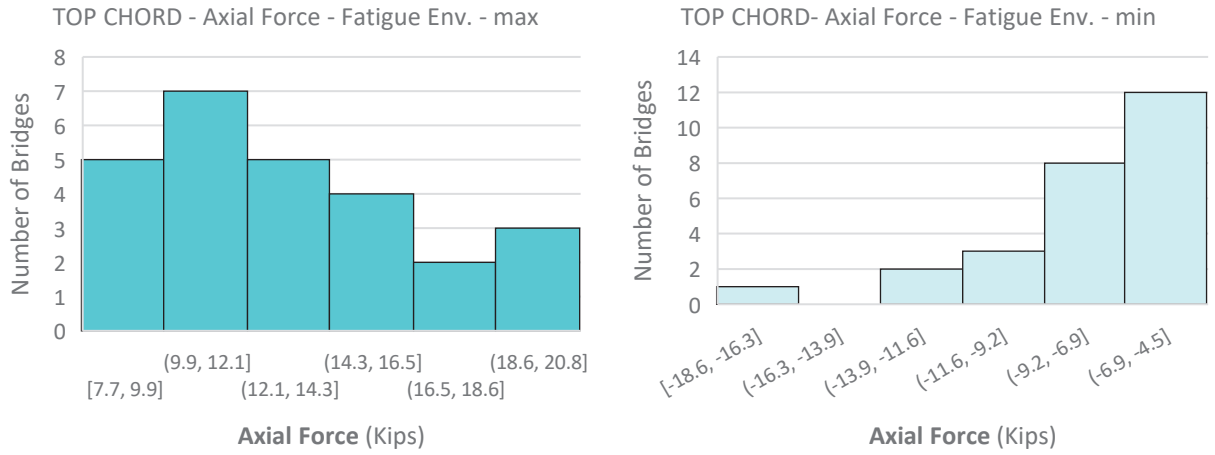

Figure 2.37- Histogram for maximum tensile and compressive axial force distribution in top chord elements for fatigue envelope

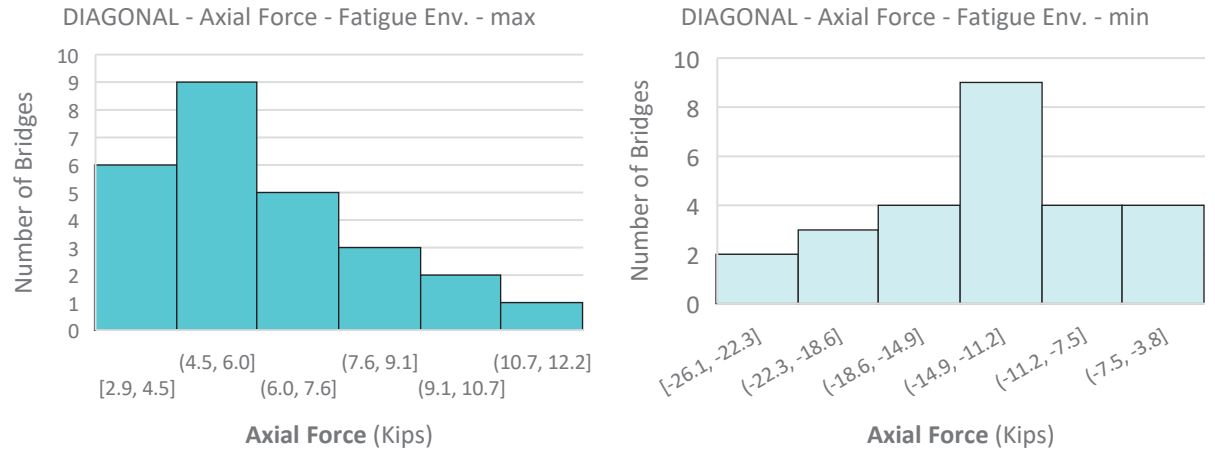

Figure 2.38- Histogram for maximum tensile and compressive axial force distribution in diagonal elements for fatigue envelope

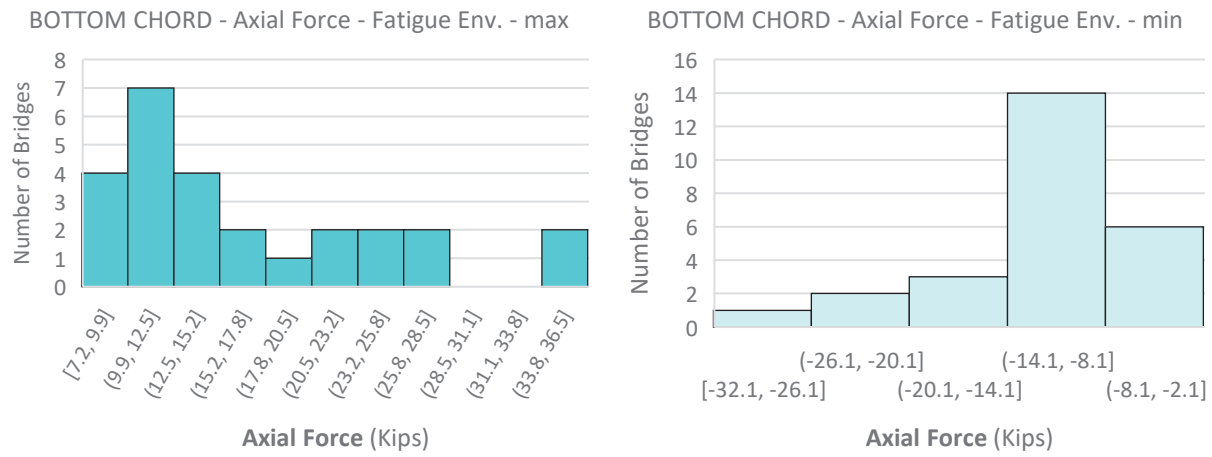

Figure 2.39- Histogram for maximum tensile and compressive axial force distribution in bottom chord elements for fatigue envelope

2.2.2 Representative Bridge Selection

The primary objective of the analyses is to select representative bridges that provide a good representation of the characteristics of all 26 bridges. The overall characteristics of these bridges are defined mostly based on their geometry configurations. The parameters considered here for selecting the representative bridges are Skew index, cross-frame member forces, steel I-girder moment of Inertia and the bridge curvature. These parameters encompass key aspects of bridges' performance and properties.

a) Skew Index (I_S)
b) Cross-frame Member Forces
c) I-Girder's Moment of Inertia
d) Curvature (L/R)- curvature parameter was addressed at the end by including both straight and curved options.

To achieve this goal, a systematic approach was followed. The bridges are sorted based on each parameter, arranging them in ascending order with respect to that parameter, and subsequently categorizing them into three distinct groups (Figure 2.40). In this classification scheme, Group 1 comprises bridges with lower parameter values, Group 2 encompasses those falling within the intermediate range, and Group 3 includes bridges with higher parameter values.

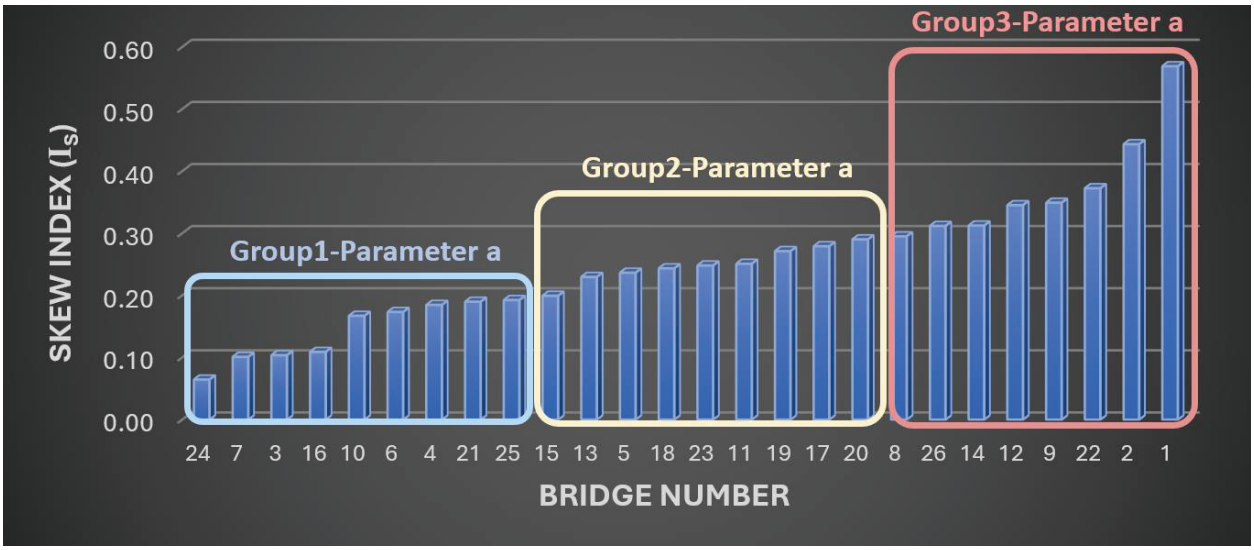

Figure 2.40- Categorizing the sorted bridges based on Skew Index (I_s)

This process is repeated for all the selected parameters. Ultimately, the aim of the study is to identify a bridge that is common to each group, for all the parameters.

Figure 2.41 below shows bridges sorted for the skew index and the three groups with respect to the skew index.

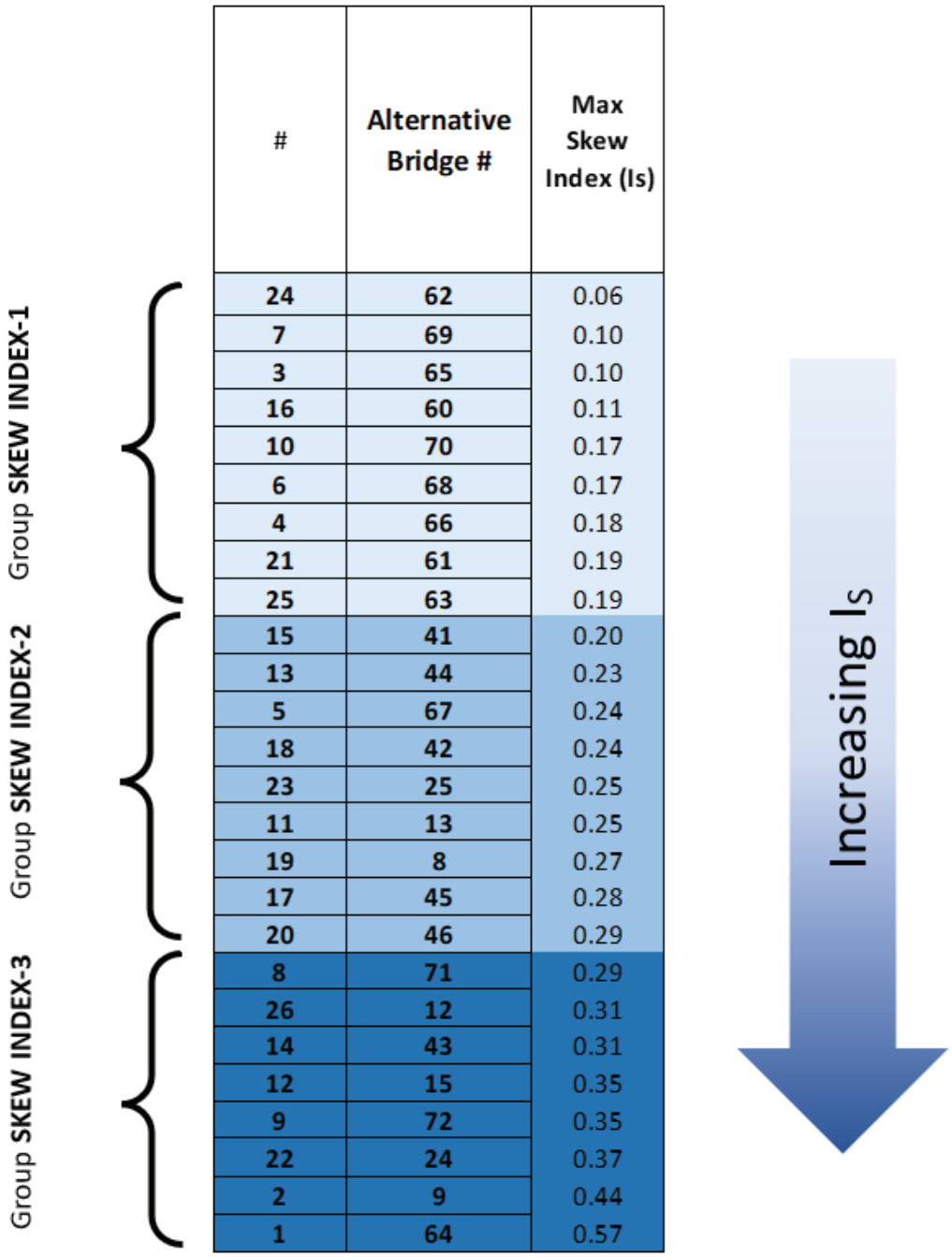

#	Alternative Bridge #	Max Skew Index (Is)
24	62	0.06
7	69	0.10
3	65	0.10
16	60	0.11
10	70	0.17
6	68	0.17
4	66	0.18
21	61	0.19
25	63	0.19
15	41	0.20
13	44	0.23
5	67	0.24
18	42	0.24
23	25	0.25
11	13	0.25
19	8	0.27
17	45	0.28
20	46	0.29
8	71	0.29
26	12	0.31
14	43	0.31
12	15	0.35
9	72	0.35
22	24	0.37
2	9	0.44
1	64	0.57

Figure 2.41- Bridges sorted for skew index and grouping

Figure 2.42 below provides a tabulation of bridges sorted for end cross-frame member forces and the bridges are divided into three groups with that respect. The bridges are sorted with respect to the bottom chord forces.

	#	Alternative Bridge #	DESIGN Envelope ---- Axial FORCE (kips)					
			TOP CHORD		DIAGONAL		BOT CHORD	
			min	max	min	max	min	max
Group FORCE-1	20	46	-17.6	28.8	-30.4	18.1	-5.5	15.1
	22	24	-14.1	34.0	-24.4	13.7	-9.8	24.3
	25	63	-26.1	30.1	-24.2	14.6	-16.4	25.3
	19	8	-17.5	32.3	-38.8	8.9	-9.8	25.3
	24	62	-27.8	11.7	-32.9	16.6	-6.4	26.0
	3	65	-9.9	29.9	-23.5	13.0	-17.2	26.2
	14	43	-43.4	34.9	-47.7	41.3	-12.6	27.8
	16	60	-29.9	28.2	-39.9	21.5	-7.1	32.9
Group FORCE-2	23	25	-37.2	34.6	-44.7	40.6	-14.6	34.5
	13	44	-12.1	25.7	-24.6	16.6	-25.1	36.3
	4	66	-12.6	22.3	-24.3	25.0	-32.5	36.6
	26	12	-36.3	30.3	-33.1	27.2	-13.6	38.1
	21	61	-20.3	27.9	-30.7	13.7	-18.0	41.1
	1	64	-21.7	40.5	-31.6	22.3	-8.3	41.9
	18	42	-30.8	40.4	-37.6	35.3	-12.8	50.0
	17	45	-49.8	39.5	-35.3	32.7	-13.9	50.1
	10	70	-21.4	27.7	-73.2	65.9	-16.1	50.5
Group FORCE-3	8	71	-16.5	31.1	-30.9	38.1	-20.1	50.8
	5	67	-15.9	24.1	-25.6	29.6	-32.3	54.3
	2	9	-30.8	44.2	-43.7	29.2	-18.0	62.8
	12	15	-80.7	36.0	-46.8	40.9	-26.9	64.4
	6	68	-25.7	30.0	-52.3	60.7	-32.9	70.4
	15	41	-46.0	37.1	-66.8	66.1	-27.5	74.9
	7	69	-34.0	25.2	-95.7	103.4	-91.6	84.6
	11	13	-35.9	30.7	-57.2	60.5	-69.9	117.9
	9	72	-64.2	68.4	-110.0	102.0	-155.6	145.9

Increasing Bottom Chord Forces

Figure 2.42- Bridges sorted for end cross-frame member forces and grouping

Figure 2.43**Error! Reference source not found.** below shows bridges sorted for girders' moment of inertia and the three groups with that respect.

	#	Alternative Bridge #	Moment of Inertia (in^4.)
Group **M-INERTIA-1**	**3**	**65**	87482
	25	**63**	120383
	22	**24**	124739
	13	**44**	125121
	26	**12**	146569
	8	**71**	148616
	24	**62**	165927
	19	**8**	172129
Group **M-INERTIA-2**	**1**	**64**	175633
	6	**68**	193652
	2	**9**	194282
	14	**43**	247481
	10	**70**	254693
	16	**60**	258549
	23	**25**	285765
	21	**61**	302493
	20	**46**	360252
Group **M-INERTIA-3**	**5**	**67**	383969
	12	**15**	420383
	9	**72**	437652
	17	**45**	462049
	11	**13**	462635
	4	**66**	463520
	18	**42**	535552
	7	**69**	559878
	15	**41**	800755

Increasing Moment of Inertia

Figure 2.43- Bridges sorted for girders' moment of inertia and grouping

After grouping of the bridges with respect to skew index, cross-frame member forces, and girders moment of inertia, VENN DIAGRAMS was used to find individual bridges that are common in each group for the three parameters considered. As it can be seen in Figure 2.44, for the bridges with

lower parameter values, Bridge 65 was identified as a representative candidate for the group. For bridges with intermediate range of parameters, Bridge 25 is a candidate representative of the group, and for bridges with higher parameter values, Bridge 72 is a candidate representative of the group. Also, these selected bridges have a variety based on curvature because they represent both curve and straight bridges. For example, Bridge 25 and 65 are straight bridges and Bridge 72 has a significant degree of horizontal curvature. To assure that the "group representative bridge" covers all bridges in its group, each representative connection was sized for the highest level of forces in the respective group.

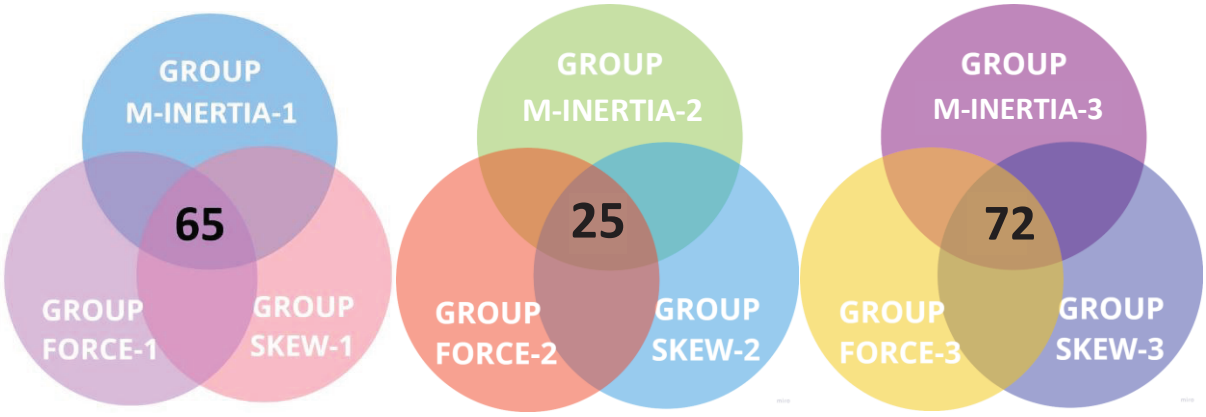

Figure 2.44- Venn diagram for finding the representative bridges considering key parameters

A review of cross-frame member fatigue forces reveals that there is no strong correlation between these forces and the envelope of cross-frame member design forces.

In summary, the major parameters for these representative bridges are shown in the following table.

Table 2.14- The major parameters for the representative bridges for Level II analysis

#	Alternative Bridge #	Max Skew Index (Is)	Cross-frame Member Forces						I-Girder's Moment of Inertia (in.^{4})	I-Girder's Height (in.)	Curvature (L/R)	
			TOP CHORD		DIAGONAL		BOT CHORD					
			min	max	min	max	min	max				
3	65	0.10	-12.6	27.8	-47.7	41.3	-43.4	34.9	87,482	66	0.0	Straight
23	25	0.25	-21.4	27.7	-73.2	65.9	-16.1	50.5	285,765	90	0.0	Straight
9	72	0.35	-64.2	68.4	-110.0	102.0	-155.6	145.9	437,652	96	0.3	Curved

Note: For Bridges 65, 25, and 72, the envelope forces associate with Bridges 43, 70, and 72 are considered that are the highest in their respective bridge groups, respectively.

2.2.3 Analytical Study - Level II

2.2.3.1 Finite Element Method General Assumptions

After determining the end cross-frame forces for all selected bridges, a Level II analysis utilizing the refined Finite Element Method (FEM) model of the HRBS connection, and its vicinity was carried out. This analysis was performed to obtain the stress distribution within the connection detail, with the aim of sizing the HRBS connections. A generic representative example, a pier end cross-frame connection to the steel girder is selected and depicted in Figure 2.45.

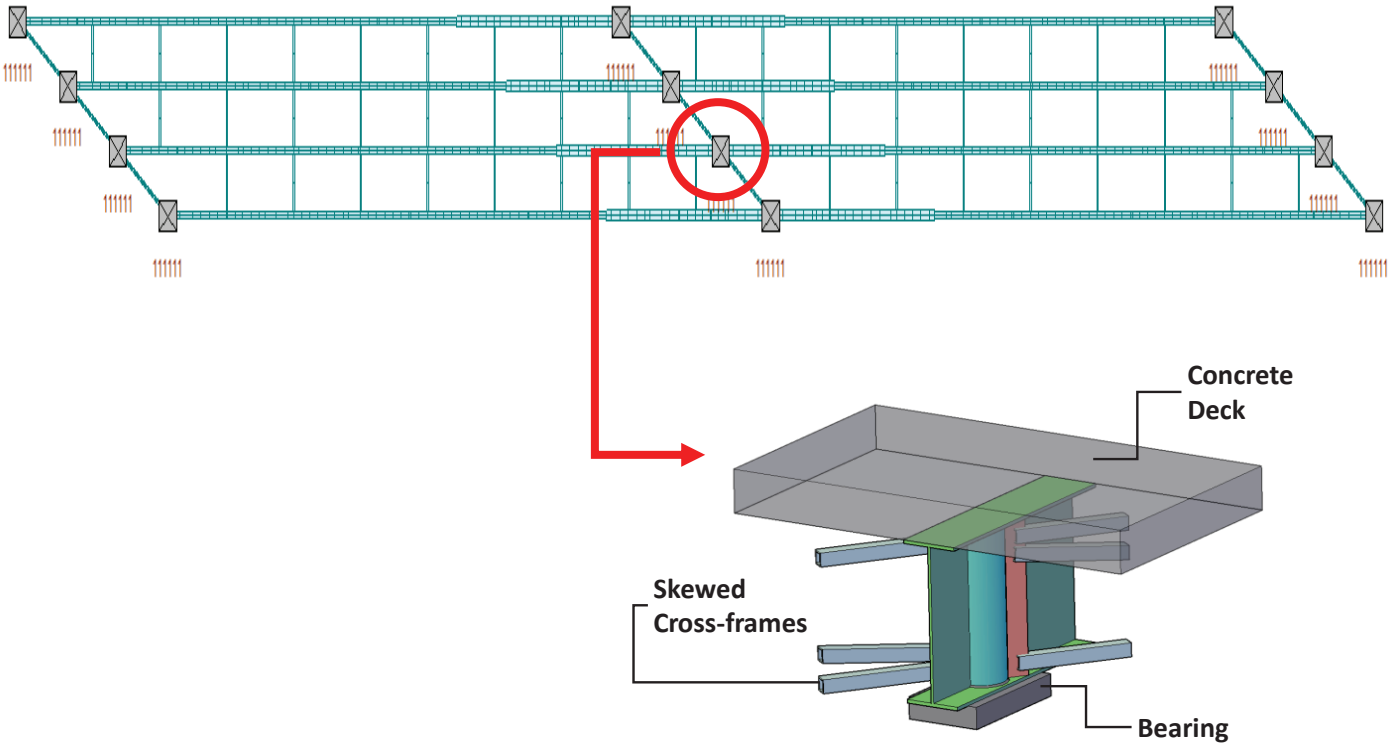

Figure 2.45- Half-Round Bearing Stiffener (HRBS) representative connection for FEM modeling

The representative HRBS connection and its vicinity includes a portion of the steel I-girder, half-round bearing stiffener plate, and stiffener plate, as well as the surrounding structural elements, including the concrete deck, skewed pier end cross-frame members, and the support bearing. In

order to achieve a Finite Element Method (FEM) modeling approach with an adequate degree of refinement, the model must focus on the pier section with appropriate boundary conditions simulating the composite girder, HRBS and pier end cross-frame.

2.2.3.2 Boundary Conditions

In the Level II analysis, for creating a model with sufficient detail and refinement, the focus will be on the behavior of a section of a continuous girder over a pier. The forces generated in the end cross-frames consisted of the force envelope magnitudes determined from the Level I analyses. The boundary conditions of the girder section must reflect the restraint provided by the composite deck as well as the support section. Given that the concrete and bearing components offer ample stiffness and support to the top and bottom flange of the steel I-girder, respectively, the lateral and vertical restraints provided by these components can be simulated through supports to the girder cross-section as demonstrated in Figure 2.46. The location of the supports along the girder can coincide with the location of jacking stiffeners if applicable. Because of the high stiffness provided by the concrete deck and bearing supports, now replaced by solid supports to the girder, the impact of the HRBS connection and members connected on one side of the girder web on the stress distribution in the connection of the other side is considered negligible. Accordingly, as it relates to sizing of connection details, further simplification can be applied by considering only connection details and connected cross-frame elements from one side, as illustrated in Figure 2.47.

Furthermore, in lieu of modeling the cross-frame members that are connected concentrically to stiffener plate, point loads were applied to the stiffener plates at the same direction as the cross-frame members distributed at bolt locations. Figure 2.48 shows the simplified model after the incorporation of these assumptions. If loading eccentricity exists, as it is in the case of single angles, T shapes and channel sections, the model was built differently to simulate the eccentricity. For this purpose, the exact configuration of cross-frame members and the gusset plates were included in the model and the loading was applied along the centroid of the cross-frame members. In the Level II analyses, the design load was composed of the envelope of cross-frame member forces from the Level I analysis. The connections were then checked for fatigue

using critical fatigue cross-frame member forces (maximums and minimums for the range). An FE model with the corresponding mesh and boundary condition for the connection is shown in Figure 2.49.

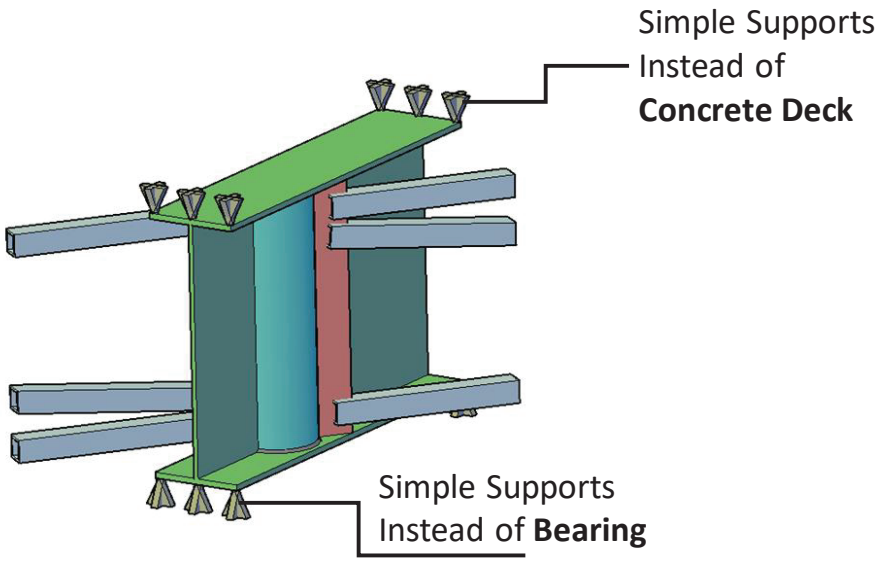

Figure 2.46- Utilizing simple supports instead of concrete deck and bearing

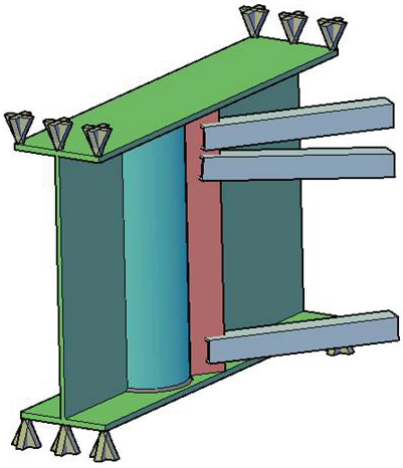

Figure 2.47- Eliminating the other side cross-frame elements

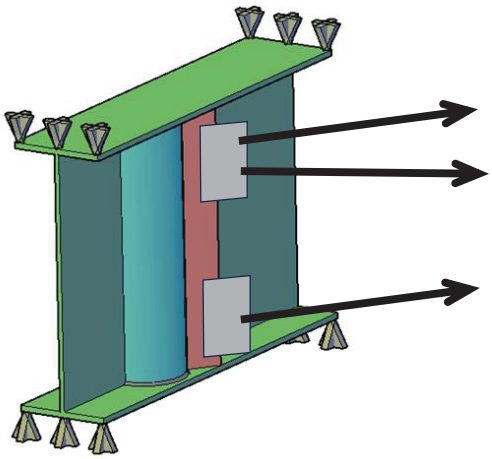

Figure 2.48- Simplified the representative HRBS connection for FEM modeling

Figure 2.49- Boundry condition for FEM models defined in Midas FEA NX

2.2.3.3 Materials

In the preceding section, the Finite Element Method (FEM) for the Level II models were outlined with “the area of interest” that includes a portion of the girder, HRBS, and stiffener plate connected to the girder from one side modeled using a refined mesh. As defined in Section 2.2.1.3.1.1, the material utilized in the steel I-girder is ASTM A 709 GRADE 50 structural steel, with properties identical to those specified in Table 2.6.

2.2.3.4 Consideration of Support Conditions

Analysis was performed to determine the effects of modeling the intermediate pier structure and neoprene bearing pad under the bridge superstructure. Three cases were considered: simple supports for girders, girders supported on neoprene bearing pads (pier not modeled), and girders supported by bearing pads and pier included in the model. The results indicated that as it relates to the stress range in the top flange over the intermediate support, these three cases produce similar results. In any case, because neoprene pads can deform vertically and laterally, potentially affecting the cross-frame member forces, the FE modeling included the neoprene bearing pads.

2.2.3.5 Geometry and Assembly

In this study, Finite Element Models (FEM) are composed of discrete components that include the steel I-girder beam, HRBS, and stiffener plate. These components are interconnected through a rigid connection, referred to as a weld connection in MIDAS FEA NX, to assemble a refined complete model. For example, for Bridge 72, as depicted in Figure 2.50, the primary steel girder component was characterized by the top and bottom flanges, a web, and two end stiffener plates (jacking plates), which were amalgamated into a single entity. The geometric properties and dimensional specifics for each model were presented in Table 2.15. The diameter of the HRBS was chosen so that they end on the flange at least 2 in. from the free edge of the flange.

Table 2.15- FEM models geometric properties

Bridge Number	Steel I-Girder Beam						Half-Round Plate					Stiffener Plate		
	Web Height (in.)	Web Thickness (in.)	Top Flang Width (in.)	Top Flang Thickness (in.)	Bot Flang Width (in.)	Bot Flang Thickness (in.)	OutSide Diameter (in.)	Thickness (in.)				Width (in.)	Thickness (in.)	Skew Angle (Degree)
72	96	0.75	24	3	28	3	16	3/8	1/2	5/8	3/4	8	1	57
25	90	0.625	22	2.63	22	2.63	16	3/8	1/2		5/8	8	1	54
65	66	0.5625	16	2	16	2	11	1/2		5/8		8	1	25

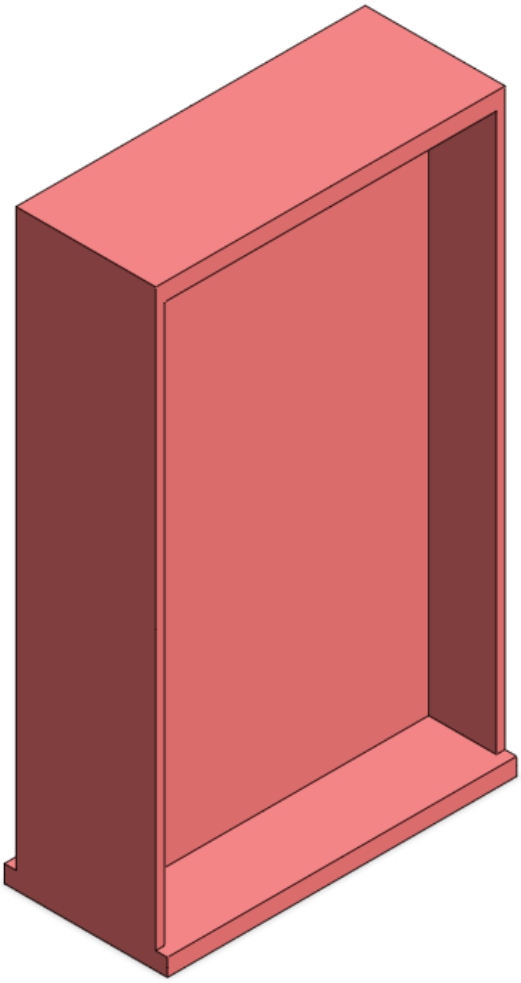

Figure 2.50- 3D model for the steel I-girder beam part with jacking stiffener plates in Bridge 72

The focus of this segment was on the sizing of the HRBS connection and the analysis of stress within the connection. Consequently, for the analysis, four different thicknesses for the HRBS plates were selected consisting of 3/8, 1/2, 5/8, and 3/4 inches. The simulations for the first connection model for Bridge 72 was performed with all these thicknesses. Since it was expected

that the stress levels in the connection has a strong correlation with the end cross-frame member forces, for Bridges 65 and 25, the analysis focused on thickness values that would satisfy closely the specific conditions considered for each case. Furthermore, to examine the influence of a 1.5 by 1.5-inch clipping at the corners of the HRBS, to better accommodate the steel girder web-to-flange weld in built-up sections, these plates were considered under two scenarios: with and without the clipping. As an example, Figure 2.51 and Figure 2.52 illustrated the HRBS plate components under both clipped and unclipped conditions for Bridge 72.

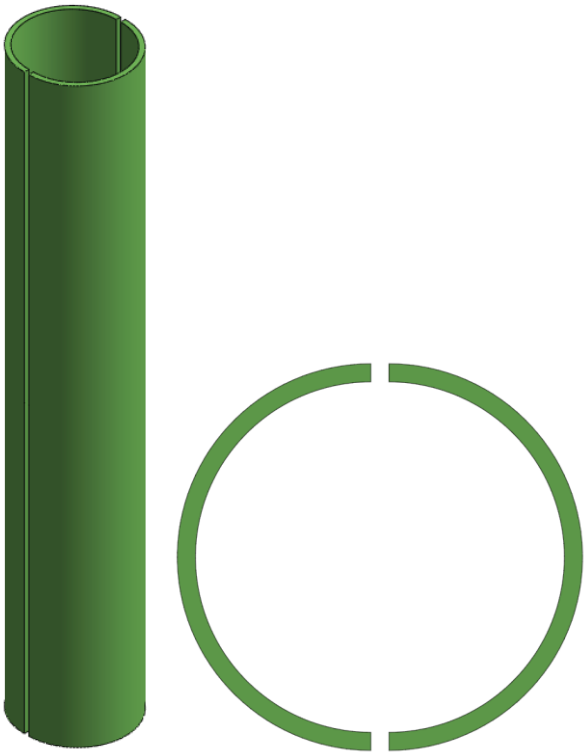

Figure 2.51- 3D model for the non-clipped HRBS plates with 3/4 inch thickness in Bridge 72. a) 3D view, b) Section

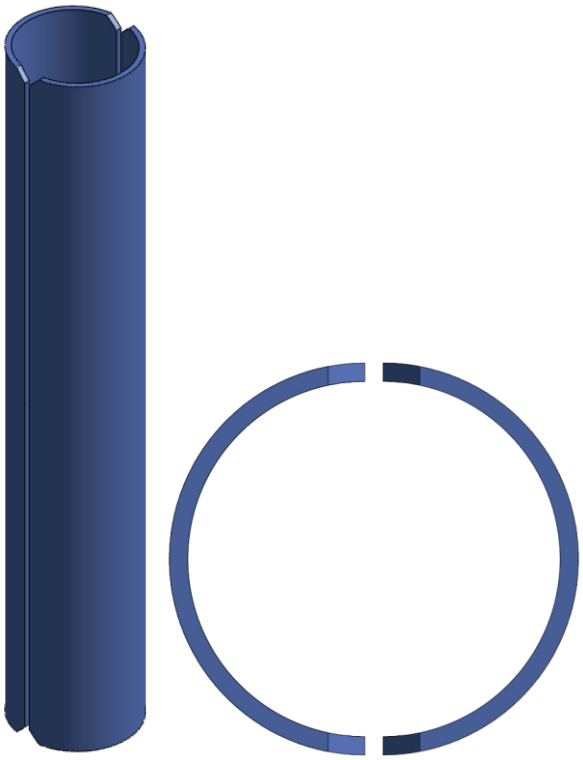

Figure 2.52- 3D model for the clipped HRBS plates with 3/4 inch thickness in Bridge 72. a) 3D view, b) Section

In the modeling process, another factor to be considered is the connection of the stiffener plate to the girder flanges. The stiffener plate that is attached to the HRBS through welding, can also be welded to the steel I-girder top and bottom flanges, referred to as a "welded stiffener," or it could be connected only to the HRBS, in which case it is termed an "unwelded stiffener." Note that, for the purpose of modeling, the condition where the stiffener plate may be connected to the flanges through bolted connections is also represented using “welded stiffener” model assuming the bolted connection is capable of transferring forces from the stiffener plate to the flanges. To reflect these different setups, for example, two types of stiffeners were designed for Bridge 72: one that matched the depth of the web and welded to the flanges, and another that was 2 inches shorter, one inch from each side, to avoid attachment to the beam's top and bottom flanges for the unwelded stiffener, as depicted in Figure 2.53. For Bridges 65 and 25, the gap between the stiffener plate and flanges was increased to 2 inches. This is to represent a more critical condition for stresses in the HRBS resulted from clipping of the stiffener plate where it intersects HRBS weld to flanges.

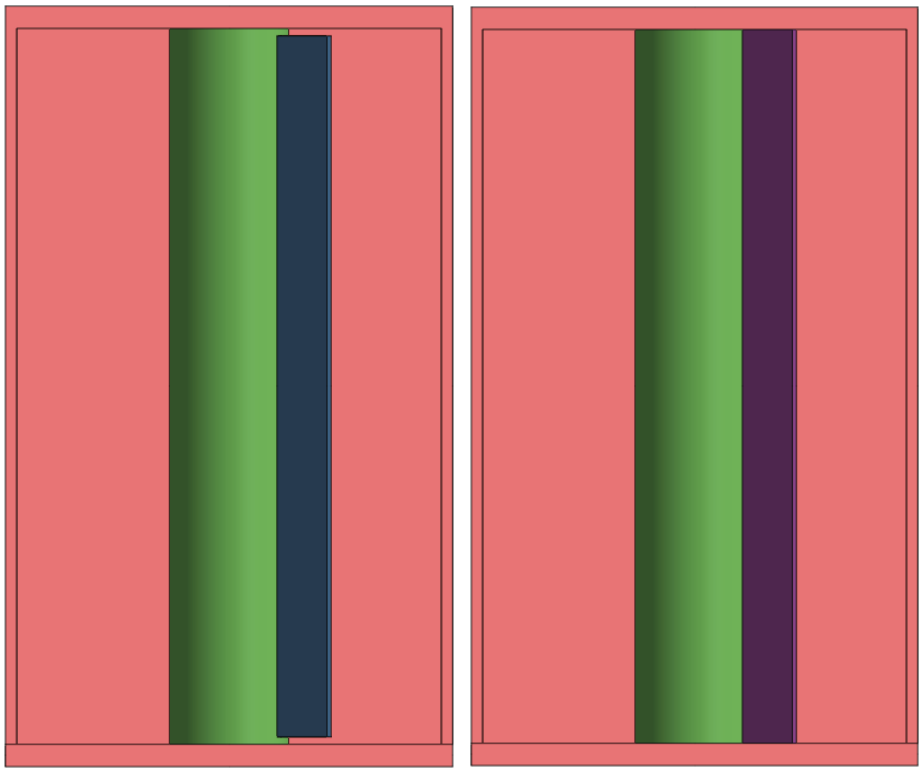

a) b)

Figure 2.53- Side view of; a) Unwelded stiffener and b) Welded stiffener

2.2.3.6 Structural Elements and Meshing

Midas FEA NX provides an extensive library of elements for a variety of applications in civil and structural engineering. These elements are categorized into one-dimensional, two-dimensional, and three-dimensional types, each tailored to meet specific structural analysis and modeling requirements. In the context of this study, specifically at level II, the area of interest has been modeled using Solid 3D elements.

The mesh generation process in MIDAS FEA NX employs a hybrid mesh shape, which is a sophisticated approach to meshing complex structures. This technique is illustrated in Figure 2.54, where the hybrid mesh shape integrates both Tetrahedral and Hexahedral elements, seamlessly connected by pyramid element types. This methodology is particularly effective in modeling intricate geometries with high precision.

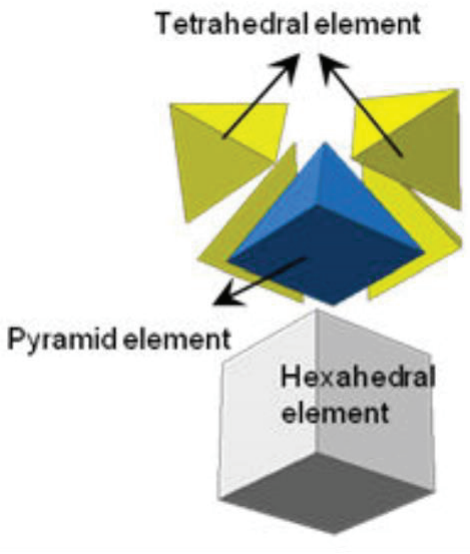

Figure 2.54- Hybrid mesh shape [129]

In this study, the predominant use of Hexahedral elements showcases their suitability for creating meshes in most parts of the model. Hexahedral elements are preferred for their structured layout and computational efficiency, making them ideal for the majority of the model where the geometry is relatively simpler. However, for specific parts of the model characterized by complex geometry, Tetrahedral elements are employed. These elements are adept at conforming to irregular shapes and contours, thereby providing a more accurate representation of the complex region.

For the refined models in this part of the research, the default size control has been set to 1 inch in all parts. However, in half-round plates, in order to detect the effect of the moment in the thickness of the plate, the thickness of the plate was divided into three layers of meshes.

An example of detailed views of an advanced hybrid mesh system, applied to the Finite Element Analysis (FEA) models of Half-Round Bearing Stiffener (HRBS) connections for Bridge 72 are presented in the following figures.

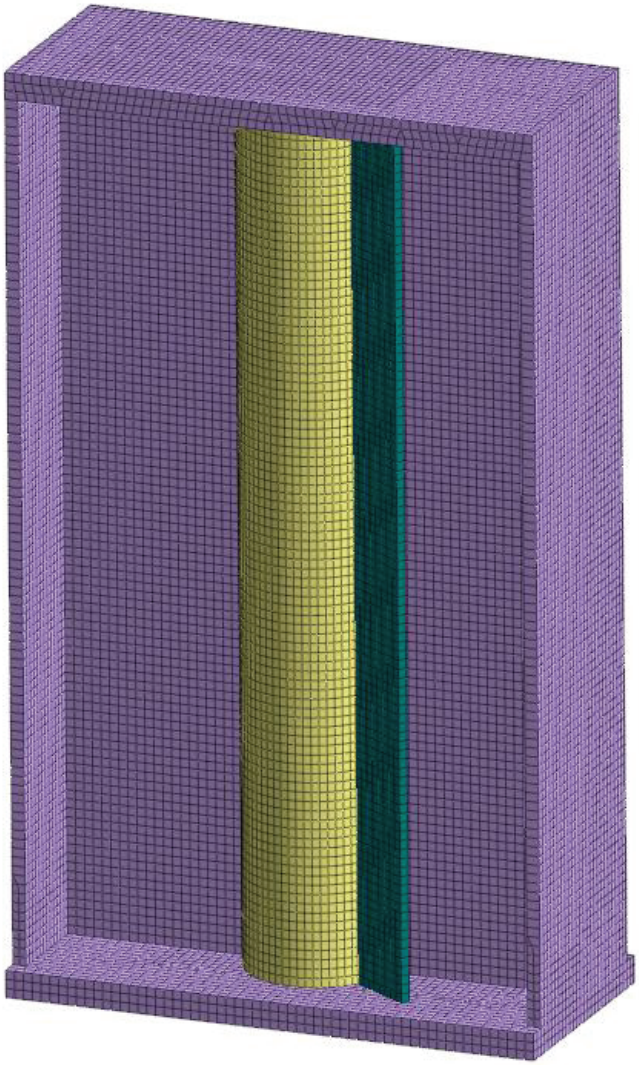

Figure 2.55- Hybrid mesh in FEA model of HRBS connection for Bridge 72: 3D view

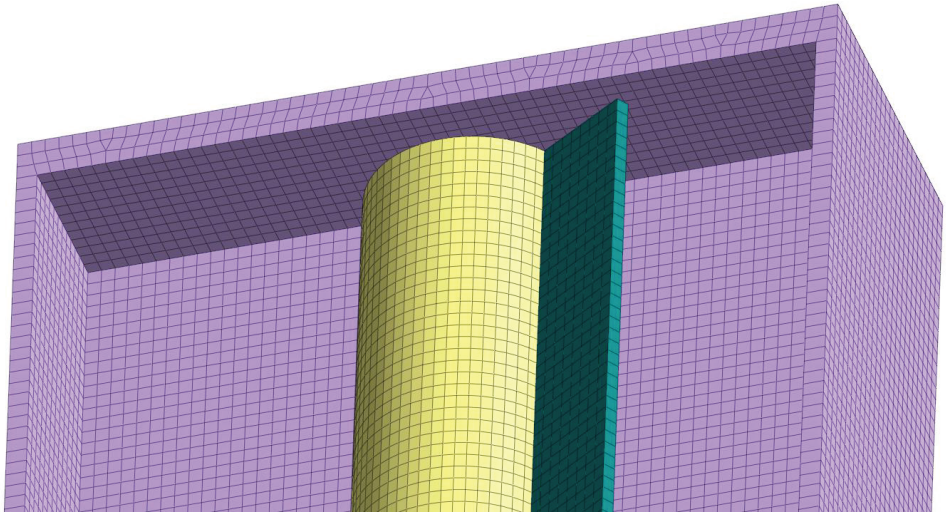

Figure 2.56- Hybrid mesh in FEA model of HRBS connection for Bridge 72: Top flange view

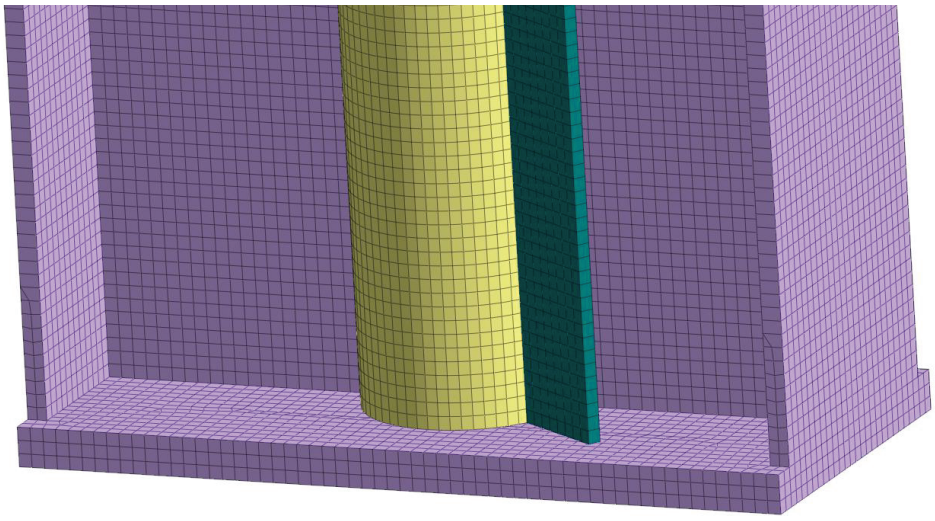

Figure 2.57- Hybrid mesh in FEA model of HRBS connection for Bridge 72: Bottom flange view

2.2.3.7 Static Load

The 26 skewed bridges identified in the state of Florida have been subjected to a comprehensive analytical study in Level I, utilizing Midas civil software for modeling. The application of loads to these bridges was guided by the AASHTO LRFD provision, ensuring consideration of possible loadings. Following the analysis, the results were extracted for the purpose of sizing the HRBS for representative bridges. The focus of the Level II analyses is directed towards the HRBS connections located on the supports of the representative Bridges 72, 25, and 65, especially those over the intermediate pier. As noted earlier, to make sure the "group representative bridge" covers all bridges in its group, the HRBS was sized for the highest level of forces determined from the Level I analyses within the specific group which are summarized in Table 2.16. Consequently, the maximum tension and compression forces of cross-frame members, including two load types - the Design Envelope load and Fatigue loading, derived from the Level I analysis were considered in this study. While the cross-frame internal forces used for design represent the envelope of forces generated by the design truck in every possible location on the bridge deck, the approach for determining fatigue force ranges included the case where the fatigue truck traverses a single lane known to induce the most critical internal forces in the end cross-frames among all possible lanes. This is consistent with provisions of AASHTO LRFD regarding positioning of the fatigue truck. These calculated internal force ranges, regarded as tensile loads, were assumed conservatively to simultaneously impact the cross-frames.

Table 2.16- Cross-frame internal forces used for analysis Level II

		Cross-frame Member Forces								
		Design Envelope (Kips)						Fatigue I Force Range (Kips)		
		TOP CHORD		DIAGONAL		BOT CHORD		TOP CHORD	DIAGONAL	BOT CHORD
#	Alternative Bridge #	min	max	min	max	min	max			
24	**65**	-12.6	27.8	-47.7	41.3	-43.4	34.9	22.1	27.7	18.3
23	**25**	-21.4	27.7	-73.2	65.9	-16.1	50.5	13.3	16.1	34.8
9	**72**	-64.2	68.4	-110.0	102.0	-155.6	145.9	17.3	13.3	53.0

The collection of the maximum tension and compression internal forces of cross-frame members from the Level I analysis represents the peak values for all skewed HRBS connections over the supports in a specified bridge. It is realized, for instance, when the upper chord force in a cross-frame member attains its maximum tension force, other elements within that cross-frame may not simultaneously reach their respective maximum forces. Consequently, considering the maximum of forces to happen at the same time generally results in a conservative sizing of the connection. The Level I analyses also revealed that, for the identification of a critical load combination, the internal forces of the chord (top or bottom) and the diagonal member connected to that chord, should exhibit identical characteristics, simultaneously manifesting as either tension or compression. However, the internal force in the other chord (not connected to a diagonal) may exhibit either a similar or an opposite direction. Therefore, the most critical load combination for the sizing of the connection can encompass four load combinations, as shown in Table 2.17.

Table 2.17- Critical load combinations for desgining HRBS connection

Load Comcination	**1**	**2**	**3**	**4**
Top Chord Force	C[1]	C	T	T
Diagonal Force	C	C	T	T
Bottom Chord Force	C	T[2]	C	T

1- C= Compression 2- T= Tension

2.2.3.8 Bridge FE Modeling

2.2.3.8.1 Modeling of Bridge 72

Figure 2.58 depicts the pier cross-frame detail for Bridge 72. The combination of top chord and diagonal elements, as well as the bottom chord element, each attach to the stiffener plate through a gusset plate with 12 bolts. In the FE model for Bridge 72, the cross-frame members forces are applied directly at the location of bolts on the stiffener plate.

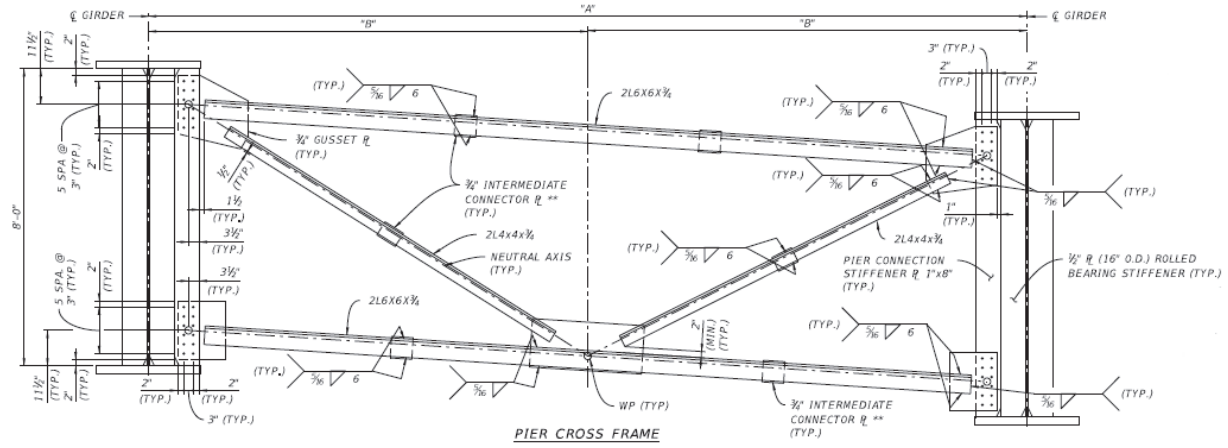

Figure 2.58- Pier cross-frame detail for Bridge 72

Figure 2.59 displays how these forces are applied at the precise locations of the cross-frame connection to the stiffener plate in Bridge 72. In this specific case, where the cross-frame members connect concentrically to the stiffener plate with 12 bolts, the FEA models show that the force from each cross-frame member is evenly distributed and applied uniformly to all bolts. Here concentrical refers to both the line of the application of the cross-frame member loads being in the plane of the stiffener plate and passing through the center of the gravity of the bolt group. The forces of the top chord and diagonal elements of the cross-frame are applied to the upper part of the model, whereas the forces of the bottom chord are applied to the lower part.

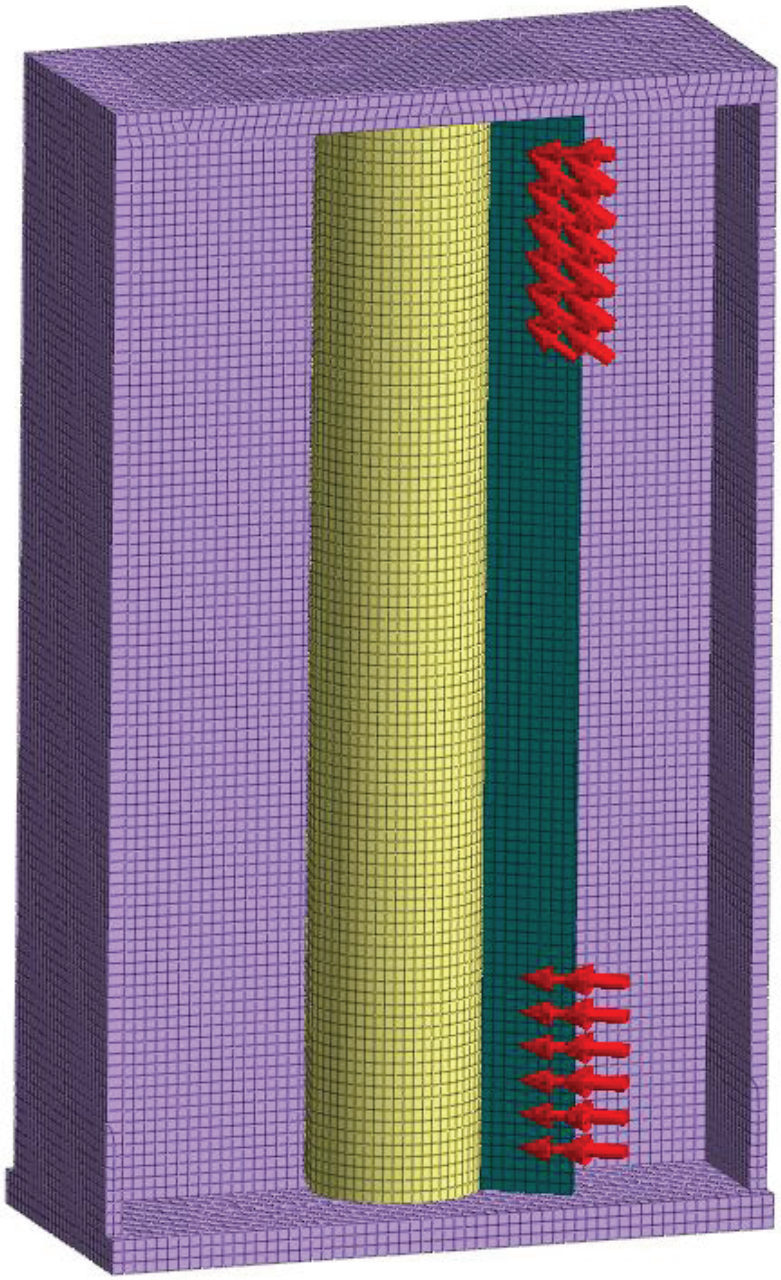

Figure 2.59- Distribution of internal forces in cross-frame connections to HRBS in Bridge 72

2.2.3.8.2 Modeling of Bridges 65 and 25

For the FE models of Bridges 65 and 25, the loading was applied to the cross-frame members connected to stiffener plates through gusset plates to introduce eccentricity. For Bridge 65, because of shallow skew angle, the length available for welding the stiffener plate to the flanges

is too small to accommodate effective weld length. Therefore, for this bridge only unwelded condition for the stiffener plate was modeled. Accordingly, this bridge was analyzed only for the clipped and unwelded condition (Figure 2.60). However, Bridge 25 was modeled for both the clipped-welded and clipped-unwelded conditions (Figure 2.61). Considering the clipped condition for both these bridges represents a more critical case compared to unclipped. This was verified by the analysis performed for Bridge 72.

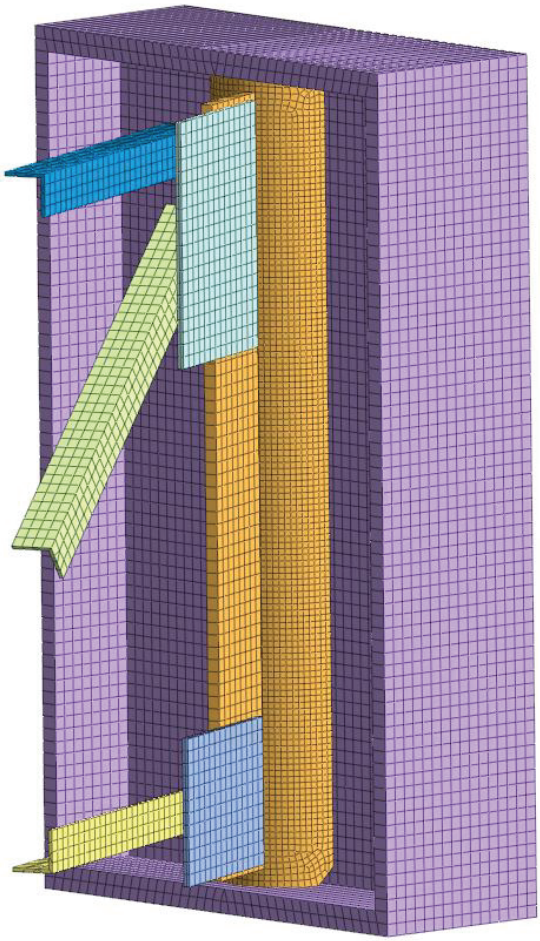

Figure 2.60- The FE model used for Bridge 65

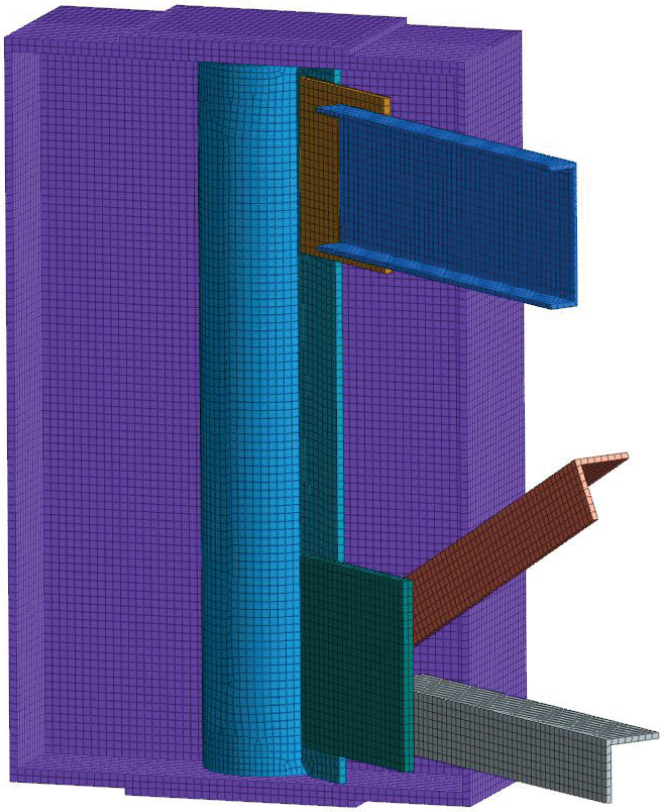

a)

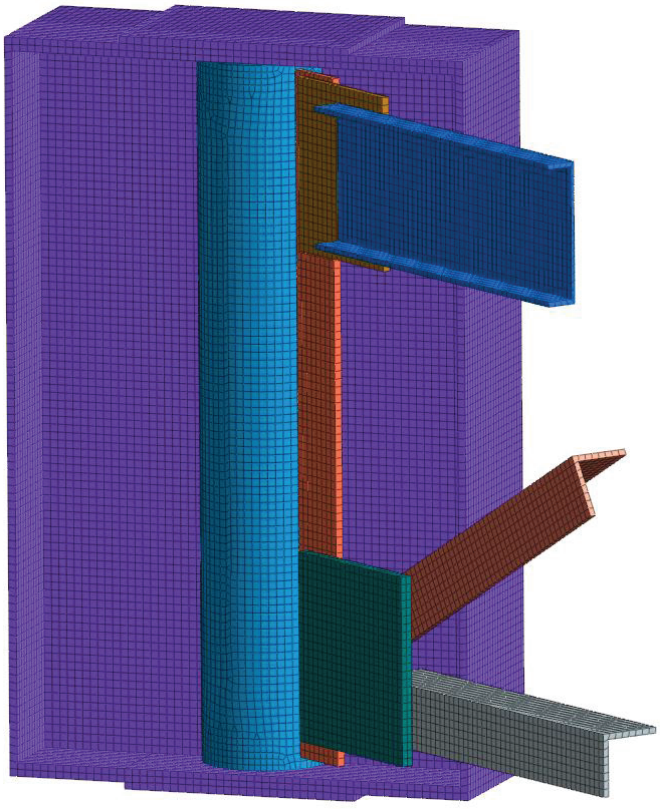

b)

Figure 2.61- FE models used for Bridge 25-2, a) Clipped & Welded, b) Clipped & Unwelded

2.2.3.9 Results

2.2.3.9.1 Results for Bridge 72

Table 2.18 presents the collected data on the highest von Mises stresses at the nodes of the Half-Round Bearing Stiffener (HRBS), experienced at the connection of the HRBS to the girder for Bridge 72 for all load combinations. These models vary in size, weld status, clipping condition, and load combinations.

Table 2.18- Maximum von Mises stress in HRBS plates based on FEM analysis results in Bridge 72

HRBS Dimensions (in.)		Stiffener Connection to Flanges	Clipping Type	Load Combination	Max Nodal Average von Mises Stress in HRBS σ_{max} (ksi)
D	t				
16	3/4	Welded	Non-Clipped	CCC	16.2
				TTT	15.7
				TTC	14.7
				CCT	15.3
			Clipped	CCC	19.9
				TTT	19.3
				TTC	18.3
				CCT	18.9
		Unwelded	Non-Clipped	CCC	37.5
				TTT	36.2
				TTC	35.8
				CCT	37.1
			Clipped	CCC	50.6
				TTT	48.9
				TTC	48.6
				CCT	50.3
	5/8	Welded	Non-Clipped	CCC	20.1
				TTT	19.5
				TTC	19.4

HRBS Dimensions (in.)		Stiffener Connection to Flanges	Clipping Type	Load Combination	Max Nodal Average von Mises Stress in HRBS σ_{max} (ksi)
D	t				
				CCT	20.0
			Clipped	CCC	26.2
				TTT	25.3
				TTC	25.6
				CCT	26.4
		Unwelded	Non-Clipped	CCC	70.0
				TTT	67.7
				TTC	68.0
				CCT	70.2
			Clipped	CCC	87.5
				TTT	84.7
				TTC	84.1
				CCT	86.9
	1/2	Welded	Non-Clipped	CCC	24.8
				TTT	24.0
				TTC	23.5
				CCT	24.3
			Clipped	CCC	37.5
				TTT	36.4
				TTC	36.2
				CCT	37.4
		Unwelded	Non-Clipped	CCC	101.0
				TTT	97.8
				TTC	98.2
				CCT	101.3
			Clipped	CCC	140.2
				TTT	135.8
				TTC	135.2

HRBS Dimensions (in.)		Stiffener Connection to Flanges	Clipping Type	Load Combination	Max Nodal Average von Mises Stress in HRBS σ_{max} (ksi)
D	t				
				CCT	139.6
	3/8	Welded	Non-Clipped	CCC	33.0
				TTT	32.0
				TTC	28.5
				CCT	29.5
			Clipped	CCC	33.7
				TTT	32.7
				TTC	32.1
				CCT	33.1
		Unwelded	Non-Clipped	CCC	153.3
				TTT	148.6
				TTC	147.5
				CCT	152.3
			Clipped	CCC	151.4
				TTT	146.7
				TTC	144.5
				CCT	149.2

2.2.3.9.2 Results for Bridges 65 and 25

The maximum von Mises stresses in the HRBS for Bridges 65 and 25 are summarized in the Table below for all load conditions.

Table 2.19- Maximum von Mises stress in HRBS plates based on FEM analysis results for Bridges 65 and 25

Bridge	HRBS Plate Dimensions (in.)		Stiffener Connection to Flanges	Clipping Type	Load Combination	Max Nodal Average von Mises Stress in HRBS σ_{max} (ksi)
	D	t				
Bridge 25	16	5/8	Welded	Clipped	CCC	13.4
					TTT	18.7
					CTT	18.2
					TCC	12.8
			Unwelded	Clipped	CCC	34.2
					TTT	46.1
					CTT	46.0
					TCC	34.1
		1/2	Welded	Clipped	CCC	11.2
					TTT	14.7
					CTT	14.1
					TCC	10.7
			Unwelded	Clipped	CCC	45.5
					TTT	64.5
					CTT	63.9
					TCC	44.9
		3/8	Welded	Clipped	CCC	24.3
					TTT	32.9
					CTT	31.4
					TCC	22.7
			Unwelded	Clipped	CCC	58.0
					TTT	81.9
					CTT	81.8
					TCC	57.9
Bridge 65	11	5/8	Unwelded	Clipped	CCC	33.7
					TTT	38.6
					TTC	36.0
					CCT	31.1
		1/2	Unwelded	Clipped	CCC	60.4
					TTT	71.0
					TTC	67.1
					CCT	56.4

2.2.3.10 Sizing of the HRBS

This section focuses on the sizing of HRBS plates and their welds to the main steel I-girder and the stiffener plate. The strength of the plates (in tension or compression) is the main parameter in these plates. According to AASHTO's article 6.8.2.1, the factored tensile resistance, P_r, should be determined as the minimum of the values obtained from Equations 2.1 and 2.2 presented below.

$$P_r = \emptyset_y P_{ny} = \emptyset_y F_y A_g \quad (2.1)$$

$$P_r = \emptyset_u P_{nu} = \emptyset_u F_u A_n R_p U \quad (2.2)$$

In this context, P_{ny} represents the nominal tensile resistance due to yielding across the gross section, measured in kips, where F_y denotes the specified minimum yield strength in ksi. A_g refers to the member's gross cross-sectional area in square inches. F_u stands for the material's tensile strength, which for Steel A709 Grade 50 is 68 ksi. A_n is the net cross-sectional area defined in AASHTO Article 6.8.3, in square inches. R_p is a coefficient adjusting for the presence of holes, set at 0.90 for fully punched bolt holes and 1.0 for bolt holes that are either fully drilled or punched and then reamed to size. U is a factor that adjusts for shear lag, with a default value of 1.0 for elements where forces are distributed evenly across all parts, and varying values as outlined in AASHTO Article 6.8.2.2 for different scenarios. ϕ_y is the yielding resistance factor for tension components as provided in AASHTO Article 6.5.4.2, fixed at 0.95, and ϕ_u is the fracture resistance factor for tension members as stated in the same AASHTO article, set at 0.80.

Thus, in the sizing process of the HRBS plates, the factored tensile resistance stress is established by applying the appropriate parameters to Equations 1 and 2. Consequently, the factored tensile resistance stress is calculated to be 47.5 ksi.

$$Factored\ Tensile\ Resistance\ Stress = min\left\{\frac{P_r}{A_g} = \emptyset_y F_y \ \ \& \ \ \frac{P_r}{A_n R_p U} = \emptyset_u F_u\right\}$$

$$= min\{0.95 \times 50\ (ksi) = 47.5\ (ksi) \quad \& \quad 0.8 \times 68(ksi) = 54.4\ (ksi)\} = 47.5\ (\text{ksi})$$

2.2.3.10.1 Sizing of HRBS for Bridge 72

In the previous section, the highest average von Mises stresses in the HRBS for Bridge 72, were summarized in Table 2.18. For the sizing of the HRBS plates, the maximum von Mises stresses at the nodes of the HRBS for all load combinations were selected and provided in Table 2.20.

Upon examining the maximum stresses in HRBS subjected to design envelope loadings detailed in Table 2.20, and considering the established factored tensile resistance stress of 47.5 ksi, it is observed that the stresses within HRBS remain within acceptable limits when stiffeners plates are welded to both the HRBS and the flanges of the Steel I-girders (welded stiffener condition) Table 2.21. However, in scenarios where stiffener plates are only attached to the HRBS (unwelded stiffener condition) and the HRBS is in non-clipped condition, acceptable stress levels were only observed in HRBS with a thickness of 3/4 inch, suggesting that plates of thinner thickness values will not meet the required tensile strength. When the HRBS is clipped, the von Mises stress slightly exceeds the specified factored tensile resistance (50.6 versus 47.5 ksi). Nonetheless, this minor excess stress, due to its localized nature (See Figure 2.62) and the conservative assumptions in force estimations, can be disregarded.

Consequently, for Bridge 72, HRBS with a 16-inch outer diameter and a thickness of 1/2 inch for the welded stiffener condition, and HRBS plates with a 16-inch outer diameter and a thickness of 3/4 inch for the unwelded stiffener condition have been selected for use in both clipped and unclipped HRBS configurations.

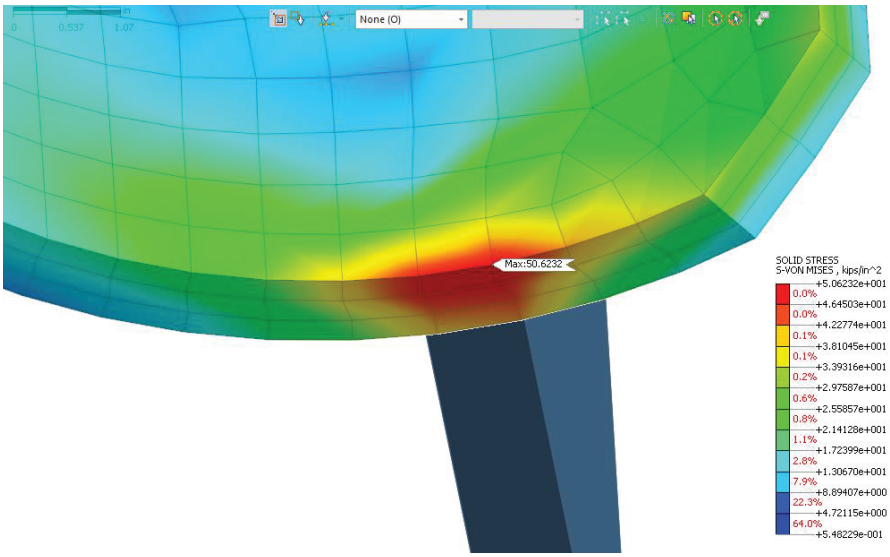

Figure 2.62- Von Mises stress contour in clipped and unwelded condition in HRBS for Bridge 72 under design envelope load (CCC condition)

Table 2.20- Envelope FEA results for nodal average von Mises stress in HRBS for design envelope loads in Bridge 72

HRBS Dimensions		Stiffener Weld to Flanges Condition	Clipping Type	Max Nodal Average von Mises Stress in HRBS σ_{max} (ksi)
D	t			
16"	3/4"	Welded	Non-Clipped	16.2
			Clipped	19.9
		Un-Welded	Non-Clipped	37.5
			Clipped	50.6
	5/8"	Welded	Non-Clipped	20.1
			Clipped	26.4
		Un-Welded	Non-Clipped	70.2
			Clipped	87.5
	1/2"	Welded	Non-Clipped	24.8
			Clipped	37.5
		Un-Welded	Non-Clipped	101.3
			Clipped	140.2
	3/8"	Welded	Non-Clipped	33.0
			Clipped	33.7
		Un-Welded	Non-Clipped	153.3
			Clipped	151.4

Table 2.21- Stress control summary in HRBS plates for Bridge 72 for the envelop design loading

HRBS Dimensions (in.)		Stiffener Weld to Flanges Condition	Clipping Type	Factored Resistance Tensile Stress (ksi)	Max Nodal Average von Mises Stress in HRBS σ_{max} (ksi)	Stress Control
D	t					
16	3/4	Unwelded	Non-Clipped	47.5	37.5	OK
			Clipped	47.5	50.6*	OK
	**1/2	Welded	Non-Clipped	47.5	24.8	OK
			Clipped	47.5	37.5	OK

*Because the stress is concentrated in small, the slight overstress deemed acceptable

**A minimum thickness of 1/2 inch was considered for practical purposes and due to large girder size

2.2.3.10.2 Comparing Connection Deformation for Welded and Unwelded Stiffener

This section provides a summary of the difference between the welded and unwelded stiffener plate details in relation to both deformations and stress/strain concentration. Among the details representing three selected bridges, the detail for Bridge 72 with the largest magnitude of cross-frame member forces was selected for this purpose. Therefore, all results outlined in this section pertain to Bridge 72. Contour plots representing displacement, von-Mises stress, von-Mises strain are superimposed on the deformed shapes for HRBS connections under critical design envelope Load (CCC) are shown in Figure 2.63, Figure 2.64, and Figure 2.65,respectively. The details that are shown are for the case with the HRBS with stiffener plate not welded to the flange and with the HRBS corners clipped at the flange-to-web juncture. The same information for clipped and welded condition is included in Figure 2.66, Figure 2.67, and Figure 2.68 respectively. The results including maximum displacement, von-Mises stress and strain are also included in Table 2.22. The sizing of the welded and unwelded details are provided in Table 2.21. The contours indicate the location of maximum displacement or stress on the HRBS. The displacements that are reported refer to the total translation relative to the unloaded condition. For clarity, the deformed shape is scaled up to a value such that the maximum displacement equals 1/20 the maximum dimension of the entire model that is girder depth of 96 in.

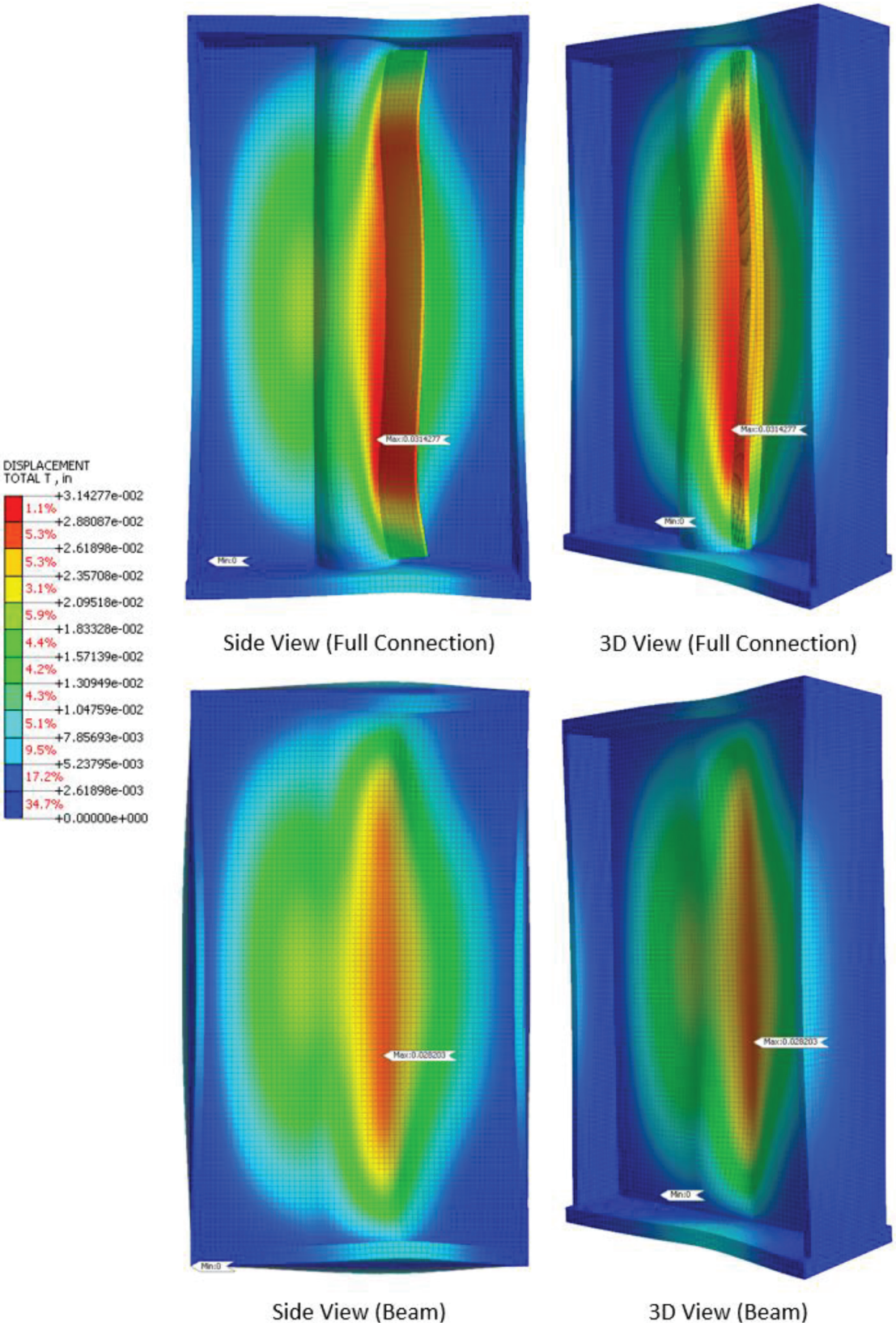

Figure 2.63- Deformed shape with displacement contours in HRBS connection for clipped and unwelded condition in Bridge 72 under critical design envelope Load

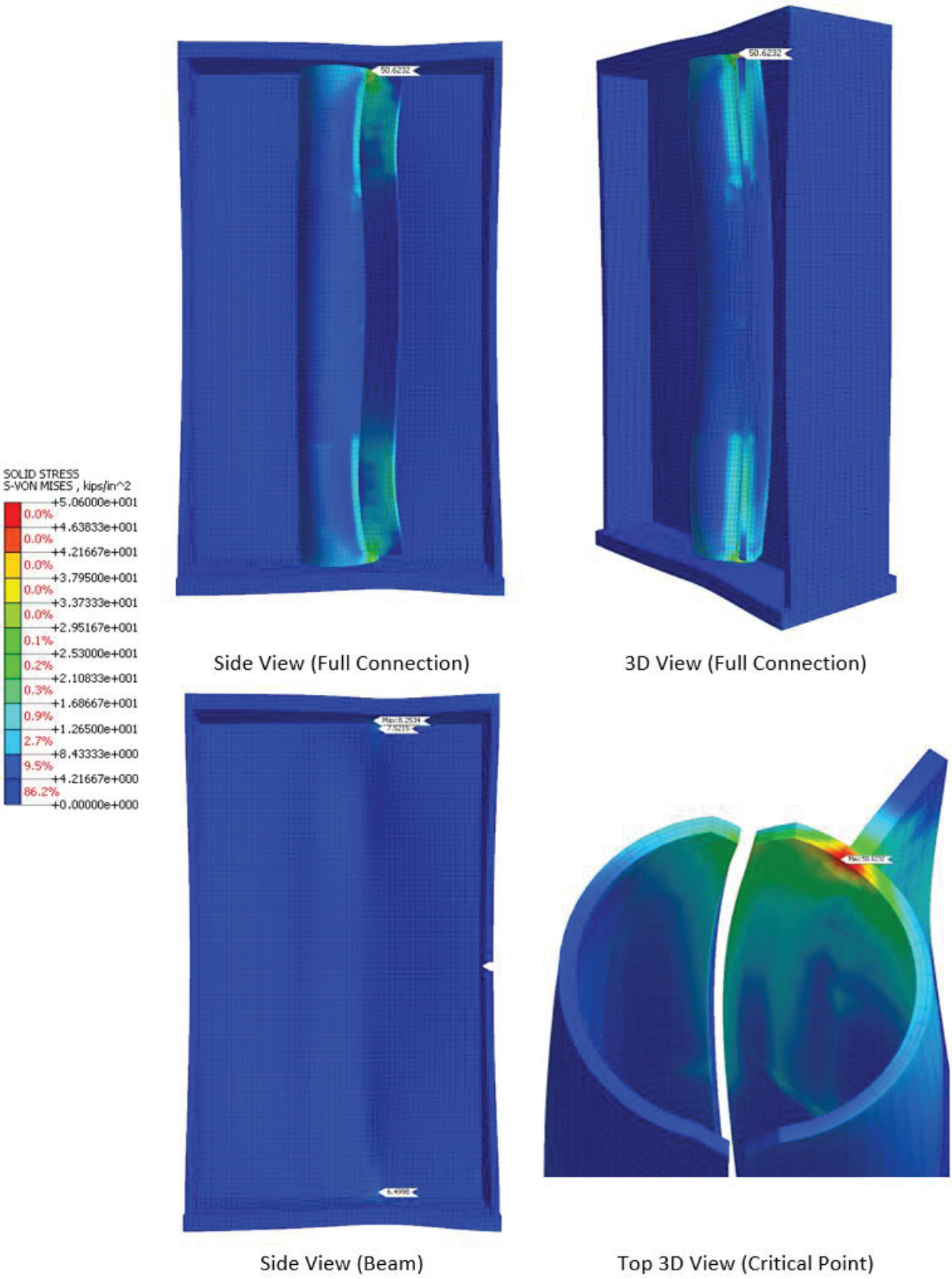

Figure 2.64- Deformed shape with von-Mises stress contours in HRBS connection for clipped and unwelded condition in Bridge 72 under critical design envelope load

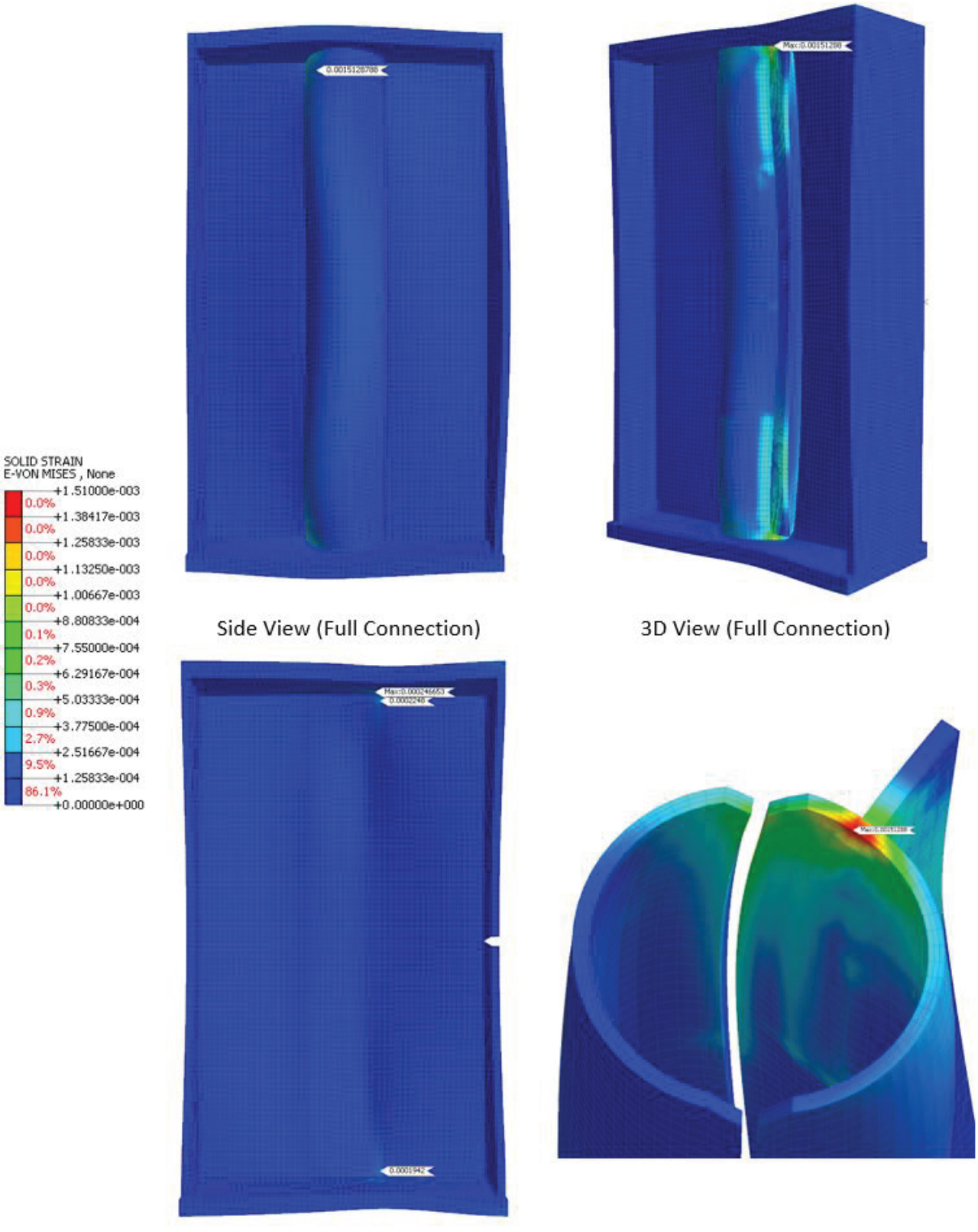

Figure 2.65- Deformed shape with von-Mises strain contours in HRBS connection for clipped and unwelded condition in Bridge 72 under critical design envelope load

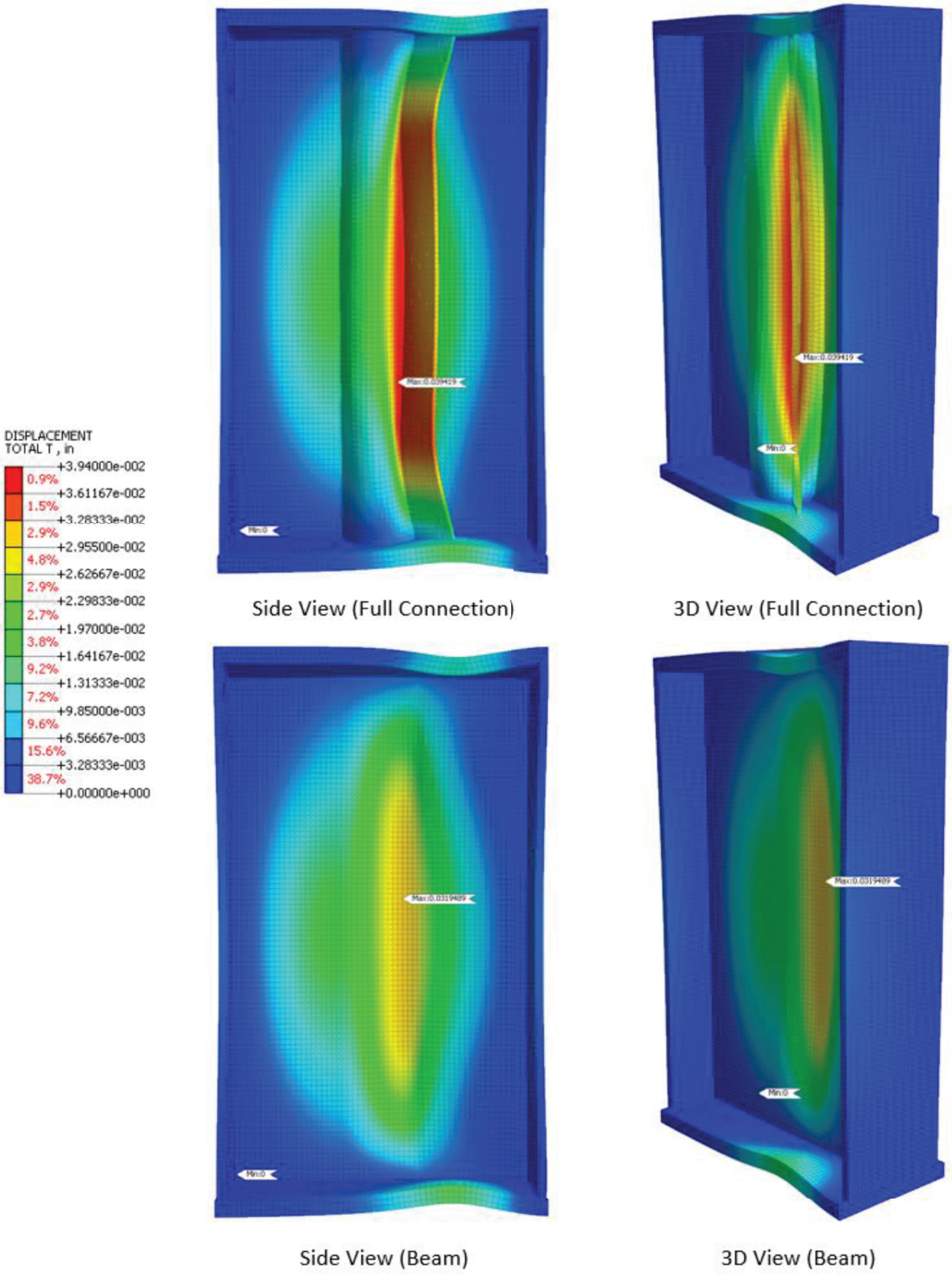

Figure 2.66- Displacement Contours with Deformed Shape in HRBS connection for Clipped and welded condition in Bridge 72 under design envelope load (CCC condition)

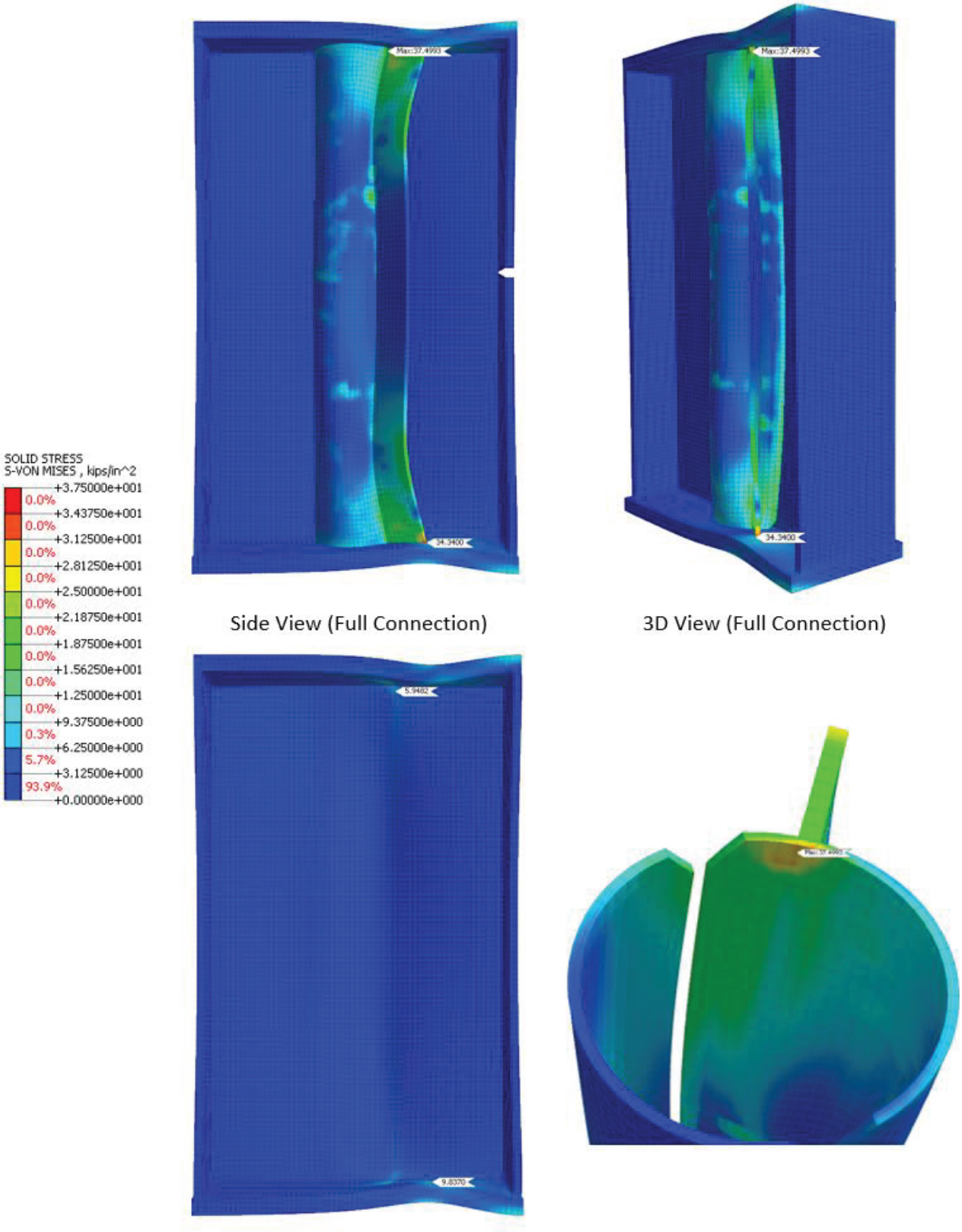

Figure 2.67- Von Mises stress Contours with Deformed Shape in HRBS connection for Clipped and welded condition in Bridge 72 under design envelope load (CCC condition)

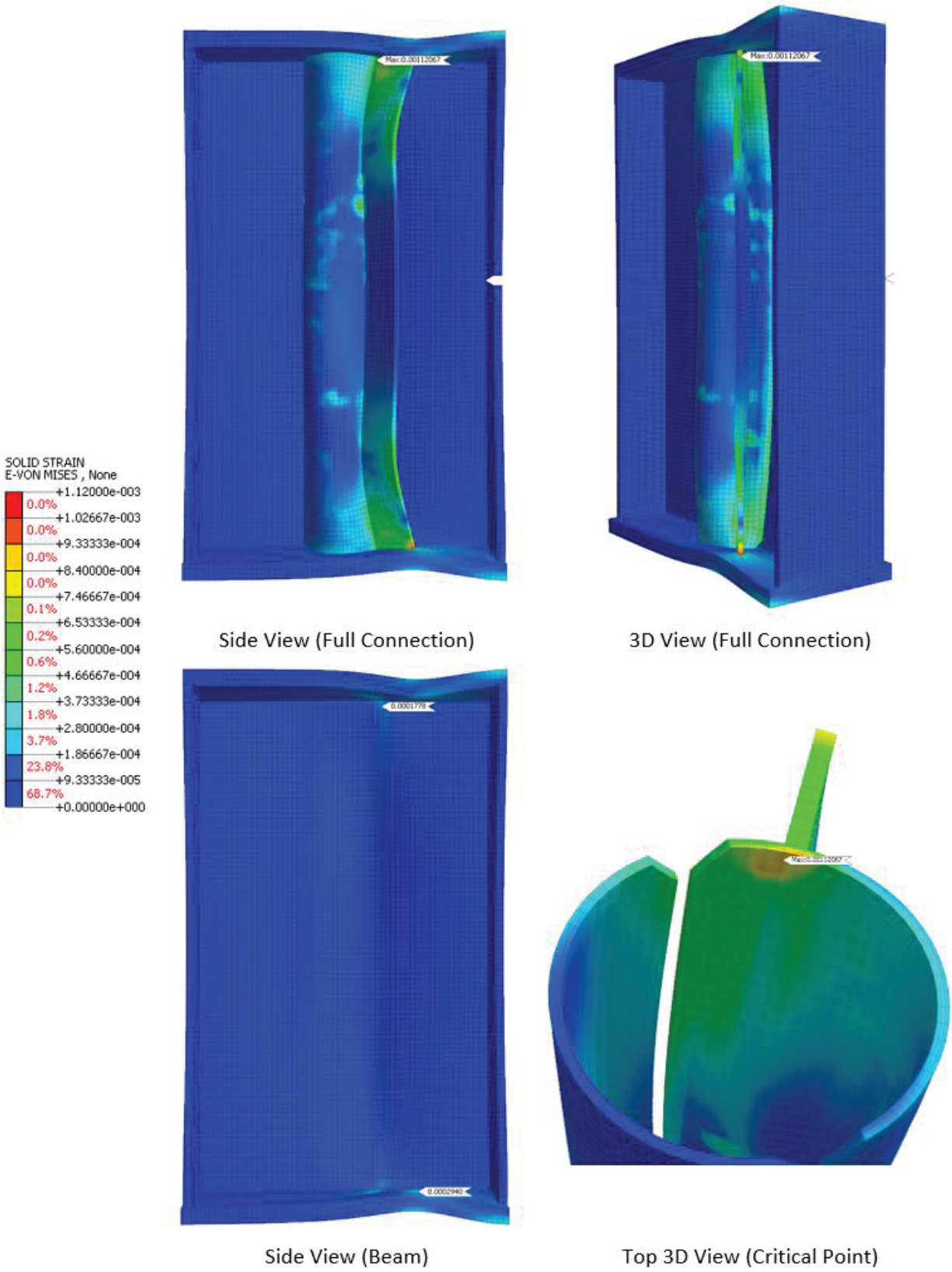

Figure 2.68- Von Mises Strain Contours with Deformed Shape in HRBS connection for Clipped and welded condition in Bridge 72 under design envelope load (CCC condition)

The maximum value of the von-Mises stress, von-Mises strain, and displacement are summarized in Table 2.22. The results show that welding the stiffener plate to the flanges considerably reduces the stress, strain and displacement when compared to values corresponding to the unwelded condition. It should be noted that the thickness of the Half-Round for the welded connection in the analysis is 1/2 in. compared to the unwelded condition that is 3/4 in. Another observation is that the stress and strain in the web of the girder from cross-frame forces in both conditions are relatively low.

Table 2.22- FEA results in HRBS connection components due to Design Envelope forces

Condition	Variables	Stiffener Plate	Half-Round Plate	Girder Web
Unwelded	Von-Mises Stress (ksi)	46.36	50.62	7.52
	Von-Mises Strain	0.001385	0.00151	0.000225
	Displacement (in.)	0.03085	0.03142	0.0282
Welded	Von-Mises Stress (ksi)	34.34	37.50	5.95
	Von-Mises Strain	0.001026	0.00112	0.000178
	Displacement (in.)	0.0383	0.0394	0.0319

2.2.3.10.3 Sizing of HRBS for Bridges 65 and 25

Based on the results shown in Table 2.19, the maximum stresses among all load conditions for HRBS in Bridges 65 and 25 are summarized in Table 2.23. Consequently, the HRBS for these bridges are sized as per Table 2.24. For completeness, the sizing of Bridge 72 is also included in this table.

Table 2.23- Stress control summary in HRBS plates for Bridges 65 and 25 for the envelop design loading

Bridge	**HRBS Plate Dimensions** (inch)		**Stiffener Welded to Flanges**	**Clipping Type**	**Factored Resistance Tensile Stress** (ksi)	**Max Nodal Average von Mises Stress in HRBS** σ_{max} (ksi)	**Stress Control**
	D	**t**					
Bridge 25	**16**	**5/8**	**Un-Welded**	**Clipped**	47.5	46.1	OK
		3/8	**Welded**	**Clipped**	47.5	32.9	OK
Bridge 65	**11**	**5/8**	**Un-Welded**	**Clipped**	47.5	38.6	OK

Table 2.24- Summary of HRBS sizing suggested for representatives of three bridge groups

Bridge #	Stiffener Welded to Flanges	Clipping Type	HRBS Plate Dimensions (in.)	
			D	t
Bridge 72	Unwelded	Non-Clipped	16	3/4
		Clipped		3/4
	Welded	Non-Clipped	16	1/2
		Clipped		1/2
Bridge 25	Unwelded	Clipped	16	5/8
	Welded	Clipped		3/8
Bridge 65	Unwelded	Clipped	11	5/8

2.2.3.11 Sizing of the Welds

Sizing of the welds was performed for Bridge 72 which had the highest level of forces. The same weld sizes are then conservatively recommended for Bridges 65 and 25. To determine the appropriate size for the fillet weld, it's necessary to compute the factored resistance, R_n, of the welded connections for various weld widths for unit weld length by applying the equation below. Within this equation, F_{exx} represents the electrode strength classification in ksi, which, for the purpose of this analysis, is chosen to be 70 ksi. Additionally, the electrode resistance factor, denoted as $\emptyset_{ee2}$, is outlined in AASHTO Article 6.5.4.2 and is determined to be 0.80.

$$R_n = 0.6\emptyset_{e2}F_{exx} \quad (2.3)$$

In which,

$\emptyset_{ee2}$= electrode resistance factor=0.80 (AASHTO Article 6.5.4.2)

F_{exx} = electrode strength classification = 70 ksi

The sizing process involves ensuring that the maximum shear force per unit length at the weld contact point remains below the factored resistance of the fillet weld per unit length of its effective area. Figure 2.69 illustrates the effective area, also known as the failure plane, which is determined to be 0.707 times the width of the weld (w).

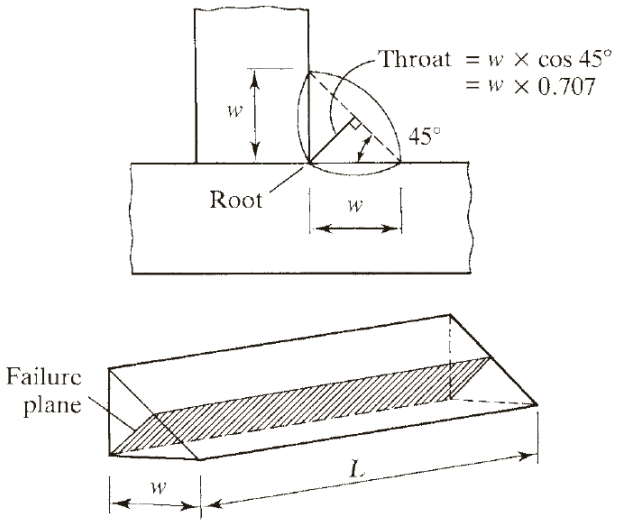

Figure 2.69- Fillet weld effective area or failure plane [134]

Therefore,

$A_{eff\times}R_n = 0.707 \times w \times L \times 0.6 \times 0.80 \times 70 = 23.75 \times w \times L$

While larger fillet welds will result in a shorter length weld required, for efficiency, the largest fillet weld that can be made with a single pass will generally be the most efficient from a fabrication perspective. The maximum fillet weld size that can be achieved with a single pass is 5/16 in. Therefore, the force per inch of a 5/16-in. fillet weld in this case is:

$$A_{eff\times}R_n = 0.707 \times w \times L \times 0.6 \times 0.80 \times 70 = 23.75 \times \frac{5}{16} \times 1 = 7.42\ kips/in$$

To determine the size of the fillet weld, first the effective weld length that transfers the cross-frame internal forces was estimated. Two sets of welds were considered: the stiffener plate to the HRBS and the HRBS to the steel I-girder. This necessitated the evaluation of two distinct weld lines. As depicted schematically in Figure 2.70 and Figure 2.71 (for welded and unwelded conditions), the first weld line (weld Line 1), which connects the stiffener plate to the HRBS, is illustrated with a blue line, while the second weld line (Weld Line 2), linking the HRBS to the steel I-girder, is represented by the red line. In assessing these weld lines, a reasonable assumption is that the stress within the steel plates propagates at a 45-degree angle from where the force is applied, which is a common assumption for limit states such as effects around concentrated forces. Figure 2.72 illustrates the stress contours produced by the cross-frame member design

envelope forces in the HRBS and the stiffener plate. As observed in this figure, the stress transmission within the steel plates agrees with an approximate 45-degree angle.

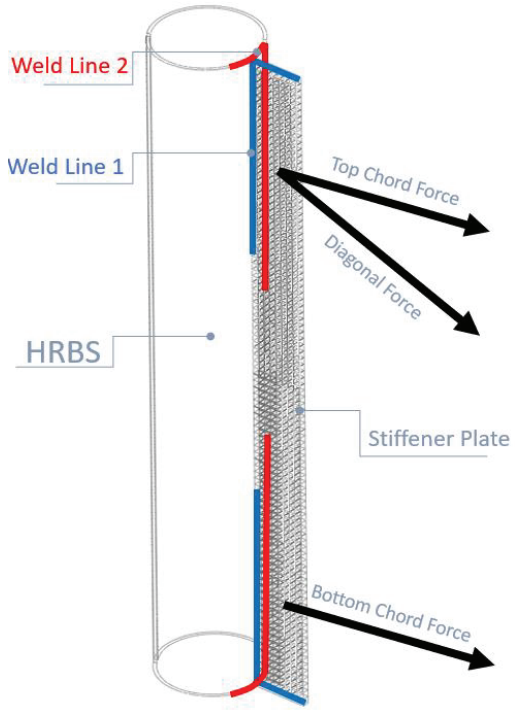

Figure 2.70- HRBS connection fillet weld effective lines for welded condition

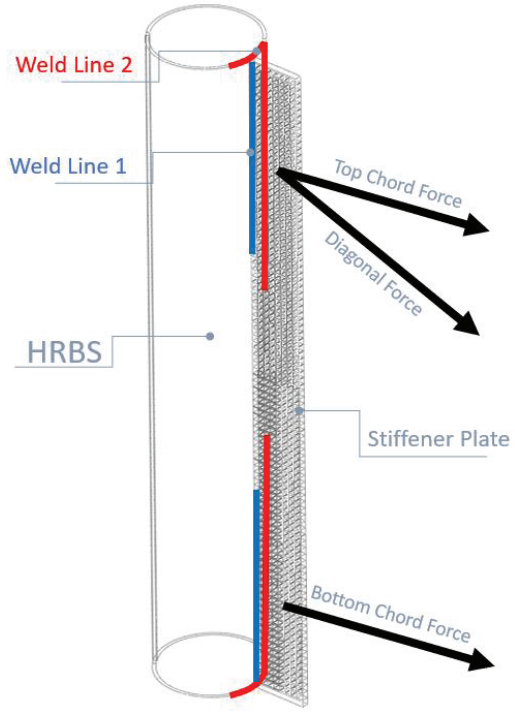

Figure 2.71- HRBS connection fillet weld effective lines for unwelded condition

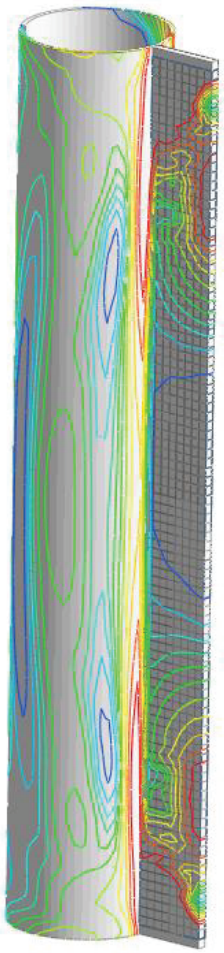

Figure 2.72- Stress distribution in HRBS and stiffener of Bridge 72 with all cross-frame members under tension

In Bridge 72, the height of the steel I-girder is sufficiently large to ensure that the stresses originating from the top chord and diagonal elements do not influence the stresses generated by the bottom chord noticeably. Consequently, the effective weld lines can be identified separately for the top and bottom portions of the connection. Given that the combined horizontal design envelope forces from the top chord and diagonal elements normally exceed those from the bottom chord, the weld lines at the top are considered to be more critical. This calculation represents the total horizontal component of the forces from the top chord and diagonal element (θ is the angle of diagonal chord with respect to the horizontal, which was 33 deg (Figure 2.73). in Bridge 72):

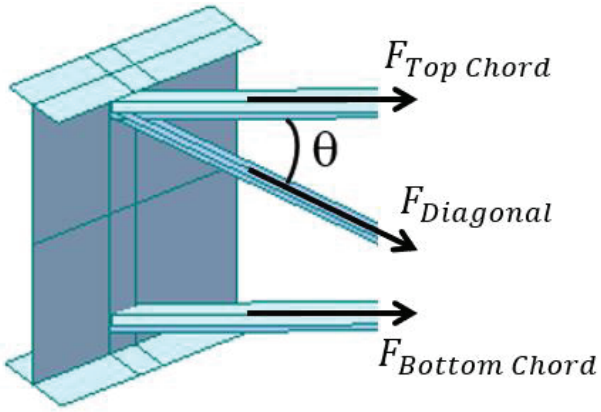

Figure 2.73- Positive direction of end cross-frame internal forces in Bridge 72

$$F_{Total-H} = F_{Top\ Chord-H} + F_{Diagonal-H} = F_{Top\ Chord} + F_{Diagonal} \times \cos\theta$$

$$F_{Total-H} = 68 + 102 \times \cos(33°) = 154\ kips$$

The minimum required length of 5/16-in. fillet weld therefore is:

$$\frac{154}{7.42} = 20.75\ inch$$

Figure 2.74 and Figure 2.75 illustrates the stress transfer process within the stiffener plate. The top chord and diagonal element are attached to the stiffener plate through 12 bolts, with the forces assumed equally divided among these bolts. Every square depicted in the figure measures 1 inch by 1 inch, resulting in a total length of 33 and 25 inches for Weld Line 1 for welded and unwelded conditions, respectively. Considering that welding can be performed on both sides of the stiffener plate to the HRBS, the overall lengths of Weld Line 1 for welded and unwelded condition amounts to 66 and 50 inches, respectively. Both of these lengths are significantly greater than the required 20.75 in.

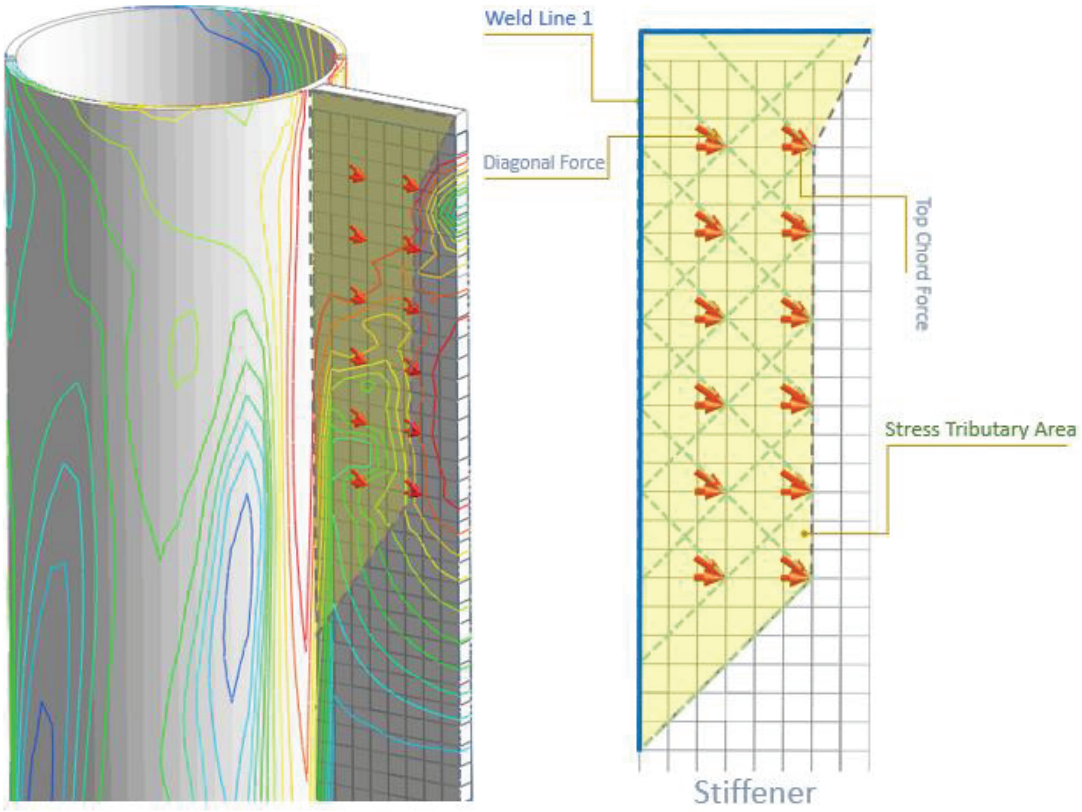

Figure 2.74- Stress transferring in the stiffener plate for welded condition

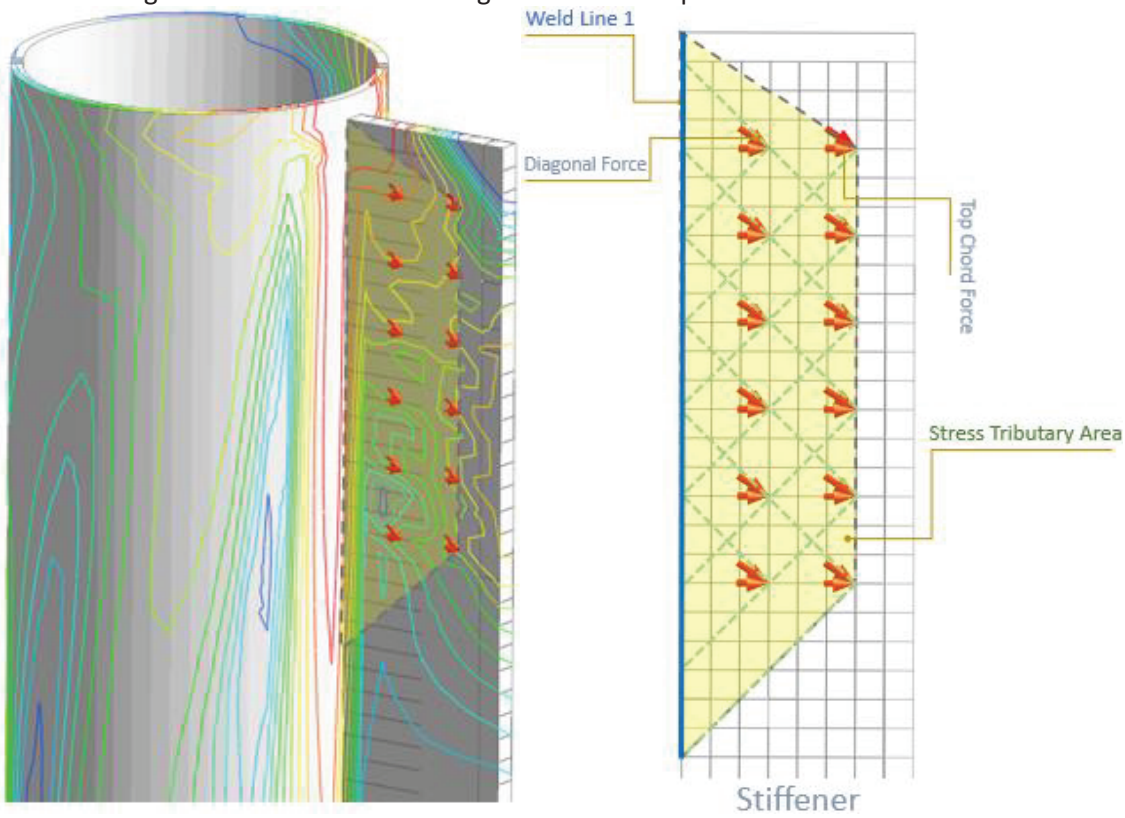

Figure 2.75- Stress transferring in the stiffener plate for unwelded condition

With similar approach, the Weld Line 2 (Figure 2.70 and Figure 2.71) that links the HRBS to steel I-girder can be determined. However, although Weld Line 2 is only on one side, further distribution of the forces toward Weld Line 2 will create a weld length much larger than 50/2 = 25 in. estimated for Weld Line 2, therefore, indicating that 5/16 fillet weld will be adequate also for Weld Line 2. This applies to all configurations of the HRBS connections in Bridge 72. Furthermore, for Bridges 65 and 25 where the level of forces is significantly lower than those considered in Bridge 72, this weld size will also suffice.

2.2.3.12 Fatigue Consideration

The overall objective of this study is to develop a testing plan for fatigue categorization of the HRBS connection as it relates to the girder flange in tension. As outlined earlier, AASHTO LRFD [73] requires fatigue performance evaluation for structural elements under net tensile stress for the Fatigue load combinations based on detail categories defined in AASHTO Table 6.6.1.23-1. These categories are established through comprehensive studies and experimental tests. The Level I analyses in this study were used to determine the stress ranges the girder flange may experience from fatigue loading taking into account the 3D effect of the cross-frame members. The connection components were also sized through the Level 2 analyses. The resulting procedures should suffice for sizing of the girder specimens for fatigue testing.

Furthermore, fatigue can also be a consideration for the connection components. The fatigue category for the connection itself, mainly for the HRBS, has not been defined. There is no detail in Table 4.5 of the AWS D1.1/D1.1M [135] or Table 6.6.1.2.3-1 of the AASHTO LRFD [73] that could represent the HRBS connection. One could draw similarity between connections featured in Table 4.5 of the AWS D1.1/D1.1M [135] or Table 6.6.1.2.3-1 of the AASHTO LRFD [73] and possibly choose a category. However, there is not a well-defined process for determining the effective tensile stress range. Evaluating the connection for fatigue in the absence of suitable experimental fatigue testing is not feasible. Consequently, this section aims only to identify potential fatigue-prone zones to predict the likely locations of fatigue crack initiation within these connections, and stress risers that may affect the fatigue performance of the connection.

The Level I analyses included Fatigue I load combinations for all 26 bridges, with the results documented earlier in this report. These findings represent the maximum and minimum fatigue internal forces in the end cross-frames induced by the fatigue load truck (HS-20) traversing the bridge along the viable bridge lanes. However, as described earlier, the approach for determining fatigue force ranges for the use in the refined FEM models are for a case where the fatigue truck traverses a single lane known to induce the most critical internal forces in the end cross-frames when compared to all other possible lanes. This is consistent with provisions of AASHTO LRFD regarding positioning of the fatigue truck. These calculated internal force ranges, regarded as tensile loads, were assumed conservatively to simultaneously impact the cross-frames.

2.2.3.12.1 Maximum Fatigue Stress Concentration Ranges

The half-round bearing stiffener connection models as per the configurations shown in Table 2.24 were analyzed through Finite Element Method (FEM) by subjecting them to various Fatigue I load ranges. It should be emphasized that the forces applied to the model are force ranges obtained by adding the absolute value of minimum envelope force (compression) to the absolute value of the maximum envelope force (tension), therefore, they include the entire range from compression to tension. There have been discussions on which stress is more critical for fatigue considerations with most supporting the argument for the principal stress. Accordingly, for completeness, Table 2.25 displays absolute value of both the highest Von Mises and principal stress concentration ranges detected in the connections of the three bridge models.

Table 2.25- FEA maximum von Mises and principal fatigue I stress concentration ranges for bridge models

Bridge No.	Weld Condition	Clipping Condition	HRBS thickness (in.)	Max Fatigue I Stress Range in I-girder (ksi)		Max Fatigue I Stress Range in Stiffener (ksi)		Max Fatigue I Stress Range in Half Round (ksi)	
				$\sigma_{von\ Misses}$	$\sigma_{Principal}$	$\sigma_{von\ Misses}$	$\sigma_{Principal}$	$\sigma_{von\ Misses}$	$\sigma_{Principal}$
72	Unwelded	NC	3/4	2.14	2.47	13.71	16.58	11.27	11.48
		C		2.34	2.62	13.46	16.42	15.12	14.71
	Welded	NC	1/2	3.38	4.60	11.87	14.54	7.56	8.83
		C		3.22	4.33	11.21	13.71	7.49	8.00
25	Unwelded	C	5/8	3.36	3.52	19.66	24.45	21.09	18.1
	Welded		3/8	3.86	3.55	9.64	9.93	13.59	8.25
65	Unwelded	C	5/8	3.50	3.22	18.93	25.47	27.95	26.86

2.2.3.12.2 Detailed Description of Fatigue Stress Concentration Ranges for Bridge 72

In Bridge 72, four distinct connection scenarios, each with varying detailing, have been put forward. Following includes a detailed discussion of the maximum principal stress concentration ranges and their location in the connection associated with Bridge 72.

2.2.3.12.2.1 Unwelded and Non-Clipped Detail

In this detail, the highest principal Stress Concentration Range (SCR) was observed in the stiffener plate at the point where the unwelded stiffener plate connects to the HRBS, with tensile SCR of 16.58 ksi, as illustrated in Figure 2.76. This SCR range reduces to 11.48 ksi upon reaching the HRBS where it joins the bottom flange of the steel I-girder, as depicted in Figure 2.77. Within the core section of the steel I-girder itself, as Figure 2.78 reveals, the peak Fatigue I SCR occurs at the bottom flange where it intersects with the HRBS, marking the SCR at 2.47 ksi. This critical point on the stiffener plate, HRBS, and steel I-girder represent areas most likely susceptible to fatigue in such connection configurations.

Owing to the almost symmetrical characteristics of the detail, similar conditions apply to the upper part of the connection. Figure 2.79 depicts the zones prone to fatigue in the un-clipped HRBS connection with the unwelded stiffener condition, in Bridge 72.

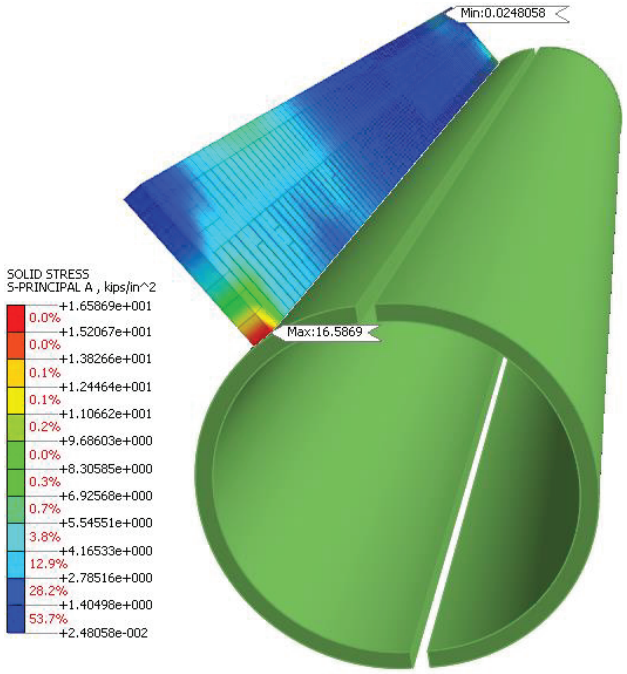

Figure 2.76- SCR contours in stiffener plate for non-clipped & unwelded condition model in Bridge 72 - bottom view

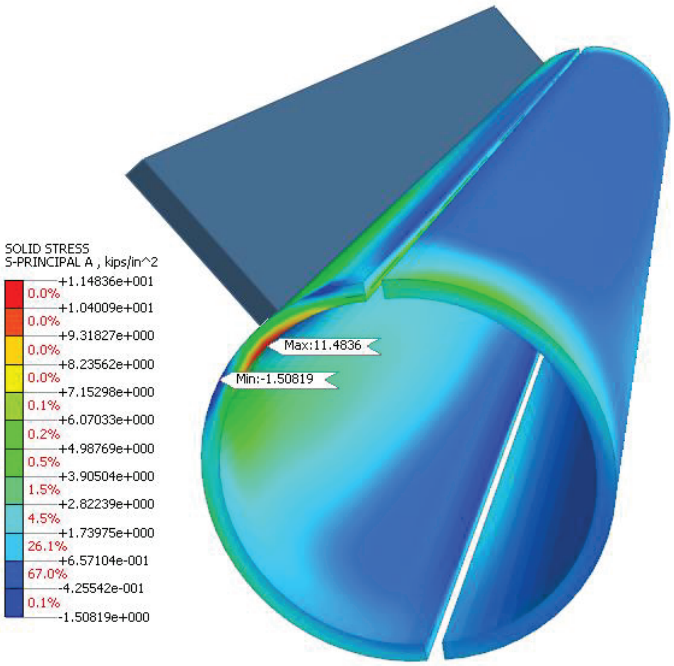

Figure 2.77- SCR contours in HRBS for non-clipped & unwelded condition model in Bridge 72 - bottom view

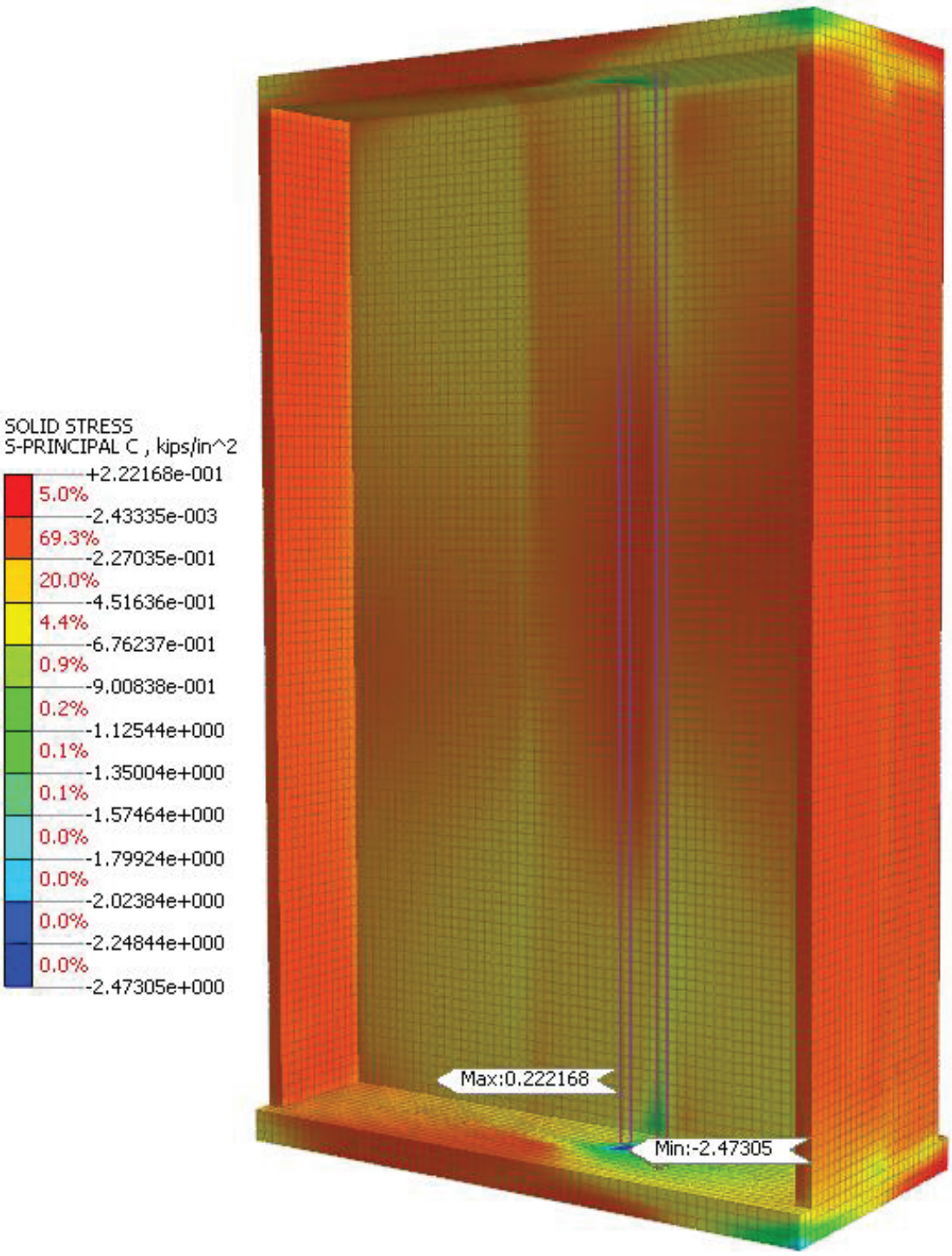

Figure 2.78- SCR contours in steel I-girder for non-clipped & unwelded condition model in Bridge 72 – 3D view

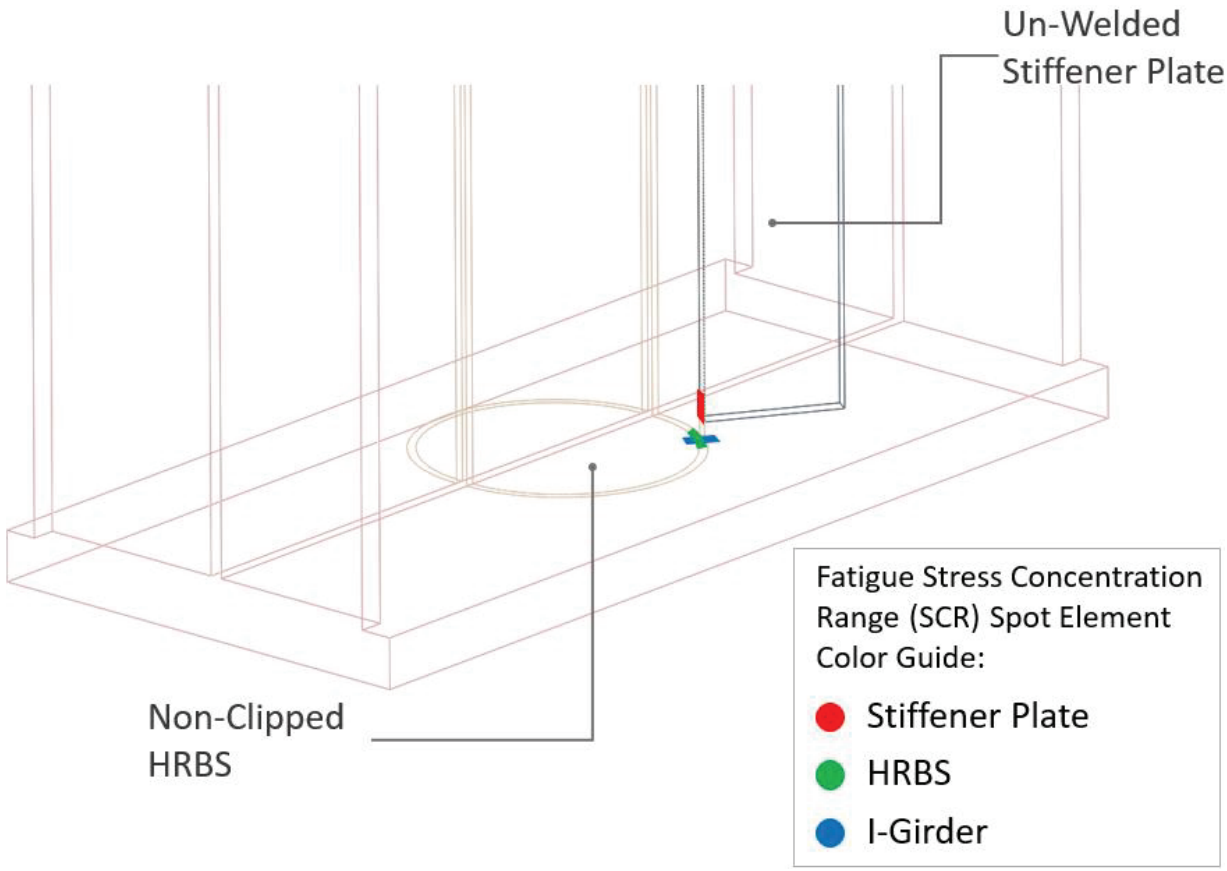

Figure 2.79- Locations of maximum SCR in non-clipped & unwelded connection model in Bridge 72

2.2.3.12.2.2 Unwelded and Clipped Detail

For clipped HRBS and unwelded stiffener plate, Figure 2.80 reveals that the peak (principal) SCR occurs on the inner surface of the clipped HRBS at the point where it meets the bottom flange, reaching 14.71 ksi. Following closely, the unwelded stiffener plate records the highest SCR of 16.42 ksi where it attaches to the HRBS near the bottom flange, as shown in Figure 2.81. Additionally, Figure 2.82 shows SCR of 2.62 ksi on the steel I-girder in the bottom flange where the HRBS connects to the web.

These crucial SCR points on the stiffener plate, HRBS, and steel I-girder highlight the potential fatigue vulnerabilities in such connection detail.

Similar stress concentration conditions are expected on the upper part of the connection. Figure 2.83 displays the areas susceptible to fatigue in the connection of the clipped HRBS with the unwelded stiffener plate in Bridge 72.

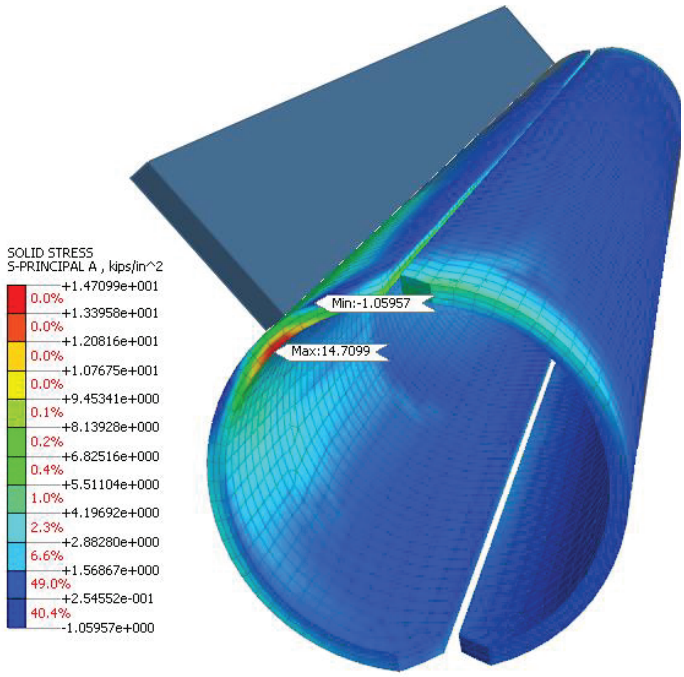

Figure 2.80- SCR contours in clipped HRBS for clipped & unwelded condition model in Bridge 72 - bottom view

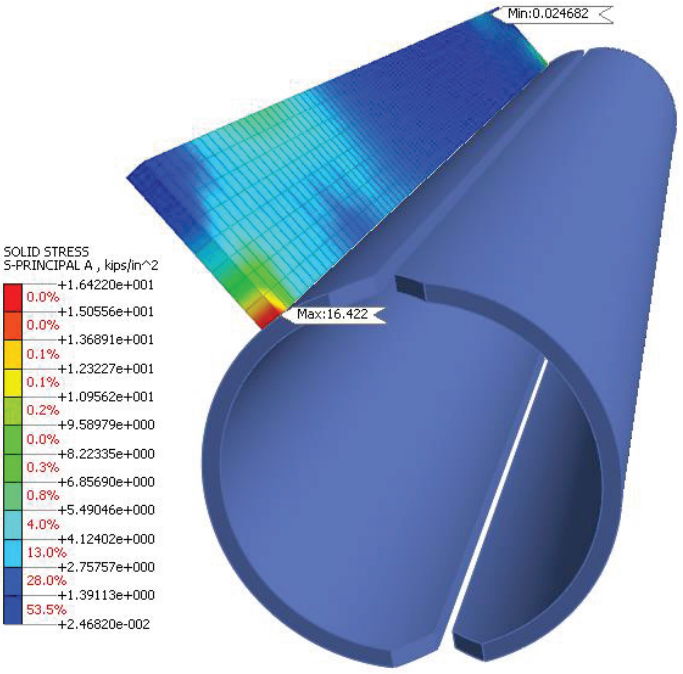

Figure 2.81- SCR contours in stiffener palte for clipped & unwelded condition model in Bridge 72 - bottom view

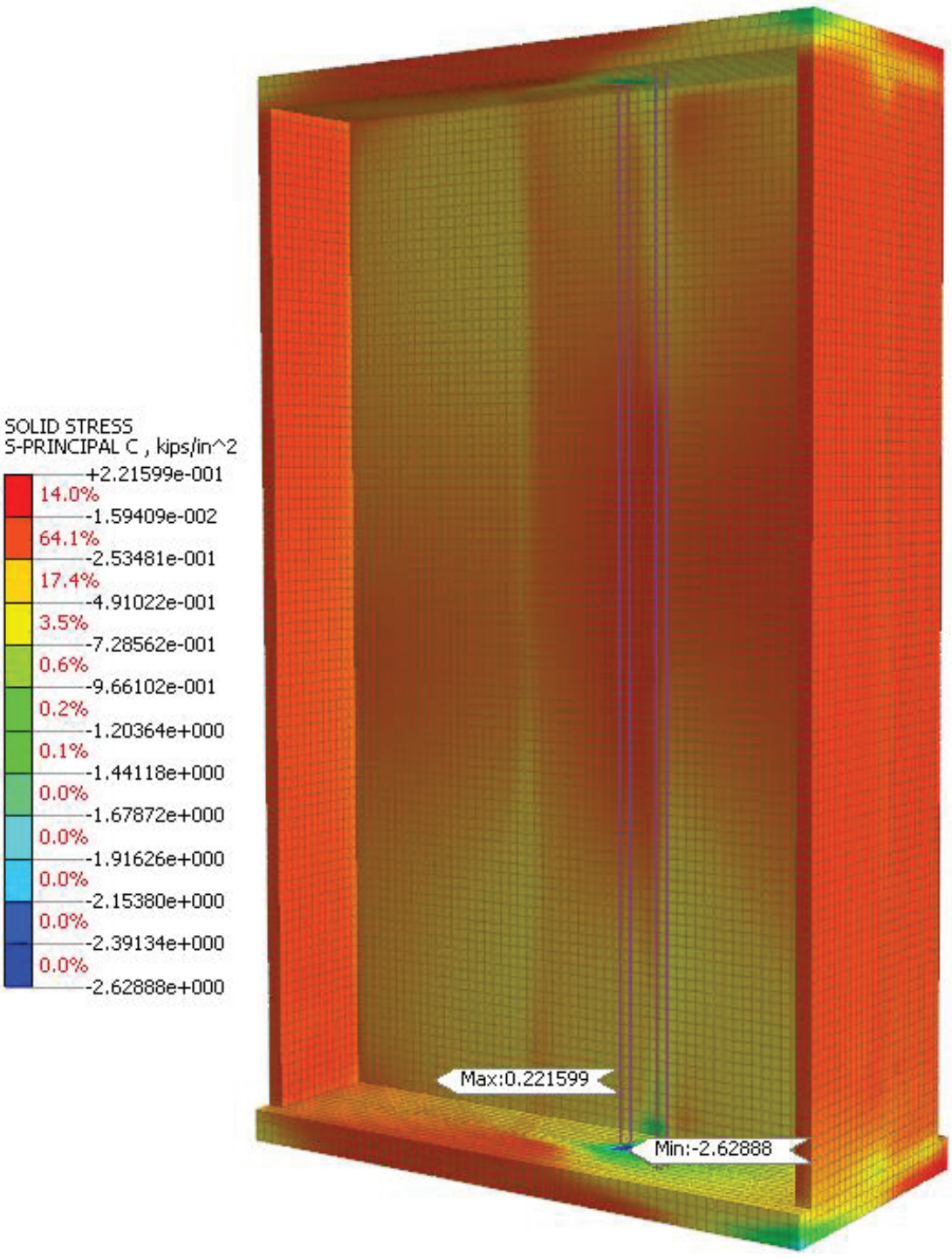

Figure 2.82- SCR contours in steel I-girder for clipped & unwelded condition model in Bridge 72 – 3D view

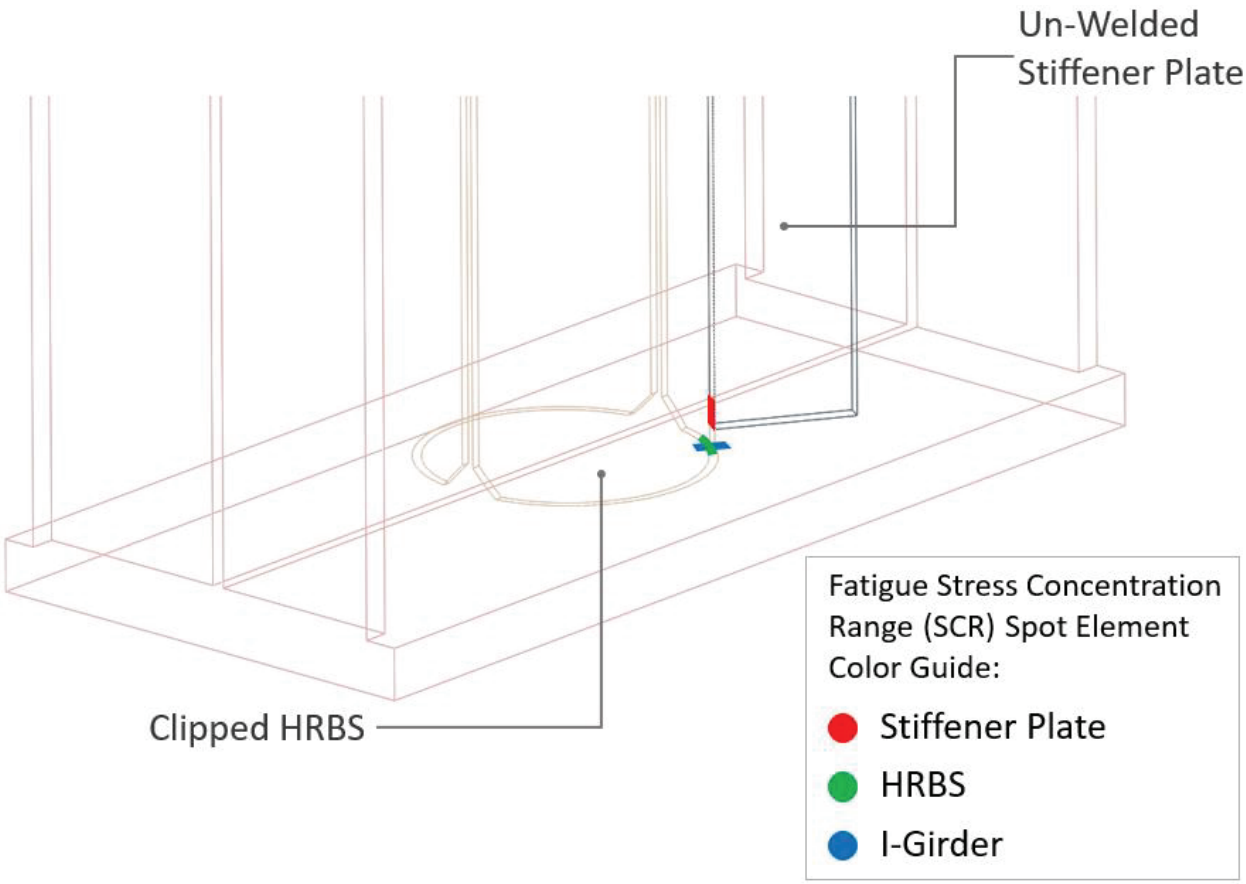

Figure 2.83- SCR positions in clipped HRBS & unwelded stiffener plate model in Bridge 72

2.2.3.12.2.3 Welded and Non-Clipped Detail

In a non-clipped HRBS with a welded stiffener plate, the most significant SCR is 14.5 ksi, located at the stiffener plate toe where it attaches to the bottom flange, as illustrated in Figure 2.84. This indicates a shift in the fatigue-sensitive zone to the stiffener toe in welded conditions. The HRBS itself exhibited the second highest SCR at 8.83 ksi, occurring at the inner layer where the stiffener plate, HRBS, and bottom flange intersect (Figure 2.85). Figure 2.86 shows the SCR within the steel I-girder for this type of connection, revealing the highest SCR of 4.60 ksi just below the toe of the welded stiffener. Figure 2.87 presents the SCR position for the non-clipped HRBS in a welded stiffener condition.

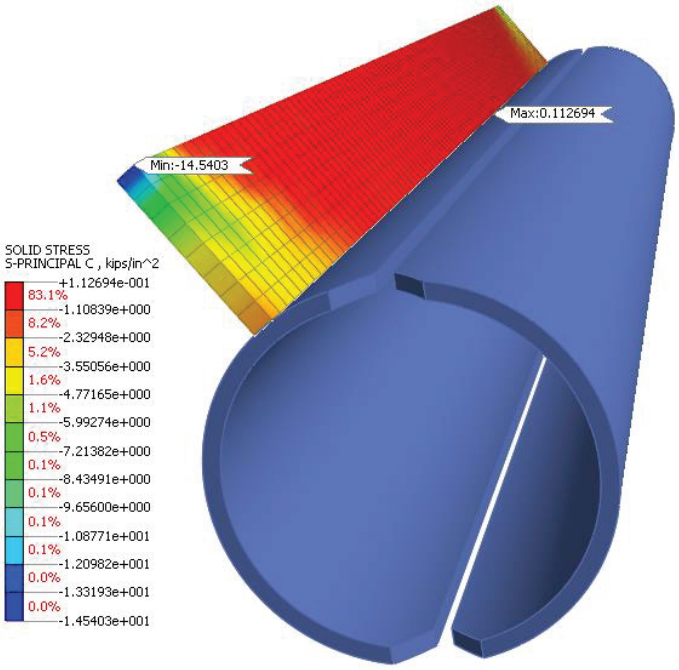

Figure 2.84- SCR contours in welded stiffener plate for non-clipped & welded condition model in Bridge 72 - bottom view

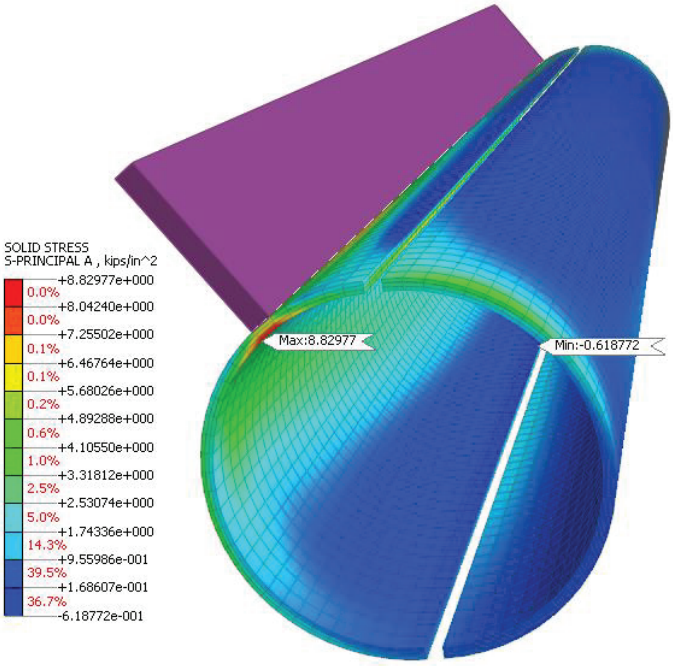

Figure 2.85- SCR contours in non-clipped HRBS for non-clipped & welded condition model in Bridge 72 - bottom view

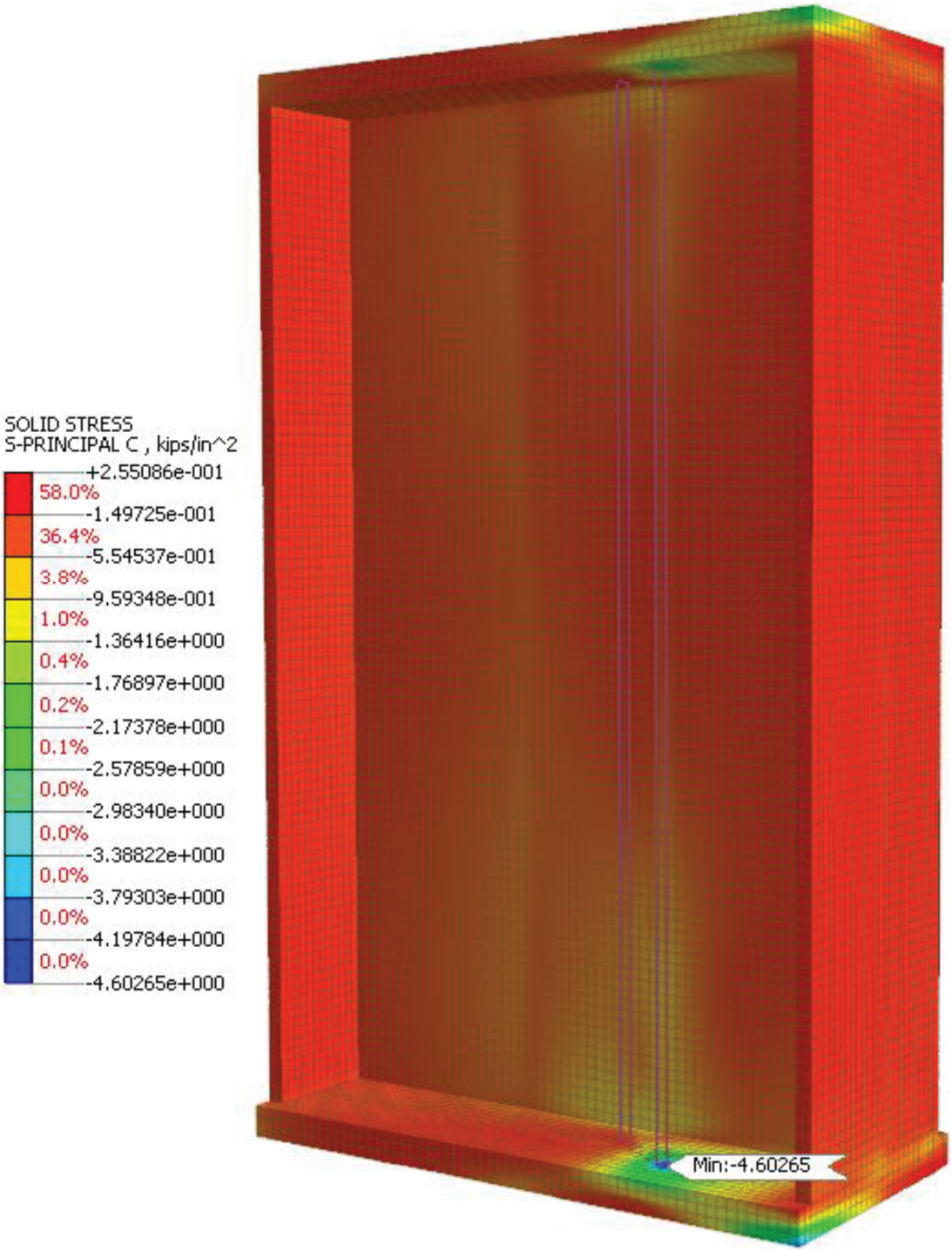

Figure 2.86- SCR contours in steel I-girder for non-clipped & welded condition model in Bridge 72 – 3D view

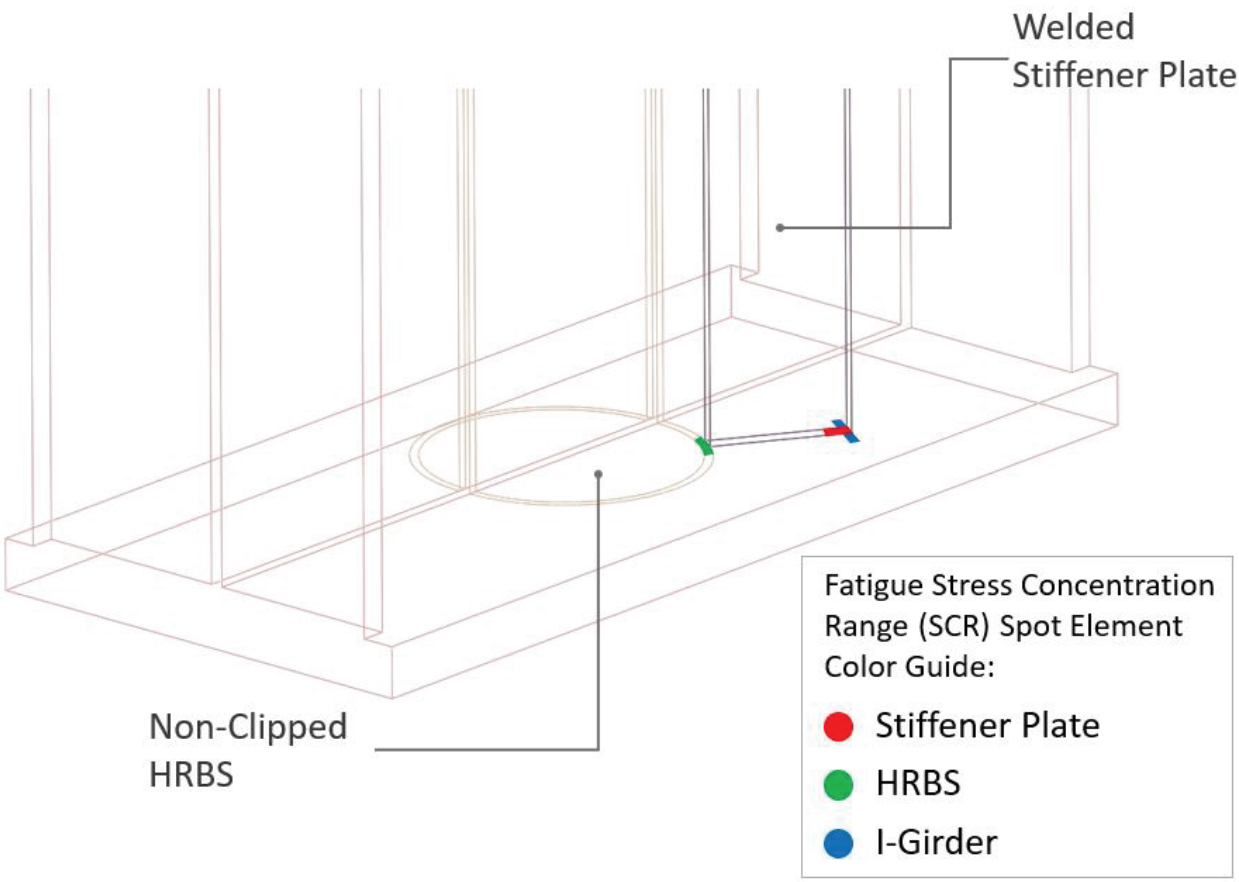

Figure 2.87- SCR positions in non-clipped HRBS with welded stiffener plate in Bridge 72

2.2.3.12.2.4 Welded and Clipped Detail

For the clipped HRBS paired with a welded stiffener, Figure 2.88 reveals that the stiffener plate's toe experiences the (principal) SCR measuring at 13.71 ksi. The clipped HRBS shows a SCR of 8.00 ksi at the juncture where it meets the bottom flange and the welded stiffener plate, as depicted in Figure 2.89. As for the steel I-girder, the peak SCR, noted is 4.34 ksi, located directly beneath the stiffener plate's toe, highlighted in Figure 2.90. Figure 2.91 details the critical SCR locations within each element of the connection. Due to approximate symmetrical behavior, similar critical points can also be identified on the connection's upper side.

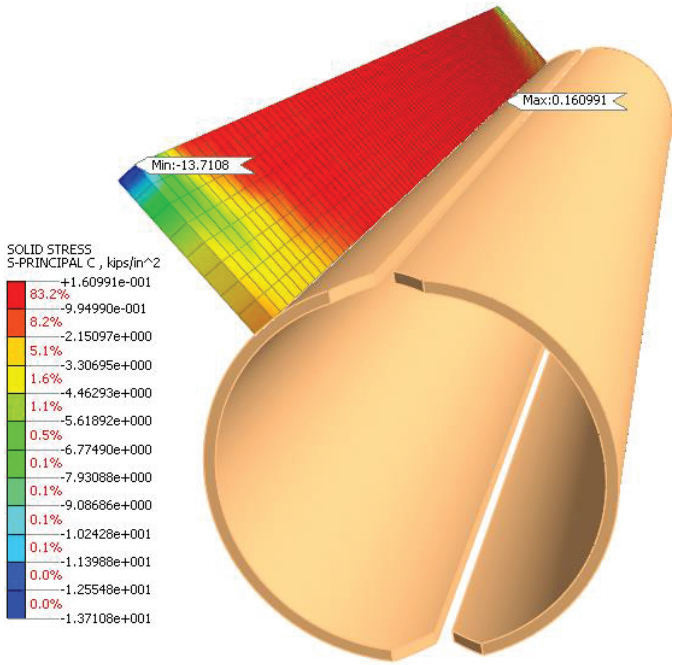

Figure 2.88- SCR contours in welded stiffener plate for clipped & welded condition model in Bridge 72 - bottom view

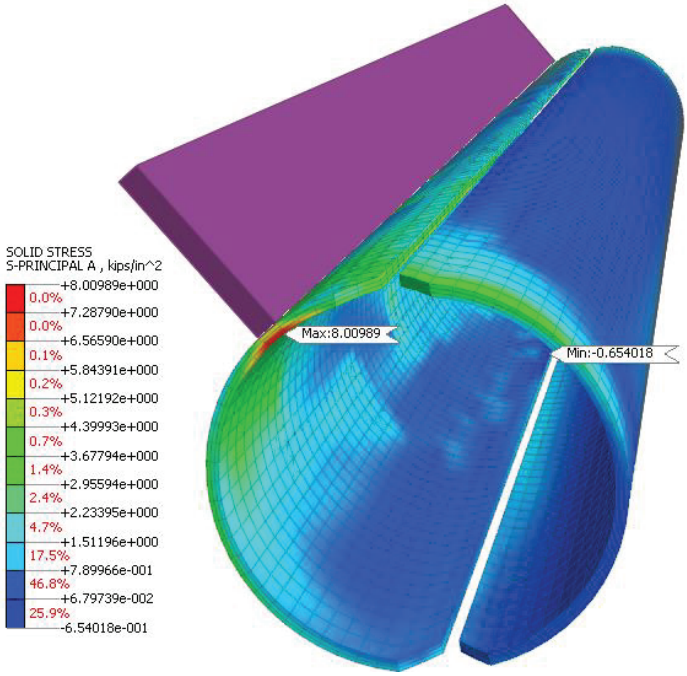

Figure 2.89- SCR contours in clipped HRBS for clipped & welded condition model in Bridge 72 - bottom view

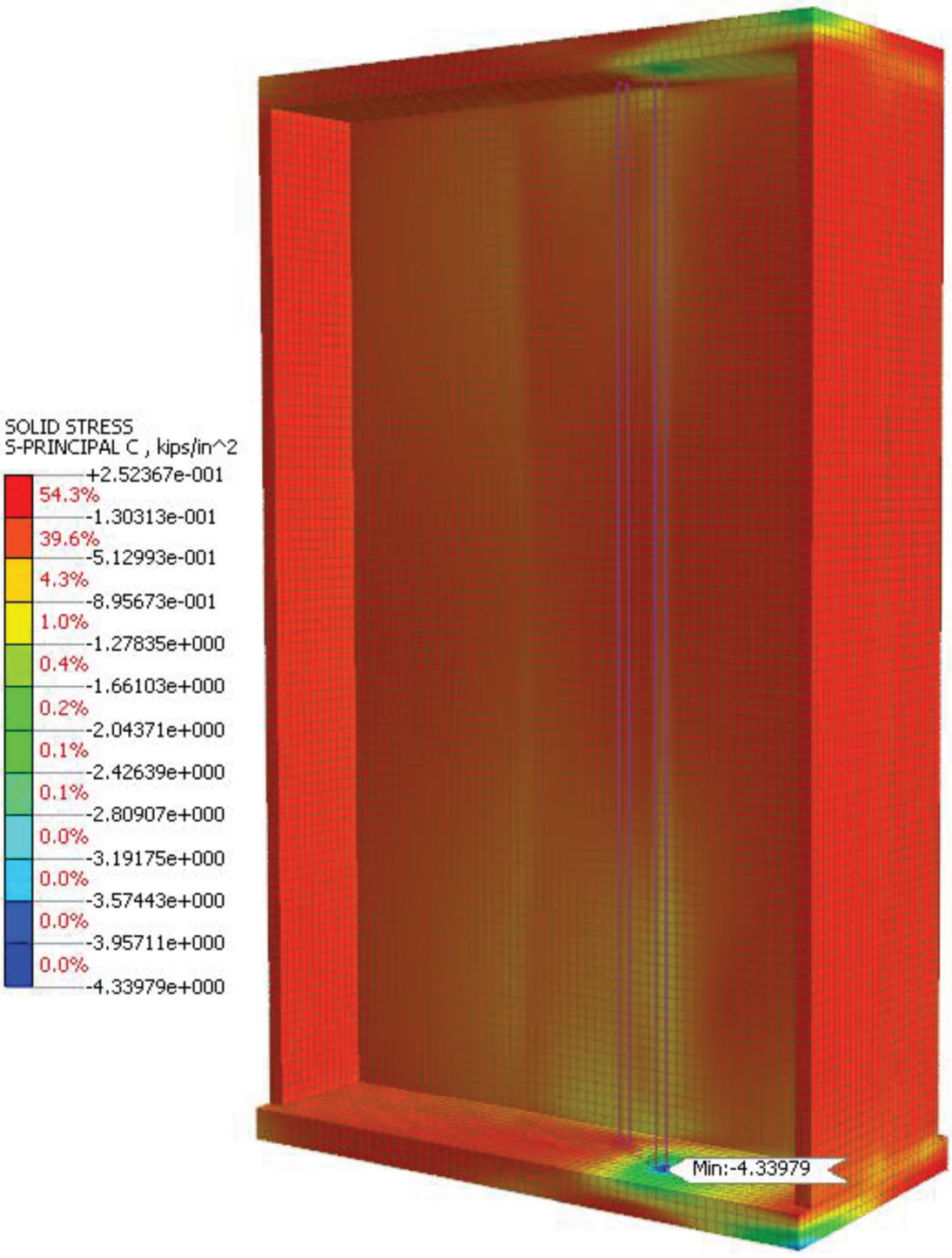

Figure 2.90- SCR contours in steel I-girder for clipped & welded condition model in Bridge 72 – 3D view

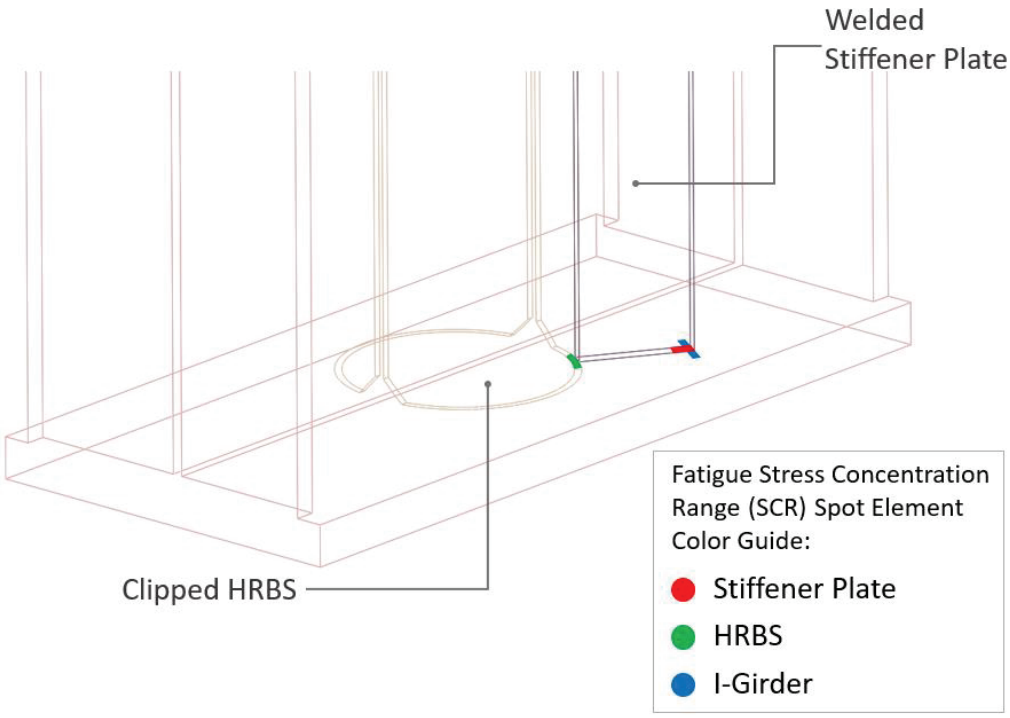

Figure 2.91- SCR positions in clipped HRBS with welded stiffener plate in Bridge 72

2.2.3.12.3 Distortion Effects for the Case of Unwelded Stiffener Plate

Stress and strain concentration ranges for the condition of unwelded stiffener plate were calculated and compared to correspondign values in the welded condition to provide a measure of the effects of distortion. Among the details representing the three selected bridges, the detail for Bridge 72 with the highest level of cross-frame member forces was selected for this purpose. Therefore, all discussions in this section pertain to details in Bridge 72. Contour plots of the principal stress and principal strain for HRBS connection subjected to the critical Fatigue-I Load (TTT) are shown in Figure 2.92 and Figure 2.93, respectively. The detail shown consists of the HRBS with clipped corners at the flange to the web junction and the stiffener plate not welded to the flanges. Similar contour plots for clipped and welded condition are provided in Figure 2.94 and Figure 2.95. The results, including the maximum principal stress and principal strain, are also summarized in Table 2.26. The sizing of the welded and unwelded details follows those selected for Bridge 72 in Table 2.21. The location of the maximum values of the specific variables is also shown in the figures. The deformed shapes in these figures are caused from Fatigue-I force ranges and have been scaled up such that the maximum displacement equals to 1/20 size of the maximum dimension of the model that is the girder depth of 96 in.

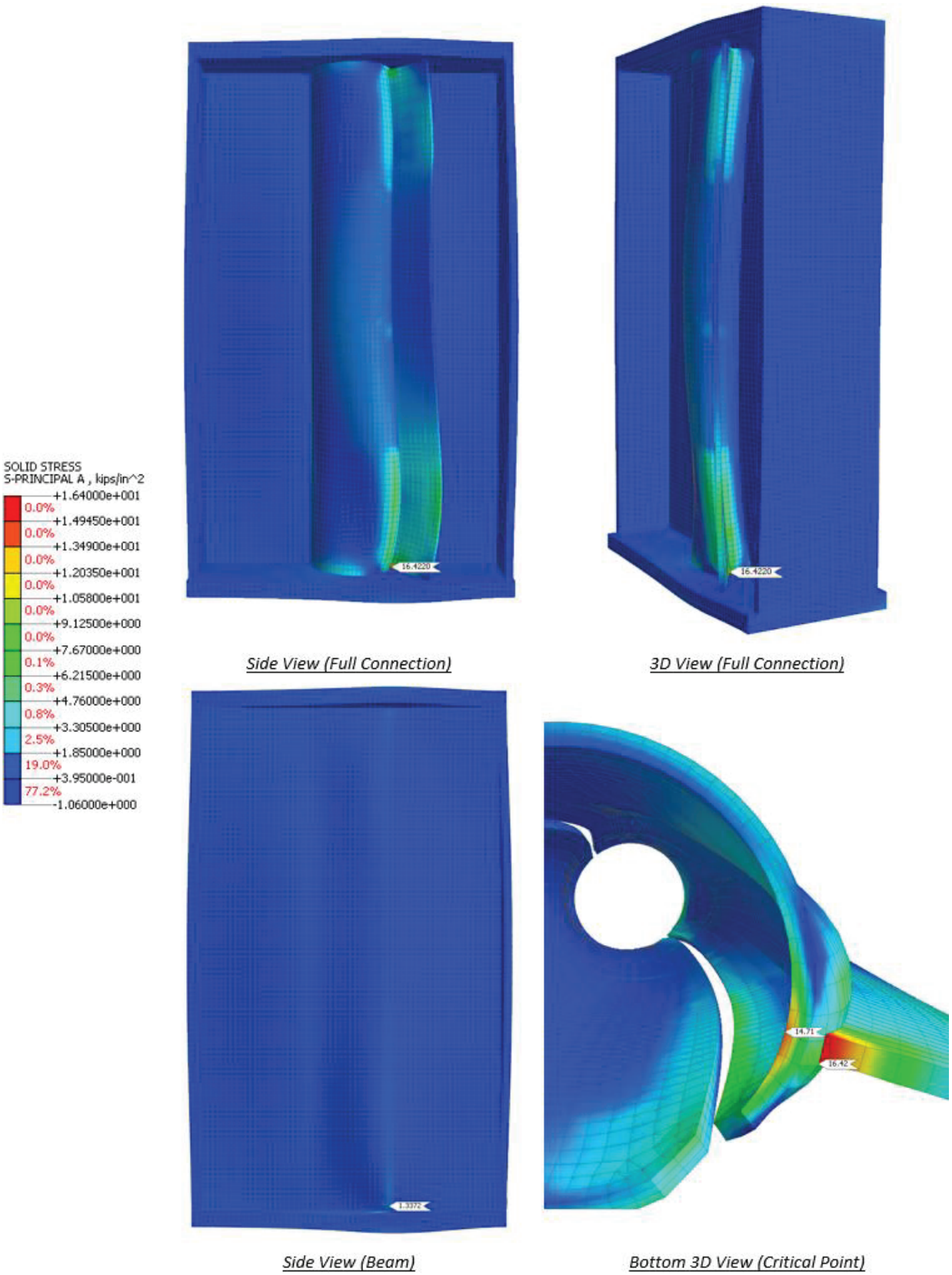

Figure 2.92- Principal stress contour with deformed shape for unwelded and clipped HRBS connection in Bridge 72 under Fatigue-I loading (TTT condition)

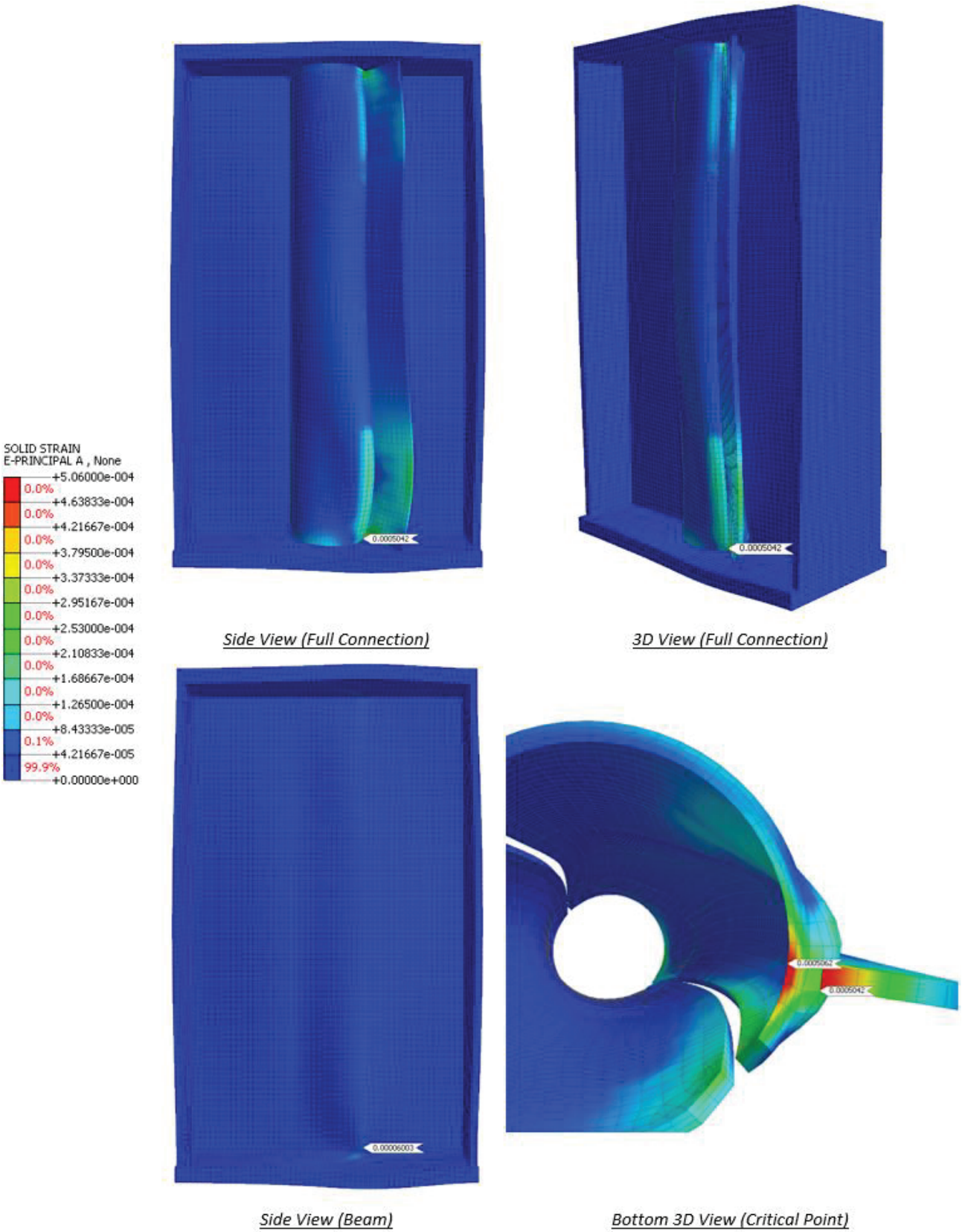

Figure 2.93- Principal strain contour with deformed shape for unwelded and clipped HRBS connection in Bridge 72 under Fatigue-I loading (TTT condition)

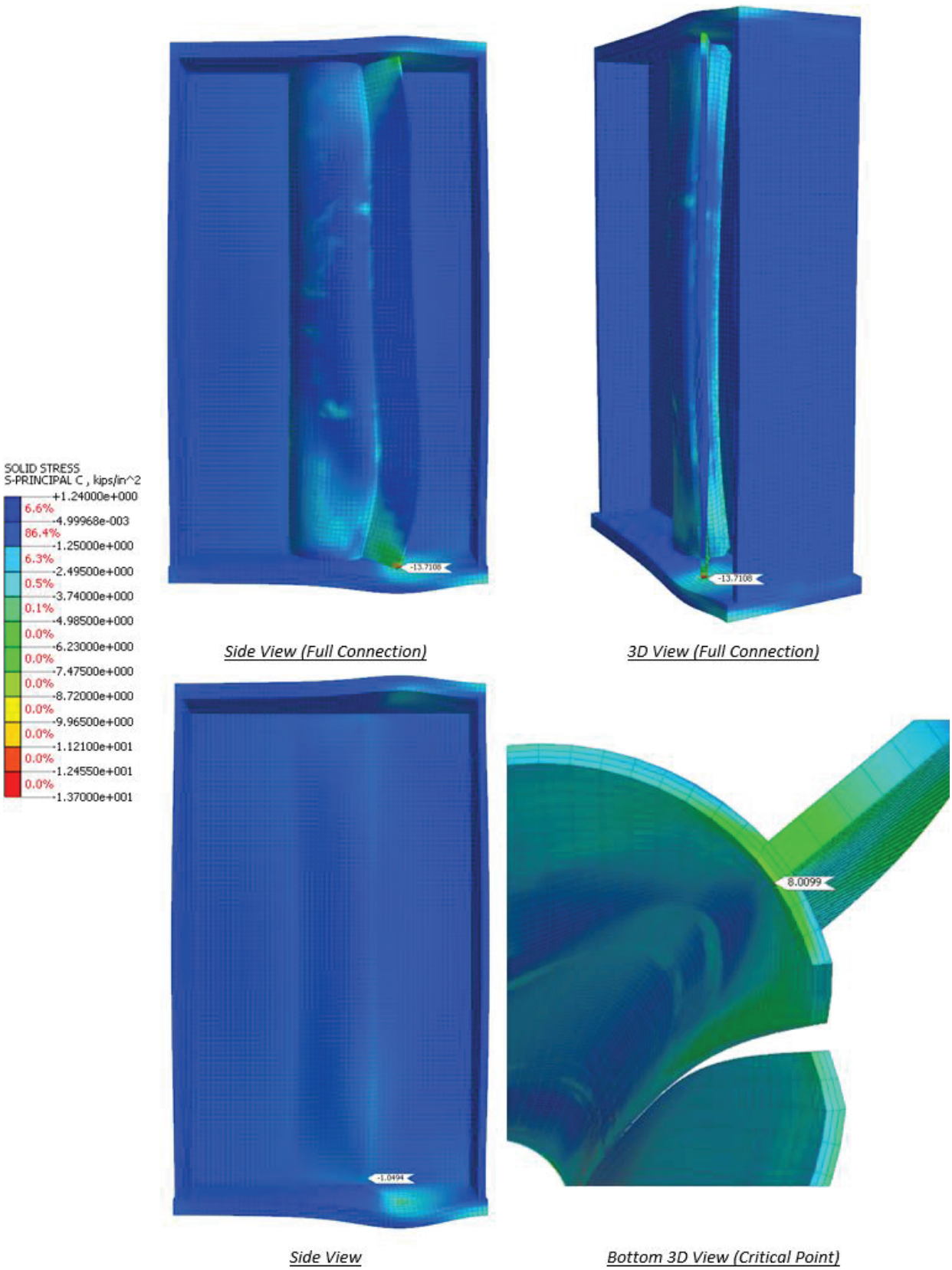

Figure 2.94- Principal stress contour with deformed shape for welded and clipped HRBS connection in Bridge 72 under Fatigue-I loading (TTT condition)

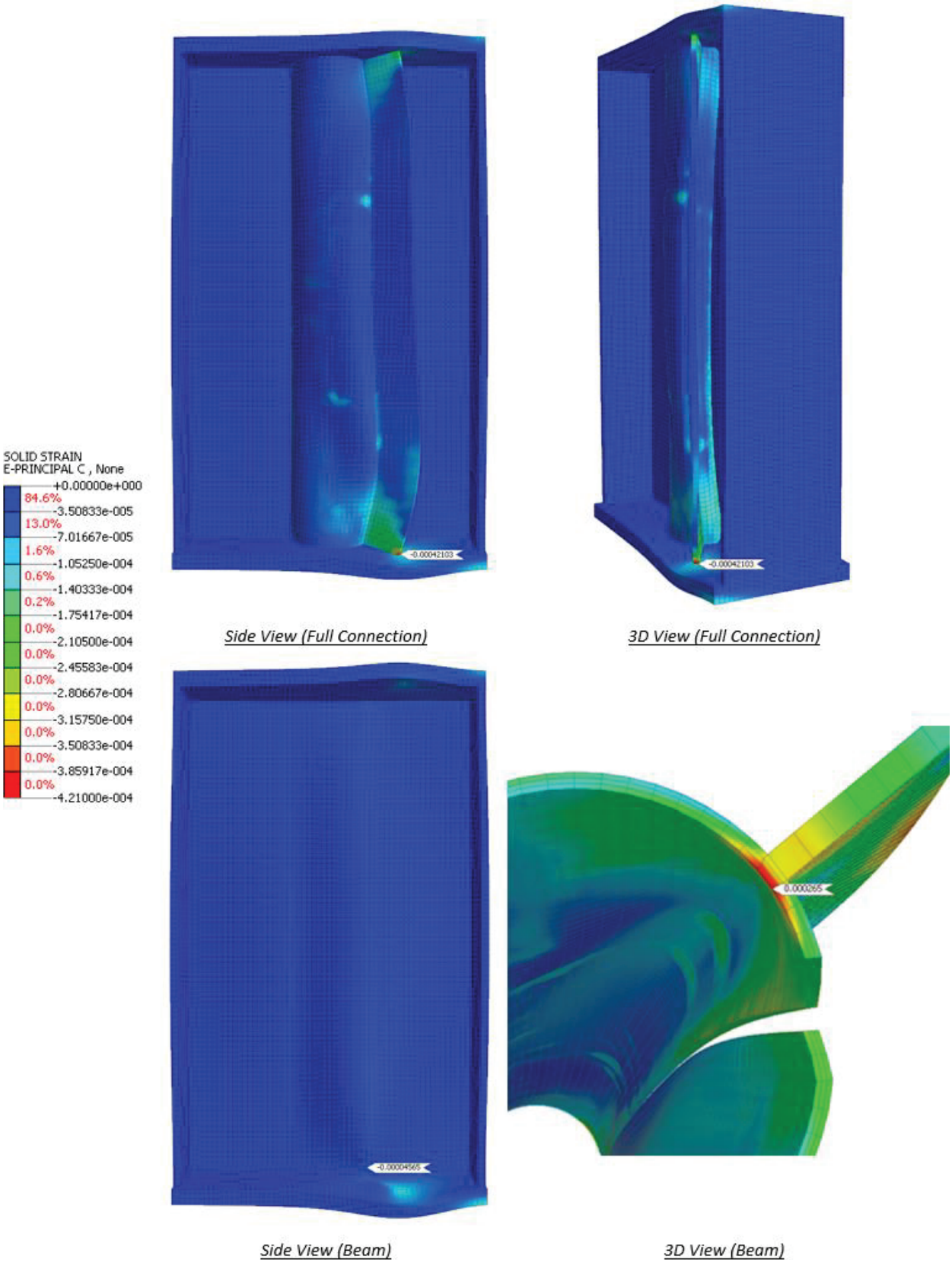

Figure 2.95- Principal strain contour with deformed shape for welded and clipped HRBS connection in Bridge 72 under Fatigue-I loading (TTT condition)

The maximum values of the principal stress concentration range and principal strain concentration range for the details discussed above under the critical Fatigue-I loading are summarized in Table 2.26. The results show that welding the stiffener plate to the flanges considerably reduces the stress and strain when compared to the unwelded condition. It should be noted that the thickness of the Half-Round for the welded connection in the analysis was 1/2 in. compared to a value of 3/4 in. for the unwelded condition. Another observation is that the stress and strain ranges in the web of the girder in both conditions are relatively low.

Table 2.26- FEA results in HRBS connection components due to Fatigue-I force range

Condition	Variables with max. Absolute value	Stiffener Plate	Half-Round Plate	Girder Web
Unwelded	Principal Stress Concentration Range (ksi)	16.42	14.7	1.3372
	Principal Strain Concentration Range	0.0005042	0.0005062	0.0000600
Welded	Principal Stress Concentration Range (ksi)	-13.71	8.01	-1.049
	Principal Strain Concentration Range	0.000421	0.000265	0.00004565

2.2.3.12.4 Maximum Fatigue Stress Concentration Ranges and their Locations

Analysis was performed to obtain the maximum fatigue stress concentration ranges and their locations for the cases modeled for Bridges 65 and 25. Table 2.27 shows the maximum fatigue principal stress concentration ranges and their locations for the connections corresponding to all three bridges.

Table 2.27- SCR and positions in HRBS, Stiffener Plate, and Girder from Fatigue I for representative bridges

Bridge #	Stiffener Welded to Flanges	Clipping Type	HRBS Plate Dimensions (inch)		Maximum Principal Stress Concentration Range and Position in I-girder	Maximum Principal Stress Concentration Range and Position in Stiffener Plate	Maximum Principal Stress Concentration Range and Position in HRBS
			D	t			
Bridge 72	Unwelded	Non-Clipped	16	3/4	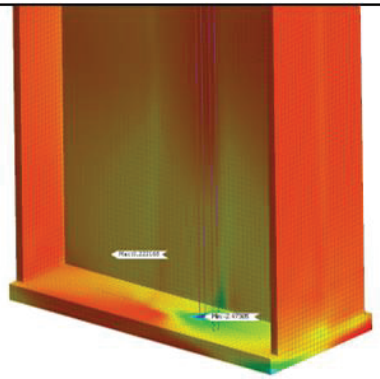 Max SCR = 2.47 (ksi)	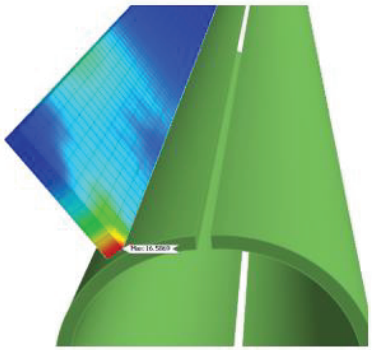 Max SCR = 16.58 (ksi)	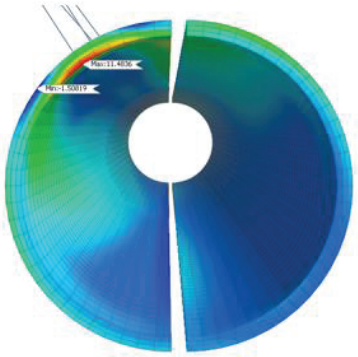 Max SCR = 11.48 (ksi)
		Clipped		3/4	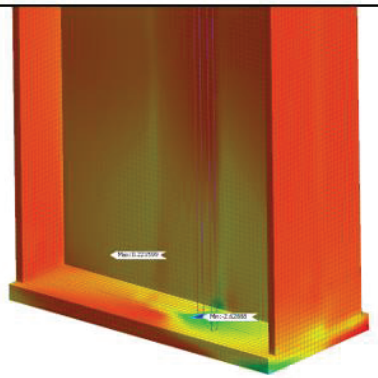 Max SCR = 2.62 (ksi)	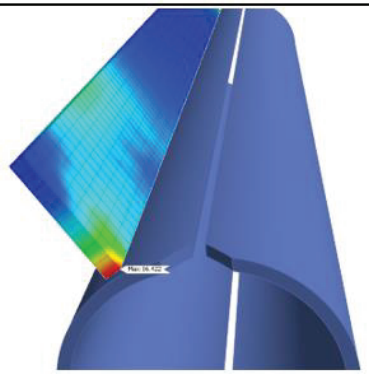 Max SCR = 16.42 (ksi)	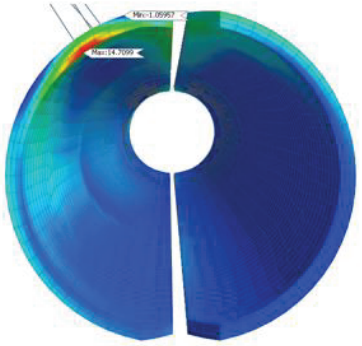 Max SCR = 14.71 (ksi)

Bridge #	Stiffener Welded to Flanges	Clipping Type	HRBS Plate Dimensions (inch)		Maximum Principal Stress Concentration Range and Position in I-girder	Maximum Principal Stress Concentration Range and Position in Stiffener Plate	Maximum Principal Stress Concentration Range and Position in HRBS
			D	t			
	Welded	Non-Clipped	16	1/2	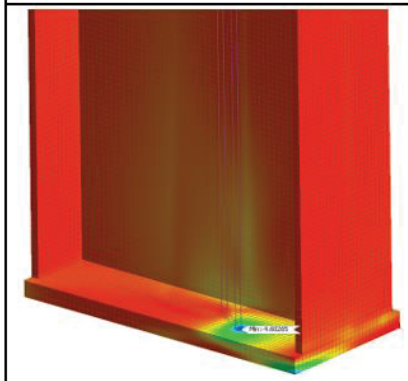 Max SCR = 4.60 (ksi)	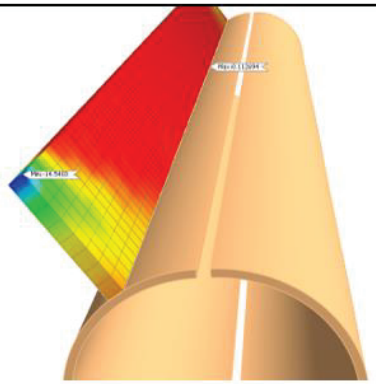 Max SCR = 14.54 (ksi)	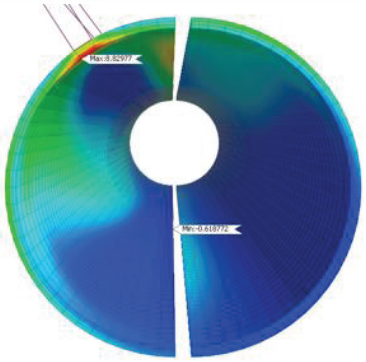 Max SCR = 8.83 (ksi)
		Clipped		1/2	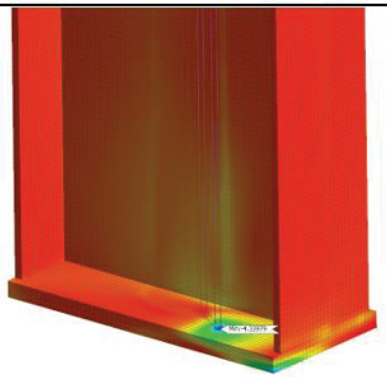 Max SCR = 4.34 (ksi)	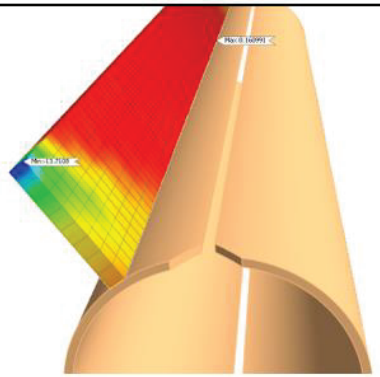 Max SCR = 13.71 (ksi)	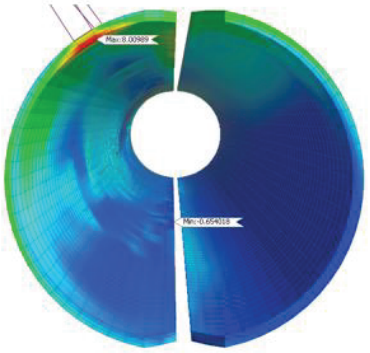 Max SCR = 8.00 (ksi)

Bridge #	Stiffener Welded to Flanges	Clipping Type	HRBS Plate Dimensions (inch)		Maximum Principal Stress Concentration Range and Position in I-girder	Maximum Principal Stress Concentration Range and Position in Stiffener Plate	Maximum Principal Stress Concentration Range and Position in HRBS
			D	t			
Bridge 25	Unwelded	Clipped	16	5/8	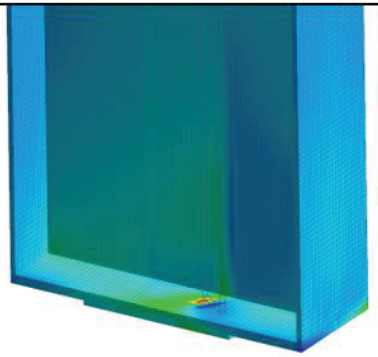 Max SCR = 3.52 (ksi)	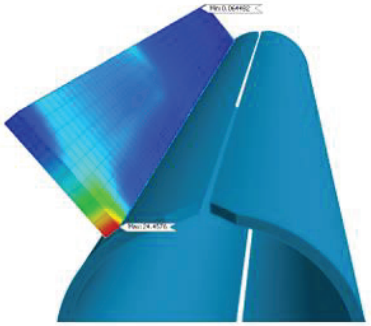 Max SCR = 24.45 (ksi)	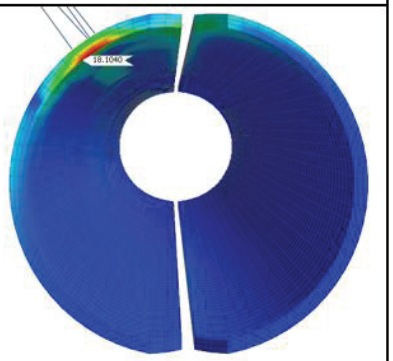 Max SCR = 18.10 (ksi)
	Welded	Clipped		3/8	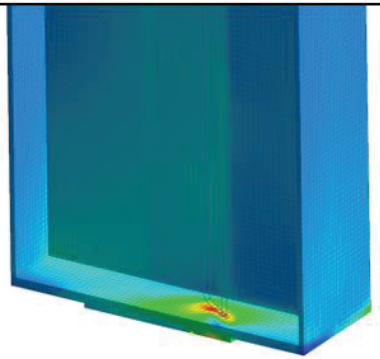 Max SCR = 3.55 (ksi)	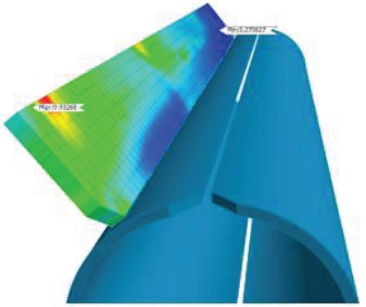 Max SCR = 9.93 (ksi)	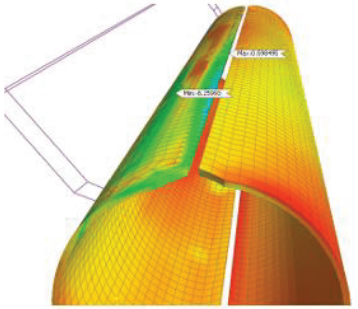 Max SCR = 8.25 (ksi)

Bridge #	Stiffener Welded to Flanges	Clipping Type	HRBS Plate Dimensions (inch)		Maximum Principal Stress Concentration Range and Position in I-girder	Maximum Principal Stress Concentration Range and Position in Stiffener Plate	Maximum Principal Stress Concentration Range and Position in HRBS
			D	t			
Bridge 65	Unwelded	Clipped	11	5/8	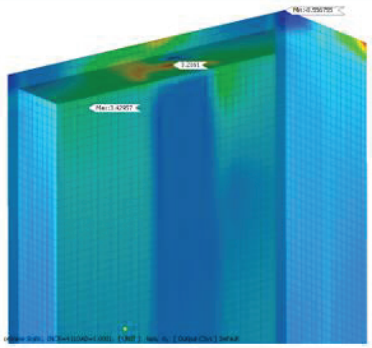 Max SCR = 3.22 (ksi)	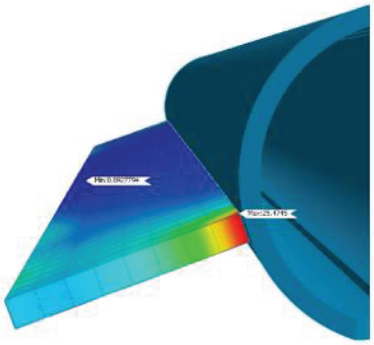 Max SCR = 25.47 (ksi)	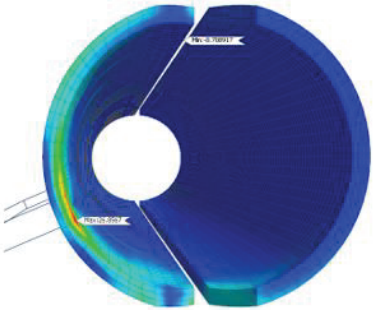 Max SCR = 26.86 (ksi)

2.2.4 Summary and Recommendations

The aim of this task was to develop common sizing and configuration details for half-round bearing stiffener connection for the end cross-frames of a representative subsets of 26 bridges in the state of Florida that were identified for this study. These configurations provide realistic input towards the experimental test plan for the evaluation of a fatigue categorization for the top flanges of continuous steel girders over intermediate skew supports. For this purpose, 3D FEM were performed on all 26 bridges to obtain the fatigue stress range in the top flanges, design forces for end cross-frame members, and fatigue force ranges for cross-frame members. These analyses have been referred to as Level I Analyses. It is important to note that the 3D analyses represented detailed models to accurately capture trends in cross-frame forces and girder flange stresses. The top flange fatigue Stress range from Fatigue I factored loading showed a range between 1.24 to 3.57 ksi with an average of 2.34 ksi. Design and fatigue envelope forces for end cross-frames are summarized in Table 2.12 and Table 2.13.

The results from the Level I analyses, provided valuable input for densely-meshed models that focus on the connections between support cross-frames, the half-round stiffeners, and the girders. The densely-meshed models are referred to as Level II analyses. For Level II analysis, the identified bridge population was subdivided into three groups based upon key parameters consisting of the level of force in the cross-frame members, skew index, and girders moment on inertia. Considering the range of these key parameters, Group 1 represented girders in the lower third of the population of the key parameters, Group 2 represented the middle third, and Group 3 the upper third. Considering the girders within each group, three representative bridges, Bridges 65, 25, and 72, were identified that are common for Group 1, Group 2, and Group 3, respectively. The connection assembly for each representative bridge consisting of half-round bearing stiffener (HRBS), stiffener plate, and a portion of girder between the jacking stiffener plates was then modeled in detail for the Level II analyses. To ensure that the analysis case was representative of the most critical for each group, the highest level of forces obtained from the Level I analysis in each group was applied for each refined model. The diameter of the HRBS was selected so that the flange extends at least 2-in. beyond the HRBS. A variation of thickness for

the HRBS ranging from 3/8 to 3/4 in. was used to determine the appropriate thickness. In the analyses, clipped and non-clipped conditions were considered for the HRBS. In addition, two stiffener connection plate details were modelled consisting of both welded and non-welded conditions with the girder flanges where applicable. The sizing of the HRBS and welds were first performed using the envelope of design forces obtained from Level I analyses and combined for all possible arrangements. The results are summarized in Table 2.28. Because the cross-frame force envelopes and most critical combination of the cross-frame members were utilized, these results represent a conservative yet reasonable condition to what should be found in practice.

Subsequently, the fatigue force ranges obtained from the Level I analyses for cross-frame members were applied to each model to identify the range and location of stress concentrations. The results are summarized in Table 2.27.

Based on these analyses, the three details recommended as prototypes for consideration in the fatigue tests in the next phase of the study are included in the table below. For completeness, the welded and unwelded options for the stiffener plates, as well as clipped and non-clipped options for the HRBS are included in the table. However, it is the recommendation of this study to use only welded stiffener plates wherever possible. This is because the fatigue stress ranges in the top flange estimated in this study are relatively low, minimizing the effects of inclined weld on the flange, and that the welded stiffeners will perform better in regards with distortion fatigue in the connection itself. In addition, welding the stiffener plates is consistent with past details that have been used on cross-frame connection plates to avoid distortional-induced fatigue. The choice between the clipped and non-clipped HRBS options will depend on the results of corrosion testing as per the plan introduced in Task 3. It is also noted that the configurations recommended here will need to be scaled down to accommodate the capacity of the testing laboratory.

Table 2.28- Sizing of the steel I-girder, HRBS, stiffener and welds

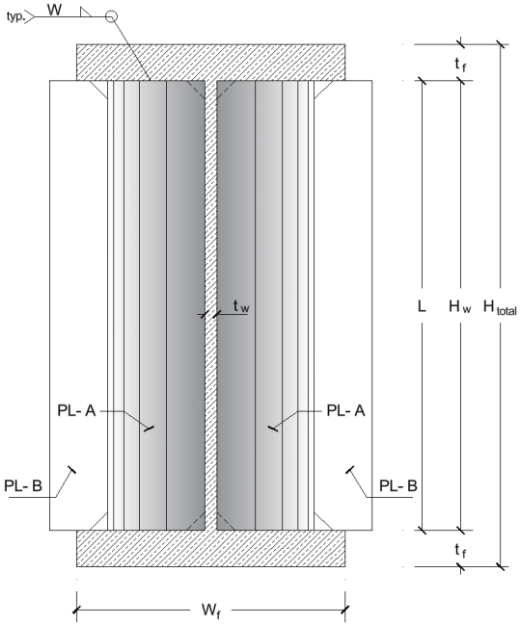

a) Front View

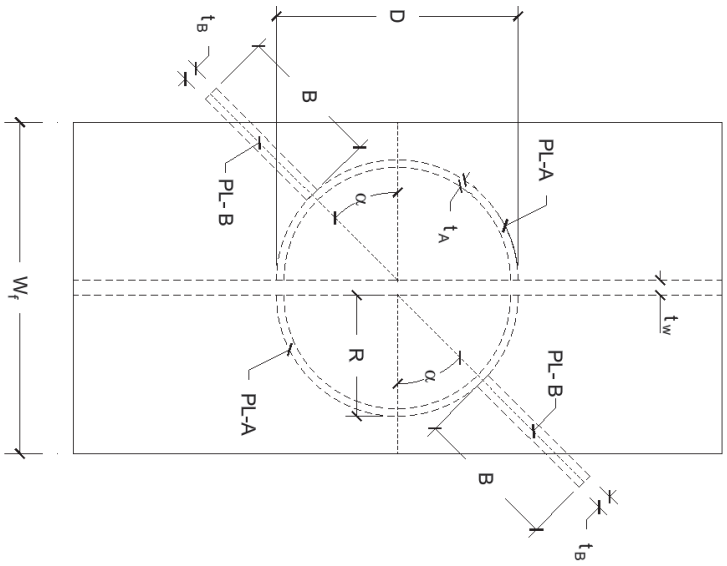

b) Top View

Detail #	Steel I-girder (in.)				Stiffener Welded to Flanges	Clipping Type	PL-A (HRBS) (in.)			PL-B (in.)				Typical Weld Size (in.)
	W_f	t_f	H_w	t_w			D	R	t_A	L	B	t_B	α	W
Detail 1	24	3	96	$\frac{3}{4}$	Unwelded	Non-Clipped	16	8	3/4	94	8	1	57°	5/16
						Clipped								
					Welded	Non-Clipped			1/2	96	8	1	57°	
						Clipped								
Detail 2	22	$2\frac{5}{8}$	90	$\frac{5}{8}$	Unwelded	Clipped	16	8	5/8	87	**8**	1	54°	
					Welded	Clipped			3/8	90				
Detail 3	16	2	66	$\frac{9}{16}$	Unwelded	Clipped	11	5.5	5/8	63	**8**	1	23°	

Chapter 3- Corrosion Study Plan

3.1 Introduction

This task aims at developing a test plan for evaluation of available methods for the assessment and prevention of steel half-round bearing stiffener corrosion. Methods to be investigated will consider, but are not limited to, 1) environmental exposure and material corrosion performance, 2) stiffener connection details, and 3) preventative corrosion measures.

Environmental exposure considerations include the natural external environment and the environment developed within the occluded space of the stiffener including humidity, moisture, surface salt contamination, detritus and atmospheric pollutants. Material corrosion performance include consideration of steel alloy types prescribed by ASTM and API (including carbon steel and weathering steel), stiffener fabrication (i.e., pipe or sheet), presence of seams and welds, and metallographic considerations such as presence and condition of mill scale and protective patina, surface defects and stresses developed in the stiffener. Stiffener connection detail considerations include vented (clipped) stiffeners, sealed stiffeners, and interfaces between connection surfaces. Preventative corrosion measures include the use of filler materials in the interior stiffener volume, protective paints for internal and external stiffener surfaces, and use of vapor-phase inhibitors.

Corrosion assessment of the half-round bearing stiffener material include the regions susceptible to elevated corrosion (Figure 3.1), including 1) the external surface subject to the natural exposure environments; 2) the internal surfaces of the stiffener subject to possible elevated accumulation of salt contamination, poor surface wash off, accumulated water and debris, and elevated time-of-wetness; and 3) joints and weldment at the connection interfaces of the stiffener to the steel girder, that can be subject to crevice corrosion and detrimental galvanic and localized stress interactions to elevate corrosion damage.

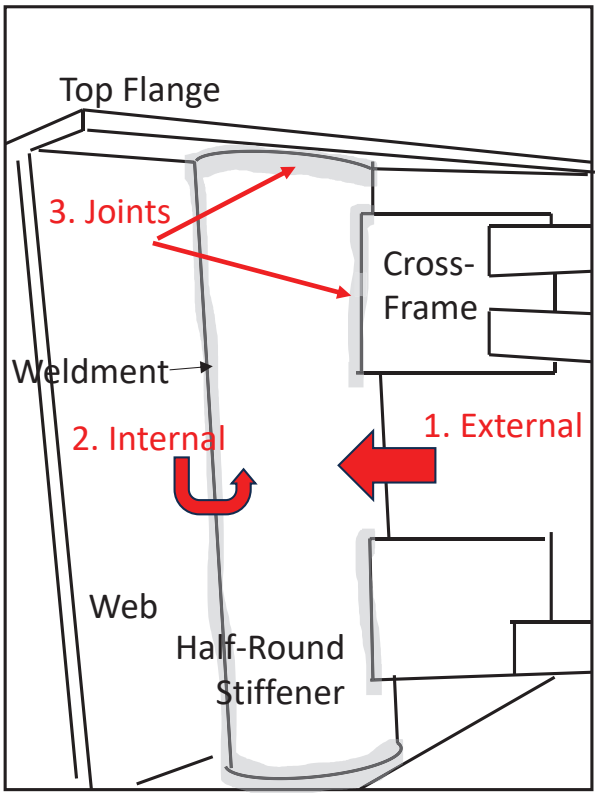

Figure 3.1 Possible Locations for Corrosion of Half-Round Stiffeners.

Figure 3.2 and Figure 3.3 show the general proposed research approach and research parameters that are further elaborated later. The categories in the Venn diagram in Figure 3.3 shows system parameters related to the exposure environment, stiffener design/detailing, and corrosion mitigation. The intersection of the categories represents research parameters to be elucidated by testing.

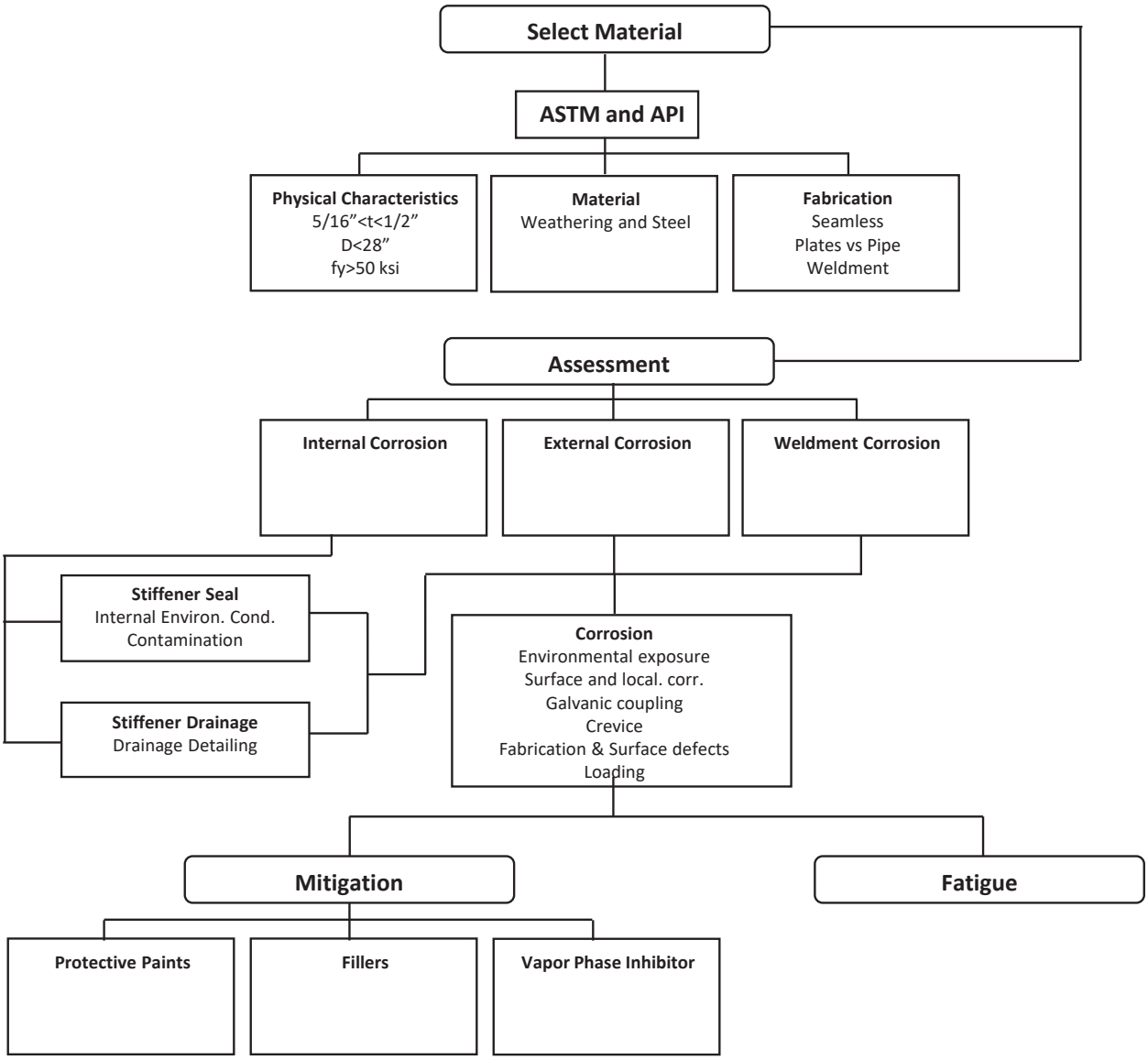

Figure 3.2 Research Approach

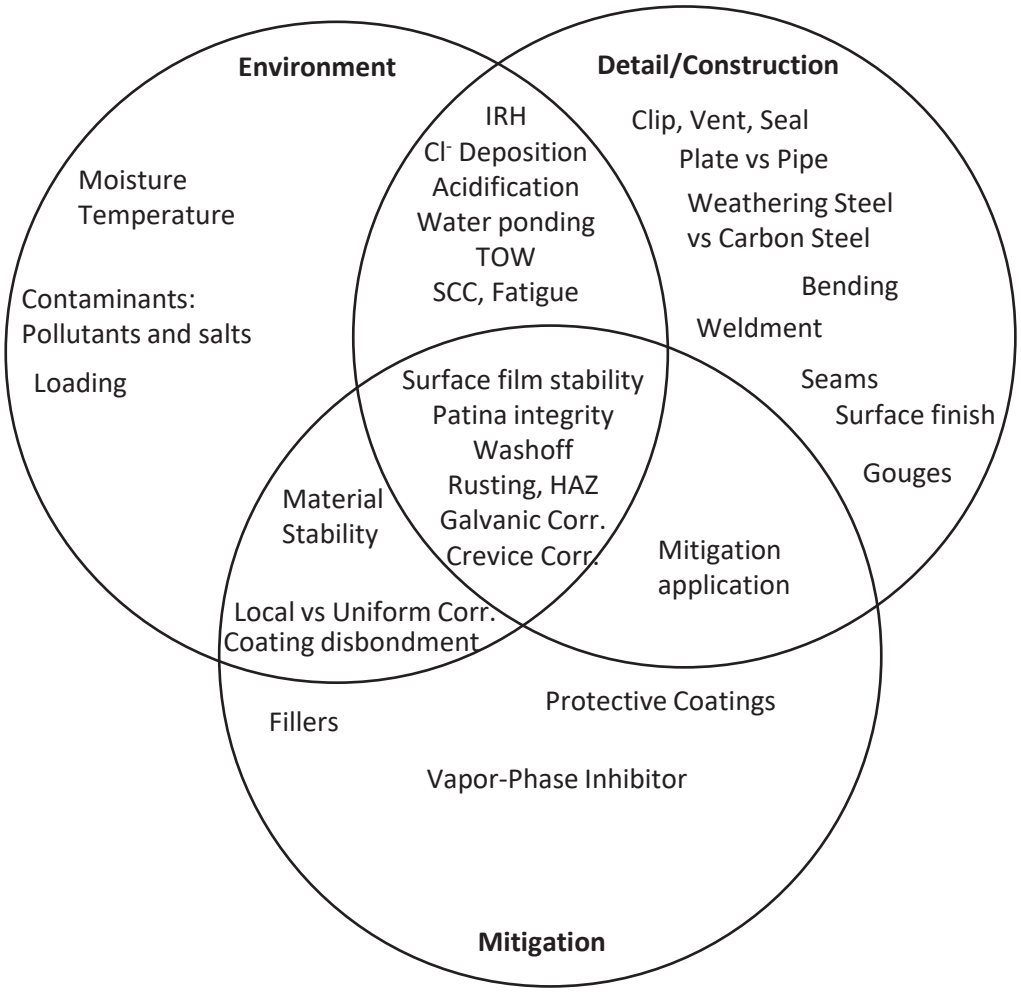

Figure 3.3 Research Test Parameters

3.2 Steel Materials

The AASTHO LRFD Bridge Design Specifications has the following material specifications:

> Quenched and tempered alloy steel structural shapes and seamless mechanical tubing with a specified maximum tensile strength not exceeding 140 ksi for structural shapes or 145 ksi for seamless mechanical tubing may be used provided that, the material meets all other mechanical and chemical requirements of AASHTO M270M/M 270 (ASTM A709/A709M), Grade HPS 100W, and the design is based upon the minimum properties for AASHTO M 2770M/ M270 (ASTM A709/709M), Grade HPS 100W. Structural tubing shall be either cold-formed welded or seamless tubing conforming to ASTM A500, Grade B or Grade C, or ASTM A847; or hot-formed welded or seamless tubing conforming to ASTM A501 or ASTM A618. Thickness limitations

relative to rolled shapes and groups shall comply with AASHTO M 160M/M 160 (ASTM A6/A6M).

Commentary: ASTM A500 cautions that the structural tubing manufactured to the specifications may not be suitable for applications involving dynamically loaded elements in welded structures where low temperature notch-toughness properties may be important… Consideration should be given to requiring that the material satisfy the Charpy V-notch toughness requirements specified in Article 6.6.2.

The available steel materials applicable for half-round bearing stiffeners with ASTM specifications are listed in Table 3.1 for plates and Table 3.2 for tubes/pipes. Notes on applicability for bridge applications are listed as well. Previous discussions with the research advisory members indicated that pipe materials specified by API may have limitations on availability due to the high commercial demands from the oil and gas distribution industries. However, inclusion of API 5L PSL 2 materials should be considered as well.

The listed ASTM specifications had various applications in mind during its development and include steel plates (that can be fabricated to half-round shapes), tubes, pipes, and round hollow structural sections of various specified geometries and strengths. Some materials may not necessarily be recommended for bridge applications, and plates that require rolling to pipe geometry and seam welding are not recommended. The listed specifications also include various steel alloys, some with enhanced corrosion mitigation. For consideration of half-round stiffeners, the geometries and strengths are dependent on the details for the bridge steel I-girders and stress development. Half-round stiffener thickness (t) and diameter (D) was selected to be 5/16” < t <1/2” and D < 28” to accommodate the select representative bridge cases considered in the research. Also, in consideration of the preliminary bridge analysis, a steel yield strength f_y > 50 ksi was considered to be appropriate.

With these assumptions, the materials in Table 3.3 are proposed for material corrosion assessment and durability testing, especially for consideration of weathering steel that is currently specified by the Department. For half-round bearing stiffeners fabricated from plates, ASTM A709 Gr50 steel can be compared to ASTM A709 Gr50W/A588 weathering steel. For stiffeners using pipes, A500 GrC welded and seamless pipes can be compared to A847 welded

and seamless weathering steel pipes. Although not recommended due to the need for welded joints, A1085 HSS pipes can also be considered for research purposes for larger members and in consideration of its welded joints. ASTM A709 Gr50 can be compared with ASTM A500 and API 5L.

Table 3.1 Specifications for Structural Plates

Covers	Grades	Weldability	Corrosion Resistance	Thickness	Tensile Strength	Toughness	FDOT/AWS
A709-21 Structural Steel for Bridges							
High-strength, low-alloy steel -W Corten	GR36, 50, 50W, HPS-50W, etc.	ASTM A6 –X3	50W and HPS50W G101 index>6.0 Unpainted	GR50 <4" GR50W <4" GR70W<4"	65 ksi 70 ksi 85-110 ksi	Y[1]	Y
A588-19 High-Strength Low-Alloy Structural Steel, up to 50 ksi Minimum Yield Point, with Atmospheric Corrosion Resistance							
High-strength, low-alloy steel Corten	Corten A Corten B (load-bearing) Corten K (high strength)	ASTM A6 –X3	G101 Substantially better than carbon steel Unpainted	<8"	<4" 70 ksi 4-5" 67 ksi >5" 63 ksi	Y	Y
A242-13 High-Strength Low-Alloy Steel							
High-strength, low-alloy steel Corten		ASTM A6 –X3	G101 Substantially better than carbon steel Unpainted	<4"	<3/4" 70 ksi <1.5" 67 ksi >1.5 67 ksi	Y	NA
A572-21 High-Strength Low-Alloy Columbiuim-Vanadium Structural Steel							
High-strength low-alloy steel	Gr 42, 50, 55, 60, 65	ASTM A6 –X3	-	<6"	<2" 65 ksi <2.5" 60 ksi <4" 50 ksi <6" 42 ksi	Y[2]	NA
A606-23 Steel, Sheet and Strip, High-Strength, Low-Alloy, Hot-Rolled and Cold-Rolled, with Improved Atmospheric Corrosion Resistance							
High-strength, low-alloy cold rolled sheets and strips	Type 2 Type 4/5 Gr 50 hot-rolled Gr 45 cold rolled	ASTM A6 –X3	Type 2: 0.2% Cu Type 4/5: Substant better than carbon steel. Unpainted. G101 index>6.0	<0.23"	Gr 50: 70 ksi Gt 34: 65 ksi	N[3]	NA

Notes,

1-For structural products to be used as tension components requiring notch toughness testing

2-For applications, such as welded bridge construction, where notch toughness is important, notch toughness requirements are to be negotiated between the purchaser and the producer.

3-The purchaser has the option to require minimum Charpy V-notch impact properties of 15 ft-lbs [20 J] or more at a specified test temperature, based on a full-size test specimen of 0.3937 in [10 mm] thickness. Typically, the test temperature is the lowest anticipated service temperature of the application. The minimum thickness permitted in accordance with Table 9 of Test Methods A370 for a subsize Charpy V-notch specimen is 0.100 in [2.5 mm].

Table 3.2 Specifications for Tubing/Pipes

Covers	Grades	Weldability	Corrosion Resistance	Thickness	Tensile Strength	Toughness	FDOT/ AWS
A847-21 Cold-Formed Welded and Seamless High-Strength, Low-Alloy Structural Tubing with Improved Atmospheric Corrosion Resistance							Y
Cold-formed *welded* and *seamless* high-strength, low-allow round tubular shapes Weathering steel		5.2 Welded tubing made from flat-rolled steel by the electric-resistance welding or electric-fusion welding process. The weld not located within the radius of tubular shapes.	G101 Substantially better than carbon steel Unpainted	Welded D=28" max; th=1" max Seamless D=10"; th=0.5" max	70 ksi	N[1]	NA
A871-20 High-Strength Low-Alloy Structural Steel Plate with Atmospheric Corrosion Resistance							
high-strength low-alloy steel plate intended for use in tubular structures	Gr 60 and 65	ASTM A6 –X3	G101 index>6.0 Unpainted	Plate thickness to meet required capacity	60 or 65 ksi	Y[2]	NR
A500-21a Cold-Formed Welded and Seamless Carbon Steel Structural Tubing in Rounds and Shapes							
Cold-formed *welded* and *seamless* carbon steel round shapes	Gr B, C, D	Welded tubing made from flat-rolled steel by the electric-resistance-welding process. The longitudinal butt joint of welded tubing welded across its thickness to assure design strength	-	D=28" max; th=1" max	GR B 58 ksi GR C 62 ksi GR D 58 ksi	N[3]	Seamless Y. Welded NR
A1085-22 Cold-Formed Welded Carbon Steel Hollow Structural Sections							
cold-formed *welded* carbon steel hollow structural sections (HSS)	HSS	HSS made from electric resistance welding	-	Tolerances vary for dia <1.9" and >2"	50-70 ksi	Y	NR
A252-19 Welded and Seamless Steel Pipe Piles							
Nominal wall steel pipe piles of cylindrical shape…in which the steel cylinder acts as a permanent load-carrying member. …produced as both welded and seamless products	GR 1, 2, 3	The piles shall be made by the seamless, electric resistance welded, flash welded, or fusion welded process. The seams of welded pipe piles shall be longitudinal, helical-butt, or helical-lap.	-	D=6-18" Th=0.134 to 0.5"	GR 1 50 ksi GR 2 60 ksi Gr 3 66 ksi	NR	NR
A501-21 Hot-Formed Welded and Seamless Carbon Steel Structural Tubing							
Black and hot-dipped galvanized hot-formed welded and seamless carbon steel…round… structural tubing for welded… construction of bridges…	A, B, C	Tubing made seamless; furnace-butt-welding (continuous welding); electric-resistance welding or submerged arc welding…			A, 58 ksi B, 65 ksi C, 70 ksi	Y[4]	NR

A618 Hot-Formed Welded and Seamless High-Strength Low-Alloy Structural Tubing							
Hot-formed welded and seamless high strength low-alloy… round… structural tubing for welded… construction of bridges….	Ia, Ib, II, III, IV, V, VI, VII	Made by the seamless, furnace-butt-welded (continuous-welded), or hot-stretch-reduced electric-resistance-welded process	Gr Ia and Ib: G101 index>6.0. Gr III. For enhanced corrosion resistance allow min 0.20% Cu by heat (0.18% by product)	D=1-48 in 0.095<t<2.5 in	**<3/4"** Ia, Ib, II:70 ; III:65; IV:80 ; V:100; VI:112; VII:139 ksi. **¾-1.5** Ia, Ib, II:67; III:65; IV:78; V:100; VI:104; VII: 133 ksi. **1.5-2.5** Ia, Ib, II:67; III:50; IV:67; V:90; VI:100; VII:129 ksi.	Y[5]	NR
API 5L PSL2							
API Specification for line pipe	X52	Seamless (SMLS) or welded (HFW, SAWL, SAWH)	-	th<0.984 in	52.2 ksi pipe body, 66.7 ksi seam	Y[6]	-

Notes,

1-Products manufactured to this specification may not be suitable for those applications where low temperature notch toughness properties may be important, such as dynamically loaded elements in welded structures, unless ordered with toughness tests. See the Supplementary Requirements. However, the customer may request Charpy Impact testing in their purchase order.

2-The steel, as represented by the Charpy V-Notch test, shall conform to the impact test requirements.

3-Products manufactured to this specification may not be suitable for those applications such as dynamically loaded elements in welded structures, etc., where low-temperature notch-toughness properties, which are typically measured by Charpy Impact testing, may be important.

4-The Charpy V-notch impact test specimens shall conform to requirements. Impact tests are not required for thicknesses smaller than or equal to 0.250 in. [6.3 mm], unless specified.

5-For Grades III, IV, V, VI, VII the Charpy V-notch impact test specimens shall conform to the requirements. Impact tests are not required for thicknesses smaller than or equal to 0.250 in. [6.3 mm], unless specified.

6. SMLS- pipe body, Welded – pipe body, weld, HAZ

Table 3.3 Proposed Test Materials

	Specification	Carbon Steel	Weathering Steel	Specifications
Plates	A709-21	Grade 50	Grade 50W (G101 index >6.0)	t < 4”, f_y =50 ksi
	A588-19	-	Grade B and K (G101 better than carbon steel)	t < 8”, f_y = 50 ksi
Pipe/Tube	A847-21	-	Seamless (G101 better than carbon steel)	Welded t < 1”, D < 28”, f_y = 50 ksi Seamless t < 0.5”, D < 10”, f_y = 50 ksi
	A500-21	Grade C (Seamless)	-	t < 1”, D < 28”, f_y = 50 ksi
API 5L PSL 2 X52	PSL X52	Seamless (SMLS)		f_y = 52.2 ksi

3.3 Internal Stiffener Corrosion

Testing to assess corrosion of the inner surfaces of the half-round bearing stiffeners should consider venting/drainage details, material corrosion behavior, and corrosion mitigation. Figure 3.4 shows a general schematic on locations of clips on the stiffener and possible aggravating corrosion conditioning.

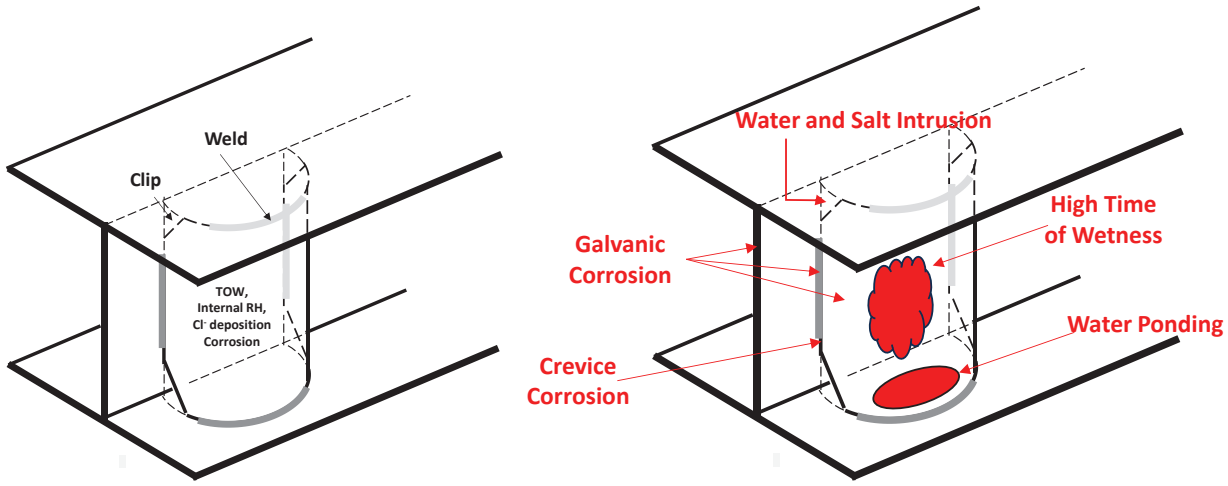

Figure 3.4 Internal Corrosion of Half-Round Bearing Stiffeners (HRBS)

Left: Location of clips and weldment, Right: Aggravated corrosion conditions

3.3.1 Assessment of Seal, Venting and Drainage Efficacy

3.3.1.1 Description

Imperfect seal of the half-round stiffener can allow for aggressive environmental conditions to develop in the internal spaces of the stiffener. An imperfect seal can develop due to the presence of clips required to fit the half-round bearing stiffener on to the I-girder that have welded web-to-flange connections, incomplete weldment, and presence of vents and drains. If left unsealed with improper drainage, high internal relative humidity (IRH), accumulation of salt and atmospheric pollutants, long time-of-wetness (ToW) and accumulation of water can develop. Carbon steel and weathering steel both do not have good corrosion resistance in these aggressive environmental conditions. Furthermore, the inability for washoff of the internal surfaces negatively affects the formation of the protective weathering steel patina. Larger vents and drains may alleviate some of the contaminant and moisture accumulation but the larger openings attract wildlife activity causing accumulation of corrosive detritus and can create localized stresses that can facilitate environmentally induced corrosion cracking (EIC) such as stress corrosion cracking (SCC) of the stiffener. Weldments create heat-affected zone (HAZ) that may have greater susceptibility to corrosion and create adverse galvanic coupling conditions. Incomplete weldments also can create crevice environments between the stiffener and I-girder surfaces allowing for localized corrosion to develop.

Scaled mockups of half-round bearing stiffeners welded to a top and bottom flange and web with alternative details of the clips made on the stiffener to accommodate weldments for the I-girder, sealing materials, and other venting details are to be made to assess the environmental conditions that can develop within the occluded spaces of the half-round stiffeners.

Details for the clips include its dimensions (height and width), geometry (angular or rounded), and use of sealing materials should be considered (Table 3.4). It is noted that fabricators in Florida typically use rounded clipped ends. Testing will consider fabricator preferences. Vents to aerate the internal space and drainage to prevent water ponding within the internal space should be

considered. Vents may cause localized stresses (affecting structural capacity and facilitate environmentally induced corrosion cracking) and allow accumulation of environmental contaminants and animal detritus. Assessment of localized corrosion associated with the weldment and incomplete weldment is warranted.

Table 3.4 Half-Round Stiffener Detailing Affecting Corrosion Performance

Detail	Stiffener Detail		Corrosion Environmental Factors
Material	Carbon steel vs Weathering steel	Steel grade	Atmospheric corrosion resistance
	Fabricated plate vs pipe	Presence of gouges, notches, arc strikes, Welded, Seamless	Localized corrosion, galvanic coupling, HAZ
Clip	Angular vs Round	Geometry (h, w, r)	IRH, ToW, salt contamination
	Open vs Sealed	Material (epoxy, silicone, etc)	IRH, ToW, salt contamination, washout, patina development
Vent/Drainage	Location, total orifice area, and geometry	Rate of ingress, rate of drainage, Stress concentrations	IRH, ToW, water ponding, salt contamination, detritus accumulation, EIC, SCC, washout, patina development,
Weldment	Complete vs Incomplete weldment; Standard vs Weathering electrodes	Perimeter length of weld, electrode type, HAZ	Crevice conditions, Galvanic coupling, HAZ
Crevice	Finish, fit and roughness at connection interface	Crevice height/ surface area	Crevice corrosion

3.3.1.2 Proposed Testing

Stiffener Seal. Scaled specimens with half-round stiffeners welded to a web and flanges (that include various clip, vent, drain, and weldment details) are to be exposed in laboratory controlled environmental conditions including 1) different relative humidities ranging from 75% to near 100% IRH controlled by saturated salt solutions, 2) temperature cycling, and 3) salt-fog environment. The specimens will be instrumented with temperature and RH sensors. It is noted that Florida designs identify the adverse effects of RH>80%. The internal humidity within the occluded space within the stiffener and the role of moisture due to condensation is to be examined. Wet candle chloride deposition apparatuses will also be placed within the stiffener internal space. Chloride test strips will also be periodically used to measure chloride deposition on various surfaces within the internal space. It is noted that the east coast of Florida averages a chloride deposition rate of 16.8 mg/m^2/day and the west coast of Florida averages 33.1 mg/m^2/day. Atmospheric pollution in the form of sulfur dioxide gas has been noted to be largely mitigated in Florida due to policies set by the Florida Dept of Environmental Protection. 0.01% was considered the threshold for concern. Surface moisture presence can also be measured using small 4-point resistance arrays. In this way, the environmental conditions within the internal space of the stiffener with the various connection details to the girder can be assessed. For example, it may be determined that certain stiffener connection details to the girder may allow for high ToW, surface contaminants, and accumulated water by condensation that can adversely affect the development of protective patinas for certain weathering steel alloys. The resulting test outcomes would then ideally provide information for more durable designs and material selection.

Stiffener Drainage. Similar test specimens can be used to not only assess moisture accumulation as described above, but also to determine drainage rates. Water can be introduced into the stiffener such as by inundation of the section to identify intrusion rate and then the effectiveness of the drainage detail can be compared by the rate of drainage. Possible design considerations include drainage via the clips, drainage introduced to the stiffener, or drainage introduced to the bottom girder flange.

Corrosion Development. Visual inspection of corrosion development can be made on these test specimens after completion of the environmental monitoring and testing. Visual assessment can include corrosion location (relative to clips, weldment, and orientation of surface), modality (general vs localized corrosion) and severity (surface area and thickness loss). The surface finish of the steel with the presence of notches and gouges up to 3/16" thick for welding purposes and modified by grinding in the direction of the primary stress may affect corrosion development and should be considered. Metallographic assessment of cut sections would be warranted.

3.3.2 Steel Corrosion on Internal Surfaces

3.3.2.1 Description

The parameters for various internal environmental conditions that can develop will in part take into consideration the results of testing described in Section 3.3.1. In addition, a multi-level factorial test setup (Table 3.5) will be considered to identify the importance of the various environmental conditions. These environmental parameters include internal relative humidity, surface salt and pollutant deposition, temperature, surface wash-off, and cyclic wetting/drying.

The material conditions described in Section 3.2 (carbon steel, weathering steel, welded, seamless, fabrication effects on microstructure) as well as subjected to constant loading conditions inducing stresses, crevices, and coupling of dissimilar metals (galvanic coupling) will be considered.

The testing in the I) environmental chamber will be used to identify the importance of various environmental exposure conditions for the different steel materials so that recommendations for appropriate connection detailing (in complement to testing in Section 3.3.1) can be made. The testing in the II) salt-fog chamber provides information on susceptibility of the materials to elevated corrosion in aggressive chloride environments. The testing according to III) ASTM G36 ideally provides indication for material susceptibility to SCC.

Test specimens with similar geometries and microstructural effects and loading will be maintained in IV) neutral pH 3% NaCl solutions in part as an extreme condition such as what may

develop in crevice environments and also so that comparative electrochemical testing can be conducted. Testing include open-circuit potential (OCP) measurements, linear polarization resistance (LPR), anodic and cathodic potentiodynamic polarization, electrochemical impedance spectroscopy (EIS), and macrocell testing. These tests will help elucidate the effects of the microstructural effects of fabrication, welding, and loading on the relative corrosion performance (including oxide film development, anodic and cathodic characteristics, and galvanic coupling of dissimilar steel surfaces and welded components) of the tested materials. Similar test specimens will be prepared and conditioned as in I) and II) for archival purposes for future fatigue testing on exposed steel coupons.

The presence of surface oxide scales and cracks in the scale due to fabrication can affect the localization of corrosion. It is anticipated that all materials are to be blast-cleaned by the fabrication shop. Other surface conditions as described earlier including notches, gouges, and grinding can be present in construction and is to be considered in lab testing. Notes on the surface condition of test specimens should be recorded. Fabrication of plates into half-round shapes will consider requirements required by Florida Standard Specifications 460-4.3.2 including cold bending (and hot bending pending on interest of the department), with radii at 5t for structural steel or 1.5t for cross frames using A709 steel. More extreme bending may be considered as well for laboratory material corrosion testing. Surface preparation of the half-round will also consider the role of surface blast clean per FDOT Standard Specifications 460-7.2.2. Gouges, notches, arc strikes on the steel surface will also be considered in testing.

Table 3.5 Material and Environmental Factors for Study

Exposure	Experimental Factors	Materials				
		A709 -50	A709 -50W	A847	A500 -C	API 5L PSL 2 X52
I Environmental Chamber	Microstructural effect	Straight (seamless, welded), Mild bend, Deep bend, Blast clean	Straight (seamless, welded), Mild bend, Deep bend, Blast clean	Seamless, welded	Seamless, welded	Seamless, welded
	RH	75, 95%	75, 95%	75, 95%	75, 95%	75, 95%

	Salt contamination (NaCl)	Zero, low, high	Zero, low, high	Zero, low, high	Zero, low, high	Zero, low, high
	Pollutant (SO_2)	Zero, low	Zero, low	Zero, low	Zero, low	Zero, low
	Temp. and cycling	Ambient, High, Cycling	Ambient, High, Cycling	Ambient, High, Cycling	Ambient, High, Cycling	Ambient, High, Cycling
	Loading On Straight (ASTM G30-22)	Zero, Constant	Zero, Constant	-	-	-
	Crevice	Yes, No	Yes, No	Yes, No	Yes, No	Yes, No
	Galvanic coupling	A709 50 to 50W	A709 50W to 50W	A847 to A709 50W	A500 C to A709 50W	API 5L to A709 50W
II Salt fog (ASTM G85-19)	Microstructural effect	Straight (seamless, welded), Mild bend, Deep bend, Blast clean	Straight (seamless, welded), Mild bend, Deep bend, Blast clean	Seamless, welded	Seamless, welded	Seamless, welded
	Loading on Straight (ASTM G30-22)	Zero, Constant	Zero, Constant	-	-	-
	Surface Wash-off	Yes, No	Yes, No	Yes, No	Yes, No	Yes, No
	Crevice (No Wash off)	Yes, No	Yes, No	Yes, No	Yes, No	Yes, No
	Galvanic coupling	A709 50 to 50W	A709 50W to 50W	A847 to A709 50W	A500 C to A709 50W	API 5L to A709 50W
III SCC (ASTM G36-94)	Microstructural effect	Straight (seamless, welded), Mild bend, Deep bend, Blast clean	Straight (seamless, welded), Mild bend, Deep bend, Blast clean	Seamless, welded	Seamless, welded	Seamless, welded
	Loading on Straight (ASTM G30-22)	Zero, Constant	Zero, Constant	-	-	-
IV Electrochem Testing	Microstructural effect	Straight (seamless, welded), Mild bend, Deep bend, Blast clean	Straight (seamless, welded), Mild bend, Deep bend, Blast clean	Seamless, welded	Seamless, welded	Seamless, welded
	Loading on Straight (ASTM G30-22)	Zero, Constant	Zero, Constant	-	-	-
	Macrocell testing	Straight to fabricated, Loaded to unloaded, Straight to welded.	Straight to fabricated, Loaded to unloaded, Straight to welded.	Pipe to straight, Pipe to welded.	Pipe to straight, Pipe to welded.	Pipe to straight, Pipe to welded.
		A709 50 to 50W	A709 50W to 50W	A847 to A709 50W	A500 C to A709 50W	API 5L to A709 50W

3.3.2.2 Proposed Testing

Corrosion Gravimetric Testing and Cracking. Test specimens in the form of cut coupons with various levels of fabrication bending, surface preparation, presence of welded seams, seamless, dissimilar metal coupling, and constant loading will be placed in I) environmental exposures in environmental chambers, in II) accelerated SCC testing in magnesium chloride solution. In the environmental chambers, the test specimens will have three levels of NaCl contamination (made by deposition and evaporation of an applied solution of known concentration), two levels of sulfur dioxide gas (controlled at a fixed concentration and pressure), two temperatures (at documented lab ambient temperatures or heated by lamp or other temperature controller), with and without temperature cycling (to promote condensation in the latter), and with and without constant load (following ASTM G-30-22 in the former). Other specimens with similar microstructural effects and loading conditions will be placed in boiling magnesium chloride solution (following ASTM G36-94).

Subsets exposed to the environmental chamber will be removed and cleaned using conventional methods such as submerging in Clark's solution prior to weighing and thickness measurements. Such testing will be conducted at minimum at 500, 1000, 1500, 2000, 3000, 4000 hours. Specimens placed in the magnesium chloride solution will be tested at earlier times and more regular intervals. All test specimens will be periodically visually examined and photo documented. The specimens subjected to loading following ASTM G30 and G36 (including with welded sections) will be examined for cracks and localized corrosion by digital photography and metallographic cross-sections.

Electrochemical Corrosion Characterization. Test specimens will be immersed in a III) neutral pH 3% NaCl solution. The OCP will be continuously monitored using a high-input impedance voltmeter and a standard reference electrode. Testing using a three-electrode configuration including LPR, EIS, and potentiodynamic polarization will be made using the coupon as the working electrode, a standard reference electrode as reference, and activated titanium (ATR) rods as counter electrodes. Macrocell current tests will be made by electrically coupling dissimilar steel/welded steel coupons with various surface areas across an electrical switch where period

current measurements can be made. Test setups such as the Rapid macrocell test (ASTM A955) utilizing a salt-bridge across separate cells for the individual electrodes in each pair can be implemented. Electrochemical noise (EN) measurements can be considered as well for macrocell coupling experiments.

Fatigue Testing. Test specimens exposed in I and II conditions made from plates and welded plates will be made into dog-bone geometric shapes (or other standardized shape) for future fatigue testing. Test specimens made from half-pipes and welded half-pipes will utilize smaller diameter geometries to facilitate future development for a jig for testing. The specimens will be exposed for a minimum of 4000 hours but may be extended. Because of the significant time period required for this test, it is recommended that the test is considered for a future complementary program.

3.3.3 Corrosion Mitigation

Corrosion mitigation of the internal surfaces of the half-round stiffener will include the use of an inorganic zinc (IOZ) coating system per Florida Standard Specifications Section 560, use of flexible filler per Section 938-5, and use of a vapor-phase inhibitor (such as film forming agents). Test setup as described in Section 3.3.1 will be employed to assess the efficacy for the paint, wax, and inhibiting film. In addition to the interior surfaces of the half-round bearing stiffener, additional coupons placed within the test volume may be considered to facilitate mass and thickness loss measurements. Experience by FDOT has shown that differentiation in performance for weathering steels was observed around 3,000 hours. Testing is envisioned for up to 4,000 hours of exposure but may be extended depending on the outcomes after initial testing.

3.4 External Stiffener Corrosion

3.4.1 Steel Corrosion on External Surfaces

The testing procedures described in Section 3.3.2 will also account for corrosion behavior of external surfaces. In this case, attention to the convex surface of fabricated plates and pipes will be considered instead of the concave surface of the specimens.

3.4.2 Corrosion Mitigation

Similar test setup and materials described in Section 3.3.1 and 3.3.3 will be considered for the corrosion assessment of the external surface with protective coating systems such as a three-coat system with IOZ. The role of the oxide scale, surface preparation, moisture, and surface contaminants on the application and durability of coatings will be assessed in terms of coating disbondment, coating degradation, and corrosion development.

3.5 Test Plan

The test plan described below is presented for one type of material. For example, carbon Steel Plate A709-21 50 counts as one type of material and Weathering Steel Plate A709-21 50W counts as another material type. The proposed tests can be repeated exactly for other material types. To this end, material selection shown in Table 3.3 is proposed. Per Table 3.3, 2 material types for plates (one available in both carbon steel and weathering materials), 2 for pipe/tube (both only seamless shapes), and 1 for API are identified (a total of 5 types of materials). The D.1.1 and D.1.5 welding codes identify weldability of the metals. Surface preparation should include near-white metal blasting following SP-10 and SP-11. The proposer for the performance of the tests can suggest for approval truncations to the test matrix for the subsequent materials/configurations based on the information obtained from preceding tests.

It is assumed/recommended that:

- Type of material for the half round (carbon steel or weathering) matches that of the girder. (i.e., the web and stiffener need to be made of the same material).
- Complete fillet weldment for the entire contact line is made
- Weathering steel electrode is used for weathering steel material
- Angular and round clips are used with specified (standard) size that can serve as vents and drain for the half round bearing stiffener
- It is assumed that all surfaces are white blasted before application of paint
- Number of test specimens for all testing subsets follow the associated ASTM (if specified) or propose a statistically acceptable number (if not specified)

Table 3.6 Test 1 Scaled Half-Round Bearing Stiffener Assembly

Test Subset		Test Specimen Parameters	Test Conditions
Without corrosion mitigation (3.1 b)	- Seal Condition - Drainage - Corrosion development	Clip type variation 1	- Environmental exposure with relative humidity variation (3.1 b) - Temperature cycling (3.1 b) - Salt fog (3.1 b) Note: Coupon specimen of relevant test subset to be placed in the test volume to facilitate thickness and loss measurement
		Clip type variation 2	
		Seal welded	
With corrosion mitigation	Internal surfaces (3.3)	Inorganic zinc	
		Flexible filler	
		Vapor-phase inhibitors	
	External surfaces (performed on specimens with any type of seal condition) (4.2)	Coating variation 1	
		Coating variation 2	

Table 3.7 Test 2 Coupons

Test Subset		Test Specimen Parameters	Test Conditions
Internal surface – (3.3.2) attention to concave side	Corrosion Gravimetric Testing and Cracking (3.3.2.2)	- Level of bending, diameter 1-Straight - Level of bending, diameter 2 - Level of bending, diameter 3 - Mitigation variation 1 - Mitigation variation 2 - With welded seam - Without welded seam - With loading - Without loading - Crevice variation 1 - Crevice variation 2 (3.3.2.2)	I) Environmental exposures in environmental chambers (3.3.2.2)
			II) Accelerated SCC testing in magnesium chloride solution (3.3.2.2)
	Electrochemical Corrosion Characterization (3.3.2.2)		III) Immersion in neutral pH 3% NaCl solution (3.3.2.2)
	Fatigue testing (3.3.2.2)		Specimens exposed to I and II conditions cut into standardized shape for future fatigue testing (3.3.2.2)
External surface (3.4.1)	Use or repeat the above test only with attention to convex side of the coupons		

3.6 Test Specimens

3.6.1 Half-Round Bearing Stiffener Assembly for Test 1

Conceptual schematics of test specimens for Table 3.1 is shown in Figure 3.5 and Figure 3.6. Environmental chambers will be conditioned by saturated salt solutions with circulation provided by small fans, and temperature controlled by heated lamps. The salt-fog chamber will conform to ASTM G85-19. Table 3.8 lists the test matrix per selected materials as shown in Table 3.3.

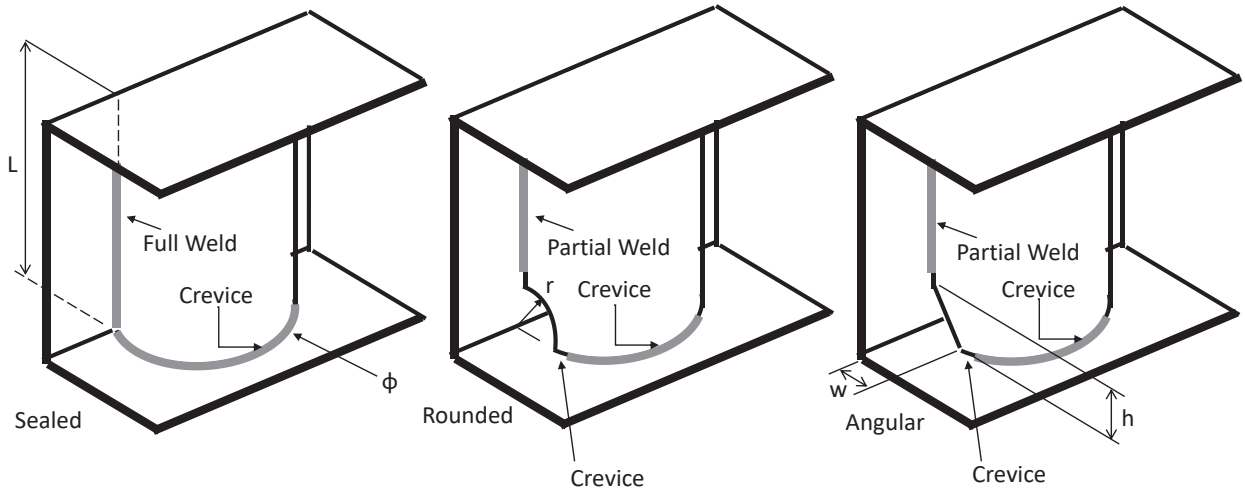

Figure 3.5 Examples of Vented Clip Parameters. Fabricator preferences (ie rouned clips will be considered)

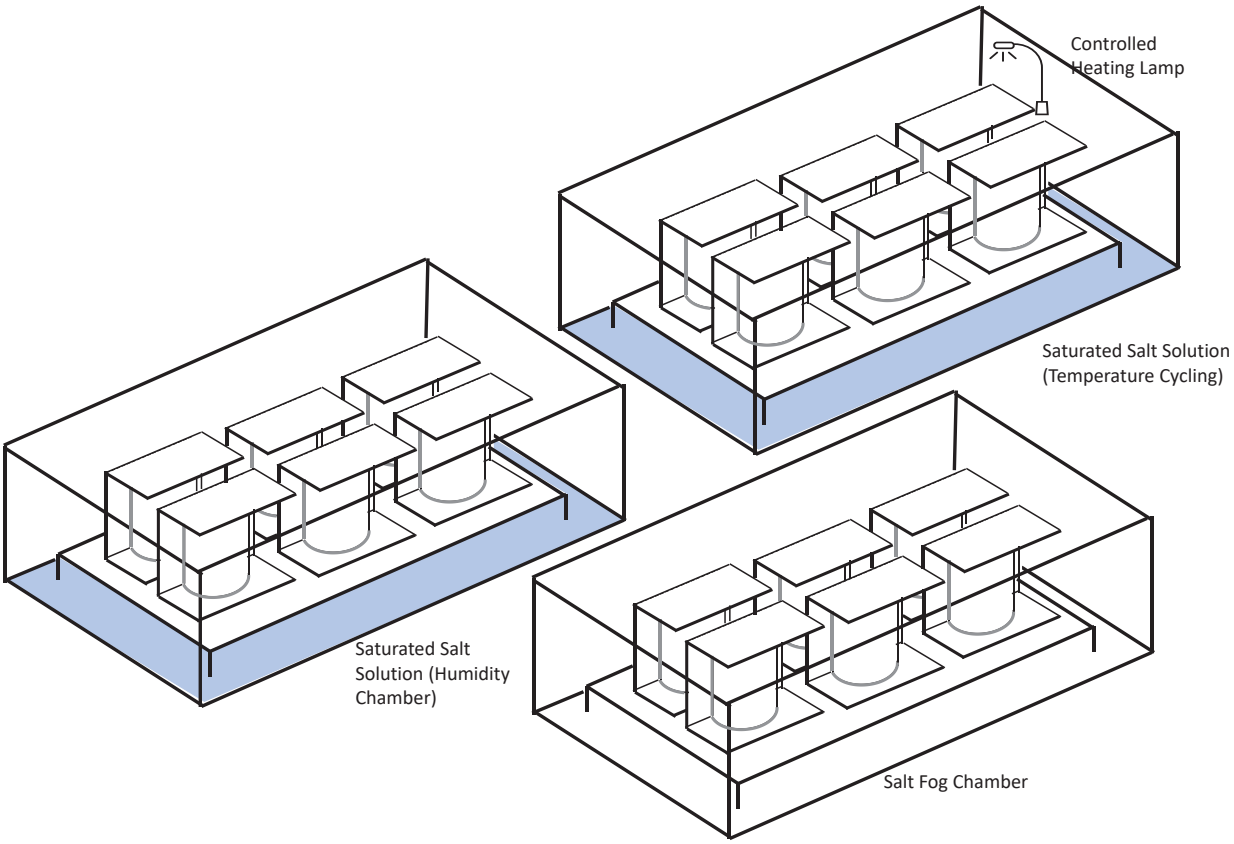

Figure 3.6 Example of Environmental Conditioning

Table 3.8 Test 1 Matrix per Material (384xM)

		Sealed	Rounded Clip	Angular Clip
No Mitigation	Humidity	M#-C-N-H75-L	M#-R-N-H75-L	M#-A-N-H75-L
		M#-C-N-H75-H	M#-R-N-H75-H	M#-A-N-H75-H
		M#-C-N-H95-L	M#-R-N-H95-L	M#-A-N-H95-L
		M#-C-N-H95-H	M#-R-N-H95-H	M#-A-N-H95-H
		M#-C-N-H100-L	M#-R-N-H100-L	M#-A-N-H100-L
		M#-C-N-H100-H	M#-R-N-H100-H	M#-A-N-H100-H
	Salt-Fog	M#-C-N-S	M#-R-N-S	M#-A-N-S
		M#-C-N-S	M#-R-N-S	M#-A-N-S
Paint	Humidity	M#-C-P-H75-L	M#-R-P-H75-L	M#-A-P-H75-L
		M#-C-P-H75-H	M#-R-P-H75-H	M#-A-P-H75-H
		M#-C-P-H95-L	M#-R-P-H95-L	M#-A-P-H95-L
		M#-C-P-H95-H	M#-R-P-H95-H	M#-A-P-H95-H
		M#-C-P-H100-L	M#-R-P-H100-L	M#-A-P-H100-L
		M#-C-P-H100-H	M#-R-P-H100-H	M#-A-P-H100-H
	Salt-Fog	M#-C-P-S	M#-R-P-S	M#-A-P-S

		M#-C-P-S	M#-R-P-S	M#-A-P-S
Filler	Humidity	M#-C-F-H75-L	M#-R-F-H75-L	M#-A-F-H75-L
		M#-C-F-H75-H	M#-R-F-H75-H	M#-A-F-H75-H
		M#-C-F-H95-L	M#-R-F-H95-L	M#-A-F-H95-L
		M#-C-F-H95-H	M#-R-F-H95-H	M#-A-F-H95-H
		M#-C-F-H100-L	M#-R-F-H100-L	M#-A-F-H100-L
		M#-C-N-H75-L	M#-R-N-H75-L	M#-A-N-H75-L
	Salt-Fog	M#-C-N-H75-H	M#-R-N-H75-H	M#-A-N-H75-H
		M#-C-N-H95-L	M#-R-N-H95-L	M#-A-N-H95-L
Inhibitor	Humidity	M#-C-I-H75-L	M#-R-I-H75-L	M#-A-I-H75-L
		M#-C-I-H75-H	M#-R-I-H75-H	M#-A-I-H75-H
		M#-C-I-H95-L	M#-R-I-H95-L	M#-A-I-H95-L
		M#-C-I-H95-H	M#-R-I-H95-H	M#-A-I-H95-H
		M#-C-I-H100-L	M#-R-I-H100-L	M#-A-I-H100-L
		M#-C-I-H75-L	M#-R-I-H75-L	M#-A-I-H75-L
	Salt-Fog	M#-C-I-H75-H	M#-R-I-H75-H	M#-A-I-H75-H
		M#-C-I-H95-L	M#-R-I-H95-L	M#-A-I-H95-L

Material (M); Clip/Vent: Sealed, Rounded, Angular (C, R, A);
Mitigation: None, Paint, Filler, Inhibitor (N, P, F, I)
Environment: Humidity 75, 95, 100 (H75, H95, H100); Temp cycling: Ambient, Heated (L, H); or Salt-Fog (S)

3.6.2 Coupons for Test 2

Figure 3.7 and Figure 3.8 show conceptual schematics of test coupon specimens to be placed in environmental chambers as well as SCC and electrochemical testing. Specimens will be sectioned from steel plates and tubes. The effect of fabrication will be made using U-bend specimens (including stock from pipes) conforming to ASTM G30-22. Stressing in the specimens include the use of U-Bend specimens per ASTM G30-22 for both plate and pipe steel materials.

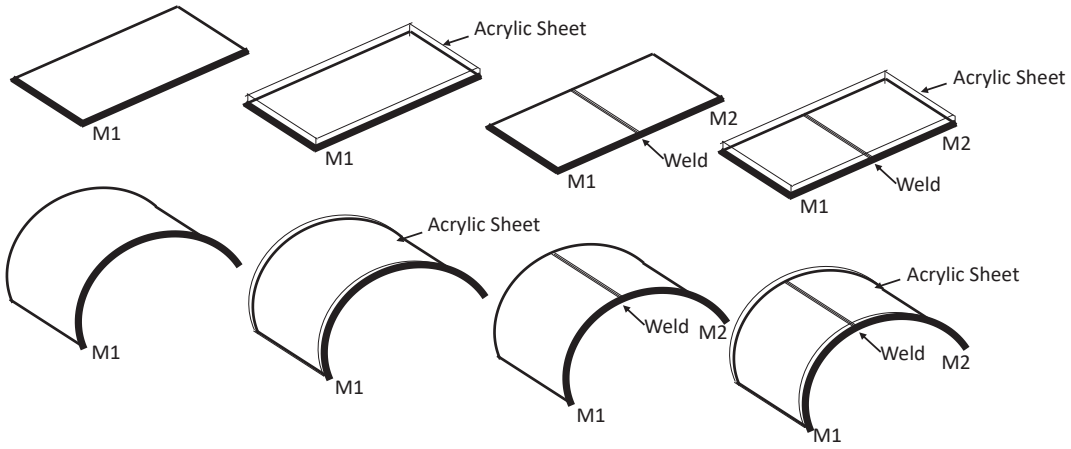

Figure 3.7 Schematic of Steel Coupons Showing Straight, Bent, Welded, and Crevice Conditions

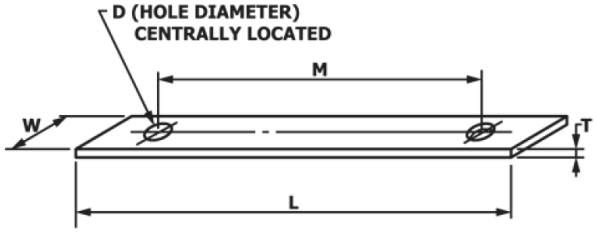

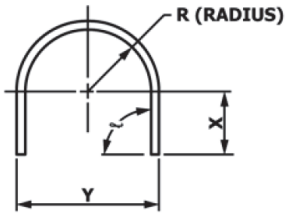

Examples of Typical Dimensions (SI Units)

Example	L, mm	M, mm	W, mm	T, mm	D, mm	X, mm	Y, mm	R, mm	α, rad
a	80	50	20	2.5	10	32	14	5	1.57
b	100	90	9	3.0	7	25	38	16	1.57
c	120	90	20	1.5	8	35	35	16	1.57
d	130	100	15	3.0	6	45	32	13	1.57
e	150	140	15	0.8	3	61	20	9	1.57
f	310	250	25	13.0	13	105	90	32	1.57
g	510	460	25	6.5	13	136	165	76	1.57
h	102	83	19	3.2	9.6	40	16	4.8	1.57

Figure 3.8 Excerpt of ASTM G30-22 Specimen Geometry

The test matrix is separated into 2 levels (Table 3.9). Level 1 includes material and fabrication characteristics and Level 2 describes environmental conditions. Table 3.10 lists the Level 1 test matrix for the test specimens that represent the material and fabrication. Table 3.11 lists the Level 2 test matrix that represent environmental parameters.

Table 3.9. Test 2 Test Matrix Organization

LEVEL 1: MATERIAL	LEVEL 2: ENVIRONMENT AND LOAD
Material (M);	Environment:
Welded Seam: Seamless, Welded (W0, W1);	Humidity 75, 95 (H75, H95);
Bend: Straight, Shallow, Deep (B0, B1, B2);	Salt Contamination: Zero, Low, High (S0, S1, S2)
Mitigation: None, Paint (N, P);	Pollutant: Zero, Low (P0, P1);
	Temp and cycling: Ambient, Cycling (T0, T1)
	Stress: Loading: Zero, Constant (L0, L1);
	Crevice: None, Yes (Z0, Z1);
	Galvanic Coupling: None, Yes (G0, G1)

Table 3.10. Test 2 Level 1 Test Matrix per Material. (12xM)

	Seamless (W0)	Welded (W1)
Straight (B0)	M#-W0-B0-N	M#-W1-B0-N
	M#-W0-B0-P	M#-W1-B0-P
Shallow Bend (B1)	M#-W0-B1N	M#-W1-B1N
	M#-W0-B1-P	M#-W1-B1-P
Deep Bend (B2)	M#-W0-B2-N	M#-W1-B2-N
	M#-W0-B2-P	M#-W1-B2-P

MATERIAL LEVEL 1:
Material (M); Welded Seam: Seamless, Welded (W0, W1);
Bend: Straight, Shallow, Deep (B0, B1, B2); Mitigation: None, Paint (N, P);

Table 3.11. Test 2 Level 2 Matrix for Environment and Loading per Material Level 1. (192x(12xM))=2,304xM

	75% RH (H75)			95% RH (H95)		
	S0	S1	S2	S0	S1	S2
P0-T0	M#-W#-B#-#-H75-S0-P0-T0-L0-Z0-G0	M#-W#-B#-#-H75-S1-P0-T0-L0-Z0-G0	M#-W#-B#-#-H75-S2-P0-T0-L0-Z0-G0	M#-W#-B#-#-H95-S0-P0-T0-L0-Z0-G0	M#-W#-B#-#-H95-S1-P0-T0-L0-Z0-G0	M#-W#-B#-#-H95-S2-P0-T0-L0-Z0-G0
	M#-W#-B#-#-H75-S0-P0-T0-L0-Z0-G1	M#-W#-B#-#-H75-S1-P0-T0-L0-Z0-G1	M#-W#-B#-#-H75-S2-P0-T0-L0-Z0-G1	M#-W#-B#-#-H95-S0-P0-T0-L0-Z0-G1	M#-W#-B#-#-H95-S1-P0-T0-L0-Z0-G1	M#-W#-B#-#-H95-S2-P0-T0-L0-Z0-G1
	M#-W#-B#-#-H75-S0-P0-T0-L0-Z1-G0	M#-W#-B#-#-H75-S1-P0-T0-L0-Z1-G0	M#-W#-B#-#-H75-S2-P0-T0-L0-Z1-G0	M#-W#-B#-#-H95-S0-P0-T0-L0-Z1-G0	M#-W#-B#-#-H95-S1-P0-T0-L0-Z1-G0	M#-W#-B#-#-H95-S2-P0-T0-L0-Z1-G0
	M#-W#-B#-#-H75-S0-P0-T0-L0-Z1-G1	M#-W#-B#-#-H75-S1-P0-T0-L0-Z1-G1	M#-W#-B#-#-H75-S2-P0-T0-L0-Z1-G1	M#-W#-B#-#-H95-S0-P0-T0-L0-Z1-G1	M#-W#-B#-#-H95-S1-P0-T0-L0-Z1-G1	M#-W#-B#-#-H95-S2-P0-T0-L0-Z1-G1
	M#-W#-B#-#-H75-S0-P0-T0-L1-Z0-G0	M#-W#-B#-#-H75-S1-P0-T0-L1-Z0-G0	M#-W#-B#-#-H75-S2-P0-T0-L1-Z0-G0	M#-W#-B#-#-H95-S0-P0-T0-L1-Z0-G0	M#-W#-B#-#-H95-S1-P0-T0-L1-Z0-G0	M#-W#-B#-#-H95-S2-P0-T0-L1-Z0-G0
	M#-W#-B#-#-H75-S0-P0-T0-L1-Z0-G1	M#-W#-B#-#-H75-S1-P0-T0-L1-Z0-G1	M#-W#-B#-#-H75-S2-P0-T0-L1-Z0-G1	M#-W#-B#-#-H95-S0-P0-T0-L1-Z0-G1	M#-W#-B#-#-H95-S1-P0-T0-L1-Z0-G1	M#-W#-B#-#-H95-S2-P0-T0-L1-Z0-G1
	M#-W#-B#-#-H75-S0-P0-T0-L1-Z1-G0	M#-W#-B#-#-H75-S1-P0-T0-L1-Z1-G0	M#-W#-B#-#-H75-S2-P0-T0-L1-Z1-G0	M#-W#-B#-#-H95-S0-P0-T0-L1-Z1-G0	M#-W#-B#-#-H95-S1-P0-T0-L1-Z1-G0	M#-W#-B#-#-H95-S2-P0-T0-L1-Z1-G0
	M#-W#-B#-#-H75-S0-P0-T0-L1-Z1-G1	M#-W#-B#-#-H75-S1-P0-T0-L1-Z1-G1	M#-W#-B#-#-H75-S2-P0-T0-L1-Z1-G1	M#-W#-B#-#-H95-S0-P0-T0-L1-Z1-G1	M#-W#-B#-#-H95-S1-P0-T0-L1-Z1-G1	M#-W#-B#-#-H95-S2-P0-T0-L1-Z1-G1
P0-T1	M#-W#-B#-#-H75-S0-P0-T1-L0-Z0-G0	M#-W#-B#-#-H75-S1-P0-T1-L0-Z0-G0	M#-W#-B#-#-H75-S2-P0-T1-L0-Z0-G0	M#-W#-B#-#-H95-S0-P0-T1-L0-Z0-G0	M#-W#-B#-#-H95-S1-P0-T1-L0-Z0-G0	M#-W#-B#-#-H95-S2-P0-T1-L0-Z0-G0
	M#-W#-B#-#-H75-S0-P0-T1-L0-Z0-G1	M#-W#-B#-#-H75-S1-P0-T1-L0-Z0-G1	M#-W#-B#-#-H75-S2-P0-T1-L0-Z0-G1	M#-W#-B#-#-H95-S0-P0-T1-L0-Z0-G1	M#-W#-B#-#-H95-S1-P0-T1-L0-Z0-G1	M#-W#-B#-#-H95-S2-P0-T1-L0-Z0-G1
	M#-W#-B#-#-H75-S0-	M#-W#-B#-#-H75-S1-	M#-W#-B#-#-H75-S2-	M#-W#-B#-#-H95-S0-	M#-W#-B#-#-H95-S1-	M#-W#-B#-#-H95-S2-

	P0-T1-L0-Z1-G0	P0-T1-L0-Z1-G0	P0-T1-L0-Z1-G0	P0-T1-L0-Z1-G0	P0-T1-L0-Z1-G0	P0-T1-L0-Z1-G0
	M#-W#-B#-#-H75-S0-P0-T1-L0-Z1-G1	M#-W#-B#-#-H75-S1-P0-T1-L0-Z1-G1	M#-W#-B#-#-H75-S2-P0-T1-L0-Z1-G1	M#-W#-B#-#-H95-S0-P0-T1-L0-Z1-G1	M#-W#-B#-#-H95-S1-P0-T1-L0-Z1-G1	M#-W#-B#-#-H95-S2-P0-T1-L0-Z1-G1
	M#-W#-B#-#-H75-S0-P0-T1-L1-Z0-G0	M#-W#-B#-#-H75-S1-P0-T1-L1-Z0-G0	M#-W#-B#-#-H75-S2-P0-T1-L1-Z0-G0	M#-W#-B#-#-H95-S0-P0-T1-L1-Z0-G0	M#-W#-B#-#-H95-S1-P0-T1-L1-Z0-G0	M#-W#-B#-#-H95-S2-P0-T1-L1-Z0-G0
	M#-W#-B#-#-H75-S0-P0-T1-L1-Z0-G1	M#-W#-B#-#-H75-S1-P0-T1-L1-Z0-G1	M#-W#-B#-#-H75-S2-P0-T1-L1-Z0-G1	M#-W#-B#-#-H95-S0-P0-T1-L1-Z0-G1	M#-W#-B#-#-H95-S1-P0-T1-L1-Z0-G1	M#-W#-B#-#-H95-S2-P0-T1-L1-Z0-G1
	M#-W#-B#-#-H75-S0-P0-T1-L1-Z1-G0	M#-W#-B#-#-H75-S1-P0-T1-L1-Z1-G0	M#-W#-B#-#-H75-S2-P0-T1-L1-Z1-G0	M#-W#-B#-#-H95-S0-P0-T1-L1-Z1-G0	M#-W#-B#-#-H95-S1-P0-T1-L1-Z1-G0	M#-W#-B#-#-H95-S2-P0-T1-L1-Z1-G0
	M#-W#-B#-#-H75-S0-P0-T1-L1-Z1-G1	M#-W#-B#-#-H75-S1-P0-T1-L1-Z1-G1	M#-W#-B#-#-H75-S2-P0-T1-L1-Z1-G1	M#-W#-B#-#-H95-S0-P0-T1-L1-Z1-G1	M#-W#-B#-#-H95-S1-P0-T1-L1-Z1-G1	M#-W#-B#-#-H95-S2-P0-T1-L1-Z1-G1
P1-T0	M#-W#-B#-#-H75-S0-P1-T0-L0-Z0-G0	M#-W#-B#-#-H75-S1-P1-T0-L0-Z0-G0	M#-W#-B#-#-H75-S2-P1-T0-L0-Z0-G0	M#-W#-B#-#-H95-S0-P1-T0-L0-Z0-G0	M#-W#-B#-#-H95-S1-P1-T0-L0-Z0-G0	M#-W#-B#-#-H95-S2-P1-T0-L0-Z0-G0
	M#-W#-B#-#-H75-S0-P1-T0-L0-Z0-G1	M#-W#-B#-#-H75-S1-P1-T0-L0-Z0-G1	M#-W#-B#-#-H75-S2-P1-T0-L0-Z0-G1	M#-W#-B#-#-H95-S0-P1-T0-L0-Z0-G1	M#-W#-B#-#-H95-S1-P1-T0-L0-Z0-G1	M#-W#-B#-#-H95-S2-P1-T0-L0-Z0-G1
	M#-W#-B#-#-H75-S0-P1-T0-L0-Z1-G0	M#-W#-B#-#-H75-S1-P1-T0-L0-Z1-G0	M#-W#-B#-#-H75-S2-P1-T0-L0-Z1-G0	M#-W#-B#-#-H95-S0-P1-T0-L0-Z1-G0	M#-W#-B#-#-H95-S1-P1-T0-L0-Z1-G0	M#-W#-B#-#-H95-S2-P1-T0-L0-Z1-G0
	M#-W#-B#-#-H75-S0-P1-T0-L0-Z1-G1	M#-W#-B#-#-H75-S1-P1-T0-L0-Z1-G1	M#-W#-B#-#-H75-S2-P1-T0-L0-Z1-G1	M#-W#-B#-#-H95-S0-P1-T0-L0-Z1-G1	M#-W#-B#-#-H95-S1-P1-T0-L0-Z1-G1	M#-W#-B#-#-H95-S2-P1-T0-L0-Z1-G1
	M#-W#-B#-#-H75-S0-P1-T0-L1-Z0-G0	M#-W#-B#-#-H75-S1-P1-T0-L1-Z0-G0	M#-W#-B#-#-H75-S2-P1-T0-L1-Z0-G0	M#-W#-B#-#-H95-S0-P1-T0-L1-Z0-G0	M#-W#-B#-#-H95-S1-P1-T0-L1-Z0-G0	M#-W#-B#-#-H95-S2-P1-T0-L1-Z0-G0
	M#-W#-B#-#-H75-S0-P1-T0-L1-Z0-G1	M#-W#-B#-#-H75-S1-P1-T0-L1-Z0-G1	M#-W#-B#-#-H75-S2-P1-T0-L1-Z0-G1	M#-W#-B#-#-H95-S0-P1-T0-L1-Z0-G1	M#-W#-B#-#-H95-S1-P1-T0-L1-Z0-G1	M#-W#-B#-#-H95-S2-P1-T0-L1-Z0-G1

	M#-W#-B#-#-H75-S0-P1-T0-L1-Z1-G0	M#-W#-B#-#-H75-S1-P1-T0-L1-Z1-G0	M#-W#-B#-#-H75-S2-P1-T0-L1-Z1-G0	M#-W#-B#-#-H95-S0-P1-T0-L1-Z1-G0	M#-W#-B#-#-H95-S1-P1-T0-L1-Z1-G0	M#-W#-B#-#-H95-S2-P1-T0-L1-Z1-G0
	M#-W#-B#-#-H75-S0-P1-T0-L1-Z1-G1	M#-W#-B#-#-H75-S1-P1-T0-L1-Z1-G1	M#-W#-B#-#-H75-S2-P1-T0-L1-Z1-G1	M#-W#-B#-#-H95-S0-P1-T0-L1-Z1-G1	M#-W#-B#-#-H95-S1-P1-T0-L1-Z1-G1	M#-W#-B#-#-H95-S2-P1-T0-L1-Z1-G1
P1-T1	M#-W#-B#-#-H75-S0-P1-T1-L0-Z0-G0	M#-W#-B#-#-H75-S1-P1-T1-L0-Z0-G0	M#-W#-B#-#-H75-S2-P1-T1-L0-Z0-G0	M#-W#-B#-#-H95-S0-P1-T1-L0-Z0-G0	M#-W#-B#-#-H95-S1-P1-T1-L0-Z0-G0	M#-W#-B#-#-H95-S2-P1-T1-L0-Z0-G0
	M#-W#-B#-#-H75-S0-P1-T1-L0-Z0-G1	M#-W#-B#-#-H75-S1-P1-T1-L0-Z0-G1	M#-W#-B#-#-H75-S2-P1-T1-L0-Z0-G1	M#-W#-B#-#-H95-S0-P1-T1-L0-Z0-G1	M#-W#-B#-#-H95-S1-P1-T1-L0-Z0-G1	M#-W#-B#-#-H95-S2-P1-T1-L0-Z0-G1
	M#-W#-B#-#-H75-S0-P1-T1-L0-Z1-G0	M#-W#-B#-#-H75-S1-P1-T1-L0-Z1-G0	M#-W#-B#-#-H75-S2-P1-T1-L0-Z1-G0	M#-W#-B#-#-H95-S0-P1-T1-L0-Z1-G0	M#-W#-B#-#-H95-S1-P1-T1-L0-Z1-G0	M#-W#-B#-#-H95-S2-P1-T1-L0-Z1-G0
	M#-W#-B#-#-H75-S0-P1-T1-L0-Z1-G1	M#-W#-B#-#-H75-S1-P1-T1-L0-Z1-G1	M#-W#-B#-#-H75-S2-P1-T1-L0-Z1-G1	M#-W#-B#-#-H95-S0-P1-T1-L0-Z1-G1	M#-W#-B#-#-H95-S1-P1-T1-L0-Z1-G1	M#-W#-B#-#-H95-S2-P1-T1-L0-Z1-G1
	M#-W#-B#-#-H75-S0-P1-T1-L1-Z0-G0	M#-W#-B#-#-H75-S1-P1-T1-L1-Z0-G0	M#-W#-B#-#-H75-S2-P1-T1-L1-Z0-G0	M#-W#-B#-#-H95-S0-P1-T1-L1-Z0-G0	M#-W#-B#-#-H95-S1-P1-T1-L1-Z0-G0	M#-W#-B#-#-H95-S2-P1-T1-L1-Z0-G0
	M#-W#-B#-#-H75-S0-P1-T1-L1-Z0-G1	M#-W#-B#-#-H75-S1-P1-T1-L1-Z0-G1	M#-W#-B#-#-H75-S2-P1-T1-L1-Z0-G1	M#-W#-B#-#-H95-S0-P1-T1-L1-Z0-G1	M#-W#-B#-#-H95-S1-P1-T1-L1-Z0-G1	M#-W#-B#-#-H95-S2-P1-T1-L1-Z0-G1
	M#-W#-B#-#-H75-S0-P1-T1-L1-Z1-G0	M#-W#-B#-#-H75-S1-P1-T1-L1-Z1-G0	M#-W#-B#-#-H75-S2-P1-T1-L1-Z1-G0	M#-W#-B#-#-H95-S0-P1-T1-L1-Z1-G0	M#-W#-B#-#-H95-S1-P1-T1-L1-Z1-G0	M#-W#-B#-#-H95-S2-P1-T1-L1-Z1-G0
	M#-W#-B#-#-H75-S0-P1-T1-L1-Z1-G1	M#-W#-B#-#-H75-S1-P1-T1-L1-Z1-G1	M#-W#-B#-#-H75-S2-P1-T1-L1-Z1-G1	M#-W#-B#-#-H95-S0-P1-T1-L1-Z1-G1	M#-W#-B#-#-H95-S1-P1-T1-L1-Z1-G1	M#-W#-B#-#-H95-S2-P1-T1-L1-Z1-G1

MATERIAL LEVEL 1: Material (M); Welded Seam: Seamless, Welded (W0, W1);
Bend: Straight, Shallow, Deep (B0, B1, B2); Mitigation: None, Paint (N, P);
ENVIRONMENT AND LOAD LEVEL 2:
Humidity 75, 95 (H75, H95); Salt Contamination: Zero, Low, High (S0, S1, S2)
Pollutant: Zero, Low (P0, P1); Temp and cycling: Ambient, Cycling (T0, T1)
Stress: Loading: Zero, Constant (L0, L1); Crevice: None, Yes (Z0, Z1);
Galvanic Coupling: None, Yes (G0, G1)

Chapter 4- Experimental Testing Plan

4.1 Test Matrix

As described earlier in the literature review conducted in the study, an effective test plan requires an organizational structure described by clear figures and tables showing the specimens, major detail variables including sizes and configurations, stress levels, and guidelines for determining the number of specimens to be tested for each stress level. Determining the applicability of an available fatigue category (S-N curve) to a specific detail through testing can be costly. As a result, a statistically valid approach should be used that provides clear answers while minimizing the number of experiments.

4.1.1 Determining Test Variables- Geometry and Configurations

This section describes the process of selecting test variables representative of the population of bridges considered in the analyses.

4.1.1.1 Prototypes

Figure 4.1 provides views of the Half-Round Bearing Stiffener (HRBS) and girder cross-section and identifies the important geometric variables. PL-A refers to the HRBS, while PL-B refers to the stiffener plate to which the cross-frame or diaphragm members connect at the support. The prototype details representing the selected bridge population that were analyzed in the study are included in Table 4.1. The girder dimensions were obtained from design drawings and the sizing of the connection details are based on the results obtained in the previous tasks.

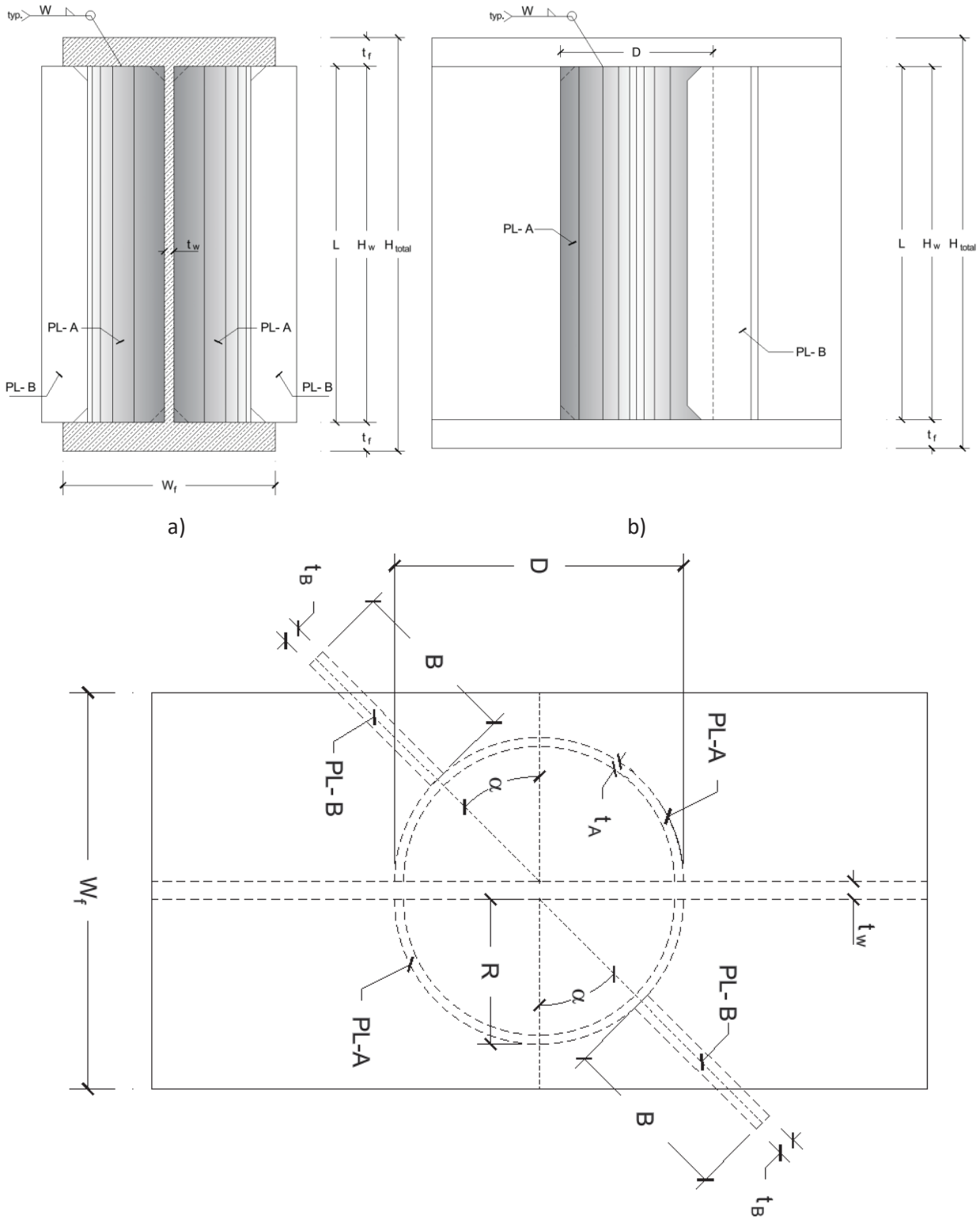

Figure 4.1- HRBS skewed connection parametric details a) Front view, b) Side view, and c) Top view

Table 4.1- Sizing of the prototype steel I-girder, HRBS, stiffener, and welds

Detail #	Steel I-girder (in.)				Stiffener Welded to Flanges	Clipping Type	PL-A (HRBS) (in.)			PL-B (in.)			
	W_f	t_f	H_w	t_w			D	R	t_A	L	B	t_B	α
1	24	3	96	$\frac{3}{4}$	Unwelded	Non-Clipped	16	8	3/4	94	8	1	57°
						Clipped							
					Welded	Non-Clipped			1/2	96	8	1	57°
						Clipped							
2	22	$2\frac{5}{8}$	90	$\frac{5}{8}$	Unwelded	Clipped	16	8	5/8	87	8	1	54°
					Welded	Clipped			3/8	90			
3	16	2	66	$\frac{9}{16}$	Unwelded	Clipped	11	5.5	5/8	63	8	1	23°

4.1.1.2 Scaling

Due to limitations in the experimental facilities regarding both space and loading, as well as to simplify the testing program, scaling of the prototype details is necessary. Two girder depth scaling options were considered in the draft test plan. Option 1 makes use of an overall girder depth of 34 in. while Option 2 uses a girder depth of 50 in. Option 1 results in the smallest dimensions that would accommodate acceptable plate thicknesses and weld sizes, whereas Option 2 provides details closer to practical sizes and dimensions including the weld size.

4.1.1.3 Option 1- Girder Depth of 34 in.

To provide guidelines for proportioning the test specimens, the starting point was to select scaled sizes for the component dimensions, including plate thickness values, assuming there were no limitations in the availability of practical thickness values. This was done to provide an indication of the target specimen. The first prototype for the 34 in. option makes use of a 1/3-scale of the

girders from Bridge 72, which is provided in the first row of Table 4.2. Subsequently, the second and third rows of the table summarize the respective scaled models for Bridges 25 and 65, which were assumed to have a total height of 34 in., and the resulting scale factor for each girder. Other dimensions in Rows 2 and 3 (for Bridges 25 and 65) were calculated simply by multiplying the prototype dimensions by $34/H_{total}$, where H_{total} is the depth of the prototype. Coincidently, with minor exceptions, the resulting scaled dimensions for all three details were close to each other. A scale factor of about 0.36 was obtained for Bridge 25 and 0.49 for Bridge 65. The plate width and thickness values are not that different with the exception of the thickness values of PL-A and PL-B. Therefore, except for the thickness of the half-round bearing stiffener, a single girder size will fit all variations, let it be with slight variations in scaling factors. Furthermore, according to similitude rules, the strains and stresses remain constant between the prototype and scaled model. Therefore, the variation of scale factor among prototypes representing the selected bridges does not affect the stress levels to be targeted in the girder flange.

Table 4.2- Scaling down to the total height of 34 inches for test specimen sizing (Option 1)

Detail #	**H_{total}** (in.)	**Scale Factor**	**Steel I-girder** (in.)				**Stiffener Welded to Flanges**	**Clipping Type**	**PL-A (HRBS)** (in.)			**PL-B** (in.)			
			W_f	**t_f**	**H_w**	**t_w**			**D**	**R**	**t_A**	**L**	**B**	**t_B**	**α**
1	34	0.33	8.00	1.00	32.00	0.25	**Unwelded**	**Non-Clipped**	5.33	2.67	0.25	31.33	2.67	0.33	57°
								Clipped							
							Welded	**Non-Clipped**			0.17	32.00	2.67	0.33	57°
								Clipped							
2	34	0.36	7.96	0.72	32.55	0.23	**Unwelded**	**Clipped**	5.79	2.89	0.23	31.47	2.89	0.36	54°
							Welded	**Clipped**			0.14	32.55			
3	34	0.49	7.77	0.97	32.06	0.27	**Unwelded**	**Clipped**	5.34	2.67	0.30	30.60	3.89	0.49	23°

4.1.1.3.1 Test Groups and Treatments

According to the scaling performed in the previous section, a single girder size will represent all variations for Option 1. The remaining parameters, namely welded or unwelded stiffener plate, clipped or non-clipped half-round, and thickness of the half-round will be represented with the cases included in the Table 4.3.

Table 4.3- Test specimen sizing details for the total height of 34 inches (Option 1)

Detail #	**Case**	**Steel I-girder** in.				**Weld Size** (Typ.) in.	**Stiffener Welded to Flanges**	**Clipping Type**	**PL-A (HRBS)** in.			**PL-B (Stiffener)** in.			
		W_f	**t_f**	**H_w**	**t_w**	**w**			**D**	**R**	**t_A**	**L**	**B**	**t_B**	**α**
1	1	8	1	32	1/4	1/8	**Unwelded**	**Non-Clipped**	5.5	2.75	1/4	30	3	0.4	30°
	2							**Clipped**	5.5	2.75	1/4	30	3	0.4	30°
2	1						**Welded**	**Non-Clipped**	5.5	2.75	3/16	32	3	0.35	60°
	2							**Clipped**	5.5	2.75	3/16	32	3	0.35	60°
3	1							**Non-Clipped**	5.5	2.75	3/16	32	3	0.35	30°
	2							**Clipped**	5.5	2.75	3/16	32	3	0.35	30°

4.1.1.3.2 Proposed Test Setup

With the space and load level limitations following closely those in the FDOT structures laboratory, Figure 4.2 through Figure 4.4 shows the test setup for the proposed fatigue test setup for Option 1.

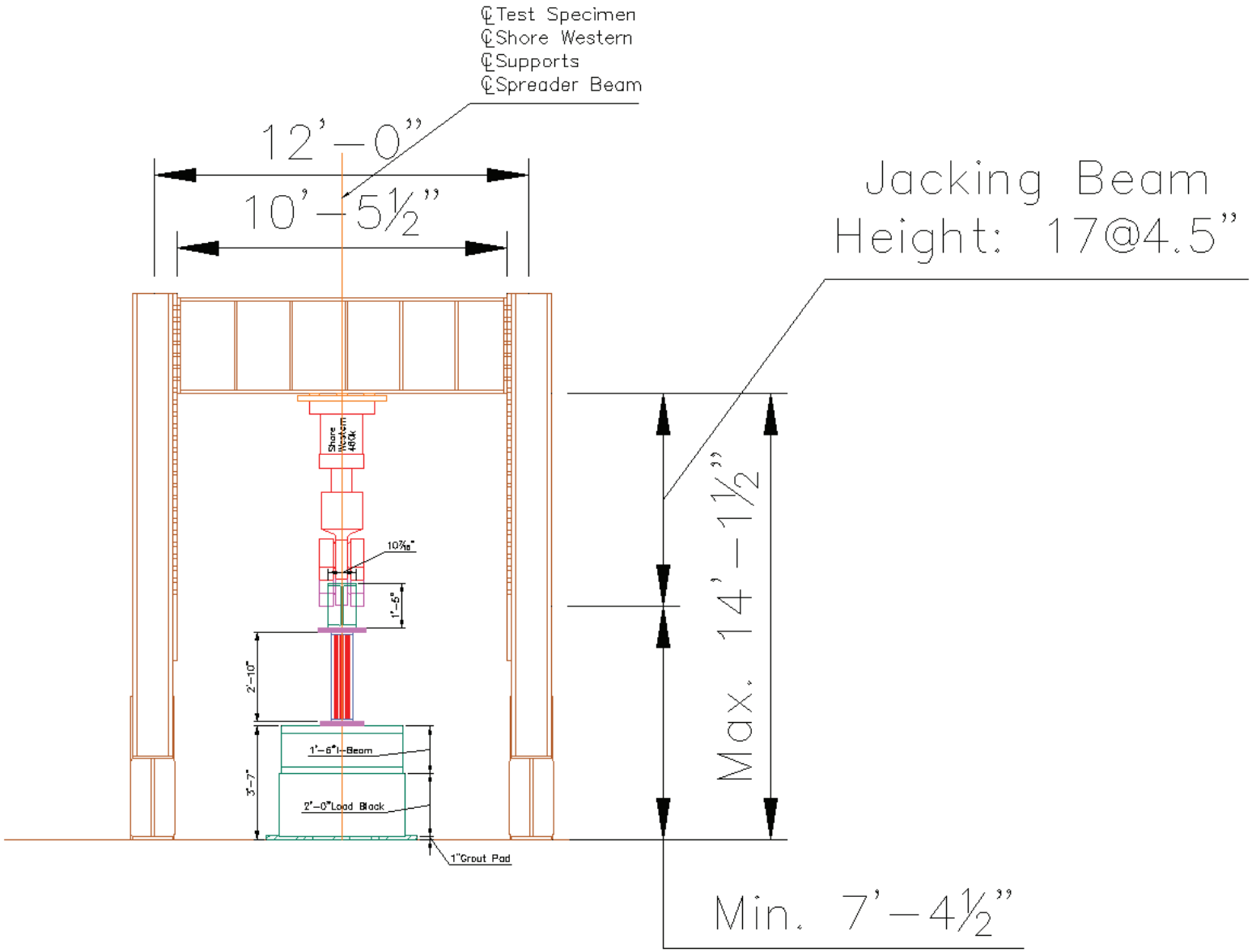

Figure 4.2- Test setup drawings for fatigue testing for Option 1 (Side view)

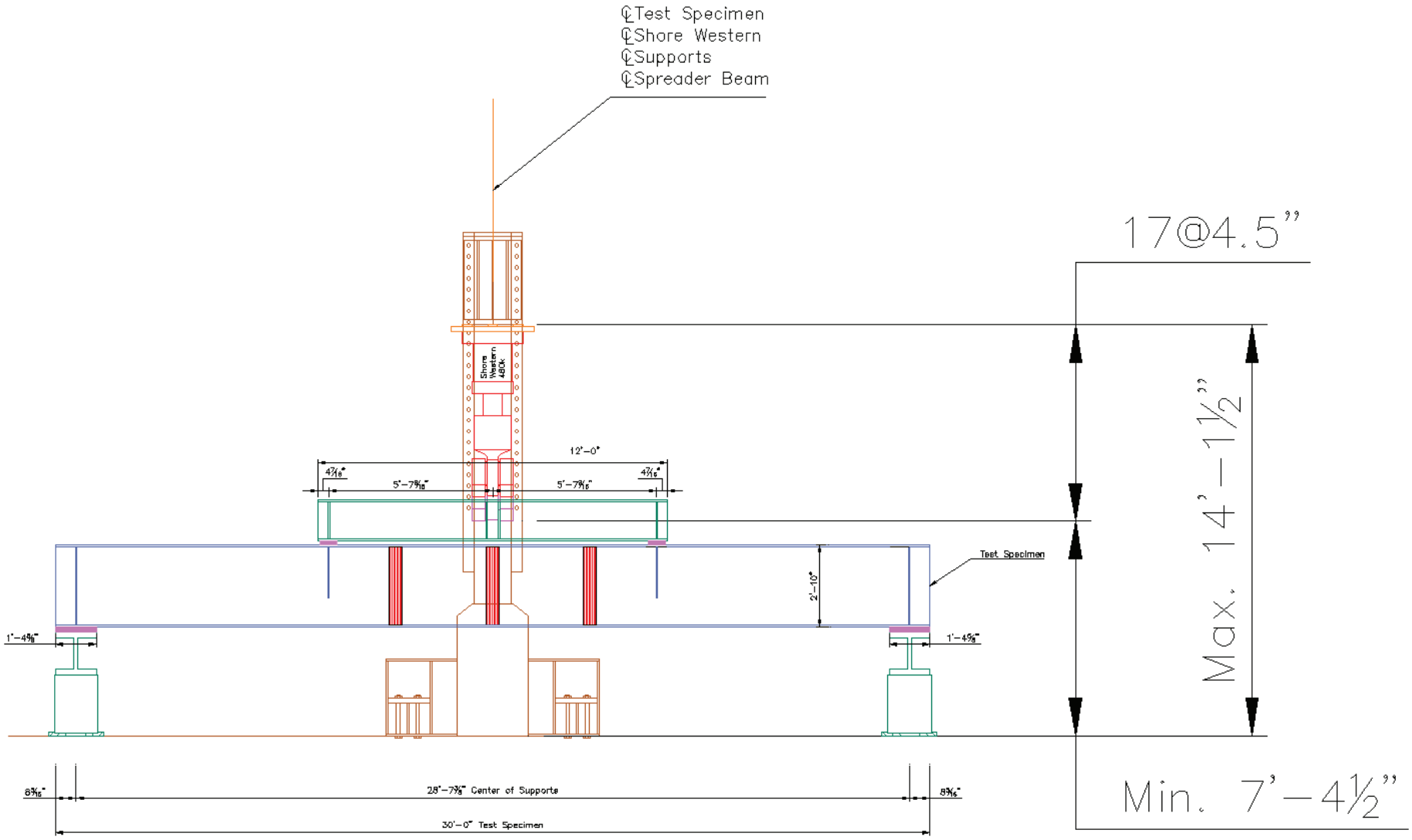

Figure 4.3- Test setup drawings for fatigue testing for Option 1 (Front view)

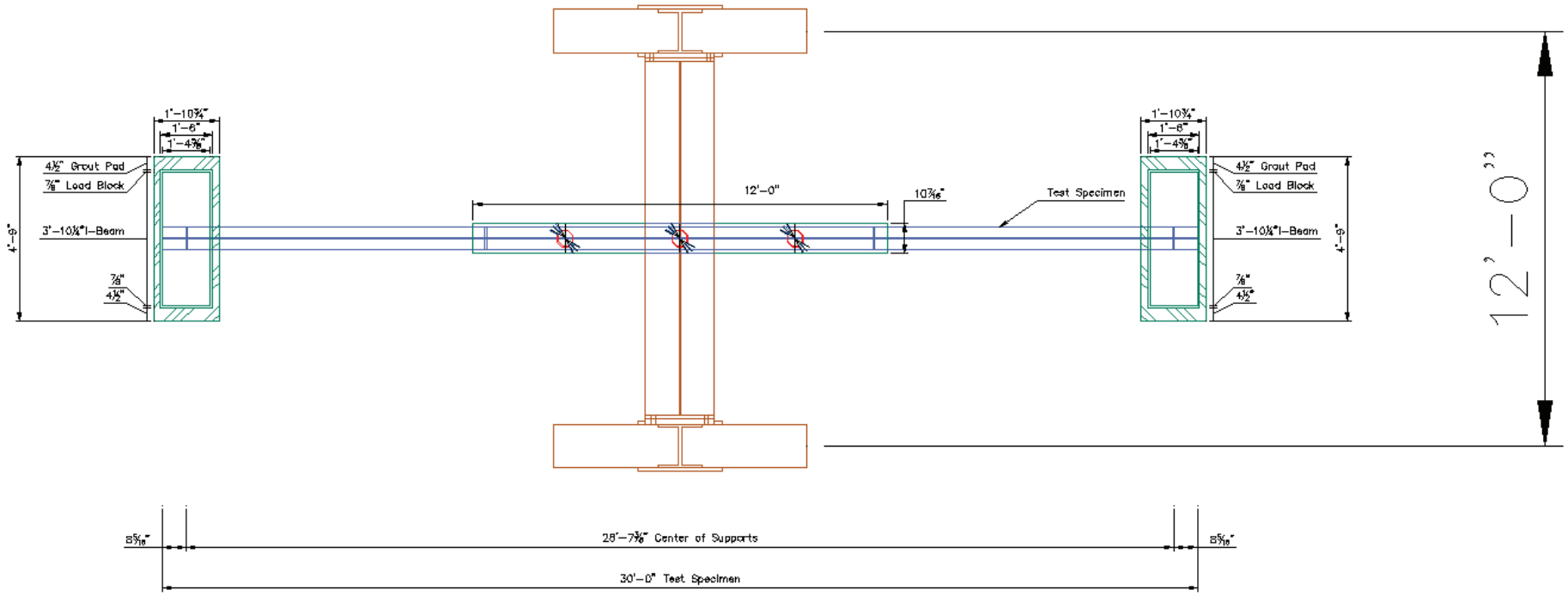

Figure 4.4- Test setup drawings for fatigue testing for Option 1 (Top view)

4.1.1.3.3 Test Specimen Details

Figure 4.5 shows in detail a girder specimen with three potential half-round bearing stiffeners for Option 1. Drawings in Figure 4.1 depict the details and dimensions of test variations included in Table 4.3. A total of six types of test specimens are proposed. The Table 4.3, outlines the configurations and parameters for different test specimens. The table categorizes the specimens based on three main details. The steel I-girder dimensions (W_f, t_f, H_w, t_w) and the typical weld size (w) are consistent across all details, representing a steel I-girder with a flange width (W_f) of 8 inches, a flange thickness (t_f) of 1 inch, a web height (H_w) of 32 inches, and a web thickness (t_w) of 1/4 inch, with a weld size of 1/8 inch. The specimens are divided into unwelded and welded categories, representing whether or not the connection plate (PL-B) is welded to the flanges. In addition, the specimens are further differentiated by whether the HRBS plate is clipped or non-clipped. For all types of specimens, the dimensions for the HRBS plate (PL-A) are given with details on the clipping type and parameters such as diameter (D), radius (R), and thickness (t_A), and the dimensions for the stiffener plate (PL-B) are given with parameters such as plate length (L), plate width (B), plate thickness (t_B), and skew angle (α). For unwelded specimens, in which the stiffeners are not welded to the top and bottom flanges of the steel I-girder, the skew angle is constant at 30 degrees, while for welded conditions, the skew angle is considered at two different degrees, 30 and 60 degrees.

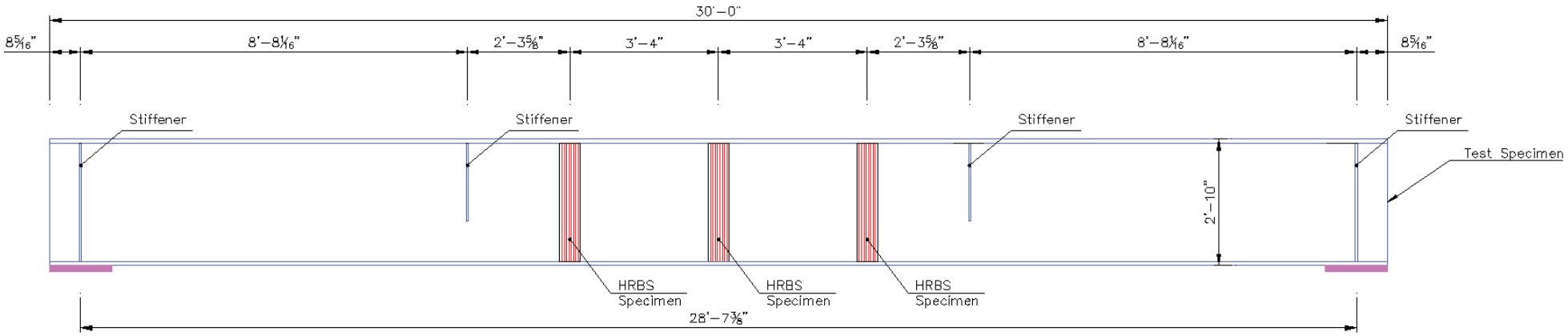

Figure 4.5- Side view of the test girder specimen for Option 1

4.1.1.4 Option 2- Prototype Girder Depth of 50 in.

Option 1 provided specimens with dimensions scaled to a total girder depth of 34 in. While the 34 in. girder depth is desirable with respect to clearance in the laboratory, the scaled weld sizes and HRBS diameter might raise questions related to the impact on the fatigue performance. Therefore, the goal of Option 2 is to increase the girder depth to 50 in., resulting in girder dimensions that are closer to what might be found in practice with regard to flange widths, HRBS diameter, and weld sizes. The process for scaling the specimen dimensions was the same as applied in Option 1 with the difference being the scaling factors based upon the overall height of 50 in. for the scaled model.

Table 4.4 shows the scaled dimensions of the connection elements for Bridge 72. Subsequently, the scaled model for Bridges 25 and 65 was assumed to be the same as that for Bridge 72, and the resulting scale factor for each girder and connection element was calculated for all dimensions involved for the two bridges. With minor exceptions, the scaling factor across each bridge was consistent. Therefore, except for the thickness of the half-round bearing stiffener, one model seems to fit all variations, let it be with slight variations in scaling factors. Furthermore, according to similitude rules, the strains and stresses remain constant between the prototype and scaled model. Therefore, the variation of scale factor among prototypes representing the selected bridges does not affect the stress levels to be targeted in the girder flange.

Table 4.4- Scaling down to the total height of 50 inches for test specimen sizing (Option 2)

Detail #	H_{total} (in.)	Scale Factor	Steel I-girder (in.)				Stiffener Welded to Flanges	Clipping Type	PL-A (HRBS) (in.)			PL-B (in.)			
			W_f	t_f	H_w	t_w			D	R	t_A	L	B	t_B	α
Detail 1	50	0.49	11.76	1.47	47.06	0.37	Unwelded	Non-Clipped	7.84	3.92	0.37	46.08	3.92	0.49	57°
								Clipped							
							Welded	Non-Clipped			0.25	47.06	3.92	0.49	57°
								Clipped							
Detail 2	50	0.53	11.70	1.06	47.87	0.33	Unwelded	Clipped	8.51	4.26	0.33	46.28	4.26	0.53	54°
							Welded	Clipped			0.20	47.87			
Detail 3	50	0.71	11.43	1.43	47.14	0.40	Unwelded	Clipped	7.86	3.93	0.45	45.00	5.71	0.71	23°

4.1.1.4.1 Test Groups and Treatments

According to the scaling performed in the previous section, a single girder size was selected to represent all variations for Option 2. Note that in this case, the weld size was kept unchanged at 5/16 in. The 5/16 in. weld represents the largest fillet that can be made in a single pass and is generally the most common fillet size that is used by fabricators. The selection of the 5/16 in. fillet is, therefore, representative of the likely welds that will be used on the HRBS and connection plate stiffener and alleviates concerns about the potential impact in fatigue vulnerabilities from reduced weld size. The remaining parameters namely welded or unwelded stiffener connection plate (PL-B), clipped or non-clipped HRBS, and thickness of the HRBS will be represented with the cases included in the Table 4.5.

Table 4.5- Test specimen sizing details for the total height of 50 inches (Option 2)

Detail #	**Case**	**Steel I-girder** in.				**Weld Size (Typ.)** in.	**Stiffener Welded to Flanges**	**Clipping Type**	**PL-A (HRBS)** in.			**PL-B (Stiffener)** in.			
		W_f	**t_f**	**H_w**	**t_w**	**w**			**D**	**R**	**t_A**	**L**	**B**	**t_B**	**α**
1	1	12	1.5	47	3/8	5/16	**Unwelded**	**Non-Clipped**	8	4	3/8	45	4	0.5	30°
	2							**Clipped**	8	4	3/8	45	4	0.5	30°
2	1						**Welded**	**Non-Clipped**	8	4	1/4	47	4	0.5	60°
	2							**Clipped**	8	4	1/4	47	4	0.5	60°
3	1							**Non-Clipped**	8	4	1/4	47	4	0.5	30°
	2							**Clipped**	8	4	1/4	47	4	0.5	30°

4.1.1.4.2 Proposed Test Setup

With the space and load level limitations following closely those in the FDOT structures laboratory, Figure 4.6 through Figure 4.8 shows the test setup for fatigue testing for Option 2.

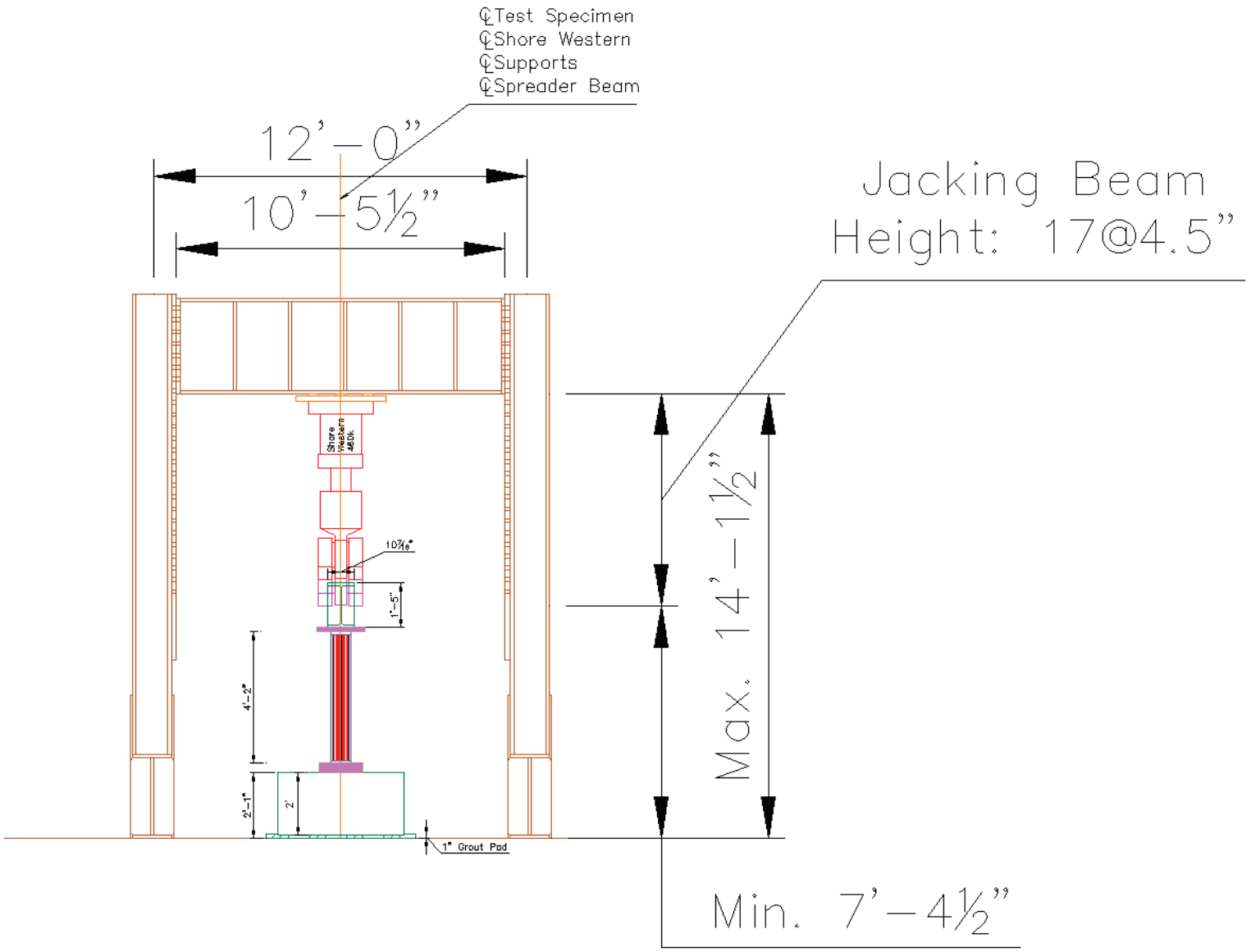

Figure 4.6- Test setup drawings for fatigue testing for Option 2 (Side view)

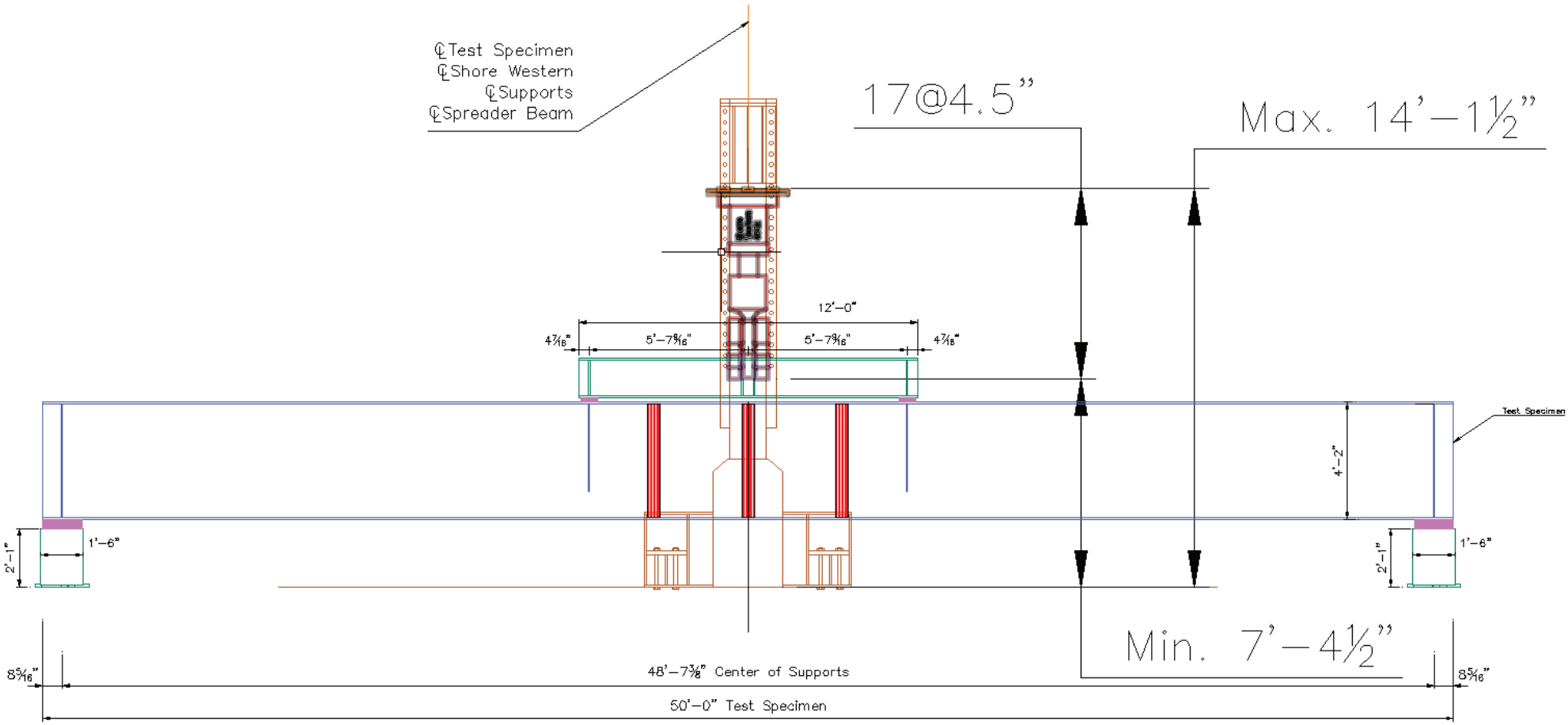

Figure 4.7- Test setup drawings for fatigue testing for Option 2 (Front view)

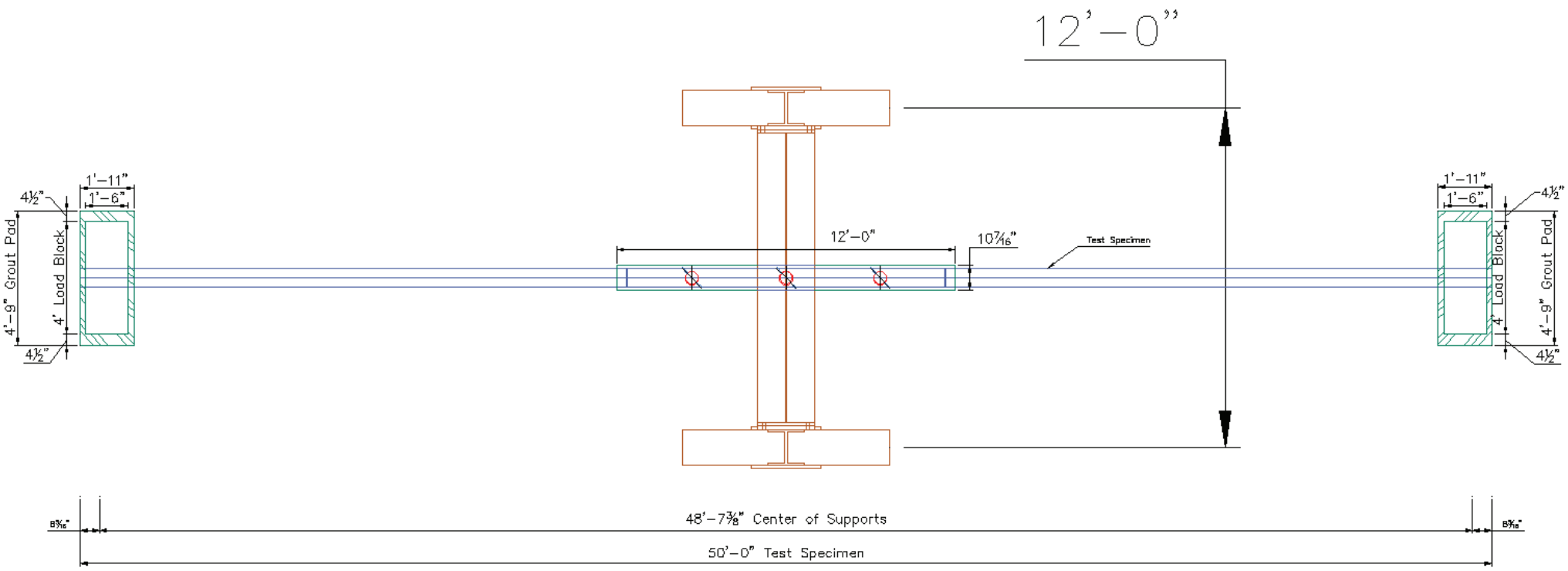

Figure 4.8- Test setup drawings for fatigue testing for Option 2 (Top view)

4.1.1.4.3 Test Specimen Details

Figure 4.9 shows in detail a girder specimen with three potential Half-Round Bearing Stiffener weldments for Option 2. For details on the HRBS connection on this girder, refer to Figure 4.1 and Table 4.5. A total of six types of test specimens are proposed.

The table categorizes the 50-in. deep specimens into three primary groups based on specific details. The Steel I-girder dimensions (W_f, t_f, H_w, t_w) and the typical weld size (w) remain consistent across all categories, featuring a steel I-girder with a flange width (W_f) of 12 inches, a flange thickness (t_f) of 1.5 inches, a web height (H_w) of 47 inches, and a web thickness (t_w) of 3/8 inch, with a fillet weld size of 5/16 inch.

The specimens are divided into unwelded and welded categories with respect to the connection plate stiffener plate (PL-B). Further differentiation is also utilized based on whether the HRBS plate is clipped or non-clipped. For all specimen types, the dimensions for the HRBS (PL-A) include diameter (D), radius (R), and thickness (t_A), while the connection plate stiffener (PL-B) dimensions include length (L), width (B), thickness (t_B), and skew angle (α).

Unwelded specimens, where the connection plate stiffeners (PL-B) are not attached to the top and bottom flanges of the steel I-girder, have a constant skew angle of 30 degrees. For welded connection plate stiffeners, the skew angle is either 30 or 60 degrees. This classification comprehensively covers variations in welding and clipping types to ensure representative data regarding the fatigue performance of the various details are obtained in the experiments.

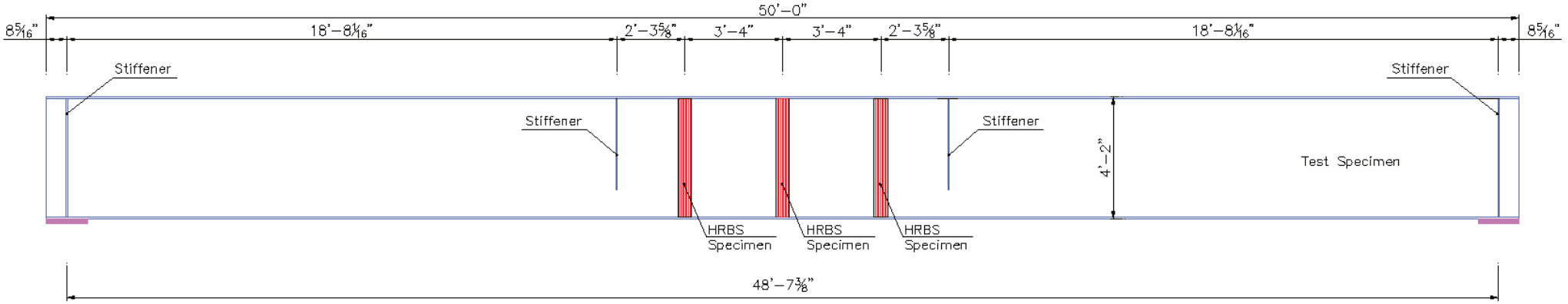

Figure 4.9- Side view of the test girder specimen for Option 2

4.1.1.5 Optimized or Reduced Scope

Regardless of which option is selected, it is recommended to start with the cases that are presumed to be the most critical with respect to performance. The case of unwelded connection stiffener plate (PL-B) with non-clipped HRBS (PL-A) that is Detail 1 - Case 1 in Table 4.3 and Table 4.5, and the case of welded stiffener plate with non-clipped half-round stiffener and skew angle of 60 degrees that is Detail 2 - Case 1 in Table 4.3 and Table 4.5, are expected to generate more critical details for fatigue testing among 6 cases.

4.1.2 Approach for Fatigue Testing

During the Task 1 of this project, the following topics were explored:

- Statistical Planning Guidelines for Fatigue Experiments
    - Fundamental Concepts in the Statistical Planning of Fatigue Experiments
    - Planning S-N Tests
        - Recommendation for the number of Stress Levels and Replication
        - Fatigue Strength and Fatigue Limit Tests

The objective of the current project is to develop a test plan for determining which AASHTO fatigue category more closely applies to the half-round stiffener connection detail for steel girder designs. Therefore, among the approaches suggested by STP588 [75] design allowable test plan seems to be the proper type to choose. The number of test specimens depends on the number of required stress levels and replications. Figure 4.10 shows the typical S-N curves for the current AASHTO fatigue categories, which provide a Log_{10} scale of the cycles to failure (N) for a given stress range. The horizontal portions of the curves indicate the threshold stress representing infinite fatigue life.

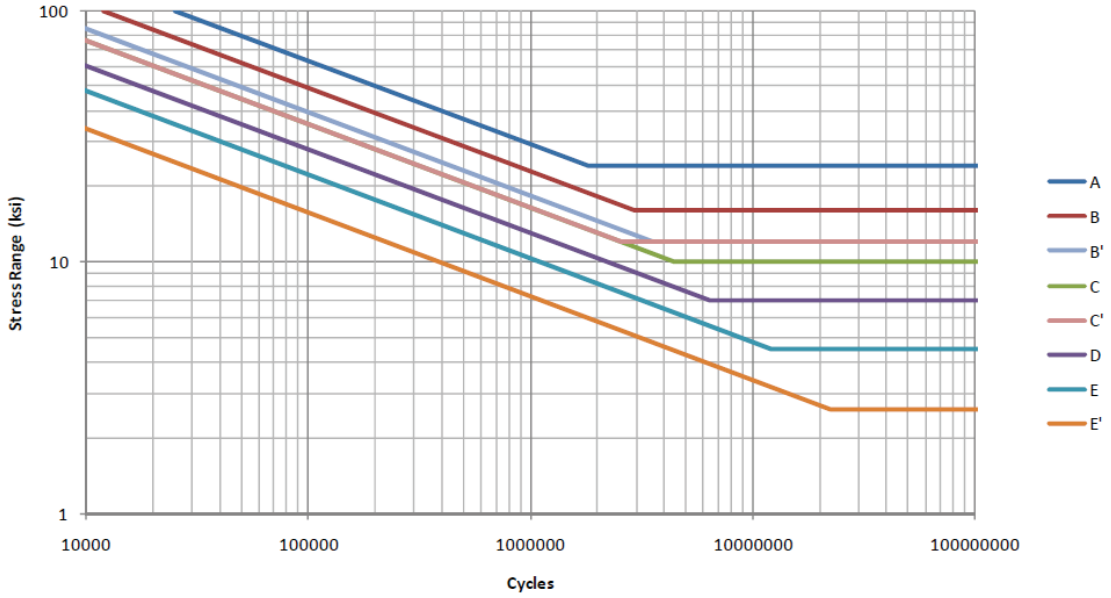

Figure 4.10 S-N curves corresponding to AASHTO fatigue categories [44]

4.1.2.1 Linear Descending Branch

Two stress range levels are recommended to be used for a linear descending branch, which is the common trend for AASHTO fatigue. The replication percentage and number of replications for the design allowable test plan have been recommended by the guidelines in STP588 [75] to be 50 to 75% and 12 to 24 specimens, respectively. Accordingly, a minimum of 6 replications for each of the two stress range levels can be used to match this recommendation. This is illustrated by S_1 and S_2 stress ranges in Figure 4.11. After obtaining at least 6 successful tests (failed) at each stress level, the median and standard deviation for each group will be determined. Then, the points on Log_{10} coordinates at median minus 2 times standard deviation will be determined and connected with a line. The AASHTO category with the closest descending line to the left of this line will be representative of the appropriate category for the connection detail. Alternatively, to reduce the total duration of the testing related to total number of cycles, higher number of tests can be selected for S_2 and lower number of tests for S_1 with a total of 12 tests for two levels. As an example, 9 tests can be performed at S_2 level and 3 at S_1. In this case, the points on Log_{10} coordinates at median minus 2 times standard deviation for stress level S_2 will be used to identify the corresponding category among AASHTO categories, and the results of test at S_1 will be used for confirming the selection and demonstrating the linear inclination.

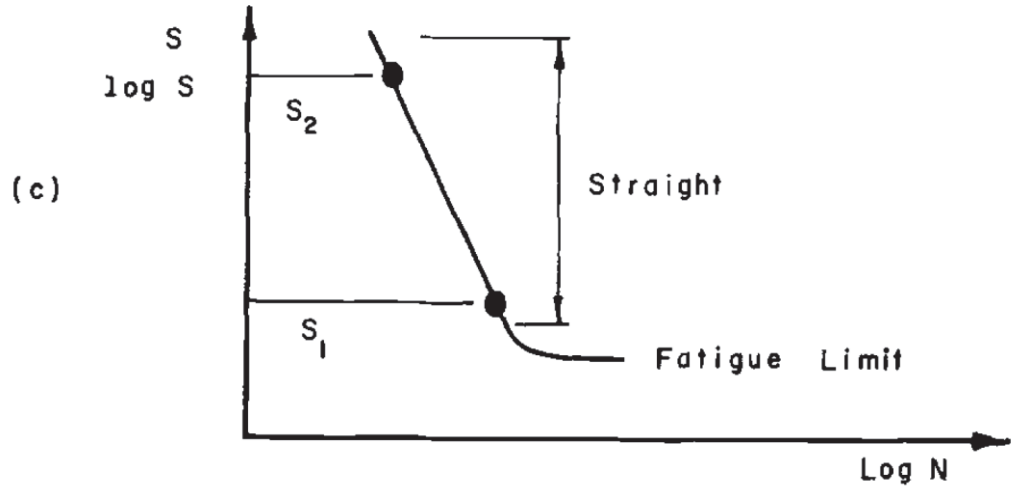

Figure 4.11 S-N curves with the straight descending branch [75]

4.1.2.2 Fatigue Threshold

For the objectives of this project, that is determining the fatigue category for design of the top flange in continuous steel girder of skew bridges over the intermediate support, it is the opinion of the authors that determining the descending line would suffice. If there would be a choice between two categories in relation with differing threshold, one could conservatively select that with the lower threshold. The process for determining the actual fatigue threshold requires a significantly higher number of test specimens tested under a higher number of cycles. Nevertheless, for completeness, the method for determining the fatigue threshold is described in this section. For reference purposes, the literature review performed in this project documents methods for determining the fatigue strength threshold [75], [84], [83].

4.1.2.3 Summary of Approach

The objective of this project is to develop a test plan for determining which fatigue category applies to the half-round bearing connection for the purpose of fatigue design of the girder top flange. As stated above, this objective can be achieved by determining which descending line among the existing categories better represent the referenced detail for each test configuration determined earlier (Table 4.3 and Table 4.5). Owing to a linear assumption for the descending line, two stress levels (S1 and S2) can be selected for this zone, and an equal number of tests, as described above are conducted for each stress level. A line can be drawn for these two stress

levels that crossed the median number of cycles for each level minus 2 times the standard deviation. An existing AASHTO category with an inclined line immediately on the left of this line can be taken as the category for this detail. Alternatively, to reduce the total duration of the testing related to a total number of cycles, higher number of tests can be selected for a higher stress range (S2) and lower number of tests for a lower stress range (S_1) with the same total number of tests for each configuration. In this case, the points on Log_{10} coordinates at median minus 2 times standard deviation for stress level S_2 will be used to identify the corresponding category among AASHTO categories, and the results of the test at S_1 will be used for confirming the selection and demonstrating the linear inclination.

It is the opinion of the authors that determining the descending line would suffice for the purpose of this project. If there would be a choice between two categories in relation to differing thresholds (e.g., for the cases of AASHTO Categories B', C, and C'), one could conservatively select the category with the lower threshold.

The procedure will be repeated for all types of test specimens determined in Table 4.3 or Table 4.5 depending on the option selected. It is recommended to start the testing with the cases that are presumed to be the most critical with respect to performance. The case of unwelded connection stiffener plate (PL-B) with non-clipped HRBS (PL-A) that is Detail 1 - Case 1 in Table 4.3 and Table 4.5, and the case of welded stiffener plate with non-clipped half-round stiffener and skew angle of 60 degrees that is Detail 2 - Case 1 in Table 4.3 and Table 4.5, are expected to generate more critical details for fatigue testing among 6 cases.

4.1.3 Test Matrix

Using the information described above, the test matrix is shown in Table 4.6 for each type of detail to be tested. This will be repeated for all other types. The number of tests shown in this table for linear descending line refers to successful tests at the location of each detail, that is, connection details for which the fatigue cracking occurs in the flange of the girder at the location of the connection. Two options are proposed for the number of tests at each stress level: Option A and Option B. Option B results in a shorter test duration with fewer total cycles.

It is understood that each girder specimen can accommodate multiple connections along the constant moment region, such as that proposed here, with 3 connection details in each girder. Therefore, each girder can potentially produce multiple successful test results if the first fatigue cracking does not degrade the girder's behavior noticeably. In some cases, repair/rewelding of the girder at cracks for one detail may restore its ability to continue the test for crack development for other details. Nevertheless, it is likely that some connection details may remain partly unused for the purpose of this program. However, even details for which fatigue cracking is not observed can provide some insight into fatigue performance those details.

Table 4.6- Test matrix for each detail configuration (multiply this table by the number of details selected for testing)

Item	Purpose	Stress levels	Cycles	Min. Number of tests	
				Option A	Option B
1	**Inclined Line portion**	S1	Determined by test	6	3
2		S2	Determined by test	6	9

Note: If determining the fatigue threshold is decided or becomes necessary, the test matrix can be amended accordingly.

4.2 Test Specimens

4.2.1 Introduction

Two levels of analysis were conducted as part of the investigation. The Level I analyses consisted of an analysis on the full bridge system to obtain the force range for key elements of cross-frame system at the supports. The Level II analyses consisted of detailed three-dimensional models of the half-round bearing stiffener (HRBS) and cross-frame systems. In Task 2, after completing the Level I analyses on 26 representative bridges, three bridges were selected for the Level II analyses. Based on the Level II analytical study conducted in Task 2b, three test prototype details were presented. In the previous task, these details were scaled to be compatible with the available FDOT laboratory testing facilities in Tallahassee. This section provides additional details for the test specimens and testing procedure.

4.2.2 Material

In Task 3 of this project, a list of materials was proposed for HRBS connection detail (see Table 3 in Deliverable for Task 3). The materials included both the plate and pipe/tube elements. This investigation is focused on the material for the HRBS and considered either A709-21 or A588-19 Grade 50. The research team recommends using the same material for both the steel girder and connections elements. For fatigue testing, considering the availability and the common use by designers, ASTM A 709 Grade 50 steel is recommended for fabricating the steel I-girders and HRBS, and plate elements. Since this fatigue testing is focused on the details and configurations, selecting a single material is practical and will provide the required information.

ASTM A 709 Grade 50 is a high-strength, low-alloy structural steel specification commonly used in bridge construction. The steel grade offers a combination of strength, weldability, and toughness, making the material a good choice for structural applications that require enhanced performance.

4.2.3 Fabrication

For fabrication, the testing agent shall prepare a complete set of design drawings depicting the information required for fabrication including material and construction specifications. The fabricator shall prepare shop drawings for fabrication and submit for approval to the testing agent. A complete record of the fabrication process shall be maintained and included with the testing phase deliverable.

Fabrication is a critical process in the construction of steel structures, involving cutting, bending, and assembling steel materials into the desired shapes and configurations. This process ensures that the structural components meet design specifications and performance requirements. For this project, the fabrication of the steel I-girders and Half-Round Bearing Stiffeners (HRBS) from ASTM A 709 Grade 50 steel will follow several key steps:

- **Cutting**:

  Precision Cutting: The steel plates shall be cut into the required shapes and sizes. Precision cutting ensures minimal material waste and high accuracy.
- **Bending and Shaping**:

  Bending: Hydraulic presses or rolling machines are used to bend and shape the steel plates into HRBS sections. The bending process is carefully controlled to avoid compromising the material integrity.

  Shaping: Specialized tools and machinery shape the Half-Round Bearing Stiffeners (HRBS) to match the design requirements.
- **Welding**:

  Preparation: Edges of the steel components are prepared for welding by cleaning to ensure strong and clean welds.

  Welding Process: Steel components are assembled and welded together. Welders ensure that the joints meet the specified standards. Attention shall be paid to specific details provided in the design and shop drawings including but not limited to seal-welding for the cases with unclipped HRBS.

Post-Weld Treatment: If required by the specifications, welded areas are treated to relieve stress and minimize defects. This might include heat treatment.

- **Assembly**:

  Component Assembly: The individual fabricated parts are assembled into larger structures, such as girders and stiffeners, according to the design specifications.

  Fit-Up: Each part is aligned and temporarily held in place to ensure proper fit before final welding.

- **Surface Treatment**:

  Cleaning: The assembled components are cleaned to remove contaminants, such as oil, dirt, or rust.

  Coating: Because of the relatively short duration of the testing and the need for inspection of details during testing, no coating is required.

- **Inspection and Quality Assurance**:

  Dimensional Inspection: All dimensions are checked against the design specifications to ensure the geometry is within tolerances.

  Weld Inspection: Welds are inspected using non-destructive testing methods as prescribed by the specifications. Dye penetrant, magnetic particle, or Eddy current on a larger weld population, and ultrasonic testing or radiography on selective welds can be applied to detect potential internal defects that might adversely impact the performance.

  Final Approval: The fabricated components undergo a final quality check to ensure they meet all required specifications.

- **Transportation and Installation**:

  If the test specimens are fabricated in a facility other than the testing lab, care should be taken that the finished components are not damaged during transportation to testing laboratory.

4.2.4 Instrumentation

Section 1.3 in the Literature Review discusses various techniques and strategies used for the detection and monitoring of crack initiation and progression in the structural elements of the test specimens. The methods are divided into two main categories:

1. **Real-time Monitoring Techniques**: These techniques continuously monitor the structure and can automatically signal the initiation and progression of cracks. Examples of real-time monitoring techniques identified earlier include Acoustic Emission (AE), Laser Vibrometry, Vision-Based Inspection Methods, and Piezoelectric Sensors and Strain Gauges.

2. **At-interval (non-real-time) Monitoring Techniques**: These techniques can be applied during pauses in the experimental tests or when the real-time monitoring system provides an indication of potential cracks to verify the presence and propagation of the cracks. Visual examination (aided or not), dye penetrant testing, magnetic particle inspection, electromagnetic testing, and eddy current testing are some of the potential methods of testing.

Choosing appropriate crack detection strategies during the fatigue test is important. Therefore, it is suggested that multiple methods (e.g., Acoustic Emission (AE), Vision-Based Inspection, and Piezoelectric Sensors and Strain Gauges), along with all at-interval monitoring techniques be used on the first test specimen. The testing agent can propose other methods if warranted by their performance. This will allow for a comparison of the methods to identify the most effective techniques for the project. The research team conducting the experimental tests will make the final selection of the methods to be used for the rest of the tests based on the results of the first test.

4.3 Safety

As with all experimental testing, proper safety protocols are paramount to protect both personnel and equipment. This safety section outlines comprehensive procedures to ensure that

all aspects of the fatigue test are conducted in a controlled and secure environment, minimizing the risk of accidents and ensuring compliance with industry standards. These protocols aim at maintaining a high standard of safety while achieving accurate and reliable test results. Specifically, for fatigue testing that require sometimes continuous operation for a long duration, the safety and operational effectiveness is of a paramount importance. Appendix A includes a detailed safety protocol that can be compared to the safety protocols of the testing agent.

4.4 Loading Protocols

The loading protocol for fatigue testing of steel I-girders with Half-Round Bearing Stiffeners (HRBS) under different loading conditions are provided in this section. Each test will be conducted with constant-amplitude cyclic loading.

4.4.1 Loading Procedure

A schematic of the setup and test specimens are provided in Figure 12. The geometry of the components and specimen need to be evaluated for proper alignment to avoid undesirable misalignments that might introduce stresses or constraints that impact the behavior. The test setup, as illustrated in Figure 1, consists of a structural steel I-girder specimen supported at both ends by relatively rigid fixtures. Multiple stiffeners are installed/welded to the girder at locations of concentrated loads as well as the three HRBS details positioned in a region of constant stress gradient from the applied loads.

The setup makes use of a spreader beam positioned above the steel I-girder to evenly distribute the applied load from the actuator (F) into two load points (P) on the steel I-girder, creating a constant moment region between these load points. Figure 13 shows the moment and shear diagrams produced in the fatigue test specimen from the cyclic load. This setup allows for applying a desired stress in the tension flange and a detailed examination of the fatigue performance of the steel I-girder with the HRBS details, under controlled and repeatable conditions.

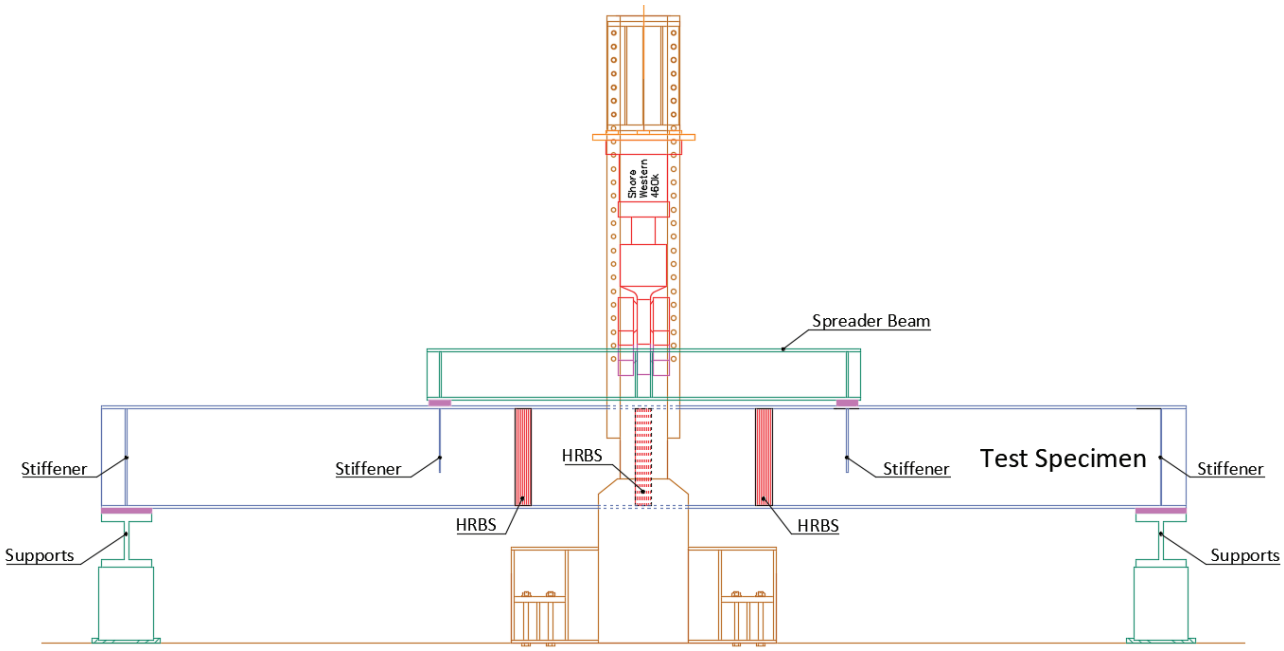

Figure 12- Test setup

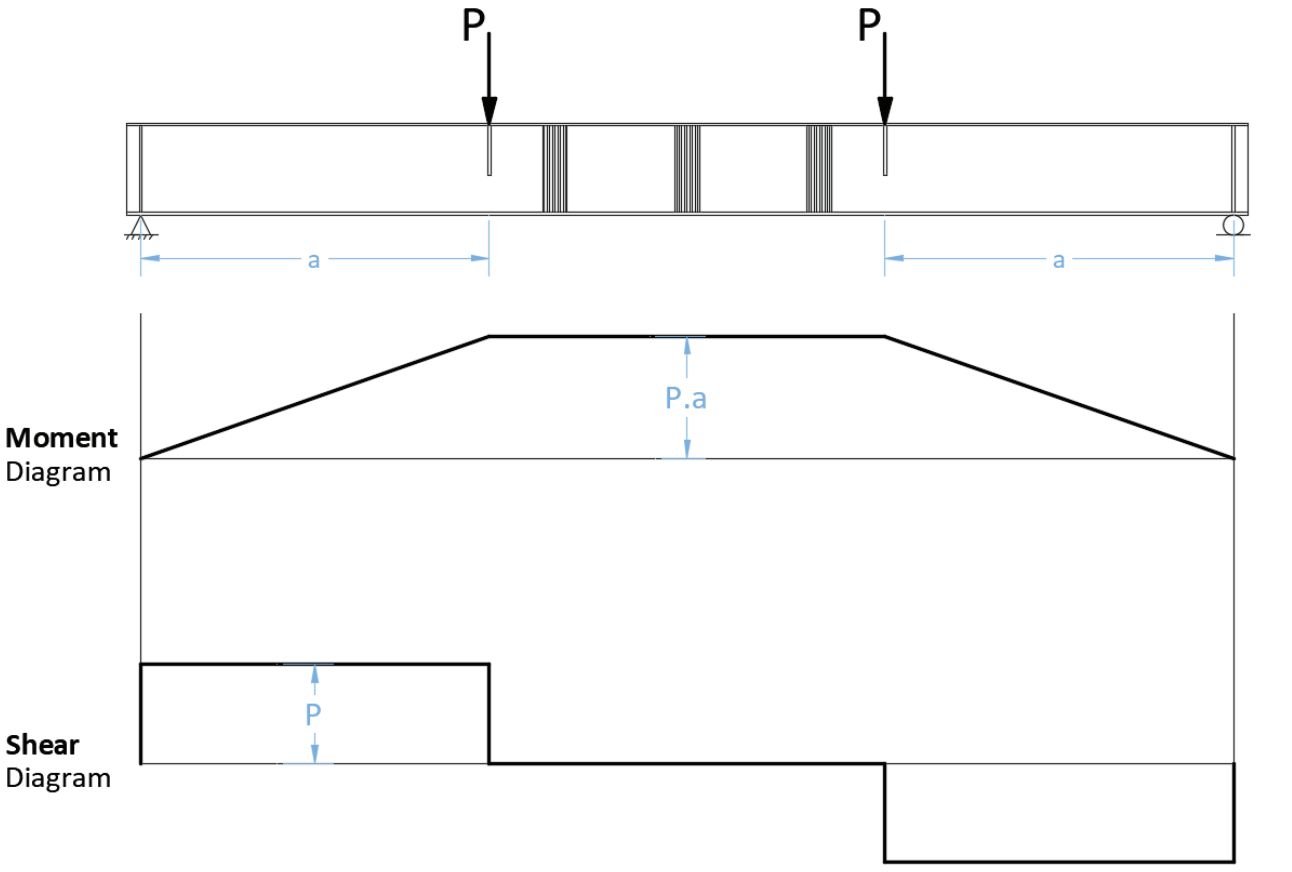

Figure 13- Moment and shear diagrams produced in the fatigue test specimen

Fisher et al., in NCHRP Report 102 [136], assert that the two most significant factors influencing fatigue strength are the stress range and the type of structural detail. They reported that the minimum stress above which the tensile stress range varies did not have a noticeable effect. The stress range is determined by the difference between the maximum and minimum stress levels resulting from the cyclic load. Accordingly, unless necessitated otherwise, the loading could begin with only dead load that is at the actuator load of zero. As an example, the dead load stress in the tension flange at the mid-span of the test girder for Option 2 of the test setup suggested in Task 4a is estimated to be around 1 ksi. The dead load includes the weight of girder and attachments, the spreader beam and attachments, and related loading fixtures below the load cell.

Figure 14 shows the actuator constant-magnitude cyclic loading over the time. The applied loading is intended to keep the actuators in compression so that loading fixtures remain in constant contact with the specimen. A minimum load level (F_{min}) should be established so that the cyclic load level does not result in a stress reversal. A stress reversal will not significantly impact the fatigue performance of the details; however, producing constant compression between the loading fixtures and the top flange of the beam simplifies the setup details. A minimum load of a few kips is usually satisfactory for most setups. The loading itself is applied cyclically to simulate the repeated stresses that occur during normal use. The frequency of these cycles will dictate the duration of the test. However, the load frequency depends on the capacity of the hydraulic jack, hydraulic servo-valves, and the hydraulic capacity of the testing lab, including the hydraulic pumps and pipe network. The loading frequency shall be determined by the testing lab and receive approval from FDOT. The loading frequency does not impact the fatigue rating of the details, but has a dramatic impact on the duration of the test. A frequency of 1 Hz. results in 86,400 cycles per day (assuming 24 hours/day testing), so a test that was expected to take 500,000 constant amplitude stress cycles would last approximately 6 days.

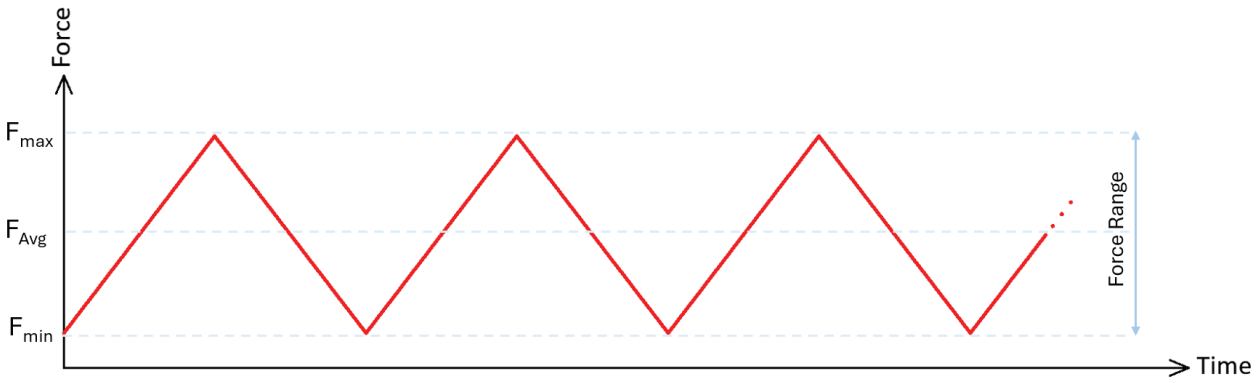

Figure 14- Actuator constant-magnitude cyclic loading pattern

The relationship between the stress in the tension flange of a steel I-girder (σ) and the force generated by the actuator (**F**) is shown by the following equation:

$$\sigma = \frac{M \times c}{I} = \frac{P \times a \times c}{I}$$

The equation shows that the stress σ is calculated using the moment M, the distance c from the point of interest (the outer layer of the tension flange or the location of welded detail) to the section's centroid, and the moment of inertia I of the steel I-girder's cross-section.

Since the actuator force, F, is evenly distributed by the spreader beam into two-point loads, represented as P in Figure 13, the stress can also be expressed as:

$$F = 2 \times P$$

$$\sigma = \frac{M \times c}{I} = \frac{F \times a \times c}{2 \times I} = F \times \left(\frac{a \times c}{2 \times I}\right)$$

In the test setups, the term $\left(\frac{a \times c}{2 \times I}\right)$ remains constant, establishing a linear relationship between the stress in the tension flange of a steel I-girder (σ) and the actuator force (F). Consequently, the stress in the tension flange of the steel I-girder (σ) generated by the actuator follows a pattern

similar to that shown in Figure 14. Figure 15 illustrates the cyclic tension stress pattern of constant magnitude in the girder's tension flange, as generated by the actuator.

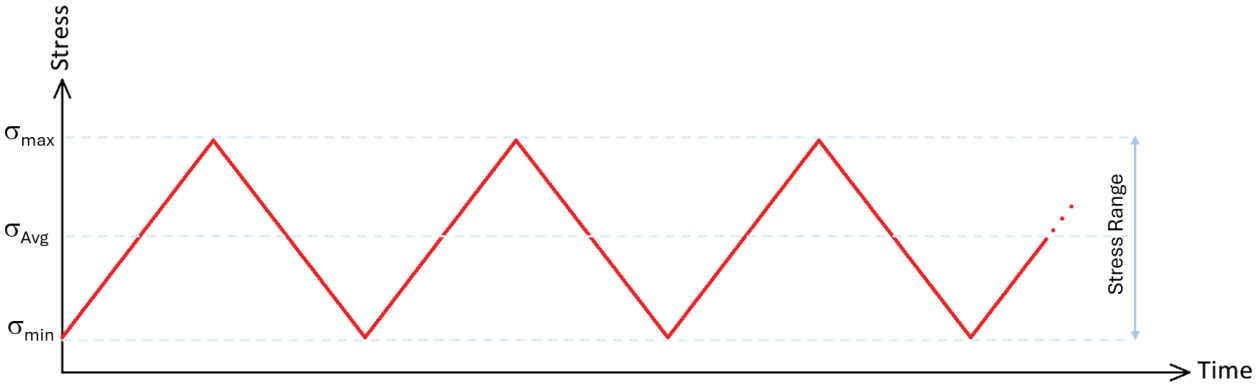

Figure 15- Cyclic tension stress pattern of constant magnitude in the girder's tension flange generated by the actuator

During the test, the load magnitude and direction should be carefully controlled as needed to maintain the desired stress range conditions. If one of the HRBS details reaches a critical crack size prior to the other stiffeners, weld repair or other retrofitting of the failed stiffener can be completed to extend the test for evaluation of the other HRBS locations. Retrofits such as this enables the gathering of additional data on the rest of the specimen to obtain multiple data points for a given detail. It is not uncommon to have scatter in the performance of a specific detail and these procedures allow for efficient use of the test specimens.

As an example, for the Option 2 setup suggested in Task 4a, to develop a stress of σ = 20 ksi, the maximum force in the jack, F_{max}, is estimated to be approximately 170 kips.

4.4.2 Determining the Stress Ranges

As described in Task 4a, the objective of the testing can be achieved comparing the fatigue performance from the experiments with the descending line among existing categories that best represents the detail for each test configuration. By assuming a linear relationship, two stress levels (S_1 and S_2) would suffice. The lower stress level, S_1, should be selected to be above the threshold level. For example, assuming that the AASHTO fatigue category is expected to be

similar to the B or C', S_1 will need to be higher than 15 ksi. S_2 can then be selected within the suitable range.

4.4.3 Span and Loading Points

The span and position of loading points should follow the option selected between two options suggested in Task 4a. Variation to those options can be suggested by the testing lab as long as it serves the main purpose of the testing program and approved by FDOT.

4.4.4 Failure Definition

In fatigue tests, the definition of failure is crucial as it determines the endpoint of the test and the interpretation of the material's or structure's endurance under cyclic loading. Failure in fatigue is generally characterized by the initiation and propagation of microscopic cracks that grow over time until they reach a critical size, leading to a significant reduction in the load-bearing capacity or complete fracture. Fatigue failure in welded details typically originates at the weld toes due to stress concentrations and the presence of micro-flaws, such as weld imperfections. Ideally, the onset of cracking should be detected with real-time monitoring instrumentation and/or at-interval inspection. On the other hand, the failure would be defined with further propagation of the crack that would result in noticeable structural response changes, e.g., variations from linear elastic deflection. A deflection failure criterion similar to that used for the studies reported in NCHRP Report 102 [136] is suggested for this program. For example, an increase of deflection by 0.020 inches should signal failure and activate a microswitch to stop the loading. Failure is often identified when the crack has significantly reduced the cross-sectional area, leading to yielding of the material and, eventually, a complete fracture. Once identified, the crack propagation can be monitored and the test stopped prior to the point of brittle fracture. As noted previously, potential retrofitting of a crack that is nearing critical size can be desirable to obtain additional data from other details.

4.4.5 Loading Pauses/Cycles Increments for Crack Inspection

In the fatigue testing, the intervals at which the tests should be stopped to inspect for cracks are critical for understanding the connection detail fatigue behavior and verifying the crack presence and propagation. The inspections are often carried out after specific portion of the fatigue life has elapsed. For example, it is suggested that, unless an event is registered by the instrumentation, the inspection pauses can begin after an approximately 75% of the expected fatigue life is consumed. Such an inspection frequency will avoid unnecessary pauses and delays in testing. Therefore, it is recommended that the most critical fatigue category expected for the detail is specified and the number of cycles to failure for the applied stress range, N_i, is determined. Then the inspection intervals to begin when 75% of N_i has been applied to the test specimen. The pause intervals after the start point can be chosen to provide for a reasonable inspection opportunity, e.g., interval cycles of $N_i/20$ unless an event is registered by the instrumentation. This approach ensures that emerging cracks are detected early to allow for appropriate interventions before failure occurs. As crack propagation accelerates, the experiments can be changed from 24 hours/day to testing during laboratory business hours so that crack propagation can be monitored.

4.4.6 Splicing and Continuing Post-Failure

Following an initial failure, regardless the failure occurs at the expected details or elsewhere, the girders can be repaired or retrofitted so that a stable and linear deflection can be achieved, and continue the testing for the other remaining details. The repair process can for example involve welding lap plates on the tension flange if the cracking has propagated in the flange. To further reinforce the cracked section, particularly in cases where the web exhibits cracking, a doubler plate can be welded to the beam web.

4.5 Data collection, Management, and Quality Control

Due to the volume and importance of the data collected in testing, a comprehensive data management plan shall be developed by the testing agent and approved by FDOT. At the minimum, the plan shall set out naming, processing, and storage conventions for all data

collected at the experimental and observational stages, as well as training in annotating datasets with necessary metadata. A data repository source is needed to track the research efforts in a timely manner. All data shall be identified by the standardized metadata formats according to the data curation guidelines in the plan.

The plan shall also include the expected data formats, data quality and quality assurance, data formatting and processing, data storage and sharing, and reporting quality control.

4.5.1 Data Quality

During Test- Data quality control in during test have two main purposes: first, to ensure that the data collected from any source shall be stored appropriately; second, data shall be screened for errors in sensors, data acquisition systems, or meta-data specifying correspondence for each data set, image, etc. All notes and collected data shall be backed up digitally on a memory drive, and transferred to server as soon as possible or in real time.

4.5.2 Data Quality/Assurance

Post Test- Data quality control is integral to the continued success of any test program involving measurement. Quality control shortly after test completion can help identify test issues and prevent costly errors in future tests. The data quality assurance process shall assess whether the appropriate protocols were implemented for all processed or interpreted data before it is formatted and archived.

4.5.3 Data Formatting and Processing

Data available in its ASCI format shall be formatted to fit Microsoft Excel worksheets or similar. Formatted data shall be archived and uploaded to the server. Data processing and analysis shall be performed in Microsoft Excel worksheets or similar and stored accordingly for reporting purposes.

4.5.4 Data Storage and Transfer/Sharing

All raw data and images, formatted and processed data shall be stored on the server for future use, back-up and transfer. Preferably, a cloud-based repository will enable the researchers and FDOT to share, update, and archive the data after each task is completed so that the data can be retrieved for tracking of the ongoing efforts.

4.5.5 Reporting Quality Control

All reports shall be reviewed by at least one PI or Co-PI (other than the author) for accuracy and completeness.

4.6 Data Analysis

Table 6 of the Task 4a report provided two options for testing of each HRBS and stiffener plate configuration. These include Option A requiring a minimum of 6 results (failure cycles) at each stress range level or Option B with 9 results at lower stress range level and 3 at higher stress range level. After these results are obtained, for the case of Option A, a line can be drawn through these points, intersecting the median number of cycles for each stress range level minus two standard deviations. The corresponding AASHTO category is identified as the inclined category line to the left of this line. To shorten testing time in Option B, more tests can be done at the higher stress level (S2) and fewer at the lower stress level (S1), with results used to confirm the category and demonstrate linearity. In this case, a line can be drawn from a point coinciding with the median minus two times the standard deviation of results for the lower stress with a slope parallel to the descending lines representing the AASHTO categories. If this line passes to the left of the results for the higher stress range level, then the corresponding AASHTO category is identified as the one with an inclined line immediately to the left of the line.

Chapter 5- Summary and Conclusion

A new connection type, the Half-Round Bearing Stiffener (HRBS) connection, has been developed and investigated by others as an alternative to bent plate connection for joining end cross-frames to steel girders in skewed bridges. The configuration of this connection assures the connection stiffener plate is perpendicular to the Half-Round plate regardless of the skew angle and avoids using bent connection plates. Over the intermediate support and negative moment region in continuous bridges, the upper flanges of the girders experience tensile stress variations from the live load and, therefore, create susceptibility to fatigue at the connection of the HRBS to the tension flange at that location. This also generates potential stress risers and concentration, adding to the overall concerns about the fatigue behavior of this connection detail. A more in-depth investigation of the fatigue behavior of the half-round bearing stiffener connection and its variations is therefore desirable. The objective of this research project was to analytically determine the fatigue sensitivity of the half-round bearing stiffener connection over the intermediate support in continuous skewed steel girder bridges and to develop a testing plan for categorization of the detail in accordance with the AASHTO LRFD existing fatigue categories. The project also evaluated the effect of welding the stiffener (connection) plate to the flange. This was accomplished through a review of the literature on the skew bridge and cross-frame connections, the selection of 26 candidate bridges in the state of Florida for analytical study, identifying the factors affecting the fatigue behavior of this connection detail, and establishing a test matrix, plan, and setup for laboratory fatigue testing that accounts for these parameters. A corrosion study plan was also developed to review the effects of material type and sizes, application of coatings, use of fillers, and venting by analysis or testing for this configuration.

There are two sets of information expected from the analytical studies planned for this project; tensile stress variation in the girder top flange over the intermediate pier for the purpose of fatigue test planning (Level I analysis) and end cross-frame member internal forces for the purpose of sizing and detailing of the HRBS connection as well as for stress concentration considerations for the connection (Level II Analysis).

Twenty-six bridges in the state of Florida were selected to represent bridges for which the HRBS connection was recognized as an appropriate detail for end cross-frames. Level I analysis through 3D finite element analysis of 26 candidate bridges indicated that the top flange fatigue stress ranges between 1.24 and 3.57 ksi with an average is 2.34 ksi. These analyses also resulted in envelop forces for the end cross-frames to be used in the subsequent detailed analyses.

For Level II analysis, the bridge population identified previously was divided into three groups based on key parameters: cross-frame member force levels, skew index, and girder moment of inertia. These parameters were segmented into thirds, with Group 1 representing the lower third, Group 2 the middle third, and Group 3 the upper third. Within each group, a representative bridge was selected; Bridge 65 for Group 1, Bridge 25 for Group 2, and Bridge 72 for Group 3, each representing the key parameters defining the respective group. Afterward, the connection assembly for each representative bridge consisting of the Half-Round Bearing Stiffener (HRBS), stiffener plate, and a portion of girder between the jacking stiffener plates was then modeled in detail using refined 3D finite element modeling for the Level II analyses. To ensure that the analysis case was representative of the most critical case for each group, the highest level of forces obtained from the Level I analysis in each group was applied for each refined model. The diameter of the HRBS was selected so that the flange extends at least 2-in. beyond the HRBS. This resulted in a diameter range of 11 to 16 in. for representative bridges based on the width of the girder flange. The thickness for the HRBS, ranging from 3/8 to 3/4 in., was found to be satisfactory depending on the size of the girder, the condition of weld for stiffener plate to the girder flanges, and clipped or non-clipped conditions for the HRBS. The sizing of the HRBS and welds was first determined using the envelope of design forces obtained from Level I analyses and combined for all possible arrangements.

To study the distortional effects, the stress and strain concentration ranges for the condition of unwelded stiffener plates (to the girder flanges) were calculated and compared to corresponding values in the welded condition to provide a measure of the effects of distortion for the representative bridge with the highest level of cross-frame member forces. The results show that welding the stiffener plate to the flanges considerably reduces the stress and strain when compared to the unwelded condition. Another observation was that the stress and strain ranges in the web of the girder in both conditions are relatively low.

Subsequently, the fatigue force ranges obtained from the Level I analyses for cross-frame members were applied to each model to identify the range and location of stress concentrations. The applied forces represent the full range from compression to tension, which is calculated by

adding the absolute values of the minimum (compression) and maximum (tension) envelope forces. The principal stress concentration ranges (SCR) in HRBS (rounded plate) varied from 14.7 to 26.9 ksi for the case of clipped HRBS and stiffener plate unwelded to the girder flange, and from 8 to 8.25 ksi for the case of clipped HRBS and stiffener plate welded to the girder flange. The stress concentration in the stiffener plate was slightly higher but very limited to a small transition point. The stress concentration range on the girder flange was minimal. Welding the stiffener plate to the girder flanges was observed to reduce the stress concentration level in general.

Based on the results of Level II analyses, it is the recommendation of this study to use welded stiffener plates wherever possible. This is because the fatigue stress ranges in the top flange estimated in this study are relatively low, minimizing the effects of inclined weld on the flange, and the welded stiffeners will perform better regarding distortion fatigue in the connection itself. In addition, welding the stiffener plates is consistent with past details that have been used on cross-frame connection plates to avoid distortional-induced fatigue. The choice between the clipped and non-clipped HRBS options will depend on the corrosion testing results as per the plan developed in Task 3 of this project.

A comprehensive corrosion testing plan was developed for the steel Half-Round Bearing Stiffeners (HRBS) that are likely to be used in bridge construction, emphasizing the evaluation of methods for assessing and improving corrosion performance. The plan focuses on key aspects such as environmental exposure, material corrosion performance, stiffener connection details, and preventative measures. The test plan includes a rigorous testing regime to assess the effectiveness of the identified methods for improving the corrosion performance. Specific tests include assessments of seal venting and drainage efficacy, corrosion development on internal and external surfaces, and the impact of different welding techniques on corrosion resistance. The materials selected for testing were also identified including various grades of carbon steel and weathering steel plates and pipes, and the rationale behind these choices.

Based on the results of analytical studies, a detailed experimental testing plan aimed at determining the most appropriate fatigue category for the Half-Round Bearing Stiffener (HRBS)

connection detail in steel girder designs was developed in the study. The test matrix was outlined in accordance with the variables involved, the prototypes used, and the scaling options. The test plan was developed to follow a statistically valid approach that minimizes the number of experiments while ensuring that the results are reliable and applicable. The study first identified the test variables, focusing particularly on the geometry and configurations of the HRBS and girder cross-sections. The test prototypes were chosen based on a representative sample of bridges. Development of the representative test specimens was organized to cover all significant variables, such as sizes and configurations. Scaling is an essential aspect of the testing program due to limitations in the experimental facilities, specifically regarding space and loading capacities. Prototypes considering two scaling options were developed: Option 1 involves a girder depth of 34 inches, while Option 2 proposes a depth of 50 inches. Detailed dimensions of the test specimens, test setup, and testing protocols were introduced for these options. The choice between these options is based on the need to balance practical dimension-scaling and weld-size considerations, ensuring the test specimens are as representative as possible of real-world conditions while fitting the limitations of the testing facility. It is recommended to start with the cases that are presumed to be the most critical with respect to performance. among all cases included in the test plan, the case of unwelded connection stiffener plate with non-clipped HRBS and the case of welded stiffener plate with non-clipped half-round stiffener and skew angle of 60 degrees are expected to generate more critical details for fatigue testing.

Chapter 6- Reference

1. Solae, C., *Field and nonlinear finite element model based investigations of skewed bridges constructed using accelerated bridge construction*. 2019, University of Georgia.

2. Wang, L., *Cross -frame and diaphragm behavior for steel bridges with skewed supports*. 2002, University of Houston: Ann Arbor. p. 295.

3. Menassa, C., et al., *Influence of skew angle on reinforced concrete slab bridges.* Journal of Bridge Engineering, 2007. **12**(2): p. 205-214.

4. Bishara, A.G., M.C. Liu, and N.D. El-Ali, *Wheel load distribution on simply supported skew I-beam composite bridges.* Journal of Structural Engineering, 1993. **119**(2): p. 399-419.

5. Rakshit, K., *Design & Construction Of Highway Bridges*. 2004: New Central Book Agency.

6. Marx, H.J., N. Khachaturian, and W.L. Gamble, *Design criteria for right and skew slab-and-girder bridges.* Transportation Research Record, 1991(1319).

7. Rajagopalan, N., *Bridge superstructure*. 2006: Alpha Science Int'l Ltd.

8. Almoosi, Y., J. McConnell, and N. Oukaili. *Structural Modeling of Cross-Frame Behavior in Steel Girder Bridges*. in *2019 12th International Conference on Developments in eSystems Engineering (DeSE)*. 2019. IEEE.

9. Grunauer, T.A.S., *Influence of bracing systems on the behavior of curved and skewed steel I-girder bridges during construction*. 2011, Georgia Institute of Technology.

10. Ozgur, C., *Influence of cross-frame detailing on curved and skewed steel I-girder bridges*. 2011: Georgia Institute of Technology.

11. White, D.W., *Guidelines for analysis methods and construction engineering of curved and skewed steel girder bridges*. Vol. 725. 2012: Transportation Research Board.

12. Norton, E.K., D.G. Linzell, and J.A. Laman, *Examination of response of a skewed steel bridge superstructure during deck placement.* Transportation research record, 2003. **1845**(1): p. 66-75.

13. Ahmadi, A., R. Henney, and D. Thompson. *Lessons Learned from the Construction of a Sharply Skewed, Two-span, Steel MultI-girder Bridge*. in *International Bridge Conference*. 2005.

14. Fasl, J., et al. *Field Measurements on Steel Girder Bridge with Skewed Supports Utilizing Lean-On Bracing*. in *Structures Congress 2009: Don't Mess with Structural Engineers: Expanding Our Role*. 2009.

15. Linzell, D.G., et al., *Guidelines for analyzing curved and skewed bridges and designing them for construction*. 2010, Pennsylvania. Dept. of Transportation. Bureau of Planning and Research.

16. Chavel, B. and C. Earls, *Construction of a horizontally curved steel I-girder bridge. Part II: Inconsistent detailing.* Journal of Bridge Engineering, 2006. **11**(1): p. 91-98.

17. Gull, J.H. and A. Azizinamini, *Simplified Method to Determine the Effect of Detailing on Cross-Frame Forces.* ENGINEERING JOURNAL-AMERICAN INSTITUTE OF STEEL CONSTRUCTION, 2019. **56**(4): p. 187-200.

18. Gull, J.H., A. Azizinamini, and T.A. Helwig, *Comparison of detailing methods for straight skewed steel I-girder bridges.* Journal of Constructional Steel Research, 2017. **136**: p. 24-34.

19. Wang, L., *Cross-frame and diaphragm behavior for steel bridges with skewed supports*. 2002: University of Houston.

20. Nguyen, C.T., J. Moon, and H.-E. Lee, *Lateral–torsional buckling of I-girders with discrete torsional bracings.* Journal of Constructional Steel Research, 2010. **66**(2): p. 170-177.

21. Schaefer, A.L., *Crossframe analysis of highly-skewed and curved steel I-girder bridges*. 2012, University of Colorado at Denver.

22. Morera, F.J., *Lateral flange bending in heavily skewed steel bridges*. 2010: North Carolina State University.

23. Almoosi, Y. and N. Oukaili, *The Response of a Highly Skewed Steel I-Girder Bridge with Different Cross-Frame Connections.* Engineering, Technology & Applied Science Research, 2021. **11**(4): p. 7349-7357.

24. Butz, T., *Cross Frame Design for Curved and Skewed Bridges Using AASHTO LRFD, 8thEdition*.

25. Herman, R.S., T.A. Helwig, and C. Zhou, *Use of Lean-On Cross-Frame Bracing in Steel Girder Bridges*, in *New Horizons and Better Practices*. 2007. p. 1-6.

26. Bishara, A.G. and W.E. Elmir, *Interaction between cross frames and girders.* Journal of Structural Engineering, 1990. **116**(5): p. 1319-1333.

27. McConnell, J., K. Ambrose, and M. Radovic. *Cross-Frame Forces in Skewed Steel I-Girder Bridges: Field Testing and Analytical Results*. in *Structures Congress 2013: Bridging Your Passion with Your Profession*. 2013.

28. Helwig, T. and J.A. Yura, *Steel bridge design handbook: Bracing system design*. 2012, United States. Federal Highway Administration. Office of Bridge Technology.

29. Radovic, M. and J. McConnell. *Evaluation of cross-frame designs for highly skewed steel i-girder bridges*. in *Proceedings of 31st Annual International Bridge Conference. IBC*. 2014.

30. McConnell, J., M. Radovic, and K. Ambrose, *Cross-Frame Forces in Skewed Steel I-Girder Bridges: Field Measurements and Finite Element Analysis.* University of Delaware Center for Bridge Engineering, Final Report to Delaware Department of Transportation, 2014.

31. Battistini, A., et al. *Effectiveness of bent plate connection for end cross-frames in skewed steel bridges*. in *Structures Congress 2009: Don't Mess with Structural Engineers: Expanding Our Role*. 2009.

32. Astaneh-Asl, A., et al., *Seismic performance of steel bridges during the 1994 Northridge earthquake*. 1994: University of California at Berkeley.

33. Bruneau, M., J.C. Wilson, and R. Tremblay, *Performance of steel bridges during the 1995 Hyogo-ken Nanbu (Kobe, Japan) earthquake.* Canadian Journal of Civil Engineering, 1996. **23**(3): p. 678-713.

34. Ballantyne, D., et al., *The Hanshin-Awaji earthquake of January 17, 1995: performance of lifelines*. 1995, National Center for Earthquake Engineering Research.

35. Carden, L., A. Itani, and I. Buckle. *An Experimental Study into the Distribution of Earthquake Forces in Steel Plate Girder Bridges*. in *Proceedings of the Pacific Conference on Earthquake Engineering, Christchurch, New Zealand. Paper*.

36. Carden, L., et al. *Buckling restrained braces for ductile end cross frames in steel plate girder bridges*. in *Proceedings of the 13th World Conference on Earthquake Engineering*. 2004.

37. Zahrai, S.M. and M. Bruneau, *Ductile end-diaphragms for seismic retrofit of slab-on-girder steel bridges.* Journal of structural engineering, 1999. **125**(1): p. 71-80.

38. Zahrai, S.M. and M. Bruneau, *Cyclic testing of ductile end diaphragms for slab-on-girder steel bridges.* Journal of structural engineering, 1999. **125**(9): p. 987-996.

39. TRANSPORTATION, F.D.O., *STRUCTURES DESIGN GUIDELINES*, in *STRUCTURES MANUAL, VOLUME 1*. 2023.

40. Kloiber, L.A., *Orthogonal and Skewed Shear Connections - Design and Detailing Requirements.* 2004.

41. AASHTO, *AASHTO LRFD bridge design specifications*. 2012: Sixth edition. Washington, D.C. : American Association of State Highway and Transportation Officials, c2012-.

42. AASHTO, *AASHTO LRFD bridge design specifications*. 2010: Fifth edition. Washington, D.C. : American Association of State Highway and Transportation Officials, c2010-.

43. Collaboration, A.N.S.B., *Guidelines for Design Constructability*. 2003.

44. Quadrato, C., et al., *Cross-frame connection details for skewed steel bridges*. 2010, University of Texas at Austin. Center for Transportation Research.

45. Quadrato, C.E., *Stability of skewed I-shaped girder bridges using bent plate connections*. 2010.

46. Winter, G., *Lateral bracing of columns and beams.* Transactions of the American Society of Civil Engineers, 1960. **125**(1): p. 807-826.

47. Yura, J.A., *Fundamentals of beam bracing.* Engineering journal-American institute of steel construction, 2001. **38**(1): p. 11-26.

48. Wang, L. and T.A. Helwig, *Stability bracing requirements for steel bridge girders with skewed supports.* Journal of Bridge Engineering, 2008. **13**(2): p. 149-157.

49. Battistini, A.D., et al., *Stiffness behavior of cross frames in steel bridge systems.* Journal of Bridge Engineering, 2016. **21**(6): p. 04016024.

50. Quadrato, C., et al., *Increasing Girder Elastic Buckling Strength Using Split Pipe Bearing Stiffeners.* Journal of Bridge Engineering, 2014. **19**(4): p. 04013017.

51. Transportation, T.D.o., *Bridge Design Manual - LRFD*, G. Bettis, Editor. 2007, Texas Departmant of Transportation.

52. Transportation, T.D.o., *Miscellaneous Details Steel Girders and Beams*. 2006.

53. Ojalvo, M. and R.S. Chambers, *Effect of warping restraints on I-beam buckling.* Journal of the Structural Division, 1977. **103**(12): p. 2351-2360.

54. Roy, S., J.W. Fisher, and B.T. Yen, *Fatigue resistance of welded details enhanced by ultrasonic impact treatment (UIT).* International Journal of Fatigue, 2003. **25**(9-11): p. 1239-1247.

55. Yu, D., C. Bennett, and A. Matamoros. *Retrofitting distortion-induced fatigue in skewed girders to cross-frame connections*. in *Structures Congress 2017*. 2017.

56. Hassel, H., et al., *Parametric analysis of cross-frame layout on distortion-induced fatigue in skewed steel bridges.* J. Bridge Eng, 2013. **10**(1061): p. 601-611.

57. Roddis, W.K., P. Kulseth, and Z. Liu, *Torsional Analysis for Exterior Girders Version 2.0*. 2002.

58. FDOT, *Standard specifications for road and bridge construction*. 2023-2024 ed. ed. 2023.

59. Gull, J.H. and A. Azizinamini, *Steel plate girder diaphragm and cross bracing loads*. 2014, Florida. Dept. of Transportation.

60. Grubb, M.A., et al., *Load and Resistance Factor Design (LRFD) For Highway Bridge April 2007 Superstructures-Design Manual*. 2007, United States. Department of Transportation. Federal Highway Administration.

61. Institute, N.H., *Analysis and design of skewed and curved steel bridges with LRFD : reference manual*. 2011, U.S. Dept. of Transportation, Federal Highway Administration, National Highway Institute.

62. Richardson, G., *Analysis and Design of Horizontally Curved Steel Bridge Girders, United States Steel Structural Report*. 1963, ADUSS 88-6003-01.

63. Mertz, D.R., *Simplified live load distribution factor equations*. Vol. 592. 2007: Transportation Research Board.

64. Ahmed, M.Z. and F.E. Weisgerber, *Torsion constant for matrix analysis of structures including warping effect.* International journal of solids and structures, 1996. **33**(3): p. 361-374.

65. Reichenbach, M., et al., *Proposed Modification to AASHTO Cross-Frame Analysis and Design*. 2021.

66. Chang, C.-J. and D.W. White, *An assessment of modeling strategies for composite curved steel I-girder bridges.* Engineering Structures, 2008. **30**(11): p. 2991-3002.

67. Chang, C.-J., *Construction simulation of curved steel I-girder bridges*. 2006: Georgia Institute of Technology.

68. Collaboration, A.N.S.B., *G13. 1 Guidelines for Steel Girder Bridge Analysis*. 2011, Washington, DC.

69. Wang, W., *A study of stiffness of steel bridge cross frames.* 2013.

70. Gurney, T.R., *Cumulative damage of welded joints*. 2006: Woodhead Publishing.

71. Fisher, J.W., et al., *Effect of weldments on the fatigue strength of steel beams*. 1970: TRB.

72. Fisher, J.W., et al., *Fatigue strength of steel beams with welded stiffeners and attachments.* NCHRP report, 1974(147).

73. AASHTO, *AASHTO LRFD bridge design specifications*. 2020: 9th edition. Washington, D.C. : American Association of State Highway and Transportation Officials, 2020.

74. Connor, R.J. and C. Korkmaz, *Fatigue Categorization of Obliquely Oriented Welded Attachments.* 2020.

75. Little, R.E., *Manual on statistical planning and analysis for fatigue experiments*. Vol. 588. 1975: ASTM International.

76. Little, R.E. and E.H. Jebe, *Statistical design of fatigue experiments*. 1975: Applied Science Publishers.

77. Hald, A., *Statistical theory, with engineering applications.* 1952.

78. BROWKER, A.H. and G.J. Lieberman, *Engineering statistics.* 1972.

79. Standardization, P., *Test of metal fatigue - Basic terms and general guidelines for preparing of samples and carry out tests*. 1976

80. ISO-12107, *Metallic materials - fatigue testing – statistical planning and analysis of data*. 2003.

81. Testing, A.S.f. and Materials. *ASTM E739-10 Standard Practice for Statistical Analysis of Linear Or Linearized Stress-Life (SN) and Strain-Life ([epsilon]-N) Fatigue Data*. 2010. ASTM.

82. Kuroda, M., et al., *Historical Review on Origin and Application to Metal Fatigue of Probit and Staircase Methods and Their Future Prospects.* 材料, 2021. **70**(3): p. 221-228.

83. Strzelecki, P. and J. Sempruch, *Experimental method for plotting SN curve with a small number of specimens.* Polish Maritime Research, 2016(4): p. 129--137.

84. Kuroda, M., et al., *Historical review on origin and application to metal fatigue of probit and staircase methods and their future prospects.* 材料, 2020. **69**(3): p. 190-196.

85. Anami, K., R. Sause, and H.H. Abbas, *Fatigue of web-flange weld of corrugated web girders: 1. Influence of web corrugation geometry and flange geometry on web-flange weld toe stresses.* International Journal of Fatigue, 2005. **27**(4): p. 373-381.

86. Anami, K. and R. Sause, *Fatigue of web-flange weld of corrugated web girders: 2. Analytical evaluation of fatigue strength of corrugated web-flange weld.* International Journal of Fatigue, 2005. **27**(4): p. 383-393.

87. Roberts, R., *Determination of tolerable flaw sizes in full size welded bridge details.* 1977.

88. Fisher, J.W., *Detection and repair of fatigue damage in welded highway bridges.* NCHRP Report, 1979(206).

89. Takamori, H. and J.W. Fisher, *Tests of large girders treated to enhance fatigue strength.* Transportation research record, 2000. **1696**(1): p. 93-99.

90. Mehrabi, A., et al., *Redundancy of Twin Steel Box Girder Bridges.* 2021.

91. Khedmatgozar Dolati, S.S., et al., *Non-Destructive Testing Applications for Steel Bridges.* Applied Sciences, 2021. **11**(20): p. 9757.

92. Dolati, S.S.K., et al. *NDT methods for damage detection in steel bridges*. in *Health Monitoring of Structural and Biological Systems XVI*. 2022. SPIE.

93. Kosnik, D.E. and D.R. Marron, *Acoustic emission evaluation of retrofits on the I-80 Bryte Bend Bridge, Sacramento, California.* Proceedings, AEWG-50/ICAE-6. Acoustic Emission Working Group, Colorado, USA, and Acoustic Emission Group, Encino, California, USA, 2007.

94. Staszewski, W., B. Lee, and R. Traynor, *Fatigue crack detection in metallic structures with Lamb waves and 3D laser vibrometry.* Measurement science and technology, 2007. **18**(3): p. 727.

95. Zhang, Y., *In situ fatigue crack detection using piezoelectric paint sensor.* Journal of Intelligent Material Systems and Structures, 2006. **17**(10): p. 843-852.

96. Hopwood II, T., et al., *Nondestructive Evaluation of Steel Bridges: Methods and Applications.* 2016.

97. Tabatabai, H., *Inspection and maintenance of bridge stay cable systems: A synthesis of highway practice*. Vol. 353. 2005: Transportation Research Board.

98. Mehrabi, A.B., *In-service evaluation of cable-stayed bridges, overview of available methods and findings.* Journal of Bridge Engineering, 2006. **11**(6): p. 716-724.

99. Mehrabi, A.B., *Performance of cable-stayed bridges: evaluation methods, observations, and a rehabilitation case.* Journal of Performance of Constructed Facilities, 2016. **30**(1): p. C4014007.

100. Mehrabi, A.B. and H. Tabatabai, *Unified finite difference formulation for free vibration of cables.* Journal of Structural Engineering, 1998. **124**(11): p. 1313-1322.

101. Stephen, G., J. Brownjohn, and C. Taylor, *Measurements of static and dynamic displacement from visual monitoring of the Humber Bridge.* Engineering Structures, 1993. **15**(3): p. 197-208.

102. Zhuang, Y., et al., *A Review of Computer Vision-Based Structural Deformation Monitoring in Field Environments.* Sensors, 2022. **22**(10): p. 3789.

103. Xu, Y., J. Brownjohn, and D. Kong, *A non-contact vision-based system for multipoint displacement monitoring in a cable-stayed footbridge.* Structural Control and Health Monitoring, 2018. **25**(5): p. e2155.

104. Ye, X.-W., C.-Z. Dong, and T. Liu, *A review of machine vision-based structural health monitoring: methodologies and applications.* Journal of Sensors, 2016. **2016**.

105. Feng, D. and M.Q. Feng, *Vision-based multipoint displacement measurement for structural health monitoring.* Structural Control and Health Monitoring, 2016. **23**(5): p. 876-890.

106. Ihn, J.-B. and F.-K. Chang. *Multicrack growth monitoring at riveted lap joints using piezoelectric patches*. in *Smart Nondestructive Evaluation for Health Monitoring of Structural and Biological Systems*. 2002. SPIE.

107. Zhang, Y. *Piezoelectric paint sensor for real-time structural health monitoring*. in *Smart Structures and Materials 2005: Sensors and Smart Structures Technologies for Civil, Mechanical, and Aerospace Systems*. 2005. SPIE.

108. Wang, C.S., F. Wu, and F.-K. Chang, *Structural health monitoring from fiber-reinforced composites to steel-reinforced concrete.* Smart materials and Structures, 2001. **10**(3): p. 548.

109. Huang, H., et al., *Fatigue Performance Test and Numerical Analysis of Composite Girders with CSW-CFST Truss Chords.* Applied Sciences, 2022. **12**(11): p. 5459.

110. Al-Karawi, H., R.U.F. von Bock und Polach, and M. Al-Emrani, *Crack detection via strain measurements in fatigue testing.* Strain, 2021. **57**(4): p. e12384.

111. Wang, Y., et al., *Insight into atmospheric corrosion evolution of mild steel in a simulated coastal atmosphere.* Journal of Materials Science & Technology, 2021. **76**: p. 41-50.

112. Melchers, R., *Transition from marine immersion to coastal atmospheric corrosion for structural steels.* Corrosion, 2007. **63**(6): p. 500-514.

113. Odnevall Wallinder, I. and C. Leygraf, *A critical review on corrosion and runoff from zinc and zinc-based alloys in atmospheric environments.* Corrosion, 2017. **73**(9): p. 1060-1077.

114. Schindelholz, E., B. Risteen, and R. Kelly, *Effect of relative humidity on corrosion of steel under sea salt aerosol proxies: I. NaCl.* Journal of The Electrochemical Society, 2014. **161**(10): p. C450.

115. Schindelholz, E., B. Risteen, and R. Kelly, *Effect of relative humidity on corrosion of steel under sea salt aerosol proxies: II. MgCl2, artificial seawater.* Journal of the Electrochemical Society, 2014. **161**(10): p. C460.

116. Ambler, H. and A. Bain, *Corrosion of metals in the tropics.* Journal of Applied Chemistry, 1955. **5**(9): p. 437-467.

117. Alcántara, J., et al., *Airborne chloride deposit and its effect on marine atmospheric corrosion of mild steel.* Corrosion Science, 2015. **97**: p. 74-88.

118. Alcántara, J., et al., *Marine atmospheric corrosion of carbon steel: A review.* Materials, 2017. **10**(4): p. 406.

119. Revie, R.W., *Uhlig's corrosion handbook*. Vol. 51. 2011: John Wiley & Sons.

120. Davis, J.R., *Corrosion of weldments*. 2006: ASM international.

121. Jiang, C., et al., *Fatigue assessment of fillet weld in steel bridge towers considering corrosion effects.* Engineering Failure Analysis, 2022: p. 106901.

122. Nyrkova, L., *Stress-corrosion cracking of pipe steel under complex influence of factors.* Engineering Failure Analysis, 2020. **116**: p. 104757.

123. Gkatzogiannis, S., et al., *Correlation of laboratory and real marine corrosion for the investigation of corrosion fatigue behaviour of steel components.* International Journal of Fatigue, 2019. **126**: p. 90-102.

124. Kogler, R., *Steel bridge design handbook: Corrosion protection of steel bridges*. 2015, United States. Federal Highway Administration. Office of Bridges and Structures.

125. Figueira, R., et al., *Corrosion of hot-dip galvanized steel reinforcement.* Corros. E Prot. Mater, 2014. **33**(3): p. 51-61.

126. Middle East, F., *Quantitative Evaluation of Volatile Corrosion Inhibitors.* 2022.

127. Abedin, M., et al., *Reliability evaluation of twin steel box girder bridges using a simplified method.* Engineering Structures, 2022. **259**: p. 114122.

128. MIDAS, *MIDAS Civil (Software)*. 2024, MIDAS IT.

129. MIDAS, *MIDAS FEA NX (Software)*. 2024, MIDAS IT.

130. SA, N.I.T., *mBrace3D*. 2023.

131. COLETTI, D.A., D.W. WHITE, and T.V. NGUYEN, *FIT-UP CONSIDERATIONS FOR STEEL I-GIRDER BRIDGES.*

132. 962), N.N.C.H.R.P.R., *Proposed Modification to AASHTO Cross-Frame Analysis and Design. .* 2021.

133. Transportation, F.D.o., *Structures Design Guidelines (SDG)*. 2023, Florida Department of Transportation.

134. Segui, W.T., *Steel Design (International Student Edition).* Penerbit Thomson, USA, 2007.

135. Code–Steel, S.W., *AWS D1. 1/D1. 1M.* American Welding Society 2020, 2020.

136. Keating, P.B. and J.W. Fisher, *Review of fatigue tests and design criteria on welded details, Final Report, July 1986, 180p.(NCHRP Report 286) Publication 86-21.* Fritz Engineering Laboratory Report Paper 524 (July): 188. http://digital. lib, 1986.

APPENDIX A - Information used as Input for Level I Analysis for All Bridges

A-1 Overall Geometric Information

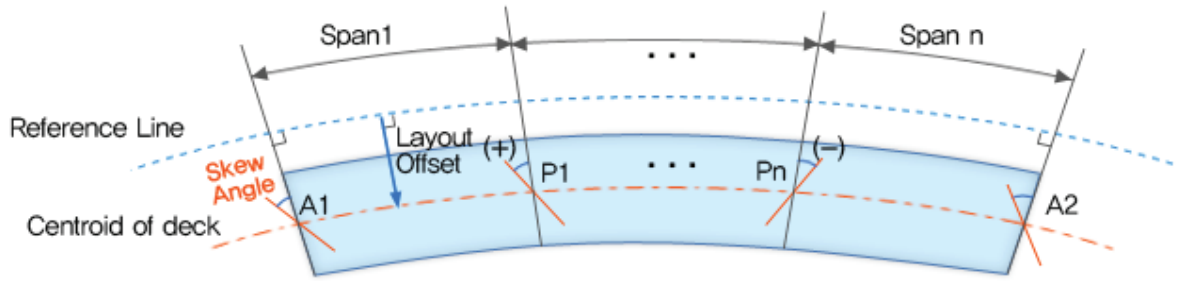

#	Alternative Bridge #	Unit	Curvature Category	Span Length (ft)												
				1	2	3	4	5	6	7	8	9	10	11	12	SUM
1	64	-	Semi-Curved	188.5	138.9	-	-	-	-	-	-	-	-	-	-	327.5
2	9	-	Streight	203.3	159.4	-	-	-	-	-	-	-	-	-	-	362.7
3	65	-	Streight	121.8	135.7	-	-	-	-	-	-	-	-	-	-	257.5
4	66	-	Streight	217.2	234.2	-	-	-	-	-	-	-	-	-	-	451.4
5	67	-	Curved	210.4	234.4	-	-	-	-	-	-	-	-	-	-	444.7
6	68	1	Curved	185.6	166.0	155.2	166.6	207.5	168.3	169.9	169.9	169.9	-	-	-	506.8
7	69	-	Curved	218.1	249.9	-	-	-	-	-	-	-	-	-	-	468.0
8	71	3	Curved	164.3	178.5	155.2	155.2	178.5	150.5	185.5	153.1	147.7	144.7	165.6	115.0	486.4
9	72	-	Curved	160.2	241.2	236.7	177.5	-	-	-	-	-	-	-	-	815.6
10	70	-	Curved	195.4	211.0	-	-	-	-	-	-	-	-	-	-	406.4
11	13	-	Streight	171.5	252.7	252.7	202.1	-	-	-	-	-	-	-	-	879.0
12	15	-	Semi-Curved	191.8	158.8	160.9	230.8	-	-	-	-	-	-	-	-	742.4
13	44	-	Streight	154.7	143.7	-	-	-	-	-	-	-	-	-	-	298.4
14	43	-	Streight	169.4	169.4	-	-	-	-	-	-	-	-	-	-	338.9
15	41	-	Semi-Curved	260.9	253.7	-	-	-	-	-	-	-	-	-	-	514.7
16	60	-	Streight	177.3	177.3	-	-	-	-	-	-	-	-	-	-	354.5
17	45	-	Streight	252.0	252.0	-	-	-	-	-	-	-	-	-	-	504.0
18	42	-	Streight	251.0	251.0	-	-	-	-	-	-	-	-	-	-	502.0
19	8	-	Streight	147.8	172.4	-	-	-	-	-	-	-	-	-	-	320.2
20	46	-	Streight	227.5	207.5	-	-	-	-	-	-	-	-	-	-	435.0
21	61	-	Streight	207.4	208.0	-	-	-	-	-	-	-	-	-	-	415.5
22	24	-	Streight	169.8	169.8	-	-	-	-	-	-	-	-	-	-	339.6
23	25	-	Streight	198.3	198.3	-	-	-	-	-	-	-	-	-	-	396.5
24	62[4]	-	Semi-Curved	179.4	172.4	-	-	-	-	-	-	-	-	-	-	351.8
25	63	2	Streight	99.9	167.1	185.1	-	-	-	-	-	-	-	-	-	352.2
26	12	-	Streight	197.0	188.9	178.2	-	-	-	-	-	-	-	-	-	564.2

#	Alternative Bridge #	Skew Angle at Pier												
		Pier 1	Pier 2	Pier 3	Pier 4	Pier 5	Pier 6	Pier 7	Pier 8	Pier 9	Pier 10	Pier 11	Pier 12	Pier 13
1	**64**	52.80	56.12	57.23	-	-	-	-	-	-	-	-	-	-
2	**9**	56.18	56.18	56.18	-	-	-	-	-	-	-	-	-	-
3	**65**	23.00	23.00	23.00	-	-	-	-	-	-	-	-	-	-
4	**66**	39.75	39.75	39.75	-	-	-	-	-	-	-	-	-	-
5	**67**	36.05	39.20	42.72	-	-	-	-	-	-	-	-	-	-
6	**68**	40.77	27.00	0.00	0.00	-	-	-	-	-	-	-	-	-
7	**69**	40.63	45.00	45.00	-	-	-	-	-	-	-	-	-	-
8	**71**	-	-	-	-	-	-	41.05	50.90	34.70	0.00	-	-	-
9	**72**	0.00	57.00	50.52	39.73	0.00	-	-	-	-	-	-	-	-
10	**70**	44.08	48.67	46.75	-	-	-	-	-	-	-	-	-	-
11	**13**	0.00	50.08	50.08	50.08	0.00	-	-	-	-	-	-	-	-
12	**15**	53.00	36.00	8.00	45.00	45.00	-	-	-	-	-	-	-	-
13	**44**	40.47	40.47	40.47	-	-	-	-	-	-	-	-	-	-
14	**43**	55.02	55.02	55.02	-	-	-	-	-	-	-	-	-	-
15	**41**	52.15	53.30	54.67	-	-	-	-	-	-	-	-	-	-
16	**60**	25.63	25.63	25.63	-	-	-	-	-	-	-	-	-	-
17	**45**	50.37	50.37	50.37	-	-	-	-	-	-	-	-	-	-
18	**42**	50.18	50.18	50.18	-	-	-	-	-	-	-	-	-	-
19	**8**	23.42	23.42	23.42	-	-	-	-	-	-	-	-	-	-
20	**46**	43.82	43.82	43.82	-	-	-	-	-	-	-	-	-	-
21	**61**	36.67	35.97	35.27	-	-	-	-	-	-	-	-	-	-
22	**24**	52.65	52.65	52.65	-	-	-	-	-	-	-	-	-	-
23	**25**	54.45	54.45	54.45	-	-	-	-	-	-	-	-	-	-
24	**62**[4]	25.00	0.00	25.00	-	-	-	-	-	-	-	-	-	-
25	**63**	-	35.50	35.50	35.58	-	-	-	-	-	-	-	-	-
26	**12**	44.23	44.65	58.72	58.72		-	-	-	-	-	-	-	-

#	Alternative Bridge #	Curvature			Girder Spacing (in.)	No. of Lanes	No. of Girders	Deck Width (ft)	Deck Thickness (in.)	Average Haunch (in.)	w_g (ft)
		θ	R (ft)	L/R							
1	**64**	1° 44' 46"	3281.4	0.06	123.00	3	6	58.21	8.5	5.1	51.25
2	**9**	-	-	0.00	114.00	3	6	54.27	8.50	4.97	47.50
3	**65**	-	-	0.00	120.00	2	4	37.08	8.50	4.20	30.00
4	**66**	-	-	0.00	144.00	3	5	56.08	8.50	3.98	48.00
5	**67**	1° 30' 0"	3819.7	0.06	144.00	4	6	67.08	9.00	3.43	60.00
6	**68**	4° 45' 0"	738.2	0.28	149.60	2	4	48.39	9.45	3.82	37.40
7	**69**	1° 59'59"	2865.0	0.09	132.00	1	3	30.08	8.50	4.76	22.00
8	**71**	5°	1145.9	0.16	111.00	2	5	43.08	8.00	3.20	37.00
9	**72**	8° 14' 38"	695.0	0.34	144.00	1	4	44.00	9.50	4.86	36.00
10	**70**	7° 04' 25"	810.0	0.26	116.00	1	4	37.29	8.50	6.24	29.00
11	**13**	-	-	0.00	144.00	2	4	43.08	9.50	2.02	36.00
12	**15**	15° 34' 32"	5725.1	0.04	147.63	3	5	60.20	7.87	4.36	49.21
13	**44**	-	-	0.00	117.00	2	5	47.08	8.00	4.85	39.00
14	**43**	-	-	0.00	150.00	2	4	47.08	9.00	2.77	37.50
15	**41**	0° 29' 14"	11758.0	0.02	144.00	2	4	43.08	8.50	5.95	36.00
16	**60**	-	-	0.00	161.00	2	4	50.17	9.00	4.55	40.25
17	**45**	-	-	0.00	139.99	2	6	65.00	8.50	3.90	58.33
18	**42**	-	-	0.00	153.00	2	5	59.00	9.00	3.64	51.00
19	**8**	-	-	0.00	159.96	4	8	101.08	9.00	5.66	93.31
20	**46**	-	-	0.00	126.75	4	7	71.08	8.50	3.51	63.38
21	**61**	-	-	0.00	127.01	3	6	59.08	8.50	4.34	52.92
22	**24**	-	-	0.00	96.50	2	7	55.25	8.50	3.74	48.25
23	**25**	-	-	0.00	141.00	2	4	43.08	9.00	3.45	35.25
24	**62**[4]	1° 48'	3183.1	0.06	96.00	1	4	30.08	8.50	3.98	24.00
25	**63**	-	-	0.00	108.26	3	6	54.37	8.46	3.53	45.11
26	**12**	-	-	0.00	105.00	2	5	42.46	8.50	5.92	35.00

A-2 Bearing Information

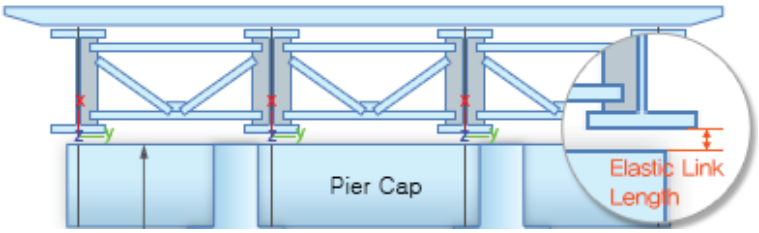

#	Alternative Bridge #	ABUTMENT BEARING STIFFNESS		PIER BEARING STIFFNESS		ELASTIC LINK LENGTH (MAX BEARING THICKNESS) (in.)
		Vertical Stiffness (K_X) (Kips/inch)	Horizontal Stiffness (K_Y)(K_Z) (Kips/inch)	Vertical Stiffness (K_X) (Kips/inch)	Horizontal Stiffness (K_Y)(K_Z) (Kips/inch)	
1	64	5067	14.9	8356	19.1	4.13
2	9	1622	9.2	3654	14.8	5.38
3	65	3117	13.7	4702	19.3	3.00
4	66	2505	7.9	13644	24.2	5.53
5	67	2505	7.9	7724	16.4	5.81
6	68	1040	5.2	7353	23.6	4.94
7	69	2873	11.3	11012	20.6	5.44
8	71	1040	5.2	7353	23.6	4.94
9	72	3361	10.9	13494	24.7	5.69
10	70	4775	16.0	25933	30.2	5.69
11	13	568	4.7	3888	13.0	5.75
12	15	2388	9.6	6966	18.0	5.51
13	44	1474	8.9	7143	19.9	3.44
14	43	7391	14.3	47471	56.9	2.69
15	41	3294	13.0	3294	13.0	3.75
16	60	1720	8.6	5486	20.5	4.16
17	45	2755	10.9	2755	10.9	3.81
18	42	2755	10.9	2755	10.9	3.81
19	8	1816	8.2	1816	8.2	3.38
20	46	2533	10.1	6098	15.6	3.84
21	61	2505	7.9	6621	13.9	6.78
22	24	5235	17.6	9265	24.3	2.56
23	25	1622	9.2	3654	14.8	5.38
24	62[4]	1720	8.6	5486	20.5	4.16
25	63	1865	9.4	7933	22.5	2.95
26	12	2505	7.9	3654	14.8	6.78

#	Alternative Bridge #	Wind Load Pressure on Girder Web (ksf) (V=180 mph)
1	**64**	0.2036
2	**9**	0.2034
3	**65**	0.2080
4	**66**	0.1846
5	**67**	0.1845
6	**68**	0.2079
7	**69**	0.1801
8	**71**	0.2016
9	**72**	0.1839
10	**70**	0.1857
11	**13**	0.1802
12	**15**	0.1776
13	**44**	0.2035
14	**43**	0.1910
15	**41**	0.1737
16	**60**	0.1964
17	**45**	0.1852
18	**42**	0.1842
19	**8**	0.2044
20	**46**	0.1890
21	**61**	0.1991
22	**24**	0.2024
23	**25**	0.1852
24	**62**[(4)]	0.2225
25	**63**	0.2241
26	**12**	0.2051

A-3 Girders Information

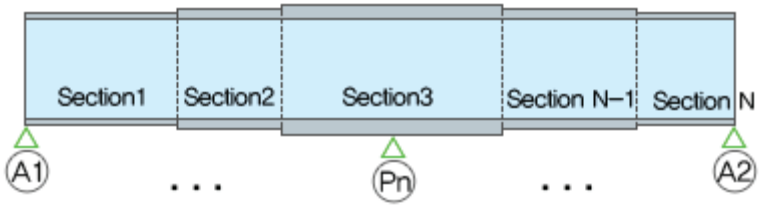

#	Alternative Bridge #	Girder 1 Length (ft)																					
		G1	G2	G3	G4	G5	G6	G7	G8	G9	G10	G11	G12	G13	G14	G15	G16	G17	G18	G19	G20	G21	G22	SUM
1	64	23.6	66.5	28.4	48.0	54.8	21.6	84.6																327.5
2	9	27.4	65.0	30.0	56.0	50.0	27.2	60.0	47.1															362.7
3	65	83.0	24.8	26.0	24.8	99.0																		257.5
4	66	148.7	32.0	25.0	25.0	25.0	25.0	170.7																451.4
5	67	142.8	30.0	25.0	25.0	25.0	22.0	174.9																444.7
6	68	122.2	35.1	19.7	16.4	18.0	29.5	55.4	31.5	18.0	16.4	19.7	35.1	89.7										506.8
7	69	39.7	77.5	40.0	18.5	16.0	54.0	16.0	25.7	39.0	94.0	47.7												468.0
8	71	25.9	117.0	16.0	10.0	26.0	20.0	64.0	14.0	34.0	20.0	111.0	28.5											486.4
9	72	124.6	25.4	40.0	47.8	112.6	33.8	50.0	42.4	118.1	28.8	40.0	38.9	113.1										815.6
10	70	123.6	51.9	42.0	44.3	144.7																		406.4
11	13	80.0	21.0	21.0	22.0	36.0	24.0	23.0	126.0	24.0	20.0	40.0	20.0	24.0	126.0	23.0	22.0	38.0	19.0	24.0	105.5	40.5		879.0
12	15	36.1	103.0	38.3	26.0	36.1	93.5	14.8	17.6	14.6	59.7	39.4	60.7	24.6	141.1	37.1								742.4
13	44	20.7	90.0	32.0	25.0	37.0	69.0	24.7																298.4
14	43	36.0	50.0	40.0	25.0	36.9	25.0	40.0	50.0	36.0														338.9
15	41	50.0	89.0	93.0	61.0	94.0	83.0	44.7																514.7
16	60	39.3	84.0	30.9	46.0	26.9	88.0	39.3																354.5
17	45	51.8	125.0	60.0	30.3	60.0	125.0	51.8																504.0
18	42	50.8	122.7	28.0	29.5	40.0	29.5	28.0	122.7	50.8														502.0
19	8	92.7	25.0	60.0	25.0	117.5																		320.2
20	46	41.0	130.0	31.8	53.0	28.0	121.2	30.0																435.0
21	61	143.5	40.0	46.0	40.0	146.0																		415.5
22	24	117.8	40.0	24.0	40.0	117.8																		339.6
23	25	32.3	112.0	24.0	15.0	30.0	15.0	24.0	112.0	32.3														396.5
24	62[4]	30.0	89.1	48.0	28.0	40.0	86.7	30.0																351.8
25	63	40.9	78.6	27.9	37.7	27.9	98.2	40.9																352.2
26	12	146.3	41.0	34.0	41.0	68.4	32.0	34.0	23.0	144.4														564.2

#	Alternative Bridge #	Girder Web Height (in.)																					
		G1	G2	G3	G4	G5	G6	G7	G8	G9	G10	G11	G12	G13	G14	G15	G16	G17	G18	G19	G20	G21	G22
1	64	71.0	71.0	71.0	71.0	71.0	71.0	71.0															
2	9	71.0	71.0	71.0	71.0	71.0	71.0	71.0	71.0														
3	65	66.0	66.0	66.0	66.0	66.0																	
4	66	91.0	91.0	91.0	91.0	91.0	91.0	91.0															
5	67	91.0	91.0	91.0	91.0	91.0	91.0	91.0															
6	68	66.9	66.9	66.9	66.9	66.9	66.9	66.9	66.9	66.9	66.9	66.9	66.9	66.9									
7	69	100.0	100.0	100.0	100.0	100.0	100.0	100.0	100.0	100.0	100.0	100.0											
8	71	69.0	69.0	69.0	69.0	69.0	69.0	69.0	69.0	69.0	69.0	69.0	69.0										
9	72	96.0	96.0	96.0	96.0	96.0	96.0	96.0	96.0	96.0	96.0	96.0	96.0	96.0									
10	70	94.0	94.0	94.0	94.0	94.0																	
11	13	96.0	96.0	96.0	96.0	96.0	96.0	96.0	96.0	96.0	96.0	96.0	96.0	96.0	96.0	96.0	96.0	96.0	96.0	96.0	96.0	96.0	
12	15	102.4	102.4	102.4	102.4	102.4	102.4	102.4	102.4	102.4	102.4	102.4	102.4	102.4	102.4	102.4							
13	44	70.0	70.0	70.0	70.0	70.0	70.0	70.0															
14	43	81.0	81.0	81.0	81.0	81.0	81.0	81.0	81.0	81.0													
15	41	116.0	116.0	116.0	116.0	116.0	116.0	116.0															
16	60	78.0	78.0	78.0	78.0	78.0	78.0	78.0															
17	45	90.0	90.0	90.0	90.0	90.0	90.0	90.0															
18	42	92.0	92.0	92.0	92.0	92.0	92.0	92.0	92.0	92.0													
19	8	72.0	72.0	72.0	72.0	72.0																	
20	46	84.0	84.0	84.0	84.0	84.0	84.0	84.0															
21	61	74.0	74.0	74.0	74.0	74.0																	
22	24	70.0	70.0	70.0	70.0	70.0																	
23	25	90.0	90.0	90.0	90.0	90.0	90.0	90.0	90.0	90.0													
24	62[4]	56.0	56.0	56.0	56.0	56.0	56.0	56.0															
25	63	54.5	54.5	54.5	54.5	54.5	54.5	54.5															
26	12	71.0	71.0	71.0	71.0	71.0	71.0	71.0	71.0	71.0													

#	Alternative Bridge #	Girder Web Thickness (in.)
		For all Cross-sections
1	64	0.625
2	9	0.625
3	65	0.563
4	66	0.625
5	67	0.625
6	68	0.630
7	69	0.688
8	71	0.500
9	72	0.750
10	70	0.750
11	13	0.688
12	15	0.709
13	44	0.500
14	43	0.563
15	41	0.875
16	60	0.563
17	45	0.625
18	42	0.625
19	8	0.625
20	46	0.625
21	61	0.625
22	24	0.563
23	25	0.625
24	62[4]	0.625
25	63	0.551
26	12	0.625

#	Alternative Bridge #	Girder Top Flange width (in.)																					
		G1	G2	G3	G4	G5	G6	G7	G8	G9	G10	G11	G12	G13	G14	G15	G16	G17	G18	G19	G20	G21	G22
1	64	20.0	20.0	20.0	26.0	26.0	26.0	20.0															
2	9	20.0	20.0	20.0	26.0	26.0	26.0	20.0	20.0														
3	65	16.0	16.0	16.0	16.0	16.0																	
4	66	20.0	32.0	32.0	32.0	32.0	32.0	20.0															
5	67	18.0	26.0	26.0	26.0	26.0	26.0	18.0															
6	68	17.7	25.6	25.6	25.6	25.6	25.6	17.7	25.6	25.6	25.6	25.6	25.6	17.7									
7	69	20.0	20.0	20.0	28.0	28.0	28.0	28.0	28.0	20.0	20.0	20.0											
8	71	14.0	14.0	18.0	18.0	18.0	18.0	18.0	16.0	16.0	16.0	14.0	14.0										
9	72	24.0	24.0	24.0	24.0	24.0	24.0	24.0	24.0	24.0	24.0	24.0	24.0	24.0									
10	70	20.0	20.0	20.0	20.0	20.0																	
11	13	14.0	14.0	26.0	26.0	26.0	26.0	26.0	14.0	28.0	28.0	28.0	28.0	28.0	14.0	26.0	26.0	26.0	26.0	26.0	14.0	14.0	
12	15	11.8	11.8	27.6	27.6	27.6	11.8	21.7	21.7	21.7	11.8	27.6	27.6	27.6	19.7	19.7							
13	44	12.0	12.0	16.0	16.0	16.0	12.0	12.0															
14	43	16.0	16.0	16.0	22.0	22.0	22.0	16.0	16.0	16.0													
15	41	22.0	22.0	26.0	26.0	26.0	22.0	22.0															
16	60	18.0	18.0	24.0	24.0	24.0	18.0	18.0															
17	45	24.0	24.0	30.0	30.0	30.0	24.0	24.0															
18	42	24.0	24.0	30.0	30.0	30.0	30.0	30.0	24.0	24.0													
19	8	16.0	22.0	22.0	22.0	16.0																	
20	46	26.0	26.0	28.0	28.0	28.0	22.0	18.0															
21	61	20.0	26.0	26.0	26.0	20.0																	
22	24	22.0	26.0	26.0	26.0	22.0																	
23	25	16.0	16.0	22.0	22.0	22.0	22.0	22.0	16.0	16.0													
24	62[4]	18.0	18.0	30.0	30.0	30.0	18.0	18.0															
25	63	17.7	17.7	29.5	29.5	29.5	17.7	17.7															
26	12	24.0	24.0	24.0	24.0	24.0	24.0	24.0	24.0	24.0													

#	Alternative Bridge #	Girder Top Flange Thickness (in.)																					
		G1	G2	G3	G4	G5	G6	G7	G8	G9	G10	G11	G12	G13	G14	G15	G16	G17	G18	G19	G20	G21	G22
1	64	1.00	1.25	1.00	1.25	2.25	1.25	1.00															
2	9	1.25	1.50	1.50	1.50	2.50	1.50	1.00	1.00														
3	65	1.00	1.25	2.00	1.25	1.00																	
4	66	1.00	1.25	1.88	3.00	1.88	1.25	1.25															
5	67	1.00	1.38	2.25	3.00	2.25	1.38	1.25															
6	68	1.57	1.57	1.97	2.76	1.97	1.57	1.38	1.57	1.97	2.76	1.97	1.57	1.57									
7	69	1.00	1.00	1.00	1.38	1.88	3.25	1.88	1.38	1.00	1.50	1.00											
8	71	1.00	1.63	1.00	1.50	2.38	1.50	1.00	1.50	2.63	1.50	1.00	1.00										
9	72	1.25	2.00	2.50	2.00	1.25	2.00	3.00	2.00	1.25	2.00	2.50	2.00	1.25									
10	70	0.88	1.00	2.00	1.00	0.88																	
11	13	0.75	0.75	0.75	1.50	2.50	1.50	0.75	1.00	0.75	1.50	2.75	1.50	0.75	1.00	0.75	1.50	2.75	1.50	0.75	1.13	1.00	
12	15	0.79	1.50	0.79	1.97	0.79	0.79	0.79	1.26	0.79	0.79	0.79	2.36	0.79	1.26	1.26							
13	44	0.75	1.00	1.50	2.50	1.50	0.75	0.75															
14	43	0.75	0.75	0.75	1.63	2.88	1.63	0.75	0.75	0.75													
15	41	1.00	1.25	2.00	3.63	2.00	1.25	1.00															
16	60	1.00	1.00	1.50	3.00	1.50	1.00	1.00															
17	45	1.25	1.25	2.50	3.25	2.50	1.25	1.25															
18	42	1.25	1.50	2.50	2.50	3.50	2.50	2.50	1.50	1.25													
19	8	1.25	1.25	2.50	1.25	1.25																	
20	46	1.25	1.25	1.63	3.00	1.63	1.00	1.00															
21	61	1.00	1.88	3.25	1.88	1.00																	
22	24	1.00	1.25	1.25	1.25	1.00																	
23	25	0.88	0.88	1.25	1.75	2.63	1.75	1.25	0.88	0.88													
24	62[4]	0.75	1.50	2.00	3.00	2.00	1.50	0.75															
25	63	0.79	0.79	1.50	2.36	1.50	0.98	0.98															
26	12	1.00	1.50	2.00	1.50	1.00	1.50	1.75	1.50	1.00													

#	Alternative Bridge #	Girder Bottom FlangeWidth (in.)																					
		G1	G2	G3	G4	G5	G6	G7	G8	G9	G10	G11	G12	G13	G14	G15	G16	G17	G18	G19	G20	G21	G22
1	64	20.0	22.0	22.0	26.0	26.0	26.0	22.0															
2	9	22.0	22.0	22.0	26.0	26.0	26.0	22.0	22.0														
3	65	16.0	16.0	16.0	16.0	16.0																	
4	66	24.0	32.0	32.0	32.0	32.0	32.0	24.0															
5	67	24.0	26.0	26.0	26.0	26.0	26.0	24.0															
6	68	19.7	27.6	27.6	27.6	27.6	27.6	19.7	27.6	27.6	27.6	27.6	27.6	15.7									
7	69	22.0	22.0	22.0	30.0	30.0	30.0	30.0	30.0	28.0	28.0	28.0											
8	71	18.0	18.0	20.0	20.0	20.0	20.0	20.0	18.0	18.0	18.0	18.0	18.0										
9	72	28.0	28.0	28.0	28.0	28.0	28.0	28.0	28.0	28.0	28.0	28.0	28.0	28.0									
10	70	20.0	24.0	24.0	24.0	20.0																	
11	13	16.0	16.0	28.0	28.0	28.0	28.0	28.0	16.0	28.0	28.0	28.0	28.0	28.0	16.0	28.0	28.0	28.0	28.0	28.0	16.0	16.0	
12	15	19.7	19.7	27.6	27.6	27.6	11.8	21.7	21.7	21.7	11.8	27.6	27.6	27.6	19.7	19.7							
13	44	16.0	16.0	16.0	16.0	16.0	16.0	16.0															
14	43	22.0	22.0	22.0	22.0	22.0	22.0	22.0	22.0	22.0													
15	41	22.0	22.0	26.0	26.0	26.0	22.0	22.0															
16	60	18.0	18.0	24.0	24.0	24.0	18.0	18.0															
17	45	24.0	24.0	30.0	30.0	30.0	24.0	24.0															
18	42	24.0	24.0	30.0	30.0	32.0	30.0	30.0	24.0	24.0													
19	8	16.0	22.0	22.0	22.0	16.0																	
20	46	20.0	26.0	30.0	30.0	30.0	22.0	18.0															
21	61	26.0	32.0	32.0	32.0	26.0																	
22	24	22.0	26.0	26.0	26.0	22.0																	
23	25	18.0	18.0	22.0	22.0	22.0	22.0	22.0	18.0	18.0													
24	62[4]	18.0	18.0	30.0	30.0	30.0	18.0	18.0															
25	63	17.7	17.7	29.5	29.5	29.5	17.7	17.7															
26	12	24.0	24.0	24.0	24.0	24.0	24.0	24.0	24.0	24.0													

#	Alternative Bridge #	Girder Bottom Flange Thickness (in.)																					
		G1	G2	G3	G4	G5	G6	G7	G8	G9	G10	G11	G12	G13	G14	G15	G16	G17	G18	G19	G20	G21	G22
1	64	1.25	2.00	2.00	1.25	2.25	1.25	1.00															
2	9	1.25	2.00	1.75	1.50	2.50	1.50	1.25	1.00														
3	65	1.00	1.25	2.00	1.25	1.00																	
4	66	1.25	1.38	1.88	3.00	1.88	1.38	1.38															
5	67	1.25	2.25	2.25	3.00	2.25	2.25	1.88															
6	68	1.57	1.57	1.97	2.76	1.97	1.57	1.38	1.57	1.97	2.76	1.97	1.57	1.57									
7	69	1.00	1.88	1.38	1.38	1.88	3.25	1.88	1.38	1.38	1.88	1.88											
8	71	1.25	2.50	1.13	1.75	2.50	1.75	1.13	1.50	2.88	1.50	2.00	1.25										
9	72	1.25	2.00	2.50	2.00	1.25	2.00	3.00	2.00	1.25	2.00	2.50	2.00	1.25									
10	70	0.88	1.25	2.00	1.25	0.88																	
11	13	0.75	1.38	1.50	1.50	2.75	1.50	1.50	1.75	1.50	1.75	3.25	1.75	1.50	1.50	1.50	1.75	3.25	1.75	1.50	2.00	1.00	
12	15	0.79	1.26	1.50	1.97	1.50	0.79	1.26	1.26	1.26	0.79	1.50	2.36	1.50	2.36	1.26							
13	44	0.75	1.38	1.75	2.75	1.75	1.00	0.75															
14	43	0.81	1.13	0.94	1.63	2.88	1.63	0.94	1.13	0.81													
15	41	1.25	1.88	2.00	3.75	2.00	1.88	1.25															
16	60	1.50	2.00	1.50	3.00	1.50	2.00	1.50															
17	45	1.38	1.75	2.50	3.25	2.50	1.75	1.38															
18	42	1.25	1.75	2.00	2.50	3.50	2.50	2.00	1.75	1.25													
19	8	1.50	1.25	2.50	1.25	1.50																	
20	46	1.63	1.63	1.63	3.00	1.63	1.25	1.00															
21	61	1.75	2.25	3.25	2.25	1.75																	
22	24	1.13	1.25	2.00	1.25	1.13																	
23	25	0.88	1.25	1.25	1.75	2.63	1.75	1.25	1.25	0.88													
24	62[4]	1.25	2.00	2.00	3.00	2.00	2.00	1.00															
25	63	1.26	1.77	1.50	2.36	1.50	2.36	1.77															
26	12	1.50	1.75	2.00	1.75	1.00	1.75	1.75	1.75	1.50													

A-4 Cross-Frame Information

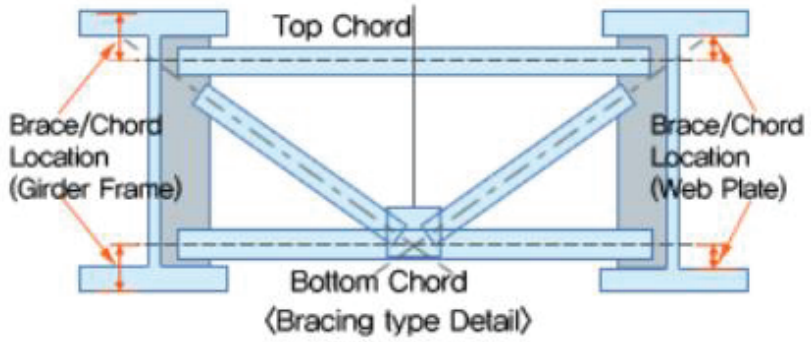

〈Bracing type Detail〉

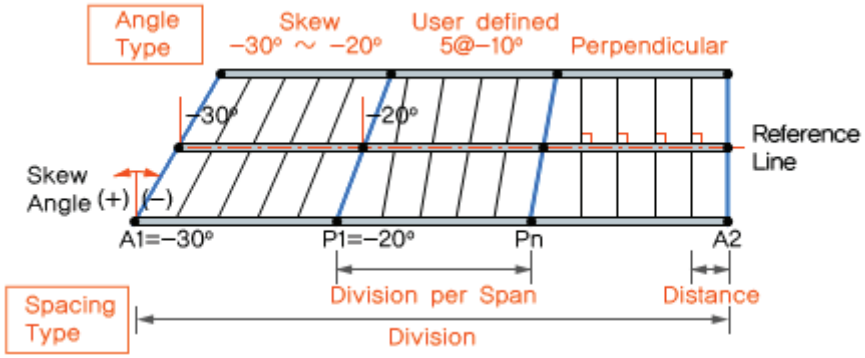

#	Alternative Bridge #	END CROSS FRAME SECTION (SKEWED)						
		TYPE	TOP CHORD	CONDITION	DIAGONAL	BOT CHORD	TOP CHORD GAP (in.)	BOT CHORD GAP (in.)
1	64	Inverted-V	C15X40	COMPOSITE	L6X6X5/8	L6X6X5/8	11	9
2	9	Inverted-V	MC18X42.7	COMPOSITE	L8X8X3/4	L8X8X3/4	12	12
3	65	Diaphragm	TOP/BOT FLNG:		PL3/4X9	WEB:	PL9/16X42	
4	66	V	C12X25	COMPOSITE	L3(1/2)X3(1/2)X3/8	L3(1/2)X3(1/2)X3/8	9	5
5	67	V	C12X25	COMPOSITE	L6X6X5/8	L6X6X5/8	9	8.5
6	68	V	C380X50 (mm)	COMPOSITE	WT 125X22.5 (mm)	WT 155X26 (mm)	13.27	5.31
7	69	Inverted-V	MC12X35	COMPOSITE	WT6X22.5	WT6X22.5	9	9
8	71	V	C15X50	COMPOSITE	L3(1/2)X3(1/2)X1/2	L3(1/2)X3(1/2)X1/2	12	5
9	72	Inverted-V	MC10X28.5	COMPOSITE	L6X6X5/8	L6X6X1	9	9
10	70	Inverted-V	C15X33.9	COMPOSITE	L6X6X3/4	L6X6X3/4	12	12
11	13	V	MC18X51.9	COMPOSITE	WT4X9	WT4X9	5	3.25
12	15	Inverted-V	W150X37(mm)	COMPOSITE	2 L 89 X 89 X 7.9(mm)	W150X37(mm)	7.87	9.06
13	44	V	C15x40	COMPOSITE	2L4X4X3/8	W24x84	8.5	10.5
14	43	Inverted-V	W12X53	COMPOSITE	L8X8X3/4	W8X40	7	9
15	41	Inverted-V	C15X33.9	COMPOSITE	L8X6X3/4	2 L8X6X3/4	12	10
16	60	Diaphragm	TOP/BOT FLNG:	COMPOSITE	PL3/4X18	WEB:	PL3/4X57	
17	45	Inverted-V	MC18X42.7	COMPOSITE	L5X5X1/2	L5X5X1/2	13	7
18	42	Inverted-V	MC18X42.7	COMPOSITE	L5X5X1/2	L5X5X1/2	13	10
19	8	Inverted-V	MC18X42.7	COMPOSITE	L6X6X1/2	L6X6X1/2	12	11.5
20	46	Diaphragm	TOP/BOT FLNG:	COMPOSITE	PL1X12	WEB:	PL5/8X72	
21	61	Inverted-V	C12X30	COMPOSITE	WT6X25	WT6X25	8.5	8
22	24	Inverted-V	W10X39	COMPOSITE	L5X5X1/2	L5X5X1/2	9	6
23	25	Inverted-V	MC18X42.7	COMPOSITE	L8X8X3/4	L8X8X3/4	12	12
24	62[4]	Inverted-V	C15X33.9	COMPOSITE	L5X5X1/2	L5X5X1/2	9.5	6.5
25	63	Inverted-V	C310X45 (mm)	COMPOSITE	L127X127X12.7(mm)	L127X127X12.7(mm)	8.66	5.71
26	12	Inverted-V	C12X30	COMPOSITE	L6X6X5/8	C12X30	10	10

#	Alternative Bridge #	INTERMEDIATE CROSS FRAME SECTION (SKEWED)						
		TYPE	TOP CHORD	CONDITION	DIAGONAL	BOT CHORD	TOP CHORD GAP (in.)	BOT CHORD GAP (in.)
1	64	---	---	---	---	---	---	---
2	9	---	---	---	---	---	---	---
3	65	---	---	---	---	---	---	---
4	66	V	L3(1/2)X3(1/2)X3/8	NON-COMP	L3(1/2)X3(1/2)X3/8	L3(1/2)X3(1/2)X3/8	5	5
5	67	V	L6X6X5/8	NON-COMP	L6X6X5/8	L6X6X5/8	10.75	8.5
6	68	V	WT 125X22.5 (mm)	NON-COMP	WT 155X30 (mm)	WT 155X33.5 (mm)	10.12	7.17
7	69	V	WT8X38.5	NON-COMP	WT8X38.5	WT8X38.5	12	10
8	71	V	L5Z5Z1/2	NON-COMP	L5X3(1/2)X1/2	L6X4X5/8	9.25	7.75
9	72	V	2L6X6X3/4	NON-COMP	2L4X4X3/4	2L6X6X3/4	11.5	115
10	70	X	L6X6X3/4	NON-COMP	L6X6X3/4	L6X6X3/4	10	10
11	13	V	WT7X24	NON-COMP	WT6X20	WT7X24	7.75	7.25
12	15	Inverted-V	W150X37(mm)	NON-COMPOSITE	2 L 89 X 89 X 7.9(mm)	W150X37(mm)	7.87	9.06
13	44	V	L3(1/2)X3(1/2)X5/16	NON-COMP	L3(1/2)X3(1/2)X5/16	L3(1/2)X3(1/2)X5/16	5	6.5
14	43	Inverted-V	W8X40	NON-COMP	L8X8X3/4	W8X40	7	9
15	41	---	---	---	---	---	---	---
16	60	Diaphragm	TOP/BOT FLNG:	NON-COMPOSITE	PL3/4X18	WEB:	PL1X57	
17	45	---	---	---	---	---	---	---
18	42	---	---	---	---	---	---	---
19	8	---	---	---	---	---	---	---
20	46	---	---	---	---	---	---	---
21	61	Inverted-V	C12X30	NON-COMPOSITE	WT6X25	WT6X25	8.5	8
22	24	Inverted-V	W10X39	NON-COMP	L5X5X1/2	L5X5X1/2	9	6
23	25	---	---	---	---	---	---	---
24	62[4]	---	---	---	---	---	---	---
25	63	Inverted-V	C310X45 (mm)	NON-COMPOSITE	L127X127X12.7(mm)	L127X127X12.7(mm)	8.66	5.71
26	12	---	---	---	---	---	---	---

#	Alternative Bridge #	INTERMEDIATE CROSS FRAME SECTION						
		TYPE	Number of Intermediate Bracing in the Bridge	TOP CHORD	DIAGONAL	BOT CHORD	TOP CHORD GAP (in.)	BOT CHORD GAP (in.)
1	64	V	15	L6X6X5/8	L5X5X1/2	L5X5X1/2	7	10
2	9	V	18	L5X5X1/2	L5X5X1/2	L5X5X1/2	10	7
3	65	V	15	L5X3X1/4	L3X3X1/4	L5X3X1/4	3	3
4	66	V	21	L3(1/2)X3(1/2)X3/8	L3(1/2)X3(1/2)X3/8	3(1/2)X3(1/2)X3/	5	5
5	67	V	23	L6X6X5/8	L6X6X5/8	L6X6X5/8	10.75	8.5
6	68	V	28	WT155x26 (mm)	WT155x37 (mm)	WT155x37 (mm)	10.63	8.66
7	69	V	20	WT6X22.5	WT6X22.5	WT6X22.5	12	8
8	71	V	22	2 L5X3(1/2)X(1/2)	2 L5X3(1/2)X(1/2)	2 L6X4X(5/8)	9.25	7.75
9	72	V	29	L6X6X1	L6X6X1	L8X8X1	9	11
10	70	X	23	L6X6X3/4	L6X6X3/4	L6X6X3/4	11.5	10
11	13	V	28	WT6X17.5	WT6X17.5	WT4X10.5	7.25	6.5
12	15	Inverted-V	33	2 L 89 X 89 X 7.9(mm)	2 L 89 X 89 X 7.9(mm)	L 89 X 89 X 7.9(mr	7.48	5.91
13	44	V	12	L3(1/2)X3(1/2)X5/16	L3(1/2)X3(1/2)X5/16	3(1/2)X3(1/2)X5/	5	5
14	43	Inverted-V	17	L4X4X3/8	L4X4X3/8	L4X4X3/8	5	5
15	41	X	23	L8X6X3/4	L6X6X5/8	L6X6X5/8	9	9
16	60	V	14	L5X5X3/8	L5X5X3/8	L5X5X3/8	6	6
17	45	Inverted-V	21	L6X6X3/4	L5X5X5/8	L6X6X3/4	6	4.5
18	42	Inverted-V	21	L6X6X3/4	L5X5X5/8	L6X6X3/4	6	4.5
19	8	Inverted-V	12	L6X6X3/4	L6X6X1/2	L6X6X3/4	5	11
20	46	V	20	2 L6X6X7/16	2 L 6X6X7/16	2WT7X66	8	16
21	61	V	15	WT7X41	WT6X25	WT7X41	11.75	7.25
22	24	V	16	L4X4X3/8	L4X4X3/8	L4X4X3/8	6	6
23	25	Inverted-V	18	L6X6X1/2	L5X5X1/2	L5X5X1/2	5	7
24	62[4]	Inverted-V	17	L5X5X1/2	L5X5X1/2	L5X5X1/2	4.5	6.5
25	63	Inverted-V	15	L127X127X9.5(mm)	L127X127X9.5(mm)	127X127X9.5(mm	3.54	7.48
26	12	V	31	L5X5X1/2	L5X5X1/2	L5X5X1/2	9.5	7

The following figures shows different views of the bridge model for all bridges modeled in this study.

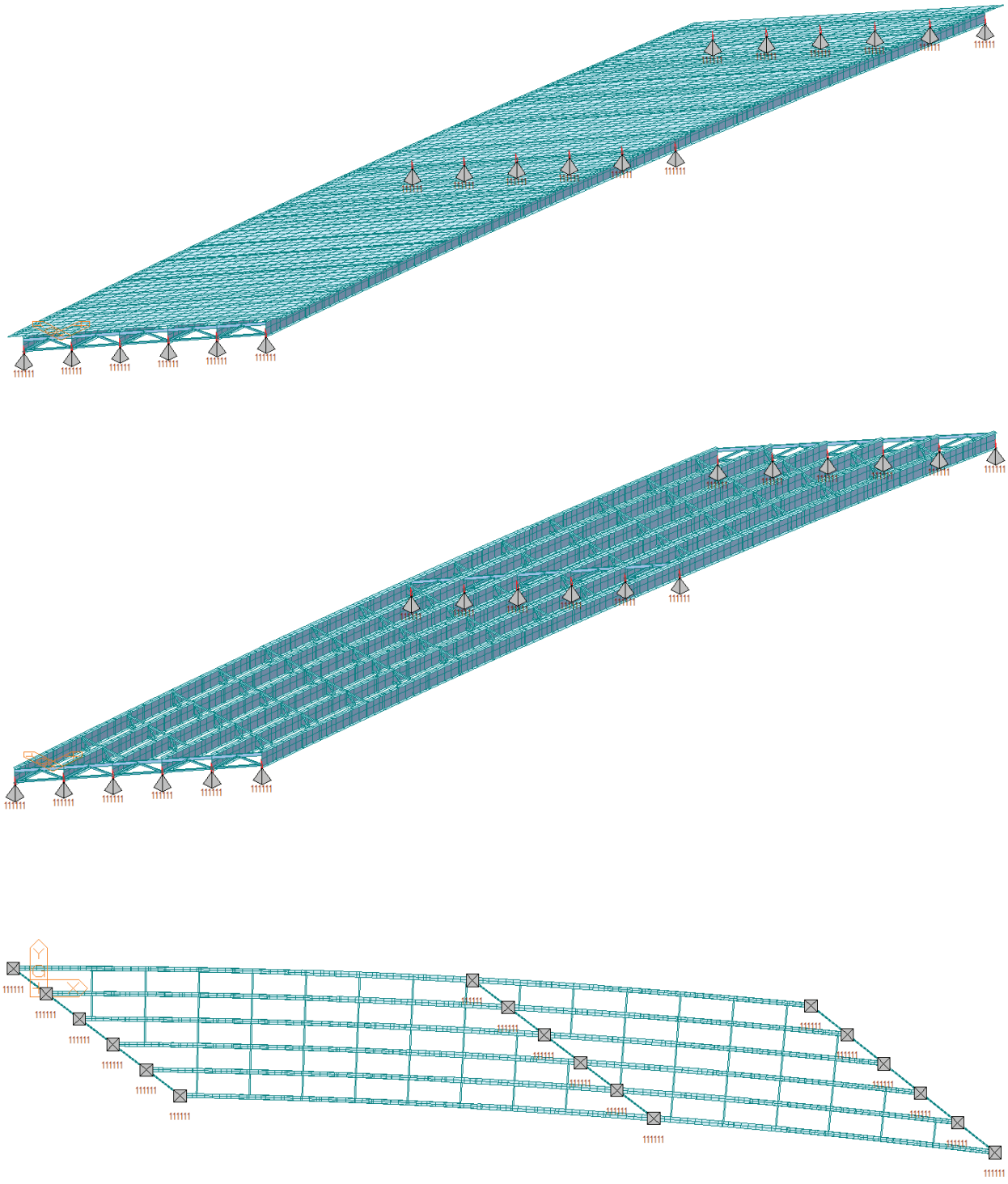

Bridge 64

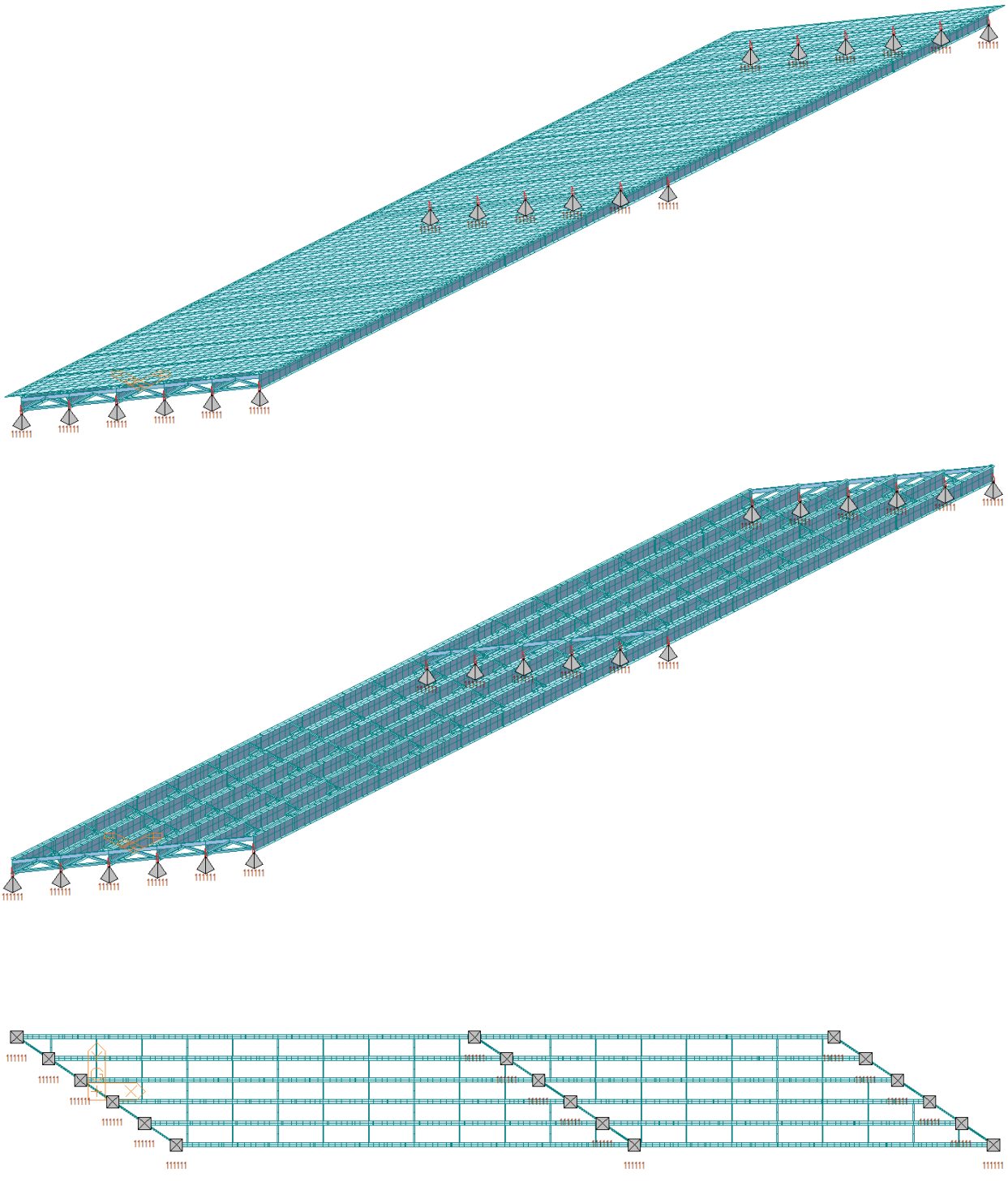

Bridge 9

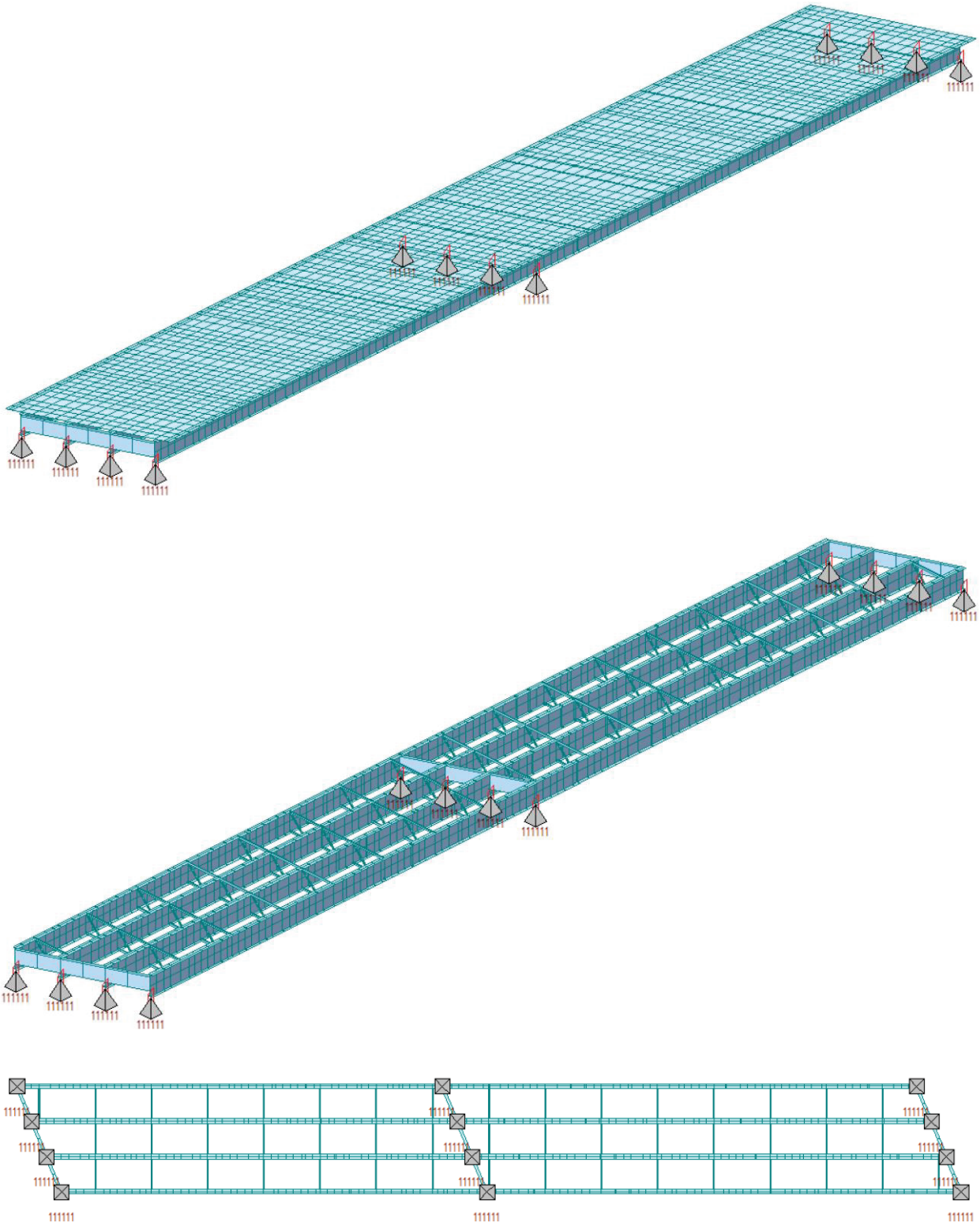

Bridge 65

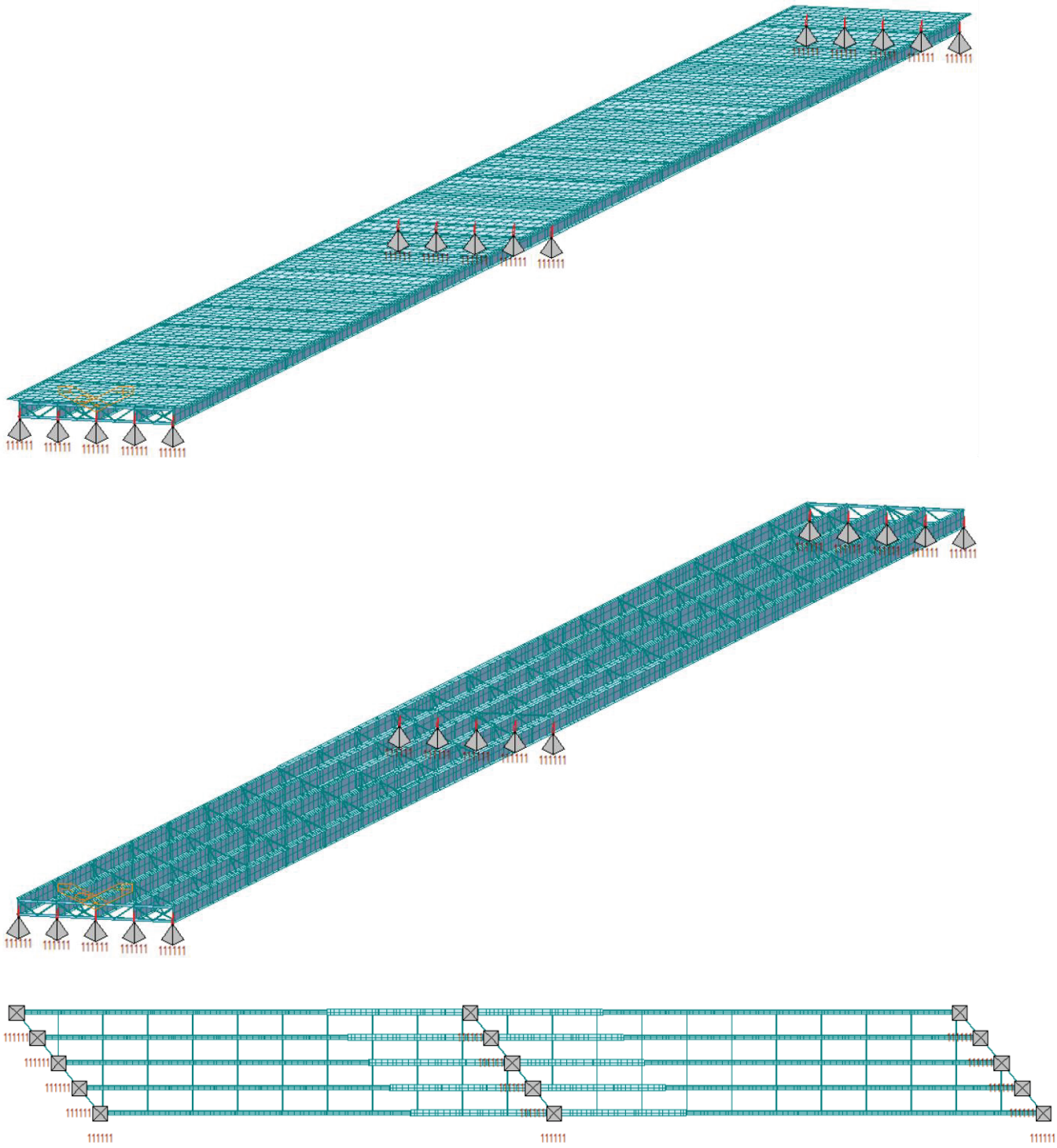

Bridge 66

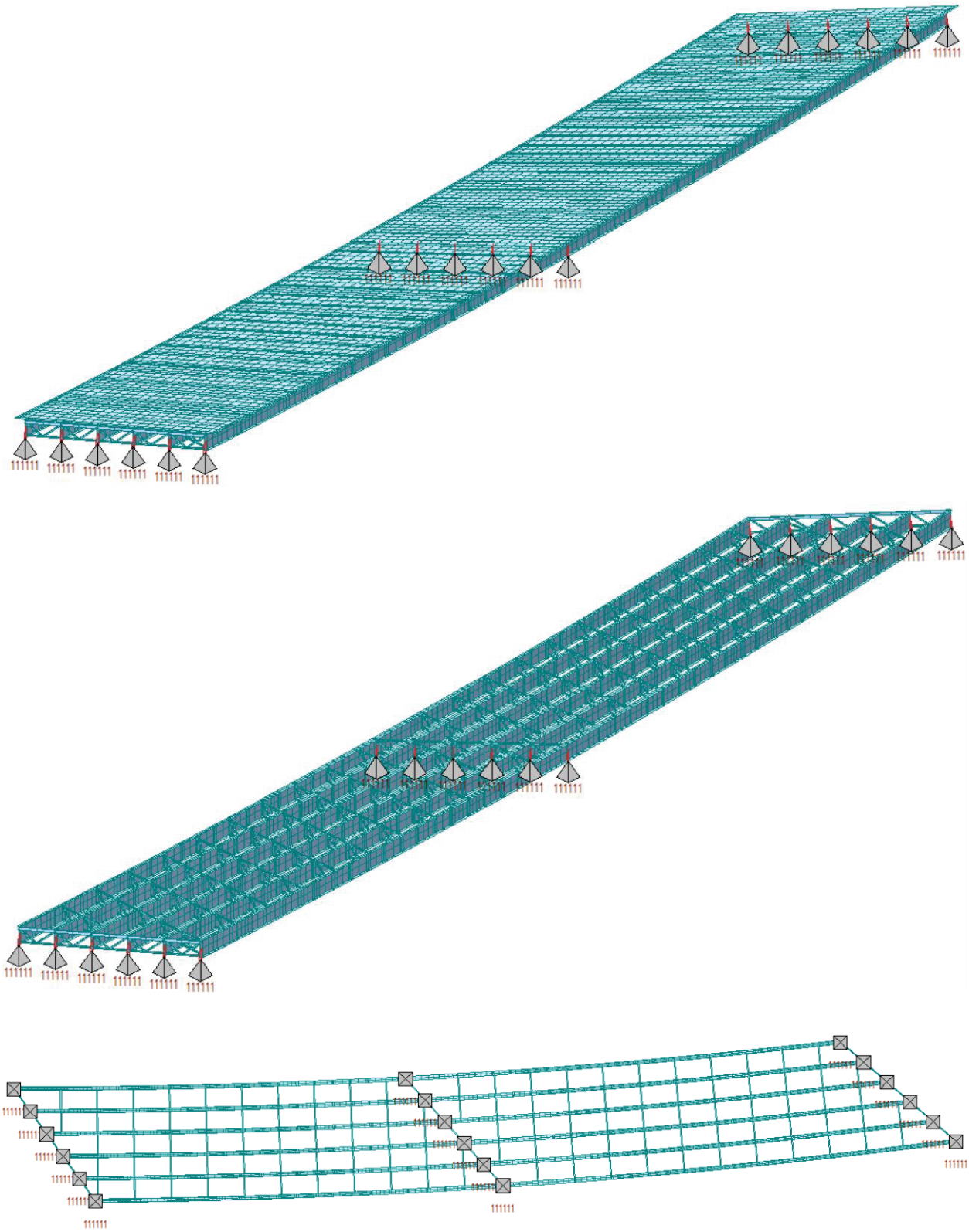

Bridge 67

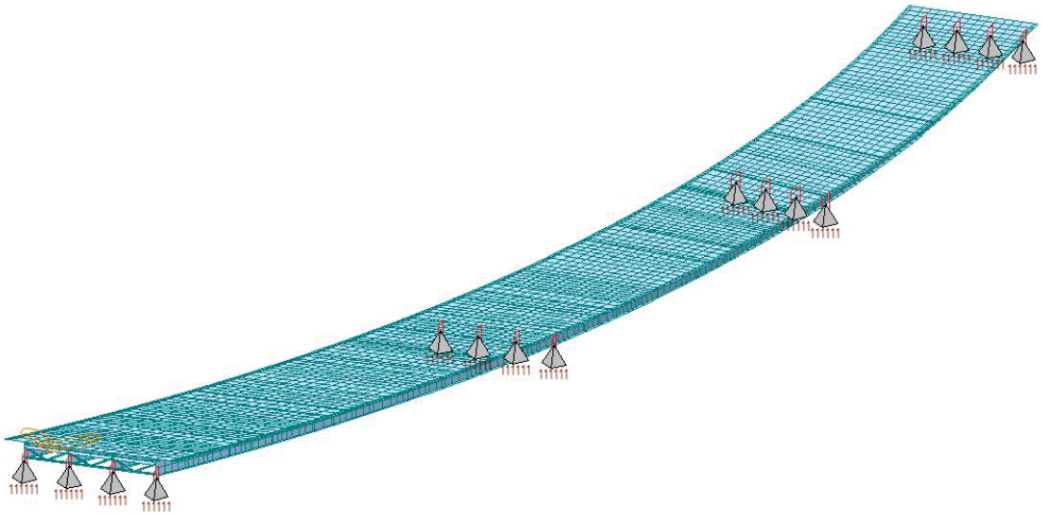

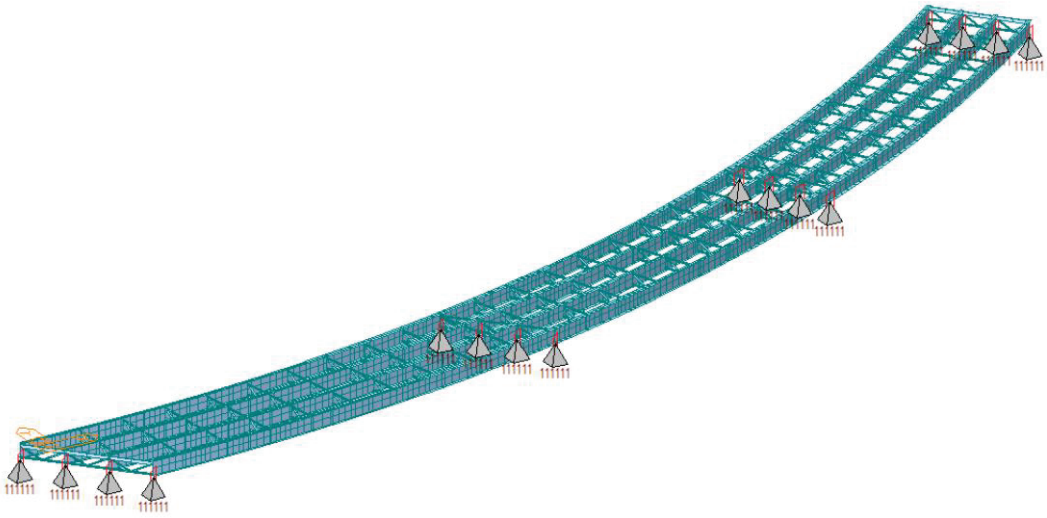

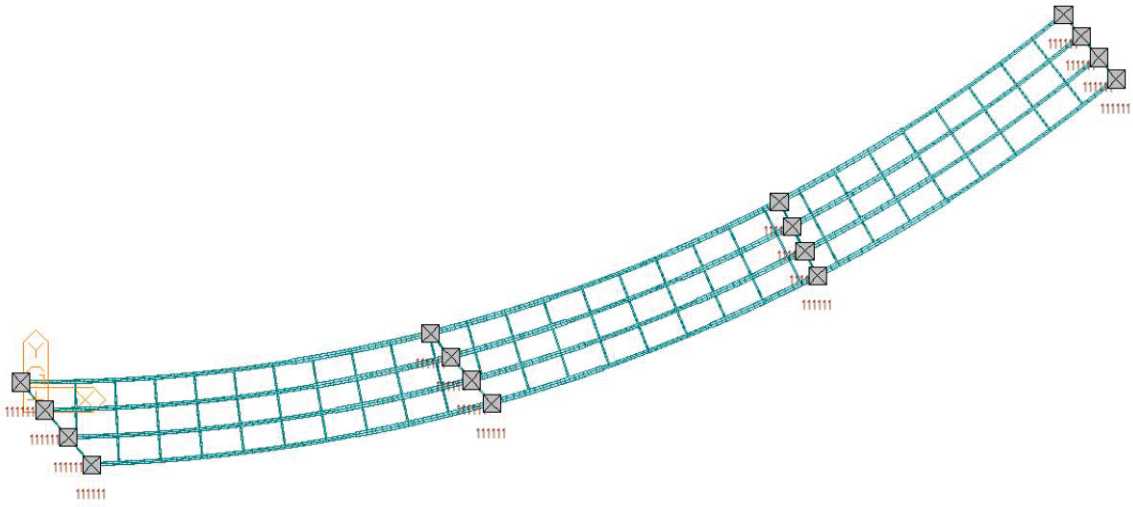

Bridge 68

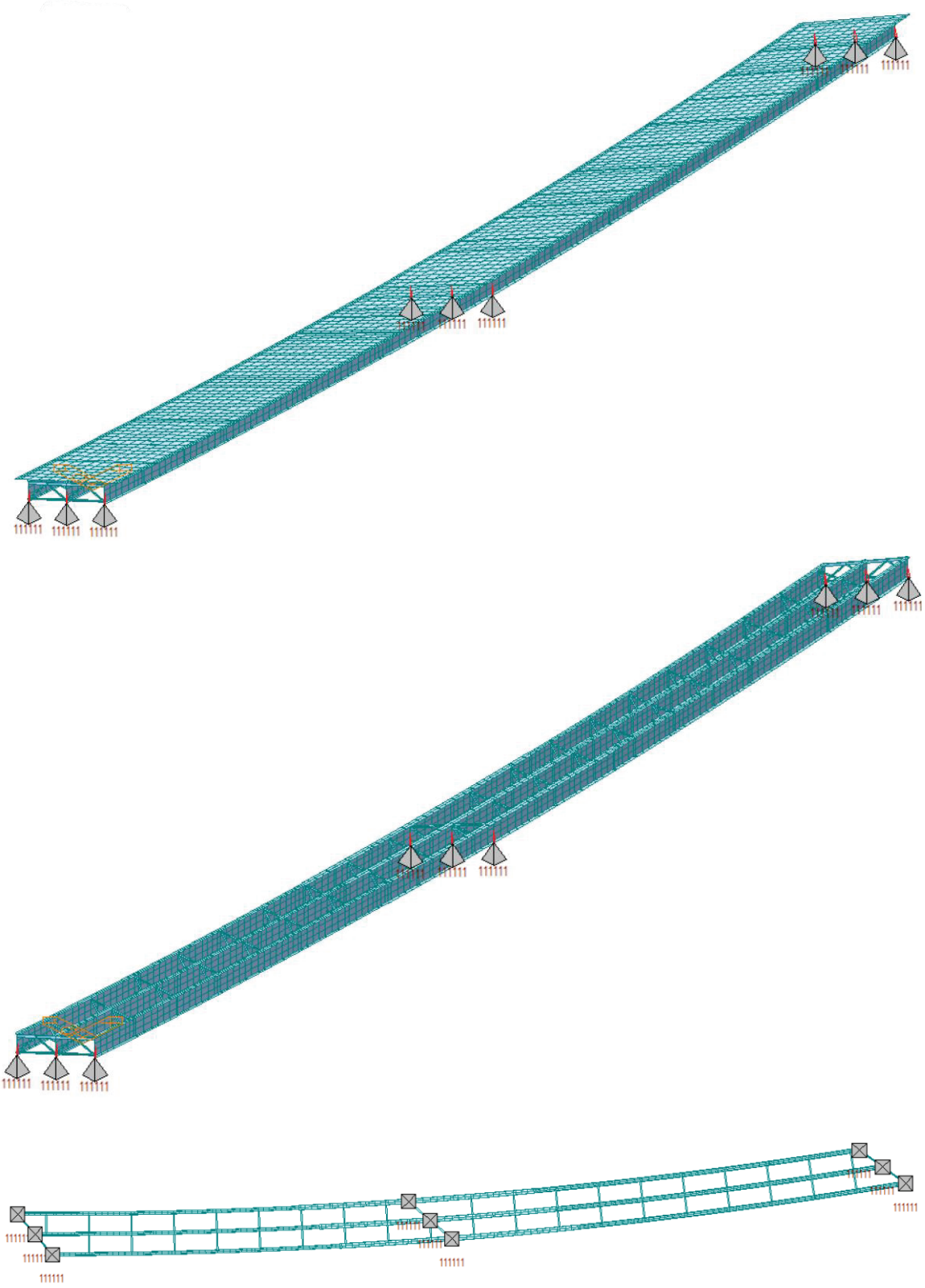

Bridge 69

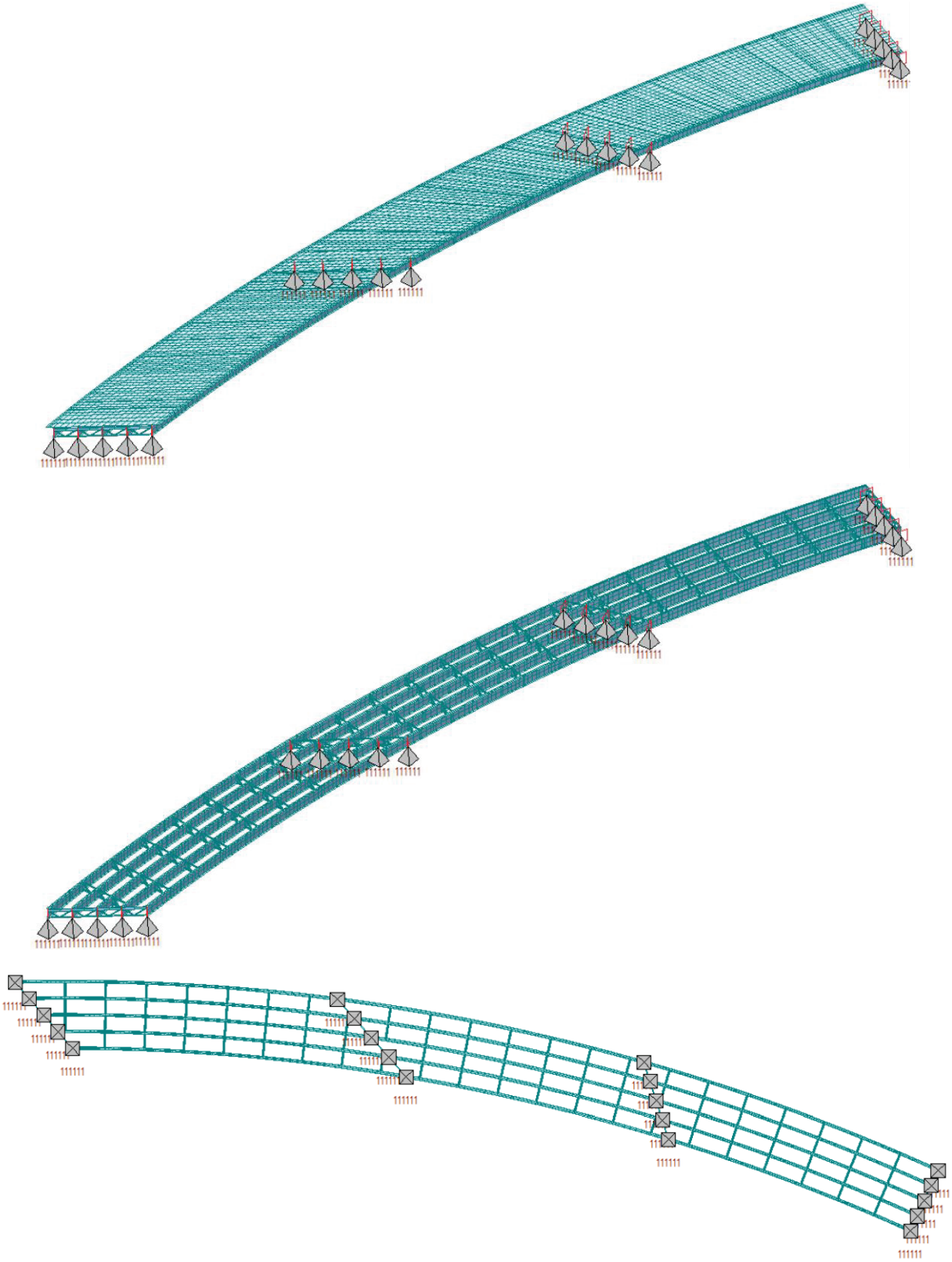

Bridge 71

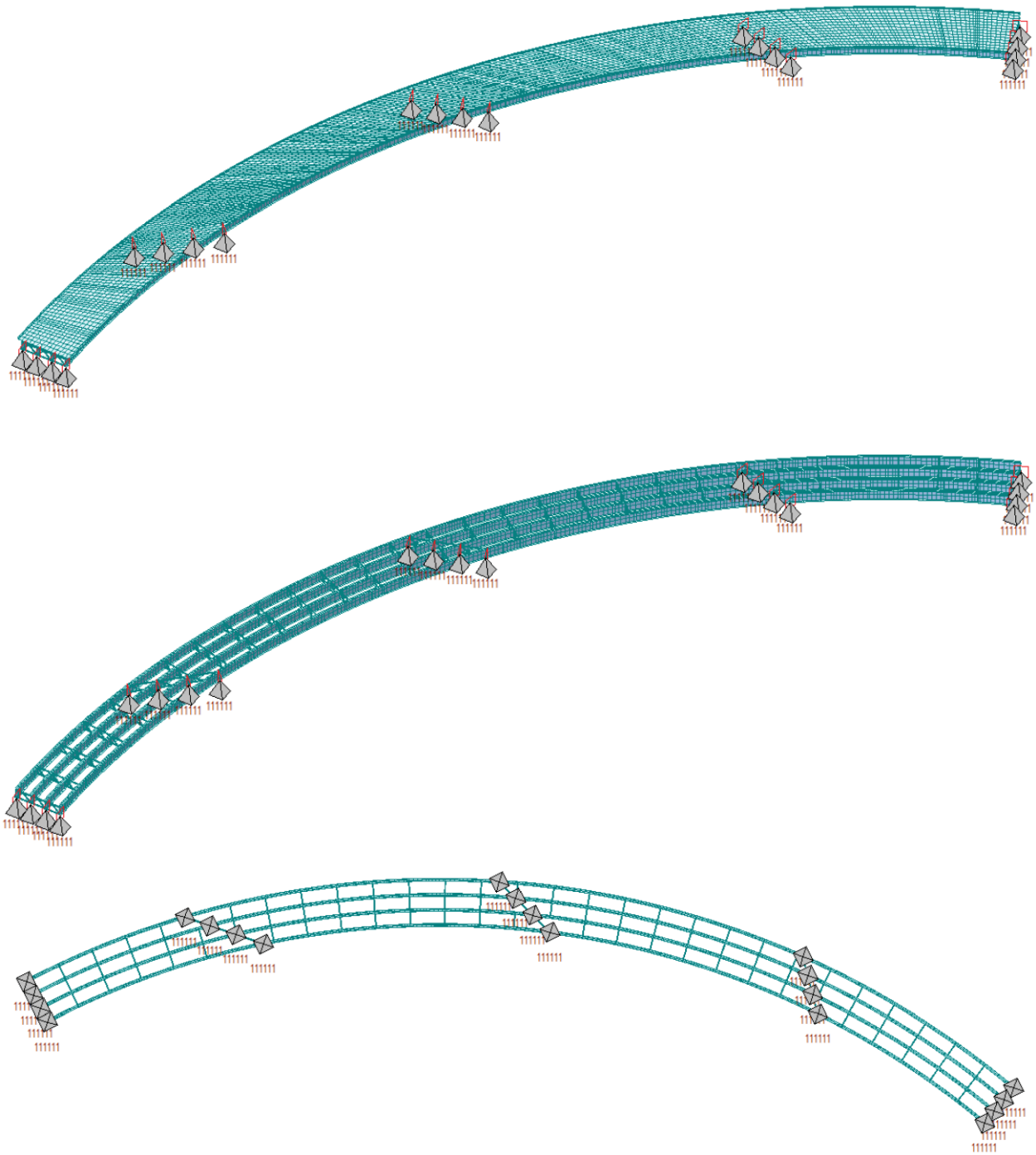

Bridge 72

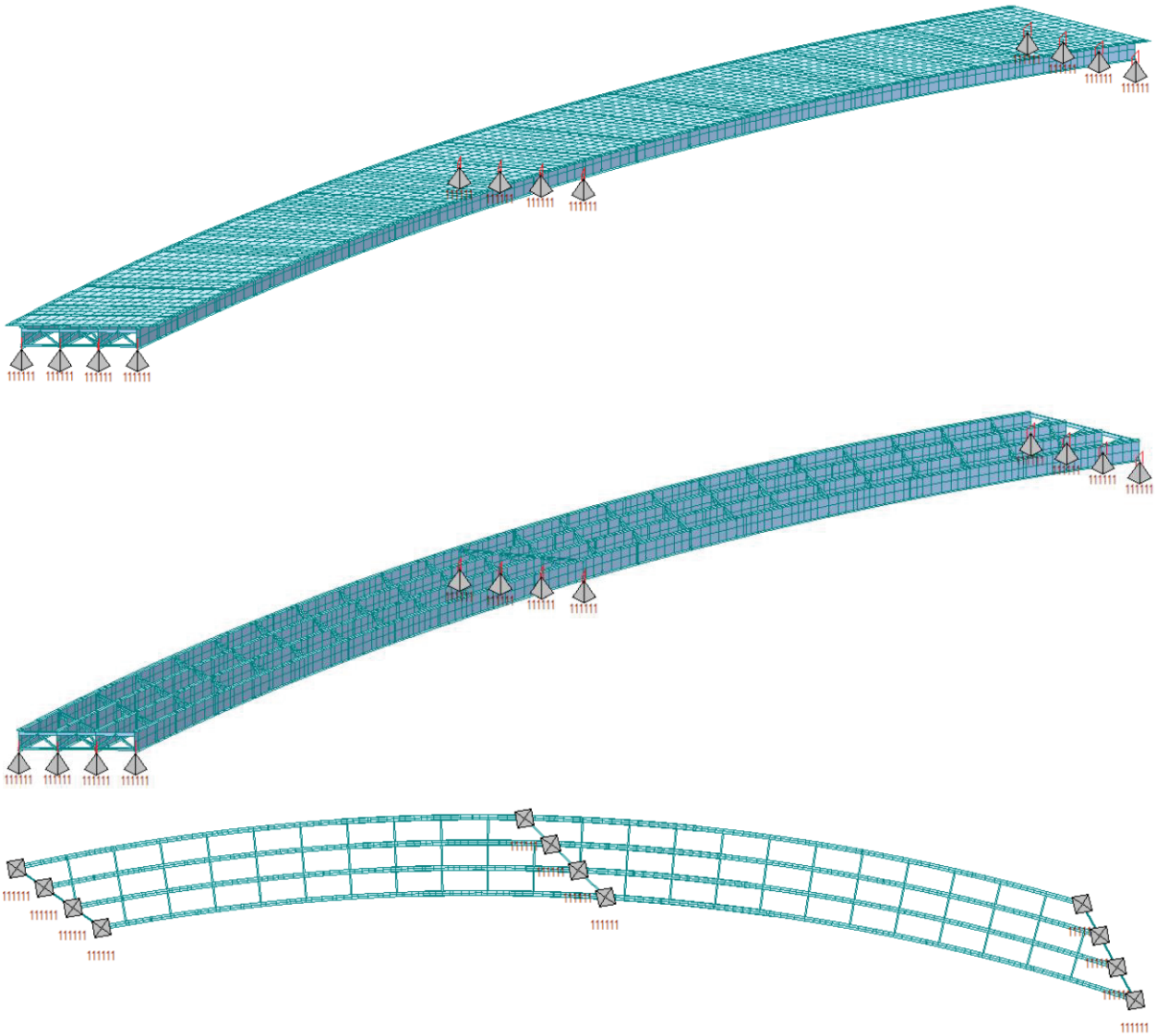

Bridge 70

Bridge 13

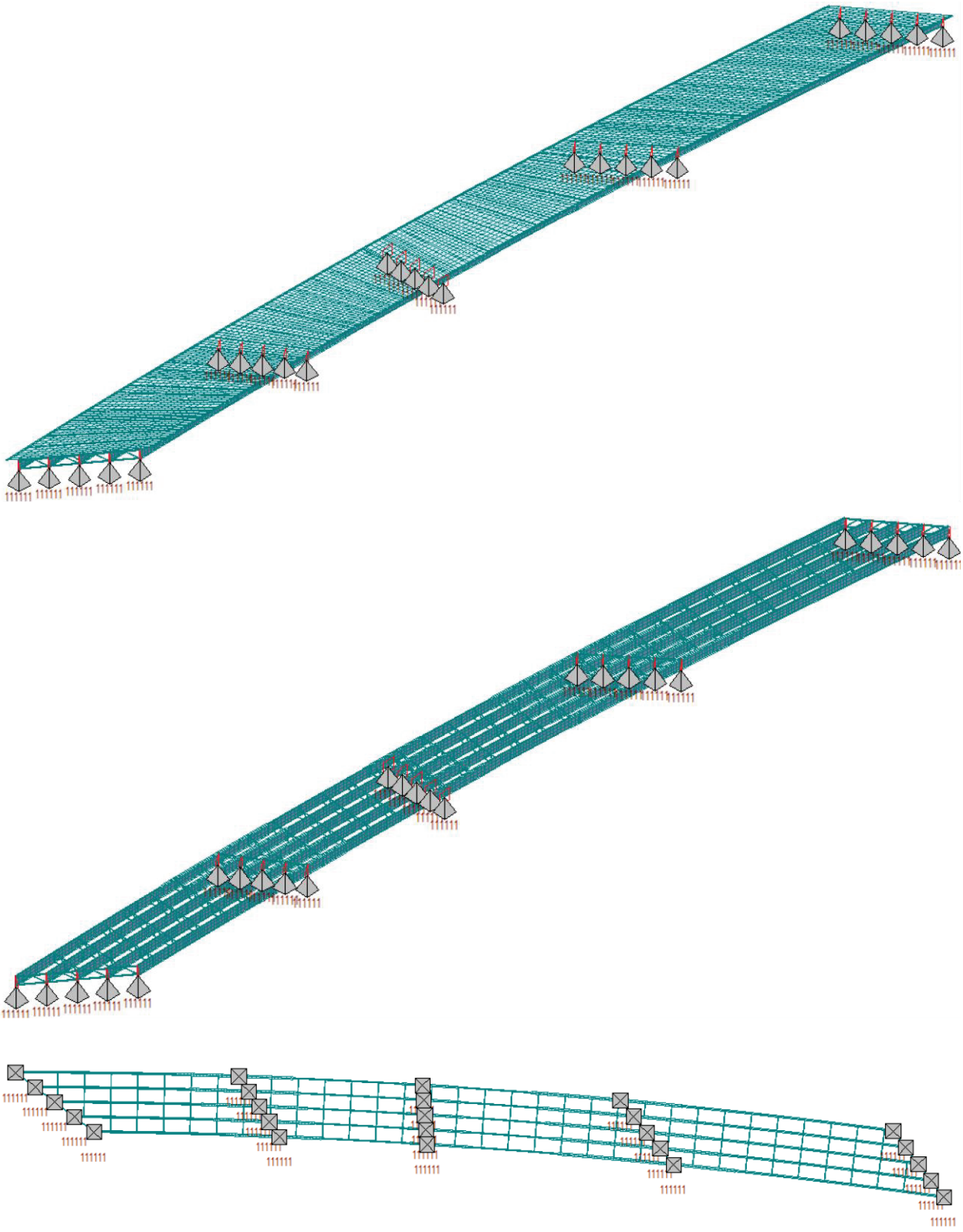

Bridge 15

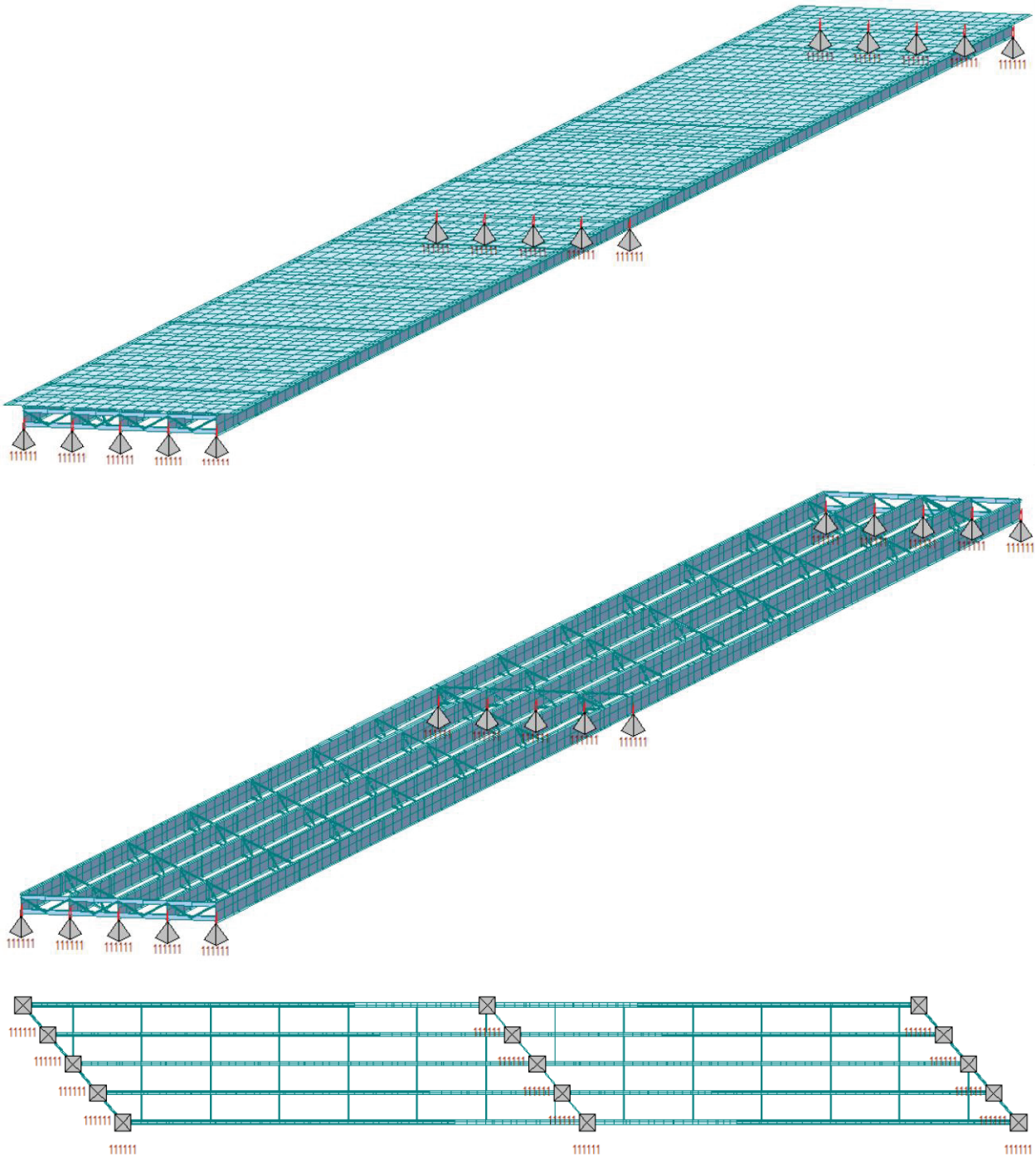

Bridge 44

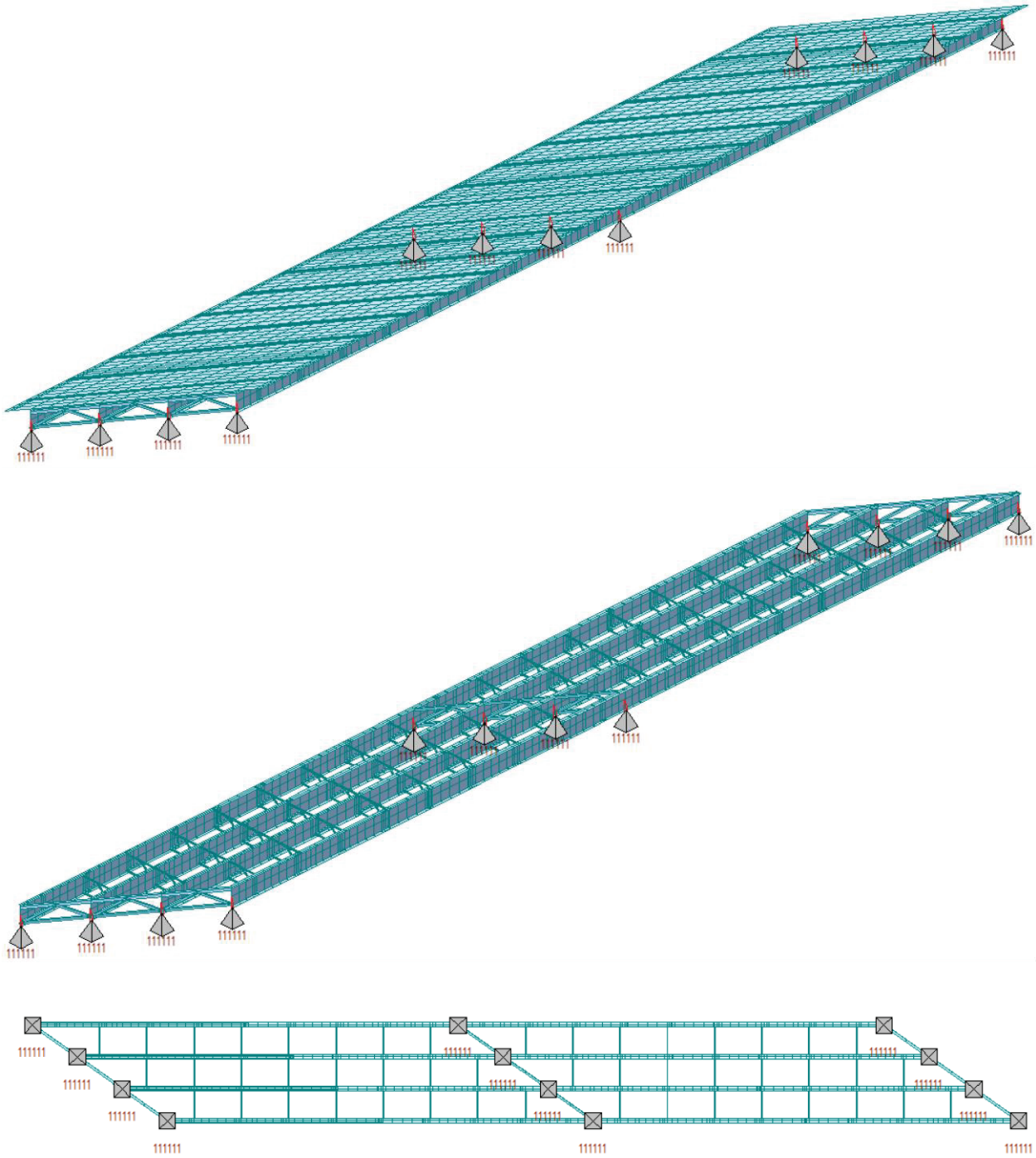

Bridge 43

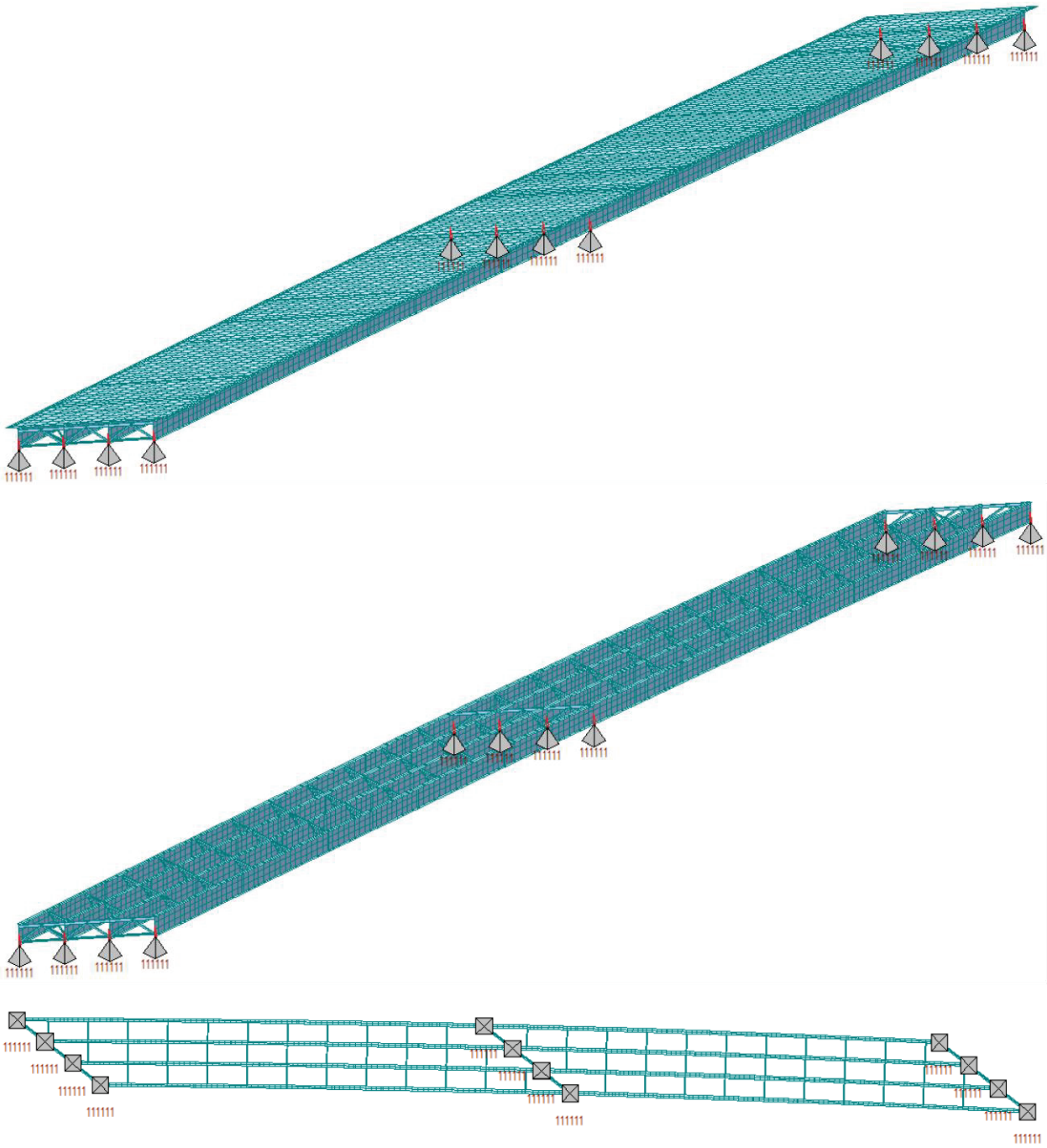

Bridge 41

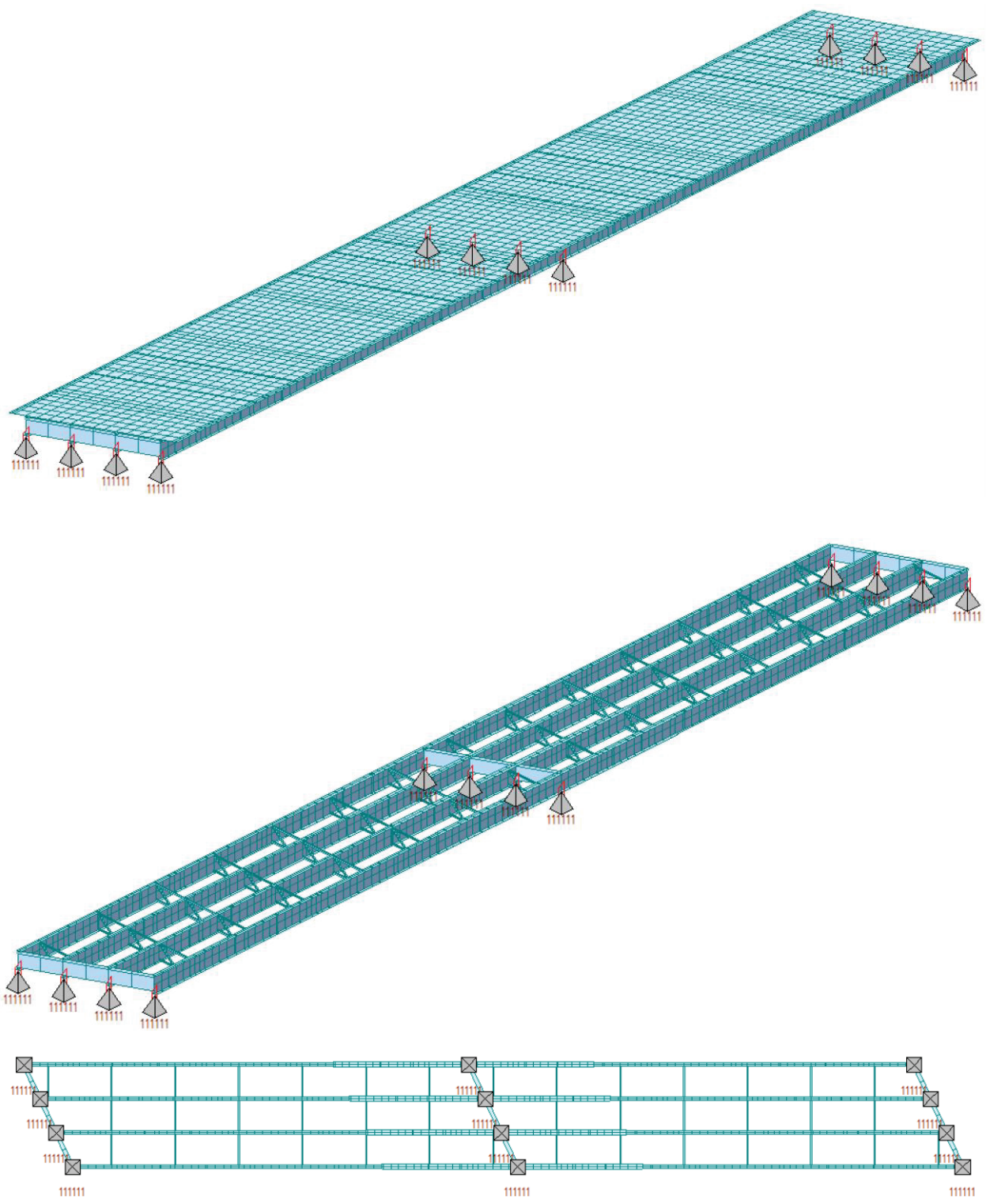

Bridge 60

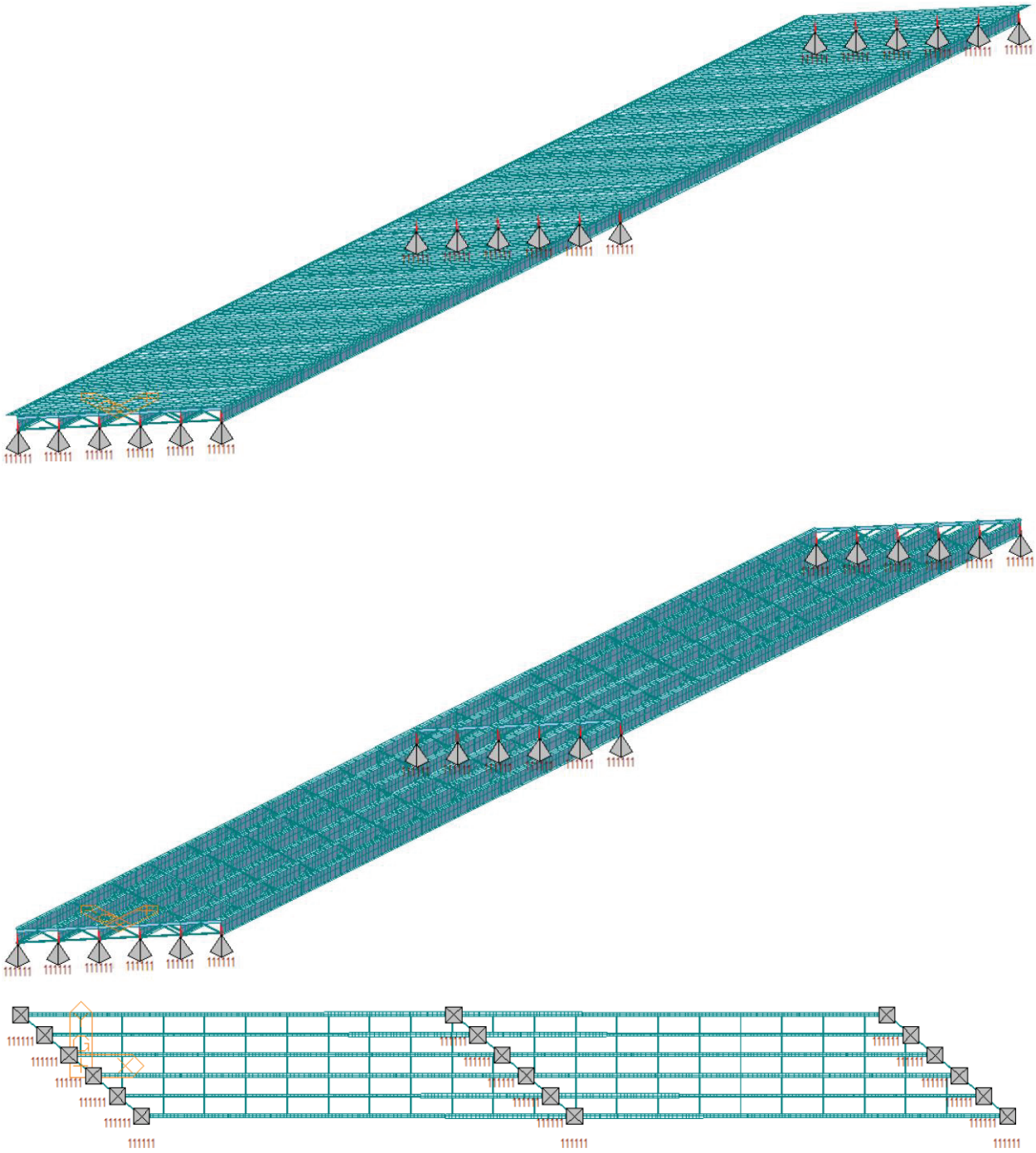

Bridge 45

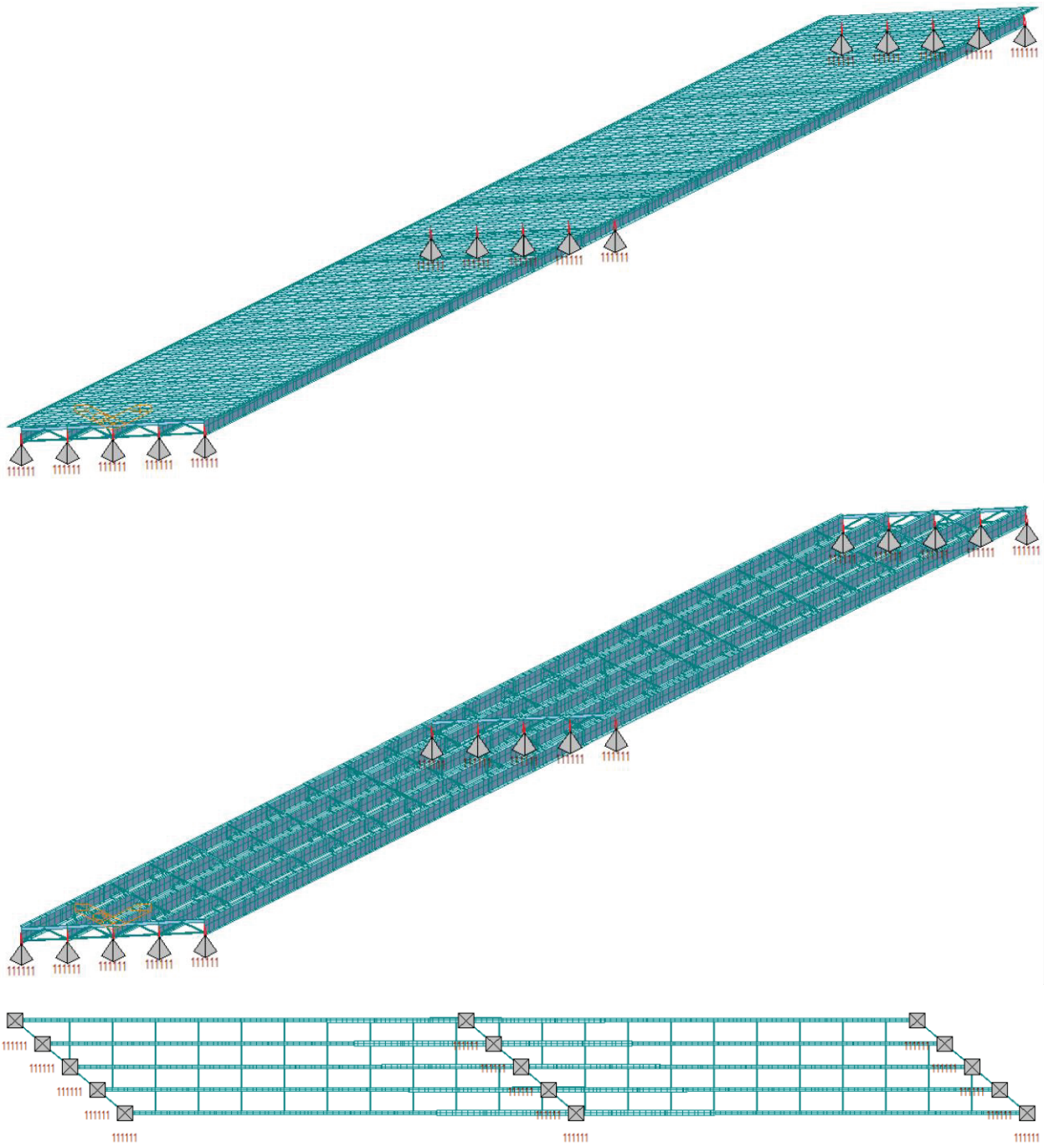

Bridge 42

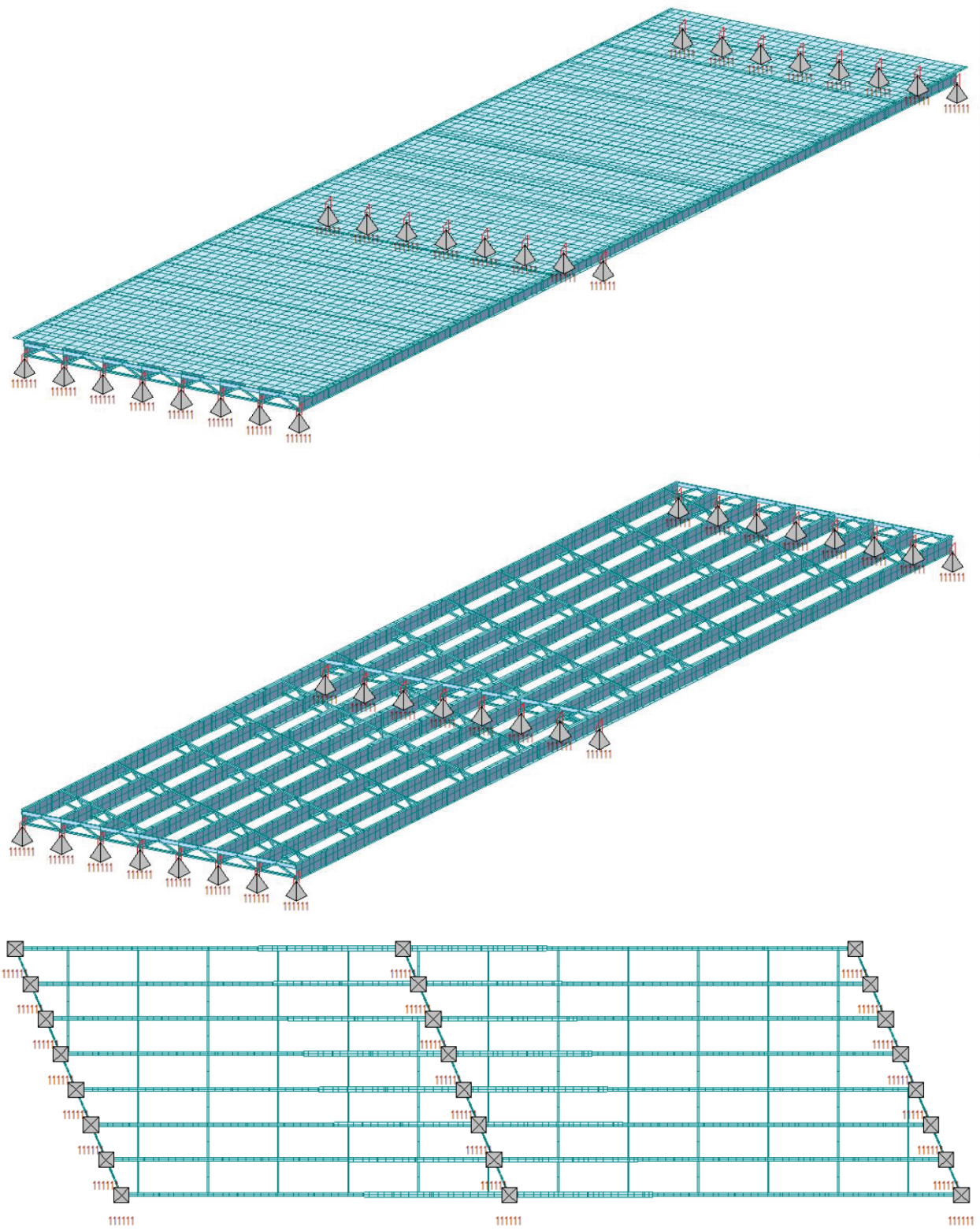

Bridge 8

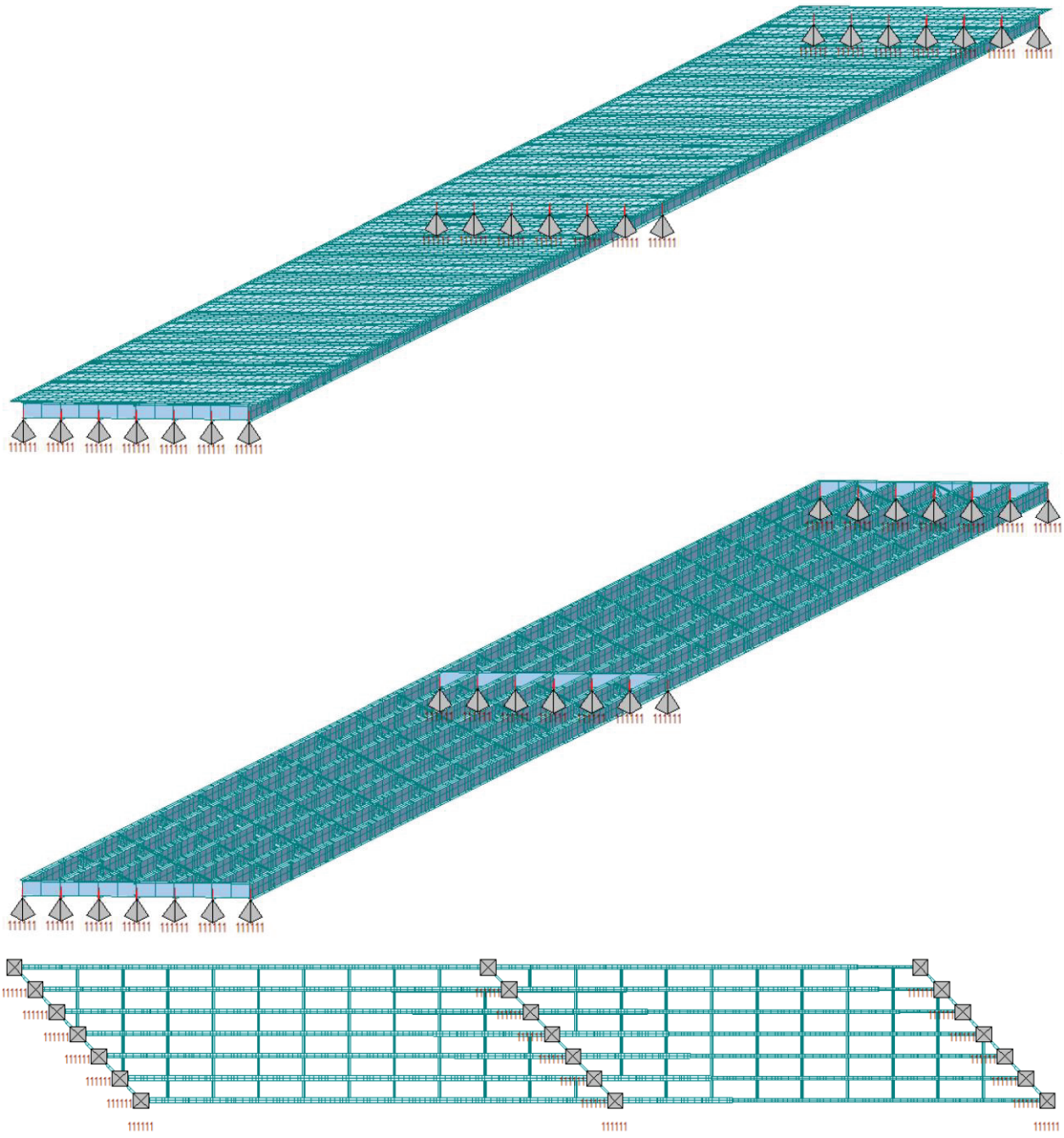

Bridge 46

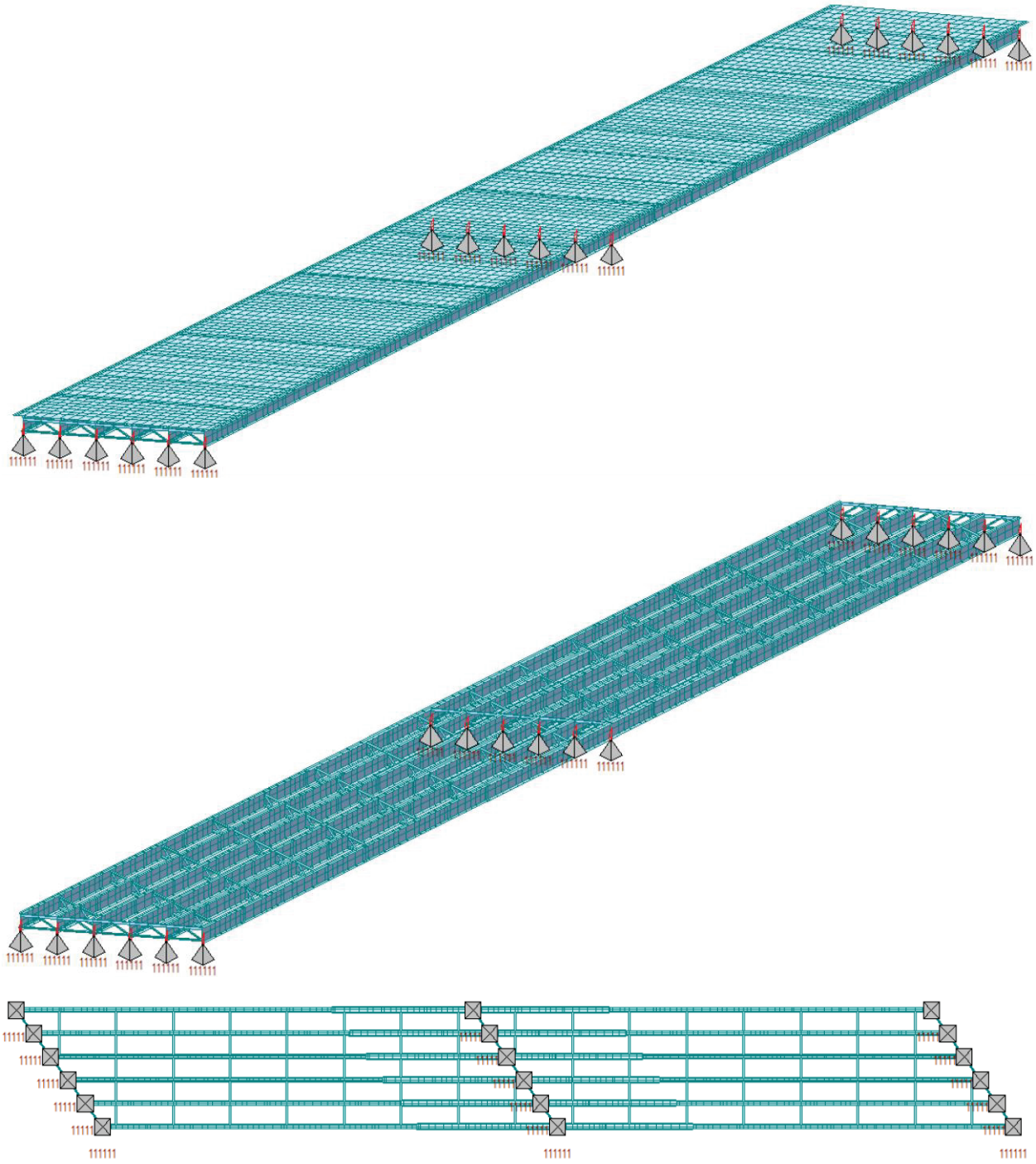

Bridge 61

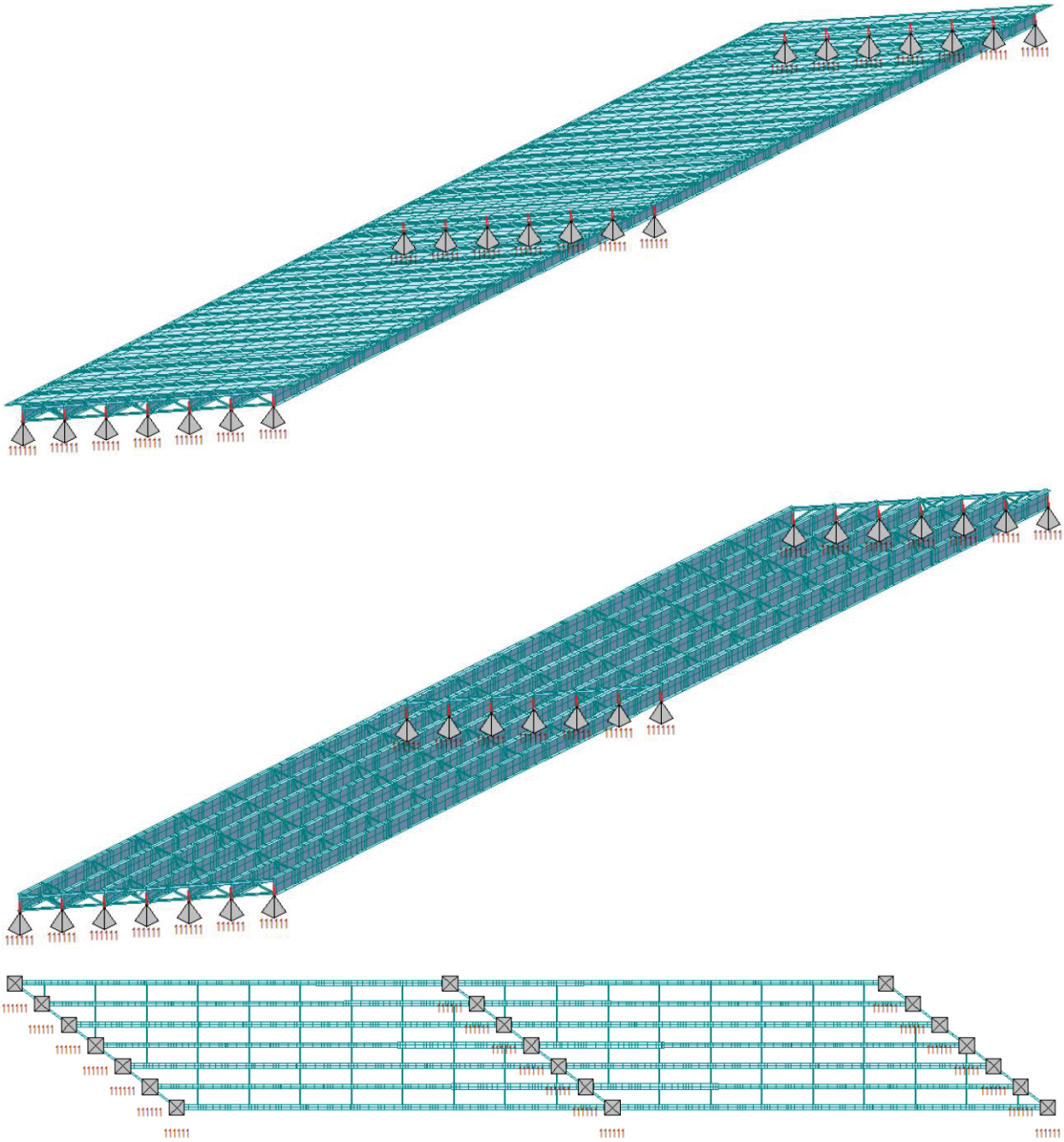

Bridge 24

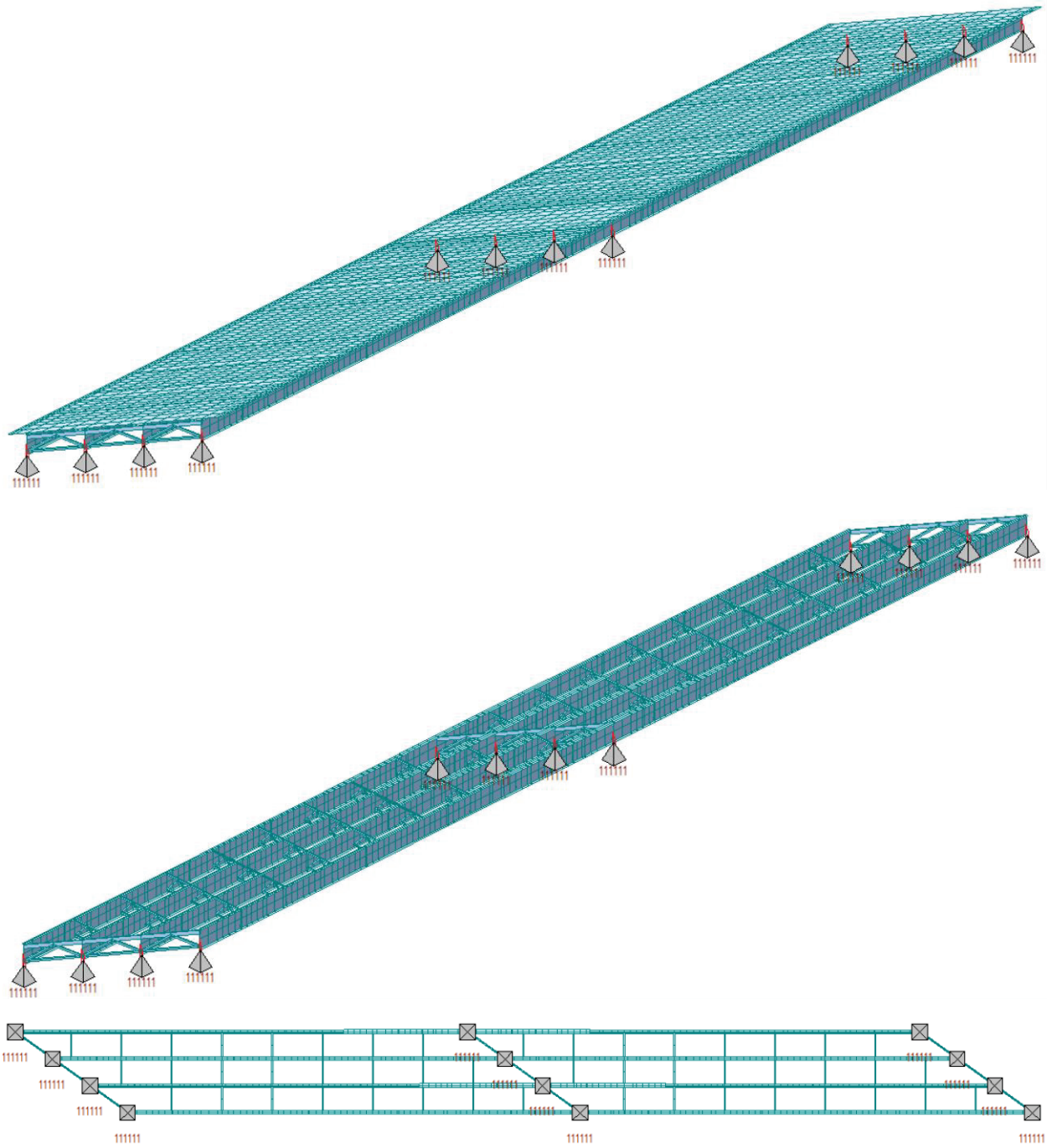

Bridge 25

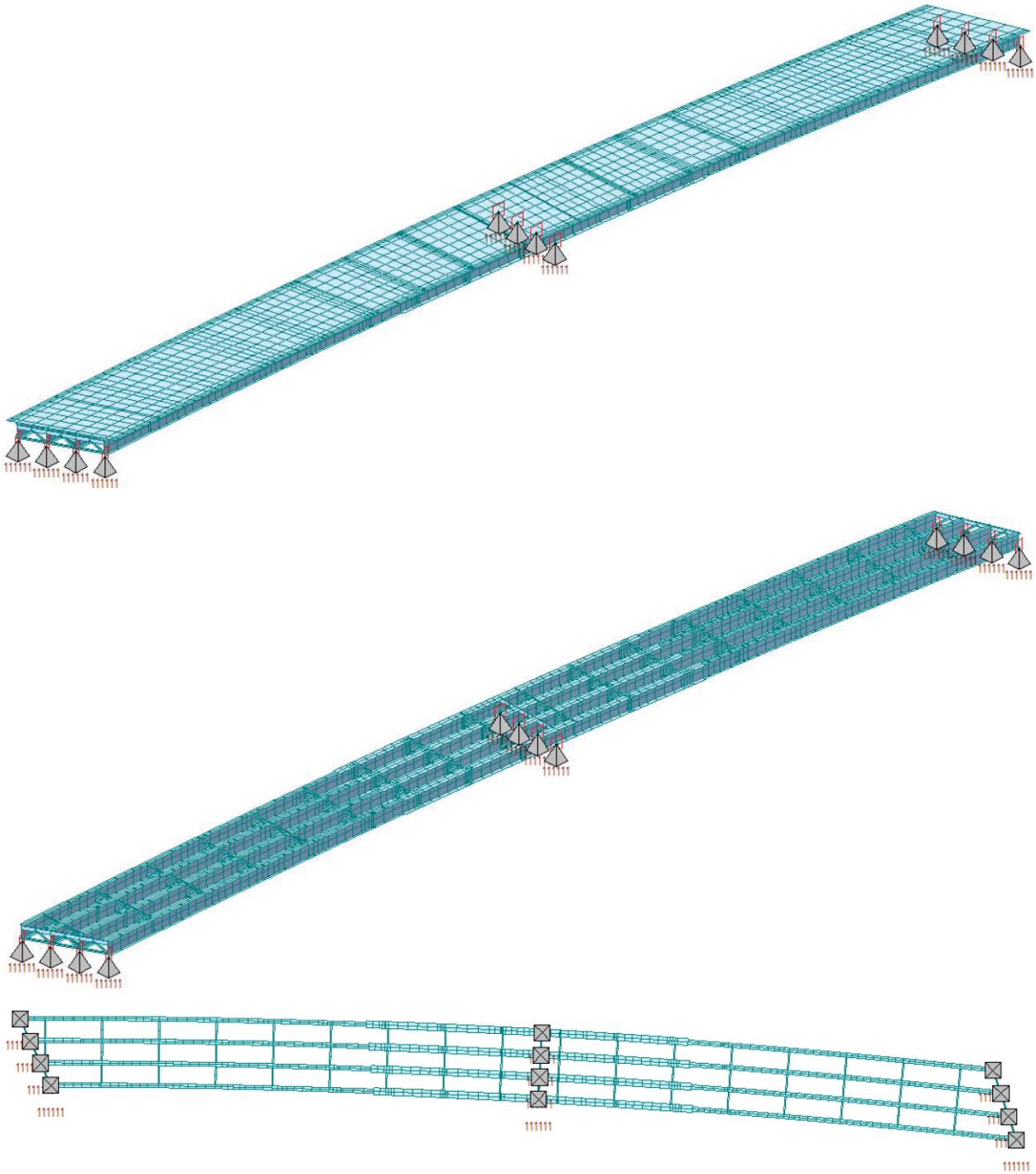

Bridge 24

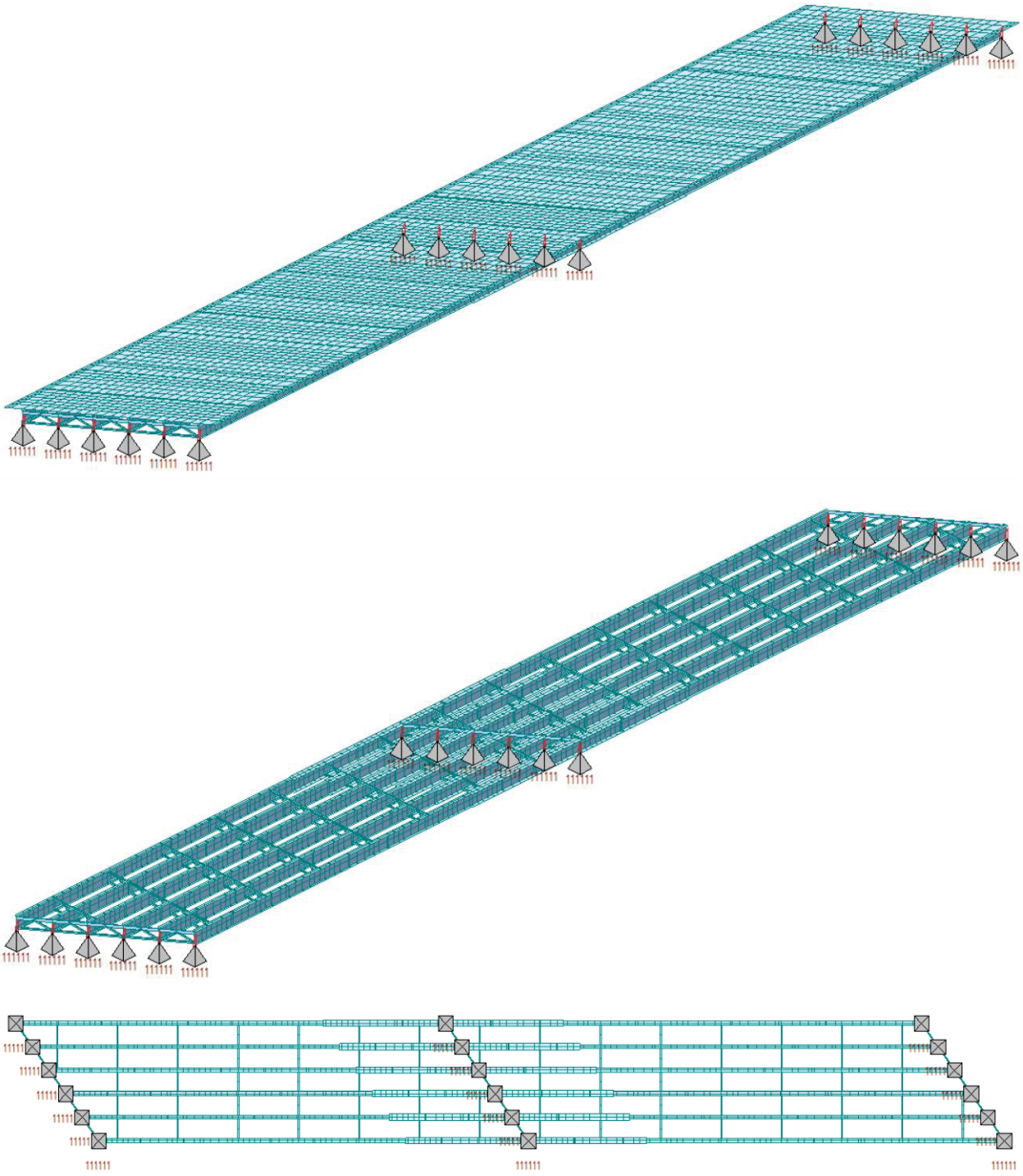

Bridge 63

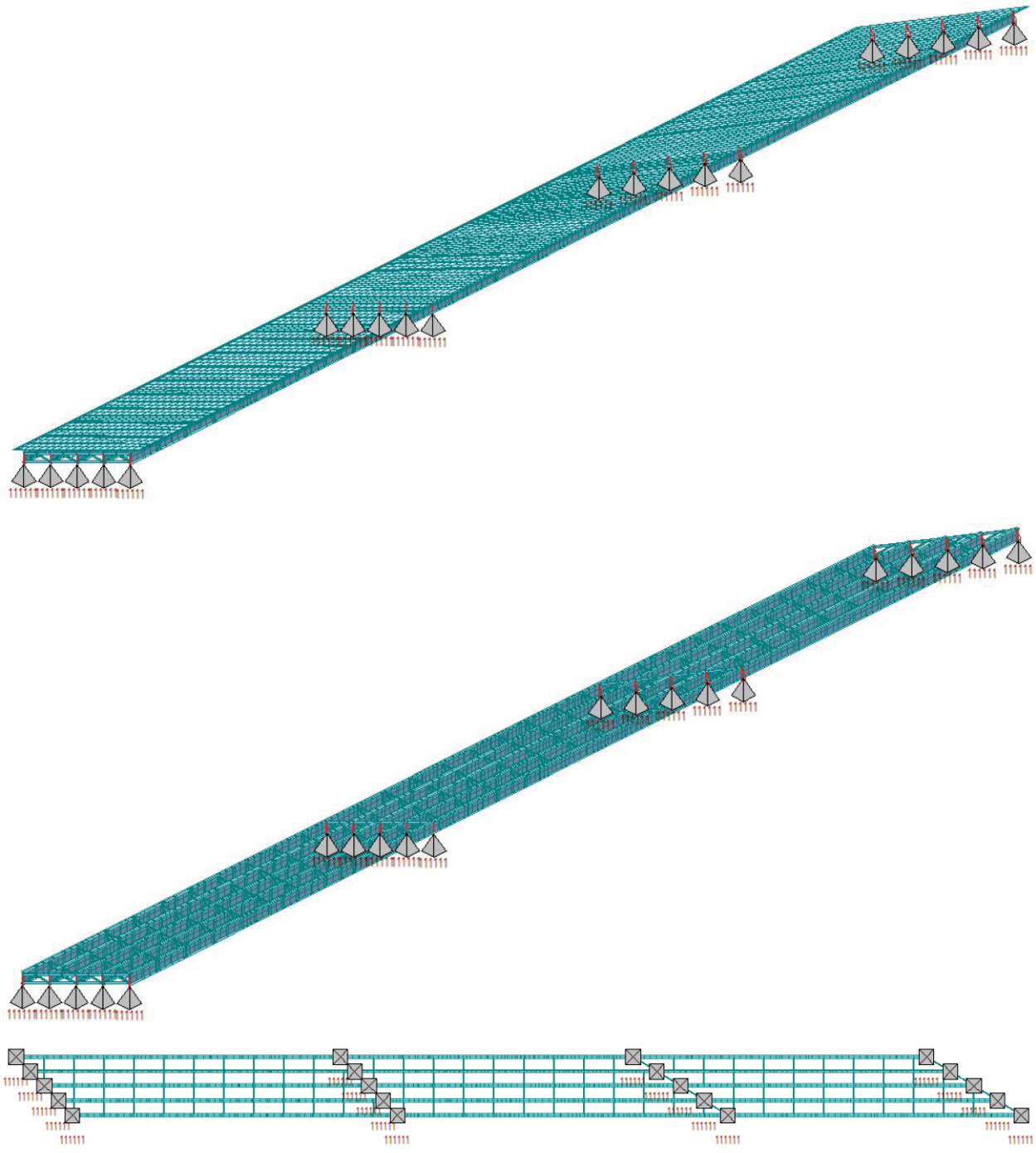

Bridge 12

APPENDIX B - Safety and Compliance Protocols for Experimental Testing

B-1 Pre-Test Preparations

- **Risk Assessment:**
    - Conduct a thorough risk assessment to identify potential hazards associated with the fatigue testing process.
    - Document all identified risks and establish control measures to mitigate these risks.
    - Ensure all personnel involved in the test are aware of the risks and have received appropriate training.
- **Training and Authorization:**
    - Only trained and authorized personnel should be allowed to operate the testing equipment and handle the test specimens.
    - Provide training on the specific fatigue testing equipment, emergency procedures, and proper use of personal protective equipment (PPE).
- **Equipment Inspection:**
    - Inspect the fatigue testing setup for any signs of wear, damage, or malfunction before use. Monitor the equipment during long-term continuous operations to assure effective performance.
    - Verify that all safety guards and interlocks are functioning properly.
    - Ensure that load cells, sensors, and other instrumentation are calibrated and in good working condition.
- **Material Handling:**

- Use appropriate lifting equipment and techniques to move and position the test specimens.
- Ensure that the test specimens are free from visible defects, such as cracks or corrosion, that could affect the test's safety or accuracy.

B-2 Personal Protective Equipment (PPE)

- **Mandatory PPE:**
  - All personnel in the testing area must wear safety helmets, safety goggles, and steel-toed boots.
  - Hearing protection should be worn if noise levels exceed safe limits.
  - Gloves and protective clothing should be worn to protect against sharp edges or rough surfaces on the steel beam.
  - All other gear required by the testing lab.
- **Specialized PPE:**
  - If the test involves high loads or high-speed cycling, consider using additional protective barriers or face shields.

B-3 Test Setup

- **Securing the Steel Girder:**
  - Ensure that the steel girder is securely positioned in the testing machine to prevent any movement during the test.
  - Double-check the alignment of the girder and loading setup and ensure all are supported and positioned properly to avoid unintended eccentricities and stress concentrations.
- **Machine Settings:**

- Make sure that the loading machine and hydraulics are capable of the prescribed loading level and frequency.

- **Environmental Controls:**

  - Maintain the testing environment within the specified temperature and humidity range to ensure consistent test results.

B-4 During the Test

- **Monitoring:**

  - Continuously monitor the test visually and by using sensors and data acquisition systems.

  - If any unusual sounds, vibrations, or movements occur, immediately halt the test and assess the situation.

- **Access Control:**

  - Restrict access to the testing area during the test to authorized personnel only.

  - Clearly mark the testing area with warning signs alarming that the fatigue test is ongoing.

- **Emergency Stop:**

  - Ensure that an emergency stop button is easily accessible to all personnel in the testing area.

  - Test the emergency stop functionality before beginning the fatigue test.

- **Communication:**

  - Maintain clear communication between all personnel involved in the test. Use radios or intercoms if the testing area is large or noisy.

B-5 Post-Test Procedures

- **Controlled Shutdown at Intervals or the End of Test:**
    - Gradually reduce the load and cycling frequency before stopping the machine.
    - Allow the steel girder to return to a stable condition before unclamping and removing it from the machine.
- **Inspection and Documentation:**
    - Conduct a post-test inspection of the steel girder and testing equipment to identify any damage or irregularities.
    - Document all test data, observations, and any incidents or near misses during the test.
- **Decontamination and Clean-Up:**
    - If any fluids or debris were generated during the test, ensure they are properly cleaned up and disposed of following environmental and safety regulations.
    - Return all tools, equipment, and PPE to their designated storage areas.

B-6 Emergency Procedures

- **First Aid:**
    - Ensure that a first aid kit is readily available in the testing area.
    - Train personnel on how to respond to common injuries that could occur during fatigue testing, such as cuts, bruises, or crush injuries.
- **Fire Safety:**
    - Verify that fire extinguishers are present and easily accessible in the testing area.

- If the test involves heating or other processes that could cause a fire, have additional fire safety measures in place.

- **Evacuation Plan:**
  - Establish an evacuation plan in case of a major incident, such as a structural failure of the girder or testing machine.
  - Conduct regular evacuation drills and ensure that all personnel are familiar with the evacuation routes and assembly points.

B-7 Regulatory Compliance

- **Standards and Guidelines:**
  - Ensure that the fatigue test complies with relevant industry standards (e.g., ASTM, ISO) and safety regulations (OSHA, etc.).
  - Keep records of all safety protocols, risk assessments, and training as required by regulatory authorities.

- **Regular Audits:**
  - Conduct regular safety audits and reviews of the fatigue testing process to identify areas for improvement.
  - Update the safety protocols as necessary based on the audit findings and any new industry developments.

B-8 Continuous Improvement

- **Incident Reporting:**
  - Implement a system for reporting and investigating any incidents or near misses during fatigue testing.

- Use the findings from these investigations to improve safety protocols and prevent future occurrences.

- **Feedback Loop:**
  - Encourage feedback from all personnel involved in the fatigue testing process.
  - Regularly review and update safety procedures based on this feedback to ensure a culture of continuous safety improvement.

B-9 Safety Culture

- **Safety Meetings:**
  - Hold regular safety meetings to discuss ongoing projects, potential hazards, and safety improvements related to fatigue testing.
  - Involve all personnel in the discussion to ensure a comprehensive understanding and commitment to safety.

- **Safety Signage:**
  - Ensure that all safety signs and labels in the testing area are clear, visible, and regularly maintained.
  - Update signage as necessary to reflect any changes in safety procedures or testing conditions.